

UNIVERSITY OF STRATHCLYDE

Department of Mechanical and Process Engineering

Division of Thermo-Fluid and Environmental Engineering

**EFFECTS OF CONDENSATION ON STEAM-WATER,
COUNTER-CURRENT FLOODING IN A VERTICAL TUBE**

by

HUSHAM MAHMOOD AHMED

Thesis presented for the degree of

DOCTOR OF PHILOSOPHY

in

MECHANICAL ENGINEERING

June 1988

**This thesis is dedicated
in loving memory of my father**

ABSTRACT

During a loss of coolant accident in a pressurised water reactor, emergency core cooling water is introduced via the downcomer annulus. The water may have to penetrate or overcome steam formed in the vessel due to the depressurisation. A typical counter-current flow situation can be created and dependent on the relative flow rates water may be prevented from reaching the reactor core with serious consequences.

This thesis considers the events leading up to this occurrence in a vertical, 54.75 mm internal diameter, 1 m long, stainless steel tube, to represent and provide a basic understanding of the situation occurring during a loss of coolant accident. Results are presented for air-water and steam-water flows with emphasis on the experimental and theoretical studies of the steam-water flow situation where direct contact heat transfer occurs. The air-water flooding data are shown to be well represented by a Wallis type flooding correlation. The steam-water flooding data are found to lie above the corresponding air-water data with their characteristic dependent on the water inlet subcooling.

The percentage of the air/steam flow extracted with the water flow at the bottom porous sinter was found

to exert a negative effect on the flooding phenomena. A theoretical model was developed to predict the liquid film thickness along the tube, and agreement with the experimental results demonstrated.

A second theoretical model was developed to evaluate the temperature across the liquid film and along the test tube and from this model, the effective turbulent diffusivity was evaluated, leading to an estimate of the turbulent viscosity of the film under conditions in which substantial condensation took place.

A semi-empirical model based on a linear stability analysis of a uniform liquid film and a counter-current flow of steam, was developed and modified for accelerating film flows. This model is shown to be capable of dealing with the steam-water flooding situation since reasonable agreement with the air-water flooding data is obtained.

A modified Wallis type flooding correlation based on the experimental data, and accounting for the non-equilibrium effect on flooding, is presented and discussed. A visualisation technique was developed and used to determine the flooding location in the test section.

CONTENTS

	<u>Page</u>
ABSTRACT	i
CONTENTS	iii
LIST OF APPENDICES	vii
LIST OF FIGURES	viii
LIST OF TABLES	xx
NOMENCLATURE	xxi
CHAPTER 1 INTRODUCTION	1
1.1 Counter-Current Annular Flow Regime	2
1.2 Industrial Applications	4
1.3 Current Project	5
CHAPTER 2 LITERATURE REVIEW	9
2.1 Mechanism of Flooding	13
2.2 Modelling Methods	17
2.3 Flooding Correlations	40
2.4 Effect of Fluid Properties	46
2.5 Effects of Tube Geometry	50
2.6 Pressure Difference	57
2.7 Entrainment	59
2.8 Mean Liquid Film Thickness	62

2.9 Counter-Current Flooding in Vapour-Liquid Systems	66
2.10 Modelling with Phase Change	69
2.11 Heat Transfer Coefficients in Condensation	74
2.12 Non-Equilibrium Condensation Effects	76
2.13 Comparison Between Vapour-Liquid and Gas-Liquid Flows	80
2.14 Conclusions on Literature Review	82
CHAPTER 3 EXPERIMENTAL APPARATUS AND OPERATING PROCEDURE	108
3.1 Test Section	108
3.2 Water Supply System	112
3.3 Air-Water System and Operation	114
3.4 Steam-Water System and Operations	116
CHAPTER 4 INSTRUMENTATION AND MEASUREMENTS	131
4.1 Air-Water Instrumentation	131
4.2 Steam-Water Instrumentation	136
4.3 Data Acquisition System	144
CHAPTER 5 VIEWING TECHNIQUES	155
5.1 Endoscope Viewing System	157
5.2 Video Camera Viewing System	159

5.3	Test Facility Modifications	160
5.4	Viewing Procedure	169
CHAPTER 6 THEORETICAL ANALYSIS		181
6.1	Film Thickness Analysis	182
6.2	Film Temperature Analysis	190
6.3	Flooding Model for Vapour-Liquid System	195
CHAPTER 7 EXPERIMENTAL RESULTS		210
7.1	Air-Water Data	210
7.2	Air-Water Flooding Data	213
7.3	Steam-Water Data	214
7.4	Steam-Water Flooding Data	217
CHAPTER 8 FLOW VISUALISATION RESULTS		228
8.1	Endoscope System	228
8.2	Video Camera System	233
8.3	Simulation of Top Flooding	248
8.4	Summary	249
CHAPTER 9 ANALYSIS AND DISCUSSION OF RESULTS		284
9.1	Effect of Air Extraction Rate on Air-Water Data	287
9.2	Effect of Steam Extraction Rate on	

Steam-Water Data	289
9.3 Compatible Flooding Data	295
9.4 Pressure Drop	298
9.5 Visualisation Technique	301
9.6 Liquid Film Thickness Analysis	303
9.7 Liquid Film Temperature Analysis	309
9.8 Flooding Model Analysis	314
9.9 Comparison with Other Data	319
CHAPTER 10 NON-EQUILIBRIUM EFFECTS AND EMPIRICAL ANALYSIS	352
CHAPTER 11 CONCLUSIONS AND RECOMMENDATIONS	371
11.1 Conclusions	371
11.2 Recommendations	374
REFERENCES	376
ACKNOWLEDGEMENTS	398
APPENDICES	400

LIST OF APPENDICES

<u>Appendix</u>	<u>Description</u>	<u>Page</u>
A	CALIBRATION METHODS AND RESULTS	400
B	AIR-WATER DATA	438
C	STEAM-WATER DATA	452
D	MATHEMATICAL ANALYSIS	497

LIST OF FIGURES

<u>Figure</u>			
<u>Number</u>		<u>Description</u>	<u>Page</u>
1.1		Smooth Counter-current Annular Two-phase Flow	7
1.2		Counter-current Two-phase Flow	7
1.3		Schematic of Loss of Coolant Accident	8
2.1		Comparison between Flooding and Deflooding Data (Bankoff and Lee (1983))	84
2.2		The Co-ordinate System of Shutt (1959)	85
2.3		The Co-ordinate System of Cetinbudaklar and Jameson (1969)	85
2.4		The Growth Rate αC_i , as a Function of the Gas Friction Velocity v_* in Air-Water System (Cetinbudaklar and Jameson (1969))	86
2.5		Comparison of Predicted Flooding Velocities with the Experimental Data of Clift et al (1966). From Cetinbudaklar and Jameson (1969)	86
2.6		The Co-ordinate System of Imura et al (1977)	87
2.7		The Co-ordinate System and Wave Profile of Shearer and Davidson (1965)	87

2.8	Analytical Model of Ueda and Suzuki (1978)	88
2.9	Hanging Liquid Films in Two Tube Sizes (Wallis and Makkenchery (1974))	88
2.10	Hanging Film Model of Wallis and Kou (1976)	89
2.11	Flow Around a pair of Sources (Wallis and Kou (1976))	89
2.12	Relationship between the Critical Air Velocity and the Tube Diameter with respect to the Reversal of the Flow of the Water Film (Pushkina and Sorokin (1969))	90
2.13	The Effect of Viscosity on Flooding in a Tube (Shires and Pickering (1965))	91
2.14	Effect of Liquid Viscosity on Flooding (Suzuki and Ueda (1977))	91
2.15	Effect of Surface Tension on Flooding (Shires and Pickering (1965))	92
2.16	Effect of Water Entering Radius on the Coefficient C, in Wallis Correlation	92
2.17	Effect of End Geometries on Flooding (Bharathan et al (1979))	93
2.18	Effect of End Cut-off on Flooding Velocity (Hewitt (1977))	94
2.19	Sketch of Geometries of Tube Ends in Various Investigations	95

2.20	Effect of Tube Diameter on Flooding (Tien et al (1979))	96
2.21	Effect of Tube Diameter on Flooding (Suzuki and Ueda (1977))	96
2.22	Effect of Tube Length on Flooding (Whalley and McQuillan (1983))	97
2.23a	Pressure Gradient in a Vertical Tube Above the Liquid Injection Point (Dukler and Smith (1979))	98
2.23b	Pressure Gradient in a Vertical Tube Below the Liquid Injection Point (Dukler and Smith (1979))	98
2.24	Generalised Sketch of Pressure Drop Variation with Gas Flow Rate in Counter-current Flow with Upper Plenum Injection (Hawley and Wallis (1982))	99
2.25	Typical Mean Thickness of Data of a Vertically Falling Film (Hawley and Wallis (1982))	100
2.26	Vertical Counter-current Steam-Water Flow Regime Map for $T_{fin} = 27^{\circ}\text{C}$ (Fan (1979))	101
2.27	Comparison between Steam-First and Water-First Data (Wallis et al (1980))	102
2.28	Flooding in Vertical Steam/Subcooled- Water Flow (Wallis et al (1980))	103

2.29	Average Heat Transfer Coefficient as a Function of Liquid Reynolds Number (Liu and Collier (1980))	104
2.30	Average Heat Transfer Coefficient as a Function of Axial Position for Several Liquid Reynolds Numbers (Liu and Collier (1980))	105
2.31	Average Heat Transfer Coefficient as a Function of Liquid Reynolds Number for Two Axial Positions (Liu and Collier (1980))	105
2.32	Saturation Length as a Function of Inlet Liquid Flow Rate for Several Inlet Temperature (Liu and Collier (1980))	106
2.33	Comparison between Pressure Drop in Air-Water and Steam-Water Systems (Liu and Collier (1980))	107
3.1	Line Diagram of Test Facility	121
3.2	Details of Test Section Assembly	122
3.3	Liquid Injector	123
3.4	Details of Extractor Guard	124
3.5	Details of Secondary Separator	125
4.1	Layout of Test Section Instrumentation	146
4.2	Mounting of Film Thickness Measuring Probe on Test Section Tube	147
4.3	Film Thickness Measuring Probe Geometry	148
4.4	Conductance Measuring Circuit	149
4.5	Conductivity Cell	150

4.6	Details of Volume Chamber	151
4.7	Layout of Water Offtake Instrumentation	152
4.8	Typical Test Section Element	153
4.9	Layout of Data Acquisition System	154
5.1	Principle of Forward Viewing Endoscope	172
5.2	Principle of Radial Viewing Endoscope	173
5.3	Endoscope Top Mounting	174
5.4	Radial Endoscope Bottom Mounting	175
5.5	Viewing Window Arrangement	176
6.1	Control Volume for Mass Balance	207
6.2	Control Volume for Momentum Balance	207
6.3	Control Volume for Energy Conservation	208
6.4	Interfacial Shear Stress Components	208
6.5	Liquid Film Flow	209
6.6	Uniform Liquid Film Flow	209
7.1	Upper Probe Film Thickness Fluctuation	219
7.2	Lower Probe Film Thickness Fluctuation	219
7.3	Measured Liquid Film Thickness (Air-Water Tests)	220
7.4	Pressure Drop Characteristics (Air-Water Tests)	221
7.5	Air-Water Flooding Data (Low Air Extraction Rate)	222
7.6	Air-Water Flooding Data (High Air Extraction Rate)	222
7.7	Measured Liquid Film Thickness (Steam-Water Tests)	223

7.8	Wall Temperature Distribution ($M_{fin} = 4.0$ l/min, $\Delta T_{sub} = 60K$)	224
7.9	Wall Temperature Distribution ($M_{fin} = 12.71$ l/min, $\Delta T_{sub} = 60K$)	224
7.10	Pressure Drop Characteristics (Steam-Water Tests)	225
7.11	Wall Temperature Distribution at Flooding Points ($\Delta T_{sub} = 60K$)	226
7.12	Wall Temperature Distribution at Flooding Points ($\Delta T_{sub} = 20K$)	226
7.13	Steam-Water Flooding Characteristic ($\Delta T_{sub} = 80K$)	227
7.14	Steam-Water Flooding Characteristic ($\Delta T_{sub} = 20K$)	227
8.1	Sequence of Events Observed through Endoscope Showing Liquid Film Behaviour, $Q_f = 4$ l/min, $\Delta T_{sub} = 10K$	250
8.2	Test Section Focussed at Different Locations with No Flow Present	251
8.3	Test Section with Various Water Flowrates and Very Low Air Flowrate	252
8.4a	Sequence of Events Showing Liquid Film Behaviour at Low and Moderate Air Flowrate, $Q_f = 4$ l/min	253
8.4b	Sequence of Events Showing Liquid Film Behaviour Before Flooding, $Q_f = 4$ l/min	254

8.4c	Sequence of Events Showing Liquid Film Behaviour at Flooding, $Q_f = 4$ l/min	255
8.5a	Sequence of Events Showing Liquid Film Behaviour at Low and High Flowrate, $Q_f = 4$ l/min	256
8.5b	Sequence of Events Showing Liquid Film Behaviour Before Flooding, $Q_f = 4$ l/min	257
8.5c	Sequence of Events Showing Liquid Film Behaviour at Flooding, $Q_f = 4$ l/min	258
8.6a	Sequence of Events Showing Liquid Film Behaviour at Low, Moderate and High Air Flowrate, $Q_f = 10$ l/min	259
8.6b	Sequence of Events Showing Liquid Film Behaviour Before and at Flooding, $Q_f = 10$ l/min	260
8.7a	Sequence of Events Showing Liquid Film Behaviour Before Flooding, $Q_f = 10$ l/min	261
8.7b	Sequence of Events Showing Liquid Film Behaviour Before and at Flooding, $Q_f = 10$ l/min	262
8.8a	Sequence of Events Showing Liquid Film Behaviour Before Flooding, $Q_f = 16$ l/min	263
8.8b	Sequence of Events Showing Liquid Film Behaviour Before and at Flooding, $Q_f = 16$ l/min	264
8.9a	Sequence of Events Showing Liquid Film Behaviour Before Flooding, $Q_f = 16$ l/min	265

8.9b	Sequence of Events Showing Liquid Film Behaviour Before and at Flooding, $Q_f = 16$ l/min	266
8.10a	Sequence of Events Showing Liquid Film Behaviour at moderate and High Steam Flowrate, $Q_f = 4$ l/min and $\Delta T_{sub} = 30K$	267
8.10b	Sequence of Events Showing Liquid Film Behaviour at Flooding, $Q_f = 4$ l/min and $\Delta T_{sub} = 30K$	268
8.11a	Sequence of Events Showing Liquid Film Behaviour at Moderate and High Steam Flowrates, 4 l/min and $\Delta T_{sub} = 80K$	269
8.11b	Sequence of Events Showing Liquid Film Behaviour at Flooding, 4 l/min and $\Delta T_{sub} = 80K$	270
8.12	Wave Motion Before Flooding, $Q_f = 4$ l/min and $\Delta T_{sub} = 20K$	271
8.13	Wave Motion Before Flooding, $Q_f = 4$ l/min and $\Delta T_{sub} = 30K$	272
8.14	Wave Motion Before Flooding, $Q_f = 4$ l/min and $\Delta T_{sub} = 70K$	273
8.15a	Sequence of Events Showing Liquid Film Behaviour at moderate and High Flowrate, $Q_f = 10$ l/min and $\Delta T_{sub} = 10K$	274
8.15b	Sequence of Events Showing Liquid Film Behaviour Before and at Flooding. $Q_f = 10$ l/min and $\Delta T_{sub} = 10K$	275

8.16a	Sequence of Events Showing Liquid Film Behaviour Before Flooding, $Q_f = 10$ l/min and $\Delta T_{sub} = 60K$	276
8.16b	Sequence of Events Showing Liquid Film Behaviour Before Flooding, $Q_f = 10$ l/min and $\Delta T_{sub} = 60K$	277
8.16c	Sequence of Events Showing Liquid Film Behaviour Before and at Flooding, $Q_f = 10$ l/min and $\Delta T_{sub} = 60K$	278
8.17a	Sequence of Events Showing Liquid Film Behaviour Before Flooding, $Q_f = 16$ l/min and $\Delta T_{sub} = 10K$	279
8.17b	Sequence of Events Showing Liquid Film Behaviour Before and at Flooding, $Q_f = 10$ l/min and $\Delta T_{sub} = 10K$	280
8.18a	Sequence of Events Showing Liquid Film Behaviour Before Flooding, $Q_f = 16$ l/min and $\Delta T_{sub} = 50K$	281
8.18b	Sequence of Events Showing Liquid Film Behaviour Before and at Flooding, $Q_f = 16$ l/min and $\Delta T_{sub} = 50K$	282
8.19	Simulated Top Flooding, $Q_f = 4$ l/min and $\Delta T_{sub} = 10K$	283
9.1	Comparison of Liquid Film Thickness Measurements with McNeil (1986)	327
9.2	Air Extraction Rates at Flooding	328
9.3	Air-Water Flooding Characteristic at Different Air Extraction Rates	329

9.4	Air Extraction Rate Profiles	330
9.5	Steam-Water Flooding Data at Different Steam Extraction Rates ($\Delta T_{\text{sub}} = 80\text{K}$)	331
9.6	Steam-Water Flooding Data at Different Steam Extraction Rates ($\Delta T_{\text{sub}} = 20\text{K}$)	331
9.7	Steam Extraction Rates ($\Delta T_{\text{sub}} = 80\text{K}$)	332
9.8	Steam Extraction Rates ($\Delta T_{\text{sub}} = 20\text{K}$)	332
9.9	Steam Extraction Rates at Different Cooling Water Flowrates ($\Delta T_{\text{sub}} = 10\text{K}$)	333
9.10	Steam-Water Flooding Data at Different Steam Extraction Rates ($\Delta T_{\text{sub}} = 10\text{K}$)	334
9.11	Air-Water Flooding Data With Extrapolated Flooding Characteristic	335
9.12	Compatible Air-Water and Steam-Water Flooding Data	336
9.13	Steam-Water Flooding Data at the Top of the Test Tube	337
9.14	Pressure Drop Characteristic at Different Liquid Injection Rates (Air-Water Tests)	338
9.15	Effect of Steam Extraction Rates on Pressure Drop Characteristic ($\Delta T_{\text{sub}} = 10\text{K}$)	339
9.16	Comparison between Prediction and Measured Film Thickness at Flooding ($\Delta T_{\text{sub}} = 80\text{K}$)	340
9.17	Comparison between Prediction and Measured Film Thickness at Flooding ($\Delta T_{\text{sub}} = 60\text{K}$)	340
9.18	Comparison between Prediction and Measured Film Thickness at Flooding ($\Delta T_{\text{sub}} = 40\text{K}$)	341

9.19	Comparison between Prediction and Measured Film Thickness at Flooding ($\Delta T_{\text{sub}} = 20\text{K}$)	341
9.20	Liquid Film Thickness Prediction at Different Condition ($\Delta T_{\text{sub}} = 80\text{K}$)	342
9.21	Liquid Film Thickness Prediction at Different Conditions ($\Delta T_{\text{sub}} = 10\text{K}$)	343
9.22	Variation of Experimental and Prediction Wall Temperature and Liquid Film Mean Temperature with Dimensionless Axial Position ($\Delta T_{\text{sub}} = 80\text{K}$)	344
9.23	Variation of Experimental and Prediction Wall Temperature and Liquid Film Mean Temperature with Dimensionless Axial Position ($\Delta T_{\text{sub}} = 20\text{K}$)	345
9.24	Variation of n and a_g in Equation (9.20) with Inlet Water Flowrate and Subcooling	346
9.25	Comparison between Proposed Flooding Model with the Air-Water Flooding Characteristic	347
9.26	Variation of V_o/U_f with Tube Dimensionless Length z^+	348
9.27	Comparison of Air-Water Flooding Data with Some Correlations	349
9.28	Comparison of Air-Water Flooding Data with Some Models	350
9.29	Comparison of Steam-Water Flooding Data with that of Bharathan et al (1980)	351
10.1	Comparison between Air-Water and Steam- Water Flooding Data	362

10.2	Comparison between Air-Water and Steam-Water Flooding Data	363
10.3	Steam-Water Flooding Characteristic, $\Delta T_{\text{sub}} = 80\text{K}$	364
10.4	Steam-Water Flooding Characteristic, ($\Delta T_{\text{sub}} = 10\text{K}$)	364
10.5	Non-Equilibrium Steam-Water Data for all Subcoolings	365
10.6	Comparison between Non-Equilibrium Data and Correlation	366
10.7	Comparison between Equilibrium Steam-Water and Air-Water Data	367
10.8	Minimum Condition for the Non-Equilibrium Correlation, ($\Delta T_{\text{sub}} = 80\text{K}$)	368
10.9	Minimum Condition for the Non-Equilibrium Correlation, ($\Delta T_{\text{sub}} = 80\text{K}$)	368
10.10	Final Non-Equilibrium Relation, ($\Delta T_{\text{sub}} = 80\text{K}$)	369
10.11	Final Non-Equilibrium Relation, ($\Delta T_{\text{sub}} = 10\text{K}$)	369
10.12	Minimum Condition for the Non-Equilibrium Correlation as a Function of J_{fin}^* and $\ln(\text{Ja})$	370

LIST OF TABLES

<u>Table</u>		
<u>Number</u>	<u>Description</u>	<u>Page</u>
9.1	Predicted Liquid Film Thickness ($\Delta T_{\text{sub}} = 80\text{K}$)	322
9.2	Predicted Liquid Film Thickness ($\Delta T_{\text{sub}} = 60\text{K}$)	322
9.3	Predicted Liquid Film Thickness ($\Delta T_{\text{sub}} = 40\text{K}$)	323
9.4	Predicted Liquid Film Thickness ($\Delta T_{\text{sub}} = 20\text{K}$)	324
9.5	Estimated Exchange Coefficients	
10.1	Turning Points for Equation (10.4)	361
10.2	Minimum Condition for Equation (10.4)	361

NOMENCLATURE

A	Area (m^2) or Wave Amplitude (m)
C	Constant
D	Diameter (m)
Fr	Froude Number
Ja	Jacob Number
K	Equation (6.29) or Kutateladze Number
L	Porous Sinter Length (m)
Nu	Nusselt Number
M	Mass Flowrate (kg/s)
p	Pressure (N/m^2)
Pr	Prandtl Number
Q	Volumetric Flowrate (l/s)
R	Radius (m) or Resistance
Re	Reynolds Number
T	Temperature (K)
U	Mean Flow Velocity in z-Direction (m/s)
V	Mean Flow Velocity in y-Direction (m/s) or Voltage
W	Mass Flowrate per Unit Width (kg/s/m)
We	Weber Number
c	Wave speed (m/s) or Conductance (S)
f	Friction Factor
g	Gravitational Constant ($9.806 m/s^2$)
h	Heat Transfer Coefficient (W/m^2K) or Enthalpy (J/kg)

i	$\sqrt{-1}$
j	Superficial Velocity (m/s)
k	Wave Number (m^{-1}) or Non-Equilibrium Factor
l	Test Tube Length (m)
p	Pressure (N/m^2)
t	Time (S)
u	Velocity Component in z-Direction (m/s)
v	Velocity Component in y-Direction (m/s)
x	Cartesian Co-ordinate (m)
y	Cartesian Co-ordinate (m)
z	Cartesian Co-ordinate (m)

Greek letters

α	Turbulent Diffusivity (m/s)
β	Contact Angle (DEG)
δ	Film Thickness (m)
ϵ	Thermal Diffusivity (m/s)
η	Perturbation (m)
μ	Viscosity (Ns/m^2)
ν	Kinematic Viscosity ($kg/s/m^2$)
σ	Surface Tension (N/m)
τ	Shear Stress (N/m^2)
ϕ	Velocity Potential (m^2/s)
λ	Salt Concentration (ppm)
γ	Fluid Conductivity ($\mu s/cm$)
ζ	Equation (6.33)

Subscripts

a	Air
B	Bottom of Test Tube
C	Critical or Condensed
f	Fluid (Liquid)
g	Gas
H	Heat
i	Interface or Imaginary
p	At Constant Pressure
r	Real
sub	Subcooled
S	Steam
SAT	Saturated
t	Top of Tube
w	Wall of Tube
∞	Evaluated at y or z tends to infinity
+	Non-Dimensional
*	Non-Dimensional

CHAPTER 1

INTRODUCTION

CHAPTER 1

INTRODUCTION

Multi-phase flow is defined as the simultaneous flow of several of the three states of matter; gas or vapour, liquid or solid. Two-phase flow is the simplest case of multi-phase flow, and gas-liquid flow is the most common class of two-phase flow. A vertical counter-current flow of gas and liquid in direct contact with each other is formed as a result of the difference in the gravitational force per unit volume on the gas and liquid. If gas and liquid are simultaneously introduced into a vertical or inclined pipe, the gas will tend to rise relative to the liquid which will flow downwards.

When a gas and a liquid flow together in a pipe, the flow can assume a number of different patterns or regimes, depending on the distribution of the two phases. The regimes of flow are governed by the flow rates and physical properties of the fluids, by the length, diameter and orientation of the pipe and by the manner in which the fluids were introduced. In counter-current flow, while many regimes such as bubbly, bubbly-slug and slug flow are possible, annular flow is the most common regime because of its occurrence in practical applications of industrial equipment and heat transfer systems. A particularly acute problem in annular counter-current flow lies in

determining the onset of liquid flow reversal i.e. the gas flow necessary to change the direction of the liquid flow from downwards to upwards, commonly referred to as "flooding".

The aim of the present research programme is to study counter-current annular two-phase flow in a vertical tube, the mechanism by which flow reversal occurs, and the effect of condensation on this mechanism.

A description of counter-current annular two-phase flow is given in Section 1.1; its application to industrial equipment in Section 1.2 and a focus on the present study in Section 1.3.

1.1 Counter-current Annular Flow Regime

A simple case of annular counter-current flow is that of gas and liquid in circular vertical tubes, in which the liquid is introduced around the inside circumference of the tube and flows along the tube wall as a continuous film, while the gas flows upwards in the centre of the tube. The type of liquid flow observed depends on the gas flowrate. For zero or low gas flowrates, the liquid film flows smoothly down the tube, appearing slightly wavy towards the bottom, Figure 1.1. As the gas flowrate is slightly increased, the interface between the gas and the liquid becomes unstable and wavy.

A gradual increase in the gas flowrate causes larger waves to develop on the interface, Figure 1.2. The gas flow gradually entrains some of the liquid droplets i.e. particles of the liquid are torn from the crest of the waves and carried up by the gas phase. When the gas flowrate reaches a limiting value, further increase results in a sudden increase in the amplitude of the ripple waves on the surface of the liquid film, and part of the liquid reverses its direction, and is carried upwards by the gas, usually accompanied by a sharp increase in the pressure difference over the tube. This condition is known as "Flooding" and it is the identification of this condition which is the main area of interest in the present investigation. At the flooding point, a further increase in the gas flow would eventually bring a complete liquid flow reversal leading to co-current upflow and resulting in the section of tube below the liquid inlet drying up. This condition is known as the "point of complete by-pass". If the gas velocity is now reduced, the annular counter-current flow could be re-established. First, a point will be reached at which part of the liquid film begins to creep down the tube wall below the injection point. This transition is termed "deflooding". Further reduction of the gas flowrate results in simultaneous climbing and falling liquid film flow, and finally downflow of all the liquid film below the injection point. Although the above description describes a fixed liquid flowrate, a similar sequence of events could be obtained for a fixed gas

flowrate and varied liquid flowrate. The former method is called liquid first, and the latter, gas first tests.

1.2 Industrial Applications

Counter-current two-phase flow has long been a subject of engineering interest and first received attention from chemical engineers in the design of packed columns. For some years, interest has been rapidly growing in problems associated with counter-current flow of a gas phase and a liquid phase in a common channel. This particular kind of two-phase flow occurs in many items of industrial equipment, for example deaeration columns for multi-stage flash distillation plants. In this situation, low oxygen concentration steam flows counter-current with the relatively high oxygen concentrated feed water through a packed column, in order to transfer oxygen from the water to the steam. The reflux condenser represents another industrial application of the counter-current two-phase flow where the incoming vapour flows counter-currently with the draining condensate. Recently, the need for a more precise knowledge of the behaviour of two-phase systems has been accentuated due to a concentration of research on nuclear reactor safety. The condition of counter-current two-phase flow and flooding can be expected to take place during a loss of coolant accident (LOCA) in a pressurised water reactor (PWR). When the loss of coolant accident

occurs in the reactor due to the break of a pipe in the primary coolant system, emergency core cooling (ECC) water is injected into the annular space which surrounds the reactor core in order to flood and cool the reactor. At the same time the depressurised water within the system flashes to steam and makes its way to the break location, thus the emergency core coolant has to flow counter-current with the upflowing steam, Figure 1.3. If the steam flowrate is sufficiently large, it could seriously limit the water supply rate to the reactor. Under such a flooding situation, core cooling can be greatly hampered. The design of the PWR must prevent the occurrence of such a situation with the proper design of an ECC system.

1.3 Current Project

The work presented in this thesis is connected indirectly with the safety of the pressurised water reactor system. When the incoming emergency coolant, which is substantially subcooled, comes into direct contact with the uprising steam in a counter-current flow arrangement, heat and mass transfer can be significant and of great importance. To examine these effects a vertical tube geometry was chosen because it provides a basic understanding of the situation occurring in counter-current two-phase flow. To aid in this investigation, two systems were used in order to obtain

flooding data:

- (i) systems where mass-transfer was not present, i.e. using air and water
- (ii) systems where mass-transfer was present, i.e. by using steam and subcooled water.

A viewing technique was developed to allow visualisation studies to be made of the counter-current flow interface and the mechanism by which the flooding process was developed. The prime object of these studies was to determine the point along the tube at which the flooding situation was initiated in both systems and to correlate this in terms of the variables involved.

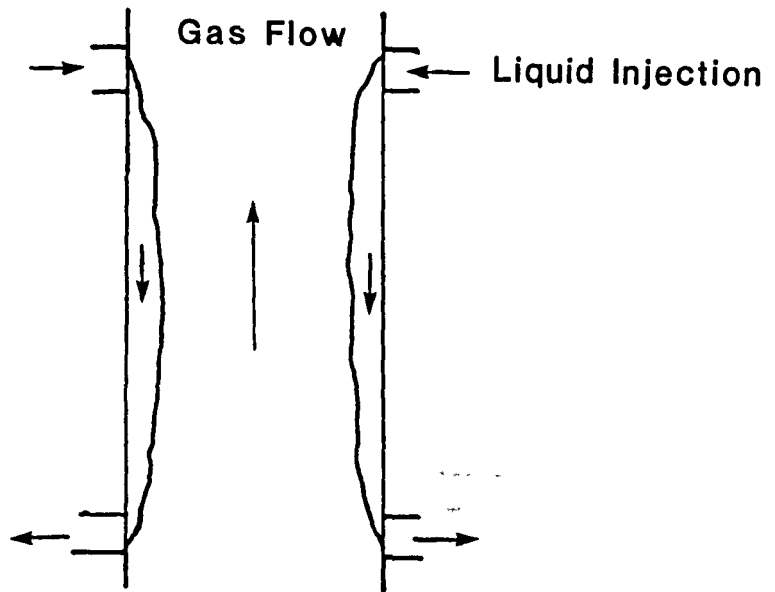


Figure 1.1 Smooth Countercurrent Annular Two-Phase Flow

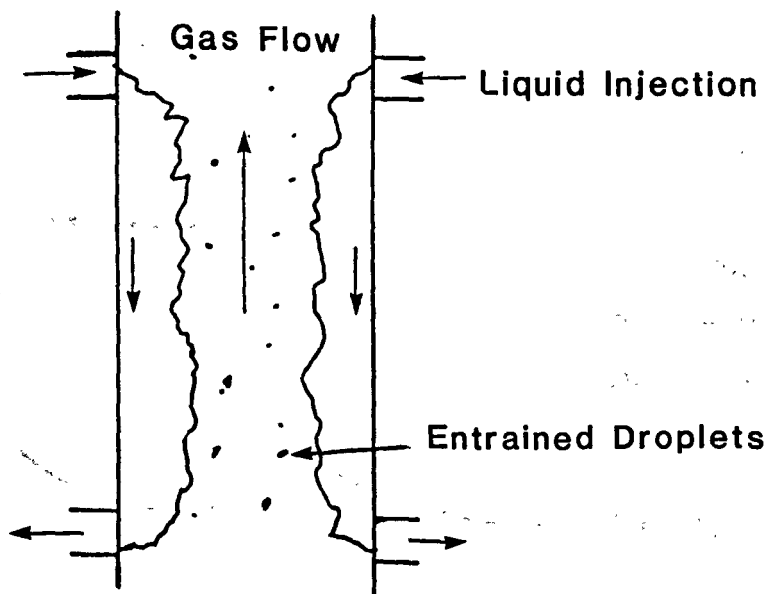


Figure 1.2 Countercurrent Two-Phase Flow

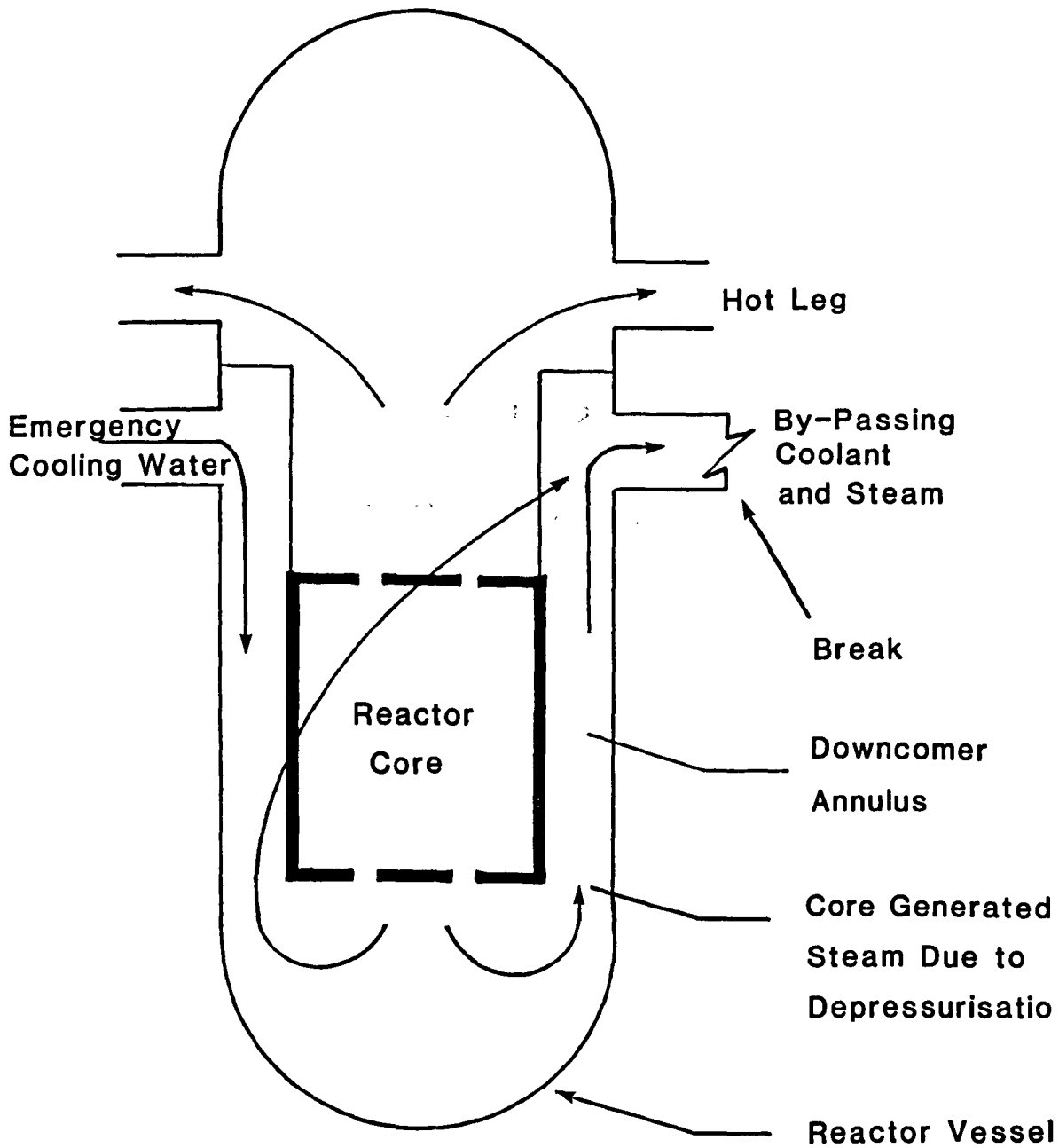


Figure 1.3 Schematic of Loss of Coolant Accident

CHAPTER 2

LITERATURE REVIEW

CHAPTER TWOLITERATURE REVIEW

In general, flooding is a term used to describe the limiting conditions for two phase countercurrent flow, mainly in vertical or steeply inclined tubes or ducts, where the liquid flows downward and the gas (or vapour) flows upwards. Flooding is basically a hydrodynamic process where the momentum and frictional drag of the ascending gas (or vapour) and the descending liquid interact with each other.

Flooding can be characterised by slugging, or bridging, of the liquid film when the film is thick enough to have large amplitude waves at the interface. Physically, the onset of flooding can appear in different guises, and is observed to be dependent on the phase flow rates, tube end conditions, the method of introducing the phases, the fluid properties of the phases and the geometry and orientation of the test section. These factors also appear to affect the location of the inception of flooding which can vary along the section being considered. The flooding transition is a very sudden process, normally accompanied by a sharp increase in the pressure gradient.

Most investigators have used visual observation in

order to determine the onset of flooding [WALLIS (1961), HEWITT and WALLIS (1963), CHUNG (1978), and WHALLEY and McQUILLAN (1983)]. Some investigators employed a sudden change in gas pressure drop measurements as a second criterion for the onset of flooding, e.g. CLIFT et al (1966), GROMES et (1974) and HAWLEY and WALLIS (1982). A few investigators even used film thickness measurements as a sign of onset of flooding e.g. D. McNEIL (1986).

The flooding condition inside a tube or duct can be reached either by gradually increasing the gas flowrate for a fixed liquid flowrate or by gradually increasing the liquid flowrate for a fixed gas flowrate. CLIFT et al (1966) reported that the flooding points determined by both methods were identical, but WALLIS et al (1975), (1980), found that not to be the case. However, most investigators did not make any distinction in the evolution of flooding in their studies. Due to the complex nature of the flooding phenomenon, studies to date have not produced a clear picture of the events. A general systematic experimental procedure also seems to be lacking which has resulted in conflicting reports throughout the literature. The main areas of the disagreement centre on the dependence of the flooding velocities on tube geometry and on the physical properties of the fluids. Thus discrepancies occur between experimenters using essentially the same conditions. This leads to speculation that the differences between the results of various authors might be due, at least in part,

to the lack of a universally accepted definition of flooding and in part to differences in experimental procedure.

Flooding conditions involve highly unsteady flow behaviour and it is difficult to determine precisely the onset of flooding. As indicated, many investigators have established different criteria for the start of flooding and some of these can be listed as follows:

- i) When the whole flow is disturbed and the liquid is carried up by the gas/vapour phase above the liquid entrance (WALLIS (1961)).
- ii) The beginning of liquid flow reversal (PUSHKINA and SOROKIN (1969) and HEWITT and WHALLEY (1979)).
- iii) When the liquid droplets started to be entrained in the gas core (DUKLER and SMITH (1979)).
- iv) The criterion of zero liquid penetration (LOVELL (1979)).
- v) When the liquid bridges the flow area (CHAUDRY (1965)).

With these varying definitions of flooding, it is not surprising that the experimental observations of flooding yield differences in the measurement of the

flooding point. A further complication of the definition of flooding arises from the converse situation of transition from upward co-current flow to countercurrent flow. This is called "deflooding". It was noted that the liquid injection rate at the deflooding point was less than that at the flooding point when the gas flow was kept constant. HEWITT and WALLIS (1963) and WALLIS et al (1963) similarly found that the deflooding gas velocity was less than the flooding gas velocity when the liquid injection rate was constant. Their experimental data are shown in Figure (2.1). This finding is confirmed by CLIFT et al (1966) and WALLIS et al (1975). On the other hand PUSHKINA and SOROKIN (1969), TIEN (1977), and LIU and COLLIER (1980) reported that the flooding velocities were nearly the same as the deflooding velocities.

Despite the large number of methods which are available to calculate flooding conditions, predictive success is limited. The empirical correlations usually fail to work for geometries or fluid properties other than those which were used to develop them, and the theoretical correlations provide a range of predictions and further suggest a range of trends. Perhaps one of the major reasons for this lack of success is the lack of understanding or agreement concerning the mechanism by which flooding occurs. Several different mechanisms and models have been postulated, but none can accurately predict flooding conditions.

Research efforts to date have mainly concentrated on flooding phenomena in the absence of phase change and little can be found where both heat and mass transfer occur. This literature review will first consider adiabatic flooding in vertical tubes with flows of gas and liquid i.e. no heat or mass transfer between the phases occurs, and then go on to consider such literature as is available which accounts for mass and/or heat transfer.

2.1 Mechanism of Flooding

The exact mechanism which underlies the flow reversal process has still to be uncovered fully. Consider a falling liquid film with countercurrent upward gas flow in a vertical tube, the available literature proposes several different mechanisms by which the flooding process takes place. One of the earliest investigations into the flooding mechanism was proposed by HEWITT and WALLIS (1963). Working with a vertical tube of 31.75 mm bore, with smooth entrance and exit conditions, and using a photographic technique to provide a high-speed cine picture of the film interface, they concluded that flooding was caused by large wave formations on the gas liquid interface. Before the flooding point, an occasional sudden pulse resembling large waves appeared on the liquid film then, at the flooding point, these waves grew so large that the flow was disrupted and became chaotic resulting in a series of

large waves being established such that some liquid was carried up above the point of water entry. The conclusions of Hewitt and Wallis were based mainly on the measurement of pressure gradient along the tube. Calculations of the effect of air drag on the liquid film, indicated that the predicted changes in the film thickness with gas flow rate up to the flooding point were small if the motion of the liquid was considered to be downwards. This led to their concluding that flooding was unlikely to occur by simple reversal of direction, but was more likely to be associated with a rapid growth of disturbances accompanied by an order of magnitude change in pressure. Their observations were confirmed by HEWITT et al (1965) and by BHARATHAN et al (1978). HEWITT et al (1965), observed that the flooding gas flow rate was strongly affected by the length of the tube, the flooding gas flow rate decreasing as the length of the tube increased, and interpreted this as an indication that flooding occurred as a result of wave growth in the falling liquid film. They claimed that, for given liquid and gas flow rates, waves which have not grown sufficiently by the time they are extracted after falling through a short distance can, in longer tubes, grow to a size which would enable them to initiate the flooding event.

However, the idea of flooding being caused by large waves on the gas-liquid interface has two schools of thought (DUKLER et al (1978)). The first speculates that once a finite amplitude wave is formed, it continues to

grow until it bridges the tube whence the liquid is carried up by the up moving gas. Suggestions of bridging being the mechanism causing flooding have appeared repeatedly in the literature, the most recent examples being those of IMURA et al (1977) and DUFFY et al (1978). However, measurements of the maximum film thickness by DUKLER and SMITH (1977) and by SUZUKI and UEDA (1977) demonstrated that bridging does not occur. When flooding takes place in large tubes, the possibility of a bridging mechanism is rejected from a consideration of the amount of liquid necessary to fill the tube compared with the small amount of liquid flowing in the tube.

The second school of thought speculates that the large waves formed are propagated upwards due to the effect of the shear and drag from the gas which results in the liquid being carried up above the feeding point. DUKLER et al (1978) thus concluded that the claim for the flooding process being connected in a primary way with wave motion or growth is purely circumstantial.

DUKLER and SMITH (1976) proposed a mechanism based on their observations of entrainment. They measured flooding condition for four water flow rates and concluded that two flooding mechanisms were possible these being associated with the onset of entrainment; one for lower flow rates and the other for higher flow rates. For lower flow rates, they postulated that flooding occurred due to the entrainment of liquid drops being torn from the

liquid film below the water entry point. Droplet deposition was observed on the wall in the section above the feed point. At these low flow rates, the film had to fall a considerable distance before the surface wave structure was fully developed. For the higher flow rates, the increased agitation of the film allowed entrainment to be initiated at the water inlet location also with the gas velocity being sufficient to carry it above the liquid entrance. With a small increase in the gas flow rate (but still below the flooding point), the water droplets above the liquid entry increased in size and number. At the flooding condition, this section of liquid film began to fall downwards in a film causing an internal recycle and a higher effective liquid flow rate than was actually fed to the tube and the gas flow suddenly sprayed liquid upwards causing flooding.

Another mechanism suggested by some investigators was based on upward flow occurring in the liquid film but no serious attention has been given to this possibility. This mechanism was rejected by HEWITT and WALLIS (1963) and, probably as a result of this, no serious study of this model has been reported, although some tentative and inconclusive explorations in a related study of upward annular flow by NICKLIN and KOCH (1969) were published. DUKLER et al (1978) suggested a mechanism by which flow reversal in the liquid film can take place. In this mechanism, the authors predicted that the process of flooding starts with the formation of waves but their

effect is indirect. When the condition of flooding is closely approached, more pronounced wave action takes place which causes the pressure gradient in the gas to increase and cause a sudden rise in interfacial shear stress, which may be sufficient to reverse the velocity in the film. The authors predicted that, for flooding to occur as a direct result of waves, either the waves must bridge the tube or be transported upwards above the water entry point as waves. For this film mechanism, the waves cause an increase in the friction loss in the gas and hence an increase in the interfacial shear stress.

2.2 Modelling Methods

The previous section illustrated how complex the process of flooding is. Despite this, a number of analytical and empirical models have been developed for flooding in vertical annular flow. Several different viewpoints have been expressed in these models and these are presented here in three categories, namely, (i) stability analysis, (ii) standing wave model and (iii) hanging film model.

2.2.1 Stability Analysis

Stability analysis has its origin in the work of SCHUTT (1959) who assumed that once growth was initiated

the process would continue until bridging occurred. The co-ordinate system used is shown in Figure 2.2. For a small diameter tube, Schutt's results showed reasonable agreement with the experimental flooding conditions except for larger diameter tubes. CETINBUDAKLAR and JAMESON (1969) used a stability analysis similar to that used by Schutt in an attempt to predict the gas velocity at which the waves became unstable. The steady laminar flow of a liquid film flowing down a vertical wall for the co-ordinate system shown in Figure 2.3 has a velocity distribution of the form

$$u = y^2 - 1 \quad (2.1)$$

with interfacial velocity being given by

$$u_0 = \frac{\rho_f g \delta^2}{2\mu_f} \quad (2.2)$$

If the free surface is disturbed by a perturbation of the form

$$\eta = a \exp(i\alpha(x-ct)) \quad (2.3)$$

where $c = c_r + ic_i$ is a complex wave velocity, the perturbation stream function has the form

$$\psi = -F(Y)\eta \quad (2.4)$$

$$\text{or } \psi = -aF(Y) \exp(i\alpha(x-ct)) \quad (2.4a)$$

Subsequent substitution of this into the Navier-Stokes equation, linearising and eliminating the pressure term,

yielded the Orr-Sommerfeld equation

$$F'''' = 2\alpha^2 F'' + \alpha^4 F = i\alpha \text{Re}_f [(u-c)(F'' - \alpha^2 F) - u''F] \quad (2.5)$$

where Re_f is the Reynolds number defined as $\frac{\rho_f u_o \delta}{\mu_f}$

The boundary conditions are

(i) Zero velocity at the wall ($y = -1$)

$$F(-1) = F'(-1) = 0 \quad (2.6)$$

(ii) Surface kinematic condition at interface ($y=0$)

$$F'(0) = c - u_o \quad (2.7)$$

The other two boundary conditions were obtained from the equality of the tangential and normal perturbation stresses in the liquid to the corresponding stresses in the gas. The perturbation to the tangential shear stress was considered as

$$\tau_{xy} = \frac{u_o \mu_f}{\delta} \eta \tau_s \quad (2.8)$$

The normal shear stress was

$$\sigma_{yy} = \frac{u_o \mu_f}{\delta} \eta \sigma_s \quad (2.9)$$

Thus the two remaining boundary conditions are

(iii) Tangential stress continuity (at $y=0$)

$$F''(0) = \tau_s - \alpha^2 (c - u_o) u''_o \quad (2.10)$$

(iv) Normal stress continuity (at $y=0$)

$$(c - u_o) F'(0) - \frac{i}{\alpha \text{Re}_f} (F'''(0) - 3\alpha^2 F'(0)) = \alpha^2 \text{We} - \alpha \frac{s}{\text{Re}_f} \quad (2.11)$$

where We is a Weber number defined as $\left\{\frac{\rho_f g \delta^2}{\sigma}\right\}$.

The first term in equation (2.11) represents the inertia of the wave and the second term represents the normal stress due to the viscosity. The term $\alpha^2 We$ is the pressure due to surface tension, σ . By arguing that the stability of the film was largely determined by the conditions near the interface and, by employing the approach of ANSHUS and GOREN (1966) in which u is regarded as constant equal to u_0 and $u'' = 2$, then equation (2.5) was reduced to a fourth order ordinary differential equation with constant coefficients and solution:

$$F = C_1 \sin \beta_1 y + C_2 \cos \beta_1 y + C_3 \sin \beta_2 y + C_4 \cos \beta_2 y \quad (2.12)$$

where

$$\beta_{1,2} = -\alpha^2 - \frac{i}{2} \alpha Re_f (u_0 - c) \pm \left[2i \alpha Re_f + \frac{i \alpha Re_f}{2} (u_0 - c) \right]^{1/2} \quad (2.13)$$

$$C_{1,2,3,4} = \text{constants.}$$

With the further assumption that the gas flow is quasi-laminar, the dimensionless stresses σ_s and τ_s can be evaluated using the approach of MILES (1957) and BENJAMIN (1959). The Solution of Orr-Sommerfield is thus given as

$$\phi(y) + f(y) = c$$

where $\phi(y)$ is the inviscid solution

and $f(y)$ is the viscous solution

Using Benjamin's integral equation, the normal stress on the boundary is given by

$$\sigma_s = -\alpha^2 \int_0^{\infty} v \phi \, dy \quad (2.14)$$

hence the inviscid solution is given as

$$v(\phi'' + \alpha^2 \phi) - v''\phi = 0 \quad (2.15)$$

and the viscous solution is given as

$$F'''' - \frac{i\alpha\rho_g}{\mu_g} (v'(y)-c)F'' = 0 \quad (2.16)$$

where $v'_0(y)$ is the velocity gradient in the gas phase at $y = 0$.

Suitable solutions were obtained for equations (2.15) and (2.16), and these were used in equation (2.14) to yield real and imaginary parts of σ_s and τ_s as

$$\sigma_{sr} = (1+0.644K\sqrt{3})A_2 \quad (2.17a)$$

$$\sigma_{si} = -0.644KA_2 \quad (2.17b)$$

$$\tau_{sr} = -0.686A_2A_1^{2/3}(1+1.288K\sqrt{3}) \quad (2.18a)$$

$$\tau_{si} = 0.686A_2A_1^{2/3}(\sqrt{3} + 1.288K) \quad (2.18b)$$

where

$$A_1 = \frac{\alpha\mu_g}{\rho_g v_*} \quad (2.19)$$

$$A_2 = \frac{2\alpha^2 v_*^2 (\rho_g/\rho_f g) I}{1+1.288K(\sqrt{3}+1/288K)} \quad (2.20)$$

$$K = A_1^{4/3} \alpha I \quad (2.21)$$

$$I = \int_0^{\infty} v^{+2} \exp(-\alpha y) dy \quad (2.22)$$

v_* is the gas friction velocity = $\frac{\tau_g \rho_g}{\mu_g}$

v^+ is the dimensionless gas velocity = $\frac{v}{v_*}$

From these results, the growth rate (αc_i) was obtained as

a function of the gas friction velocity v_* for various liquid Reynolds numbers. Figure 2.4 illustrates the variation of α_1 with v_* . The minimum frictional velocity for each curve in the unstable region (where $\alpha_1 > 0$) was taken to be the flooding velocity for the corresponding liquid Reynolds number. Figure 2.5 shows a comparison between this theory and the experimental data of CLIFT et al (1966) with the authors claiming a maximum deviation of 7%.

This analysis indicated the complexity of the problem but, despite the complex mathematics and simplifying assumptions involved, the analysis did not produce a single embracing flooding equation. Furthermore, it did not give an indication of the stability of the flow waves travelling in the direction of the gas flow. It should be noted that this analysis can only be applied to the linear stability concept, which may not fully define the flooding problem. There are further limitations inherent in this type of stability analysis, which are discussed at the end of this section.

It may be of some significance that the experimental study of a free falling film down a vertical tube by JONES and WHITAKER (1966) showed that the numerical solution of the Orr-Sommerfeld equation was in good agreement with the experimental results near the top of the film where the small disturbance assumption is expected to be valid.

Another attempt to analyse the instability of the small perturbation waves was carried out by IMURA et al (1977) and involved the coordinate system shown in Figure 2.6. The gas and the liquid were assumed to be inviscid fluids in respect of the stability of the liquid film. Using the velocity potential of the liquid and the gas, ϕ_f and ϕ_g respectively, the continuity equation could be written as:

$$\frac{\partial^2 \phi}{\partial x^2} + \frac{1}{r} \frac{\partial}{\partial r} \left(r \frac{\partial \phi}{\partial r} \right) = 0 \quad (2.23)$$

and the Bernoulli equation

$$\frac{p}{\rho} = \frac{\partial \phi}{\partial t} - \frac{1}{2} \left(\frac{\partial \phi}{\partial x} \right)^2 + \left(\frac{\partial \phi}{\partial r} \right)^2 - gx + K \quad (2.24)$$

where K is constant

The boundary conditions were defined as:

- (i) At the tube wall $r = R$
- (ii) At the tube centre $r = 0$, hence

$$\frac{\partial \phi_f}{\partial r} = 0$$

- (iii) At the interface (liquid side) $r = R - \delta$, hence

$$-\frac{\partial \phi_f}{\partial r} = \frac{\partial \eta}{\partial t} + u_f \frac{\partial \eta}{\partial x}$$

(iv) At the interface (gas side) $r = R - \delta$, hence

$$-\frac{\partial \phi_g}{\partial r} = \frac{\partial \eta}{\partial t} + u_g \frac{\partial \eta}{\partial x}$$

where η is the displacement of the wave from the average film thickness defined as

$$\eta = \eta_0(t) \sin(x - ct) \quad (2.25)$$

$$\text{with } a = 2\pi/\lambda \quad (2.26)$$

The final constraint was imposed by the relation between the surface tension effects and the pressure difference between the gas and the liquid phases (interfacial pressure) at the interface

$$P_f - P_g = \sigma \left\{ \frac{\partial^2 \eta / \partial x^2}{\left[1 + \left(\frac{\partial \eta}{\partial x} \right)^2 \right]^{3/2}} - \frac{1}{R - \delta + \eta} \right\} \quad (2.27)$$

with $\left(\frac{\partial \eta}{\partial x} \right)^2 \ll 1$ being ignored.

Combining equation (2.25) with equation (2.27) and ignoring the second order terms, gave

$$P_f - P_g = \sigma \left\{ -\frac{1}{R - \delta} + \eta (-K^2) + \frac{1}{(R - \delta)^2} \right\} \quad (2.28)$$

The velocity potentials were solved by separation of the variables in equation (2.23) employing the boundary condition (i) to (iv). The velocity potential was then substituted into equation (2.24) to solve for P_f and P_g ,

which were then inserted into equation (2.28) to obtain a stability equation based on the growth rate of $\eta(t)$

$$\text{i.e. } \frac{\partial^2 \eta_0}{\partial t^2} - \beta^2 \eta_0 = 0 \quad (2.29)$$

where

$$\beta^2 = \frac{K}{\rho_f P - \rho_g Q} [K(\rho_f P(c - u_f))^2 - \rho_g Q(c - u_g)^2 + \sigma(K^2 - (R - \delta)^{-2})] \quad (2.30)$$

$$P = [I_0\{K(R - \delta)\} + \frac{I_1(KR)}{K_1(KR)} K_0\{K(R - \delta)\}] /$$

$$[I_1\{K(R - \delta)\} - \frac{I_1(KR)}{K_1(KR)} K_1\{K(R - \delta)\}] \quad (2.31)$$

$$Q = \frac{I_0(R - \delta)}{I_1(K(R - \delta))} \quad (2.32)$$

$$\text{and } c = (u_f - \frac{\rho_g Q}{\rho_f P} u_g) / (1 - \frac{\rho_g Q}{\rho_f P}) \quad (2.33)$$

The wave was stable for $\beta^2 < 0$ whereas for $\beta^2 \geq 0$ the wave became unstable and flooding occurred due to bridging.

With further simplifications and approximations, the stability criterion could be expressed as

$$u_g + u_f = [\frac{\sigma}{\rho_g} (K - \frac{1}{R - \delta})]^{1/2} \quad (2.34)$$

The authors claimed good agreement with experimental data except at very high liquid flow rates.

This approach, which is similar to that of CENTINBUDAKLAR and JAMESON (1969), involves many assumptions and it must be concluded that, despite the wide acceptance of this approach, the evidence that the flooding process is connected with the wave motion or growth is purely circumstantial. All these theories are based on the assumption that the initial wave will grow until bridging occurs. This assumption has been rejected when flooding takes place in large tubes.

2.2.2 Standing Wave Model

SHEARER and DAVIDSON (1965) presented one of the earliest analyses which predicted the shape and amplitude of a standing wave formed on a liquid film running down a vertical surface and due to an upward flow of gas over the liquid surface. These authors observed a stationary wave in experiments with a wetted-wall column and the wave profile considered is shown in Figure 2.7. They postulated that the instability of this stationary wave was maintained in position by pressure gradients, which were induced by the acceleration of the gas flow over the front of the wave and which might lead to bridging of the liquid film by increasing the gas velocity. The wave amplitude was found to be very sensitive to gas velocity, with a critical gas velocity existing beyond which the

wave amplitude became very large. The wave profile above the leeward and the windward portions of the wave were analysed separately, and the flow pattern on both the gas and liquid side studied. The following assumptions relating to the gas side were made:

- a) The gas flow broke away from the liquid surface on the leeward side of the wave and hence the gas pressure in this region was constant.
- b) The shear stress exerted on the liquid surface by the gas was neglected.
- c) For the variation of gas pressure over the windward surface of the wave, the empirical expression

$$(P_0 - P_g) / \rho_g U_g^2 = (\pi\delta/2L)(1 + \pi\delta/4L) \quad (2.35)$$

could be used, where

P_0 = pressure far upwind from the wave

P_g = pressure at any point on the windward surface

δ = film thickness = $\left(\frac{3\mu Q_m}{\rho g}\right)^{1/3}$

L = length from the crest to the trough

U_g = velocity of the gas stream.

For the liquid side, the following assumptions were made:

- a) The inertia and viscous forces in the liquid film over the leeward part of the wave were negligible
- b) The pressure within the liquid varied linearly with height.

Thus the following wave profile was obtained

$$\delta = a + \delta_0 \left[\frac{3a}{2} \left(\frac{\rho_f g}{\sigma} \right)^{2/3} \right]^{1/3} \frac{x^3}{2} - \frac{\rho_f g}{6\sigma} x^3 \quad (2.36)$$

where 'a' denotes the amplitude of the wave crest.

The differential equation for the wave profile became

$$\sigma \frac{d^3 \delta}{dx^3} + \frac{\pi \rho_g U_g}{2L} \left(1 + \frac{\pi \delta}{2L} \right) \frac{d\delta}{dx} + \rho_f g + \frac{6}{5} \frac{\rho_f Q_f^2}{\delta^3} \frac{d\delta}{dx} - \frac{3\mu Q}{\delta^3} = 0 \quad (2.37)$$

with the boundary conditions

$$(i) \quad \text{at } x = 0, \quad \delta = \delta_0 + a$$

$$(ii) \quad \text{at } x = 0, \quad \frac{d\delta}{dx} = 0$$

$$(iii) \quad \text{at } x = 0, \quad \frac{d^2 \delta}{dx^2} = - \left[\frac{3a}{2} \left(\frac{\rho_f g}{\sigma} \right)^{2/3} \right]^{1/3}$$

$$(iv) \quad \text{at } x = L, \quad \delta = \delta_0$$

Equation (2.37) was solved numerically and the results indicated that the stationary wave was stable only in a

narrow range of gas flow rates. However, the agreement between theory and experiment was reasonable only up to liquid Reynolds numbers of 250. For higher Reynolds numbers, large discrepancies were found which were attributed by the authors to the entry conditions. It was postulated that rougher entry conditions would generate greater turbulence in the liquid film and possibly in the air.

SHEARER and DAVIDSON (1965) also compared their model predictions with the data of HEWITT and WALLIS (1963) and NICKLIN and DAVIDSON (1962), these having been obtained with smoother entry conditions. The comparison showed fairly good agreement up to Reynolds numbers of 1000 and, above this value, the disagreement was attributed to the onset of turbulence in the liquid film. However, there is little justification for this argument since the model has an assumed negligible effect of velocity distribution on the windward part of the wave profile. This can be shown by reference to equation (2.37) where the velocity profile assumption affects only the last two terms on the left-hand side. A variation of 20% in the coefficients (corresponding to a change from a laminar to a uniform velocity profile) has an insignificant effect on the solution. It is likely, therefore, that the empirical pressure distribution over the windward part of a stationary wave no longer holds for the turbulent film since it does not reasonably represent the behaviour of the wave near the crest.

Another attempt to use the standing wave model was made by UEDA and SUZUKI (1978), their model being based on previously published experimental observations by SUZUKI and UEDA (1977). They assumed the standing wave to be present and to be of the form shown in Figure 2.8 where the shape of the wave crest was considered to be flat as a result of the wave tip being continuously torn off by the gas stream. In their analysis, the following assumptions were made:

- (a) The wave was stationary.
- (b) The shear stresses at the interface and the shroud surface were negligible except for those on the liquid lump.
- (c) Both gravity force and compressibility of the gas were negligible.

They set up the force balance on the wave in both the horizontal and vertical directions with the pressure drop across the wave being considered as the effect of sudden contraction and expansion losses. The abrupt contraction loss was expressed as,

$$\Delta P_{10} = \zeta_0 \frac{\rho_g}{2} U_{g0}^2 = \zeta_1 \frac{1}{2} \rho_g V_{g1}^2 \quad (2.38)$$

with the loss coefficient ζ_0 being a function of A_{g0}/A_{g1} .

In the experiments considered, A_{g0}/A_{g1} varied within the range 0.4 to 0.83 giving the loss coefficient ζ_1 as

$$\zeta_1 = A_{g1}/A_{g0} - 1 \quad (2.39)$$

The abrupt expansion loss was calculated from

$$\Delta P_{02} = \zeta_2 \frac{\rho_g}{2} (U_{g0} - U_{g2})^2 \quad (2.40)$$

where ζ_2 was assumed to be unity, with $A_{g1} = A_{g2}$ and $U_{g1} = U_{g2}$. The total pressure drop across the wave could thus be obtained as

$$\Delta P = \frac{1}{2} \rho_g V_{g1}^2 \left(\frac{A_{g1}}{A_{g0}} \right) \left(\frac{A_{g1}}{A_{g0}} - 1 \right) \quad (2.41)$$

Applying Bernoulli's equation between sections (1) and (2) gave

$$P_{g1} - P_{g0} = \frac{1}{2} \rho_g U_g^2 \left[\left(\frac{A_{g1}}{A_{g0}} \right)^2 - 1 \right] \quad (2.42)$$

and the horizontal force balance as

$$(P_{g1} - P_{g0}) \delta = \sigma \eta_c \quad (2.43)$$

where σ is the surface tension and η_c a factor depending on the wave profile. The pressure variation in the liquid film between sections (1) and (2) was relatively very small and considered constant. The momentum balance in the vertical direction was

$$\Delta P A_{g1} = \rho_f g \delta (A_{g1} - A_{g0}) \quad (2.44)$$

From these equations, the relationship between the gas velocity and the wave height at the onset of flooding

could be deduced as

$$\eta_c = \left(\frac{\rho_g U_{g1}^2}{\rho_g 2g} \right) \left(\frac{\rho_g U_{g1}^2}{\sigma} \right) \left(\frac{A_{g1}}{A_{g0}} \right)^2 \left[\left(\frac{A_{g1}}{A_{g0}} \right)^2 - 1 \right] \quad (2.45)$$

The wave height can thus be determined knowing $\left(\frac{A_{g1}}{A_{g0}} \right)$.

The profile factor (η_c) was estimated from experiment to be 1.5. The flooding velocity was predicted by considering the intersection of equation (2.45) with empirical curves of wave height plotted against gas velocity. The authors claimed good agreement between the predicted values of flooding velocity and the measured values.

This model, with its large dependence on empiricism, is one of few to allow for some boundary layer separation effects and liquid entrainment, although it does not consider the rate of entrainment nor the subsequent increase in gas phase momentum.

2.2.3 Hanging Film Model

The hanging film phenomenon in vertical counter-current flow is a situation in which the liquid film is supported against gravity, and held at rest on the inner surface of a tube, by an upward flow of gas.

WALLIS and MAKKENCHERY (1974) noted that there was a difference between the higher critical gas velocity (above which the film attachment point rose in the tube) and the lower critical gas velocity (below which the film attachment point moved down the tube) and reported that, for small diameter tubes (<6 mm), the velocities differed by a factor of about two whereas for larger tubes these velocities were much closer. They also noted that the typical shape of the film near the gas-liquid interface was different in small and large tubes (Figure 2.9). This was confirmed by EICHHORN (1980) who also reported the existence of a range of gas velocities that would suspend the film in the tube. These velocities were inter-related with interfacial shear stress and film thickness and any one could thus be regarded as an independent variable allowing the other two to be found. Unlike the previous models, the hanging film model can only be used to predict the critical gas velocity when no penetration of liquid downflow occurs. This phenomenon was first proposed by GROLMES et al (1974) when they modelled the flooding phenomenon as a thin hanging film. The authors argued that, below the flooding velocity, the gas had some effect on the waviness of the liquid flow but did not appreciably affect the velocity profile in the liquid film. They assumed that the downward force due to the liquid weight was balanced by the viscous effects

giving

$$\mu_f \frac{d^2 U_f}{dy^2} + \rho_f g = 0 \quad (2.46)$$

with boundary conditions

(i) at the wall $y = 0$, $U_f = 0$

(ii) at the interface $y = \delta$, $\tau_i = \mu_f \frac{dU_f}{dy}$ (2.47)

where T_i is the interfacial shear stress between the phases defined as

$$\tau_i = \frac{1}{2} f_i \rho_g U_g^2 \quad (2.48)$$

where f_i is the interfacial friction factor at flooding conditions.

Using equation (2.46) and equation (2.48), with the boundary conditions (i) and (ii), gave the velocity profile equation

$$U_f = -\frac{1}{2} \frac{\rho_f g \delta^2}{\mu_f} \left[\left(\frac{y}{\delta}\right)^2 - \left(\frac{y}{\delta}\right) \right] + \frac{1}{2} \frac{\rho_g U_g^2 f_i}{\mu_f} \quad (2.49)$$

The average film velocity could thus be defined as

$$U_f = \frac{1}{\delta} \int_0^{\delta} U_f dy \quad (2.50)$$

The flooding condition was assumed to take place when the average film velocity was set to zero with the critical gas velocity being given by

$$U_g = \frac{2}{\sqrt{3}} \left(\frac{\rho_f}{\rho_g} \cdot \frac{g \cdot \delta}{f_i} \right)^{1/2} \quad (2.51)$$

where

$$\delta = \left(\frac{3\mu_f Q_m}{\rho_f g} \right)^{1/3} \quad (2.52)$$

Equation (2.51) could be used as a relation for flooding velocity provided a satisfactory correlation could be found for f_i . The authors approached this problem by looking for a correlation between the interfacial friction factor at the onset of flooding and the liquid film thickness. Their own data and the data of TOBILEVICH et al (1968) with fluids of higher liquid viscosity were used to establish such a relationship. The correlation can be expressed as

$$f_i = 0.006 + \frac{200\delta^2}{\left(\frac{\mu}{\mu_R}\right)^{0.44}} \quad (2.53)$$

where δ is film thickness (cm), μ_R is reference viscosity used to account for the higher gas velocity required to initiate flooding of liquid films with higher viscosity than water ($\mu_R = 1$ cp).

The limit of applicability of this analysis was recommended as

$$\delta_{\min} = 1.72 \left(\frac{\sigma}{\rho} \right)^{1/5} \left(\frac{v}{g} \right)^{2/5} (\gamma(\theta)_0)^{1/5} \quad (2.54)$$

where $Y(\theta)$ is a function of contact angle ($\sim 1/3$ for water on glass).

Another analysis based on the hanging film was presented by WALLIS and KUO (1976). They tackled the problem in terms of separated flow as indicated by the diagram in Figure 2.10.

By considering the Bernoulli equations for the gas and liquid phases, and the interface boundary condition of pressure continuity, these authors obtained the following relationship

$$\frac{1}{2} \left[\frac{\rho_g U_g^2}{((\rho_f - \rho_g)g\sigma)^{1/2}} \right] \left[\left(\frac{d\phi^*}{dx^*} \right)^2 + \left(\frac{d\phi^*}{dy^*} \right)^2 \right] + \frac{\frac{d^2 x^*}{dy^{*2}}}{\left[\left(1 + \frac{dx^*}{dy^*} \right)^2 \right]^{3/2}} + \frac{\frac{dx^*}{dy^*}}{r^* \left[1 + \left(\frac{dx^*}{dy^*} \right)^2 \right]^{1/2}} - (x^*_0 - x^*) = E \quad (2.55)$$

where E is a constant, x^* and y^* are the dimensionless coordinates, r^* is the dimensionless radius, and ϕ^* is the dimensionless velocity potential. These were defined respectively as:

$$x^* = x \left(\frac{\Delta\rho g}{\sigma} \right)^{1/2}$$

$$y^* = y \left(\frac{\Delta\rho g}{\sigma} \right)^{1/2}$$

$$r^* = r \left(\frac{\Delta \rho g}{\sigma} \right)^{1/2}$$

$$\phi^* = \frac{\phi}{u_g} \left(\frac{\Delta \rho g}{\sigma} \right)^{1/2}$$

The boundary conditions used were:

- (i) The hanging film is approached from infinity by a uniform stream, thus

$$\text{at } x = \infty, \quad \frac{d\phi^*}{dy^*} = 0, \quad \frac{d\phi^*}{dx^*} = 1$$

- (ii) At the stagnation point at the leading edge of the liquid film, the interfacial gradient is dependent on the contact angle, thus

$$\text{at } x = x_0, \quad r^* = r_0^*, \quad \frac{dx^*}{dy^*} = -\cot\beta$$

where β is the contact angle.

To solve for the case of a hanging film, Wallis and Kuo used the Kutateladze number, which they defined as

$$K_g = \rho_g^{1/2} U_g (\Delta \rho g \sigma)^{-1/4} \quad (2.56)$$

Equation (2.55) was then rearranged, using K and the boundary conditions, to give

$$K_g^2 = \frac{\sin^3 \beta \left(\frac{d^2 x^*}{dy^{*2}} \right) x_o + \frac{\cos \beta}{r_o^*} - \frac{d^2 x^*/dy^{*2}}{\left[1 + \left(\frac{dx^*}{dy^*} \right)^2 \right]^{3/2}} - \frac{dx^*/dy^*}{r^* \left[1 + \left(\frac{dx^*}{dy^*} \right)^2 \right]^{1/2}} + (x_o^* - x^*)}{\frac{1}{2} \left[\left(\frac{d\phi^*}{dx^*} \right)^2 + \left(\frac{d\phi^*}{dy^*} \right)^2 \right]} \quad (2.57)$$

The contact angle (β) was set at 90° , with the Bond number ($D^* = 2r_o^* = D \cdot \left(\frac{\Delta \rho g}{\sigma} \right)^{1/2}$) assumed large. The complex distance $z = x + iy$ and the velocity potential $w = \phi + i\psi$, were introduced in dimensionless form as before to reduce equation (2.57) to

$$K_g^2 = 2[(x_o^* - x^*) + \sin^3 \beta \left(\frac{d^2 x^*}{dy^{*2}} \right) x_o - \frac{d^2 x^*/dy^{*2}}{\left[1 + (dx^*/dy^*)^2 \right]^{3/2}}] \left[\frac{dw^*}{dz^*} \right]^{-2} \quad (2.58)$$

This equation was solved by introducing two sources in a uniform stream, as illustrated in Figure 2.11. If the sources have strength A , and are located at $(0, \pm a)$, the complex potential function for this arrangement becomes

$$w^* = z^* - A^* \ln(z^{*2} + a^{*2}) \quad (2.59)$$

and the dimensionless stream function

$$\psi = y^* - A^* \tan^{-1} \left(\frac{2x^*y^*}{x^{*2} + a^{*2} - y^{*2}} \right) \quad (2.60)$$

The interface is given by $\psi^* = 0$, or

$$x^* = \frac{y^*}{\tan(y^*/A^*)} + \left[\frac{y^{*2}}{\tan^2(y^*/A^*)} + y^{*2} - a^{*2} \right]^{1/2} \quad (2.61)$$

From equation (2.61) the stagnation point occurs at

$$x_0^* = A^* + (A^{*2} - a^{*2})^{1/2} \quad (2.62)$$

Equations (2.61), (2.62), and $\frac{dw^*}{dz^*}$ were put into equation (2.58), with a chosen value of a^* and A^* varied until K_g remained as constant as possible (usually with 10% of the mean value). The maximum Kutateladze number for stability was found to be 1.87, well below the known experimental value of 3.2.

This analysis may be of use in finding the flow reversal point since it allows for rewetting properties, however its application to flooding is doubtful. In addition, limitations are imposed on this model by the assumption of a 90° contact angle and of large tube diameters.

In general, these modelling methods have not been very successful in explaining the various flooding phenomena and correlating the wide range of experimental data.

2.3 Flooding Correlations

A large number of flooding correlations or equations can be found in the literature and can be separated into two main groups. The first group is based largely on experimental flooding data and were developed for particular conditions; the second group is based on some form of physical or mathematical modelling of the flooding event. However, two dimensionless parameters have emerged as being important, these being the dimensionless superficial velocity and the Kutateladze number.

WALLIS (1961), working on vertical tubes, suggested that the flooding condition could be predicted by the use of equations of the type

$$v_g^*1/2 + v_f^*1/2 = C \quad (2.63)$$

where

$$v_g^* = v_g \rho_g^{1/2} \{gD(\rho_f - \rho_g)\}^{-1/2} \quad (2.64)$$

$$v_f^* = U_f \rho_f^{1/2} \{gD(\rho_f - \rho_g)\}^{1/2} \quad (2.65)$$

where v_g^* and v_f^* are the dimensionless superficial velocities of the gas and liquid respectively. WALLIS (1969) further developed this flooding correlation into

the following

$$j_g^{*1/2} + m j_f^{*1/2} = C \quad (2.66)$$

where j_g^* , j_f^* are the Wallis dimensionless parameters for the gas and liquid respectively, being defined as

$$j_i^* = J_i \rho_i^{1/2} \{gD(\rho_f - \rho_g)\}^{-1/2} \quad (2.67)$$

where j_i is the gas or liquid superficial velocity and m and C are empirical constants. Based on a survey carried out by TIEN and LIU (1979) the value of 'C' appeared to depend mainly on tube diameter and the entry and exit conditions and ranged from 0.7 to 1.0. Similarly, the value of 'm' ranged from 0.8 to 1.0. For fully turbulent flow, the value of m was 1.0. The Wallis parameter somewhat represents the ratio of inertia force to hydrostatic force whereas the Kutateladze number expresses the balance between inertia, buoyancy and surface tension force, being defined as

$$K_i = U_i \left[\frac{\rho_i^2}{g\sigma(\rho_f - \rho_g)} \right]^{1/4} \quad (2.68)$$

where σ is the surface tension and U_i the appropriate phase superficial velocity. The use of the Kutateladze number in flooding correlations dates back to work of TOBILEVICH et al (1968) and PUSHKINA and SOROKIN (1969). Kutateladze (1972) developed a correlation similar to the

Wallis correlation which took the form

$$K_g^{*1/2} + m_1 K_f^{*1/2} = C_1 \quad (2.69)$$

The Wallis and Kutateladze correlations enjoy wide use as predictive equations and are often used without regard to the limits of the foundation data. Many experiments have been carried out to test their validity under various conditions, however neither of these correlations provide the complete answer to flooding prediction, but are useful tools for enabling solutions to be found. The two correlations out perform each other under different conditions when tested against experimental data. However, the performances should not be interpolated beyond the data range tested.

PUSHKINA and SOROKIN (1969) emphasised the differences between the two correlations by carrying out two sets of experiments. One set was performed in a 309 mm tube, the other set in a series of small tubes with internal diameters of 6.2, 8.8, 9.0, 12.2 and 13.1 mm. The analysis focussed on determining the critical air velocity required for flooding. The results presented showed that the tube diameter had no effect on the magnitude of the critical (flooding) velocity of the air and was approximately 14 to 16 m/s. (Line 1 in Figure 2.12). For the same data, the Wallis correlation predicted a varying (flooding) gas velocity which did not fit the experimental data (Line 2 in Figure 2.12).

Pushkina and Sorokin claimed these results demonstrated the superiority of the Kutateladze correlation over the Wallis correlation.

WALLIS and MAKKENCHERY (1974) offered an explanation of the results presented by Pushkina and Sorokin. They emphasised that the Wallis correlation was based on a limited amount of data taken in tubes with diameters ranging from 12.7 mm to 50.8 mm and stated that the Kutateladze correlation contained no characteristic scale dimension for the apparatus, hence would best be suited for large diameter tubes provided the liquid film remained thin. They admitted that for small diameter tubes, the surface tension effects could be important. To support their claim, Wallis and Makkenchery presented data which showed that the difference in velocity required to support a hanging film compared to that required for flow reversal was a factor of 2, greater in small tubes compared to large tubes. Wallis and Makkenchery incorporated the surface tension effect in terms of a dimensionless tube diameter D^* , where

$$D^* = D[g(\rho_f - \rho_g)/\sigma]^{1/2} \quad (2.70)$$

which is sometimes called the Bond number. They also showed that the Wallis and Kutateladze numbers could be related through the Bond number, thus

$$j^* = K/D^* \quad (2.71)$$

Recently, BANKOFF et al (1981) introduced a new dimensionless parameter H^* , based on a new characteristic length, defined as

$$H_i^* = j_i \left[\frac{\rho_i}{g\bar{w}(\rho_f - \rho_g)} \right]^{1/2} \quad (2.72)$$

where

$$\bar{w} = D^{(1-\alpha)} \left(\frac{\sigma}{g(\rho_f - \rho_g)} \right)^{\alpha/2} \quad (2.73)$$

with the value of α lying somewhere between zero and unity such that

$$\text{when } \alpha \rightarrow 0 \quad \text{then } H^* \rightarrow j^*$$

$$\text{and when } \alpha \rightarrow 1 \quad \text{then } H^* \rightarrow K^*$$

Thus the Bankoff parameter H^* represents a smooth transition scaling between the Wallis parameter, j^* , and the Kutateladze parameter K^* . The empirical exponent α is a dimensionless geometry-dependent factor. Based on this dimensionless parameter, a new correlation was suggested of the form

$$H_g^{*1/2} + m_2 H_f^{*1/2} = C_2 \quad (2.74)$$

McQUILLAN and WHALLEY (1984) collected a large number of experimental flooding data points to test the performance of the more commonly used empirical and

theoretical flooding correlations. The data contained flooding information for a wide range of flow conditions and fluid physical properties. They found that the most successful empirical correlation was that of ALEKSEEV et al (1972), based on the Kutateladze K , Weber We , and Galileo Ga , numbers. Thus

$$K_g = Fr^{-0.20} We^{-0.21} Ga^{-0.09} \quad (2.75)$$

where

$$Fr = \frac{Q_f(\rho_f - \rho_g)^{3/4}}{g^{1/2} \sigma^{3/4}} \quad (2.76)$$

$$We = \frac{\sigma}{(\rho_f - \rho_g) D^2} \quad (2.77)$$

$$Ga = \frac{g \sigma^{3/2}}{U_f^2 (\rho_f - \rho_g)^{3/2}} \quad (2.78)$$

The Alekseev et al correlation agreed well with the data over a range of tube diameters and liquid surface tensions, but over-predicted flooding gas flowrates at high liquid viscosities. In view of this, McQUILLAN and WHALLEY (1984) modified the ALEKSEEV et al (1972) correlation to become

$$K_g = 0.286 Bo^{0.26} Fr^{-0.22} \left(1 + \frac{\mu}{\mu_w}\right)^{-0.18} \quad (2.79)$$

Of the theoretical correlations tested, McQUILLAN and WHALLEY (1984) found that the modified form of the correlation presented by BHARATHAN et al (1978) was the

most successful over a range of liquid viscosities and surface tensions but overpredicted the flooding gas velocity for large tube diameter. They attempted to explain the overpredictions in terms of inaccuracies in the empirical interfacial friction factors for large tube diameters.

2.4 Effect of Fluid Properties

In further attempts to understand the phenomenon of flooding, investigations have been carried out to study the effect of liquid properties, e.g. viscosity, surface tension, and gas properties, mainly the gas density. In many cases, however, the results reported have been conflicting.

2.4.1 Liquid Viscosity Effect

Although a number of the correlations presented in the literature contain viscosity terms, few of these have any direct experimental support and the effects reported are quite confusing.

WALLIS (1962), working with a vertical tube of 191 mm diameter, reported measurements of the flooding gas rate using water, glycerol solution, and ethylene glycol as liquids in counter-current flow with air at atmospheric

pressure and with the liquid viscosity varying from 1 to 3000 centipoise. The results indicated that an increase in liquid viscosity decreased the flooding gas velocity for a fixed water flowrate. A similar trend was obtained by SHIRES and PICKERING (1965), CLIFT et al (1966), and CHUNG et al (1980), see Figure 2.13. A similar effect of liquid viscosity (but less conclusive was reported by TIEN et al (1979). They found that, for a liquid film flowing at a fixed velocity, an increase in the liquid viscosity caused an increase in the perturbed pressure in the film which increased the pressure difference across the film surface which, in turn led to waves being formed on the film surface and hence flooding to occur at lower gas velocities. They also stated, however, that the viscosity effect could be contradicted by the inertia effect, which could explain why the net liquid viscosity effect was small. Tien et al supported the claims by experimental data obtained from air-oil tests. A completely different effect of liquid viscosity was reported by SUZUKI and UEDA (1977), after experiments using liquids with five different viscosities ranging from 9.0×10^{-4} to 2.4×10^{-2} kg/ms. They found that the gas flooding velocity increased as the liquid viscosity was increased. The effect was evident for thin liquid films (see Figure 2.14) but not so clear for thick films. Similar conclusions were reported by TOBILEVICH et al (1968) and GROLMES et al (1974).

The results of HEWITT (1977) indicated only a small

effect of liquid velocity on the flooding gas velocity. A comparison of the data obtained from two solutions of glycerol (38% and 67%) with those obtained from water showed that the 67% glycerol solution data ($\mu_f = 1800 \times 10^{-5}$ kg/ms) lay only slightly above those of water ($\mu_f = 110 \times 10^{-5}$ kg/ms) whilst the data for the 38% glycerol solution ($\mu_f = 300 \times 10^{-5}$ kg/ms) lay a little below. In view of these results, Hewitt concluded that liquid viscosity influence on flooding conditions was small and only became important when the changes in viscosity were substantial.

2.4.2 Surface Tension Effect

Some studies have been carried out to ascertain the influence of surface tension, although it is not always easy to know the true surface tension of the dynamic interface since the static measurements may not be quantitatively accurate when applied to flooding conditions. According to SUZUKI and UEDA (1977), the dynamic value is slightly higher than the corresponding static value but the difference could be neglected. However, the data reported are in general agreement that a smaller surface tension value leads to lower flooding gas velocities.

The experimental findings of SHIRES and PICKERING (1965), HEWITT (1977), ZVIRIN et al (1979), and CHUNG et

al (1980) are consistent with the theoretical findings of C E T I N B U C K L A R and J A M E S O N (1969) and T I E N et al (1979) in that lower surface tension decreases the gas velocity at flooding. In principle, the reduction in surface tension means a smaller pressure difference can be sustained across a film surface without the surface forming waves with smaller radii of curvature, where small radius of curvature implies short wave length or large wave amplitude, both of which are a surface instability. Hence, for the same liquid flowrate, a reduction in surface tension will cause flooding to occur at a lower air flowrate, Figure 2.15.

T O B I L E V C H et al (1968), and S U Z U K I and U E D A (1977) obtained no conclusive effect of surface tension. The Wallis correlation takes no account of surface tension and this is sometimes considered to be a major deficiency.

2.4.3 Gas Density Effect

The dependence of the gas flowrate at flooding on the gas density has generally been neglected. However, a few investigations have been made and these will be considered here.

H E W I T T (1977) investigated the gas density effect by using two different air densities, 1.33 kg/m^3 and 2.34 kg/m^3 . The results indicated that a lower gas

velocity was required to cause flooding as the gas density increased, for a given liquid velocity. Hewitt agreed with the assumption of SHEARER and DAVIDSON (1965) that the flooding condition would occur at a fixed value of $\rho_g V_g^2 / \sigma$ for a given film thickness. Although he quoted two different air densities used in his experiments, Hewitt did not give any information about the way the higher air density was obtained, since the reported air temperature was approximately 20°C for both sets of tests.

ZVIRIN et al (1979) compared the results of their theoretical exercise with Hewitt's experimental results and predicted a slight decrease in the flooding velocity when the gas density was increased. Similar conclusions were obtained by SHIRES and PICKERING (1965), CHAUDRY (1967), and TOBILEVICH et al (1968).

2.5 Effects of Tube Geometry

The effects of tube geometry on flooding have been widely reported and these have indicated various parametric influences. However, there have been conflicting findings regarding these influences or effects on flooding.

2.5.1 End Condition Effects

A number of investigators have found that flooding conditions are sensitive to the way in which the gas and liquid enter and leave the tube. WALLIS (1961) postulated that the flooding condition was influenced by the design of the tube ends. He allowed for this influence by including a factor in his flooding correlation which was dependent on the tube end geometry. For tubes with sharp-ended flanges, the value of the factor was 0.725 whereas when end effects were minimised the value lay between 0.88 and 1.0.

A quantitative investigation on the effect of the entry radius was performed by BHARATHAN et al (1977) and Figures 2.16 and 2.17 show how the ratio of the entry radius to the tube diameter affects the factor C in the Wallis correlation. Tubes with smoother entries have higher value of C.

HEWITT et al (1965) concluded that porous sections of tube, carefully matched to the main tube, provide the closest approximation to the idea of smooth liquid injection and removal. BANKOFF and LEE (1983) reported that gas flooding velocities with porous injection were higher than those with top flooding entry, under the same conditions.

The effect of tapered liquid inlet conditions was

investigated by CHUNG et al (1980) who found that the required flooding gas velocity was much higher in a tapered liquid inlet than that in a sharp-edged inlet system. ENGLISH et al (1963) investigated the effect of the diagonal cut-off angle in the liquid exit and, by comparing the results with square ended tub results, they found that increases in flooding gas rates of 5%, 25%, and 54% were obtained when using tube ends with 30°, 60° and 75° tapers respectively. A similar effect was reported by HEWITT (1977) who showed that the gas flooding velocity was increased about 30% when using a diagonal cut tube end ($\psi = 30^\circ$) compared with a normal cut tube ($\psi = 0^\circ$) see Figure 2.18.

The tube end condition also appeared to influence the position of the inception of flooding. CHUNG et al (1980) observed that flooding (marked by liquid entrainment and highly agitated film) appeared near the liquid exit when a tapered liquid inlet was used, whereas flooding always took place at top of the tube, without prior droplet entrainment and subsequent film agitation, when a sharp-edged liquid inlet was employed. Furthermore, they observed that with a tapered liquid inlet and nozzle air supply, flooding occurred primarily as a result of interface instability developed inside the tube and not around the inlet or exit.

D. McNEIL (1986) gave an explanation as to why higher gas flooding velocities were obtained when smoother

liquid films were introduced. He suggested that rougher entry conditions induced turbulence and hence increased the effective viscosity of the liquid film thus thickening the film and consequently reducing the gas rate to induce flooding. BANKOFF and LEE (1983) suggested the cause as a higher interfacial friction factor produced by the initially imposed disturbances at the sharp liquid entry, since this is more likely to cause the formation of unstable waves. They argued that none of the available flooding correlations had sufficient adjustable parameters to account fully for the wide variety of end geometries used. However, based on a wide literature survey made, they found that the flooding model of CETINBUDAKLAR and JAMESON (1969) was the model which best accounted for the effects of the liquid entrance conditions.

Details of the tube end conditions used by various investigators are illustrated in Figure 2.19.

2.5.2 Tube Diameter Effects

The effect of tube diameter on the flooding velocity is of great interest in connection with possible scaling laws in single-channel flows. Although extensive tests have been performed, the effect of tube diameter on flooding is not very clear. The number of literature items reporting definite effects roughly equals that reporting little or no effect. Analyses by SHEARER and

DAVIDSON (1965), CENTINBUDKLAR and JAMESON (1969), and PUSHKINA and SOROKIN (1969) showed no explicit diameter dependence for the flooding velocity. GROLMES et al (1974) reported that the tube diameter has very little effect on the flooding velocity and TIEN et al (1979) showed that flooding under ideal entry conditions should only have a weak diameter dependence (Figure 2.20). On the other side, CHAUDRAY (1967), TOBILEVICH et al (1968), HEWITT (1977) and SUZUKI and UEDA (1977), reported that higher gas superficial velocities were required to initiate flooding as the tube diameter increased (for a fixed liquid superficial velocity), see Figure 2.21. DIEHL and KOPPANY (1969) also concluded that the flooding velocity was a function of the tube diameter and that there was a definite critical diameter above which the flooding velocity became independent of tube diameter. They also concluded that, for small diameter tubes, the liquid bridged across the tube opening due to surface tension effect and, in very small tubes, counter-current flow was impossible. It was also reported by WALLIS et al (1975) that MAKKENCHERY (Unpublished work) carried out a series of studies on flooding with air-water flows in tube sizes ranging from 19.1 mm to 139.7 mm. These results showed that the flooding velocity was independent of tube diameter at diameters greater than 50.8 mm. Opposing trends were reported by RICHTER et al (1978), which indicated that the flooding curves would shift to lower values of velocity with increasing pipe size.

The findings from a Literature Survey conducted by BANKOFF and LEE (1983) indicated that most of the analytical models and empirical correlations predicted a monotonic decrease of gas flooding velocity (in terms of the Wallis parameter) as the dimensionless diameter, D^* , increased for a fixed dimensionless liquid velocity. This gave an opposite trend, in terms of the gas superficial velocity which agreed with the findings of TOBELIVICH et al (1968), HEWITT (1977), SUZUKI and UEDA (1977) and CHUNG et al (1980). It also implied that the gas flooding superficial velocity was not proportional to the square root of the tube diameter as the Wallis correlation indicated.

2.5.3 Tube Length Effects

The effect of tube length on flooding conditions has been explored by many investigators and, again, contradictory results are reported. HEWITT et al (1965) observed that the flooding velocity decreased with increasing tube length but, later HEWITT (1977) reported a small tube length effect, using a different liquid discharge arrangement. NICKLIN and DAVIDSON ((1962) reported flooding data for both 6 ft and 15 ft length tubes, 25 mm diameter. Their results show that the shorter tube flooded at higher gas velocities than the larger. Similar results were obtained by CHAUDRY (1967) and SUZUKI and UEDA (1977). Furthermore, Suzuki and Ueda

found that the effect was rather significant in the high liquid flow rate range. They suggested four different correlations to account for tube length effects. HAGI et al (1977) reported that, for similar end geometries, the constant C in the Wallis correlation was essentially unaffected by the tube length. Similarly GROLMES et al (1974) did not observe any length effect. However, more recently, WHALLEY and McQUILLAN (1983) concluded that the flooding air flowrate for a given pressure and water film flow rate was strongly affected by the length of the tubes with the flooding air flow rate decreasing as the length of the tube increased, see Figure 2.22. They also provided a possible explanation for GROLMES et al (1974) not being able to observe the length effect, attributing this to the liquid exit geometries used by Grolmes. They suggested the exit geometries led to a localisation of flooding at the liquid exit, so that flooding was initiated by the flow conditions at the liquid exit and hence no length effect would be expected.

LIU and TIEN (1982) also reported that increasing the tube length would hamper the onset of flooding but only to a limited extent. According to the authors, the tube length exerted an influence on flooding through the liquid momentum (velocity) which increased with tube length up to a point whereafter it became independent of tube length, and was dependent only on the liquid injection rate.

2.6 Pressure Difference

Pressure difference measurements in counter-current flow have always been used as an indicator for the onset of flooding and for predicting flow pattern changes. The measurements are not altogether easy to make since there are connecting lines between the sensing points and the measuring point and it is essential (in the interest of manometry) to know what type of fluid exists in these lines during measurements.

Some investigators, e.g. HEWITT et al (1963), COLLIER and HEWITT (1961), interposed a separator between the sensing and measuring points to ensure air only was present in the connecting lines to the measuring instruments. Others, e.g. HEWITT et al (1962), HEWITT and TAYLOR (1970), used positive flows of liquid or air in the connecting lines, the liquid purge system being most popular and reliable.

The axial position of the pressure difference measurements has also varied with different investigators. For example, HEWITT and WALLIS (1963) situated the pressure tapping points above the injection (porous sinter) point and below the film removal (porous sinter) point thus ensuring "dry wall" connections. In contrast, DUKLER and SMITH (1979) measured the pressure difference, or pressure gradient, above and below the liquid injection

point, the results of these measurements being illustrated in Figures 2.23a and 2.23b. These results clearly demonstrate the ability of pressure difference measurements to identify the onset of flooding, due to the sharp increases which occur. The authors described the characteristics as follows. Prior to flooding, the pressure gradient slowly increased with gas flow rate but, as the flooding point is approached, the surface of the falling liquid film became wavy with a small increase in gas flowrate causing the disturbance to spread over the entire liquid falling film, resulting in a highly agitated surface and the formation of liquid slugs within the tube (bridging the tube at higher inlet liquid flows). As a preliminary to slug formation, a rough thick liquid developed, causing a considerable increase in interfacial shear stress with the pressure difference rising sharply for a small increase in gas flowrate, once a liquid slug has been formed. The onset of flooding, following the formation of slugs, generally corresponded to the point where the maximum pressure difference occurred and led to unsteady conditions. The preceding remarks apply particularly to the measurements made below the liquid injection point where the changes at the flooding point are more marked. Typical pressure difference characteristics for vertical counter-current flow with upper plenum injection are shown in Figure 2.24, these being presented by HAWLEY and WALLIS (1982) and relating to flow in a 51 mm diameter tube. Similar results were obtained by BHARATHAN et al (1979) and OSTROGORSKY et al

(1982). The pressure drop characteristics are similar to those obtained from porous injection systems before flooding takes place. Stage 5 was described by the authors as the onset of flooding following which two distinct traces of the pressure drop were obtained which depended on the flow pattern which had become established in the tube. If the flow pattern changed rapidly to a pattern similar to Bharathan's transition flooding regime, in which a smooth film region was established in the upper part of the tube with rough film flow below, then the pressure drop followed line 6a; if the flooding pattern was a full-length rough film (which was described by BHARATHAN et al (1970) as rough film flooding regime) the pressure drop followed line 6. However, both pressure drop traces continued to decrease due to the reduction of the liquid delivery rate as the gas flux increased.

From the results shown in this section, it may be concluded that the measurement of pressure drop in adiabatic counter-current vertical flow predicts the onset of flooding quite well.

2.7 Entrainment

The entrainment of liquid droplets in the gas core is an important effect associated with a gas-liquid annular two-phase flow, and it can play an important role in flooding also. In counter-current vertical flow, a

liquid film flows down the tube wall and is acted on by the ascending gas phase flowing in the core of the tube and this interaction between the two phases can produce an exceedingly complex pattern of waves. The break-up of the disturbance waves on the liquid-gas interface is usually regarded as being the source of the liquid droplet entrainment in annular flow (HEWITT and TAYLOR (1970)). Detailed studies of the onset of entrainment by COUSINS et al (1965) revealed that the disturbance waves are a necessary but not sufficient requirement for the onset of liquid entrainment. If the gas velocity is insufficient, no entrainment will take place even if the disturbance waves are present. The inception of entrainment has been assumed, by many investigators (e.g. HUTCHINSON and WHALLEY (1972), and MCCARTHY and LEE (1979)), to be the point at which the drag forces exceed the surface tension forces.

Although (i) experimental techniques have been well developed for the measurement of entrainment (ii) the link between the disturbance waves and the droplet entrainment has been clearly established by photographic studies (e.g. ARNOLD and HEWITT (1967), HEWITT and ROBERTS (1969), WHALLEY et al (1973) and WHALLEY and HEWITT (1983)), and (iii) a variety of mechanisms for the detailed breakup of the disturbance waves into entrained droplets have been proposed, the precise mechanism by which droplets are detached from disturbance waves is still uncertain.

The entrainment of liquid droplets emanating from the onset of flooding has been observed by some investigators, notably DUKLER and SMITH (1979), who postulated that it was possible that the mechanism which led to entrainment may also lead to flooding in some cases. It was also suggested that the entrained droplets from the liquid film could have some effect on the flooding process. However, the precise reason for the association between entrainment and flooding is still not clear.

A detailed study made by McCARTHY and LEE (1979), confirmed that the onset of entrainment in vertical counter-current flow coincided with the onset of flooding. The authors also concluded that, when the liquid flow rate was low, liquid carry-over was due to the entrainment of liquid drops sheared off the waves on the liquid film surface. At high liquid flow rates, where flooding was indicated by bridging or plug type flow, the liquid carry-over was due to the entrainment of drops formed by the bursting of the liquid bridge. TIEN et al (1979) extended their flooding model to include the effect of entrained droplets in the gas flow. The results of their analysis qualitatively showed that liquid entrainment reduced the gas flooding velocities in the low liquid flow regime. Experimental results obtained by the same authors also showed this qualitative trend. A possible explanation for this trend was offered in terms that the additional momentum flux from the entrained droplet in the

gas stream caused the observed shift with the effect being diminished at high liquid flowrates. Similar conclusions were obtained by TIEN and LIU (1979) and DOBRAN (1981).

HEWITT and TAYLOR (1970) reported that the location of the onset of entrainment depended on tube end conditions and the method of introducing the phases, whilst DOBRAN (1981) found that flooding with non-smooth ends was associated with higher values of entrainment and that smooth ends and more viscous liquids would tend to minimise the break down of waves and produce less entrainment. DUKLER and SMITH (1977) observed two locations for the initiation of entrainment, the first well below the liquid entry and the second at the entry. The former occurred at low liquid flowrates and the latter at high liquid flowrates. These authors also suggested that the onset of liquid entrainment was associated with onset of flooding. BANKOFF and LEE (1983) reported that entrainment took place at the bottom of the tube but could be initiated at the liquid entrance when the liquid flow rate was large enough. CHUNG et al (1980) observed that droplet entrainment was primarily a liquid exit effect.

2.8 Mean Liquid Film Thickness

The liquid film thickness is a parameter which affects the onset of flooding and several investigators, such as GROLMES et al (1974), IMURA et al (1977) and

RICHTER (1981), have incorporated empirical expressions for the mean liquid film thickness in their flooding correlations. There are two conditions of falling liquid film which should be considered:

(i) Falling film without gas flow:- An early analysis of the laminar film flow for a vertical plate was developed by NUSSELT (1916), based on a balance of the shear, gravity, and pressure forces on the element of liquid. The classical expression was expressed in the form:

$$\delta^* = 1.442 \text{ Re}^{1/3} \quad (2.80)$$

where δ^* was the dimensionless film thickness and Re_f the Reynolds number, these being defined by

$$\delta^* = \delta \left(\frac{\rho_f (\rho_f - \rho_g) g}{\mu_f^2} \right)^{1/3} \quad (2.81)$$

$$\text{Re}_f = \frac{\rho_f Q_f}{\mu_f} \quad (2.82)$$

Although equation (2.80) was developed for flow down a flat surface, the film thickness is normally small enough for any effects of surface curvature to be neglected (BELKIN et al (1959)). KAMI et al (1954) and FEIND (1960), among other investigators, conducted experiments covering the average thickness of falling film in annular

flow without upwards gas flow. The results indicated that Nusselt's equation held quite well in the laminar flow region and HEWITT and WALLIS (1963) found that it was valid for the liquid Reynolds number up to 1000. BELKIN et al (1959) reported extensive experimental data for film thickness measurement in vertical tubes, covering a wide range of liquid Reynolds number, from 200 to 30,000. Their data closely followed the Nusselt equation in laminar flow. In turbulent flow, they proposed a new correlation for the film thickness in terms of Reynolds number and a wall shear factor:

$$\text{i.e. } \delta^* = 0.794 (Re_f \sqrt{f_w})^{2/3} \quad (2.83)$$

where f_w was the wall friction factor which could be obtained from the Blasius equation:

$$f_w = 0.0559 Re_f^{-1/4} \quad (2.84)$$

FINED (1960) correlated his experimental data, which covered a range of Reynolds number from 400 to 2000, with the following equation:

$$\delta^* = 0.532 Re_f^{1/2} \quad (2.85)$$

Similarly, WALLIS (1969), based on the experimental data of BELKIN et al (1959), found that the mean value of the liquid film appeared to follow the Nusselt equation up to Reynolds numbers of 250. At higher Reynolds numbers,

when the film became turbulent, Wallis suggested a new correlation of the form

$$\delta^* = 0.159 \text{Re}_f^{2/3} - 11.76 \quad (2.86)$$

(ii) Falling film with counter-current gas flow:- One of the main characteristics of falling liquid film is that the interface between the film and the adjacent gas phase is, in most cases, covered by a complex pattern of waves. However, the effect of the presence of the gas flow on the mean film thickness in vertical annular flow has been studied by several investigators including HEWITT and WALLIS (1963), TOBILEVICH et al (1972), and HAWLEY and WALLIS (1982). Generally, their results indicated that the mean film thickness tended to increase as the gas flow rate was increased, due to the acceleration effect produced by the interfacial shear stress. The interfacial shear stress, in general, acts to retard the liquid film flow resulting in a thicker film of lower velocity. In practice however, it has been observed that this effect is not significant because the interfacial shear stress predicted in counter-current flow, prior to the onset of flooding, is very small compared to the wall shear stress. HEWITT and WALLIS (1963) showed that the mean film thickness at low Reynolds numbers, with low gas flows, was well approximated by Nusselt's equation (2.80). This was confirmed by HAWLEY and WALLIS (1982) as shown in Figure 2-25. The data obtained by GROLMES (1974) indicated a decreasing flooding velocity with increasing

film thickness and similar results were reported by SUZUKI and UEDA (1977).

In vertical annular flow, HEWITT and TAYLOR (1970) reported that the thickness of a falling liquid film gradually decreased as the liquid film velocity increased due to gravitational acceleration. HEWITT et al (1965) found that, near the flooding condition, the film thickness was, on average, greater at the top than at the bottom of the tube.

2.9 Counter-Current Flooding in Vapour-Liquid Systems

Flooding in counter-current vapour-liquid systems differs from that in gas-liquid systems primarily because condensation is possible if the liquid is subcooled. This additional mechanism of condensation provides the means for further transport of mass, energy and momentum and its influence on the flooding characteristics is found to depend mainly on the local behaviour of the moving vapour-liquid interface. The highly transient condensation effect can lead to local pressure deficiencies in the vapour phase which can accelerate the unstable growth of large pressure waves at the vapour-liquid interface, thus causing flooding to occur as a result of this interfacial wave instability. A less dramatic effect of condensation is that it reduces the effective mass flow and momentum of the vapour phase while

increasing those of the liquid phase.

Flooding in counter-current liquid-vapour flow is a mechanism which is, at present, not completely understood. In part, this is due to the complexity of accurate theoretical modelling of the flooding phenomena and partly because of the absence of experimental data. Relatively little information can be found in the literature for the effects of subcooling on flooding in vertical tubes since most experimental work has been performed using other geometries (mainly simulated Pressurised Water Reactor (PWR) vessel geometries). The effects of condensation of a saturated or superheated vapour on a counter-current flow of subcooled liquid has been of great interest in the safety analysis of PWR during a postulated Loss of Coolant Accident (LOCA).

FAN and SCHROCK (1978) performed an experimental investigation of flooding using steam and subcooled water in a vertical glass tube 38 mm in diameter and 2410 mm long with an inlet water temperature of 27° C. They presented a flow regime map, Figure 2.26, for counter-current steam-water flow to describe the system behaviour for the tube below the liquid injection point. In this figure, three of the major boundaries are formed by the complete condensation line, the saturated liquid flooding line, and the 100% by-pass line. Region (2) represents the regime just after the onset of flooding, regions (3) and (6) represent the regimes of partial

delivery, and regions (7) and (8) represent zero penetration of liquid downflow, implying a hanging film regime. The bottom of the test section becomes dry in region (9). FAN (1979), working on the same system, presented a similar map for a lower initial liquid subcooling (inlet water temperature of 71° C) which showed the regions (8) and (9) to be closer to the 100% by-pass line.

A systematic experimental study in a vertical tube was carried out by WALLIS et al (1980). Here the test section was a lexan tube 50.8 mm i.d. and 1.52 m long which was located between two plenum chambers to ensure that the water was injected indirectly into the test section. For a series of inlet water temperatures, two categories of tests were performed, "steam first" and "water first". Their results showed that several flooding regimes were possible, depending on whether the boundaries were approached by varying the steam or the water flow, since this determined whether the bulk of the condensation took place in either the upper or lower plenum. Typical results from these experiments are shown in Figure 2.27. In addition, Wallis et al found the effect of using rounded instead of squared ends on the tube was significant. Hysteresis effects were also found in the flooding curves when the steam flow was increased from zero to the point of complete by-pass and when it was decreased to zero again (all other parameters held constant) see Figure 2.28. Hysteresis effects were also

reported by TIEN (1977), but were different from those observed by WALLIS et al (1980).

LIU and COLLIER (1980) performed similar experimental studies in the counter-current condensation of steam and subcooled water in an adiabatic tube. In general the steam-water results were similar to those obtained for air-water flow. They also observed a hysteresis effect in the flooding curves.

2.10 Modelling with Phase Change

Despite the complicated nature of the condensation effect, a few attempts have been made to analyse the effect of vapour condensation on the counter-current flooding phenomena. In general, these are modifications of existing gas-liquid flooding models or correlations.

TIEN (1977) proposed a simple correlation for a single vertical tube by modifying equation (2.66). He incorporated the condensation effect on the liquid film surface by calculating the steam flow reduction on the assumption that the condensation enthalpy change was balanced by the heat transfer required to raise the temperature of the subcooled water to the saturation temperature. Hence the effective steam flow, based on the Kutateladze number, was

$$K_{ge} = K_g - f K_f \left(\frac{C_p \Delta T_{sub}}{h_{fg}} \right) \left(\frac{\rho_f}{\rho_g} \right)^{1/2} \quad (2.87)$$

where f was an empirical constant characterising the fraction of steam actually condensed. By substituting K_{ge} into the flooding equation (2.69) a subcooled flooding correlation was obtained in the form

$$(K_g - B f \Delta T_{sub} K_f)^{1/2} + m K_f^{1/2} = C \quad (2.88)$$

where B was a property constant defined as

$$B = \left(\frac{C_p}{h_{fg}} \right) \left(\frac{\rho_f}{\rho_g} \right)^{1/2} \quad (2.89)$$

Equation (2.88) leads to the interesting result that there is a possible hysteresis effect due to condensation. Flooding curves calculated by the above correlation for various initial liquid subcooling values, using the experimental data of WALLIS (1961), and PUSHKINA and SOROKIN (1969) for air-water flows, gave m and C as 1 and $(3.2)^{1/2}$ respectively. According to Tien's argument, there is always a minimum point in the flooding curve for subcooled liquid and the liquid injection flow rates higher than the minimum value of each flooding curve results in the hysteresis effect, since the positive slope region in the curve is unstable. It should be pointed out that the condensation efficiency, f , and the slope, m , in equation (2.88) are assumed to be independent of the liquid injection rate in the Tien correlation. This does not reflect the experimental evidence obtained by other

investigators, such as WALLIS et al (1975) and CROWLEY et al (1976). Moreover, recent experimental results show that the slope, m , is a function of the initial liquid subcooling as well as the liquid injection rate. Therefore, the Tien correlation requires modification in these respects.

LIU et al (1978) proposed a correlation to model the flooding characteristics for air-water flows and then developed a heat transfer analysis to allow for condensation effects in the case of steam-water flows. The air-water correlation bore some similarity to the Wallis correlation expressed by equation (2.66), and took the form

$$j_g^{*1/2} + \left(\frac{\rho_g}{\rho_f}\right)^{1/4} j_f^{*1/2} = C \quad (2.90)$$

The value of $(\rho_g/\rho_f)^{1/4}$ was small compared to the "m" value suggested by the Wallis correlation. They then used the annular flow model for counter-current steam-water flooding flows to determine the amount of steam condensed using a mass balance for a differential section δs to give

$$\frac{dW_s}{dx} = \frac{dW_L}{dx} \quad (2.91)$$

where W_s was the steam flowrate and W_L the water film flowrate. An energy balance for the same differential

section, assuming $h_{fg} \gg C_p (T_{sat} - T_w)$, was written as

$$W_L C_p \frac{d}{dx} (T_w) \cdot \delta x = \frac{dW_s}{dx} \cdot \delta x \cdot h_{fg} \quad (2.92)$$

where T_w was the temperature at any station of the falling film, T_w a function of x , h_{fg} the latent heat of evaporation, and C_p the specific heat at constant pressure. By substituting equation (2.91) into equation (2.92) and integrating from the initial conditions, the local film temperature could be written as

$$T_w(x) = T_{win} + \frac{h_{fg}}{C_p} \ln \left(\frac{W_L(x)}{W_{Lin}} \right) \quad (2.93)$$

The heat transferred was assumed to be due to condensation only, with the heat transfer coefficient 'h' defined by

$$h(T_{sat} - T_w) = \frac{dW_s}{dx} h_{fg} \quad (2.94)$$

Using equations (2.92), (2.93), and (2.94) gave

$$\frac{dW_s}{dx} = H - \frac{h}{C_p} \ln \left(1 + \frac{W_c}{W_{Lin}} \right) \quad (2.95)$$

where $H = \frac{h \Delta T_{sub}}{h_{fg}}$ and W_c was the condensed steam flow rate.

Assuming the mass of the condensed steam to be very much less than the liquid injected, h was considered constant and by neglecting all higher order terms, equation (2.92) was integrated to give

$$W_c = W_{Lin} \frac{C_p(T_{sat} - T_{Win})}{h_{fg}} \left[1 - \exp\left(\frac{-hx}{C_p W_{Lin}}\right) \right] \quad (2.96)$$

Equation (2.96) was put into dimensionless form compatible with equation (2.90) as

$$j_{gc}^* = j_{Lin}^* \lambda f \quad (2.97)$$

where

$$\lambda = \frac{C_p \Delta T_{sub}}{h_{fg}} \quad (2.98)$$

and the condensation efficiency

$$f = 1 - \exp\left(\frac{-hx}{C_p W_{Lin}}\right) \quad (2.99)$$

Thus equation (2.90) could be modified to account for steam condensation as follows

$$(j_g^* - f \lambda j_{Lin}^*)^{1/2} + \left(\frac{\rho_g}{\rho_L}\right)^{1/4} j_f^{*1/2} = C \quad (2.100)$$

Other correlations have been suggested to deal with the counter-current flows of steam and water in simulated PWR downcomer geometries. One such correlation, which has been adopted for use in vertical tube geometries, was presented by ROTHE and CROWLEY (1978). Their correlation was based on a modification of the Wallis correlation expressed in equation (2.66) whereby they accounted for condensation effects by reducing the effective steam flow by an amount proportional to the condensation capability

of cold water, this capability then being expressed as

$$j_{ge}^* = j_g^* - f j_{fin}^* \left(\frac{\rho_s}{\rho_g} \right)^{1/2} \left(\frac{C_p (T_{sat} - T_f)}{h_{fg}} \right) \quad (2.101)$$

or
$$j_{ge}^* = j_g^* - f \lambda j_{fin}^* \quad (2.102)$$

Incorporating this modification into the Wallis equation

gave
$$(j_g^* - f \lambda j_{fin}^*)^{1/2} + m j_f^{*1/2} = C \quad (2.103)$$

The similarity between equation (2.102) and equation (2.88) is clear.

2.11 Heat Transfer Coefficients in Condensation

Considerable experimental work on condensation heat transfer coefficients has been reported over the years although the empirical correlations derived from these experimental studies differ from each other widely. Thus detailed information on local heat transfer coefficients and interfacial areas in counter-current flooding flows of vapour and liquid is not readily available.

LIU and COLLIER (1980) carried out extensive experiments in counter-current flows of steam and water in vertical tubes, and determined heat transfer coefficients from temperature measurements at several axial positions in the test tube. They found that the average heat transfer coefficient, at the same axial point, was

proportional to the liquid Reynolds number, whilst the liquid injection rate, the inlet temperature, and the operating mode had only a minor influence. This is illustrated in Figure 2.29. The hysteresis effects present showed no obvious influence on the average heat transfer coefficient but the values did change appreciably with axial position as shown on Figures 2.30 and 2.31. Liu and Collier managed to correlate the results from three different tube diameters, by the expression

$$\frac{\bar{h}_x}{k} \left(\frac{v^2}{g}\right)^{1/3} = 1.07 \times 10^{-3} \left(\frac{x}{D}\right)^{-0.86} Re_f^{0.81} \quad (2.104)$$

Because of the large enthalpy of evaporation values involved, the authors concluded that the effect of mass transfer on the heat transfer coefficient could be ignored and suggested a correlation of similar form to predict the mass transfer coefficient.

LIU et al (1978) used the empirical correlation suggested by Akers and Rosson to predict the average heat transfer coefficients although this correlation was originally developed for horizontal steam water flows. LIU et al found it represented their experimental data reasonably well. The correlation took the form

$$Nu = 0.145 Pr_f^{0.33} \left[Re_v \left(\frac{\mu_v}{\mu_f}\right) \left(\frac{\rho_f}{\rho_v}\right)^{1/2} + Re_f \right]^{0.8} \quad (2.105)$$

2.12 Non-Equilibrium Condensation Effects

The difference between liquid-gas and liquid-vapour counter-current interactions is mainly attributed to mass and heat transfer (or condensation) effects which can be significant (and even overwhelming) depending on the temperature difference between the vapour and the liquid. Therefore in order to correlate any flooding mechanism which involves a liquid - vapour combination, the condensation effect must be separated and allowed for. The main difficulty in isolating the amount of condensation lies in the lack of knowledge regarding the degree of thermal non-equilibrium which exists during the energy exchange between the liquid and the vapour. If thermal equilibrium existed, then the amount of condensation could be determined from the energy (heat) transfer necessary to raise the liquid bulk temperature to that of the vapour. In practice, and this has been indicated by many investigators, a complete thermal equilibrium situation is not achieved. Experimental investigations have shown that the flooding curves for steam-water interactions with zero, or near zero, liquid subcoolings were very close to those for air-water when conducted in the same geometry. Therefore the experimental data obtained in vapour-liquid tests could be reduced to isolate the non-equilibrium effects, usually in terms of an equilibrium factor.

Theoretically, when steam and subcooled water come

into contact, the degree of equilibrium attained will depend mainly on

1. the residence time
2. the contact area between the phases
3. the amount of energy to be transferred

i.e. an equilibrium situation can be reached after an infinite time or at an infinitely long condensation length. The expression f in equation (2.99),

$$f = 1 - \exp\left(\frac{-hx}{C_p W_{in}}\right),$$

clearly indicates these characteristics. k has a value of 1 when either the condensation length or the heat transfer coefficient is infinite. When the liquid flowrate is relatively small, the liquid may be heated to saturation before reaching the liquid exit. The distance at which saturation is reached is known as the liquid saturation length and outside that length the liquid will be at the saturation temperature and condensation will be negligible. LIU and COLLIER (1980) plotted the saturation length as a function of the inlet liquid flowrate for several inlet water temperatures as shown in Figure 2.32. In addition, LIU et al (1978) argued that the heat transfer due to rapid bubble collapse was much larger than that of convection and conduction. This vapour bubble collapse was always noticed to occur at the vapour-liquid interface and thus could be treated as an instantaneous heat source at the interface. The

temperature of the interface increased rapidly and became very high (saturated) thus preventing further bubble collapse for a short time until the temperature at the interface was lowered by conduction heat transfer into the liquid. However, in practice, an equilibrium situation may be considered to prevail after a certain time period.

In the past decade, several attempts have been made by different investigators to present correlations for the equilibrium factor. ROONEY et al (1982, 1983), working mainly with PWR downcomer refill studies, showed that the amount of steam which must be condensed in order to remove the liquid subcooling and produce thermal equilibrium between the steam and water was given by

$$M_{sc_{eq}} = Ja M_{fin} \quad (2.105)$$

where

$M_{sc_{eq}}$ = steam condensed to achieve thermal equilibrium

M_{fin} = inlet water flowrate

Ja = Jakob number defined as

$$Ja = \frac{C_{pf}(T_{sat} - T_{fin})}{h_{fg}} \quad (2.107)$$

and hence the equilibrium factor, k was defined to indicate the degree of non-equilibrium present, with

$$k = \frac{M_{sc}}{M_{sc_{eq}}} \quad (2.108)$$

where M_{sc} was the actual steam condensed. Rearranging

equations (2.106) and (2.108) gave

$$M_{sc} = k \left[\frac{C_{p_f}(T_{sat} - T_{fin})}{h_{fg}} \right] M_{fin} \quad (2.109)$$

under equilibrium conditions, $k = 1$. ROONEY et al (1983) also presented a general correlation for the equilibrium factor in the form,

$$k = 1 - \exp\left\{ a \left[\text{Ja} j_f^* \left(\frac{\rho_f}{\rho_s} \right)^{1/2} Y^{-1/2} \right] \right\}^{-n} \quad (2.110)$$

where j_f^* was the dimensionless liquid Wallis parameter
 Y was the fraction of inlet water penetrating to
 lower plenum

a and n were constants with values of -0.24 and 0.6 respectively.

The authors found that this correlation gave a reasonable fit, to 1212 steam-water data points taken at Strathclyde, Dartmouth, Creare and BCL, with an RMS error of 20.3%. The above data covered a range of scales of PWR geometries from $1/30$ to $1/5$.

LIU et al (1978) presented a theoretical model for deducing the equilibrium factor, k . They considered a turbulent liquid film flowing down an adiabatic wall against a rising vapour with the temperature of the falling liquid assumed to be uniform across the falling film and only changing in the direction of flow. The steam was assumed to be saturated and free of non-condensable gases, the shear stress at the vapour

liquid interface was neglected and the physical properties of the liquid were assumed constant and uniform. The analysis yielded an expression for the equilibrium factor, k , given by

$$k = 1 - e^{-St} \quad (2.111)$$

where St was Stanton number defined as

$$St = \frac{hBL}{Cp_f M_{fin}} \quad (2.112)$$

Although equation (2.105) had its limits, the investigators thought it represented a significant improvement and opened the way to other empirical correlations for the equilibrium factor.

2.13 Comparison Between Vapour-Liquid and Gas-Liquid Flows

As indicated in the previous section, condensation is regarded as the major difference between vapour-liquid and gas-liquid counter-current flows. A comparison between annular counter-current flow of the two systems has been made by some investigators demonstrating some of the similarities and differences between the two systems.

WALLIS et al (1980), tried to provide such a

comparison by carrying out a systematic study using a transparent vertical tube. They found that the air-water data generally lay slightly above the steam water data although this effect could have been caused by a minor modification of the system or by some variation of the fluid properties such as the surface tension at the interface. The scatter in the data obtained in the steam-water tests was larger than that obtained in the air-water tests and hysteresis effects were found in both sets of results. They also found that the critical flooding location could be either at the liquid entry point or at the liquid exit point, depending on the geometry. In the steam-water tests, the critical flooding location could shift suddenly from the top to the bottom of the tube, and was affected by the mode of injection i.e. either water-first or steam-first tests. Their results also indicated that the vapour flooding velocity did not depend on the water velocity. Since they could never quite achieve saturated water conditions at inlet, i.e. zero subcooling, a comparison between air-water and steam-water data with no subcooling and hence no condensation could not be made.

LIU and COLLIER (1980) reported that the overall trends in steam-water system behaviour were similar to those of air-water flow, although the interactions in the steam-water tests were much more violent and chaotic due to condensation effects. The system pressure behaviour for steam-water flows was distinctly different from that

seen for air-water, as illustrated in Figure 2.33.

Many investigators, TIEN (1977), LIU et al (1978), LIU and COLLIER (1980) and BANKOFF and LEE (1983), reported no significant difference in flooding fluxes between steam-water and air-water flows. The DOBRAN (1981) results showed that higher flooding fluxes were possible in systems with heat transfer compared to adiabatic flows. TIEN (1977) also concluded that liquid subcooling could exert a significant positive effect on the flooding characteristics with a much larger steam flowrate being required to sustain flooding in the subcooled case. All the authors acknowledged that the hysteresis effects in vapour-liquid flow are unique insofar as they are more obvious and relate to a region of positive slope.

The entrainment in vapour-liquid flows may exhibit quite different features from that in gas-liquid flows. As the vapour flows upwards, the velocity decreases due to condensation so that water droplets that were initially levitated find a stable elevation, dependent on their size, and by random lateral movements may be deposited on the water film and carried downwards.

2.14 Conclusions on Literature Review

The literature reviewed indicated that most of the

theoretical approaches to flooding have been carried out for adiabatic two-phase flow, and that many different mechanisms have been proposed. Although the fundamental understanding of the flooding phenomena appears to be improving, the picture is by no means complete and more research is required. Little work has been done on the effects of condensation on flooding and more data are required. The available evidence on the effects of several parameters, including fluid properties, on the flooding phenomena have been reviewed and types of liquid entrance and exit conditions seem to have the greatest influence. In particular, the gas flooding velocity is substantially reduced if the liquid film is not introduced smoothly. This may be one factor which could account for the wide spread of flooding data reported. Most models incorporate a tube diameter effect, but the effect of the tube length is controversial. However reports supporting the idea that longer tubes require less gas flow to initiate flooding are more convincing. Viscosity and surface tension seem to exhibit opposing effects on flooding velocity. More careful experimentation is required to investigate and resolve these effects.

If a comparison is made between adiabatic and diabatic two-phase flow systems, the data should be taken from the same, or at least a similar, facility. This is the case in the research programme dealt with in this thesis.

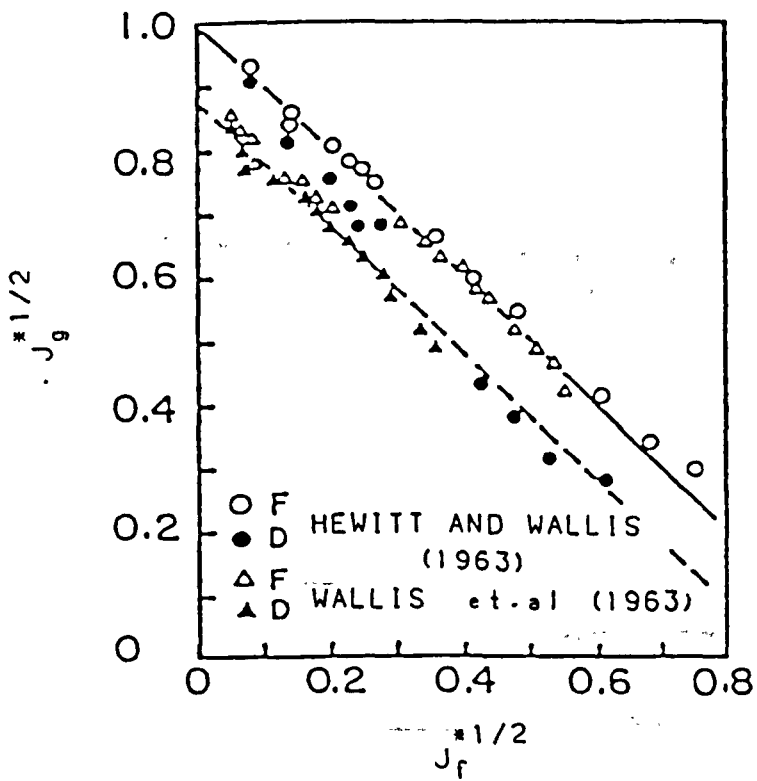


Figure 2.1 Comparison between Flooding and DeFlooding Data .
(Bankoff and Lee (1983))

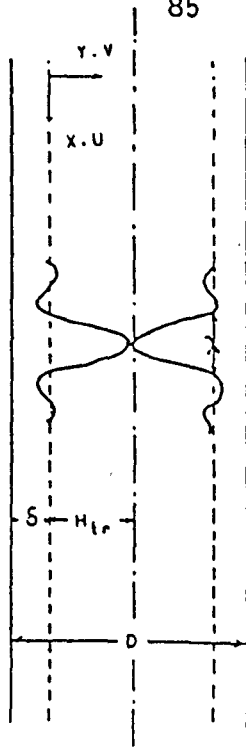


Figure 2.2 The Coordinate System of Schutt (1959).

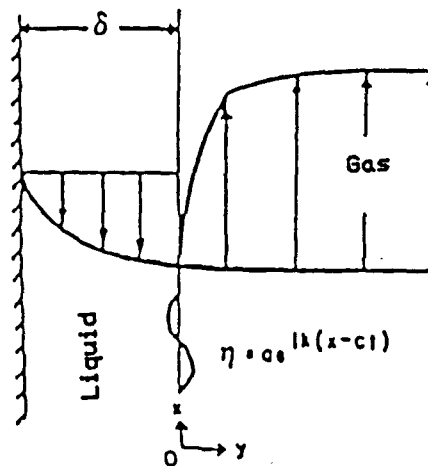


Figure 2.3 The Coordinate System of Cetinbudaklar and Jameson (1969).

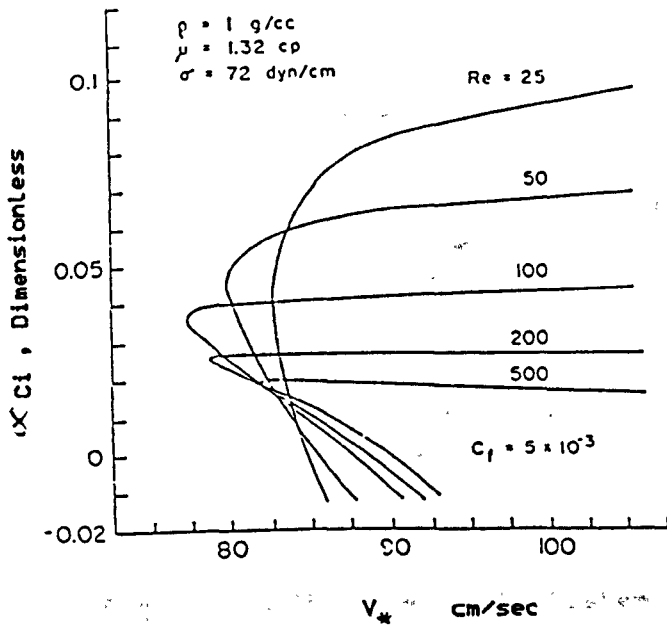


Figure 2.4 The Growth Rate C_i , as a Function of the Gas Friction Velocity V_* in Air - Water System. (Cetinbudaklar and Jameson (1969))

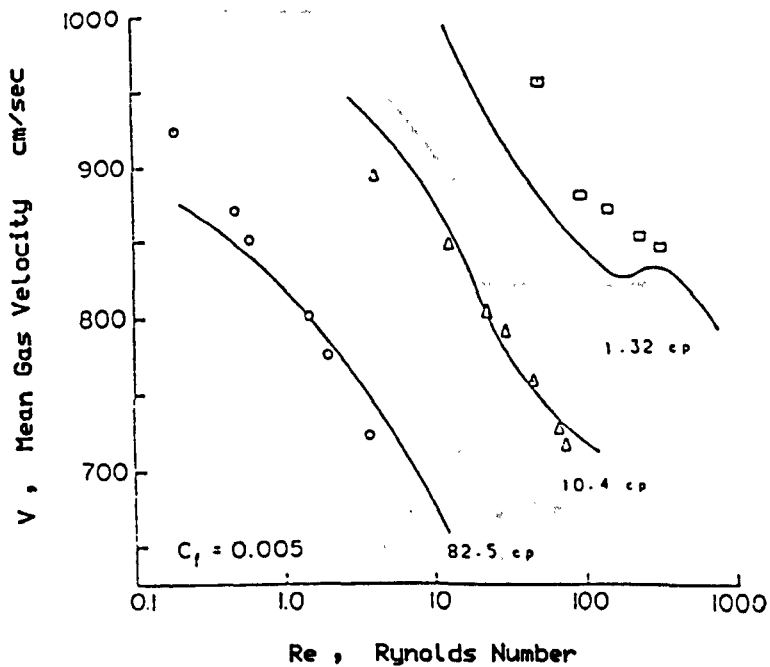


Figure 2.5 Comparison of Predicted Flooding Velocities with the Experimental Data of Clift et. al. (1966). From Cetinbudaklar and Jameson (1969).

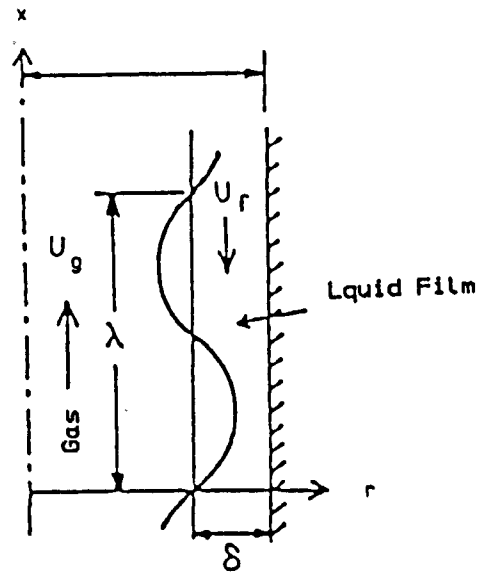


Figure 2.6 The Coordinate System of Imura et al (1977).

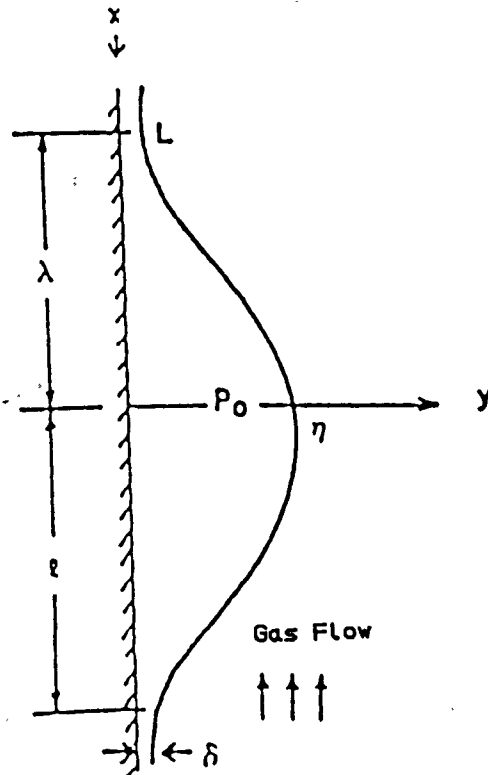


Figure 2.7 The Coordinate System and Wave Profile of Shearer and Davidson (1965).

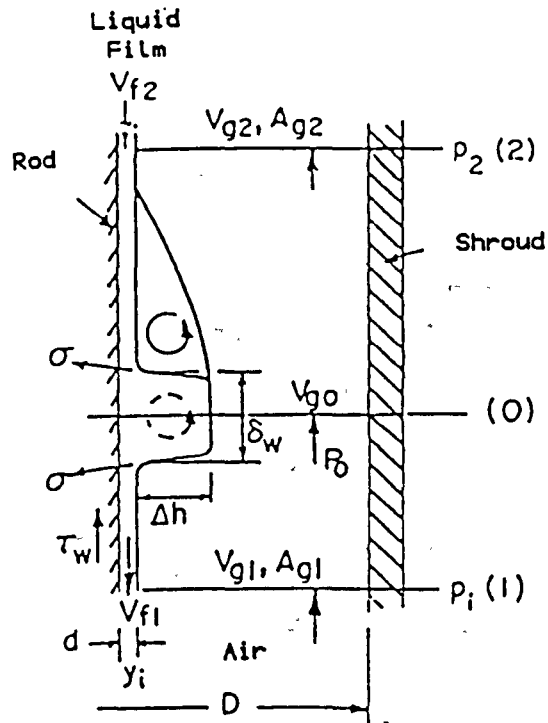
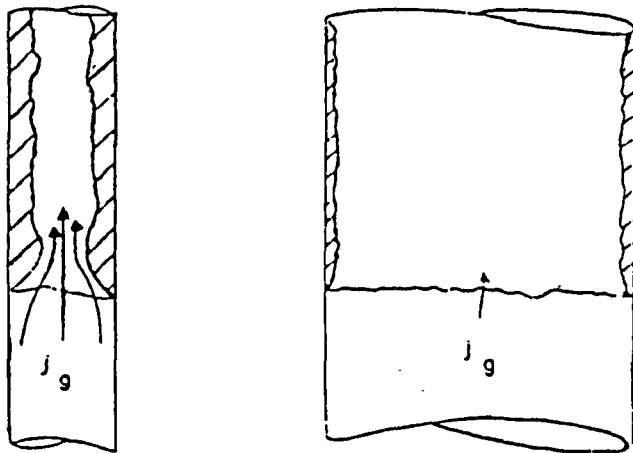


Figure 2.8 Analytical Model of Ueda and Suzuki (1978).



A. Small Tube

B. Large Tube

Figure 2.9 Hanging Liquid Films in Two Tubes Sizes. (Wallis and Makkenchery (1974)).

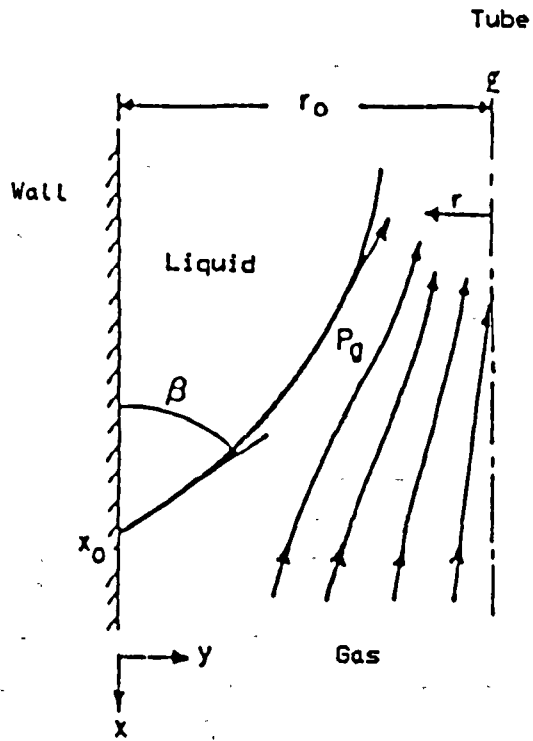


Figure 2.10 Hanging Film Model of Wallis and Kou (1976).

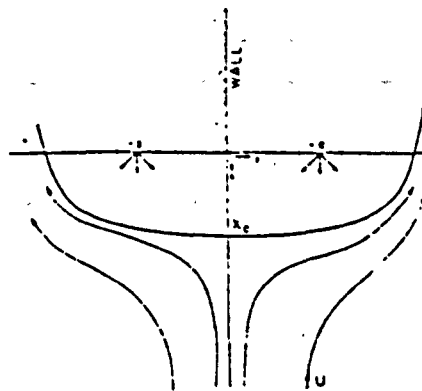


Figure 2.11 Flow Around a Pair of Sources (Wallis and Kou (1976)).

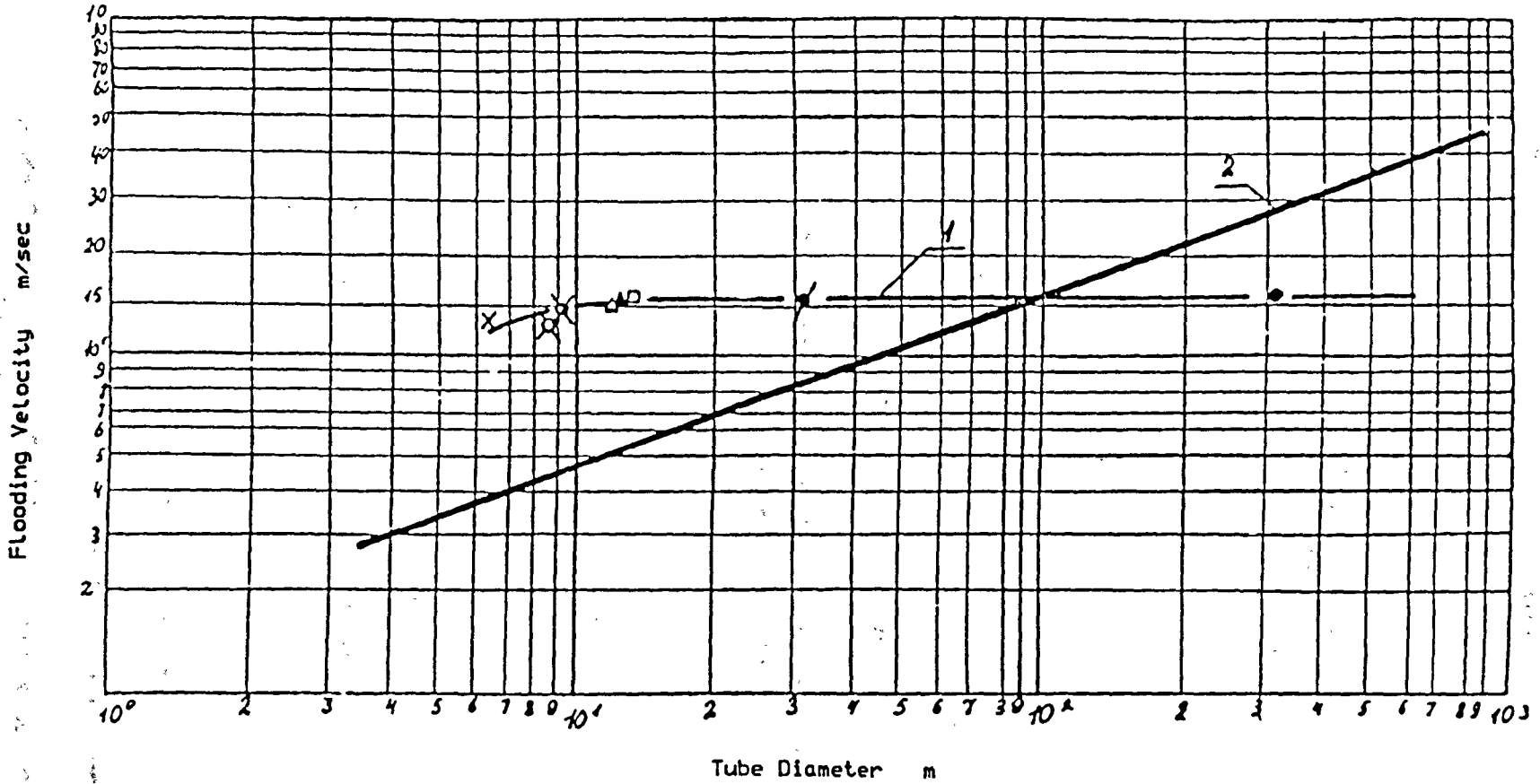


Figure 2.12 Relationship between the Critical Air Velocity and the Tube Diameter with Respect to the Reversal of the Flow of the Water Film
 1- According to Empirical Data. 2- According to the Wallis Formula.
 (Pushkina and Sorokin (1969)).

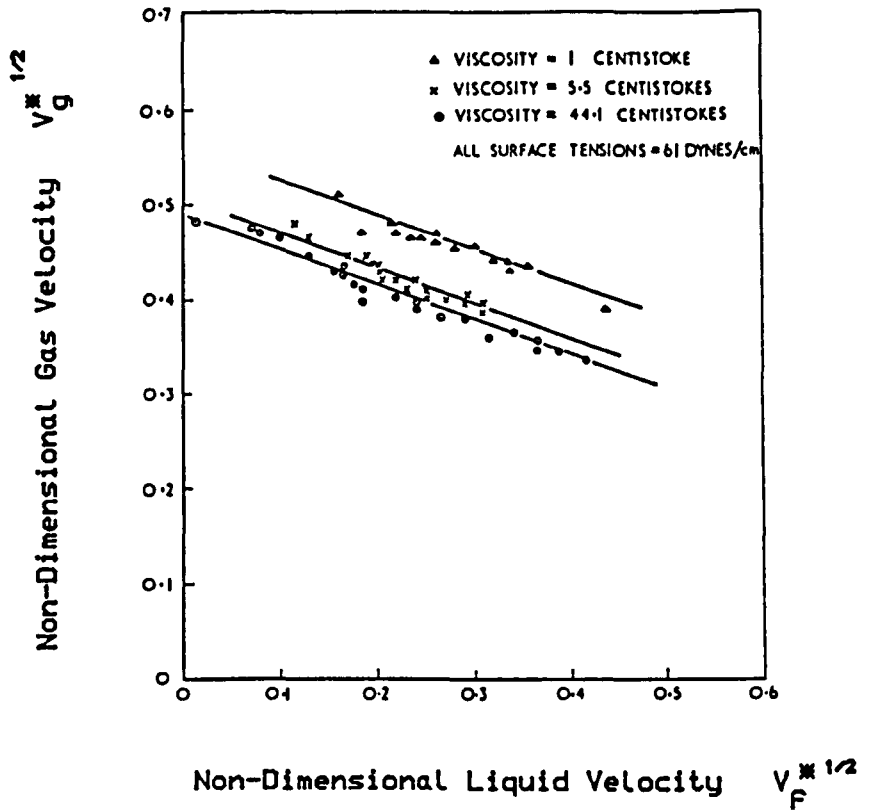


Figure 2.13 The Effect of Viscosity on Flooding in a Tube. (Shires and Pickering (1965)).

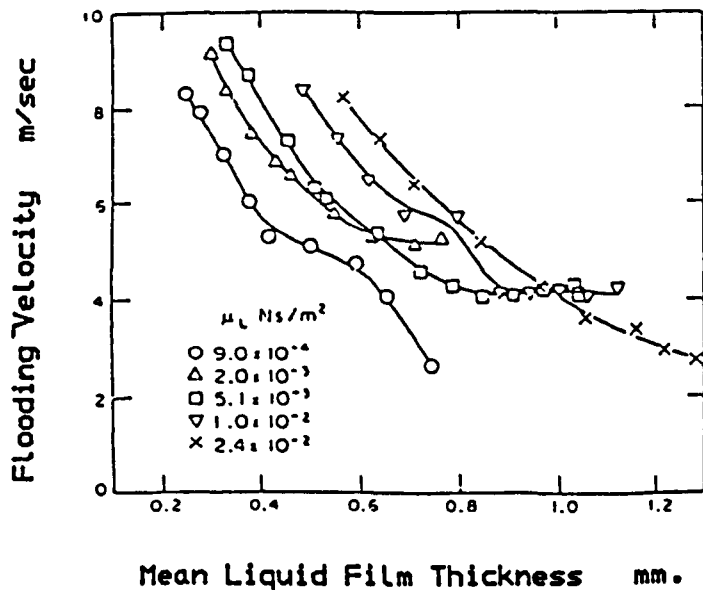


Figure 2.14 Effect of Liquid Viscosity on Flooding. (Suzuki and Ueda (1977)).

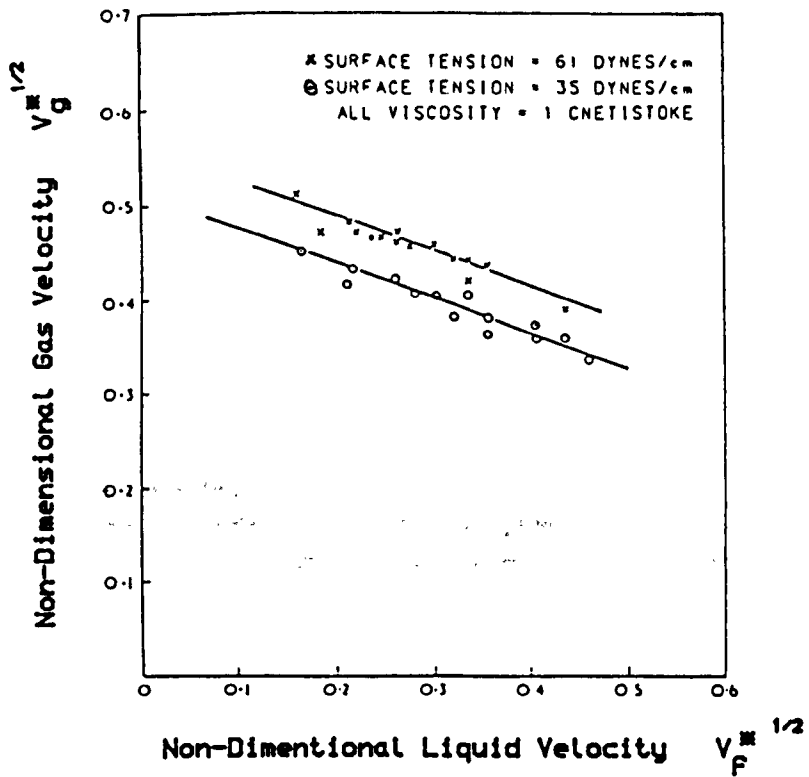


Figure 2.15 Effect of Surface Tension on Flooding (Shires and Pickering (1965)).

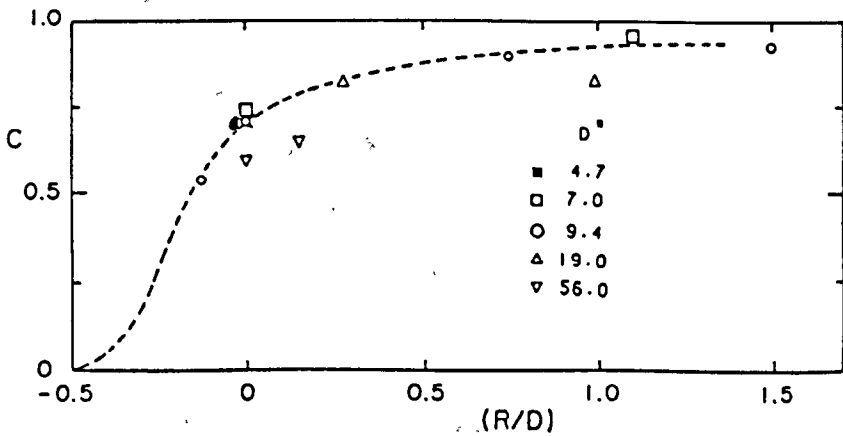


Figure 2.16 Effect of Water Entry Radius on the Coefficient C, in Wallis Correlation

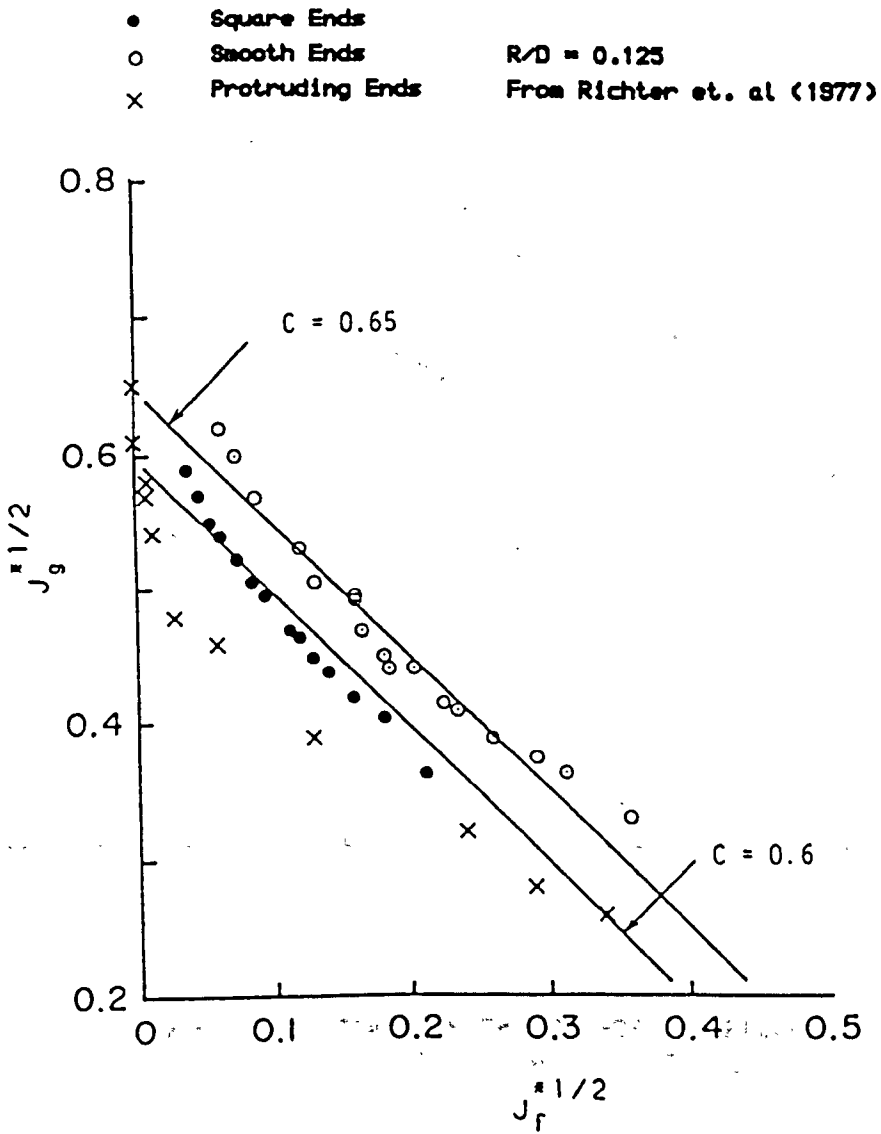


Figure 2.17 Effect of End Geometries on Flooding. (Barathan et. al (1979))

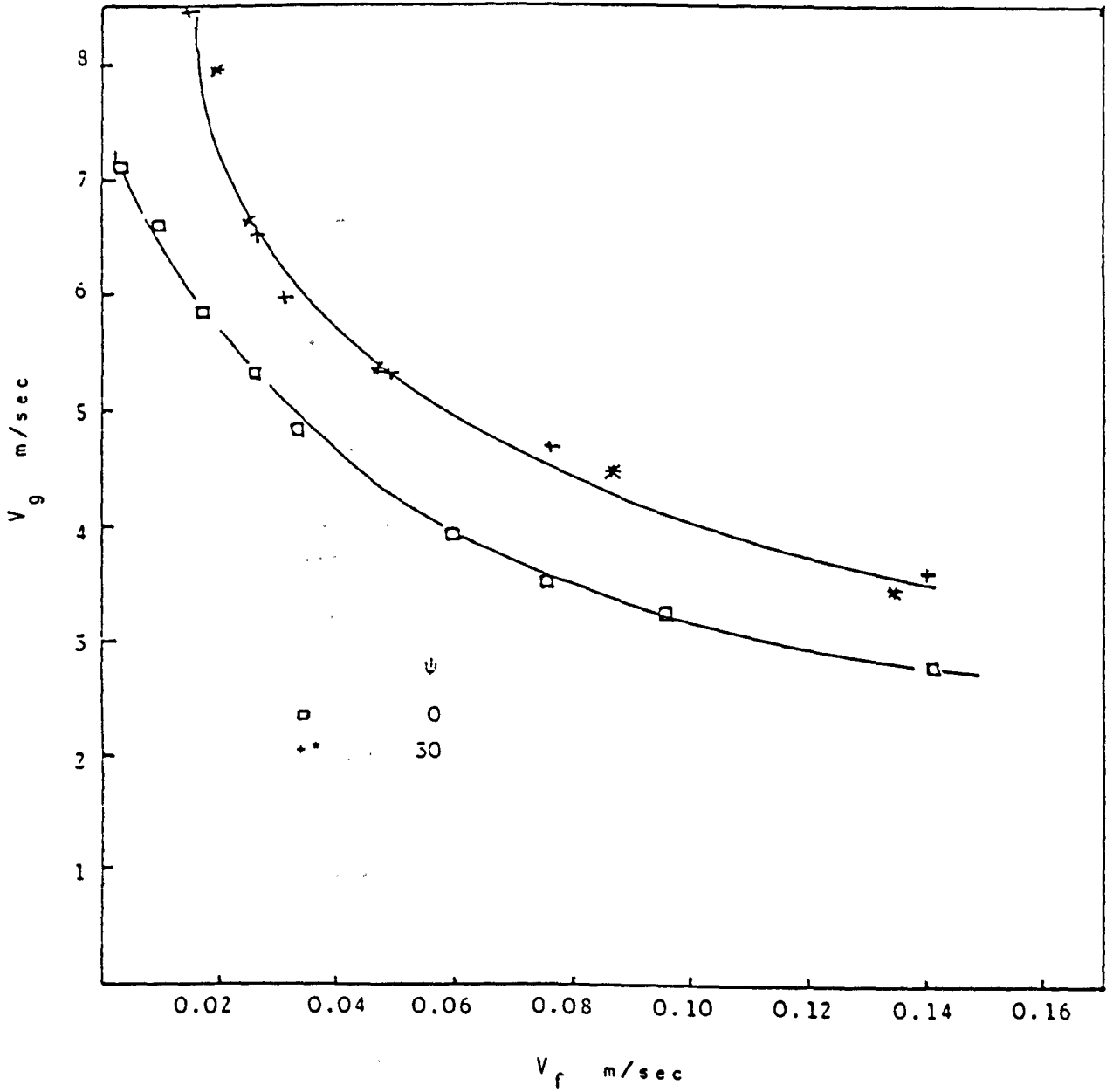


Figure 2.18 EFFECT of End Cut-OFF on Flooding Velocity. (Hewitt (1977)).

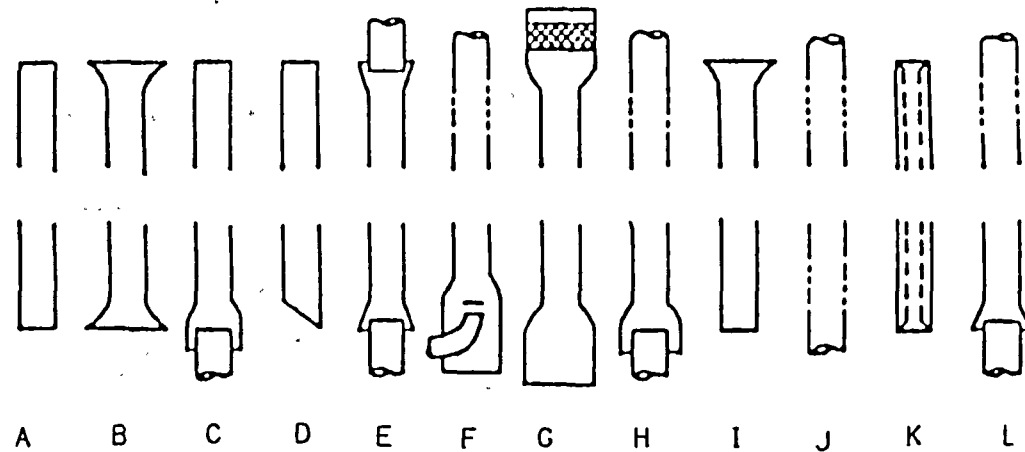


Figure 2.19 Sketch of Geometries of Tube Ends Used in Various Investigation.
 A- Wallis (1961) B- Wallis (1961) C- Kami et. al (1954)
 D- Hewitt (1977) E- Fiend (1960) F- Clift et al (1966)
 G- Grolmes et al (1974) H- Pushkina and Sorokin (1969)
 I- Pushkina and Sorokin (1969) J- Hewitt and Wallis (1963)
 K- Chang et al (1980) L- Dukler and Smith (1979)

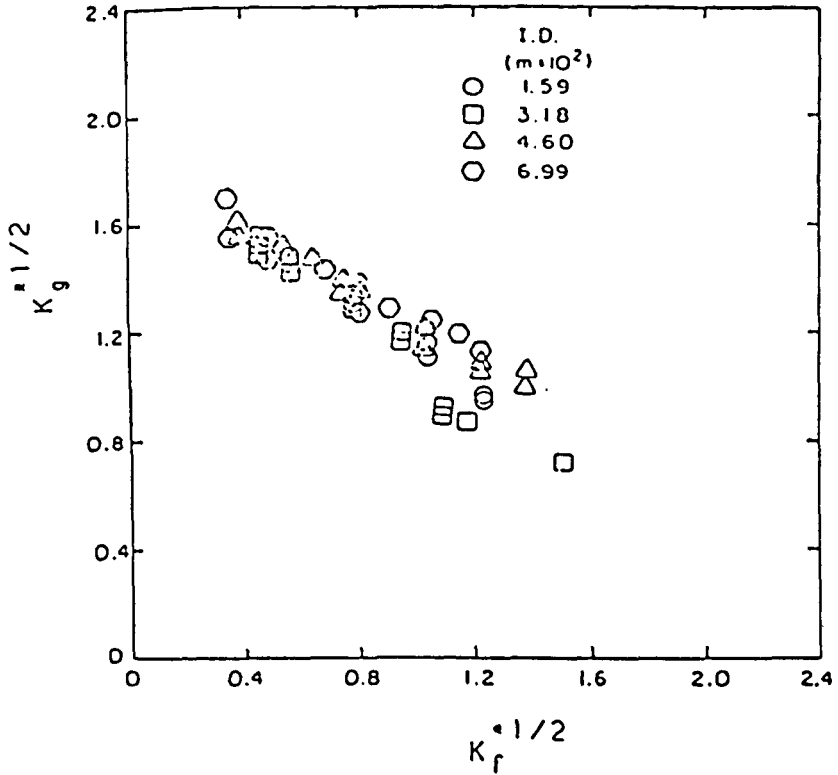


Figure 2.20 Effect of Tube Diameter on Flooding. (Tien et. al (1979)).

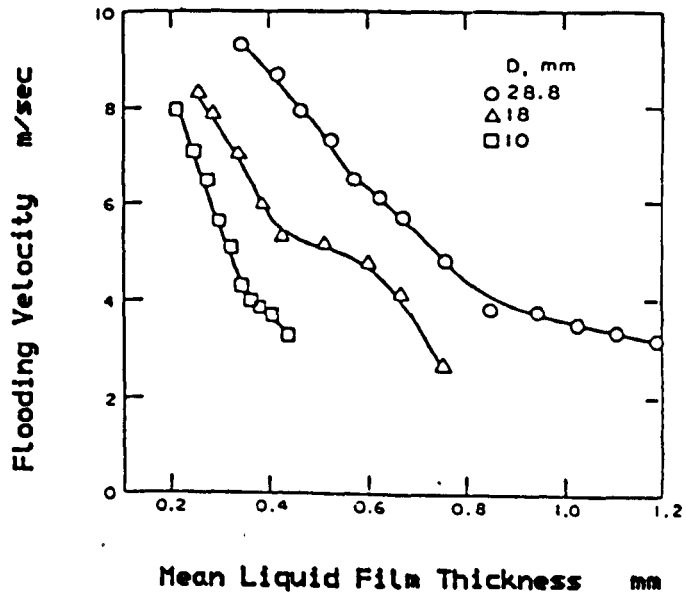


Figure 2.21 Effect of Tube Diameter on Flooding. (Suzuki and Ueda (1977)).

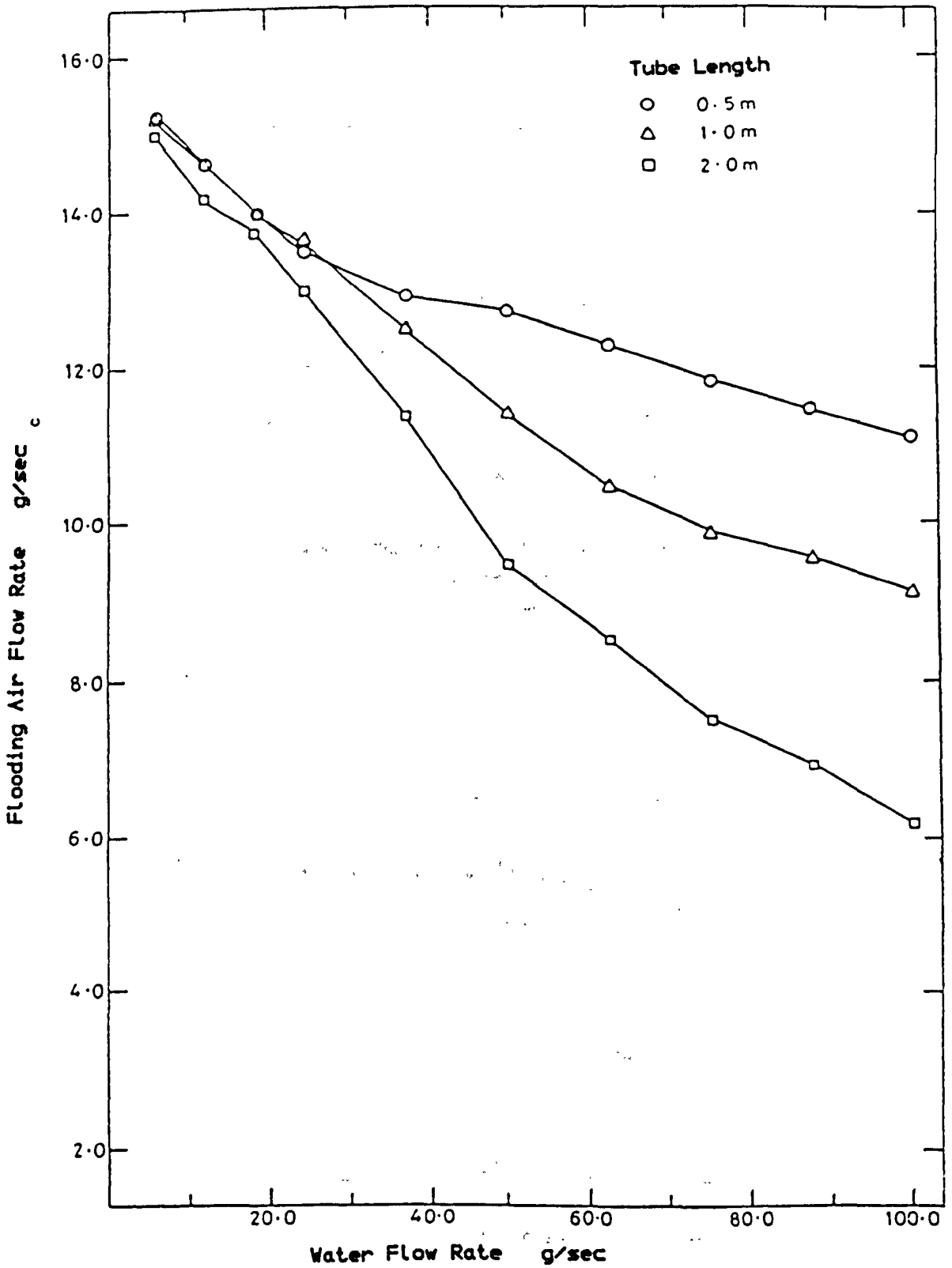


Figure 2.22 Effect of Tube Length on Flooding
(Whalley and McQuillan (1983)).

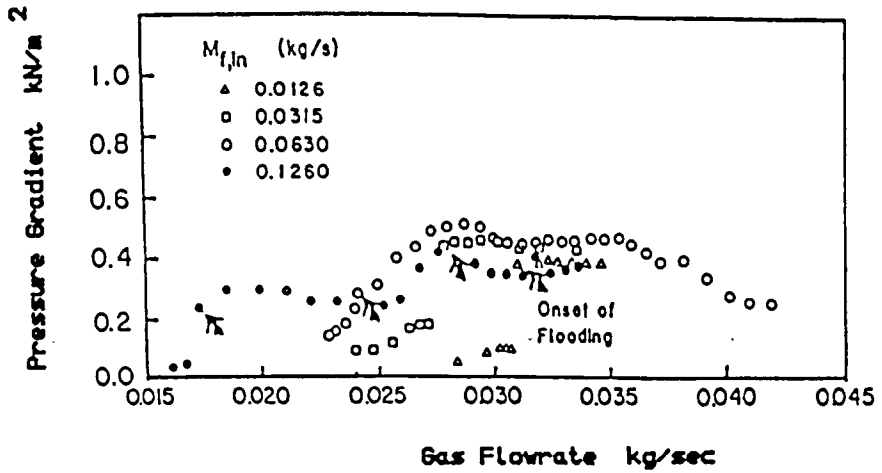


Figure 2.23a Pressure Gradient in a Vertical Tube Above the Liquid Injection Point. (Dukler and Smith (1979))

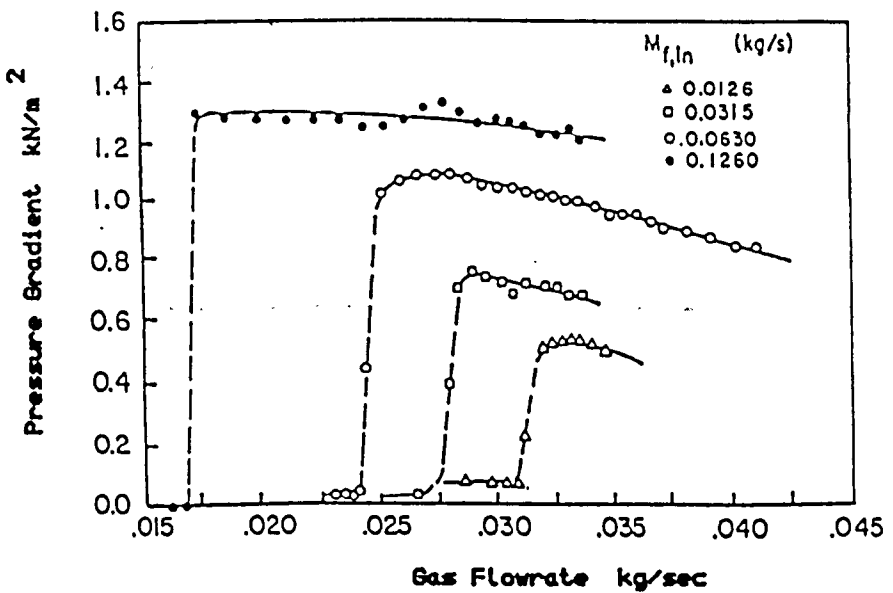


Figure 2.23b Pressure Gradient in a Vertical Tube Below the Liquid Injection Point. (Dukler and Smith (1979))

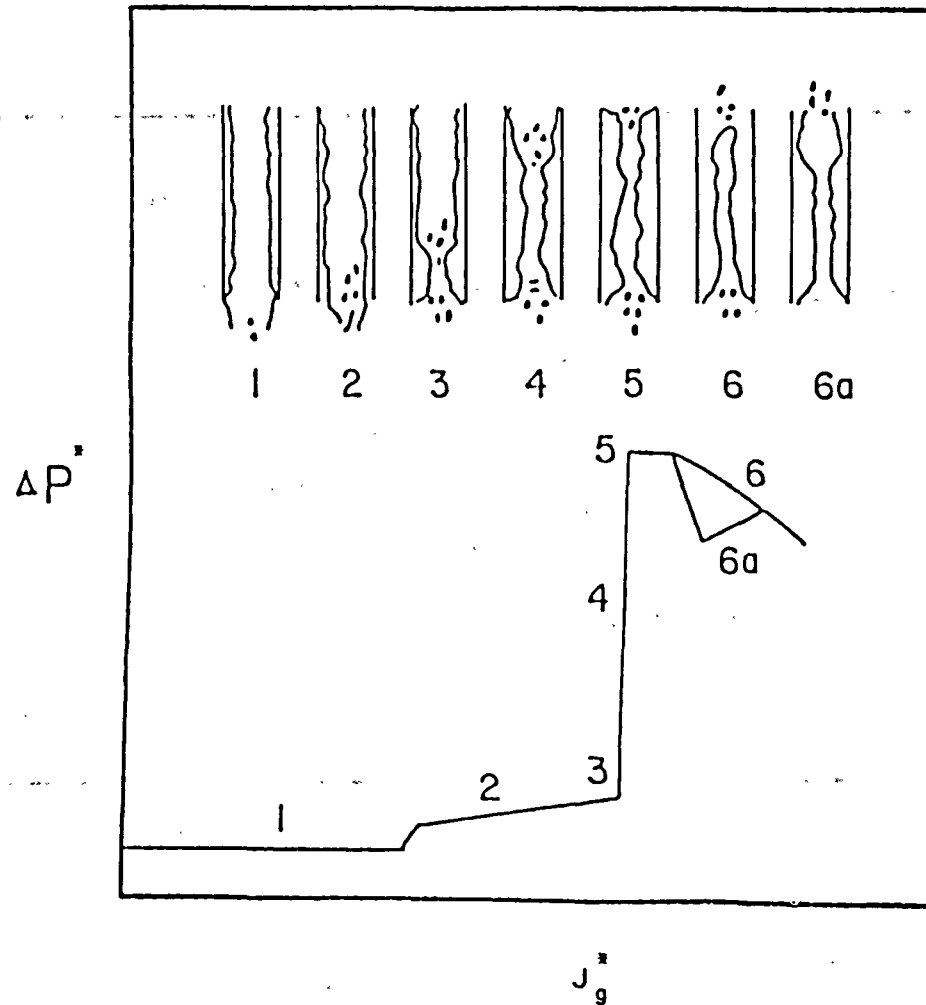


Figure 2.24 Generalised Sketch of Pressure Drop Variation with Gas Flow Rate in Counter - Current Flow with Upper Plenum Injection. (Hawley and Wallis (1982)).

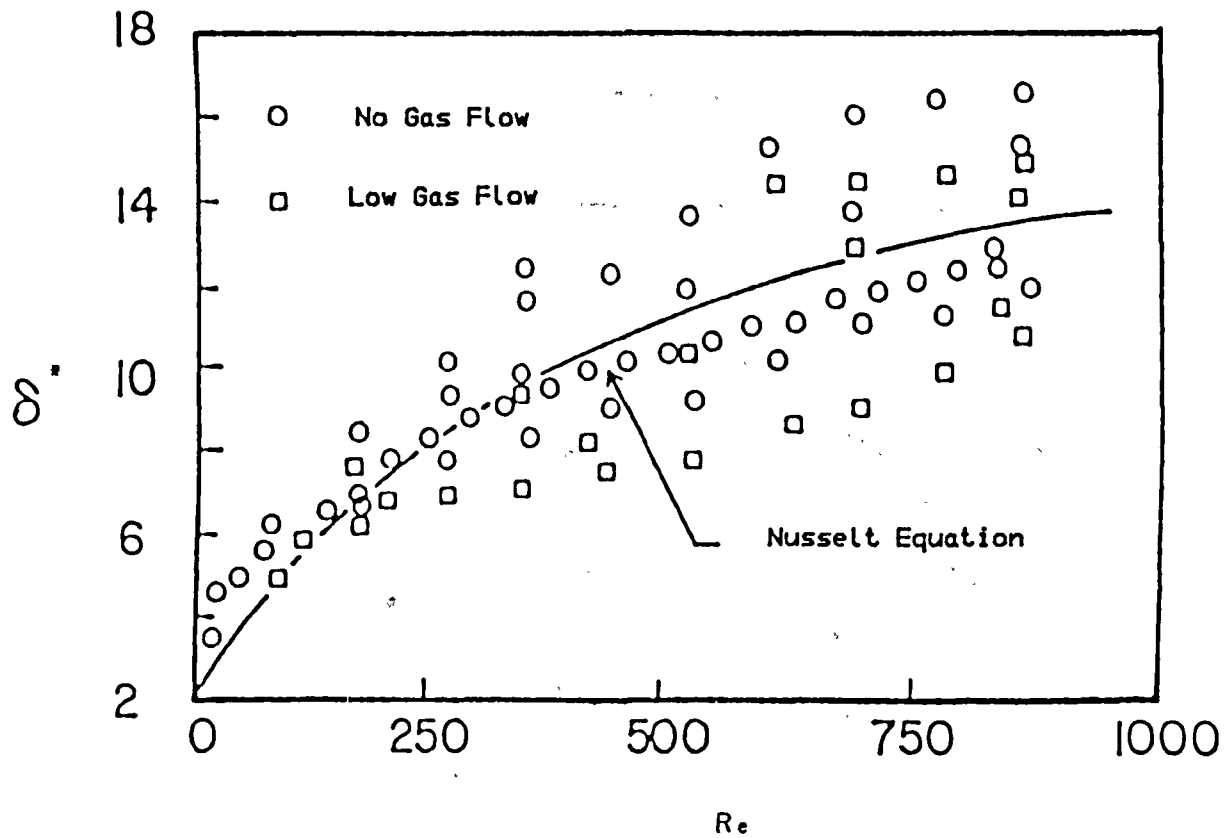


Figure 2.25 Typical Mean Thickness Data of
 a Vertically Falling Film .
 (Hawley and Wallis (1982)).

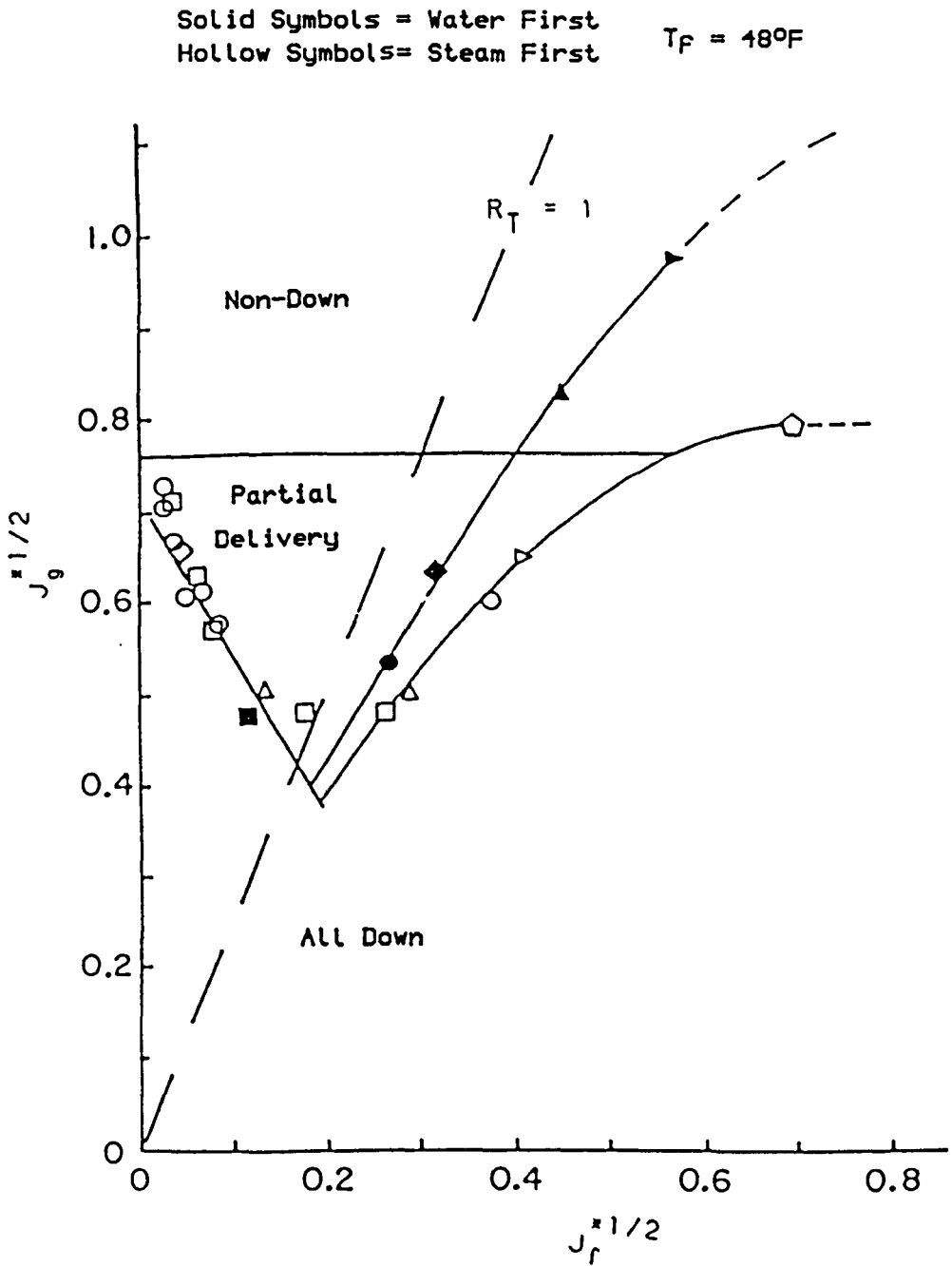


Figure 2.27 Comparison between Steam-First and Water-First Data. (Wallis et. al (1980)).

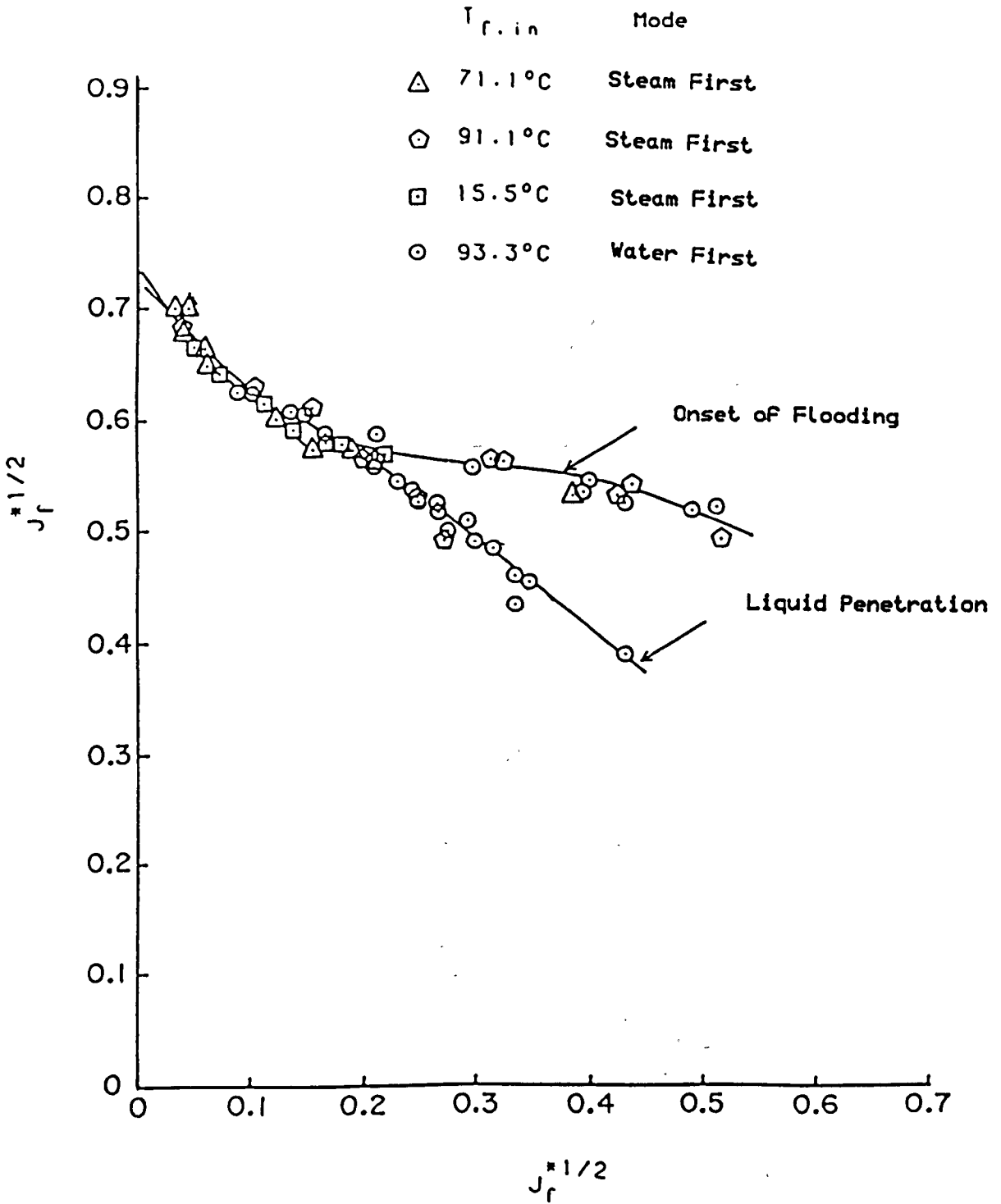


Figure 2.28 Flooding in Vertical Steam/Subcooled-Water Flow. (Wallis et. al (1980)).

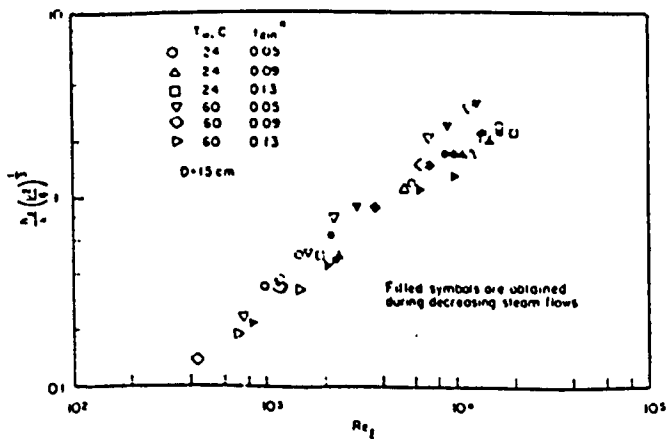
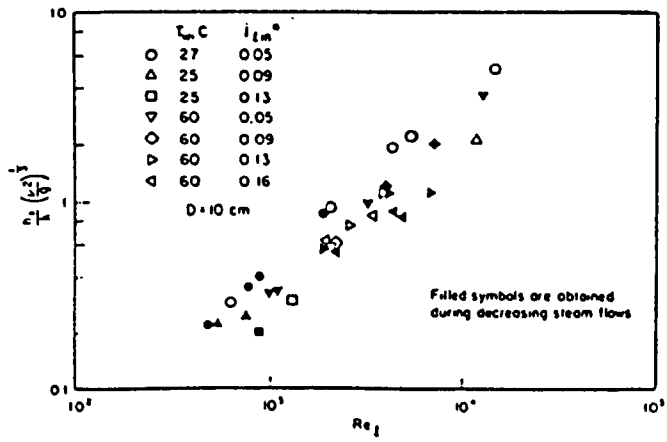
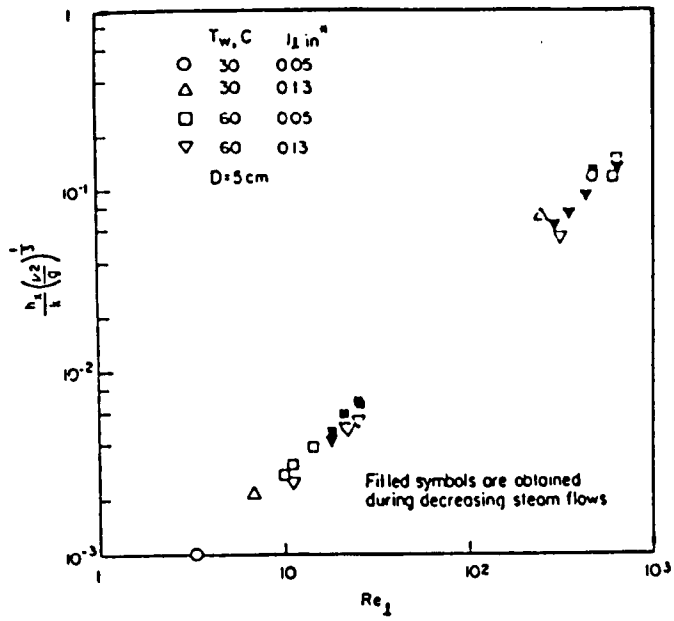


Figure 2.29 Average Heat Transfer Coefficient as a Function of Liquid Reynolds Number. (Liu and Collier (1980)).

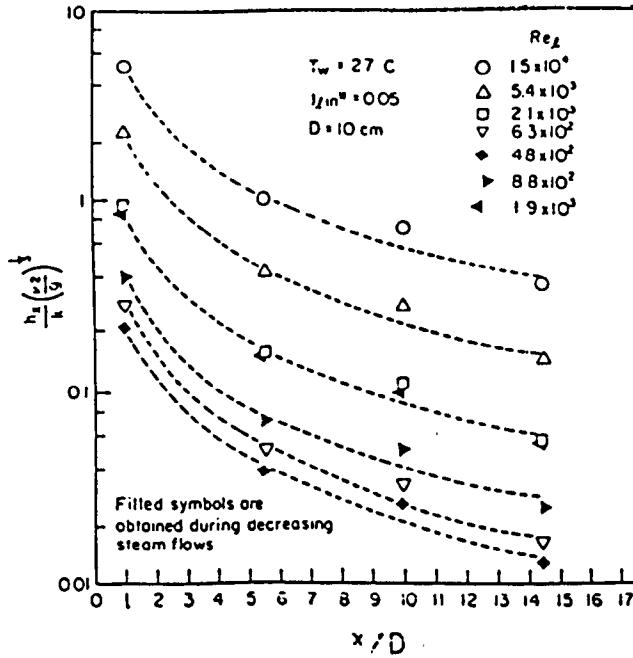


Figure 2.30 Average Heat Transfer Coefficient as a Function of Axial Position for Several Liquid Reynolds Numbers. (Liu and Collier (1980)).

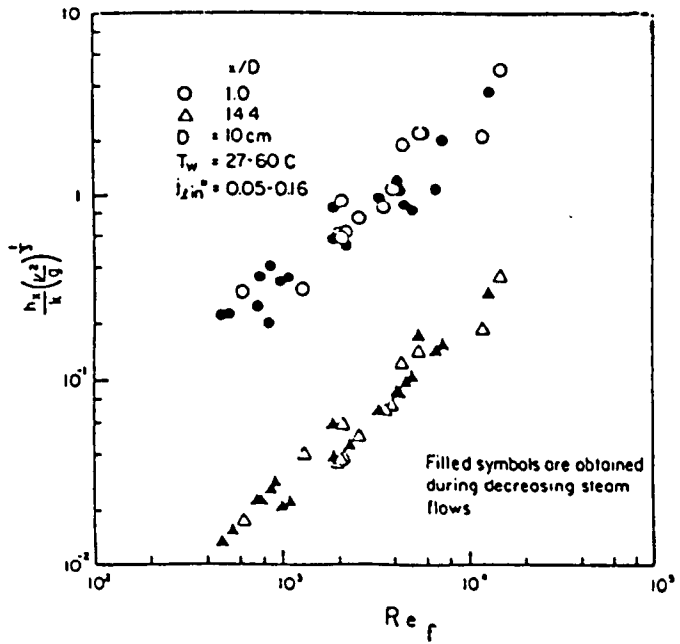


Figure 2.31 Average Heat Transfer Coefficient as a Function of Liquid Reynolds Number for Two Axial Positions. (Liu and Collier (1980)).

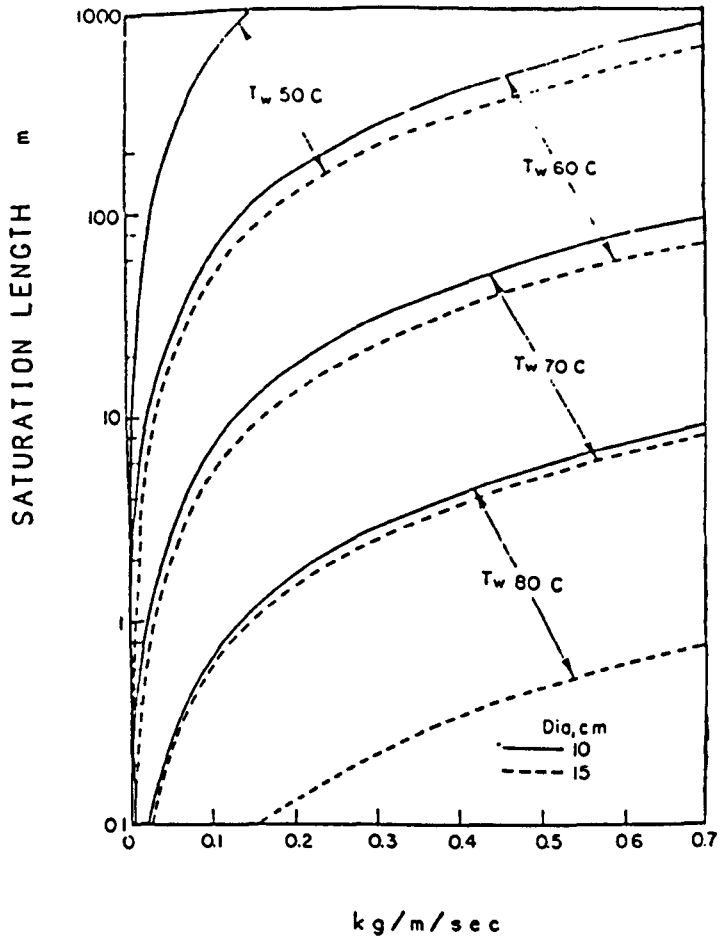


Figure 2.32 Saturation Length as a Function of Inlet Liquid Flow Rate for Several Inlet Temperature. (Liu and Collier (1980)).

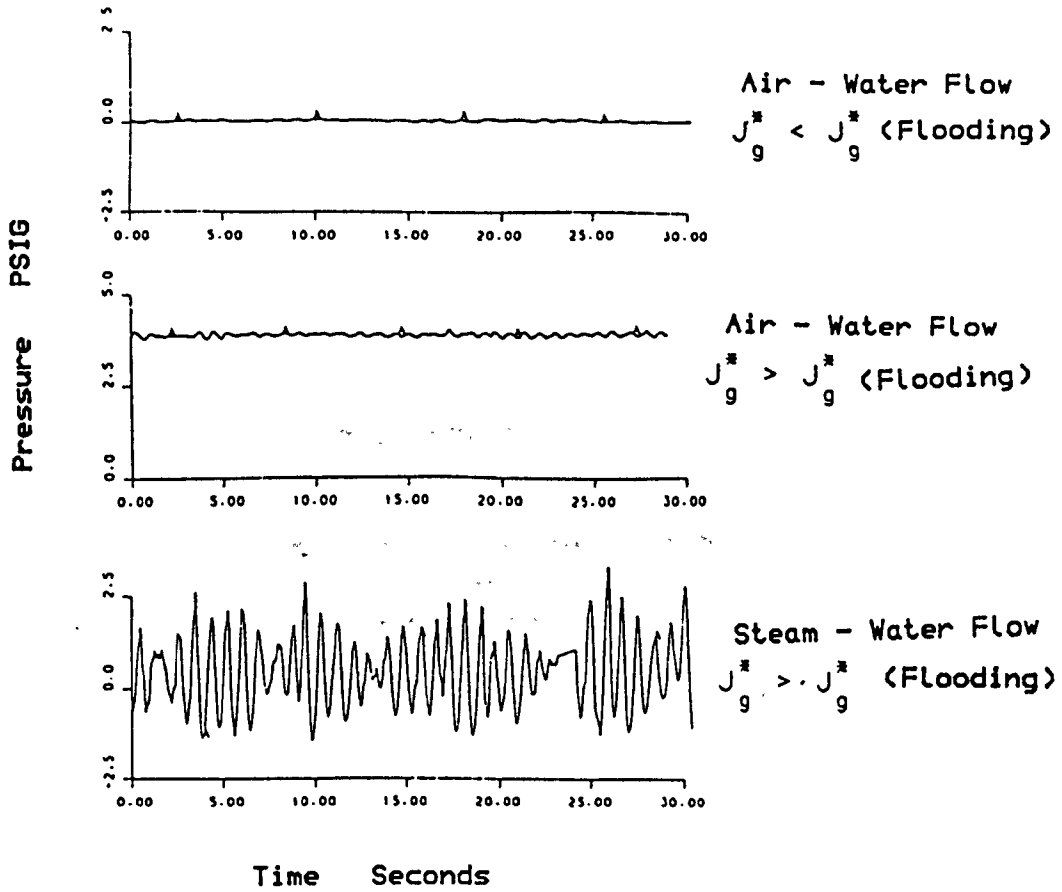


Figure 2.33 Comparison between Pressure Drop in Air - Water and Steam - Water System. (Liu and Collier (1980)).

CHAPTER 3

EXPERIMENTAL APPARATUS **AND OPERATING PROCEDURE**

CHAPTER 3

EXPERIMENTAL APPARATUS AND OPERATING PROCEDURE

The experimental apparatus was similar in many respects to that used by D. McNeil (1986) but with considerable modifications. The experiments were carried out on a test facility designed and constructed to measure the necessary flow rates, pressure drops, liquid film thicknesses and temperature distributions, in order to investigate the fluid mechanics and heat transfer parameters affecting the counter-current flooding phenomenon. To aid in the isolation of these parameters, two modes of operations were used, (i) air-water tests and (ii) saturated steam-subcooled water tests, and these are described in Sections 3.3 and 3.4 respectively. The layout of the test facility is shown in Figure 3.1.

The test facility was designed to allow a photographic technique to be used and this will be described in more detail in Chapter 5.

3.1 Test Section

Details of the test section assembly are shown in Figure 3.2. The major part of this assembly consisted of three parts, the injector, the test tube and the

extractor.

The injector was made from a 168 mm diameter stainless steel tube. To ensure a smooth introduction of annular film of water to the test section, a 60 mm length of porous sintered brass tube of slightly larger diameter than the test section tube was fitted to the inside of the injector. This difference in diameter was smoothed out over the length of the flange enclosing the injector. The water was introduced to the injector by four inlet ports each of which contained four discharge holes perpendicular to the axis of the port to ensure that no liquid directly impinged on to the sinter surface. Details of the injector are shown in Figure 3.3 and illustrated in the photographic plate 3.1.

The test tube section used in the experiments was manufactured from a 54.75 mm bore stainless steel tube and had a net length of 1000 mm exactly. It contained two sets of probes for liquid film thickness measurements which were placed 746 mm apart. The probes were contained within two 125 mm diameter stainless steel blocks, which were used as probe mount housings as can be seen in Figure 3.2 and Plate 3.2. The two blocks were machined with flats to provide a mating surface for the probe mounts, before being drilled axially in order to slip over the test section's outer diameter, and then bored out to allow the probe mounts to be matched to the test section inner surface. This method of manufacturing

ensured no protruding joints likely to interfere with the liquid film (as proved later by visual observations). The film thickness probes are described further in Chapter 4.

The liquid extractor was similar to the injector in construction but different when in operation. Basically, by applying suction to the extractor, the liquid film could be removed. Since the extractor had to deal with two-phase flow, an ideal extractor should remove all of the liquid film flow without removing any of the associated air or steam. Practically, it was found that the amount of liquid film removed through the extractor was usually less than the total amount of liquid injected, and also that a percentage of air or steam was removed along with the liquid film.

Two parameters were found, in practice, to govern the amount of liquid film and air or steam being extracted. The first parameter was the pressure difference across the extractor, which affected, mainly, the amount of air or steam being removed with the liquid film flow, i.e. by varying the pressure difference, different quantities of air or steam were removed. This will be discussed in Chapter 9 in more detail. The second parameter was the geometry, which affected the amount of liquid film and to some extent the amount of air or steam being removed. To clarify the second parameter effects, two varying methods of geometry were considered.

The first method involved systematically reducing the tube flow area by blanking off parts of it. This had the effect of increasing the average film thickness on the active sinter flow area and thus increasing the resistance to the air or steam flow. It was found that the best result was obtained when 15% of the total extraction area was blanked. This had the effect of improving the removal of the liquid flow to a value varying between 95% and 100% of the total liquid flowrate. These two values correspond to the highest and lowest liquid flowrate being used in the experimental tests. At the same time it decreased the amount of air or steam removed by about 5%. However, this method introduced problems in terms of a large pressure drop across the reduced area, and consequently required repeated cleaning.

The second method involved placing a guard, of the type shown in Figure 3.4, over the outside surface of the porous tube. This produced increased resistance to the air or steam in the slots without greatly reducing the active area of the sinter and gave a smaller pressure drop over the extractor and consequently a reduction in the number of sinter cleaning operations. This method improved the removal of the liquid film to a value varying between 98% and 100% of the total liquid flowrate and was the method used for both air-water and for steam-water tests.

A three metre long stainless steel tube of the same diameter as the test tube was joined by a matched flange to the bottom of the extractor, so that the bore was continuous. This settling length allowed air and steam to be introduced smoothly and gently to the established annular flow in the test section, Plate 3.3.

As mentioned previously, small amounts of liquid may not be removed through the extractor and these fell down through the settling length to the bottom of the tube where they were collected in the secondary separator system. The separator, which is detailed in Figure 3.5 and shown in photographic plate 3.4, was manufactured from 170 mm O.D. stainless steel tube, and located below the settling length at the air or steam inlet. The design of the secondary extractor ensured that the liquid overshooting the extractor would not interfere with the incoming air or steam and also that a build up of water could be prevented by occasionally opening the drain valve. The entire system was supported by a unitrust structure and extreme care was taken to maintain perfect vertical alignment of the test section. A general view of the test section is shown in plate 3.5.

3.2 Water Supply Systems

The water used in the experiments could be supplied to the test section from either the main service supply in

the laboratory or from two storage tanks. The first method was used for air-water tests whilst the second method was used for steam-water tests.

The storage tanks contained a steam condenser water heating unit. The upper storage tank, which was located at a height of 5.5 m above the lower tank, contained three electrical immersion heaters of 2, 4 and 6 Kw power input to provide a further temperature control. The water could be recirculated between the two tanks in order to obtain a constant head supply at a constant temperature. From the higher level tank the water was pumped to the test section. The level of water inside the lower storage tank was monitored by means of a sight glass, while a mercury manometer system was used to indicate the water level inside the upper tank. Both tanks and the connection pipes were well insulated to minimise heat loss.

Three filtering elements were used, in series, to ensure that the water supplied to the test section contained no impurities. These elements were (i) a strainer, to prevent any carry over of large deposits from supply tanks (ii) a surface filter to remove the large undissolved solids and (iii) a fine pore sintered tube similar in type to that of the injector but of smaller pore size. The porous tube filter and the surface filter had a back wash/forward flush arrangement to permit in-line cleaning, as indicated in Figure 3.1. The water

then passed through two rotameters installed in parallel to monitor the flowrate before entering the test section.

3.3 Air-Water System and Operation

The air was supplied to the test facility from the laboratory compressor at pressures up to 17.5 bar. Since the tests were to be carried out at atmospheric pressure, the air pressure was controlled by an automatic pressure regulating valve installed upstream. The air flowrate was controlled by two valves in series. The air then passed through three rotameters, installed in parallel, for measuring the flowrates, before entering the test section settling length and hence the test section.

The air entering the test section had two exit paths (i) through the water extractor system at the bottom of the test section leading to the air-water separator or (ii) through the air discharge system at the top of the test section which also led to an air-water separator. These are indicated in Figure 3.1.

The air which passed up through the test section went to a separator tank. The separator consisted of a rectangular tank, 700 x 500 x 500 mm made of plastic which contained three baffle plates. The air-water mixture entered the separator and was separated by buoyancy effects. The water passed under gravity to the waste

through an outlet at the bottom. At the same time the air discharged to the atmosphere through an outlet located at the top. The air discharging system is shown in Plate 3.5.

A vacuum pump was used to create the required pressure difference across the extractor and thus provide suction to the liquid film flow. The air removed with the film through the extractor was passed to a separation tank. The 60 x 30 x 30 mm separator was made of galvanised steel, and contained three baffle plates. The separated air passed through two air rotameters to the atmosphere while the water was pumped, after being measured by a rotameter, to waste. A certain water level in the separator was maintained so that air could not escape through the water outlet. The air-water tests were performed using the following procedures:

- (i) The vacuum pump was switched on and the air supply rate adjusted to be slightly greater than the vacuum pump flowrate.
- (ii) The water flowrate was set to the desired value.
- (iii) The water discharge pump was adjusted to a suitable flowrate in order to maintain a reasonably constant level in the separator tank.

(iv) The air supply flowrate was increased in small increments until flooding occurred, allowing time to obtain steady and stable conditions and the necessary data and measurements to be recorded.

The amount of air removed through the extractor was kept as constant as possible over the range of the liquid flowrate being tested. Flooding was identified by three methods.

- (i) A chaotic condition of the liquid film and the change in the flow pattern, as indicated by an oscilloscope. A permanent copy of the oscilloscope trace could be obtained by means of a U.V. recorded.
- (ii) A substantial increase in the test section pressure drop which was monitored by two manometers and the pressure transducer voltage output displayed on an avometer.
- (iii) A marked increase in the amount of entrainment observed through a glass tube fitted at the top of the test section.

3.4 Steam-Water System and Operation

Steam was supplied through the University boilers at about 10 bar. An automatic pressure regulating valve,

(Bailey type) was installed in the main pipe in order to reduce the steam pressure to the desired value, and maintain this constantly upstream throughout the range of flowrates being used. Beyond the pressure regulating valve, the steam flowrates and pressure were controlled by two valves, in series. Between these two valves, an orifice meter plate was installed in order to measure the steam flowrate. Before entering the test section settling length, the steam passed through a heated pipe which ensured that all the steam used in the experiments was completely saturated. The pipe was heated electrically by means of electric tape connected to a variable voltage supply which provided fine control on the temperature of the pipe and in consequence the steam temperature. Two steam traps, were installed in the main steam supply pipe while a third was fitted at the heated pipe entrance to ensure that all the condensed water was removed. As there was a possibility that during the course of the experiments, some water could escape from the bottom end of the settling length tube to the steam pipe inlet, a drainage valve was fitted to the steam pipe where it entered the secondary separator to ensure no water was left in the line.

Steam entering the test section left either (i) through the water extractor system at the bottom of the test section or (ii) through the steam discharge system at the top of the test section. The flow paths are indicated in Figure 3.1.

The steam flow which escaped through the extractor with the water, passed to a condenser type heat exchanger as part of a two-phase mixture. This two-phase mixture was condensed to subcooled water which was pumped to waste through a rotameter. The steam flowrate passing up through the test section went to a condenser and was discharged to the atmosphere, thus maintaining the test pressure close to atmospheric. All steam pipes and the test section were well insulated to minimise heat loss. Steam-Water tests were carried out using the following procedure:

- (i) The water in the storage tanks was heated to the required temperature.
- (ii) The desired cooling water flowrate was set up through the condensers.
- (iii) A low water flowrate (typically 2-3 l/min) was introduced to the test section.
- (iv) A low steam flowrate was introduced to the test section.

- (v) The valve at the outlet from the steam discharge condenser was closed. This had the effect of building up pressure inside the test section and hence forcing the heated water and the steam flow through the extractor to the condenser. The introduced steam supply rate was adjusted until the condensation effect gave the desired water extraction.
- (vi) The valve at the steam discharge condenser was opened very slowly.
- (vii) The supply steam was carefully adjusted to give steady and stable counter-current flow.
- (viii) The water flowrate was also slowly and carefully adjusted to the required value.
- (ix) Condensed water which collected in the steam supply line, and also the water which escaped to the secondary separator was drained.
- (x) The steam flowrate was gradually increased in incremental steps until flooding occurred, ensuring that enough time was allowed in each step mentioned above to obtain steady conditions.

Step (v) was the most difficult part of the steam-water test procedure, i.e. to create a pressure difference

across the extractor using the condensation effect. It was noticeably more difficult to create the condensation effect when the water subcooling was high (60-80K) and when the cooling water flow rate passing through the condenser was low (4-12 l/min). In order to speed up the process, it was easier to start the procedure with lower water subcooling (10-40K) and a higher cooling water flowrate (20-29 l/min) then, when stable counter-current flow was established, the water temperature was brought down slowly to the required value and the cooling water flow through the condenser was reduced carefully to the desired rate.

The onset of flooding was observed in the same way as for the air tests.

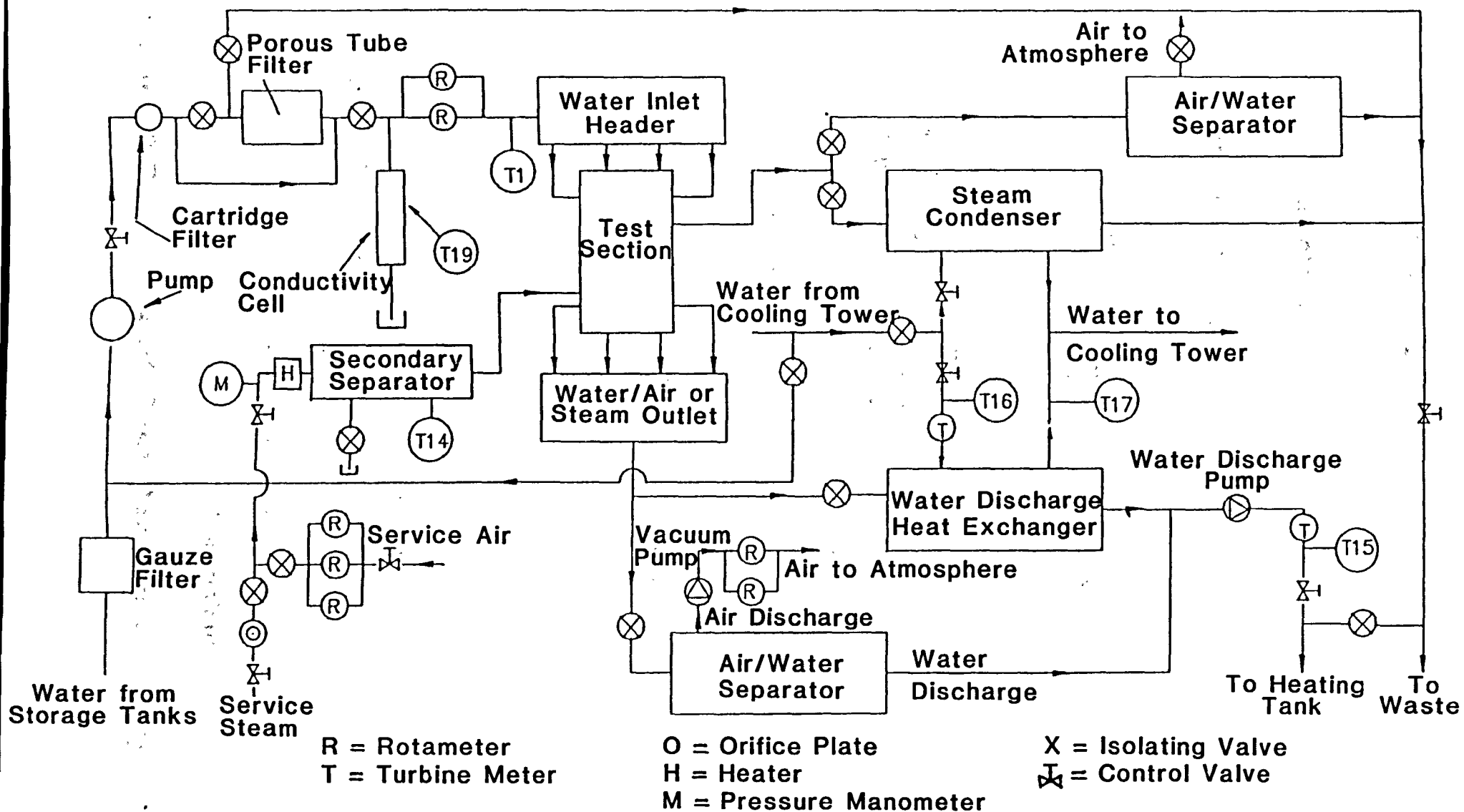


Figure 3.1 Line Diagram of Test Facility

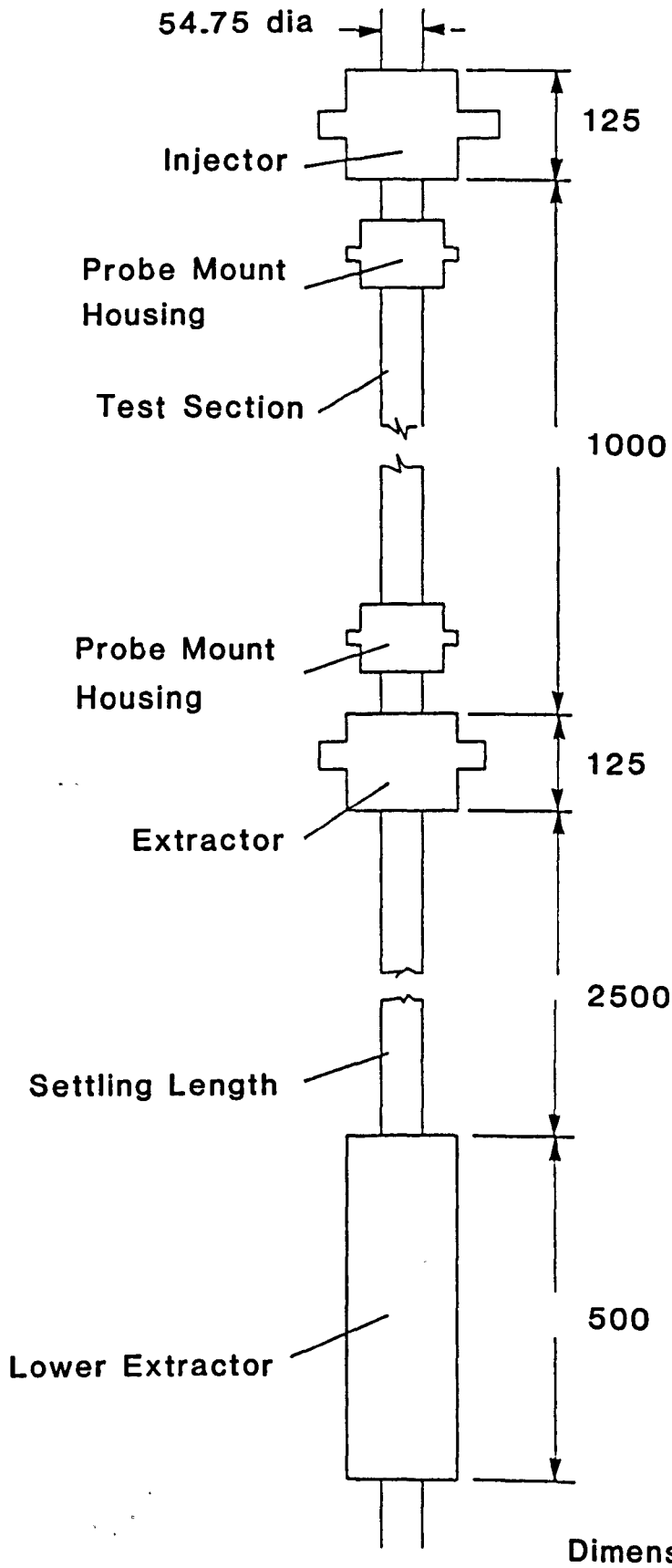
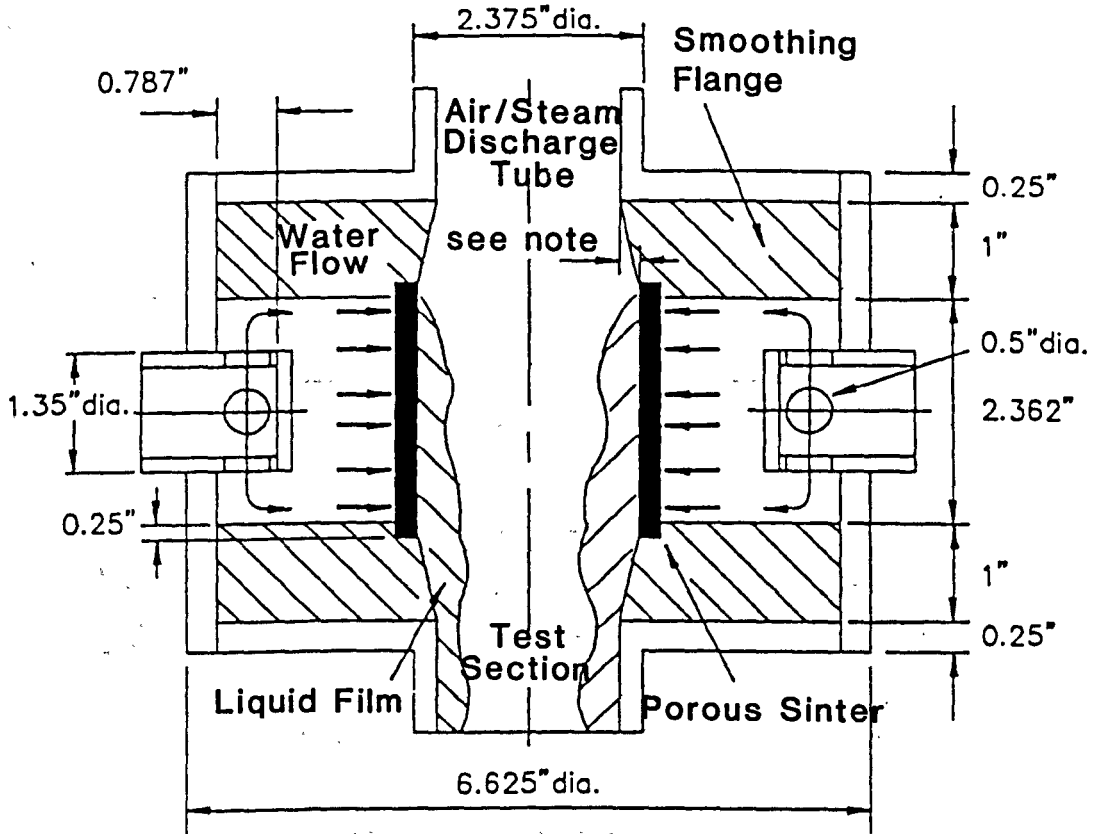
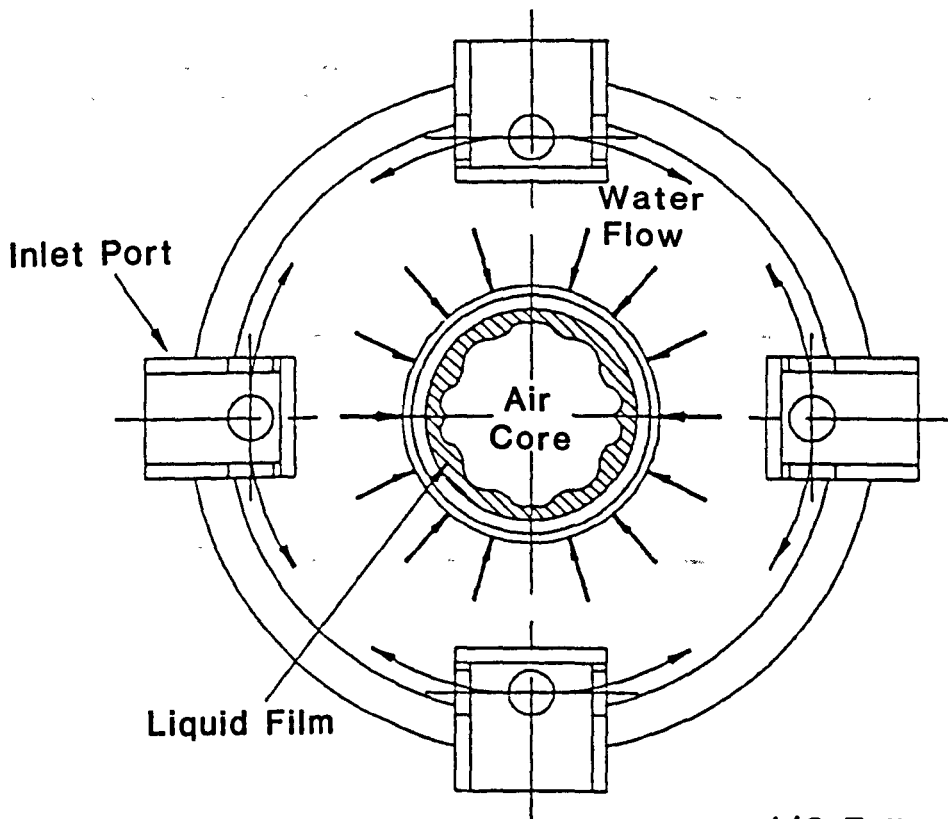


Figure 3.2 Details of Test Section Assembly

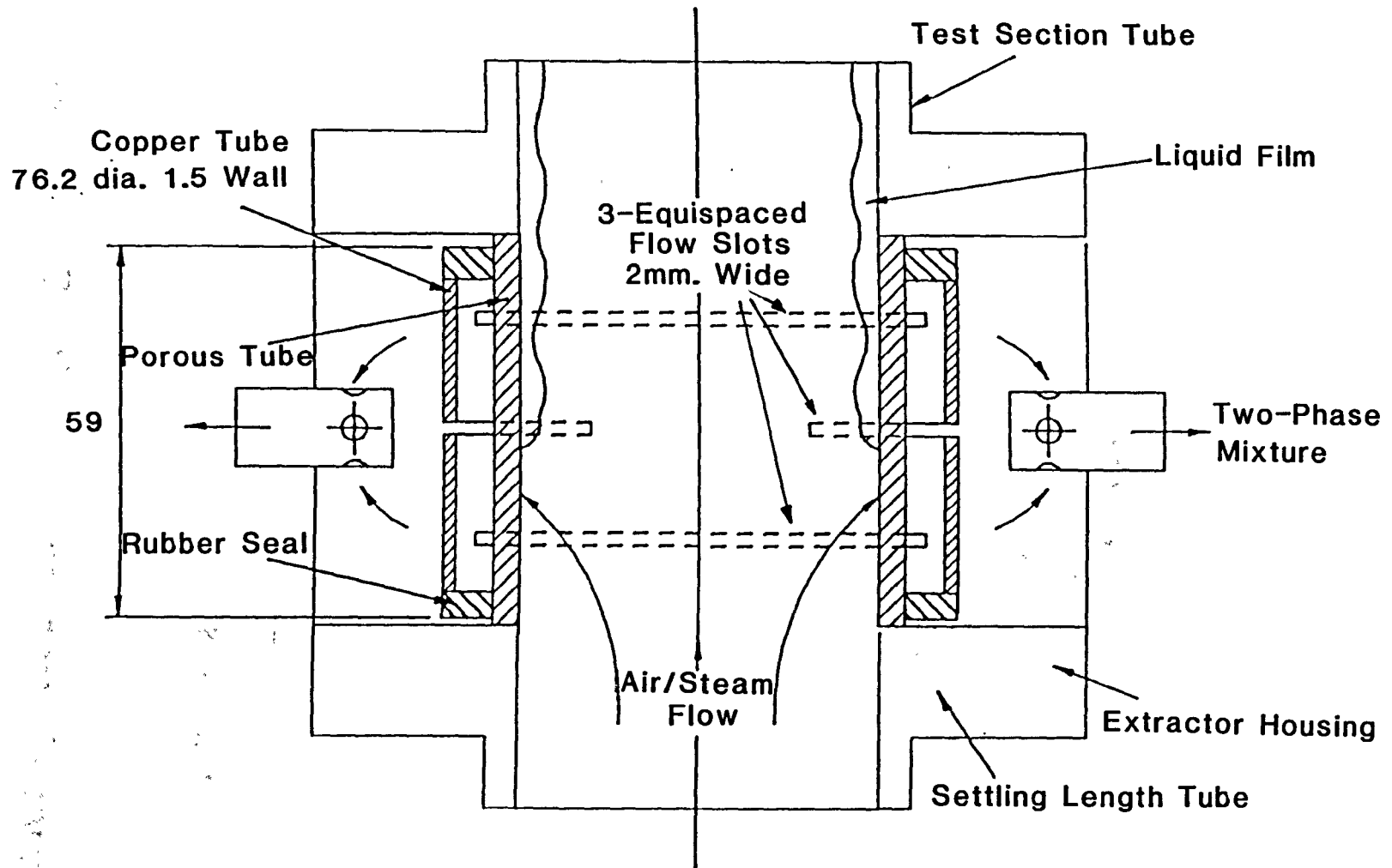


Note : Tube Bore 2 mm. less than Sinter Bore



1/2 Full Size

Figure 3.3 Liquid Injector



Dimensions in mm.

Figure 3.4 Details of Extractor Guard

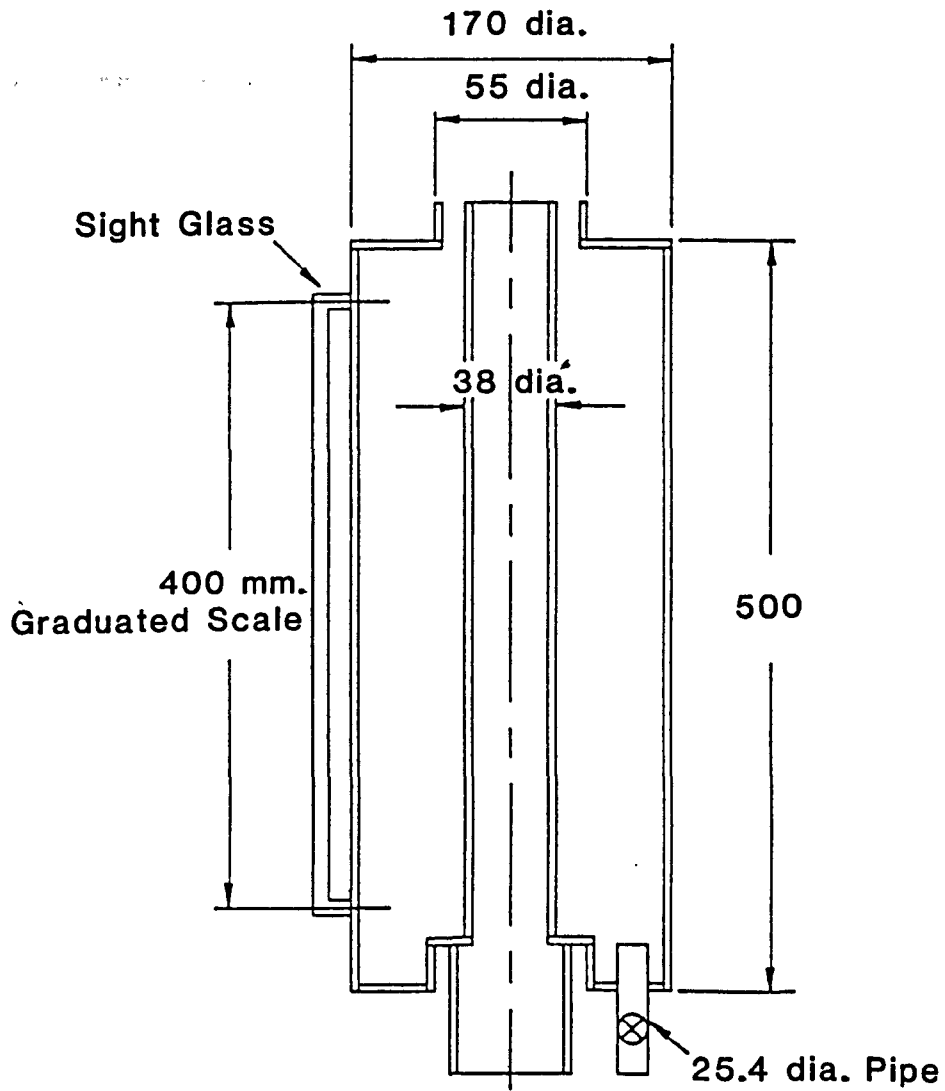
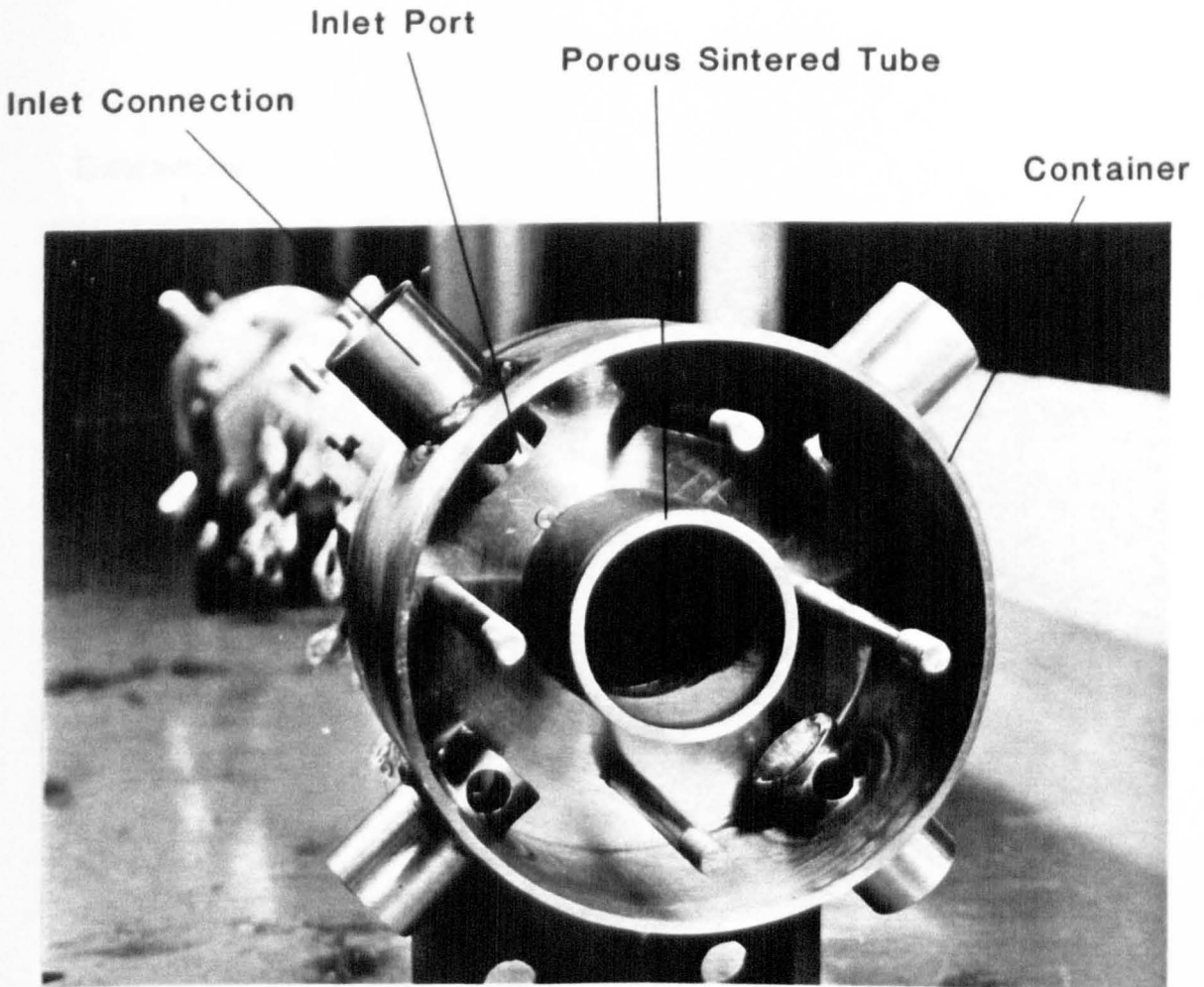
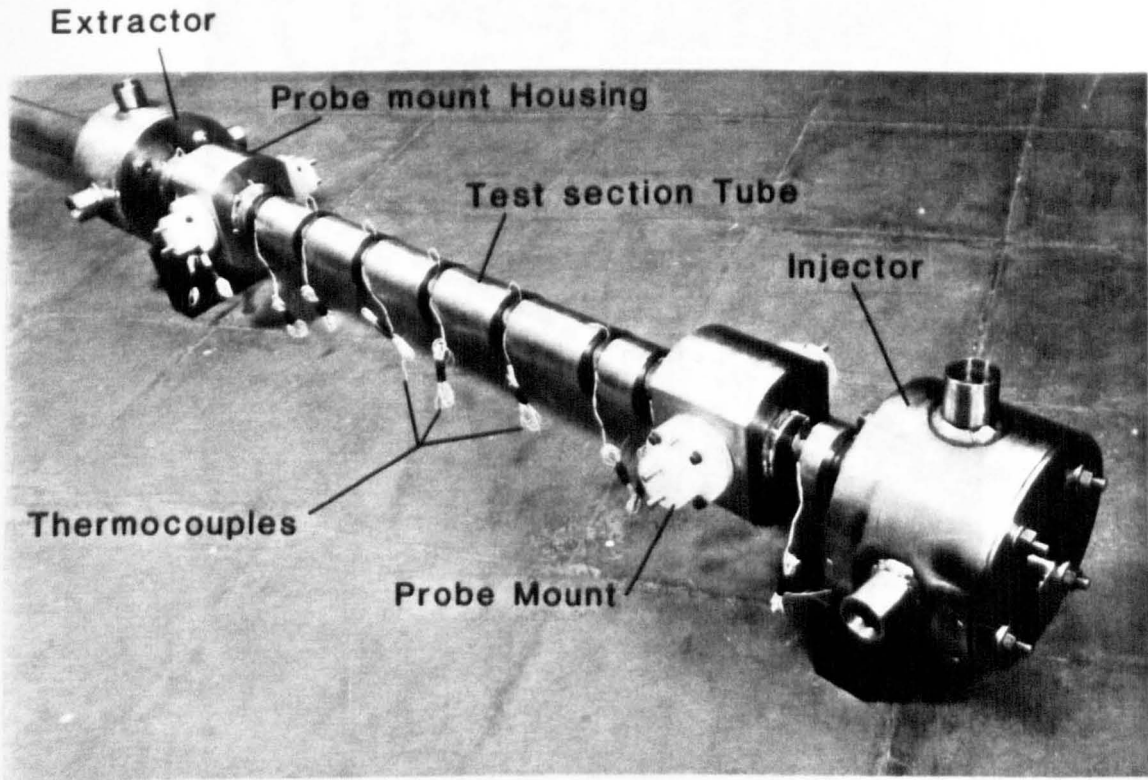


Figure 3.5 Details of Secondary Separator



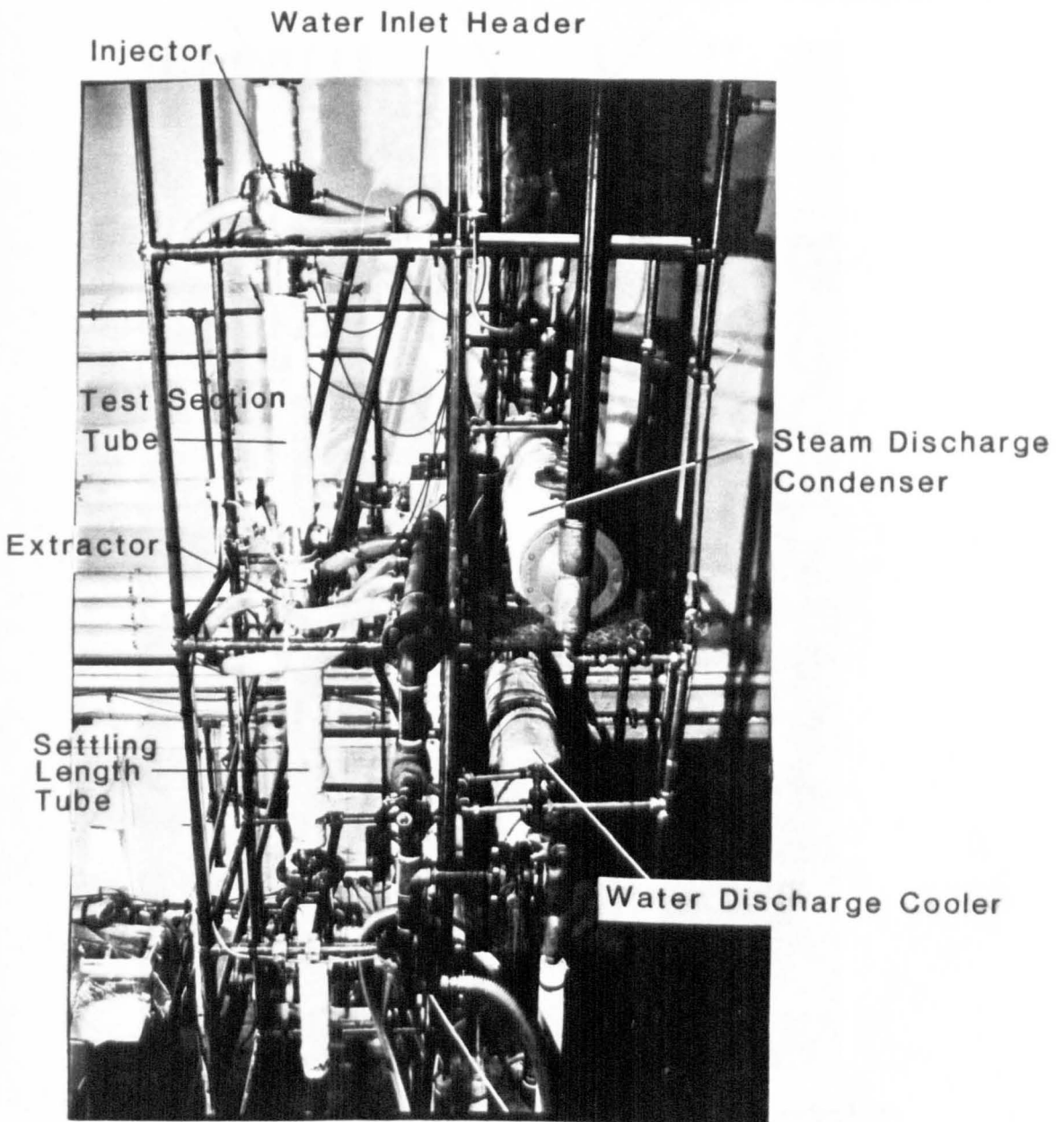
Liquid Injector System

PLATE 3.1



Test Section Assembly

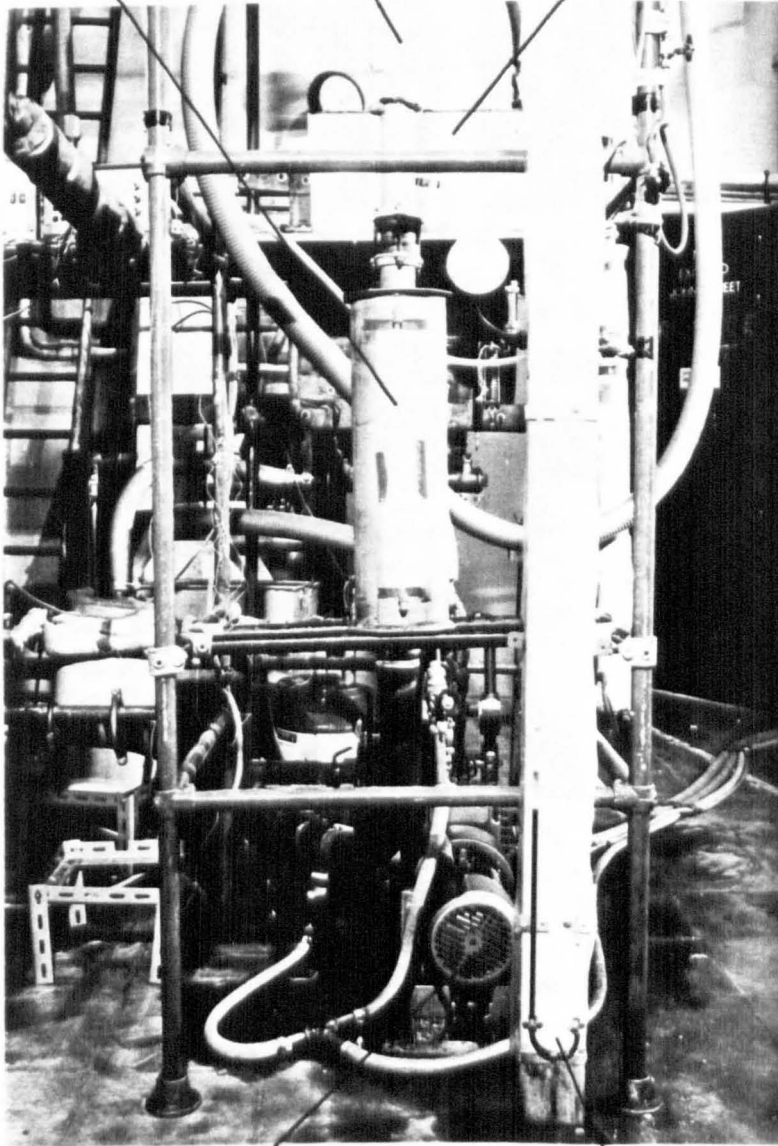
PLATE 3.2



Test Section Assembly "in situ"

PLATE 3.3

Secondary Separator
Settling Length
Water Discharge
Air-Water Separator

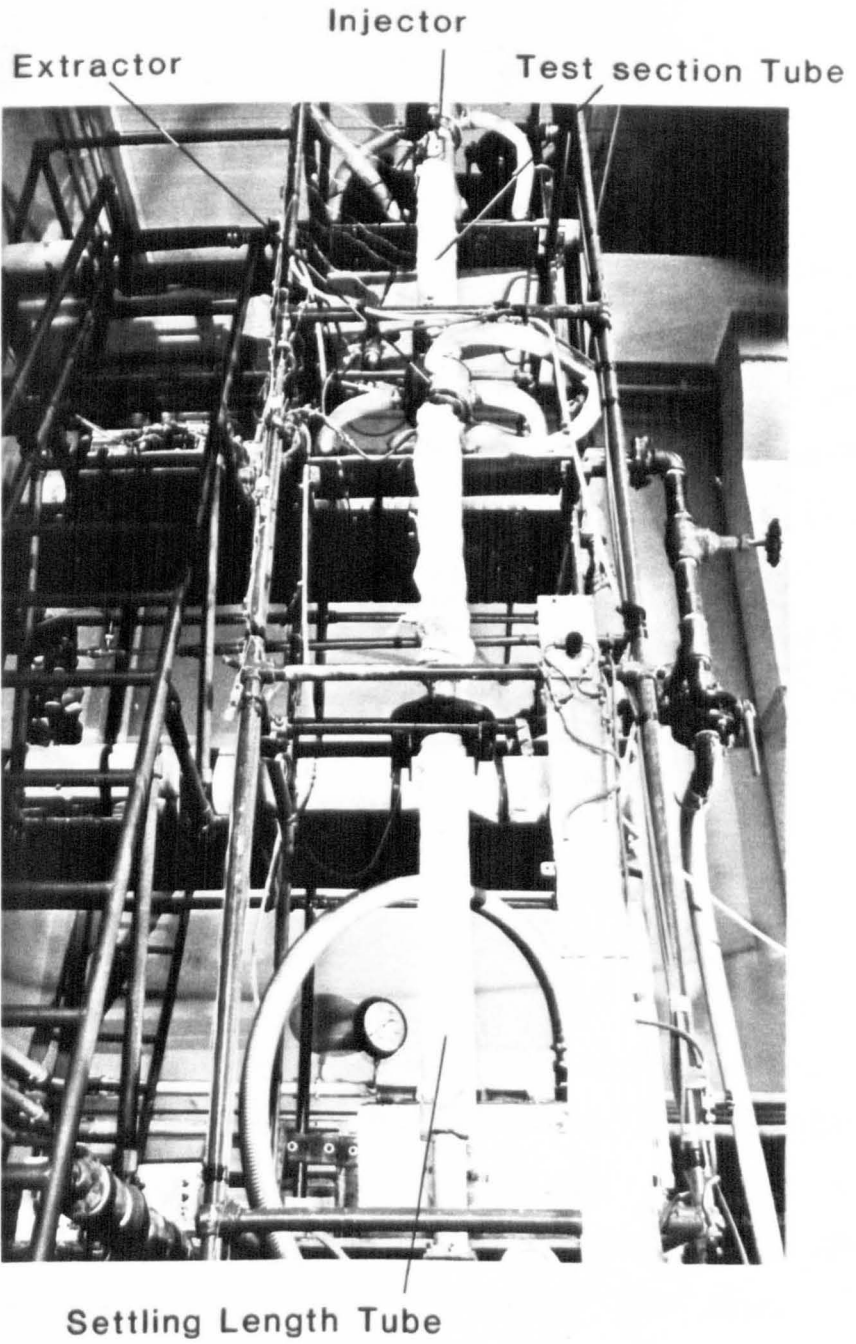


Air Vacuum Pump

Paraffin Manometer

Secondary Water Separator

PLATE 3.4



General View of Test Section

PLATE 3.5

CHAPTER 4

INSTRUMENTATION AND MEASUREMENTS

CHAPTER 4

INSTRUMENTATION AND MEASUREMENTS

During the course of the experimental programme, different sets of instrumentation were required for the two separate systems involved. There was one set for the air-water tests and an other for the steam-water tests, although some of the instrumentation was common to both systems. The air-water instrumentation is described in Section 4.1 and the steam-water instrumentation in Section 4.2. Section 4.3 contains a brief description of the data acquisition system used in the project.

4.1 Air-Water Instrumentation

The parameters measured during the air-water tests were the air and water flowrates, the test section pressure, the test section pressure drop, the air and water temperatures and the liquid film thickness. The instrumentation and the methods adopted are described below.

4.1.1 Air Flowrates

In the air-water tests, two air flowrates were

measured, the total air supply flowrate before it entered the test facility, and the air flowrate after it had passed through the water extractor system. The air flow to the test section was the difference between the two measurements.

The air-water flowrates were measured using three rotameters installed in parallel, one of which was a 35G metric tube whilst the other two were 47G metric tubes. All three rotameters were fitted with duralumin floats. The air flowrate passing through the extractor system was measured (after being separated from the water) by two rotameters installed in parallel, one a 35XG metric tube and the other a 24XG metric tube, both with duralumin floats. All the air rotameters were calibrated in accordance with the manufacturer's recommendations. The calibration details are given in Appendix A, section A1.

4.1.2 Supply Water Flowrate

The supply water flowrate was measured using two rotameters, of different ranges, each accommodated in separate flow lines to provide versatility and accuracy in the flow measurements. For high water flowrates a 47 metric series rotameter with stainless steel float was used. For lower flowrates a 0 to 10 l/min water rotameter was used. The 47 metric series tube was calibrated in situ and details are given in Appendix A

Section A2. After checking the other rotameter it was decided that no calibration equation was required.

4.1.3 Air-Water Temperature Measurements

Air and water temperatures were measured using copper-constantan thermocouples. The thermocouples fitted at the air inlet section and at the air discharge system were connected to an appropriate switching box and digital readout, whilst air and water temperatures at other positions were monitored through the data acquisition system directly. These included the temperatures of the water supply, conductivity cell and the liquid film, above and below each conductance probe, Figure 4.1.

4.1.4 Liquid Film Thickness

A conductance type method was used to measure the liquid film thickness as it is the most convenient method to use with a stainless steel tube. The conductance probes and the necessary electronic circuits were developed in the Department of Thermodynamics. The conductance probe consisted of a circular stainless steel rod, centrally placed in a polypropylene material which was used as the probe mount. This was fixed inside a stainless steel block, specially manufactured, and used as the probe mount housing. The mounting arrangement is

shown in Figure 4.2. These were then machined and welded into position on the test tube section in such a way that no protruding joints were likely to interfere with the liquid film. The probe geometry is shown in Figure 4.3.

A conductance measuring circuit, shown in Figure 4.4, was used to measure the liquid film conductance. The stainless steel rod formed one electrode while the test tube section formed the second electrode which was maintained at earth potential. The polypropylene material provided the insulation. The calibration details of the conductance measuring circuit is described in Appendix A, Section A4.

Since the conductance between two electrodes is dependent on the liquid film thickness and the conductivity, a conductivity measurement cell of the form shown in Figure 4.5 was used to measure the conductivity of the liquid film. A sample of the water entering the test section was provided to the conductivity cell through a separate line.

In the present work, two sets of conductance probes were used to measure the liquid film thickness at two locations. The upper set was placed 128 mm below the top flange of the test section with the lower set placed at 128 mm above the bottom flange of the test section. The calibration details of the two probes are described in Appendix A, section A5. The conductance probes were

connected simultaneously to the data acquisition system, an oscilloscope and a U.V. recorder. A visual observation of the film flow and the situation of flooding was given by the oscilloscope, whilst a record of the same situation was provided by the U.V. recorder. The latter was used mainly in the situation of flooding in an attempt to establish whether flooding was first observed at the upper or lower conductance probe.

4.1.5 Test Section Pressure

The test section pressure was measured by means of a mercury manometer connected to the bottom of the test section assembly at the air inlet, Figure 3.1.

4.1.6 Test Section Pressure Drop

A differential pressure transducer of TEKFL0 TF7 type in conjunction with a TR8 Transmitter was used to measure the pressure drop in the test section. The calibration details of the pressure transducer are given in Appendix A, Section A6. The test section pressure drop was also monitored by two manometers, a paraffin manometer and a mercury manometer. These were connected in parallel to each other and with the pressure transducer. The paraffin manometer, which was very sensitive to any pressure change, provided accurate and

sufficient monitoring of the pre-flooding pressure drop. Since the flooding situation was always accompanied by a substantial change in the test section pressure drop, the paraffin manometer was unable to cope with the variation, therefore it was isolated and the mercury manometer was used to assess the post-flooding pressure drop.

The pressure tappings were placed 1364 mm apart with the top pressure tapping point positioned 25 mm above the top flange of the injector. The pressure tappings and the measuring devices were connected via transparent volume chambers of the type illustrated in Figure (4.6). A certain level of water was always maintained in the chamber.

4.2 Steam-Water Instrumentation

All the parameters measured in the air-water tests were also measured in the steam-water tests, except air flowrates and air inlet and discharge temperatures. Therefore any omission here implies that the method previously outlined, in the air-water tests, was used although many additional parameters were measured for steam-water.

4.2.1 Steam Flowrates

It was only practical to measure the supply steam flowrates directly by an orifice meter. To avoid any disturbance to the liquid film flow, no measuring instruments were inserted inside the test section. The direct measurement of either the steam or water flowrate through the extractor was impossible because the mass transfer had the effect of changing the local steam and water flowrate inside the test section. Therefore, additional temperatures and flowrates were measured to overcome the situation and thus obtain the required flowrates indirectly through heat and mass transfer calculations. The methods adopted are described below.

4.2.1.1 Supply Steam Flowrate

The steam supply rate was measured by using a 20 mm diameter orifice plate which was fitted in a 55 mm diameter pipeline. The pressure difference across the orifice plate was detected by D upstream and $D/2$ downstream tapping points. The orifice design and installation was according to BS 1042. The upstream pressure and temperature were determined by a thermocouple and a Bourdon pressure gauge. Another differential pressure transducer (TEKFLO TF7 type in conjunction with a TR8 transmitter) was used to measure the pressure difference across the orifice plate. Calibration details

of the orifice plate are given in Appendix A, Section A7.

4.2.1.1 Extracted Water Flowrate

Since a mixture of water and steam passed through the extractor system, neither of them could be measured directly. Furthermore, the subcooling of the liquid could have allowed further steam condensation to take place, and/or any pressure drop in the extractor system to produce flashing. Heat and mass transfer balances were thus used to determine the liquid and vapour flowrates at the extractor inlet.

The flow pattern in the extractor is illustrated in Figure 4.7. Considering the control volume shown in the same figure, assuming steady conditions and neglecting heat losses, an energy balance can be written as

$$\begin{array}{l} \text{energy transfers} \\ \text{to the system} \end{array} = \begin{array}{l} \text{energy transfers} \\ \text{from the system} \end{array}$$

which gives

$$M_{fL}h_{fF} + M_{gL}h_g = M_{cW}(h_{fc2} - h_{fc1}) + M_D h_{fD} \quad (4.1)$$

where

$$M_{fL}h_{fF} = \text{liquid film enthalpy}$$

$$M_{gL}h_g = \text{steam enthalpy}$$

$$M_{cW}(h_{fc2} - h_{fc1}) = \text{heat transfer to cooling water}$$

$$M_D h_{fD} = \text{energy content of discharge water.}$$

The mass balance of the same control volume can be written as

$$M_{fL} + M_{gL} = M_D \quad (4.2)$$

and hence from equations (4.2) and (4.1)

$$M_{gL} = \frac{M_{cW}(h_{fc2} - h_{fc1}) - M_{fL}(h_{fF} - h_{fD})}{h_g - h_{fD}} \quad (4.3)$$

which can be closely approximated by

$$M_{gL} = \frac{M_{cW}C_p(T_{fc2} - T_{fc1}) - M_{fL}C_p(T_F - T_D)}{h_{fg} + C_p(T_{sat} - T_D)} \quad (4.4)$$

where the specific heats are assumed to be constant.

Equation (4.4) was used to calculate the amount of steam leaked through the extractor. The water flowrate to the extractor (M_{fL}) was calculated from the inlet water flowrate to the test section plus the amount of steam condensed on the liquid film within the test section which was calculated from equation (4.9) as will be indicated in the next section. It was unnecessary to measure the discharge water flowrate (M_D) as this was not taken into account in the above equation. For the sake of accuracy and as a cross check, the volumetric discharge water flowrate was measured by using a Bestobell M6 turbine flowmeter, which was converted to a mass flowrate using the water density corresponding to the measured discharge water temperature (T_D). The details of the turbine flow meter calibration are given in Appendix A, section A8.

When the pressure difference across the extractor system was very high, a very small amount of air occasionally leaked into the system. Since even a few air bubbles could affect the reading of the turbine meter and influence the accuracy, a timed collection tank mounted on a weighing device was used to measure the discharge flowrate.

The cooling water flowrate (M_{cw}) through the condenser, was obtained by measuring the volumetric flowrate using another Bestobell M6 turbine flowmeter. Its calibration details are given in Appendix A section A8. By using the density corresponding to the measured cooling temperature, the volumetric flowrate was converted to a mass flowrate.

4.2.1.3 Condensed Steam Flowrates

The amount of steam flow condensed on the liquid film inside the test section can be determined from an energy balance between the water inlet and the water outlet.

Consider the fluid element shown in Figure 4.8
A mass balance gives

$$M_g - M_{gout} = M_f - M_{fin} \quad (4.5)$$

and an energy balance gives

$$M_{fin}h_{fin} - M_f h_f = h_g(M_{gout} - M_g) \quad (4.6)$$

and using equation 4.5 in 4.6 gives

$$M_f = \frac{M_{fin} (h_g - h_{fin})}{(h_g - h_f)} \quad (4.7)$$

which can be closely approximated by

$$M_f = M_{fin} \frac{h_{fg} + C_p(T_{sat} - T_{fin})}{h_{fg} + C_p(T_{sat} - T_f)} \quad (4.8)$$

The mass flow of steam condensed on the liquid film is

$$M_{gc} = M_f - M_{fin} \quad (4.9)$$

substituting equation (4.9) in (4.8) gives

$$M_{gc} = \frac{M_{fin} C_p (T_f - T_{fin})}{h_{fg} + C_p (T_{sat} - T_f)} \quad (4.10)$$

where the specific heat C_p is assumed constant.

4.2.1.3 Test Section Steam Flowrates

The steam flowrate to the test section was determined from the difference between the steam supply flowrate and the flowrate of the steam which leaked through the extractor system

$$M_{gin} = M_{gsup} - M_{gL} \quad (4.11)$$

The steam flowrate which passed the top of the test tube was calculated from the difference between the steam flowrate to the test section and the amount of steam condensed on the liquid film inside the test tube section.

$$M_{gout} = M_{gin} - M_{gc} \quad (4.12)$$

4.2.2 Temperature Measurements

Copper-Constantan thermocouples were used to measure the temperature at the points of interest which are illustrated in Figure 3.1. Two types of thermocouple fixing were used on the test rig, (i) thermocouples whose tip projected through the centre of an Allan screw into the bulk of the flow (and thus could be removed) and (ii) thermocouples which were soldered directly on to the tube wall.

The thermocouples in the test tube section were soldered to the tube wall at a distance of 0.6 mm from the inner surface at the locations illustrated in Figure 4.1. The liquid film temperature distribution along the tube at the interface was determined from these measurements and the procedure will be discussed later in Chapter 6.

The temperatures at eighteen positions were collected directly by the microcomputer through the data

acquisition system, all these thermocouples being connected to a common cold junction in melting ice. The calibration details of these thermocouples are given in Appendix A, Section A9. Temperatures at other points were measured by connecting each thermocouple directly to a switch box and digital readout.

4.2.3 Test Section Pressure and Pressure Drop Measurements

The same instruments which were used to measure the test section pressure and pressure drop in the air-water system were also used in the steam-water system, with two minor modifications in the pressure drop measurements.

- (i) Since the second phase was steam, the two volume chambers were completely filled with the water instead of maintaining a certain level of water as in the air-water tests.
- (ii) The paraffin manometer was completely isolated from the measuring system because the high sensitivity of this type of manometer made it too difficult to be used with the sort of experimental procedure carried out in the steam-water tests.

4.3 Data Acquisition System

As described earlier, various system parameters required to be monitored during each test. This was achieved by using a data acquisition system based on an Apple II microcomputer which was developed by the Department of Thermodynamics in conjunction with the University Microprocessor laboratory. The data acquisition system was a purpose built, 64 channel, multiplexed system although, during the experimental tests, only 29 of the available 64 channels in the system were used. The layout of the system is shown in Figure 4.9. The measurements detailed previously were available in the form of voltage output from the various instruments, that is, thermocouples, liquid rotameters, pressure transducers, and conductance probes. These signals required to be digitised before they could be accepted by the computer. This was achieved by the use of the analogue to digital converter unit (ADC). The ADC unit required an input signal in the range of 0-10 V to produce a twelve byte signal for the computer. For maximum accuracy, the largest signal produced by any test parameter should give a 10 V signal to the ADC unit. Since all the instruments used could not produce signals of this magnitude or range, some signals were conditioned before connection to the data acquisition system. Signal conditioning, which involved high signal amplification, also produced large noise amplification and so a signal filtering unit was used to minimise this effect. The

microcomputer controlled the system via six output signals, three for selecting the required multiplexing chip and three for choosing which signal on the selected multiplexing chip to connect to the microcomputer input line.

The hardware necessary for the data acquisition system, therefore included signal conditioning units, a signal filtering unit, a multiplexer unit, the analogue to digital converter and the microcomputer itself. Auxiliary units such as a disc drive unit and a printer were added to the system for data processing purposes.

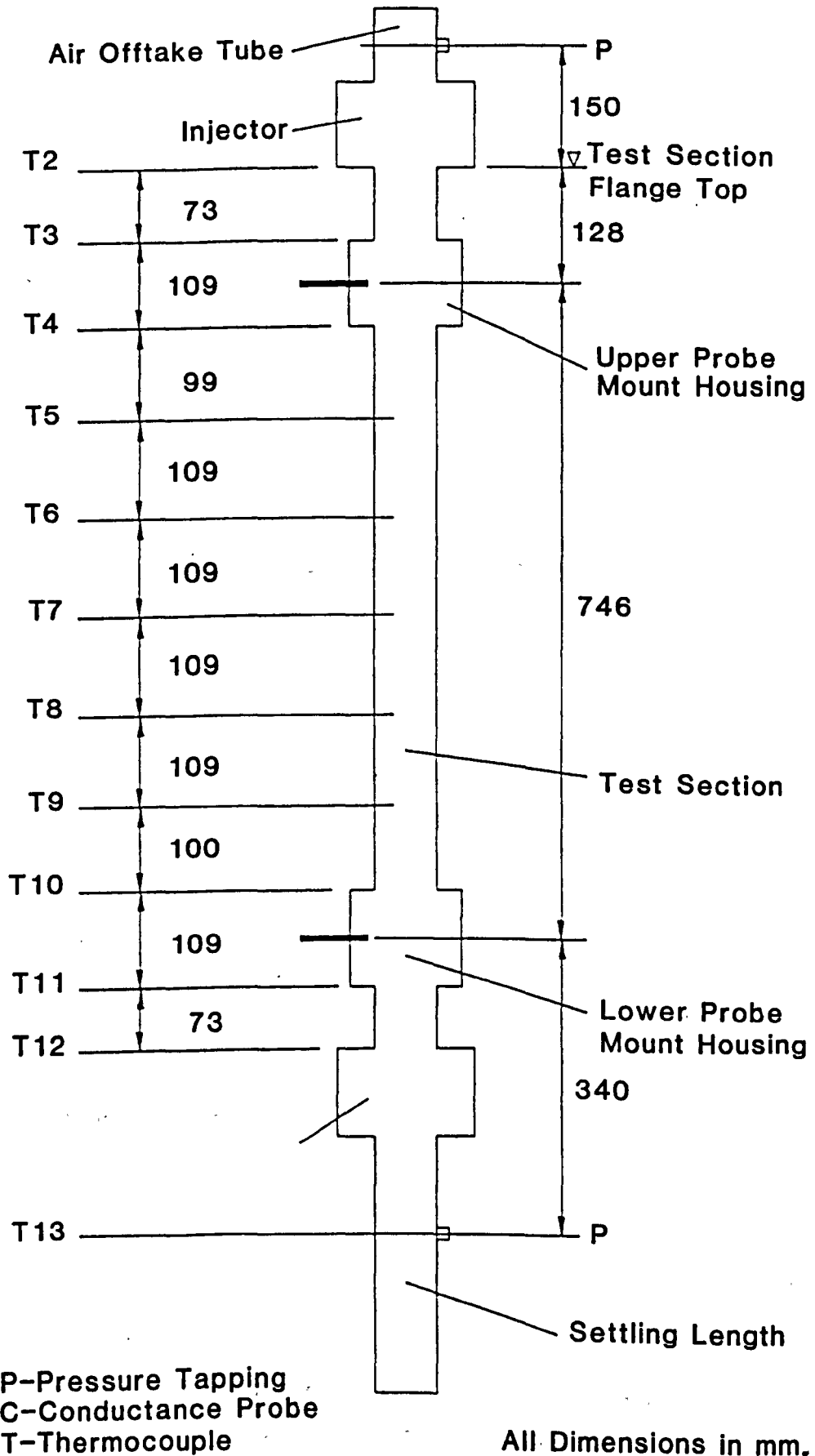


Figure 4.1 Layout of Test Section Instrumentation

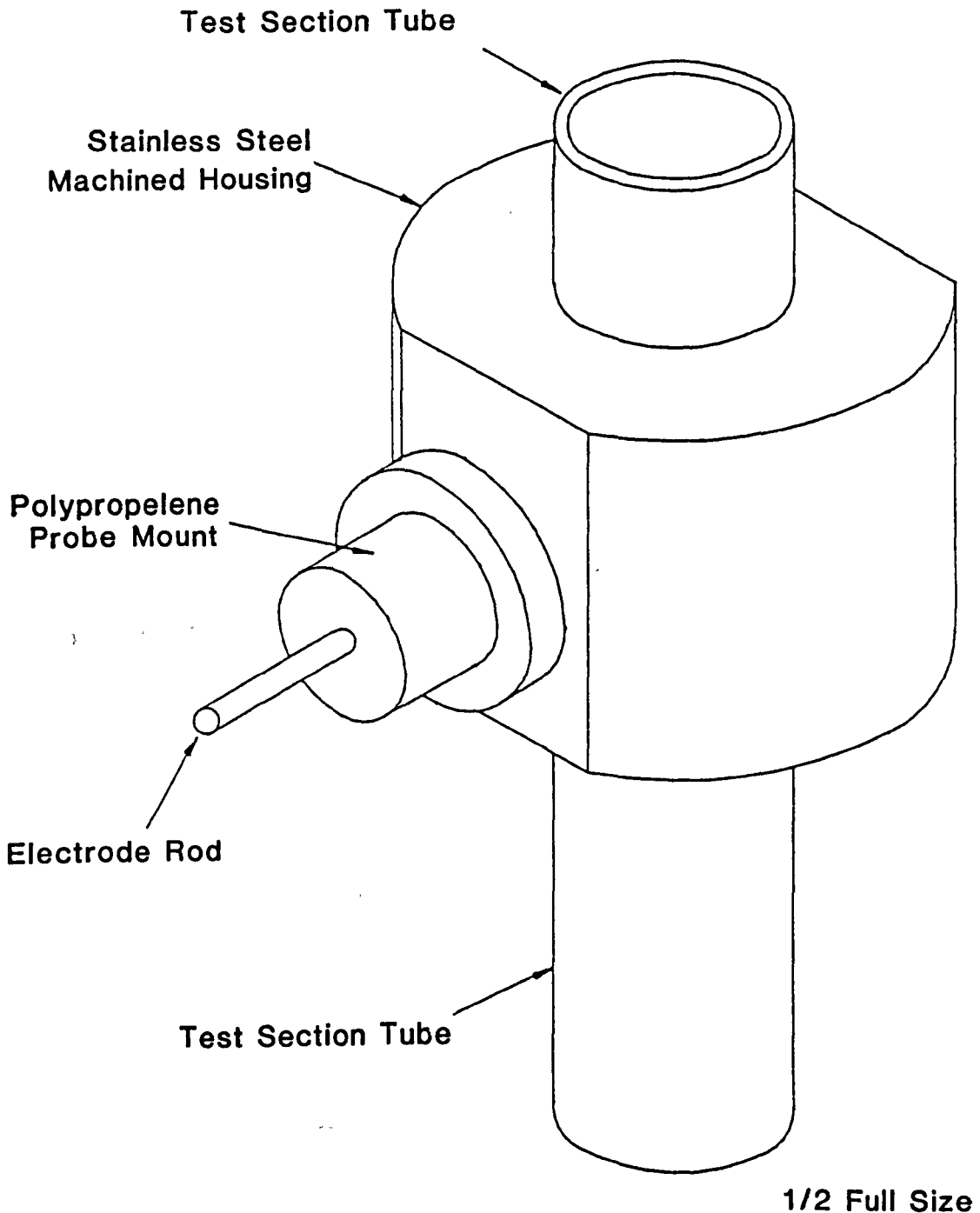


Figure 4.2 Mounting of Film Thickness Measuring Probe on Test Section Tube

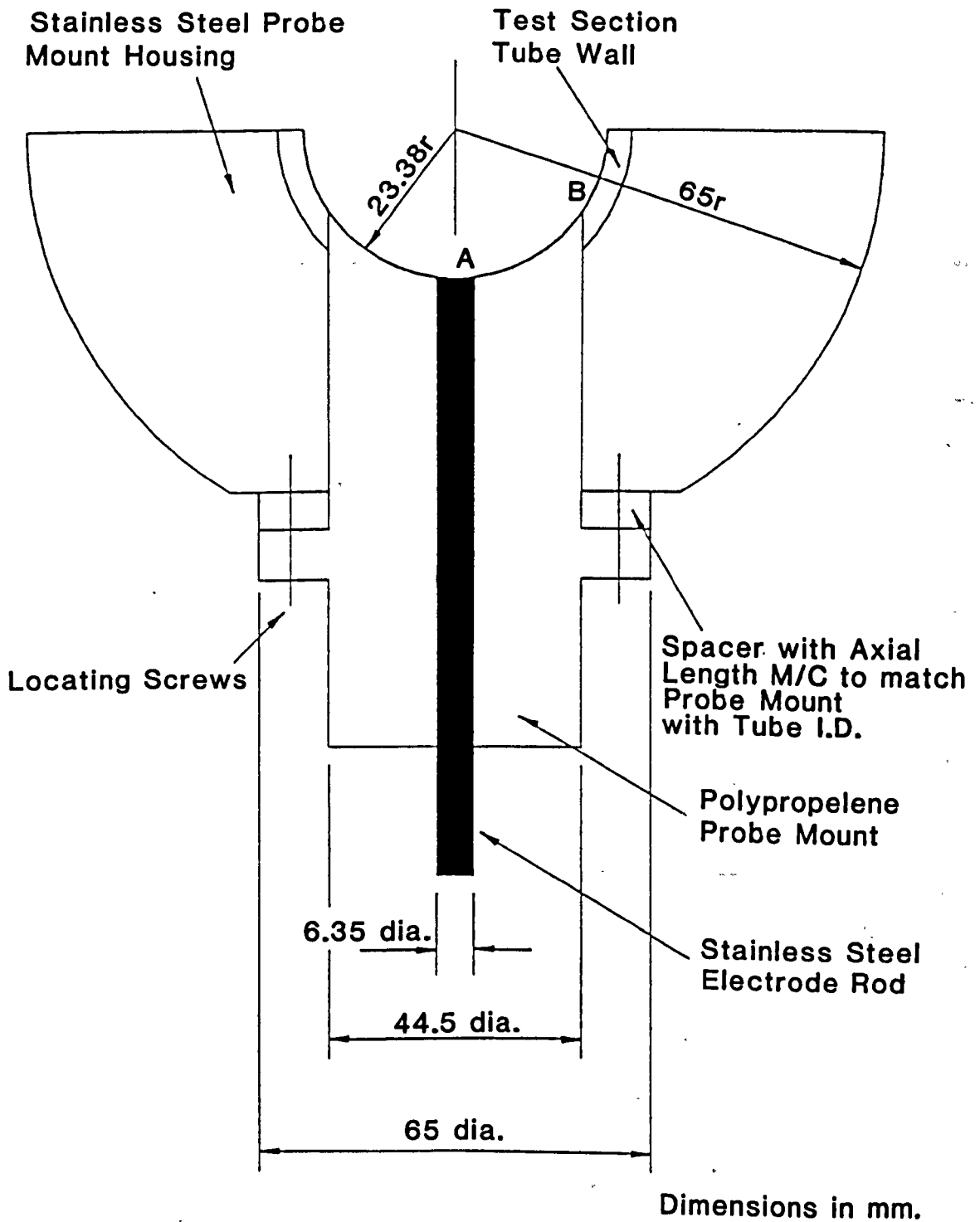


Figure 4.3 Film Thickness Measuring Probe Geometry

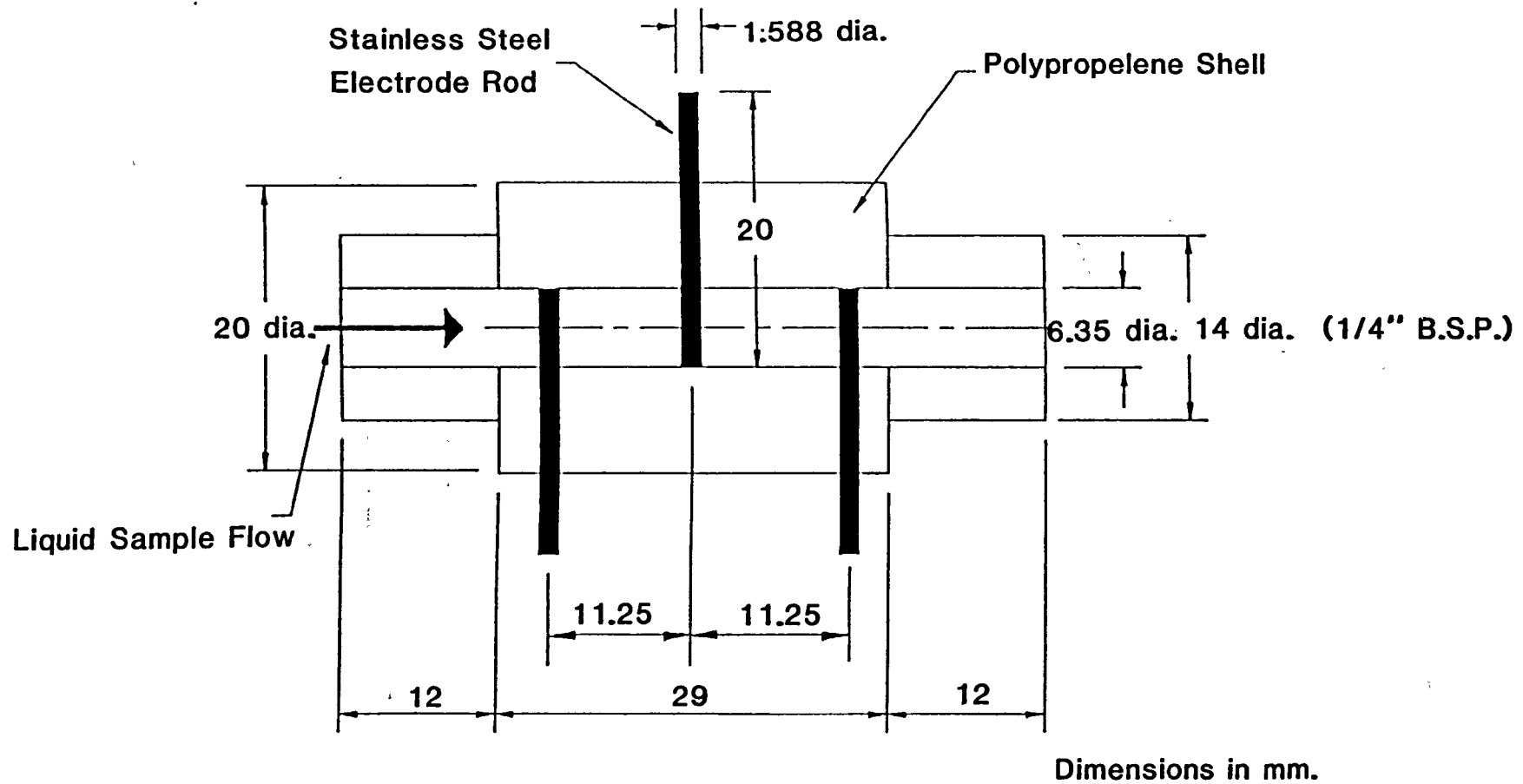


Figure 4.5 Conductivity Cell

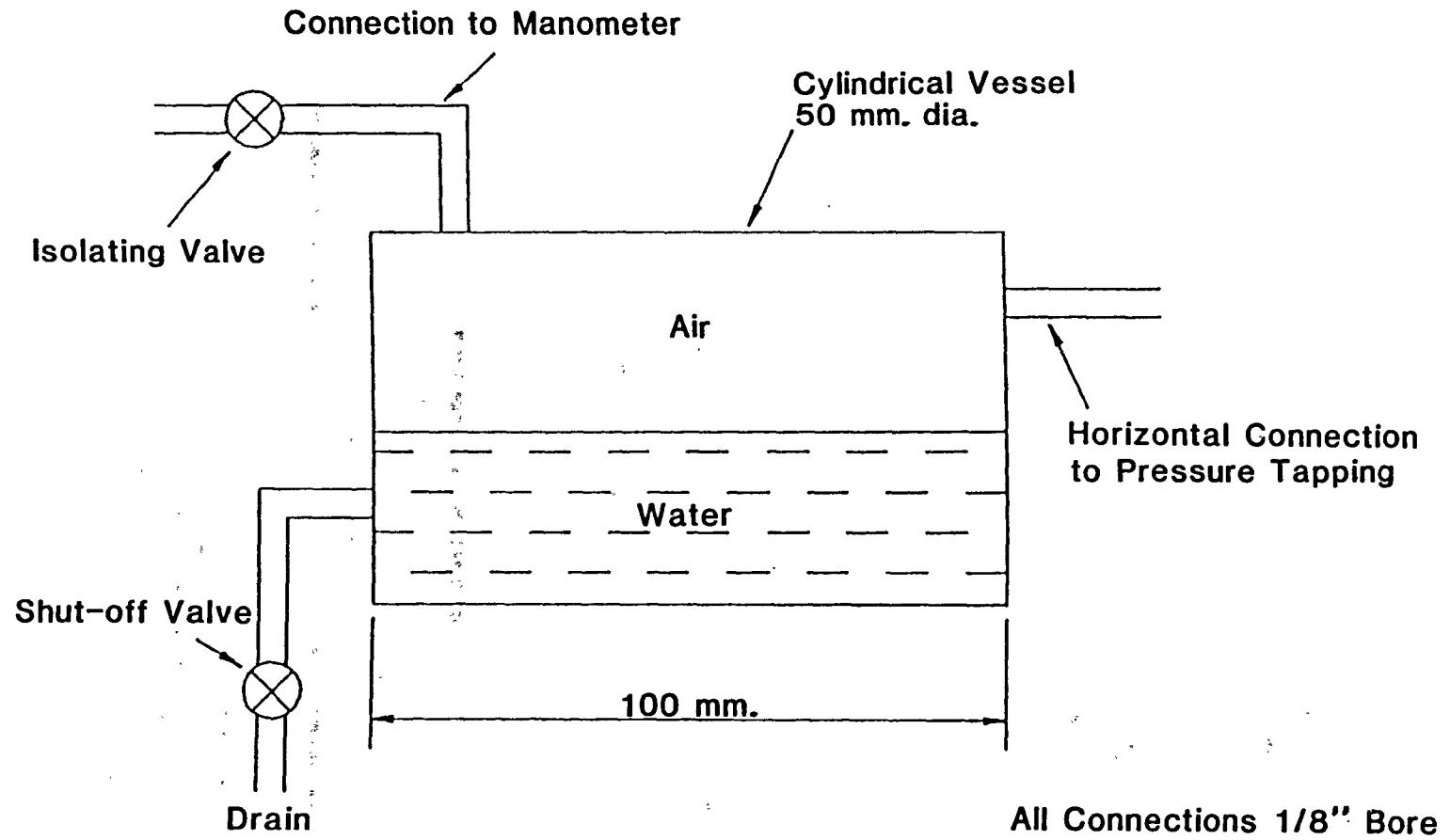


Figure 4.6 Details of Volume Chamber

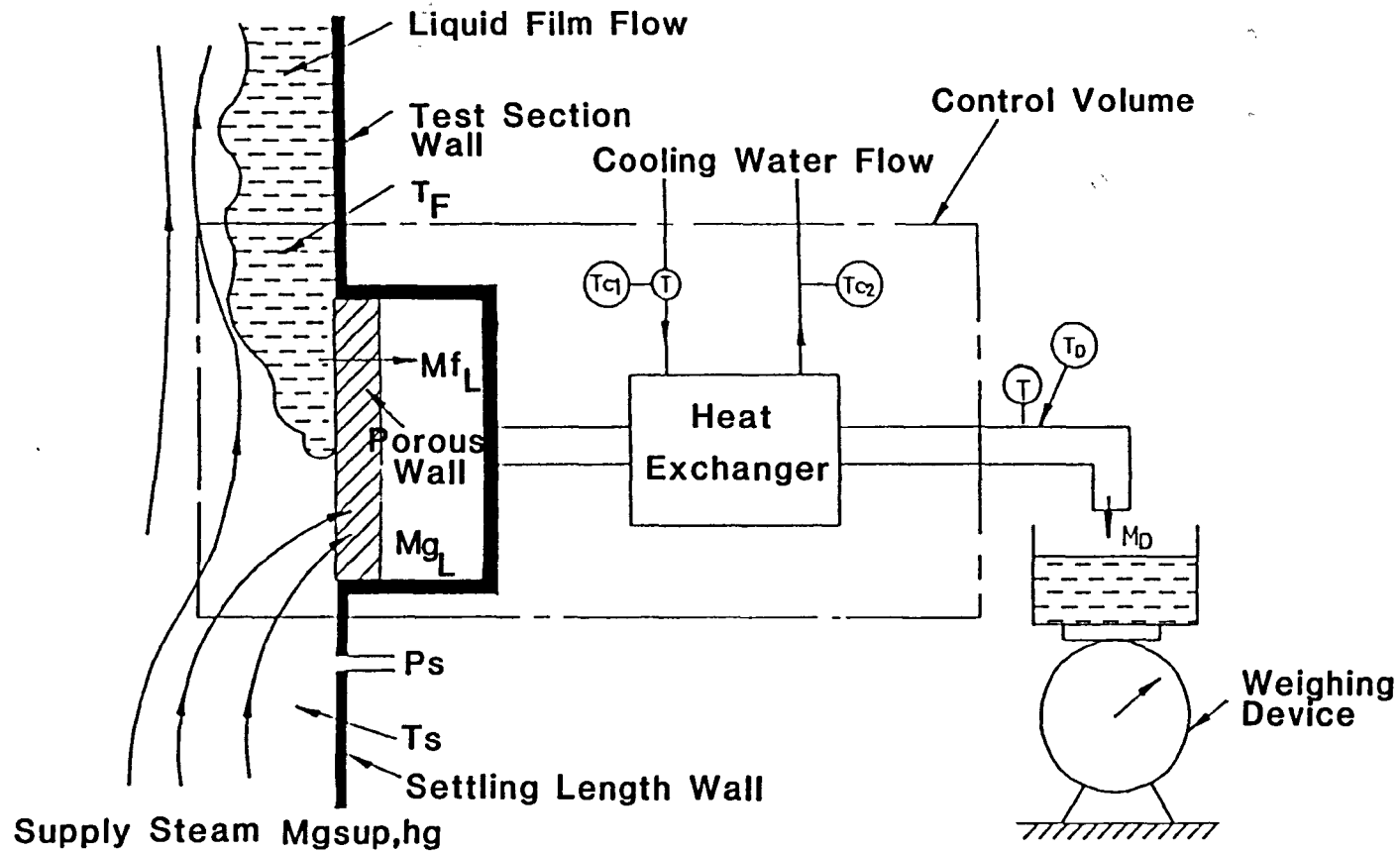


Figure 4.7 Layout of Water Offtake Instrumentation

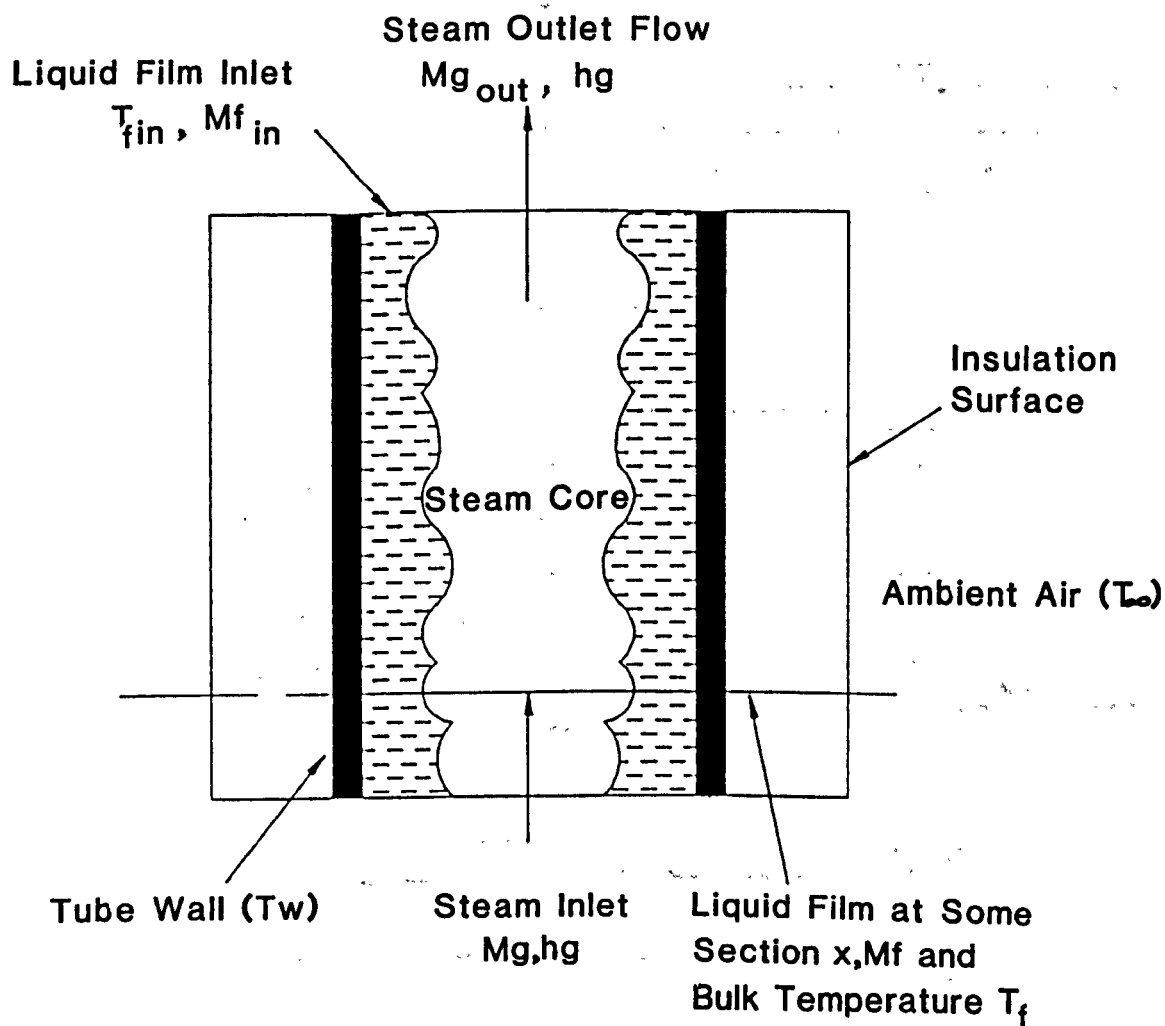


Figure 4.8 Typical Test Section Element

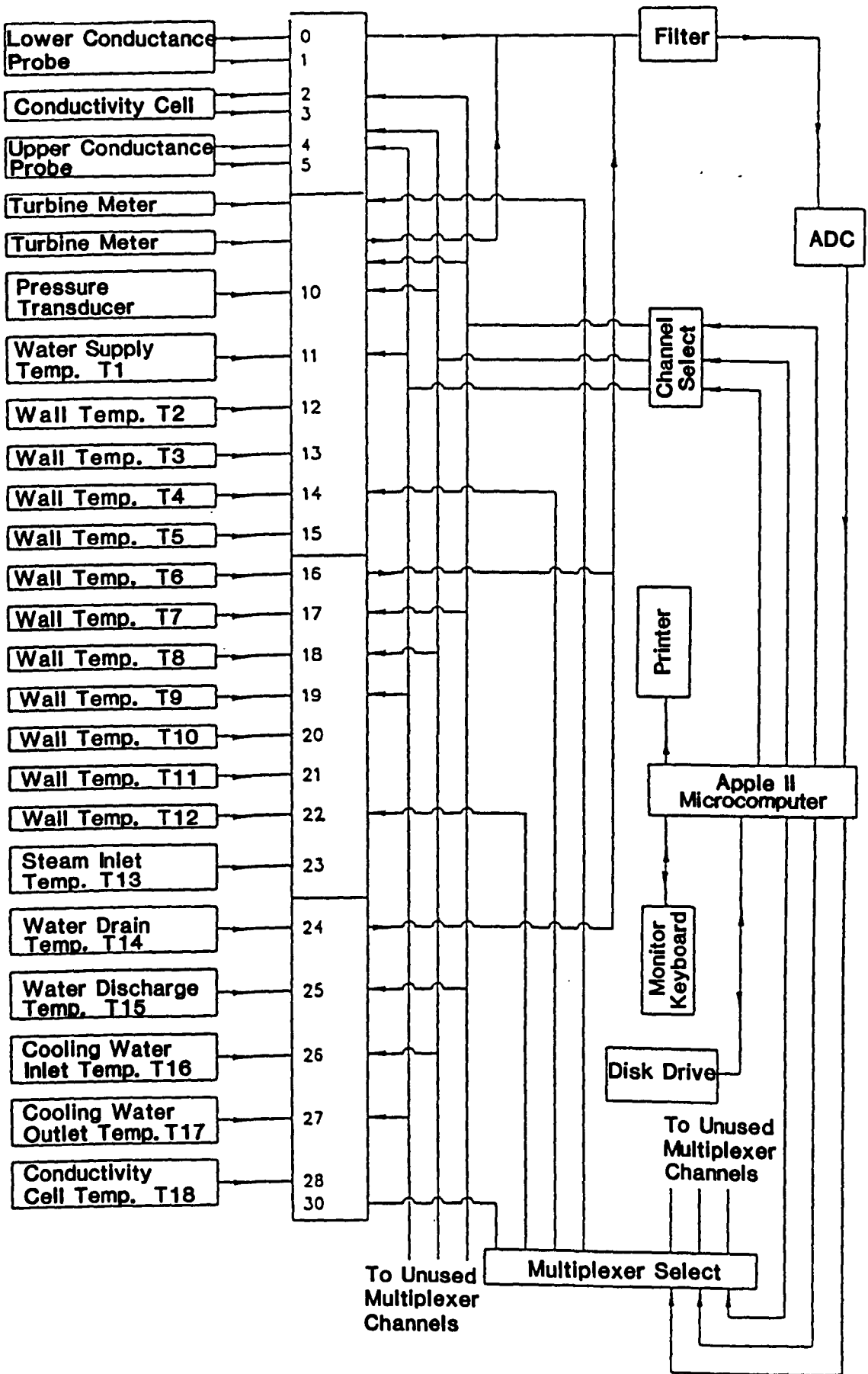


Figure 4.9 Layout of Data Acquisition System

CHAPTER 5

FILM VIEWING TECHNIQUES

CHAPTER 5VIEWING TECHNIQUES

Photographic techniques have found wide application in two-phase flow studies, since they enable more information to be obtained. The use of photography to record what was seen is an important source of qualitative deduction as it can extend the range of observation, enabling the time scale of viewing to be changed in such a way that rapidly occurring phenomena can be observed. A photographic record can also be used to provide quantitative measurements.

In earlier work employing photography in two-phase flow systems within the University a side viewing technique was used, i.e. observing the flow from the side of the channel. Recently the more advanced technique of axial photography has been employed which consisted of viewing the flow in a channel along its axis, with the camera looking directly into the flow. The application of the second technique can play an important part in the observation of annular two-phase flow systems.

The use of the photographic technique in the present work had two main objectives:

- i) To obtain information on the nature of disturbances

and their development in vertical annular two-phase flow in two different systems, i.e. air-water and steam-water systems.

- ii) To locate the position, in the test section, at which the flow reversal first developed in each of the two systems.

Developing a photographic technique had many difficulties, particularly with lighting since the test tube section was manufactured from stainless steel. The axial viewing technique adopted in the present work was carried out in two different ways:

- (i) Using endoscope systems : This viewing technique, using a self-illuminating endoscope, was developed in an attempt to overcome the lack of light inside the test section and is described in Section 5.1.
- (ii) Using video camera systems : This technique was used as an alternative to the endoscope system because of the recording problems experienced. In this system the flow is observed directly by a coloured video camera from which the name of the system is deduced, although a black and white video camera was indirectly used with the endoscope system. Details of this system are given in Section 5.2. Further details are given in Section 5.3 and viewing procedures in Section 5.4.

5.1 Endoscope Viewing System

Endoscope viewing is a new method of flow visualisation and its use here in a two-phase flow system was developed by the author. It involved inserting an endoscope device (similar in fundamental construction to that used in medical fields) inside the test section. The advantage of using such a system was that it provided a closer observation of the events taking place within the test section and also helped ensure that no undesirable protruding joints existed during the course of the experimental tests. The main disadvantage of using such a system in counter-current annular two-phase flow systems, where the onset of flooding is of special interest, was the danger that the endoscope, an alien body inside the test section, would affect the two-phase flow and the onset of the flooding process. This situation was overcome in some tests by using an endoscope with a zoom facility.

The endoscope systems consisted of seven parts most of which are shown in plate 5.1. These were:

- (i) A forward viewing endoscope : This was a stainless steel tube, 115 mm long and 11 mm in diameter with a 120° forward viewing angle. It contained an optical system which had a rigid construction of

lenses in the central core. This was enclosed by a non-coherent fibre optic bundle which was built inside the stainless steel tube. The fibre optics carried light from the source to the object being viewed. The reflected light from the object passed up through the optical core arrangement to the eyepiece and then to the viewing device, illustrated in Figure 5.1. The eyepiece assembly consisted of a viewing lens with focusing and zoom facilities.

(ii) A Radial viewing endoscope : This was a stainless steel tube 2200 mm long and 11 mm in diameter used to view the object radially. The forward viewing angle of the lens was also 120° . This endoscope had the same fundamental construction as that of the forward viewing endoscope with two minor differences :

a) Since the viewing by this endoscope was radial, a mirror was built inside the optical core, at the bottom, to reflect the light received from the object to the viewing device, as illustrated in Figure 5.2).

b) The endoscope had no zoom facility.

(iii) A low light, black and white, video camera with special lens connections manufactured to allow the

video camera to accommodate the eyepiece of the endoscope.

- (iv) A light source comprising of a 150 W quartz halogen lamp.
- (v) A fibre optic cable for interfacing the light source with the endoscope.
- (vi) A monitor to view the camera output.
- (vii) A video recorder to record the camera output.

5.2 Video Camera Viewing System

Different axial viewing techniques have been used by investigators to visualise annular two-phase flow inside a vertical tube, of which photography was the most popular. This was because it was relatively easy to use in observing and investigating, counter-current annular two-phase flow, before the onset of flooding took place. At the onset of flooding difficulties could arise because high speed cine films cover a relatively short period of time and it was difficult to predict the exact time at which the onset of flooding would occur. It was also difficult to time this to occur half way through the film. To extend the filming time to cover the whole process, a video camera technique was used in the present

work.

The video camera system was also advantageous since it produced film well suited for frame by frame analysis and, with axial viewing, it provided in situ visualisation of the events taking place inside the test section. These events could not be seen from outside, even with a transparent test section. The camera used was a Panasonic - F2 colour video camera. A colour monitor was connected to the camera in order to visualise its output. The recorder had the facility of replaying the recorded tapes in slow motion and also frame by frame in such a way that a total of 25 frames could be produced for every second recorded on the tape. This corresponded to a time interval of 40 ms. The video camera had a timing facility which could be displayed on the monitor screen and also recorded on the video tape. The video camera equipment is shown in plate 5.2.

5.3 Test Facility Modifications

The application of the viewing techniques required some modifications to the test facility. The modifications included introducing a suitable illumination system into the test tube and also placing the viewing devices in a suitable position to make the flow inside the test section visible. The necessary modifications in the test facility for both the endoscope

and the video camera techniques in the air-water system are detailed in 5.3.1 and for the steam-water system in Section 5.3.2.

5.3.1 Air-Water System

The alterations to the test facility for the air-water system were carried out so that the endoscope viewing technique and the video camera technique could function under suitable conditions. Details of both techniques are given below

(i) Endoscope technique : The modifications required for this technique were (i) to allow the endoscope to be inserted inside the test tube and (ii) to provide test tube illumination. The endoscope could be inserted into the test tube in two ways, either through the top of the test tube looking downwards, or from the bottom of the test tube looking upwards. To avoid interfering with the air settling length, the second method was initially discarded. Also the modification to the air offtake system, at the top of the test tube, was easier to carry out. The modification to the air offtake system included replacing the straight portion of the tube used previously, by a two inch T piece with the air flow taken off at 90° to the previous direction. A transparent polycarbonate disc was machined and fitted to a two inch nut, which was then tightened at the top of the T piece

as shown in Figure 5.3. The endoscope was inserted into the test tube through the straight connector. A nut, backing ring washer, and an 'O' ring were used to lock the endoscope into position and also to prevent any air from escaping by providing the necessary sealing. When the nut was loosened the endoscope could be moved up and down, sliding within the straight connector in order to position the viewing lens at any desired axial location within the test section. The arrangement is shown in plate 5.3. As previously mentioned, the endoscope device had a self-illumination system, which was provided from a light source of 150 W and gave just enough light for the radial endoscope to view a small area on the inside wall of the test section. For the forward viewing endoscope the power of the light source was not sufficient to illuminate the entire inside of the tube, and for economic reasons a more powerful light source was not available; therefore an external lighting system had to be used. It was not possible to illuminate the test section by directly projected light as the bottom of the test section was connected to the settling length, and any interference with this was undesirable, whilst the top of the test tube was occupied by the modification made for the use of the endoscope system. The only other technique available was to insert transparent sections at suitable locations above and below the test section, so that the test section was indirectly illuminated and the intensity of the light inside the test section was dependent on the reflected light. The

illuminating system had to be very powerful so that the reflected light was sufficient to illuminate the test section.

A 300 mm section was cut from the settling length tube, removed and replaced by a glass tube of the same length. The glass tube also had the same internal diameter as the settling length tube, and was manufactured to withstand pressures up to 5 bars. The distance between the top of the glass tube and the bottom flange of the extractor system was 600 mm. This distance was chosen to minimise any effect that the installation of the glass tube might have produced on the flooding process. The glass tube was then surrounded by an aluminium box containing two 800 watt photographic halogen lamps. Ventilation holes were made in the box to disperse the heat produced by the lamps. The illumination arrangement is shown in plate 5.4 .

At the top of the test tube a 200 mm long glass tube was added to the bottom of the T piece and another aluminium box made to surround it. The box contained two 250 watt halogen lamps. Although the centre of the polycarbonate disc at the top of the test tube was occupied by the endoscope, an attempt was made to send light through the rest of this disc. It was found that a 250 watt halogen lamp produced so much heat that it melted the polycarbonate disc, therefore it was replaced by a 250 watt sodium lamp which produced much less heat.

Since the endoscope could move upwards and downwards, in order to position the viewing length at different axial locations, the black and white video camera which accommodated the eye piece of the endoscope, had to move relative to this. Therefore a wooden board was manufactured containing a sliding carriage. The board was placed vertically at the top of the test tube and the camera was mounted on the sliding carriage, which provided the necessary movement. A linear scale was fitted to the board to indicate the axial position of the endoscope viewing lens inside the test tube.

The water droplets had little effect on the radial viewing endoscope as its viewing point was located on the side. In the case of the forward viewing endoscope, although the water droplets were impinging on the viewing lens, no special arrangement was needed to clear the surface since it was inserted in at the centre of the test tube. The air flowrate, with the highest velocity at the centre of the tube, helped to clear the lens viewing surface.

Although it was decided initially that inserting the endoscope from the bottom of the test tube would be undesirable because of interference and disturbance effects, an attempt was made to view the flow from the bottom of the test tube using the radial endoscope device. At 250 mm from the bottom flange of the

extractor system, a hole of 15 mm diameter was drilled at the side of the settling length tube and a 100 mm length of tube of 15 mm inside diameter was welded to the side hole. A similar arrangement made to the polycarbonate disc, in order to lock the endoscope device into position and prevent any fluid from escaping, was repeated at the other end of the side tube when the radial endoscope was inserted as shown in Figure 5.4. The viewing lens was facing up the test section from the bottom. Although this technique of viewing was acceptable to visualise the counter-current flow for the pre-flooding situation, at the flooding situation it was not reliable. As the endoscope device was inserted from the bottom of the test tube, the hole in the polycarbonate disc which had previously been used for locating the endoscope at the top of the test section became unnecessary. This disc was therefore replaced by a new polycarbonate disc and a 50 watt photospot bulb, with internal reflectors, was mounted above it. This arrangement provided the test section with direct light. The disadvantage was that the light was facing the endoscope viewing lens.

(ii) video camera technique : The colour video camera was placed at the top of the test tube and was used to view the flow inside the test section directly. The same alterations to the air offtake system used in the previous technique were employed here also except that the polycarbonate disc was replaced by a polycarbonate rectangular section which was used as a viewing window

for the video camera. The polycarbonate window which was mounted at the top of the test tube, was used to protect the video camera lens from the flow. It was carefully designed and manufactured so that it could be kept clear of all the impinging droplets by means of an air purge flowing diametrically across its lower surface. The polycarbonate window consisted of two polycarbonate plates, the dimensions of each being 300 mm x 100 mm x 10 mm. The first plate had two flat surfaces and formed the top section of the window which had the video camera lens placed on top of it. Therefore it was carefully machined and its centre was highly polished in order to give a very clear view. The second plate which formed the lower section of the window, had a hole of 54.75 mm diameter (the same as the test tube diameter) drilled at the centre and a groove of special shape was made at the top surface of the plate to join the central hole to both sides. When the two plates were joined together, the groove formed a passage for the purging air inlet and outlet. On the inlet side, the depth of the groove varied smoothly from 2 mm at the edge of the hole to 4 mm at the edge of the window. This was to direct the purging air to the bottom of the top section of the viewing window and also to increase the purging air velocity. On the outlet side, the depth of the groove was kept constant at 6.25 mm. The polycarbonate window is illustrated in Figure 5.5. The purging air flow supplied from the main line, through a pipe of 10 mm diameter, controlled by two valves in series, entered the

polycarbonate window, between the two sections from one side and left from the opposite side. Having removed the droplets, it carried on to waste through a pipe of 15 mm diameter, controlled by a manual valve.

To illuminate the glass tube inserted in the settling length tube and its associated equipment, an extra 400 watt photographic halogen lamp was fitted into the aluminium box. The illumination arrangement at the top of the tube section was removed since it was too close to the camera lens and affected the focusing and the quality of the output picture.

The main disadvantage of this illumination technique was that the light did not come from behind the video camera, but from the bottom of the test tube facing the video camera lens. Therefore when the flooding situation took place, and the liquid waves started to block the test tube cross section the light was blocked out and at the same time viewing ceased.

5.3.2 Steam-Water System

The modifications carried out to the test facility in the air-water system were all incorporated in the steam-water system with three additional alterations:

(i) As the illumination inside the test tube was found

to have decreased due to the introduction of steam instead of air, the power of the illumination system placed at the settling length tube was increased to a total of 2400 watts.

(ii) The temperature of the purging air used in the air-water system to clear the lower surface of the polycarbonate window from the impinging water droplets was too low to be used in the steam-water experiments due to the steam condensation on the window surface making viewing by the video camera lens indistinct. Thus a small heat exchanger was used to raise the purge air temperature to the steam saturation temperature before it passed to the polycarbonate window. A superheated steam line was connected to the other side at the heat exchanger for this purpose. The purging air pipe and the steam supply pipe from and to the heat exchanger were all well insulated to minimise heat losses.

(iii) In the steam water experiments, the temperature of the viewing window was close to the steam saturation temperature, and as the video camera was adjacent to this window, it could have been affected by the high temperature. To ensure that the video camera was functioning at normal temperature, a small fan was directed onto the video camera, at the same time ensuring that no air from the fan blew on to the polycarbonate viewing window. For the endoscope system, no alteration was needed as the endoscopes were manufactured to

withstand temperatures as high as 130°C.

5.4 Viewing Procedure

Photographing the flow inside the test section was much more difficult in the steam-water system than in the air-water system. The main problems were high temperature, fluctuations in the test section pressure due to condensation, and the thick layer of steam making viewing indistinct. Furthermore conducting the steam-water tests took much more time and required to be more carefully carried out. However, the viewing procedure used in the air-water system was similar to that used in the steam-water system, and is detailed below for the endoscope and video camera viewing techniques in Sections 5.4.1 and 5.4.2 respectively.

5.4.1 Endoscope Viewing Procedure

Initially the hole in the polycarbonate disc which was made as a passage for the endoscope device was blocked by means of a blank nut. Counter-current annular flow was then established as detailed in Chapter 3 (Section 3.3 for the air-water system and Section 3.4 for the steam-water system). When annular flow was established and the air/steam and the water flowrates adjusted to the desired values, the required endoscope

was inserted through the polycarbonate disc arrangement into the test section and positioned at the required axial location. The video camera was mounted at the top of the endoscope to accommodate the eye piece. The endoscope was connected to the light source and the external illumination systems were switched on. The endoscope was then focused and when the clearest view was obtained on the monitor, the video recorder was switched on and the air/steam flowrate increased in small steps until the flooding occurred.

The same procedure was used when it was decided to view the flow and the flooding situation inside the test section by the naked eye instead of the video camera.

5.4.2 Video Camera Viewing Procedure

To start the viewing procedure, the polycarbonate window was carefully cleaned, and the lower surface of the window was covered with a very thin layer of silicone grease in order to decrease the ability of the water droplets to stick to the window surface and at the same time to increase the efficiency of the impinging air in removing these droplets. The polycarbonate window was then replaced on top of the test tube and the purging air inlet and outlet valves closed. The video camera was mounted on the top of the polycarbonate to allow the camera lens to be placed as close as possible to the

window in order to obtain a satisfactory angle of view. The normal procedure of establishing annular counter-current flow of air/steam and water was then carried out as was described in Chapter 3 (Section 3.3 for air-water tests and Section 3.4 for steam-water tests). As the air/steam and water flowrates were adjusted to the required values, the purge air outlet was opened fully and remained so for the rest of the experimental test. The purge air inlet valve was then turned full on in order to clear the window of the droplets of water which had adhered to it while establishing annular flow. It was then turned down until the droplets impinged on the lower surface of the polycarbonate window and then increased just enough to clear the window. This procedure ensured that the minimum amount of purging air was used to keep the polycarbonate window and viewing surface clear and hence any side effects were kept to a minimum. The illuminating system, the video camera and the rest of the viewing system were switched on and the video camera focused at the required axial location of the test section. The procedure of increasing the air/steam flowrates in small steps was carried out until flooding was obtained. As the air flowrate increased the amount of entrained droplets also increased and so the purge air flowrate had to be readjusted after each step to keep the window as clear as possible.

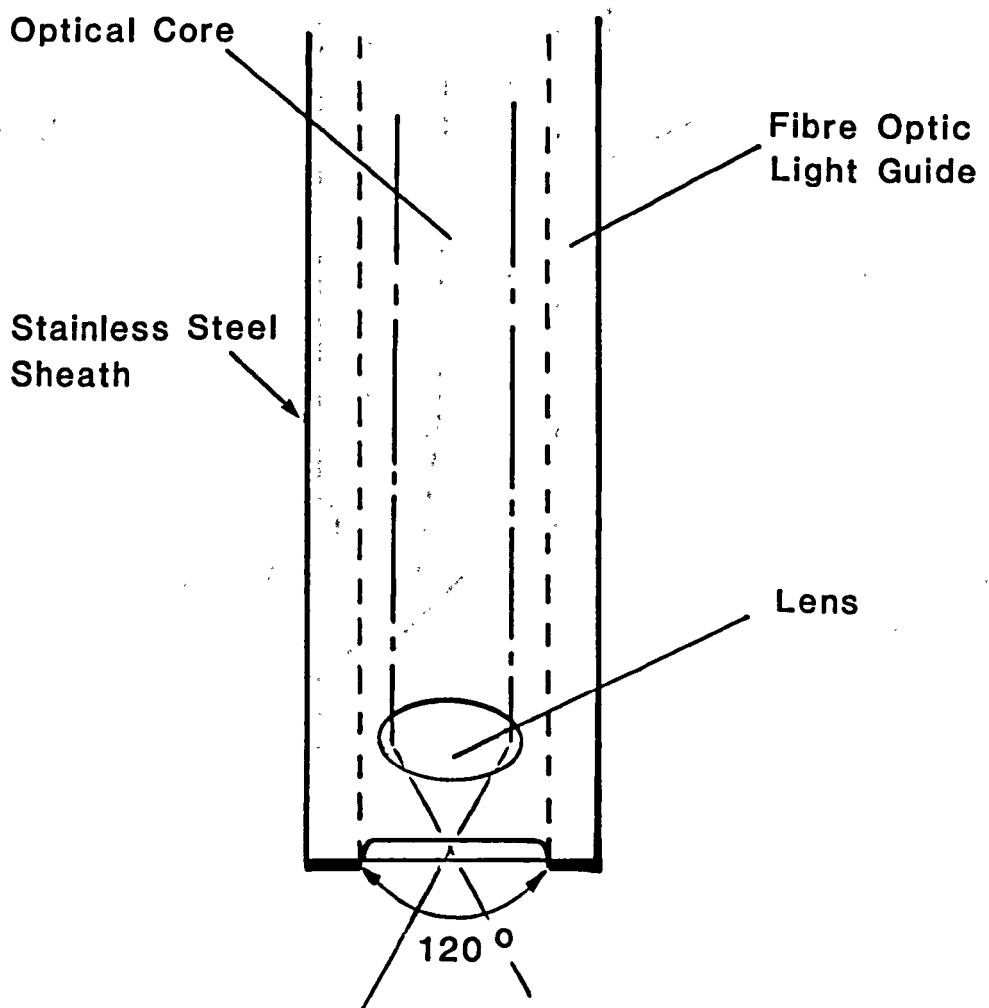


Figure 5.1 Principle of Forward Viewing Endoscope

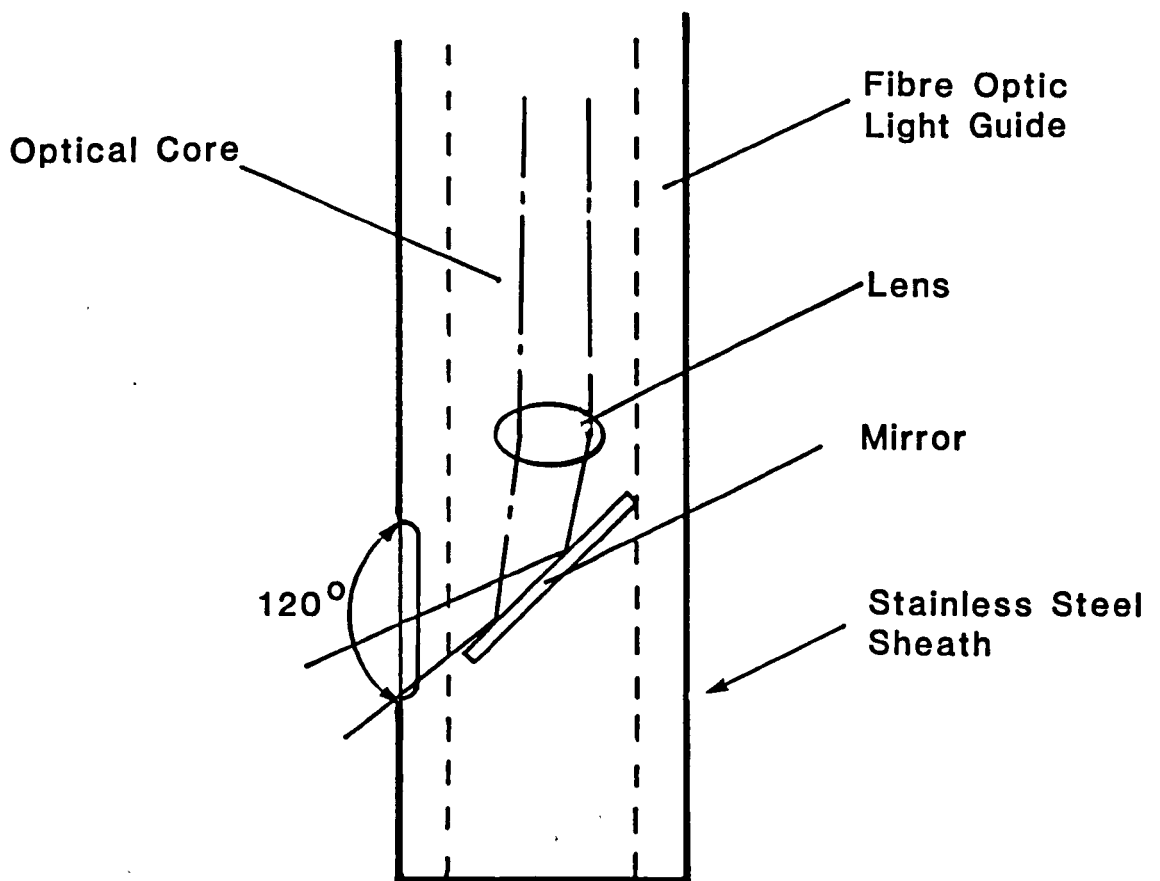


Figure 5.2 Principle of Radial Viewing Endoscope

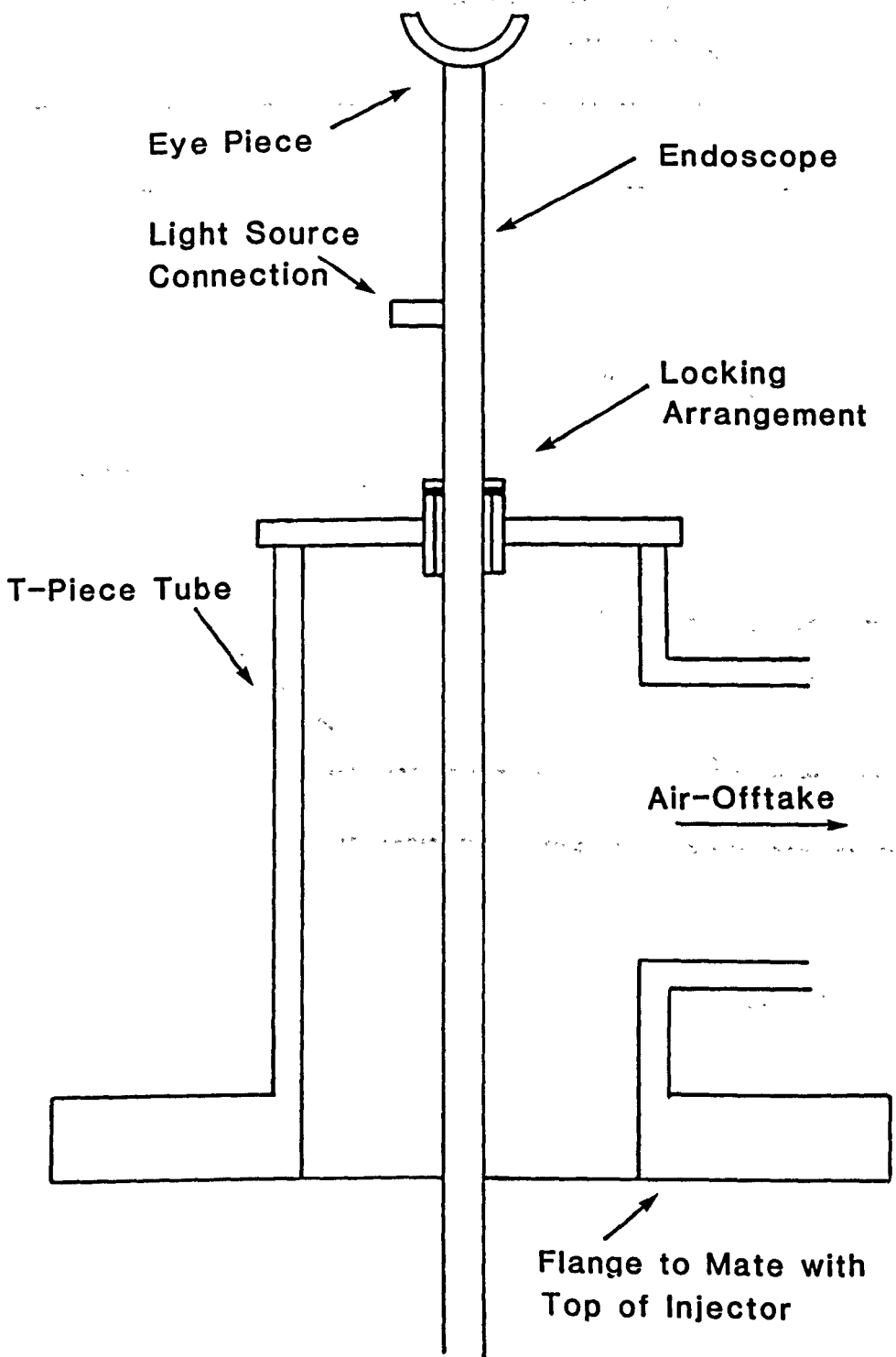


Figure 5.3 Endoscope Top Mounting

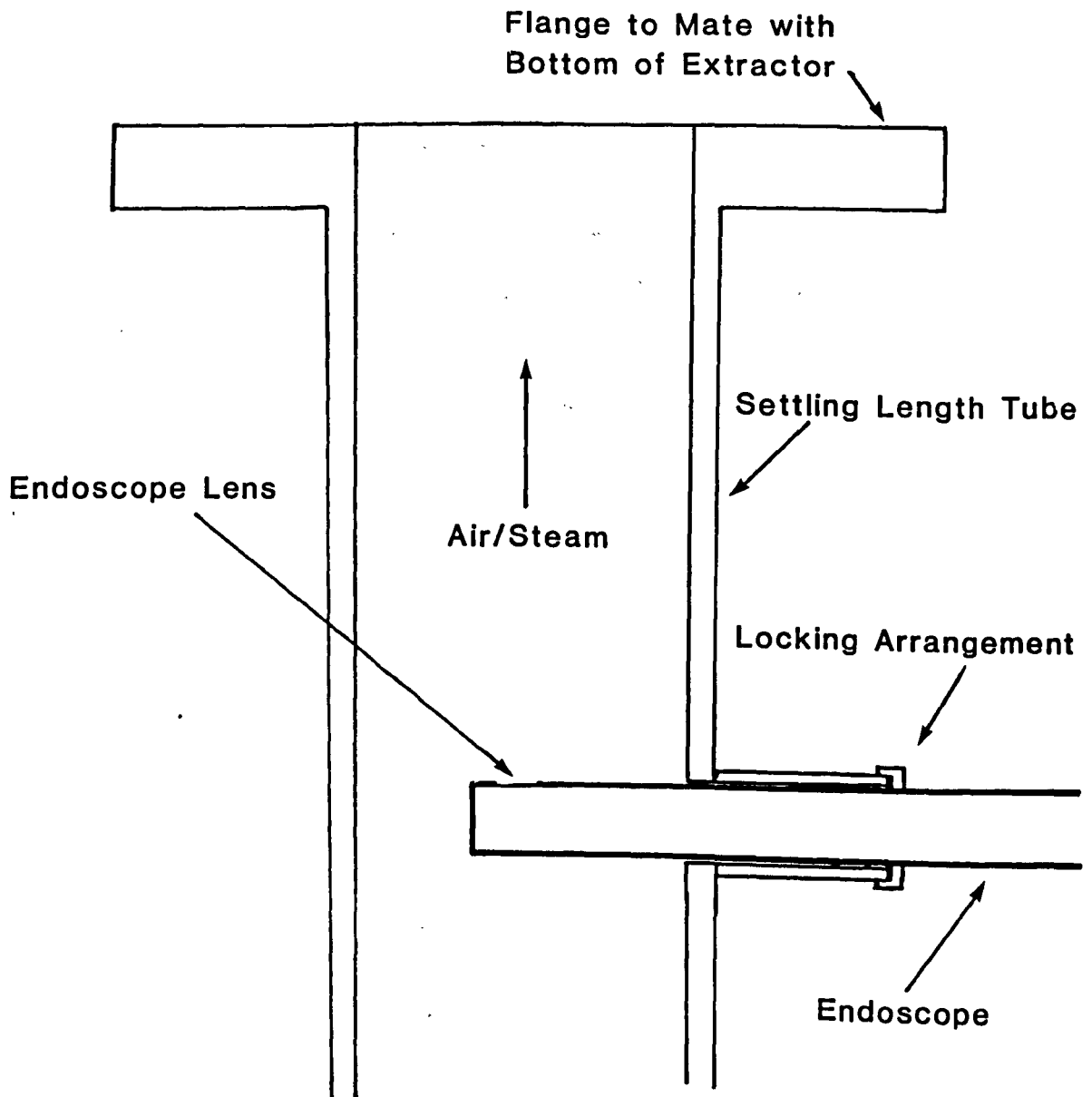


Figure 5.4 Radial Endoscope Bottom Mounting

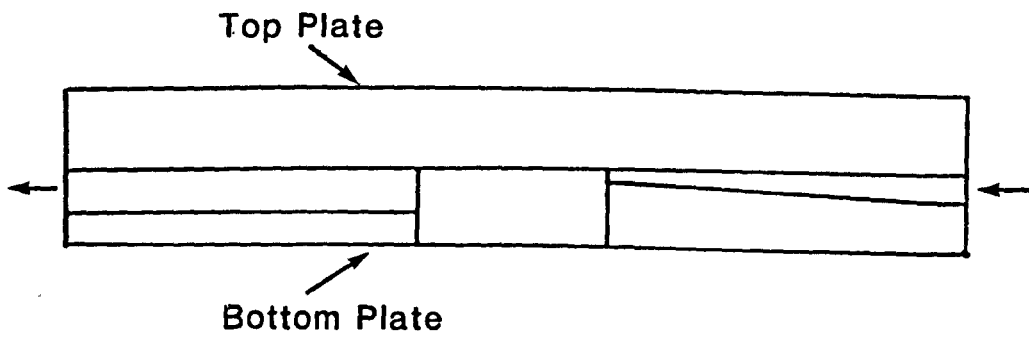
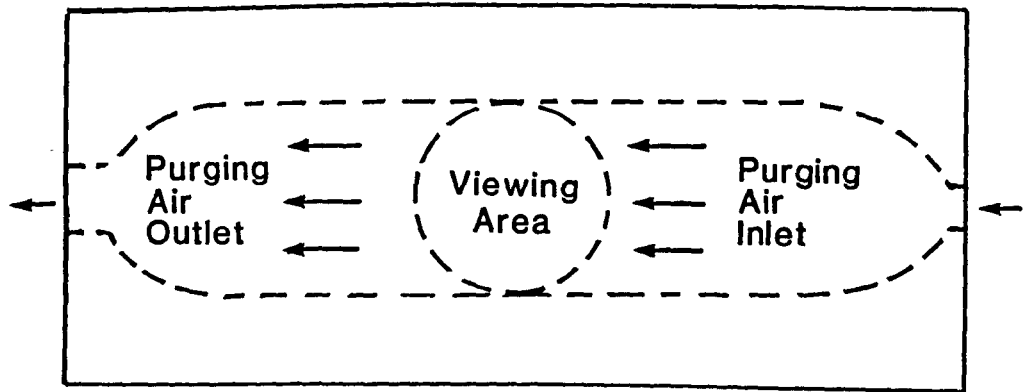
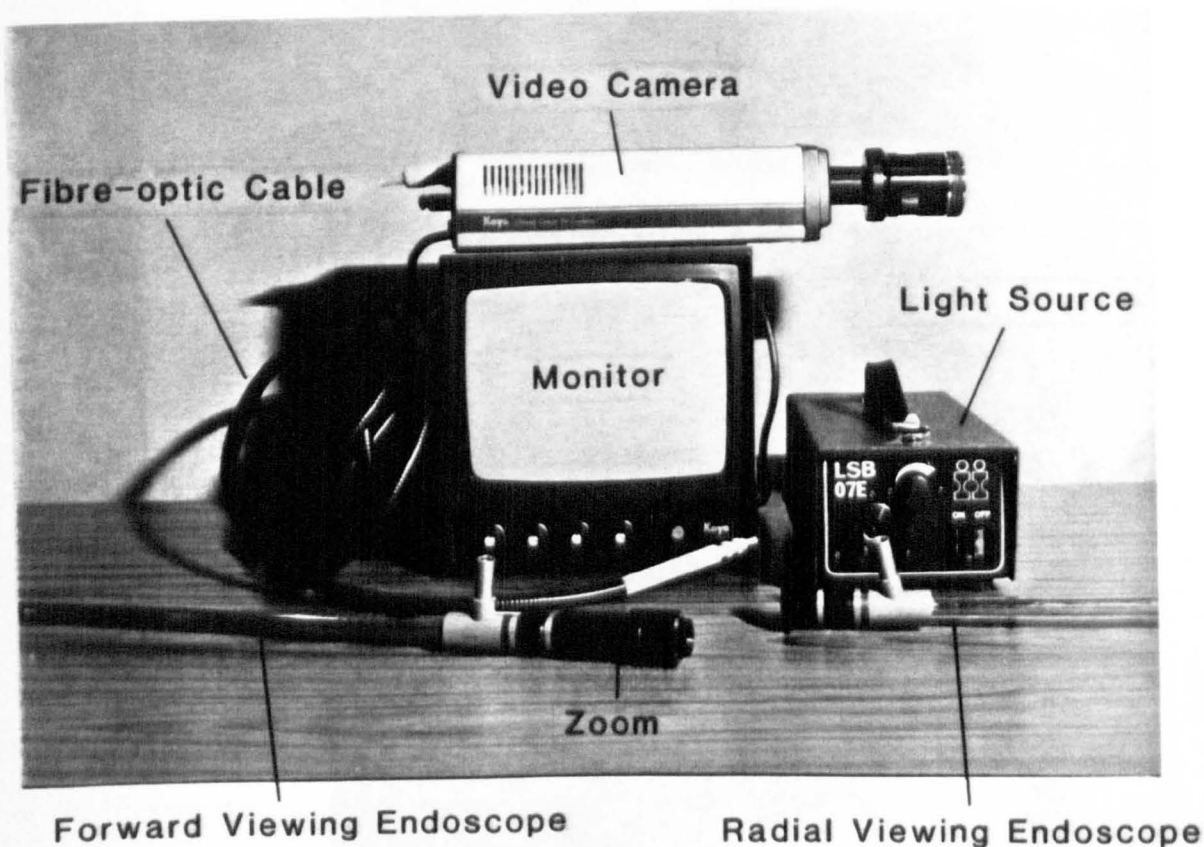
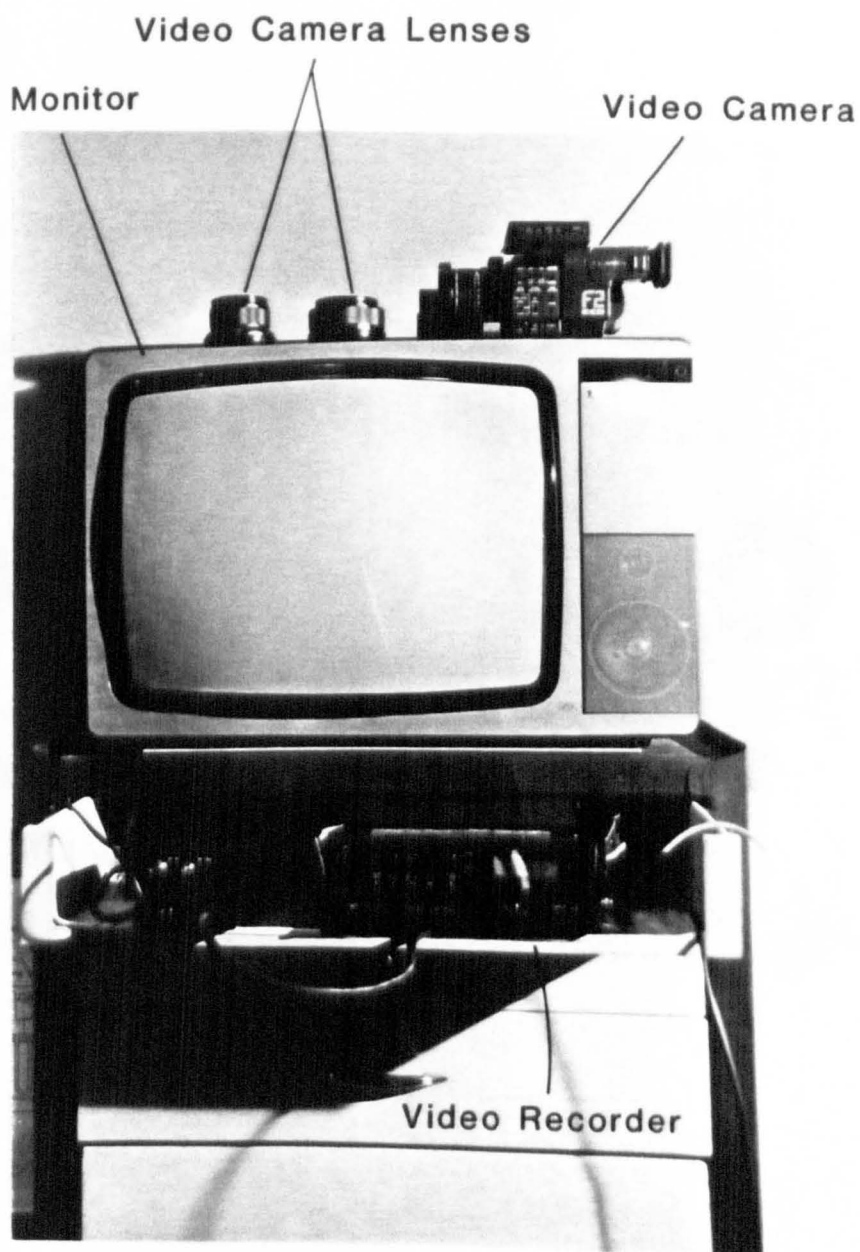


Figure 5.5 Viewing Window Arrangement



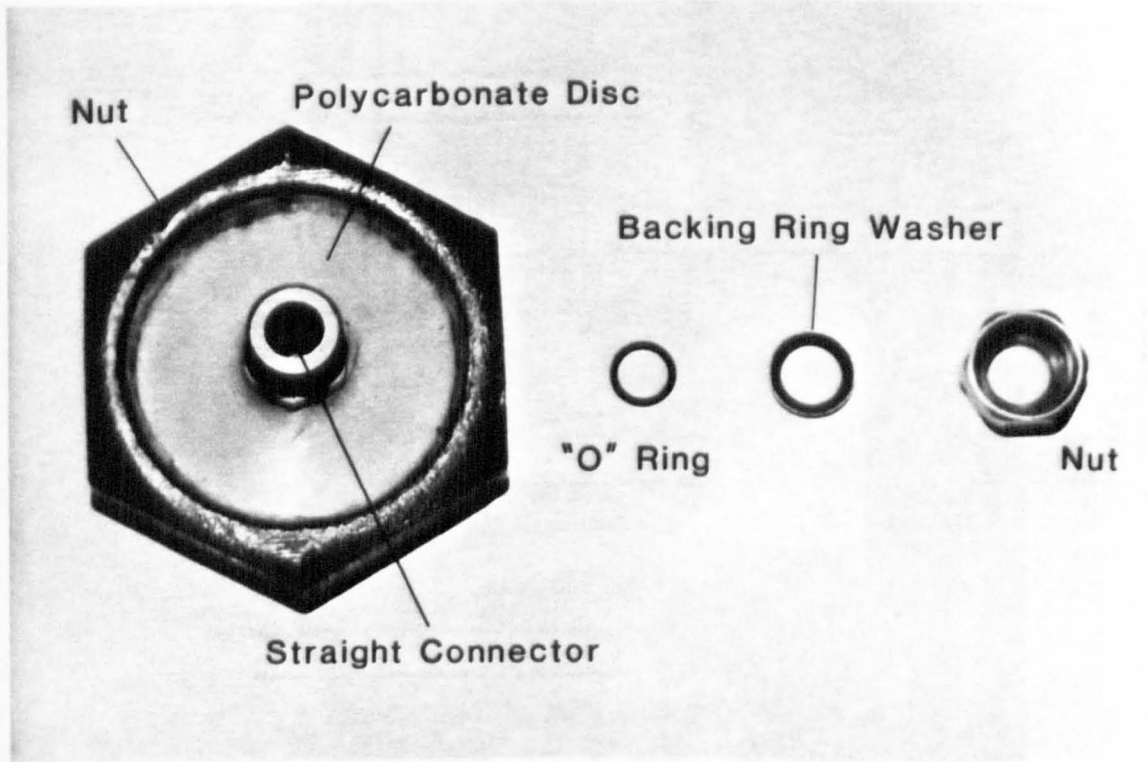
Endoscope Viewing Equipment

PLATE 5.1



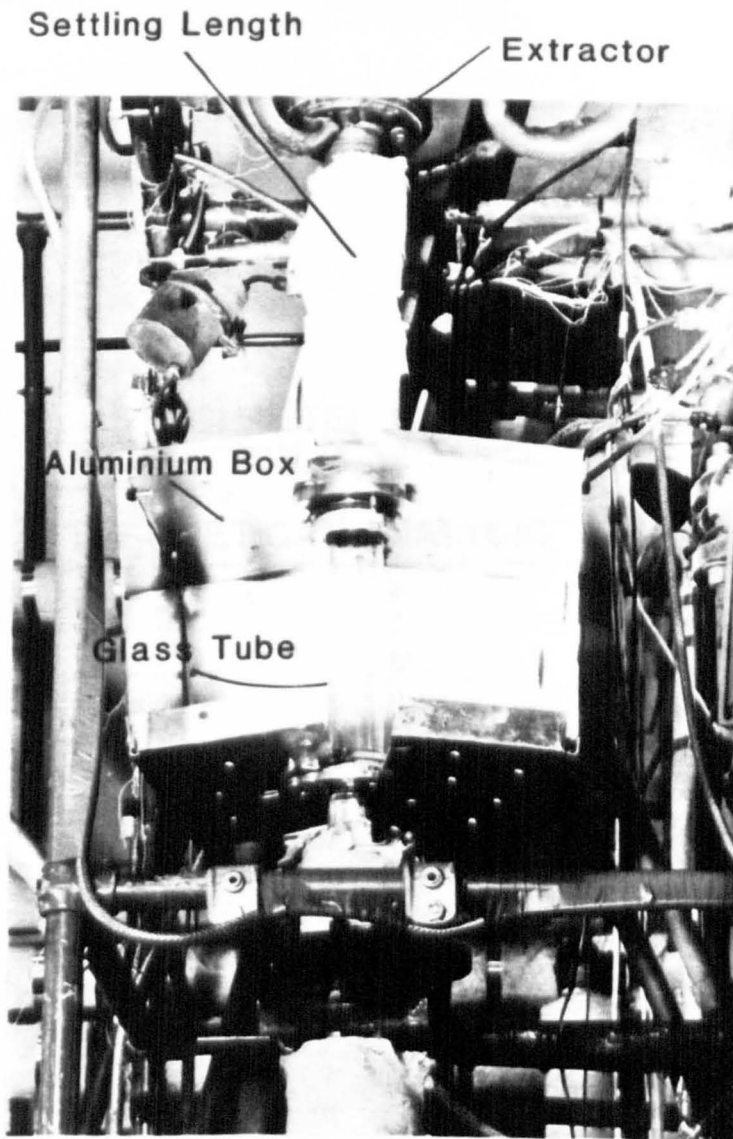
Video Camera Viewing Equipment

PLATE 5.2



Endoscope Locator Assembly

PLATE 5.3



Illumination Arrangement

PLATE 5.4

CHAPTER 6

THEORETICAL ANALYSIS

CHAPTER 6THEORETICAL ANALYSIS

It has been widely reported that the effect of condensation on flooding conditions may be very significant, especially in counter-current two-phase flow. In this chapter, a theoretical investigation into condensation effects on the liquid thickness and the flooding conditions is presented. The investigation was carried out in three stages. The first stage involved modelling the liquid film thickness along the solid wall of the tube with the continuity, momentum and energy equations being solved for the liquid film flow, as described in Section 6.1. The second stage involved modelling the temperature of the liquid film across and along the tube and this was developed by evaluating the effective turbulent thermal diffusivity, which led to an estimate of the turbulent viscosity of the film, as described in Section 6.2. The final stage produced a flooding model based on a linear stability analysis of a uniform film and was derived to accommodate the vapour-liquid flooding condition under which substantial condensation took place. This is presented in Section 6.3.

6.1 Film Thickness Analysis

In an attempt to model the film thickness and the effect of condensation in annular counter-current flow, the mass, momentum and energy balances are approximated for a liquid film flowing down the solid wall of a tube and with the vapour phase flowing up the centre of the tube. The governing equations, which describe the interaction between the vapour and liquid phases are based on the following assumptions: (i) The flow is steady, incompressible and one-dimensional (ii) The mass transfer is due to condensation (iii) The vapour phase is dry saturated and the saturation temperature remains constant (iv) Non-condensable gases are not present.

6.1.1 Mass Balance

Considering the control volume shown in Figure 6.1, the mass balance can be written as:

$$\left(M_g + \frac{d}{dz}(M_g)dz \right) - M_g + M_f - \left[M_f + \frac{d}{dz}(M_f)dz \right] = 0 \quad (6.1)$$

and hence

$$\frac{d}{dz}(M_f) = \frac{d}{dz}(M_g) \quad (6.2)$$

6.1.2 Momentum Balance

In the momentum balance, the net force acting on each phase in the direction of motion is equal to the rate of change of momentum of that phase. Applying this balance to both liquid and vapour phases, considering the control volume shown on Figure 6.2, yields:

(i) Liquid Phase:

$$\begin{aligned}
 & \left[\left(\frac{\pi D^2}{4} - \frac{\pi}{4} (D-2\delta)^2 \right) p_f \right] - \left[\left(\frac{\pi D^2}{4} - \frac{\pi}{4} \left(D - 2 \left(\delta + \frac{d\delta}{dz} dz \right) \right)^2 \right) \left(p_f + \frac{dp_f}{dz} dz \right) \right] + \\
 & \left[\left(\frac{\pi D^2}{4} - \frac{\pi}{4} \left(D - 2 \left(\delta + \frac{d\delta}{dz} dz \right) \right)^2 \right) - \left(\frac{\pi D^2}{4} - \frac{\pi}{4} (D-2\delta)^2 \right) \right] \left[- \left(p_i + \left(p_i + \frac{dp_i}{dz} dz \right) \right) \right] \\
 & - \left[\frac{1}{2} \left(\pi (D-2\delta) + \pi \left(D - 2 \left(\delta + \frac{d\delta}{dz} dz \right) \right) \right) dz \tau_{fiz} \right] - \left[\pi D dz \tau_w \right] + \\
 & \left[\rho_f g \frac{1}{2} \left(\left(\frac{\pi D^2}{4} - \frac{\pi}{4} (D-2\delta)^2 \right) + \frac{\pi D^2}{4} - \frac{\pi}{4} \left(D - 2 \left(\delta + \frac{d\delta}{dz} dz \right) \right)^2 \right) dz \right] = \\
 & \left[M_f U_f \frac{d}{dz} (M_f U_f) dz \right] - M_f U_f - U_g \frac{d}{dz} (M_g) dz \quad (6.3)
 \end{aligned}$$

where τ_{fiz} is the vertical component of τ_{fi}

and p_i is the interfacial pressure

Simplifying equation 6.3 (see Appendix D), gives

$$\frac{dp}{dz} = -\frac{(D-2\delta)}{\delta(D-\delta)} \tau_{fiz} - \frac{D}{\delta(D-\delta)} \tau_w + \rho_f g + \frac{(D-2\delta)\rho_f U_f^2}{\delta(D-\delta)} \frac{d\delta}{dz} - \frac{2U_f}{\pi\delta(D-\delta)} \frac{d}{dz}(M_f) + \frac{U_g}{\pi\delta(D-\delta)} \frac{d}{dz}(M_g) \quad (6.4)$$

(ii) Vapour Phase

$$\begin{aligned} & \left[\frac{\pi}{4}(D-2\delta)^2 p_g - \left(\frac{\pi}{4}(D-2(\delta + \frac{d\delta}{dz}))^2 \right) \left(p_g + \frac{dp_g}{dz} dz \right) \right] - \left[\frac{1}{2} \left(p_i + \left(p_i + \frac{dp_i}{dz} dz \right) \right) \right. \\ & \left. \left(\frac{\pi}{4}(D-2(\delta + \frac{d\delta}{dz}))^2 - \frac{\pi}{4}(D-2\delta)^2 \right) \right] + \left[\frac{1}{2} (\pi(D-2\delta) + \pi(D-2(\delta + \frac{d\delta}{dz}))) \right. \\ & \left. dz \tau_{giz} \right] + \left[\rho_g g \left(\frac{1}{2} \frac{\pi}{4}(D-2\delta)^2 + \frac{\pi}{4}(D-2(\delta + \frac{d\delta}{dz}))^2 \right) dz \right] = \\ & - \left[\left(M_g U_g + \frac{d}{dz}(M_g U_g) dz \right) - M_g U_g - U_g \frac{dM_g}{dz} dz \right] \quad (6.5) \end{aligned}$$

where τ_{giz} is the vertical component of τ_{gi}

Simplifying equation (6.5) (see Appendix D), gives:

$$\frac{dp}{dz} = \frac{4}{(D-2\delta)} \tau_{giz} + \rho_g g + \frac{4\rho_g U_g^2}{(D-2\delta)} \frac{d\delta}{dz} + \frac{4U_g}{\pi(D-2\delta)^2} \frac{d}{dz}(M_g) \quad (6.6)$$

6.1.3 Energy Conservation

When a saturated vapour moves counter-current to a subcooled liquid film, condensation occurs and energy is transferred. Considering the control volume shown in Figure 6.3, the energy balance is:

$$[M_f \bar{h}_{fL} + (M_g h_g + \frac{d}{dz}(M_g h_g) dz)] - [M_g h_g + (M_f \bar{h}_{fL} + \frac{d}{dz}(M_f \bar{h}_{fL}) dz)] = q_w \quad (6.7)$$

This could be deduced (see Appendix D), to give:

$$\frac{d}{dz}(M_f) = \frac{M_f C_{pf}}{h_{fg} + C_{pf}(T_s - T_f)} \frac{d}{dz}(\bar{T}_f) \quad (6.8)$$

It is assumed that there is no slip between the two phases at the interface, therefore

$$\tau_{gi} = \tau_{fi} = \tau_i \quad (6.9)$$

and since θ is a very small angle, Figure 6.4, then

$$\tau_{giz} = \tau_{fiz} = \tau_i \quad (6.10)$$

Substituting equation (6.2) into equations (6.4) and (6.6), and eliminating the pressure gradient, gives

$$\frac{d\delta}{dz} = \left\{ \frac{(D-2\delta)^2 + 4\delta(D-\delta)}{\delta(D-\delta)(D-2\delta)} \tau_i + \frac{D\tau_w}{\delta(D-\delta)} - (\rho_f - \rho_g)g + \left(\frac{2U_f - U_g}{\pi\delta(D-\delta)} + \frac{4U_g}{\pi(D-2\delta)^2} \right) \frac{dM_f}{dz} \right\} / \left\{ \frac{(D-2\delta)\rho_f u_f^2}{\delta(D-\delta)} - \frac{4\rho_g u_g^2}{(D-2\delta)} \right\} \quad (6.11)$$

6.1.4 Wall Shear Stress

The wall shear stress can be expressed by the relationship

$$\tau_w = f_w \frac{1}{2} \rho_f U_f^2 \quad (6.12)$$

where f_w is the wall friction factor.

The film thickness effect on the distribution of f_w can be neglected (WALLIS, 1970), with f_w represented by

$$f_w = \frac{C}{(Re_f)^n} \quad (6.13)$$

where in smooth tubes,

$$C = 16 \text{ and } n = 1 \text{ for laminar flow} \quad (6.14)$$

and

$$C = 0.079 \text{ and } n = 0.25 \text{ for turbulent flow.} \quad (6.15)$$

6.1.5 Interfacial Shear Stress

The interfacial shear stress is computed from the widely reported correlation for adiabatic flow:-

$$\tau_i = \frac{1}{2} \rho_g f_i (U_g - U_f)^2 \quad (6.16)$$

The interphase momentum transfer between the two phases, liquid and vapour, is not included in the above correlation because it has been taken into account in both

the liquid and vapour momentum equations, (6.3) and (6.5) respectively.

For annular counter-current flow of liquid and gas in vertical tubes, BHARATHAN et al (1979) recommended that the interfacial friction factor, f_i , be represented by the following relations

$$f_i = 0.005 + a(D^*/2)^b(1-\sqrt{\alpha})^b \quad (6.17)$$

where

$$\log_{10} a = -0.56 + 9.07/D^* \quad (6.18)$$

$$b = 1.63 + 4.74/D^* \quad (6.19)$$

and

$$D^* = \text{Bond No.} = \frac{\sigma}{g(\rho_f - \rho_g)^{1/2}} \quad (6.20)$$

Substituting the values of τ_i and τ_w into equation (6.11), and re-arranging gives

$$\frac{d\delta}{dz} = \left\{ \frac{D^2}{2(D^2\delta - 3\delta^2D + 2\delta^3)} \rho_g f_i (U_g - U_f)^2 + \frac{DC\rho_f U_g^2}{(Re_f)^n} - (\rho_g - \rho_g)g \right.$$

$$\left. \left[\frac{2U_f - U_g}{\pi\delta(D-\delta)} + \frac{4U_g}{\pi(D-2\delta)^2} \right] \frac{dM_f}{dz} \right\} / \left\{ \frac{(D-2\delta)\rho_f U_f^2}{\delta(D-\delta)} - \frac{4\rho_g U_g^2}{(D-2\delta)} \right\}$$

(6.21)

Consider the non-dimensional terms

$$\begin{aligned}
 z^+ &= z/L & Fr_f &= \frac{u_f}{(gL)^{1/2}} = \frac{Q_f}{\pi\delta(D-\delta)(gL)^{1/2}} \\
 \delta^+ &= \delta/L & Fr_g &= \frac{u_g}{(gL)^{1/2}} = \frac{4Q_g}{\pi(D-2\delta)^2(gL)^{1/2}} & (6.22) \\
 D^+ &= D/L \\
 \rho^+ &= \rho_g/\rho_f & Re_f &= \frac{\rho_f Q_f}{\pi(D-\delta)\mu_f}
 \end{aligned}$$

then equation (6.21) can be made dimensionless by using equation (6.22) and re-arranging, to give

$$\begin{aligned}
 \frac{d\delta^+}{dz^+} &= \left\{ \frac{D^{+2}}{2D^{+2}\delta^+ - 6\delta^{+2}D^+ + 4\delta^{+3}} f_i \rho^+ (Fr_g - Fr_f)^2 + \frac{D^+ C Fr_f^2}{2\delta^+(D-\delta^+)(Re_f)^n} \right. \\
 &\quad \left. -(1-\rho^+) + \left[\frac{2Fr_f - Fr_g}{\pi\delta^+(D^+ - \delta^+)} + \frac{4Fr_g}{\pi(D^+ - 2\delta^+)^2} \right] \frac{1}{\rho_f (gL)^{1/2}} \frac{dM_f}{dz} \right\} / \\
 &\quad \left\{ \frac{(D^+ - 2\delta^+) Fr_f^2}{\delta^+(D^+ - \delta^+)} - \frac{4\rho^+ Fr_g^2}{(D^+ - 2\delta^+)} \right\} & (6.23)
 \end{aligned}$$

Substituting equation (6.8) into equation (6.23) gives

$$\begin{aligned}
 \frac{d\delta^+}{dz^+} &= \left\{ \frac{D^{+2}}{2D^{+2}\delta^+ - 6\delta^{+2}D^+ + 4\delta^{+3}} f_i \rho^+ (Fr_g - Fr_f)^2 + \frac{D^+ C Fr_f^2}{2\delta^+(D-\delta^+)(Re_f)^n} \right. \\
 &\quad \left. -(1-\rho^+) + \left[\frac{2Fr_g - Fr_f}{\pi\delta^+(D^+ - \delta^+)} + \frac{4Fr_g}{\pi(D^+ - 2\delta^+)^2} \right] \frac{\pi\delta(D-\delta)U_f}{L(gL)^{1/2}} \right. \\
 &\quad \left. \frac{Cp_f}{h_{fg} + Cp_f(T_s - T_f)} \frac{d\bar{T}_f}{dz} \right\} / \left\{ \frac{(D^+ - 2\delta^+) Fr_f^2}{\delta^+(D^+ - \delta^+)} - \frac{4\rho^+ Fr_g^2}{(D^+ - 2\delta^+)} \right\} & (6.24)
 \end{aligned}$$

Consider the non-dimensional terms of

$$\begin{aligned} T^+ &= \bar{T}_f / T_{in} \\ T_s^+ &= T_s / T_{in} \\ HCP^+ &= h_{fg} / C_{p_f} T_{in} \end{aligned} \quad (6.25)$$

Substituting (6.41) into equation (6.40), gives

$$\begin{aligned} \frac{d\delta^+}{dz^+} &= \left\{ \frac{D^{+2}}{(2D^{+2}\delta - 6\delta^{+2}D^+ + 4\delta^{+2})} f_{i\rho^+} (Fr_g - Fr_f)^2 + \frac{D^+ C Fr_f^2}{2(\delta^+ D^+ - \delta^{+2})(Re_f)^n} \right. \\ &\quad \left. - (1 - \rho^+) + \left[\frac{2Fr_f - Fr_g}{(\delta^+ D^+ - \delta^{+2})} + \frac{4Fr_g}{(D^+ - 2\delta^+)^2} \right] \right. \\ &\quad \left. \frac{Fr_f \delta^+ (D^+ - \delta^+)}{HCP^+ + (T_s^+ - T^+)} \frac{dT^+}{dz^+} \right\} / \left\{ \frac{(D^+ - 2\delta^+) Fr_f^2}{(\delta^+ D^+ - \delta^{+2})} - \frac{4\rho^+ Fr_g^2}{(D^+ - 2\delta^+)} \right\} \end{aligned} \quad (6.26)$$

As $\delta \ll D$, then equation (6.26) can be written as

$$\begin{aligned} \frac{d\delta^+}{dz^+} &= \left\{ \frac{1}{2\delta^+} f_{i\rho^+} (Fr_g - Fr_f)^2 + \frac{C Fr_f^2}{2\delta^+ (Re_f)^n} - (1 - \rho^+) + \right. \\ &\quad \left[\frac{Fr_f - Fr_g}{\delta^+ D^+} + \frac{4Fr_g}{(D^+ - 2\delta^+)^2} \right] \frac{\delta^+ D^+ Fr_f}{HCP^+ + (T_s^+ - T^+)} \frac{dT^+}{dz^+} \bigg\} / \\ &\quad \left\{ \frac{Fr_f^2}{\delta^+} - \frac{4\rho^+ Fr_g^2}{(D^+ - 2\delta^+)} \right\} \end{aligned} \quad (6.27)$$

Equation (6.27) represents the variation in the film

thickness along the test tube. The first term allows for the effect of the interfacial shear stress; the second term, the wall shear stress effect; the third term the gravitational effect and the final term, the condensation effect on the variation of the film thickness. The evaluation of the liquid film mean temperature \bar{T}_f is given in the next section.

6.2 Film Temperature Analysis

For a liquid film flowing down an adiabatic vertical wall, the two dimensional energy equation for incompressible, steady flow and neglecting diffusion in the z-direction, Figure 6.5, is given as

$$u \frac{\partial T}{\partial z} = \frac{\partial}{\partial y} (\epsilon_H + K) \frac{\partial T}{\partial y} \quad (6.28)$$

where ϵ_H is the eddy diffusivity of heat, and

$$K = \frac{k_f}{\rho_f C_{p_f}} \quad (6.29)$$

where k_f is the liquid thermal conductivity.

Equation (6.28) represents the energy equation for laminar ($\epsilon_H = 0$) and turbulent flow.

Assuming u and $(\epsilon_H + K)$ are functions of z only, such that

$$u = U_f \text{ and } (\epsilon_H + K) = (\overline{\epsilon_H + K})$$

Then

$$U_f \frac{\partial T}{\partial z} = (\epsilon_H + K) \frac{\partial^2 T}{\partial y^2} \quad (6.30)$$

or

$$\frac{1}{\alpha(z)} \frac{\partial T}{\partial z} = \frac{\partial^2 T}{\partial y^2} \quad (6.31)$$

where

$$\alpha(z) = \frac{\overline{\epsilon_H + K}}{U_f} \quad (6.32)$$

z

$$\text{if, } \zeta = \int_0^z \alpha(z) dz \quad (6.33)$$

i.e.

$$d\zeta = \alpha(z) dz \quad (6.34)$$

Then equation (6.31), becomes

$$\frac{\partial T}{\partial \zeta} = \frac{\partial^2 T}{\partial y^2} \quad (6.35)$$

The boundary conditions (Figure 6.5) are:

$$(i) \quad T = T_t \text{ at } \zeta = 0$$

$$(ii) \quad \frac{\partial T}{\partial z} = 0 \text{ at } y = 0$$

$$(iii) \quad T = T_s \text{ at } y = \delta$$

$$(iv) \quad T = T_w \text{ at } y = 0$$

Equation (6.35) can be solved by separation of variables and Fourier series, in the same manner as CARSLAW and JAEGER (1953). Using the first three boundary conditions gives a solution of the form

$$T = T_s + \frac{2}{\delta} \sum_{i=0}^{\infty} \exp\left[-\frac{(2i+1)^2 \pi^2 \zeta}{4\delta^2}\right] \cos\frac{(2i+1)\pi y}{2\delta} \left\{ \frac{2\delta(-1)^{i+1}}{(2i+1)\pi} T_s + \int_0^{\delta} T_t \cos\frac{(2i+1)\pi y'}{2\delta} dy' \right\} \quad (6.36)$$

integrating equation (6.36) and re-arranging, gives

$$\frac{T - T_s}{T_t - T_s} = \frac{4}{\pi} \sum_{i=0}^{\infty} \frac{(-1)^i}{(2i+1)} \exp\left[-\frac{(2i+1)^2 \pi^2 \zeta}{4\delta^2}\right] \cos\frac{(2i+1)\pi y}{2\delta} \quad (6.37)$$

Applying boundary condition (iv) to equation (6.37) gives the variation of wall temperature T_w with ζ .

$$\frac{T_w - T_s}{T_t - T_s} = \frac{4}{\pi} \sum_{i=0}^{\infty} \frac{(-1)^i}{(2i+1)} \exp\left[-\frac{(2i+1)^2 \pi^2 \zeta}{4\delta^2}\right] \quad (6.38)$$

The mean film temperature \bar{T}_f as a function of δ , can be written as

$$\bar{T}_f = \frac{1}{\delta} \int_0^{\delta} T dy \quad (6.39)$$

Using equation (6.39) and equation (6.37) gives

$$\frac{\bar{T}_f - T_s}{T_t - T_s} = \frac{4}{\pi} \sum_{i=0}^{\infty} \frac{(-1)^i}{(2i+1)} \exp\left[-\frac{(2i+1)^2 \pi^2 \zeta}{4\delta^2}\right] \frac{1}{\delta} \int_0^{\delta} \cos \frac{(2i+1)\pi y}{2\delta} dy \quad (6.40)$$

integrating equations (6.40) and re-arranging, gives

$$\frac{\bar{T}_f - T_s}{T_t - T_s} = \frac{4}{\pi} \sum_{i=0}^{\infty} \frac{(-1)^i}{(2i+1)} \exp\left[-\frac{(2i+1)^2 \pi^2 \zeta}{4\delta^2}\right] \frac{2}{(2i+1)\pi} \sin \frac{(2i+1)\pi y}{2} \quad (6.41)$$

re-arranging, gives

$$\frac{\bar{T}_f - T_s}{T_t - T_s} = \frac{8}{\pi} \sum_{i=0}^{\infty} \frac{1}{(2i+1)^2} \exp\left[-\frac{(2i+1)^2 \pi^2 \zeta}{4\delta^2}\right] \quad (6.42)$$

dividing equation (6.42) by (6.38), gives

$$\frac{\bar{T}_f - T_s}{T_w - T_s} = \frac{2}{\pi} \frac{\sum_{i=0}^{\infty} \frac{1}{(2i+1)^2} \exp\left[-\frac{(2i+1)^2 \pi^2 \zeta}{4\delta^2}\right]}{\sum_{i=0}^{\infty} \frac{(-1)^i}{(2i+1)} \exp\left[-\frac{(2i+1)^2 \pi^2 \zeta}{4\delta^2}\right]} \quad (6.43)$$

Equation (6.43) gives the film mean temperature at a wall temperature T_w for a given value of ζ .

Since T_w values along the test tube are known (from experimental measurements), a knowledge of ζ values is required in order to evaluate \bar{T}_f .

Assuming that

$$\alpha(z) = a_0 + a_1 z + a_2 z^2 + \dots + a_n z^n \quad (6.44)$$

Then

$$\zeta = \int_0^z \alpha(z) dz = a_0 z + \frac{a_1}{2} z^2 + \frac{a_2}{3} z^3 + \dots + \frac{a_n}{n+1} z^{n+1} \quad (6.45)$$

Using equation (6.45) with (6.38) and (6.42) gives, respectively

$$\frac{T_w - T_s}{T_t - T_s} = \frac{4}{\pi} \sum_{i=0}^{\infty} \frac{(-1)^i}{(2i+1)} \exp\left\{-\frac{(2i+1)^2 \pi^2}{4\delta^2} \left[a_0 z + \frac{a_1}{2} z^2 + \dots + \frac{a_n}{n+1} z^{n+1} \right]\right\} \quad (6.46)$$

and

$$\frac{\bar{T}_f - T_s}{T_t - T_s} = \frac{8}{\pi} \sum_{i=0}^{\infty} \frac{(-1)^i}{(2i+1)^2} \exp\left\{-\frac{(2i+1)^2 \pi^2}{4\delta^2} \left[a_0 z + \frac{a_1}{2} z^2 + \dots + \frac{a_n}{n+1} z^{n+1} \right]\right\} \quad (6.47)$$

Fitting equation (6.46) to the experimental data with $T_w = T_{wexp}$, the constants a_0, a_1, \dots, a_n , and the index n can be evaluated. Substituting these values into equation (6.47) gives the liquid film mean temperature at any position along the tube and at any thickness across the liquid film.

6.3 Flooding with Uniform Film Including Condensation:

This part of the analysis is a modification to previous work carried out in this University by McNeil (1986) and it is carried out by introducing a new term to the velocity potential equation accounting for condensation velocity effect, so that the velocity potential in a stream of vapour flow with flat interface, Figure 6.6, can be defined as

$$\phi = U_f z + V_g Y \quad (6.48)$$

Then

$$u = \frac{\partial \phi}{\partial z} = U_f \quad (6.49)$$

and

$$v = \frac{\partial \phi}{\partial Y} = V_g \quad (6.50)$$

The velocity potential can be represented by

$$\phi = U_f z + V_g Y + \phi' \quad (6.51)$$

where ϕ' is the velocity potential variation due to the perturbation, then

$$\frac{\partial^2 \phi'}{\partial z^2} + \frac{\partial^2 \phi'}{\partial Y^2} = 0 \quad (6.52)$$

The solution of equation (6.52) (see Appendix D) can be given by

$$\phi' = [i(u-c)\eta_0 - \frac{V_g \eta_0}{k\delta}] \exp[-k(y-\delta)] \exp[ik(z-ct)] \quad (6.53)$$

where

$$\eta = \eta_0 \exp [ik(z-ct)] \quad (6.54)$$

Applying equation (6.53) for the liquid phase when $u = U_f'$ then

$$\phi'_f = [i(U_f - c)] \eta_0 \exp [ik(y-\delta)] \exp [ik(z-ct)] \quad (6.55)$$

and for the vapour phase where $u = -U_g$ to give

$$\phi'_g = -\left(i(U_g - c) + \frac{v_g}{k\delta}\right) \eta_0 \exp [-k(y-\delta)] \exp [ik(z-ct)] \quad (6.56)$$

Bernoulli's equation can be written as

$$\frac{p}{\rho} + \frac{\partial \phi}{\partial t} + \frac{1}{2} \left(\frac{\partial \phi}{\partial z}\right)^2 + \frac{1}{2} \left(\frac{\partial \phi}{\partial y}\right)^2 = C_1 \quad (6.57)$$

where C_1 is a constant or time dependent function.

Since $\phi = U_f z + V_g y + \phi'$, then equation (6.57) can be written as

$$\frac{p}{\rho} + \frac{\partial \phi'}{\partial t} + \frac{1}{2} \left(U + \frac{\partial \phi'}{\partial z}\right)^2 + \frac{1}{2} \left(V_g + \frac{\partial \phi'}{\partial y}\right)^2 = C_1 \quad (6.58)$$

Note that all perturbed quantities (denoted by (')) are all proportional to perturbation η .

Neglecting terms of order η^2 or above, equation (6.58)

becomes, for the liquid phase, as

$$\frac{p}{\rho_f} + \frac{\partial \phi'_f}{\partial t} + \frac{U_f^2}{2} + U_f \frac{\partial \phi'_f}{\partial z} = C_2 \quad (6.59)$$

and for the vapour phase as

$$\frac{p}{\rho_g} + \frac{\partial \phi'_g}{\partial t} + \frac{U_g^2}{2} = U_g \frac{\partial \phi'_g}{\partial z} + \frac{V_g^2}{2} + V_g \frac{\partial \phi'_g}{\partial y} = C_3 \quad (6.60)$$

The boundary condition is that at $z = 0$ all perturbed quantities are negligible, thus

$$C_2 = \frac{p_0}{\rho_f} + \frac{U_f^2}{2} \quad (6.61)$$

and

$$C_3 = \frac{p_0}{\rho_g} + \frac{U_g^2 + V_g^2}{2} \quad (6.62)$$

where p_0 is the static pressure at $z = 0$.

Defining a perturbed pressure difference by

$$p' = p - p_0 \quad (6.63)$$

allows equation (6.59) to be rewritten as

$$\frac{p_f'}{\rho_f} + \frac{\partial \phi_f'}{\partial t} + U_f \frac{\partial \phi_f'}{\partial z} = 0 \quad (6.64)$$

and equation (6.60) becomes

$$\frac{p_g'}{\rho_g} + \frac{\partial \phi_g'}{\partial t} - U_g \frac{\partial \phi_g'}{\partial z} + V_g \frac{\partial \phi_g'}{\partial y} = 0 \quad (6.65)$$

Using equation (6.55) into equation (6.64), gives for the liquid phase (see Appendix D)

$$p_f' = \rho_f k (U_f - c)^2 \eta_0 \exp[-k(y - \delta)] \exp[ik(z - ct)] \quad (6.66)$$

For the vapour phase, from equations (6.57) and (6.65) (see Appendix D), gives

$$p_g' = -\rho_g k \left[i(U_g + c) + \frac{v_g}{k\delta} \right] [i(U_g + c) + v_g] \eta_0 \exp[-k(y-\delta)] \exp[ik(z-ct)] \quad (6.67)$$

The interaction of the two phases is considered at the interface by the momentum jump balance i.e.

$$p_g - p_f = \sigma \left(\frac{\partial^2 r}{\partial z^2} + \frac{1}{(R-r)} \right) \quad (6.68)$$

where R is the tube radius, r is the film thickness at some time and place, and the liquid film surface curvature is approximated by

$$\frac{\partial^2 r}{\partial z^2} + \frac{1}{(R-r)} \quad \text{since} \quad \left(\frac{\partial r}{\partial z} \right)^2 \ll 1$$

At $z = 0$ $r = \delta$, hence

$$p_{g0} - p_{f0} = \frac{\sigma}{(R-\delta)} \quad (6.69)$$

at some location z , $r = \delta + \eta$ which from equation (6.68) gives

$$p_g - p_f = \sigma \left(\frac{\partial^2 \eta}{\partial z^2} + \frac{1}{(R-\delta-\eta)} \right) \quad (6.70)$$

which using a binomial expansion of (η^2) gives

$$p_g - p_f = \sigma \left(\frac{\partial^2 \eta}{\partial z^2} + \frac{1}{(R-\delta)} + \frac{\eta}{(R-\delta)^2} \right) \quad (6.71)$$

If terms of order $(\eta)^2$ or above are neglected, with

$$p_g - p_f = p_{g0} - p_{f0} + p_g' - p_f' \quad (6.72)$$

then, from equations (6.69) and (6.71)

$$p_g' - p_f' = \sigma \left(\frac{\partial^2 \eta}{\partial z^2} + \frac{\eta}{(R-\delta)^2} \right) \quad (6.73)$$

using equation (6.54) in equation (6.73) gives

$$p_g' - p_f' = \sigma \eta_0 \exp[ik(z-ct)] \left[\frac{1}{(R-\delta)^2} - k^2 \right] \quad (6.74)$$

Applying equation (6.66) and (6.67) at $y = \delta$, and substituting into equation (6.74) gives

$$\rho_g k \left[(U_g + c)^2 - i(U_g + c)V_g \left(1 - \frac{1}{k\delta} \right) - \frac{v_g^2}{k\delta} \right] + \frac{\rho_f k (U_f - c)^2}{\tanh(k\delta)} = \sigma \left[k^2 - \frac{1}{(R-\delta)^2} \right] \quad (6.75)$$

The wave celerity is

$$c = c_r + ic_i \quad (6.76)$$

gives from equation (6.75)

$$\begin{aligned} & \rho_g k \left[U_g^2 + 2U_g(c_r + ic_i) + c_r^2 + 2ic_r c_i - v_g \left(1 + \frac{1}{k\delta} \right) iU_g + ic_r - c_i \right] - \frac{v_g^2}{k\delta} \\ & + \frac{\rho_f k}{\tanh k\delta} \left[U_f^2 - 2U_f(c_r + ic_i) + c_r^2 - c_i^2 + 2ic_r c_i \right] = \sigma \left[k^2 - \frac{1}{(R-\delta)^2} \right] \end{aligned} \quad (6.77)$$

Equating the real and imaginary parts of equation (6.77) gives

$$\rho_g k [U_g^2 + 2U_g c_r + c_r^2 - c_i^2 + v_g (1 + \frac{1}{k\delta}) c_i - \frac{v_g^2}{k\delta}] + \frac{\rho_f k}{\tanh(k\delta)} U_f^2 - 2U_f c_r + c_r^2 - c_i^2 = \sigma \{k^2 - \frac{1}{(R-\delta)^2}\} \quad (6.78)$$

and

$$\rho_g k [2U_g + 2c_r - \frac{v_g}{c_i} (1 + \frac{1}{k\delta}) (U_g + c_r)] + \frac{\rho_f k}{\tan(k\delta)} [-2U_f + 2c_r] = 0 \quad (6.79)$$

Then

$$c_r = \frac{U_f - \frac{1}{2} \frac{v_g}{c_i} (1 + \frac{1}{k\delta}) \frac{\rho_g}{\rho_f} U_g \tanh(k\delta)}{1 + [1 - \frac{1}{2} \frac{v_g}{c_r} (1 + \frac{1}{k\delta})] \frac{\rho_g}{\rho_f} \tanh(k\delta)} \quad (6.80)$$

For a gas (vapour)-liquid system at moderate pressure,

$\frac{\rho_g}{\rho_f} \tanh k\delta$ is very small, (of order 0.001), and from experiment

it has been shown that at the flooding point U_g is of order 10

U_f . Hence equation (6.80) can be approximated by

$$c_r = U_f \quad (6.81)$$

and hence equation (6.78) gives

$$c_i = \frac{1}{2} \left\{ \left(1 + \frac{1}{k\delta}\right) \frac{\rho_g}{\rho_f} v_g \tanh(k\delta) \right\} + \left\{ \left[\left(1 + \frac{1}{k\delta}\right) \frac{\rho_g v_g}{\rho_f} \frac{\tanh(k\delta)}{2} \right]^2 + \left[\left((U_g + U_f)^2 \frac{v_g^2}{k\delta} \frac{\rho_g}{\rho_f} \tanh(k\delta) - \frac{\tanh(k\delta)\sigma}{\rho_f k} \left(k^2 - \frac{1}{(R-\delta)^2} \right) \right) \right]^2 \right\}^{1/2}$$

which, if $\tanh(k\delta) = k\delta$, can be written as (6.82)

$$c_i = \frac{1}{2} \left\{ (k\delta + 1) \frac{\rho_g v_g}{\rho_f} \right\} + \left\{ k\delta \left[k\delta \left(\frac{\rho_g}{\rho_f} (U_g + U_f)^2 - \frac{\sigma}{\rho_f k} \left(k^2 - \frac{1}{(R-\delta)^2} \right) \right) - \frac{\rho_g v_g^2}{\rho_f} \right] \right\}^{1/2} \quad (6.83)$$

or

$$\left[c_i - \frac{(k\delta + 1)}{2} \frac{\rho_g v_g}{\rho_f} \right]^2 = \left\{ (k\delta) \left[\frac{\rho_g}{\rho_f} (U_g + U_f)^2 - \frac{\sigma}{\rho_f k} \left(k^2 - \frac{1}{(R-\delta)^2} \right) \right] - \frac{\rho_g v_g^2}{\rho_f} \right\} \quad (6.84)$$

6.3.1 Flooding From Maximum Wave Growth Rate

Using equation (6.76) allows equation (6.54) to be written as

$$\eta = \eta_0 \exp(kc_i t) [\cos(kz - c_r t) + i \sin(kz - c_r t)] \quad (6.85)$$

The wave amplitude (A) is therefore given by

$$A = \eta_0 \exp(kc_i t) \quad (6.86)$$

The maximum growth of the wave will occur when (kc_i) is a maximum and hence

$$\frac{d}{dk} (kc_i) = 0 \quad (6.87)$$

Multiplying equation (6.84) by k , differentiating the result with respect to k using equation (6.139) gives

$$(U_g + U_f) = \left\{ \frac{2v_g^2}{3k\delta} - \frac{2k\delta+1}{3k\delta} c_i v_g + \frac{4\sigma}{3\rho_g k} \left(k^2 - \frac{1}{2(R-\delta)^2} \right) \right\}^{1/2} \quad (6.88)$$

Substituting equation (6.88) into equation (6.84) gives

$$c_i = \left\{ \left(\frac{k\delta+2}{6} \frac{\rho_g}{\rho_f} v_g \right) + \frac{1}{2} \left(\frac{k\delta+2}{6} \frac{\rho_g}{\rho_f} v_g \right)^2 - \frac{1}{3} \frac{\rho_g}{\rho_f} v_g^2 + \frac{1}{3} \frac{\sigma\delta}{\rho_f} \left(k^2 + \frac{1}{(R-\delta)^2} \right) \right\}^{1/2}$$

as $(\rho_g/\rho_f)^2 \ll 1$ then (6.89)

$$c_i = \left\{ \left(\frac{k\delta+2}{6} \frac{\rho_g}{\rho_f} v_g \right) + \left\{ \frac{\sigma\delta}{3\rho_f} \left(k^2 + \frac{1}{(R-\delta)^2} \right) - \frac{1}{3} \frac{\rho_g}{\rho_f} v_g^2 \right\}^{1/2} \right\} \quad (6.90)$$

6.3.2 Evaluation of Vapour Condensation Velocity

(a) Test Tube: The temperature gradient at the vapour-liquid interface, along the test tube, is obtained by differentiating equation (6.37)

$$\left(\frac{\partial T}{\partial y} \right)_{y=\delta} = \frac{2\Delta T}{\delta} \sum_{i=0}^{\infty} \exp(2i+1)\pi^2/4\delta^2 \zeta \quad (6.91)$$

The heat balance across the interface is

$$q = U\rho_f C_p \zeta \left(\frac{\partial T}{\partial y} \right)_{y=\delta} = h\Delta T \quad (6.92)$$

applying equation (6.92) to equation (6.91) gives

$$\frac{St}{2} = \frac{\zeta}{\delta} \sum_{i=0}^{\infty} \exp\left[\left((2i+1)\pi^2/4\delta^2\right)\zeta\right] \quad (6.93)$$

where

$$St = \frac{h}{\rho C_p U} \quad (6.94)$$

This surface heat transfer is due to condensation of the vapour, hence

$$q = V_g \rho_g h_{fg} \quad (6.95)$$

using equation (6.95) into equation (6.93) gives

$$\frac{V_g}{U_f} = \frac{\rho_f}{\rho_g} Ja \frac{\zeta}{\delta} \sum_{i=0}^{\infty} \exp\left[\left((2i+1)\pi^2/4\delta^2\right)\zeta\right] \quad (6.96)$$

(b) Injector Sinter: Assuming a constant film thickness, and using semi-infinite heat conduction over the top sinter, then

$$\frac{\partial T}{\partial \zeta} = \frac{\partial^2 T}{\partial y'^2} \quad (6.97)$$

where y' is the distance from the vapour-liquid interface.

The Boundary Conditions are:

- (i) $T = T_t$ at $z = 0$
- (ii) $T = T_s$ at $y' = 0$

From Carslaw and Jaeger (1953) the solution of equation (6.97) can be written as

$$(T - T_t) = (T_s - T_t) \operatorname{erfc} \frac{y'}{2\sqrt{\zeta}} \quad (6.98)$$

simplifying equation (6.98) gives

$$T = T_s + (T_t - T_s) \operatorname{erf} \frac{y'}{2\sqrt{\zeta}} \quad (6.99)$$

differentiating equation (6.99) with respect of y' , gives

$$\frac{\partial T}{\partial y'} = \frac{T_t - T_s}{\sqrt{\pi\zeta}} \left[\exp\left(-\frac{y'^2}{4\zeta}\right) \right] \quad (6.100)$$

The heat balance across the vapour-liquid interface can be written as

$$q' = V_g \rho_g h_{fg} = k_f \left(\frac{\partial T}{\partial y'} \right)_{y'=0} \quad (6.101)$$

substituting equation (6.101) into equation (6.100) gives

$$V_g \rho_g h_{fg} = \frac{k_f \Delta T}{\sqrt{\pi\zeta}} \quad (6.102)$$

$$\frac{V_g}{U_f} = \frac{(K + \epsilon_H)}{U_f} \frac{Ja}{\sqrt{\pi\zeta}} \frac{\rho_f}{\rho_g} \quad (6.103)$$

6.3.3 Application of Flooding Model to Accelerating Liquid Film

It is postulated that flooding with a uniform film is the result of the growth of an infinitesimal wave from the liquid injector until it reaches some critical height at the liquid extractor. Modifying this model to allow for acceleration effects within the film, it is assumed that the

'blowing' effect of porous injection, reduces the wave growth time between the injector and the extractor, resulting in a smaller wave height at the liquid extractor to become unstable [McNeil(1986)]. These waves of smaller height require a larger gas(vapour) flow. The critical wave height is assumed to be that given by Richtan (1980), hence

$$A_{crit} = \frac{2\sigma}{\rho_g U_g^2} = \eta_0 \exp(kc_i t) \quad (6.104)$$

Following a growing wave down a uniform film, then in equation

$$(6.104) \quad t = \frac{z}{c_r} \quad \text{and at the flooding point } z = l, \text{ then}$$

$$A = \frac{2\sigma}{\rho_g U_g^2} \exp[kc_i/c_r(z-l)] \quad (6.105)$$

where l is the length of the tube.

The waves of a smaller height at the extractor require a larger gas (vapour) flow to become unstable; or it could be assumed that the wave height distribution of an accelerating liquid film could be represented in a uniform film over a longer length $z = le$, where both systems have the same growth time,

then

$$A = \frac{2\sigma}{\rho_g U_g^2} \exp(kc_i/c_r(z-le)) \quad (6.106)$$

In terms of a mean film thickness δ_m , given by

$$\delta_m = \frac{1}{l} \int_0^l \delta \, dz \quad (6.107)$$

The ratio of the new gas (vapour) velocity for flooding to the uniform gas (vapour) velocity U_{gp} becomes [McNEIL (1986)]

$$\frac{U_g}{U_{gp}} = \exp \left[k \frac{c_i}{c_r} \frac{1}{2} \left(\frac{\delta_m}{\delta_\infty} - 1 \right) \right] \quad (6.108)$$

where δ_∞ is the liquid film thickness over the longer tube which is determined from equation (6.27), by assuming that the

film is fully developed $\left(\frac{d\delta^+}{dz^+} = 0 \right)$ and its temperature is

saturated $\left(\frac{dT^+}{dz^+} = 0 \right)$, Thus

$$\delta_\infty = \frac{1}{2} \left[\rho^+ f_i (Fr_g - Fr_f)^2 + \frac{C Fr_f^2}{(Re_f)^n} \right] \quad (6.109)$$

To complete the model it remains to determine the critical wave number and this is illustrated later in Chapter 9.

As mentioned previously, the model is similar in principle to the gas-liquid flooding model of McNeil (1986), but by introducing the new term V_g it is postulated that the effect of condensation in vapour-liquid flow is to inhibit growth and formation of the disturbance waves.

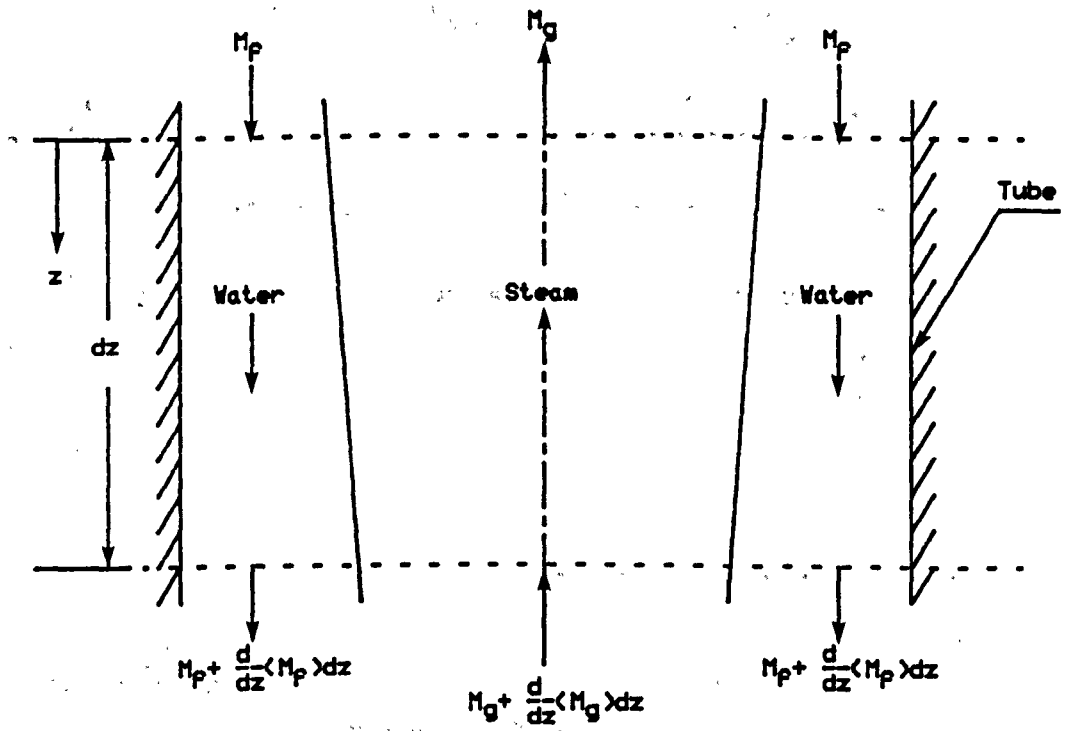


Figure 6.1 Control Volume For Mass Balance

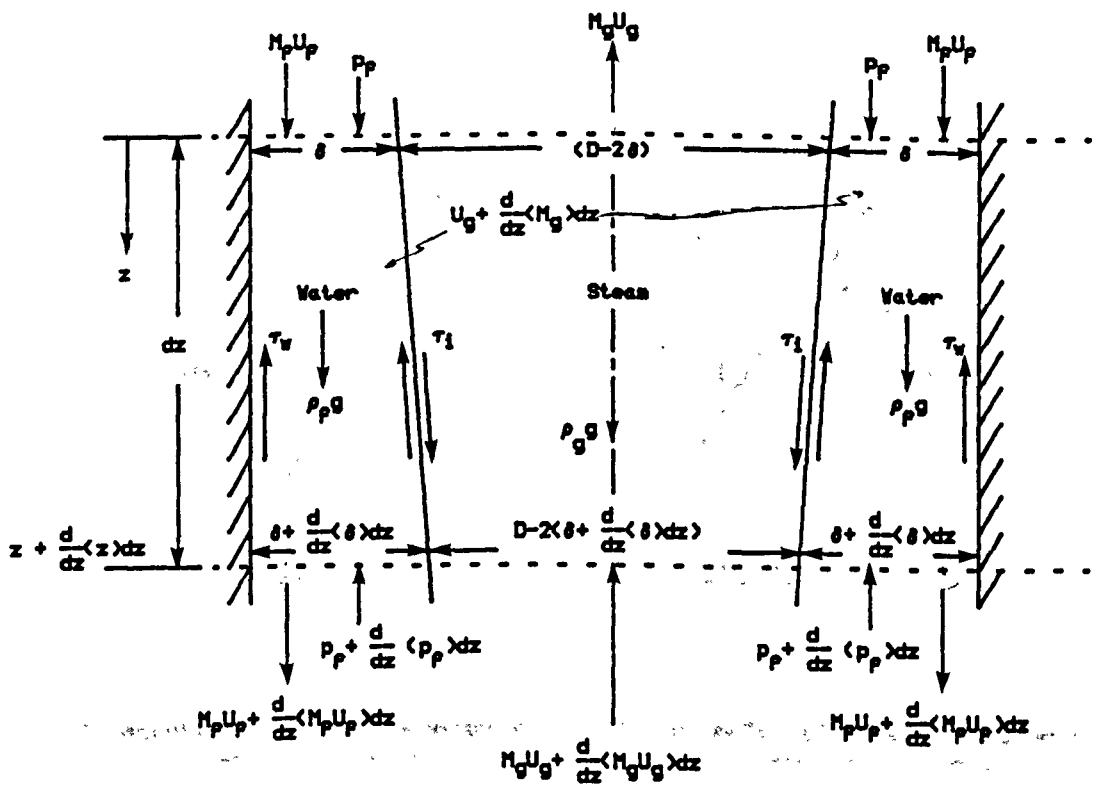


Figure 6.2 Control Volume For Momentum Balance

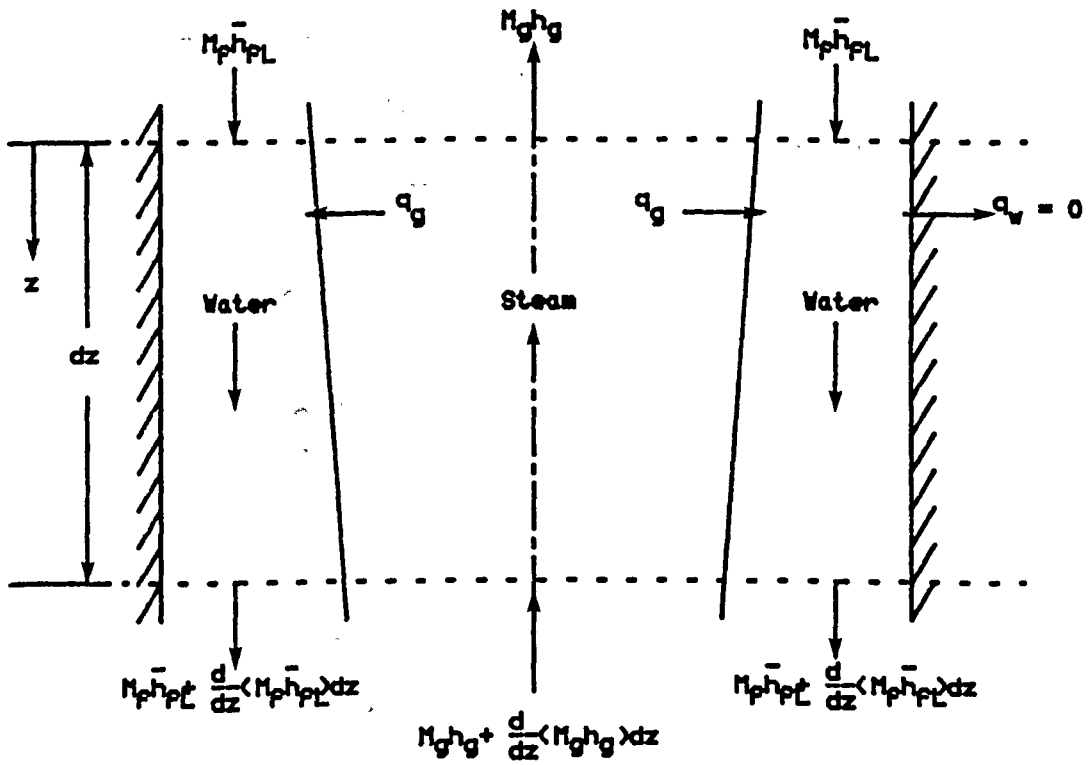
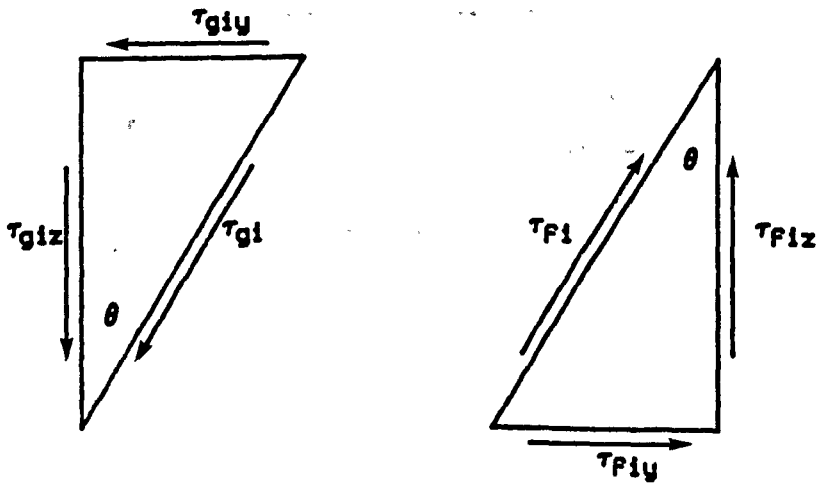


Figure 6.3 Control Volume for Energy Conservation



(a) Interfacial Shear Components on Steam Phase

(b) Interfacial Shear Components on Liquid Phase

Figure 6.4 Interfacial Shear Stress Components

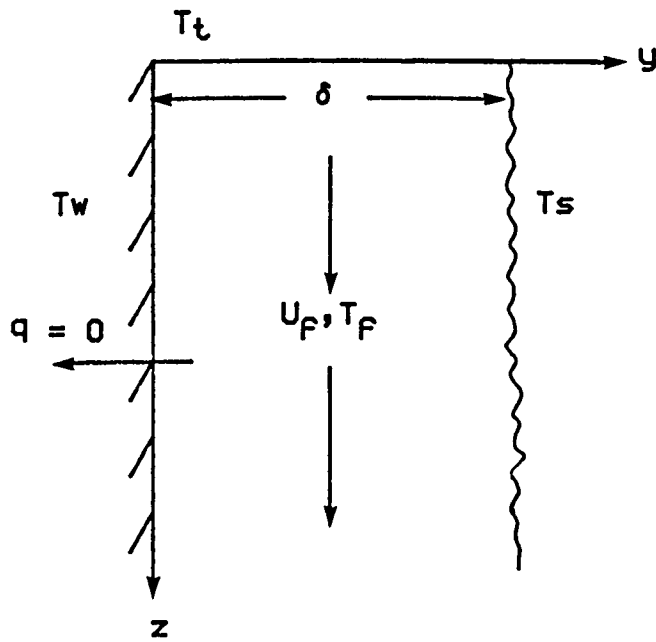


Figure 6.5 Liquid Film Flow

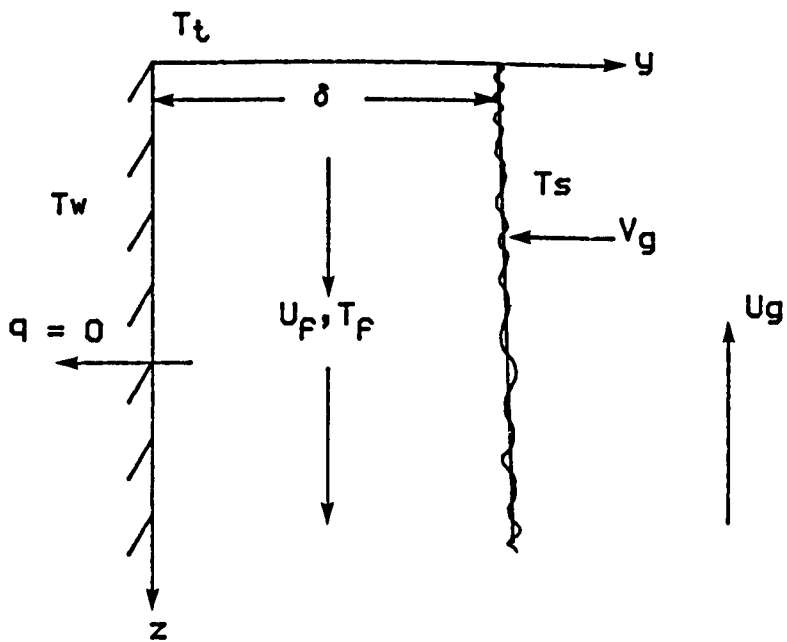


Figure 6.6 Uniform Liquid Film Flow

CHAPTER 7

EXPERIMENTAL RESULTS

CHAPTER 7

EXPERIMENTAL RESULTS

During the course of the experimental programme, data was collected with the test facility operating with either air-water or steam-water flows. The programme involved the downward flow of water with a counter-current upward flow of air or steam, the latter being increased in small incremental steps until flooding occurred. For each system or mode, tests were performed at different air or steam extraction rates with a total of 2292 test runs being recorded, 2040 of which involved steam-water interactions. The air-water data collected are described generally in Section 7.1 and the air-water flooding data presented in Section 7.2. Corresponding steam-water data are presented in Sections 7.3 and 7.4.

7.1 Air-Water Data

In the experimental programme, tests were performed with two different rates of air extraction through the extractor system. As described in Chapter 3, a vacuum pump was used to extract the falling water flow through a porous sinter placed at the bottom of the test tube and some air was always extracted with the water, the air flow depending on the vacuum pressure created by the pump.

Sets of air-water data were taken for two different extraction flowrates. In the first set, experimental data were taken with the pump vacuum pressure controlled and maintained at its lowest possible value, such that the minimum rate of air flow passed through the extractor, at the same time ensuring that all of the water flow was extracted. During these tests, the air flow was increased in small steps until flooding occurred. The data taken under these conditions are listed in Appendix B, Table B.1.

The second set of air-water tests were performed with air extraction rates at the maximum possible value. Only flooding data were recorded during these tests.

In both sets, the water flowrate was varied to cover a range between 4 and 39.6 l/min.

At the start of each air-water experimental test run, regardless of extraction rate, care was taken to ensure that the rate of air flow through the extractor was balanced by the supply air flow corresponding to zero air flow through the test section. Under these conditions, the liquid film could be considered as a free falling film and liquid film measurements were made for various water flowrates in the range 4 to 28.23 l/min. Each liquid film measurement was evaluated as the mean of 250 readings taken over a period of 5.8 secs. Typical measurements of instantaneous film thickness versus time

taken at a water flowrate of 12.71 l/min are shown in Figure 7.1 and 7.2 for the upper and lower probes respectively. It can be seen that fluctuations in the values are considerably greater at the bottom probe than at the top probe. Numerical integration of these readings (using Simpson's Rule) allowed the mean film thickness to be determined. Curves showing the mean film thickness as a function of water flowrate at the upper probe and lower probe are given in Figure 7.3. It can be seen, particularly at high water flowrates that the mean film thickness at the upper probe is considerably greater than that at the lower probe, implying that the film is accelerating as it moves down the tube.

In the air-water tests, the pressure drop data were only recorded at the low air extraction rates. Figure 7.4 shows measured pressure drop plotted as a function of flowrate at a constant water injection rate. It can be seen that the pressure drop measurements increased only slightly until the flooding situation was approached whence the pressure drop rose sharply. Hence pressure difference is a good indicator of the onset of flooding in the experimental tests. The pressure drop data will be discussed later in Chapter 9.

7.2 Air-Water Flooding Data

The air-water flooding data taken with the test facility operating at the low air extraction rate are given in Appendix B, Table B.2 with the high extraction rate in Table B.3.

Flooding data from air-water experiments in vertical tubes are frequently correlated using the Wallis parameter, which is defined as

$$j_i^* = \frac{\rho_i^{1/2} j_i}{[gD(\rho_f - \rho_a)]^{1/2}} \quad (7.1)$$

where $i = a$ for air and $i = f$ for water

D is the test tube inner diameter

and j is the superficial velocity = Q/A

On this basis, the two sets of air-water flooding results are listed in Tables B.4 and B.5 (Appendix B) and shown plotted on Figures 7.5 and 7.6 respectively. For each data plot, a Wallis type correlation for flooding was obtained using the least squares method, as follows:

(i) low air extraction rate

$$j_a^{*1/2} + 0.59j_f^{*1/2} = 0.8 \quad (7.2)$$

(ii) high air extraction rate

$$j_a^{*1/2} + 0.54j_f^{*1/2} = 0.76 \quad (7.3)$$

7.3 Steam-Water Data

Unlike the air-water tests, the rate of steam flow extracted (leaked) through the porous sinter was controlled indirectly by varying the amount of cooling water passing through the condenser. At the start of any steam-water test, both water flow and steam flow (usually at a low rate) were passed through the extraction sinter to the condenser due to the condensation of steam and the cooling down of the water creating a negative pressure (relative to the test section pressure) inside the condenser. The amount of cooling water flowing through the condenser controlled the amount of "negative" pressure created and consequently the amount of steam extracted with the water (the extracted water included the inlet water flow and the condensed steam flow). Low cooling water flowrates produced a low vacuum pressure, extracting a small steam flowrate, and vice versa. It should be noted that there must be a minimum amount of cooling water passing through the condenser to create a vacuum high enough to extract all of the water flow. If the vacuum is not high enough, some water will pass over the extraction sinter into the settling length tube. The vacuum inside the condenser is also affected by the inlet water subcooling. Both effects, i.e. cooling water flowrate and inlet subcooling, are discussed in detail in Chapter 9.

Once again, two sets of experimental data were

taken on the test facility. The first set was taken with a high steam flow extracted with the extracted water, the rate of cooling water flow through the condenser varying between 25 and 29 l/min with a small number of tests being performed at slightly lower cooling water flowrates (the minimum value never fell below 20 l/min). During these tests, experimental data were collected for eight different inlet water subcoolings in the range 10 K to 80 K in 10 K increments. The steam flowrate was increased in increments until flooding occurred. Due to the considerable amount of data taken under these conditions it has not been listed in the appendices of this thesis but it is available in the Department on request.

The second set of data were taken with low extracted steam flows. Throughout these tests, the rate of cooling water was controlled mainly within the flow range 4 to 5 l/min with only a small number of tests where the flowrate reached a higher limit of 6 l/min. During these tests, the same 8 subcoolings as mentioned previously were covered and with one extra subcooling of 3 K. In all subcoolings, the steam flowrate was increased incrementally until flooding occurred. In the 3 K subcooling tests, only flooding data were recorded. The data taken under these conditions are listed in Appendix C, Table C.1.

At an inlet water subcooling of 10 K, two extra

sets of tests were performed at two different (medium range) rates of cooling water flow corresponding approximately to 11.5 l/min and 19.1 l/min respectively. The data taken under these conditions are listed in Appendix C Table C.2. Under all conditions (high, medium and low steam extraction rates), the rate of inlet water flows covered was dependent on the inlet water subcooling and the steam extraction rate, with the maximum values covered varying between 4 l/min and 21.9 l/min.

Carrying out steam-water tests with small steam flows passing to the test tube was quite difficult because of the indirect measurement method required for the steam flowrate through the liquid extractor. However, care was taken to ensure that the liquid film thickness measurements were made with the steam flowrate well below the flooding point values. Liquid film thickness data were collected in a similar way to that for the air-water tests, for all of the 8 inlet subcoolings. Specimen mean film thickness measurements obtained from both the upper and lower probes for an inlet water subcooling of 10 K are shown plotted as a function of inlet water flowrate in Figure 7.7. Liquid film measurement data at other subcoolings, and the effect of liquid viscosity due to film temperature variation, are presented in Chapter 9.

Tube Wall Temperature measurements were made at 11 locations and these are listed in Appendix C, Table C.3. Typical measured tube wall temperature distributions are

shown in Figures 7.8 and 7.9 for two different cases in which the inlet water flowrate was kept constant and the steam flowrate varied up to the onset of flooding.

In steam-water tests pressure drop data were taken at both low and high steam extraction rates. Figure 7.10 shows measured pressure drop data plotted as a function of steam flowrate at a constant water injection rate. The presence of "negative" pressure drop can be seen and this will be discussed in detail later in Chapter 9.

7.4 Steam-Water Flooding Data

The main difficulty in processing the steam-water data was due to the indirect measurements of the extraction steam flowrate since these required a knowledge of the liquid film mean temperature and only the tube wall temperatures was measured.

Steam-water flooding data taken are listed in Appendix C, Tables C.4 and C.5 for high and low steam extraction rates respectively. Corresponding test tube wall temperatures at the flooding points for low steam extraction rate tests are listed in Appendix C, Table C.6. Figures 7.11 and 7.12 show the measured wall temperature distribution along the test section at the flooding points for two different subcoolings and several inlet water flowrates, taken at low steam extraction rates. The

calculated steam flow as outlined in Chapter 4 was obtained from

$$M_{SC} = \frac{M_f C_p (T_f - T_{fin})}{h_{fg} + C_p (T_{sat} - T_f)} \quad (7.4)$$

$$M_{SL} = \frac{M_{cw} C_{p1} (T_{c2} - T_{c1}) - M_f C_{p2} (T_f - T_D)}{h_{fg} + C_{p3} (T_{sat} - T_D)} \quad (7.5)$$

$$M_{SB} = M_{Ssup} - M_{SL} \quad (7.6)$$

and

$$M_{ST} = M_{SB} - M_{SC} \quad (7.7)$$

The water outlet temperature was calculated making use of the liquid film temperature analysis detailed in Section 6.2.

In the steam-water flooding, the data are often correlated using the Wallis dimensionless parameters with the steam flowrate being considered either as that corresponding to the water outlet section (bottom of test section), or to that at the water inlet section (top of test section). All of the steam-water flooding data were processed on this basis and the results of the low extraction data are listed in Appendix C, Table C.7. Typical flooding characteristics for low steam extraction rates are shown in Figures 7.13 and 7.14 for two different subcoolings.

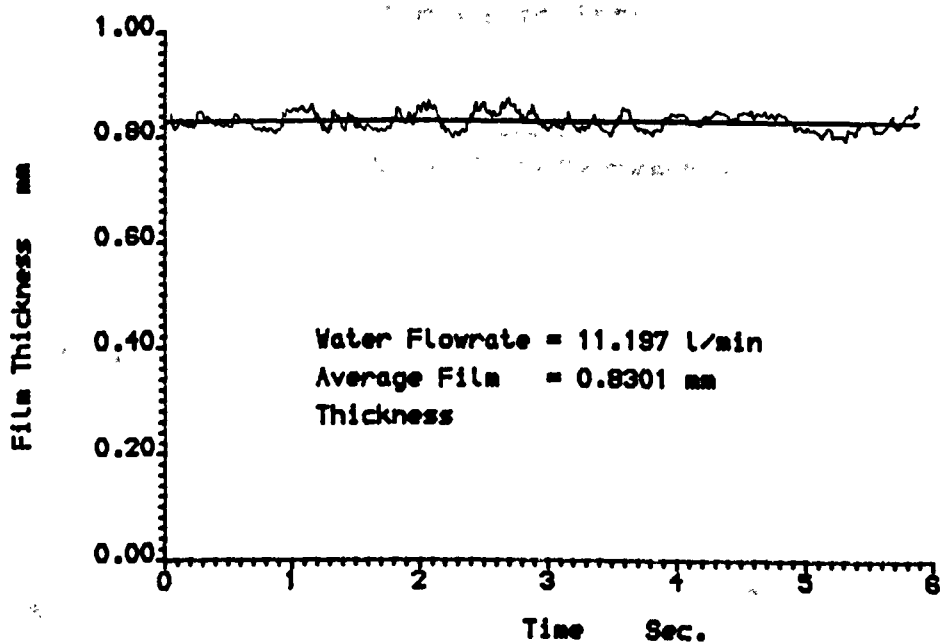


Figure 7.1 Upper Probe Film Thickness Fluctuation

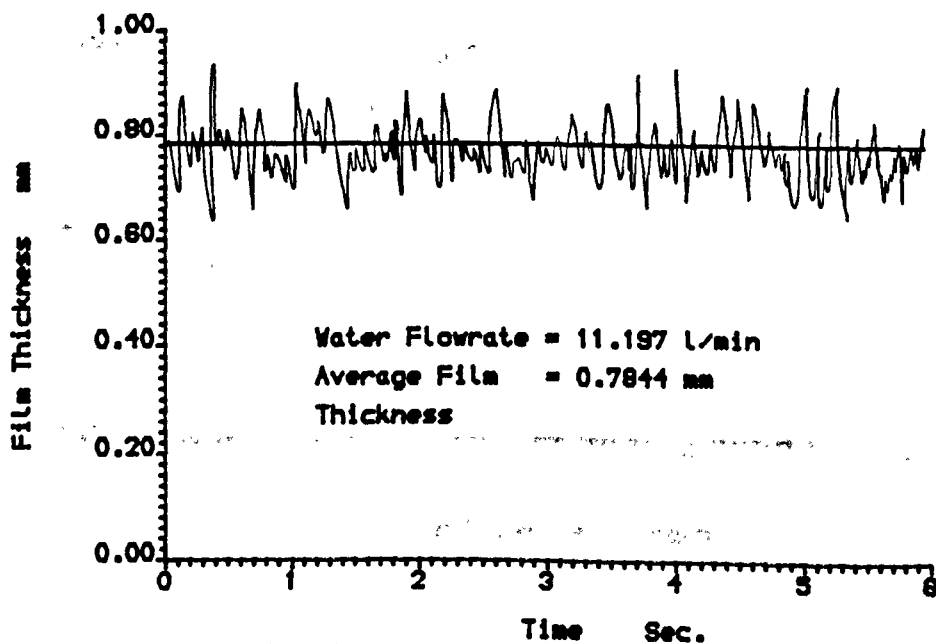


Figure 7.2 Lower Probe Film Thickness Fluctuation

Air-Water Tests

- o Upper Probe Measurements
- x Lower Probe Measurements

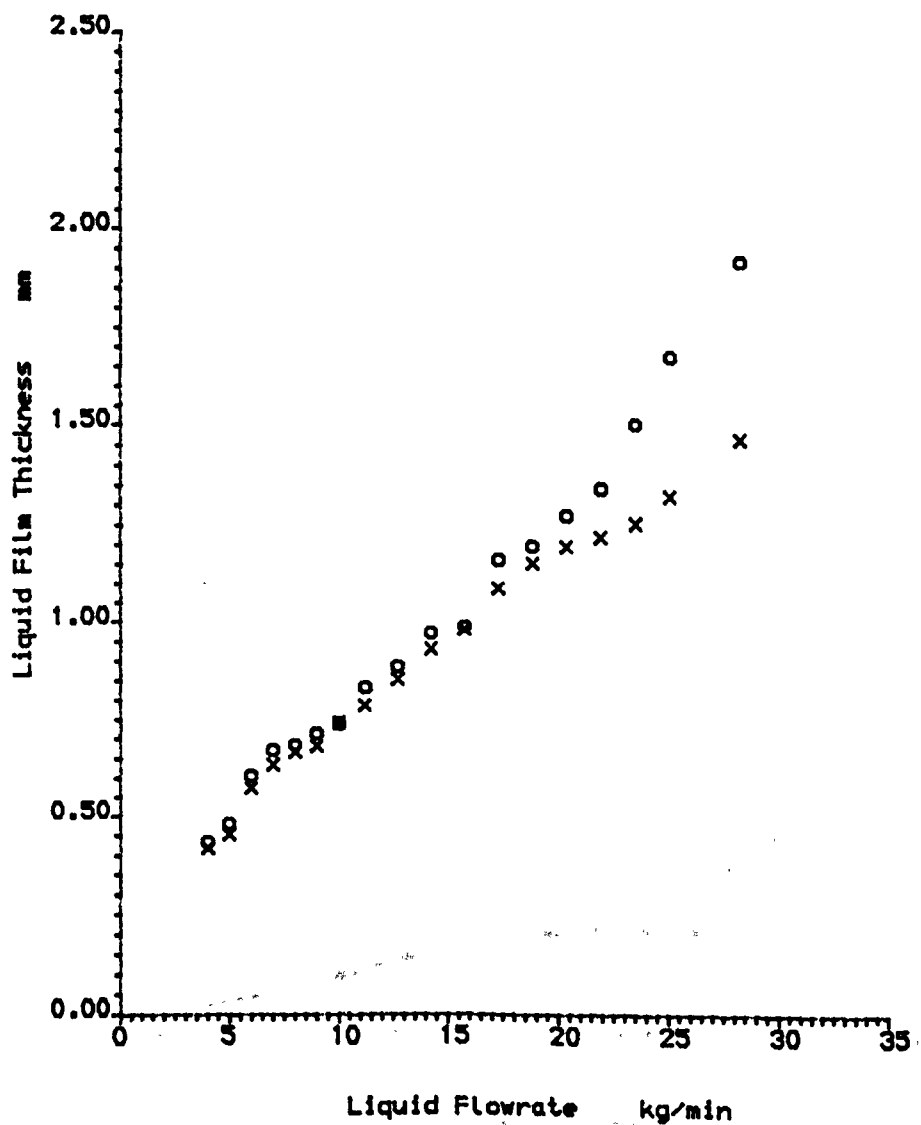


Figure 7.3 Measured Liquid Film Thickness

Air-Water Tests

Inlet Water Flowrate = 4.0 l/min

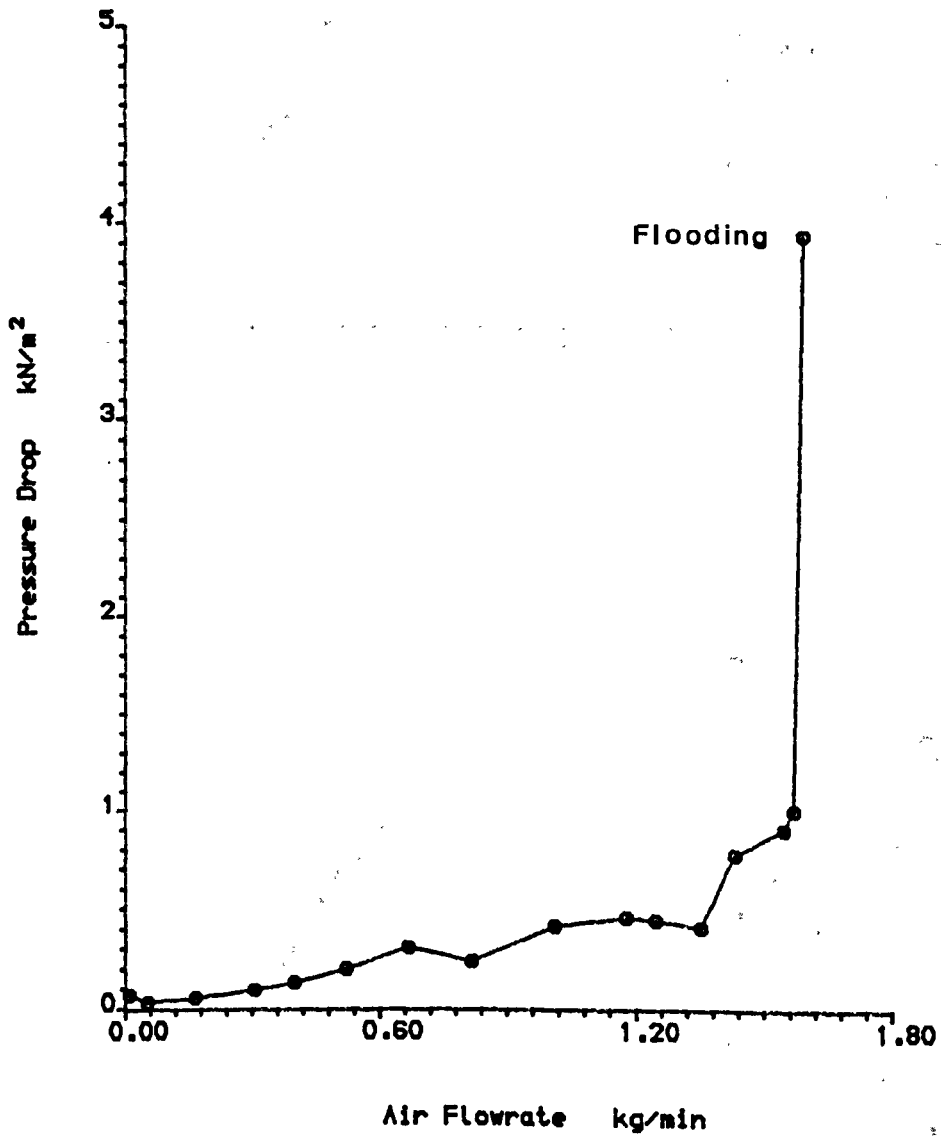
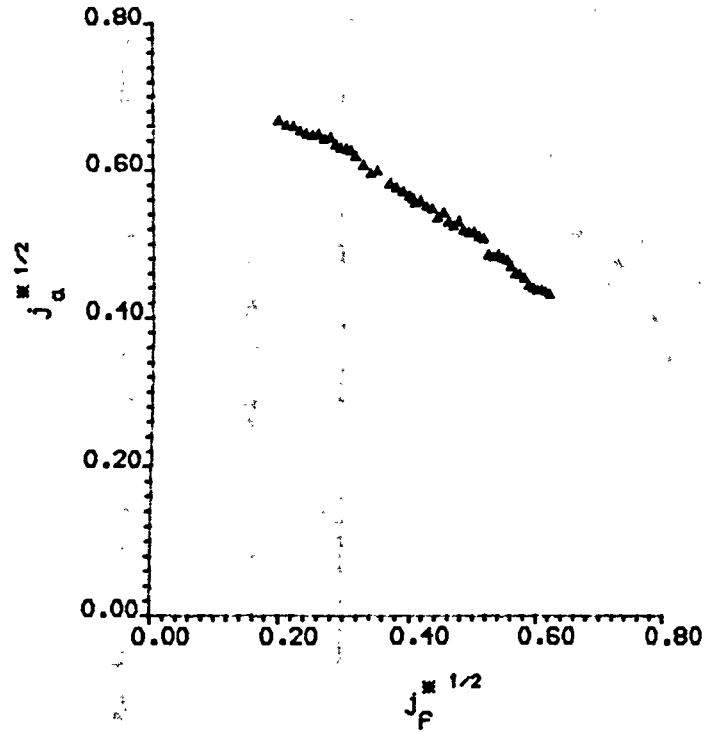


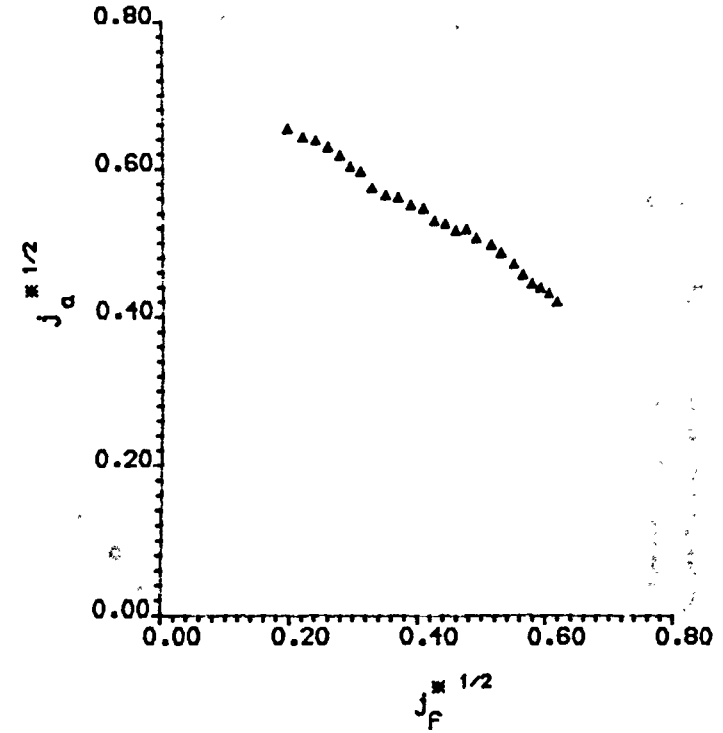
Figure 7.4 Pressure Drop Characteristics

Air-Water Tests



Air-Water Flooding Data
(Low Air Extraction Rate)

Figure 7.5



Air-Water Flooding Data
(High Air Extraction Rate)

Figure 7.6

Steam-Water Tests

o Upper Probe Measurements
x Lower Probe Measurements

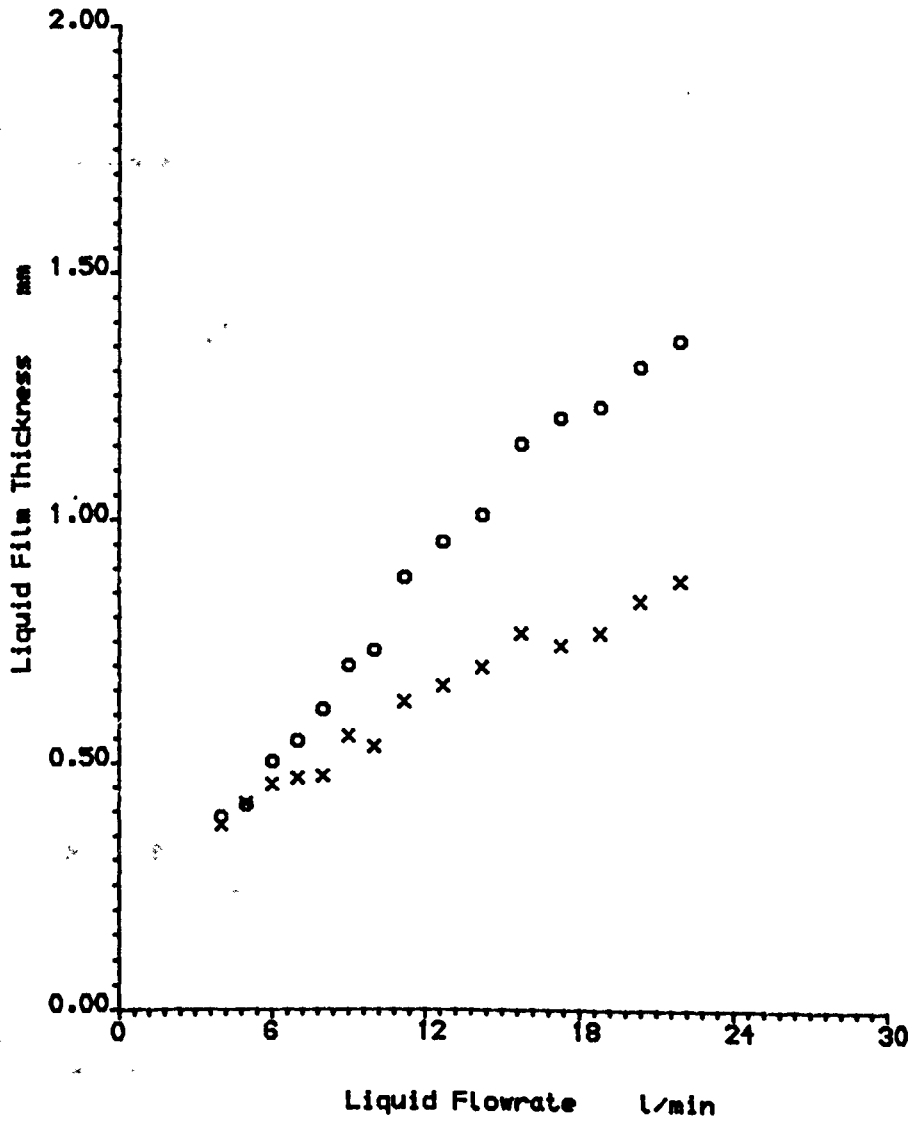
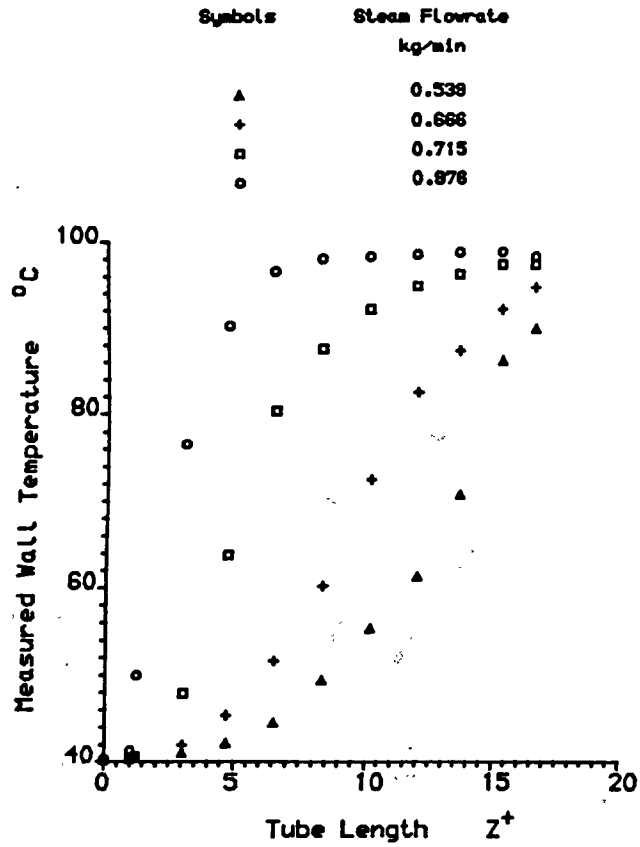


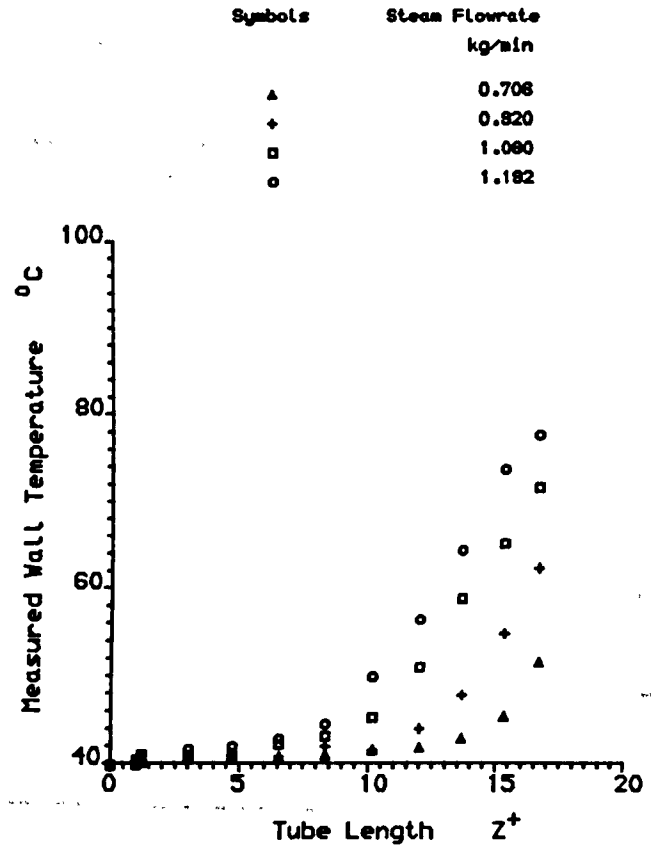
Figure 7.7 Measured Liquid Film Thickness
($\Delta T_{\text{sub}} = 10 \text{ K}$)

Steam-Water Tests



Wall Temperature Distribution
 $(\dot{M}_{Fin} = 4.0 \text{ l/min. } \Delta T_{sub} = 60 \text{ K})$

Figure 7.8



Wall Temperature Distribution
 $(\dot{M}_{Fin} = 12.7 \text{ l/min. } \Delta T_{sub} = 60 \text{ K})$

Figure 7.9

Steam-Water Tests

Inlet Water Flowrate = 4.0 l/min

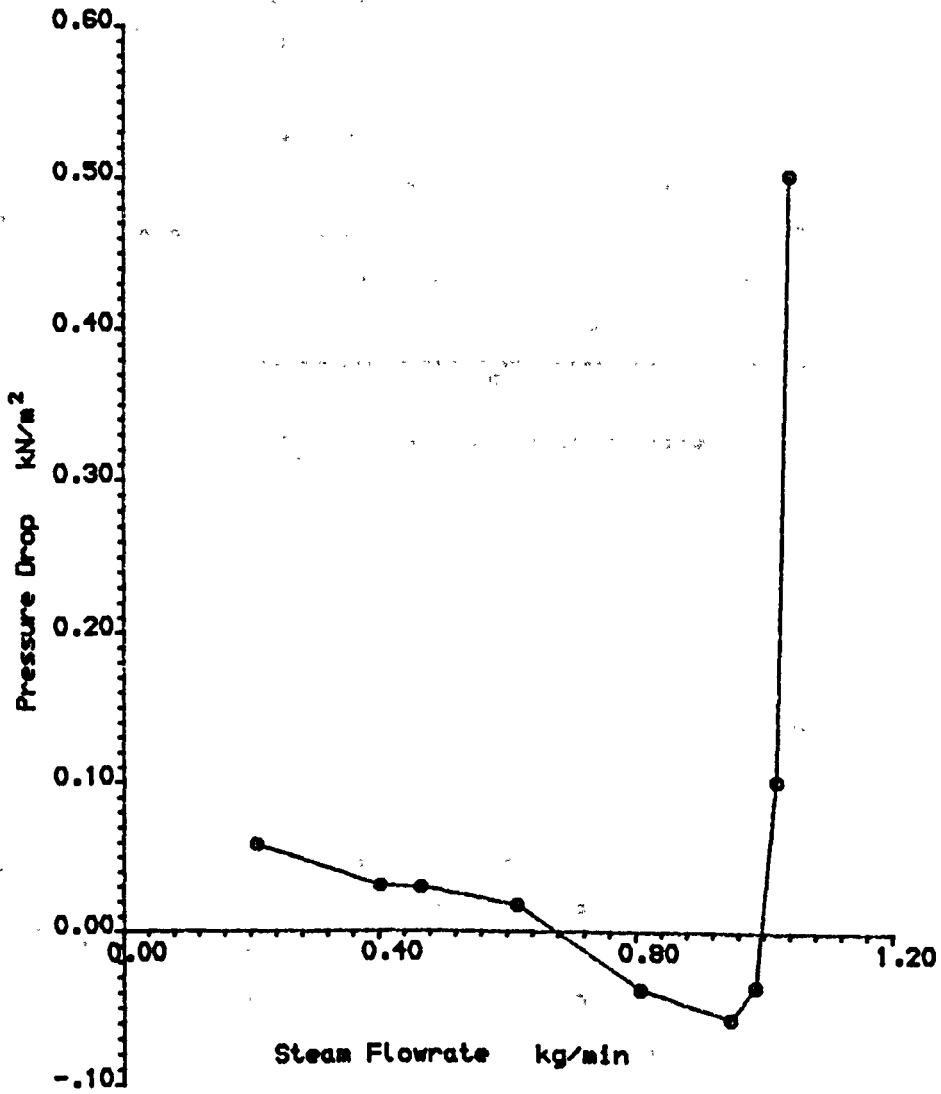
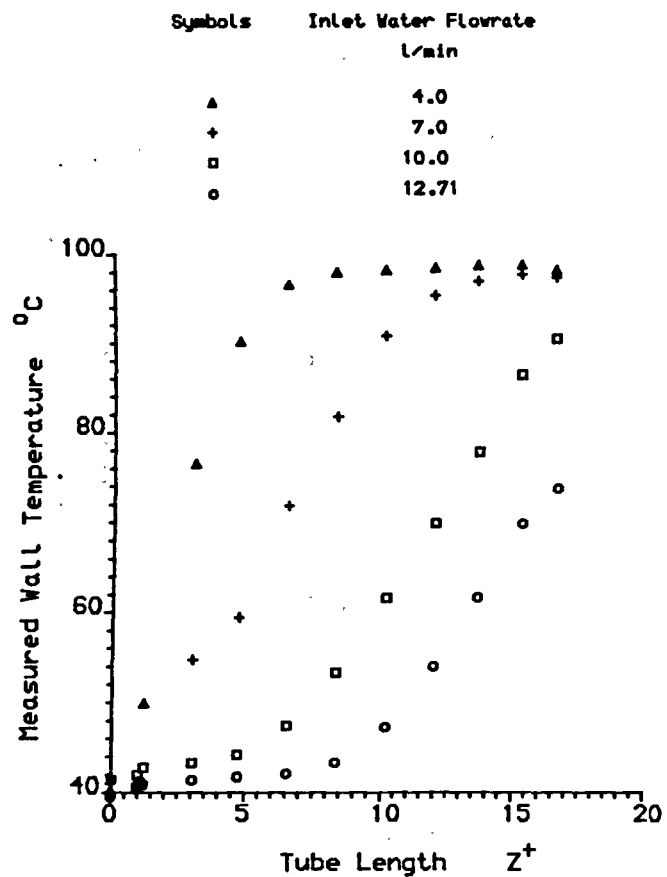


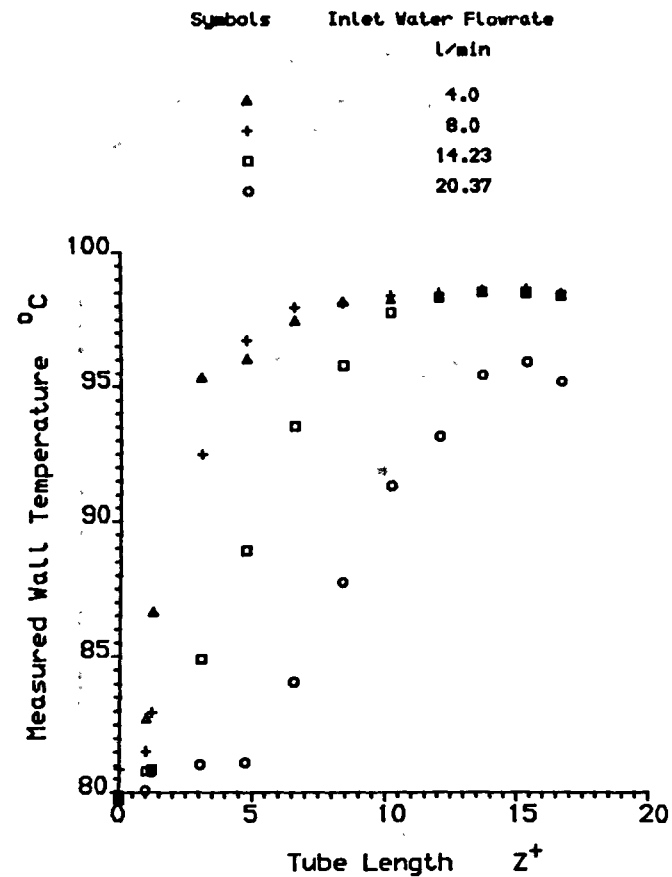
Figure 7.10 Pressure Drop Characteristic
($\Delta T_{\text{sub}} = 10 \text{ k}$)

Steam-Water Tests



Wall Temperature Distribution
at Flooding Points. $\Delta T_{\text{sub}} = 60 \text{ K}$

Figure 7.11



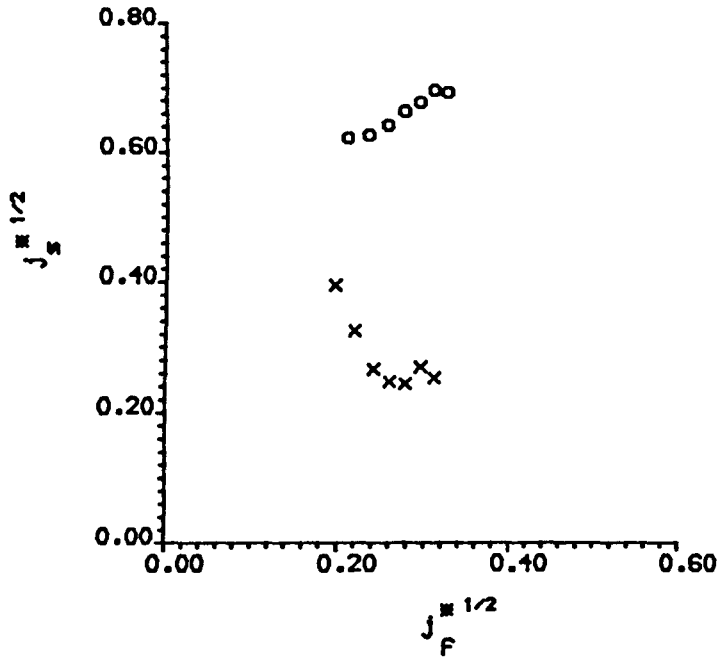
Wall Temperature Distribution
at Flooding Points. $\Delta T_{\text{sub}} = 20 \text{ K}$

Figure 7.12

Steam-Water Tests

$\Delta T_{sub} = 80 \text{ K}$

- x Top of Test Section
- o Bottom of Test Section

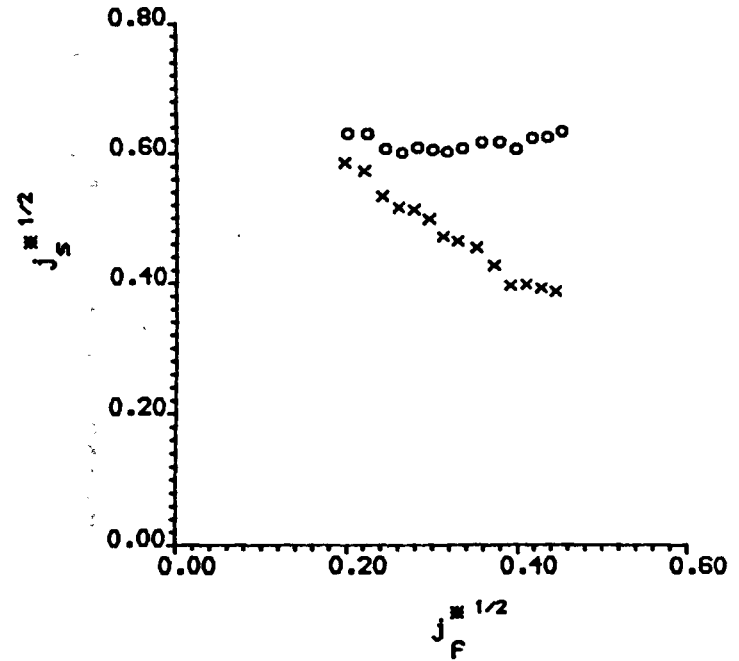


Steam-Water Flooding Characteristic

Figure 7.13

$\Delta T_{sub} = 20 \text{ K}$

- x Top of Test Section
- o Bottom of Test Section



Steam-Water Flooding Characteristic

Figure 7.14

CHAPTER 8

FLOW VISUALISATION RESULTS

CHAPTER 8FLOW VISUALISATION RESULTS

The endoscopy and the video camera systems, in conjunction with the test facility modifications described in Chapter 5, were used to view the liquid film flow at different locations within the test section and also to view the developing process leading up to the flooding situation. This was considered for both modes, i.e. air-water and steam-water. The viewing results obtained from the endoscope system are described in section 8.1, and those from the video camera system in section 8.2.

8.1 Endoscope System

As mentioned previously, two types of endoscope devices were employed to view the flow inside the test section. These were the radial viewing endoscope and the forward viewing endoscope. The radial viewing endoscope was inserted into the test section in two ways, vertically from the top of the test tube (air/steam offtake system), and horizontally from the bottom of the test tube (settling length tube). During the lead-up process to the flooding situation in both air-water and steam-water tests, and when using the first method of inserting the

radial viewing endoscope, four locations within the test section were chosen to be viewed. These were:

- a) Liquid injector
- b) Upper probe mount
- c) Lower probe mount
- d) Liquid extractor

In these cases, the radial viewing endoscope was useful in establishing that

- (i) the water was injected smoothly into the test section to form a continuous film
- (ii) the probe mount did not interfere with the liquid film
- (iii) the liquid film was extracted smoothly, with most of the water passing through the upper section of the extractor porous sinter while the extracted air or steam passed through the lower section.

Unfortunately, when using the radial viewing endoscope to observe the flooding process it provided no qualitative or quantitative information on the flooding situation, mainly because flooding developed very quickly and the viewing area covered by the endoscope as very localised. Thus the developing process of flooding which

covered a much bigger area was incompletely viewed, i.e. the sequence of events leading up to flooding was missing. Furthermore the lens of the endoscope was frequently covered by liquid droplets, making observation difficult.

The second method was carried out in an attempt to overcome the disadvantage of the first method although there was some concern that the endoscope might interfere with the introduction of the air/steam flow into the test section. In this method, the radial viewing endoscope was inserted horizontally through a side tube connected to the settling length tube so that the viewing lens was looking upward. A reasonable image was obtained for the whole length of the test section, but it was not possible to focus on a certain position. In this case the endoscope was useful to observe the wave motions and their growth along the test section. At zero air/steam flowrate, it was clearly seen that the water was injected smoothly and as it moved downwards in a continuous film, ripples of small amplitude appeared on the film surface, mainly at the bottom section of the test tube. These waves grew larger as the air/steam flowrate increased and at moderate air/steam flowrates (0.4-0.6 kg/min), it was observed that (generally) there was only one large wave present which travelled down the tube as a complete ring. The amplitude of the single waves increased as the air/steam flowrate was increased. Before the flooding point was reached, the view inside the test section became

indistinct, mainly because the endoscope lens was covered with liquid droplets, and therefore no qualitative information was obtained near or at the flooding situation. When the flow inside the test section was observed by the naked eye through the endoscope, the quality was much better than that obtained on the video recordings probably because of inadequate illumination. Figure 8.1 shows a sequence of prints taken at intervals of $1/25$ s from the monitor screen for a steam-water test. The water flowrate was 4 l/min, the inlet subcooling was 10 K and the steam flowrate was moderate (approximately 0.5 kg/min). The motion of the disturbance waves down the tube is indicated by arrows in the sequence.

The forward viewing endoscope was inserted inside the test tube through the arrangement made at the air/steam off-take system. Initially, the viewing lens of the endoscope was located just above the liquid injector, so that it would not affect the events taking place inside the test section. Also, by making use of the zoom facility attached to this endoscope it was possible to focus at different axial locations within the test section. A reasonable image for the flow was obtained and all the observations made by the radial viewing endoscope at zero or low air/steam flowrates were thus confirmed. As the air/steam flowrate was gradually increased, liquid droplet entrainment also increased and impinged on the viewing lens of the endoscope but since

the lens was located at the test tube centre line, the high speed of the air/steam cleared the water droplets from the lens face. During the lead-up process to flooding, it was observed that the waves on the water film surface grew larger, mainly at the lower end of the test section, as the air flowrate was incrementally increased, and the film surface became chaotic near the flooding situation. In the course of time, a point was reached at which large amplitude waves were observed to have formed on the film surface at or near the flow removal sinter, and were carried by the air/steam phase. The onset of flooding was achieved when one of these waves passed the water inlet section. This observation indicated that the flow reversal process started at or near the flow removal sinter.

It was also observed that the time required for the flooding process to develop was less in the steam-water tests than in the air-water tests. Also, the flooding process required more time to develop at low water flowrates than with high water flowrates. Similar observations were obtained when the axial location of the viewing lens of the endoscope was moved along the test section. When the forward viewing endoscope was used, it was not possible to observe the single wave on the film surface which could be clearly seen using the radial endoscope.

Unfortunately, it was only possible to view the events clearly inside the test section through the endoscope by looking at it with the naked eye. The recordings obtained for these events, using a black and white video camera, were of poor quality and not informative. This was mainly due to inadequate lighting and some optical problems which arose between the endoscope zoom and the video camera. The company which supplied the endoscope and the video camera was not able to solve any of these optical problems, nor was the Audio Visual Department in the University. However, the endoscope viewing technique will require further development and is expected to perform much better in a transparent test section since the illumination problem would be solved.

8.2 Video Camera System

The colour video camera was fixed at the top of the test tube and the camera lens was located as near as possible to the viewing window. A good image was obtained for the whole length of the test section as it was found, mainly in the steam/water tests, that by tilting the video camera by a few degrees (less than 10) the image could be improved. This was due to avoiding the direct light from the illumination system at the settling length which was facing the video camera lens.

The observations of the events which took place inside the test section were obtained in three ways.

- (i) In situ viewing of the flow which was obtained by the camera output being instantaneously shown on a monitor screen.
- (ii) The events were recorded on a video tape and frame by frame analysis carried out later. A selected sequence of frames has been photographically reproduced. Each plate shows the time in minutes, seconds and 1/100 seconds; the time between each frame was 1/25 second.
- (iii) The colour video camera was removed and the events inside the test section viewed by the naked eye through the viewing window system.

Before presenting the video camera results it should be noted that:-

- (i) In the description of the photographic frames four categories of air or steam flowrate were used:
 - (a) Low air/steam flowrate: less than 0.2 kg/min
 - (b) Moderate air/steam flowrate : in the range of 0.4-0.7 kg/min

- (c) Before flooding air/steam flowrate: in the range of 0.1 kg/min before the flooding flowrate
 - (d) Flooding air/steam flowrate: at the start of flooding
- (ii) The best method of observing the counter-current flow situation and the flooding process was by the naked eye directly on the test tube. When the process was recorded on a video tape there was some loss of qualitative information and even more was lost when the plate was photographed from the monitor screen. Thus the description below is compiled from the photographic information supplemented by the naked eye data.
- (iii) The length of test tube was 1 m, but because of optical effects, the movement of disturbances at the bottom of test tube appeared small (1 or 2 mm) on the photographs of successive frames which represented an actual movement of 10-20 cm in the test tube.

The results obtained from the air-water tests are described in Section 8.2.1 and the results from the steam water tests in Section 8.2.2.

8.2.1 Air-Water System

A good image was obtained of the whole test section. The video camera lens was focussed at two different locations (a) the bottom of the test section, and (b) the middle of the test section. Fig. 8.2 shows two plates for the test section with no flow at each of the two focussing positions used. This figure also indicates the position of the liquid injector, test section, extractor and the glass tube used for illumination. Three different inlet water flowrates were used in the tests viewed, 4 l/min, 10 l/min and 16 l/min, with the air flowrate being varied incrementally up to the flooding point. In general, the image obtained for the water flowrate at 4 l/min was better than that at 10 l/min and both were better than that at 16 l/min since the thicker layers of water film reflected less light and thus looked darker. This can be seen in Figure 8.3 which shows two plates of the water film at each of the three water flowrates respectively. The two plates illustrate the two focusing methods employed. The observations obtained from each of the three water flowrates which were viewed are presented separately:

(i) In air-water tests using a low water flowrate of 4 l/min, it could be clearly seen that the water was injected smoothly and continuously. The film surface at the top part of the test section was very smooth. As the

film moved downward, small ripple waves appeared and the film surface looked particularly wavy near the lower end of the test section. The waves on the film surface were relatively slow moving. As a low flowrate of air was introduced to the test section the amplitude of the waves slightly increased. These small waves can be seen in plates 1- 6 on Figure 8.4a, which shows a sequence of movements at intervals of $1/25$ s, these prints being produced from the video tape. In those sequence of plates the waves were small enough so that the top part of settling length of tube (just below the extractor) can be seen as the very dark area (near the arrows). On increasing the air flowrate incrementally, the film surface became more disturbed mainly at the bottom of the test section. This can be seen on plates 7 - 12 on Figure 8.4a. In this sequence of plates, the vertical arrows still refer to the position of the extractor sinter; it can be seen that the amplitude of the waves at that position was high enough to cover the dark area of the settling length tube; the horizontal arrows show the existence of smaller waves at the top half of the tube. Further increases in the air flowrate had the effect of increasing the amplitude of the disturbance waves and the film surface became very chaotic near the flooding situation, particularly at the lower end of the test section. When the air flowrate reached the critical point, it was noted that the developing process leading up to the flooding situation took a relatively long time.

It began with the appearance of highly disturbed waves on the water film at or near the flow removal sinter. These disturbed waves propagated slowly and spasmodically up the tube and when it was thought that they may develop and cause the flooding, they smoothly died out and disappeared into the falling film flow. At the same time other disturbed waves of high amplitude at or near the flow removal sinter started to propagate up the tube. This oscillation was repeated many times and it could run for several minutes before one of these waves eventually moved and propagated very quickly upwards past the water inlet section, signalling the onset of flooding. Most of the time this sequence took place without any increase in the air flowrate. On other occasions, the upward propagation of the disturbed waves could not reach the water inlet sinter, even after being left for a substantial time. Consequently flooding occurred with a relatively small increase in the air flowrate. Flooding was found to be sensitive to small increases in the air flowrate, so care had to be taken not to overshoot the flooding air flowrate. When flooding took place, the falling film was observed to become heavily disturbed and part of the liquid began to flow upwards. Meanwhile the amplitude of the waves near the lower end of the test section became very large so that they started to block the test section. In this situation the light inside the test tube sharply decreased, as the test section was illuminated by a system installed below it, and accordingly viewing became

difficult. Figure 8.4b shows a selection of plates demonstrating the situation just before flooding, for an inlet water flowrate of 4 l/min. In this figure, the difference in the amplitude of waves can be seen, if for example, plate 1 is compared with plate 12. The disturbance size at the extractor sinter in plate 1, the vertical arrow, was smaller than the size of the disturbance in plate 12. Furthermore, the colour of the disturbances in plate 1 was milky while those in plate 12 were very dark. The horizontal arrows again indicate much smaller waves at the top half of the test tube. Figure 8.4c shows the same situation at the critical point. This clearly shows that the time needed for the flooding process to develop is relatively large (about 10 sec. shown in the frame). In this figure, plates 1, 2 and 3 show relatively small disturbances at the extractor sinter (the vertical arrows) and plates 4, 5 and 6 show that the disturbances have increased. While the disturbances almost blocked the bottom of the tube causing it to become very dark, in plates 7, 8 and 9 and more light passed through to the test tube as the disturbances decreased. In plates 10, 11 and 12, the disturbances at the bottom of the test tube increased again and started blocking the tube. In Figure 8.4c the video camera has managed to pick some smaller disturbances at the top half of the tube (horizontal arrows) which appeared as milky lines. Figures 8.5a, 8.5b and 8.5c contain a series of plates showing the sequence of events leading up to the

flooding situation, for the same water flowrate (4 l/min), but at a focussing location positioned at the middle section of the test tube.

(ii) When experiments were carried out with an inlet water flowrate of 10 l/min (a medium flow rate), the water film appeared on the monitor screen to be slightly darker at the bottom of the test section, although it could be clearly seen by the naked eye through the viewing window. Plates 1, 2 and 3 on Figure 8.6a show the waves at the film surface for low air flowrates while plates 4, 5 and 6 show the situation at a moderate air flowrate and for the same water flowrate. Plates 7-12 in Figure 8.6a show a sequence of events leading to flooding. In this figure, it can be seen that as the air flowrate is increased, the film surface becomes darker as the surface gets rougher. The waves on the film surface were clearly seen along the tube as milky lines (horizontal arrows), while they appears as milky areas at the bottom of the tube as the amplitude of the waves was higher (vertical arrows). Figure 8.6b contains 12 plates with a time difference between each of $1/25$ s, illustrating the events at the flooding situation.

Examination of this figure, and other recordings involving a water inlet flowrate of 10 l/min, indicated that, if the air flowrate was increased to the critical point, the developing process leading up to the flooding

situation took a relatively shorter time. A comparison between the events shown by the plates in Figure 8.4c and Figure 8.6b indicate that flooding is a very quick process, but the time required for it to develop decreased substantially as the inlet water flowrate increased from 4 l/min to 10 l/min (about 10 times faster in the low flowrate). In both cases the flooding process was observed to start at the same place, which was at or near the flow removal sinter. Another sequence of events for air-water tests with an inlet water flowrate of 10 l/min is shown in Figures 8.7a and 8.7b where the viewing of the air-water interface was taken at a focussing location positioned at the middle of the test tube.

(iii) In air-water tests involving an inlet water flowrate of 16 l/min, which was regarded as a relatively high rate of flow, the film appeared darker at the bottom section of the test tube. The waves on the film could hardly be distinguished on the monitor screen, though it could be seen by the naked eye. In these tests, the results concerning the location at which the flooding was started and the speed at which the flooding process was developed were similar to those described in previous tests with a water inlet flowrate of 10 l/min with two variations. These were (a) the film surface was more agitated and its reaction to the increase of the air flowrate was more violent and (b) the time required for the flooding process to be developed was slightly shorter.

Figure 8.8a shows a selection of prints taken for an air-water test with an inlet water flowrate of 16 l/min and various air flowrates up to the flooding point. Figure 8.8b shows a sequence of prints for the same test at the flooding point. Figures 8.9a and 8.9b show another sequence of events for the same inlet flowrates where the air-water interface before, and during, the flooding process are viewed at a focussing location positioned at the middle section of the test tube.

During all air-water tests, it was observed that most of the water droplets were entrained from disturbance waves at the bottom of the test section where the wave amplitudes were higher. It was also noted that when the air flowrate reached the critical value and flooding was about to take place, the amount of water droplets being entrained increased substantially. As the inlet water flowrate was increased the size of the water droplets also increased. The difference between the time required for the flooding process to be developed in air-water tests with an inlet water flowrate of 4 l/min and that with an inlet water flowrate of 10 l/min was substantial. There was very little difference in the time required in the tests carried out with an inlet water flowrate of 10 l/min and 16 l/min.

8.2.2 Steam Water System

Flow visualisation under steam-water conditions was a much more difficult process than that under air-water conditions, since the presence of steam and the condensation effects made the situation more complicated. Therefore the viewing image obtained for the events inside the test section, as expected, was not as clear as that obtained in the air-water tests but was still a reasonable image. The viewing procedure was carried out for the same three inlet water flowrates; 4, 10 and 16 l/min, with the steam flowrate being incrementally varied up to the flooding point. For the first two flowrates, subcoolings were varied between 10K and 80K in increments of 10K, while for the largest flowrate it was only possible to obtain views up to 50K. The manoeuvring of the video camera lens on the viewing window was less flexible under steam-water conditions; therefore it was decided to concentrate the focussing location at one position i.e. at the bottom section of the test tube.

Viewing experiments involving the low inlet water flowrate of 4 l/min produced a good image when the water subcooling was low. As the inlet water subcooling was increased, the quality of the image consequently decreased slightly. At low inlet water subcoolings and low steam flowrates, small disturbance waves were observed on the film surface, particularly at the lower end of the test

section. On increasing the steam flow incrementally, these disturbance waves grew and the film surface became very agitated as the flooding situation was approached. The disturbance waves and their growth in the process leading up to flooding under steam-water conditions similar to that under air-water conditions. The main difference between the two situations was that with low inlet water subcoolings, the film surface was observed to be fractionally rougher when steam was used. This film surface roughness increased as the inlet water subcooling increased and the difference was more noticeable with high subcoolings. When the steam flowrate reached the critical point, as in the air-water tests, the developing process leading up to the flooding situation was observed to start with the appearance of highly disturbed waves at the lower end of the test section, mainly at or near the extraction sinter. In the early stages, sequences of these disturbed waves were observed to be propagated up the test section, before they lost their momentum and disappeared into the falling film flow. In the course of time, the film surface became very agitated mainly at or near the extraction sinter and when one of these disturbed waves moves upwards passing the inlet water sinter, this marked the start of the flooding process. On some occasions the final upward propagation of the disturbed waves towards the inlet water sinter required only a very small increase in the steam flowrate. At low inlet water flowrates, the developing process leading up to flooding

took less time than that required for a similar situation under air-water conditions. This time decreased as the inlet water subcooling was increased. Figures 8.10a and 8.10b show a selection of prints taken from a sequence of steam-water tests at a water inlet flowrate of 4 l/min and various steam flowrates up to the critical point. The inlet water subcooling was 30K. Again the vertical arrows refer to the disturbances at the extractor sinter while the horizontal arrows refer to the smaller disturbances existing along the test tube. Figures 8.11a and 8.11b show another selection of prints demonstrating a similar situation with an inlet water subcooling of 80K.

The disturbed waves and their upwards movement in the developing process leading up to flooding could be clearly seen in some of the steam-water tests, probably because the film surface was rougher than when air and water was used. The video camera was able to pick up and record some of the movement of the disturbed waves just before flooding, as is demonstrated in Figures 8.12, 8.13 and 8.14, which show sequences of prints for three different inlet water subcooling, 20K, 30K and 70K respectively. The disturbed waves could be clearly seen as milky areas at the bottom of the test section. Disturbances moving up the tube appeared on the photographs with sharper front edges, in contrast with disturbances moving downwards which appear to have less

sharp fronts. However the upward disturbances movement can be followed by the arrows shown on the plates. For example plates 4 and 5 in Figure 8.12 indicate a disturbance movement of about 2 to 3 mm which corresponds to about 20-30 cm along the film surface of the test section. The arrow in plate 3 points to a clear disturbance which dies out in plate 4, after a movement of about 1 mm (about 10 cm). Similar conclusions can be obtained when the arrows pointing to the disturbances in plates 1 and 2 in Figure 8.13 are followed. However this wave motion could be better followed on a monitor screen and even better when it is observed directly by the naked eye in the test tube.

Increasing the inlet water flowrate to 10 l/min had the effect of increasing the film surface roughness which also increased as the inlet water subcooling increased. At the same time the image of the flow shown on the monitor screen was slightly less distinct particularly at high inlet water subcooling. The disturbance waves on the film surface could be clearly seen up to the critical condition. At the critical condition, the upward propagated disturbance waves were not able to be distinguished on the monitor screen, but they could be clearly seen by the naked eye through the viewing window. Similarly to the air-water conditions, the flooding process was manifested by the appearance of the disturbance waves at or near the extraction sinter.

Figures 8.15a and 8.15b show a sequence of prints for steam-water tests with inlet water subcooling of 10K and a flowrate of 10 l/min. The prints 6-12, Figure 8.15b represent the situation at the critical point. These show that flooding developed faster under these conditions than in the air-water tests shown in Figure 8.10b. Similar results are demonstrated by Figures 8.16a, 8.16b and 8.16c which show a selection of prints taken for a steam-water test with an inlet water flowrate of 10 l/min and subcooling of 60K, with increasing steam flowrates up to flooding.

Increasing the inlet water flowrate to 16 l/min had the effect of increasing the roughness of the water film which also increased as the inlet water subcooling was increased from 10K to 50K. The viewing image obtained was of poor quality but the disturbance waves on the film surface could still be seen. Again it was observed that the flooding process started to develop at the lower end of the test tube and the time required for this process to develop was slightly less than in the test using an inlet water flowrate of 10 l/min. The events just before, and at flooding, for an inlet water flowrate of 16 l/min and subcooling of 10K are shown in Figures 8.17a and 8.17b. Figures 8.18a and 8.18b show a similar situation with inlet water subcooling of 50K.

8.3 Simulation of Top Flooding

The flooding process, in all of the tests being viewed, under both air-water and steam-water conditions, was seen to start at the lower end of the test section, at or near the extraction sinter. In order to compare the difference between flooding taking place at the top of the test section and, as happened in the tests, at the bottom of the test section, flooding was simulated to take place at the inlet flow sinter and a series of photographs taken. The simulation was carried out by replacing the seal, which was lodged between the porous tube and the lower flange of the water injector, with another seal of slightly smaller internal diameter. This meant that about 1/2 mm of the seal projected into the flow. A series of tests using both air and steam with water were carried out. Figure 8.19 shows a sequence of 6 prints for a steam-water test with an inlet water flowrate of 4 l/min and subcooling of 10K. The first two prints illustrate the beginning of the flooding process while the other four prints illustrate the development of the flooding process to block the top section of the test tube. It can be clearly seen, from these prints, that the flow in the test section was not disturbed, and the light inside the test section was not blocked, as was found when flooding started at the lower end of the test section.

8.4 Summary

Two systems were used to visualize the counter-current two-phase flow inside the test tube; the endoscope and the video camera systems. The recordings obtained from the endoscope system were of poor quality and the observations had to be made by the naked eye. However, using both systems, it was observed that (i) The wave amplitude increased as it moved down the tube and also increased with the air/steam flowrate (ii) Flooding always started at or near the flow removal sinter and (iii) The flooding process began with the appearance of highly disturbed waves on the liquid film at or near the flow removal sinter. These waves were continuously propagated slowly and spasmodically up the tube, before smoothly dying out and disappearing into the falling film flow. These oscillations were repeated several times before one of the waves eventually propagated very quickly upwards past the water inlet section, signalling the onset of flooding.

Although the flooding process is a very fast process, the time required for it to develop decreased as the inlet water flowrate (and subcooling) increased.

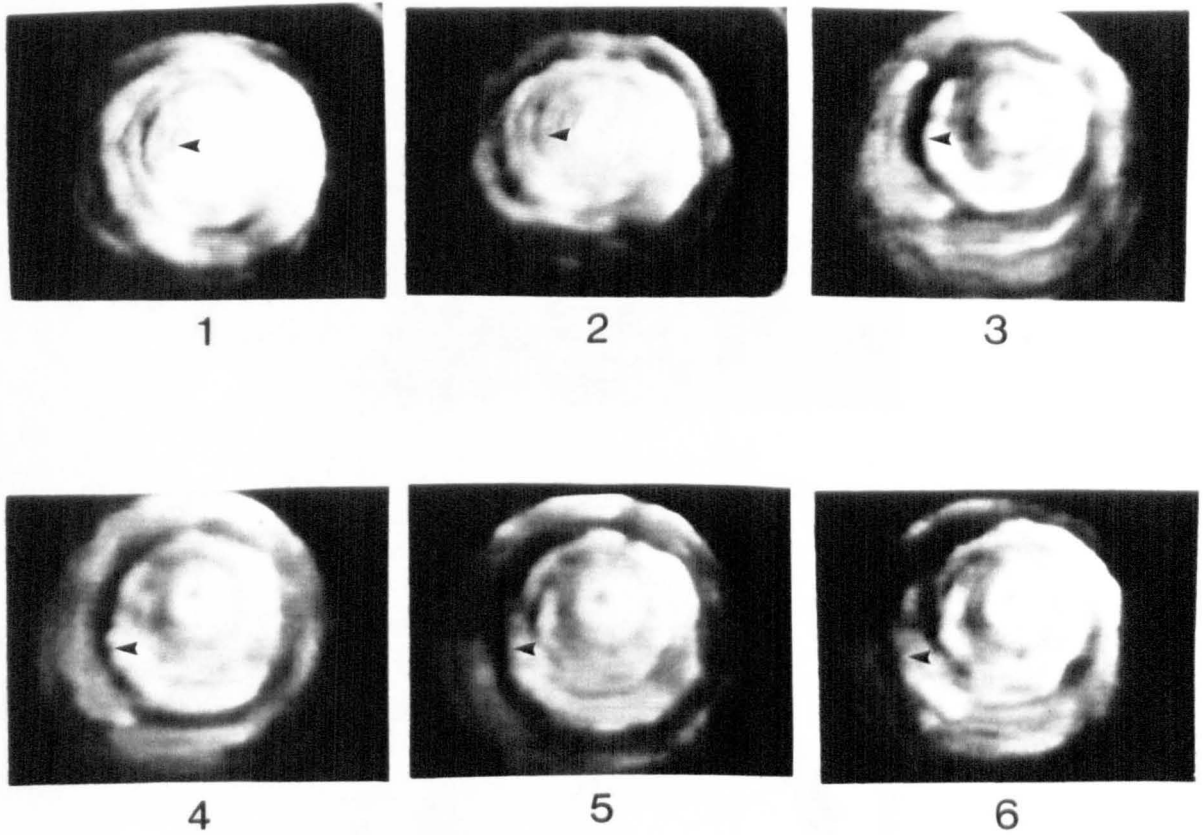
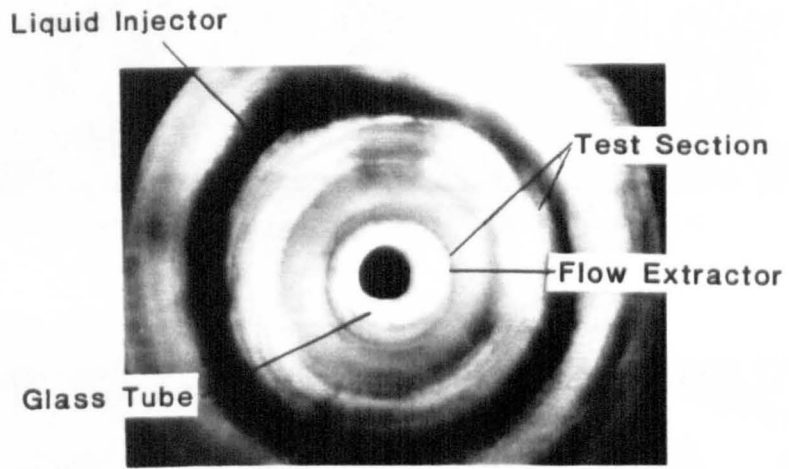
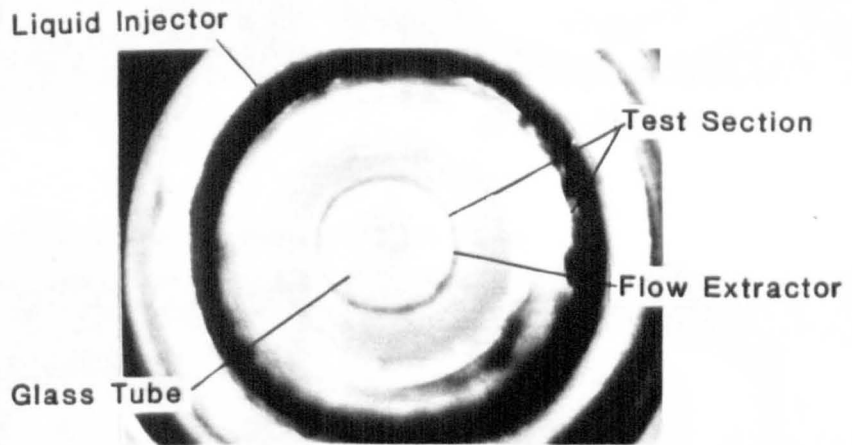


Figure 8.1 Sequence of Events observed through Endoscope showing Liquid Film Behaviour

Steam-Water Test, Inlet Water Flowrate : 4 l/min
Inlet Water Subcooling : 10K



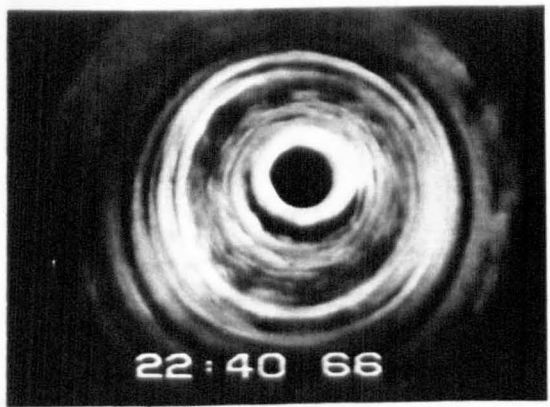
a) Focused on Bottom of Test Section



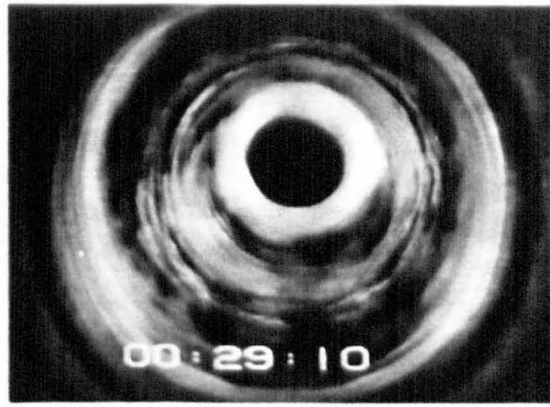
b) Focused on Middle of Test Section

Figure 8.2 Test Section Focused at Different Locations with No Flow Present

a) Inlet Water Flowrate : 4 l/min

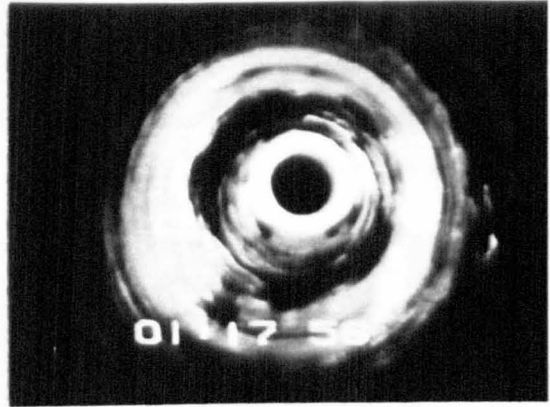


Bottom Focusing

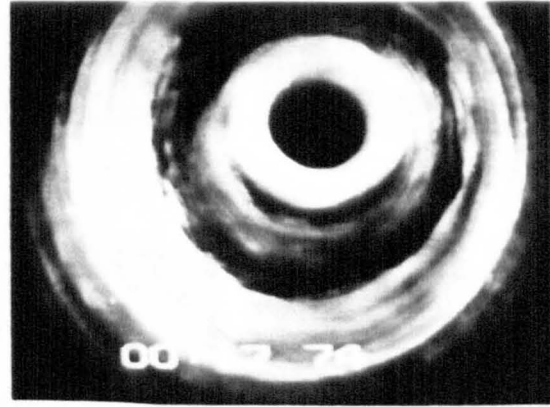


Middle Focusing

b) Inlet Water Flowrate : 10 l/min

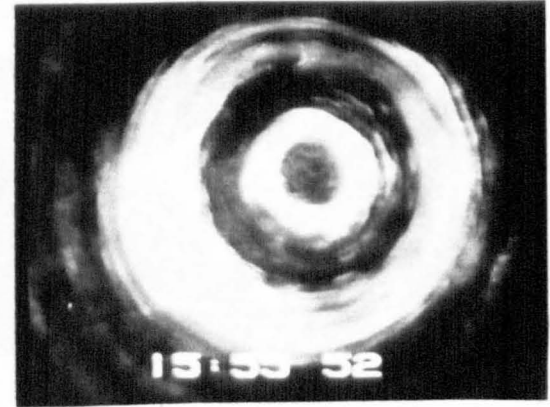


Bottom Focusing

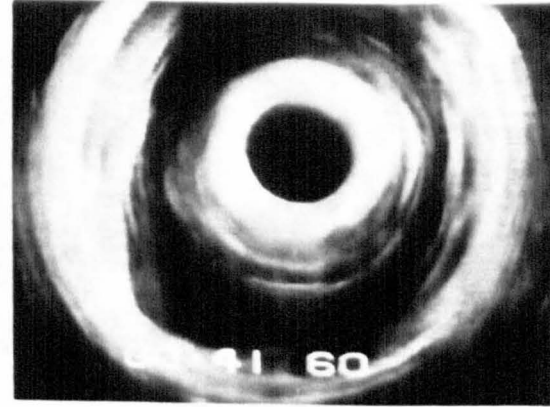


Middle Focusing

c) Inlet Water Flowrate : 16 l/min



Bottom Focusing



Middle Focusing

Figure 8.3 Test Section with Various Water Flowrates and Very Low Air Flowrate

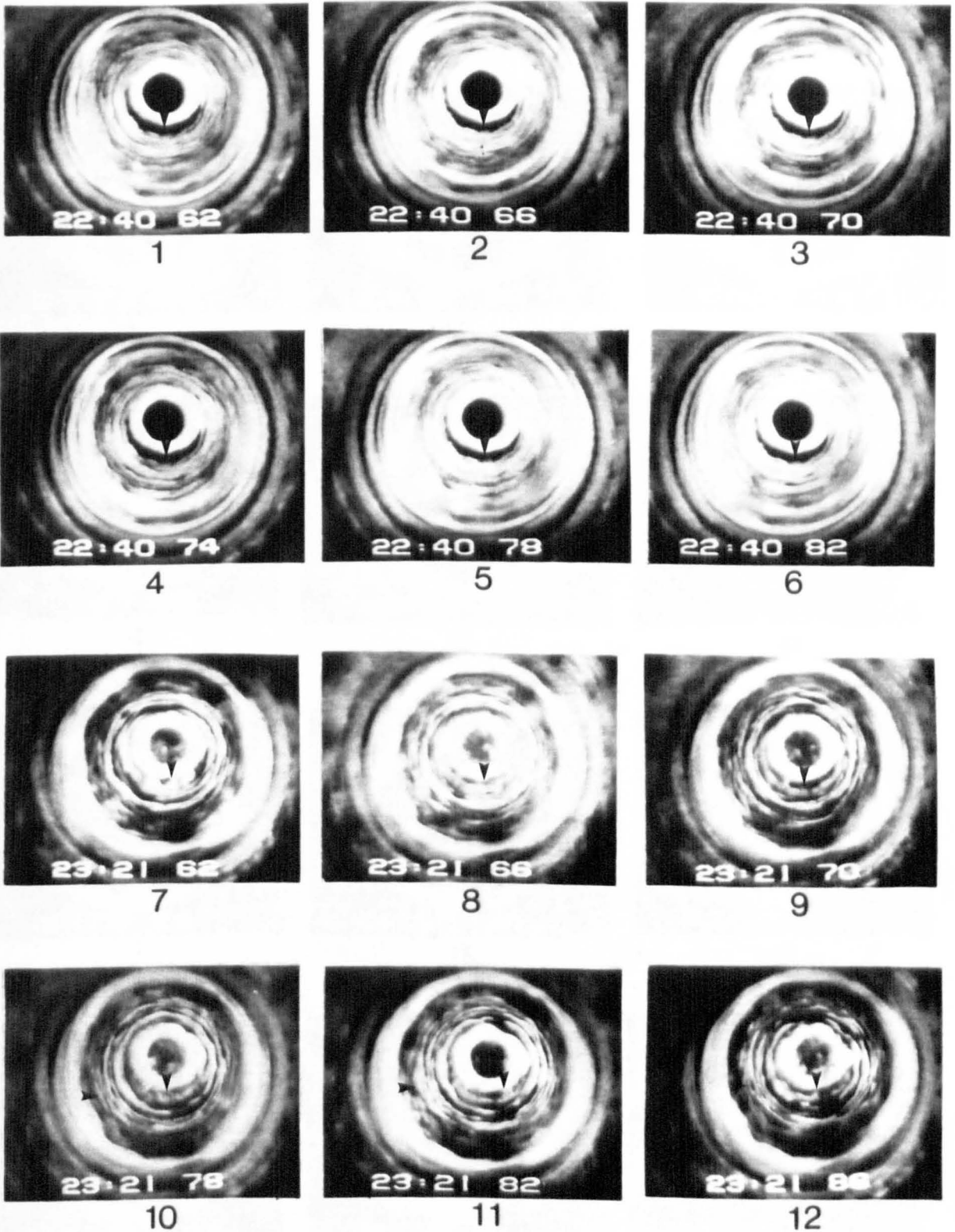


Figure 8.4a Sequence of Events Showing Liquid Film Behaviour at Low and Moderate Air Flowrate

Air - Water Test

Water Flowrate : 4 l/min

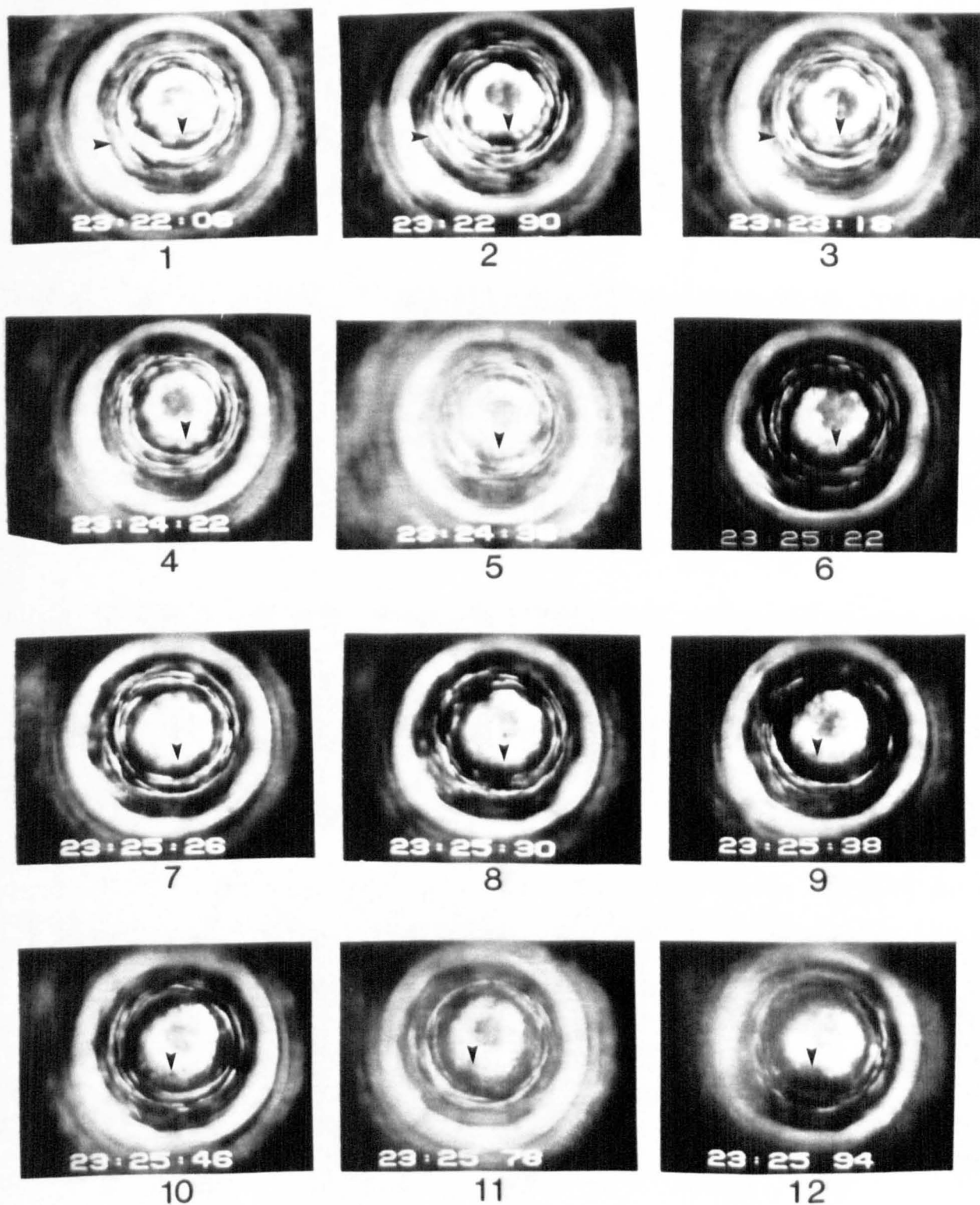


Figure 8.4b Sequence of Events Showing Liquid Film Behaviour Before Flooding

Air - Water Test

Water Flowrate : 4 l/min

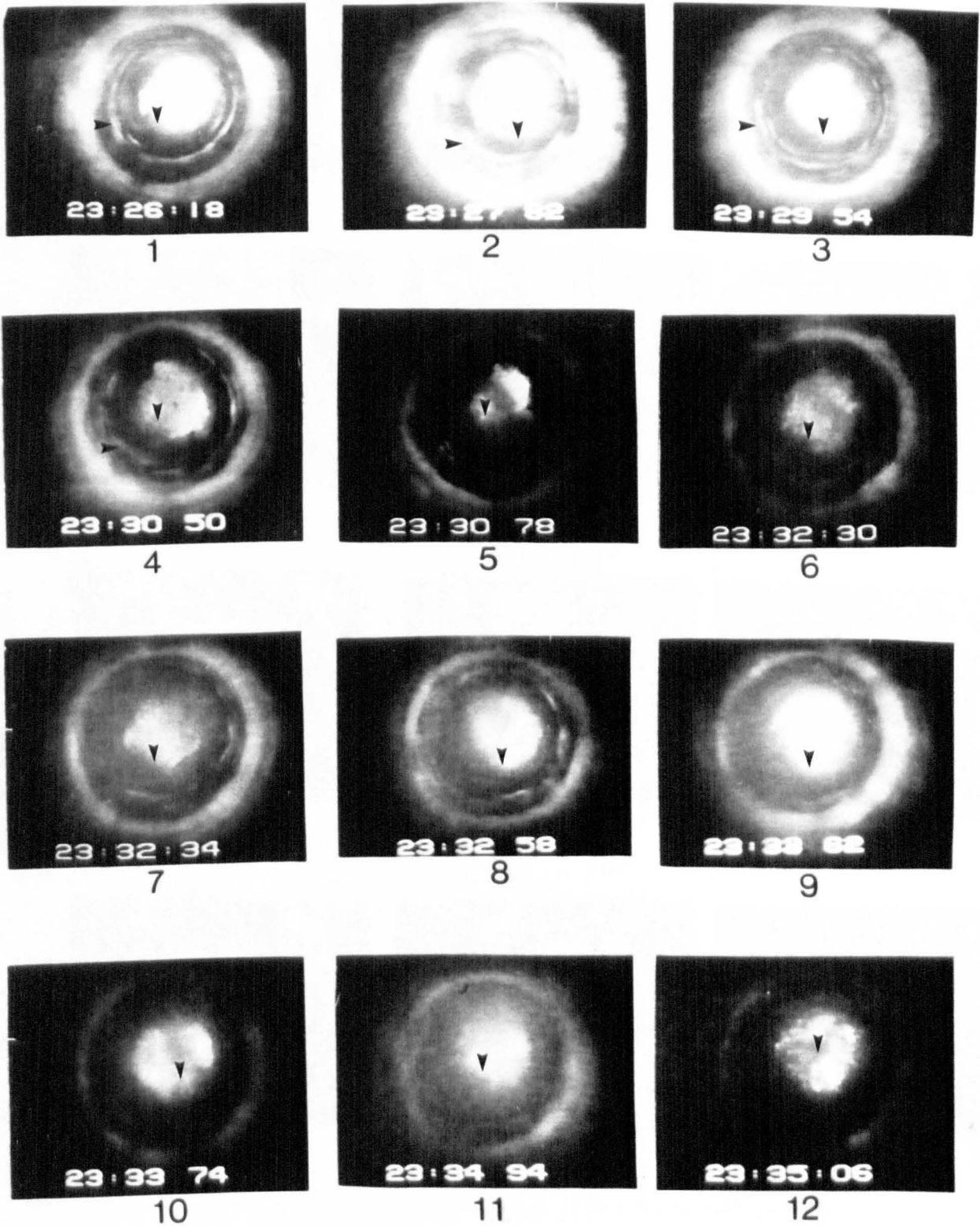


Figure 8.4c Sequence of Events Showing Liquid Film Behaviour at Flooding

Air - Water Test

Water Flowrate : 4 l/min

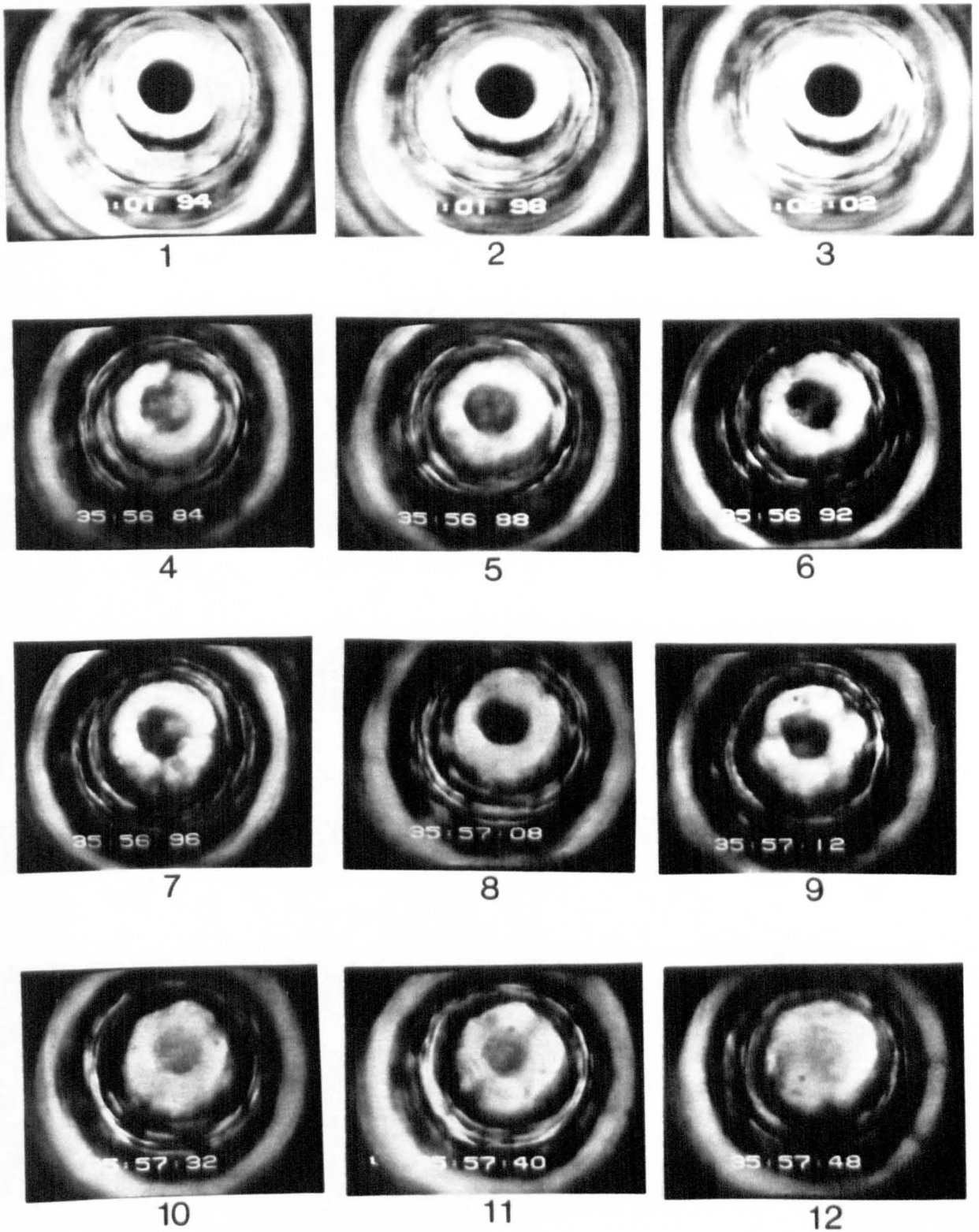


Figure 8.5a Sequence of Events Showing Liquid Film Behaviour at Low and High Air Flowrate

Air - Water Test

Water Flowrate : 4 l/min

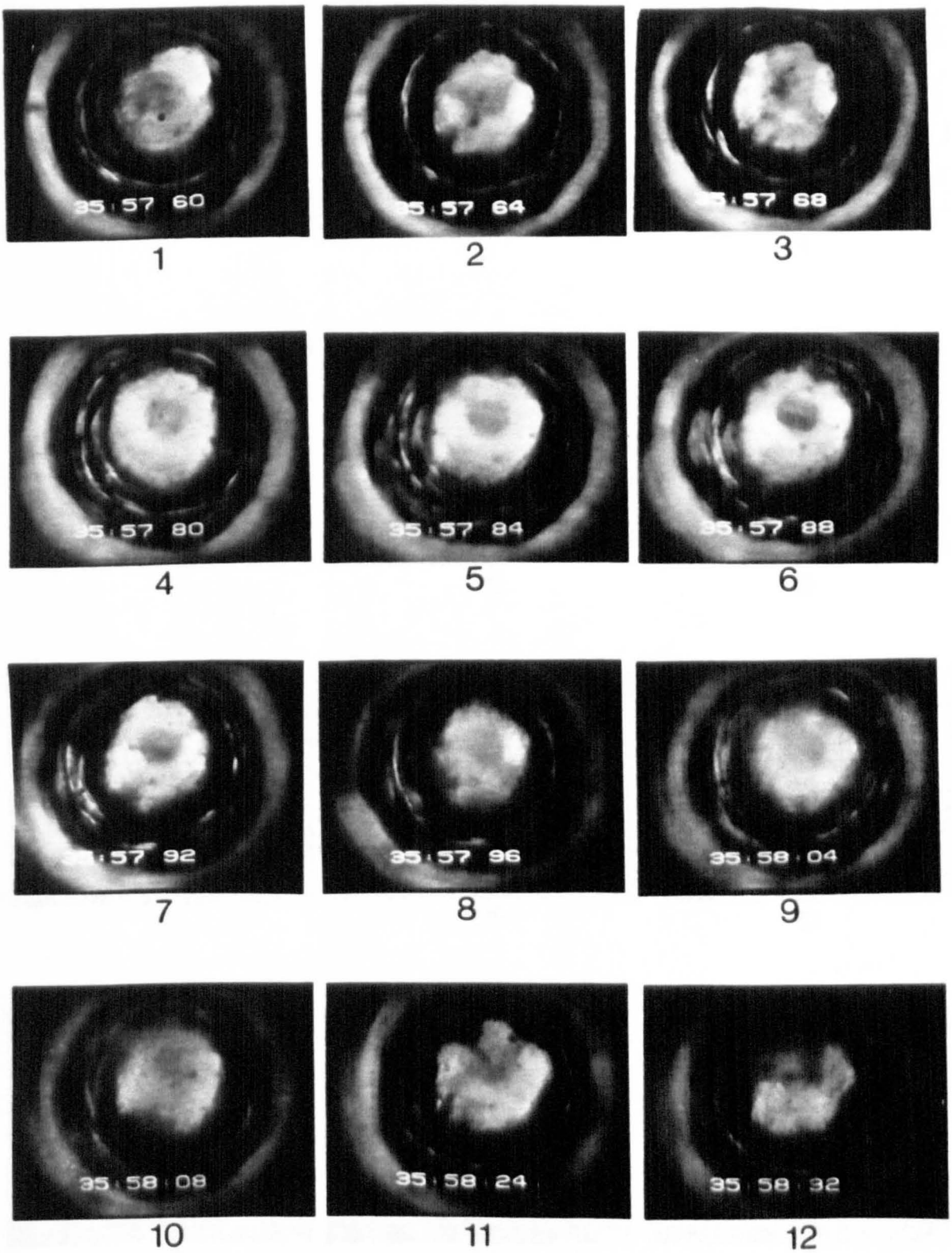


Figure 8.5b Sequence of Events Showing Liquid Film Behaviour Before Flooding

Air - Water Test

Water Flowrate : 4 l/min

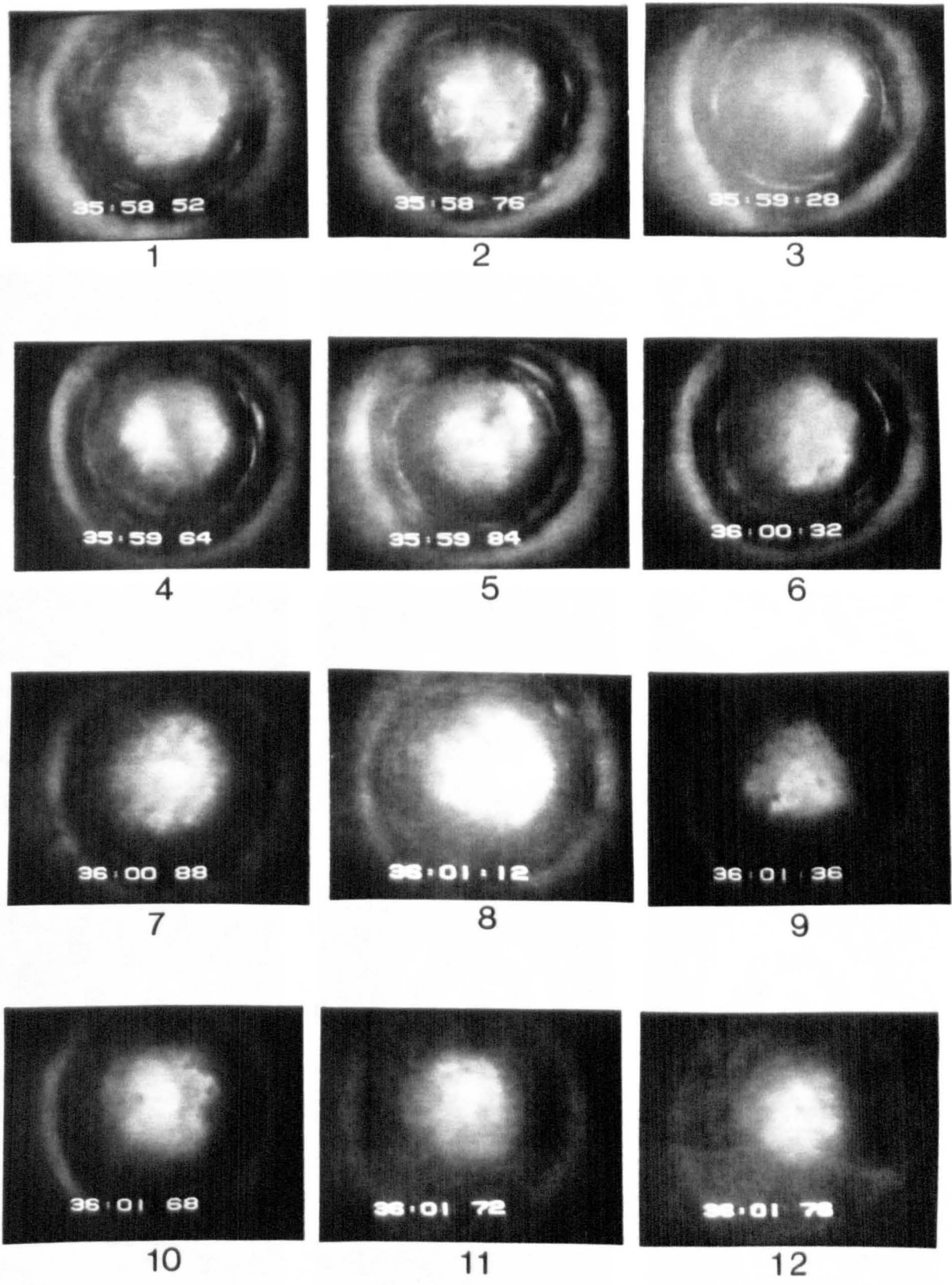


Figure 8.5c Sequence of Events Showing Liquid Film Behaviour at Flooding

Air - Water Test

Inlet Water Flowrate : 4 l/min

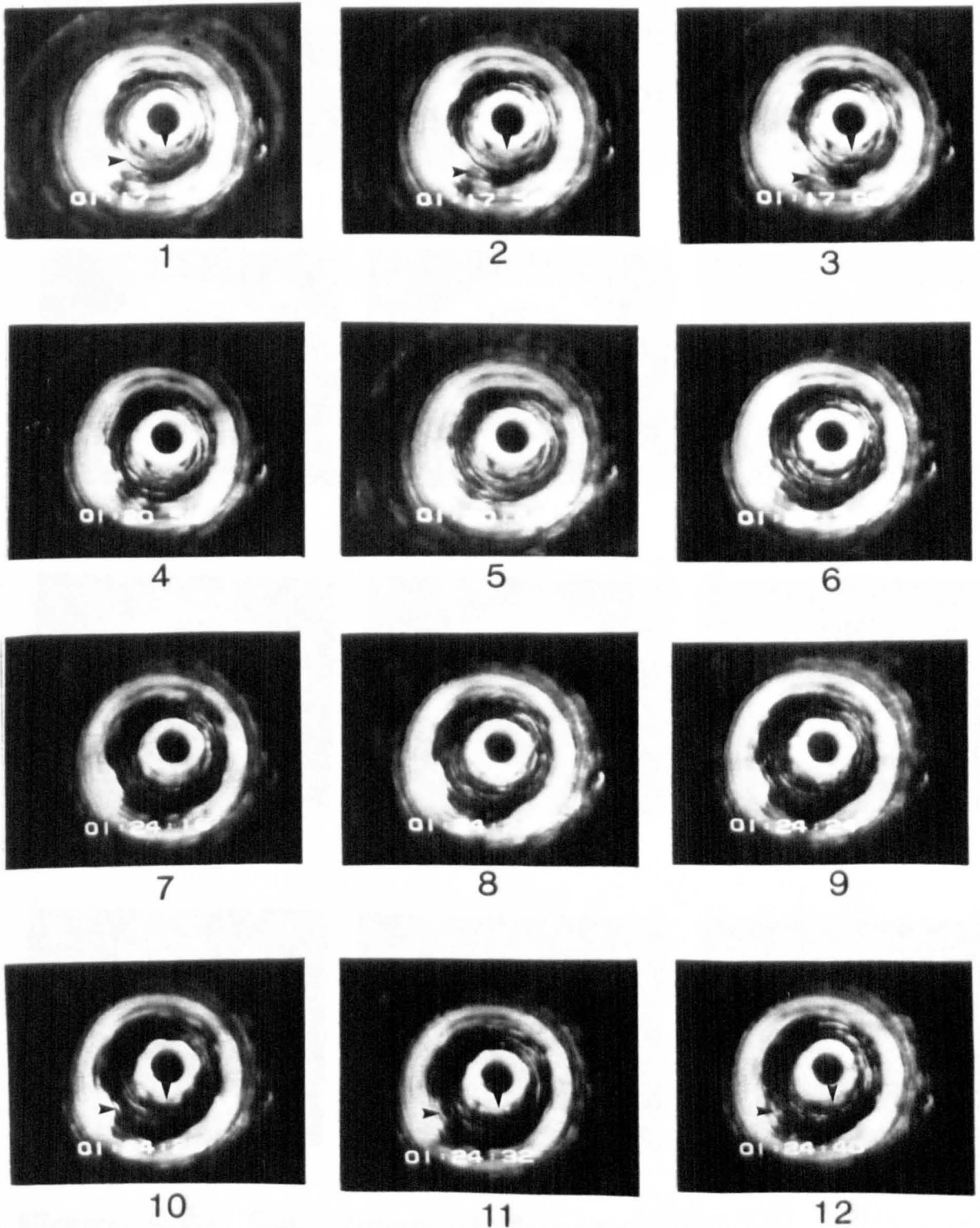


Figure 8.6a Sequence of Events Showing Liquid Film Behaviour at Low, Moderate and High Air Flowrate

Air - Water Test

Water Flowrate: 10 l/min

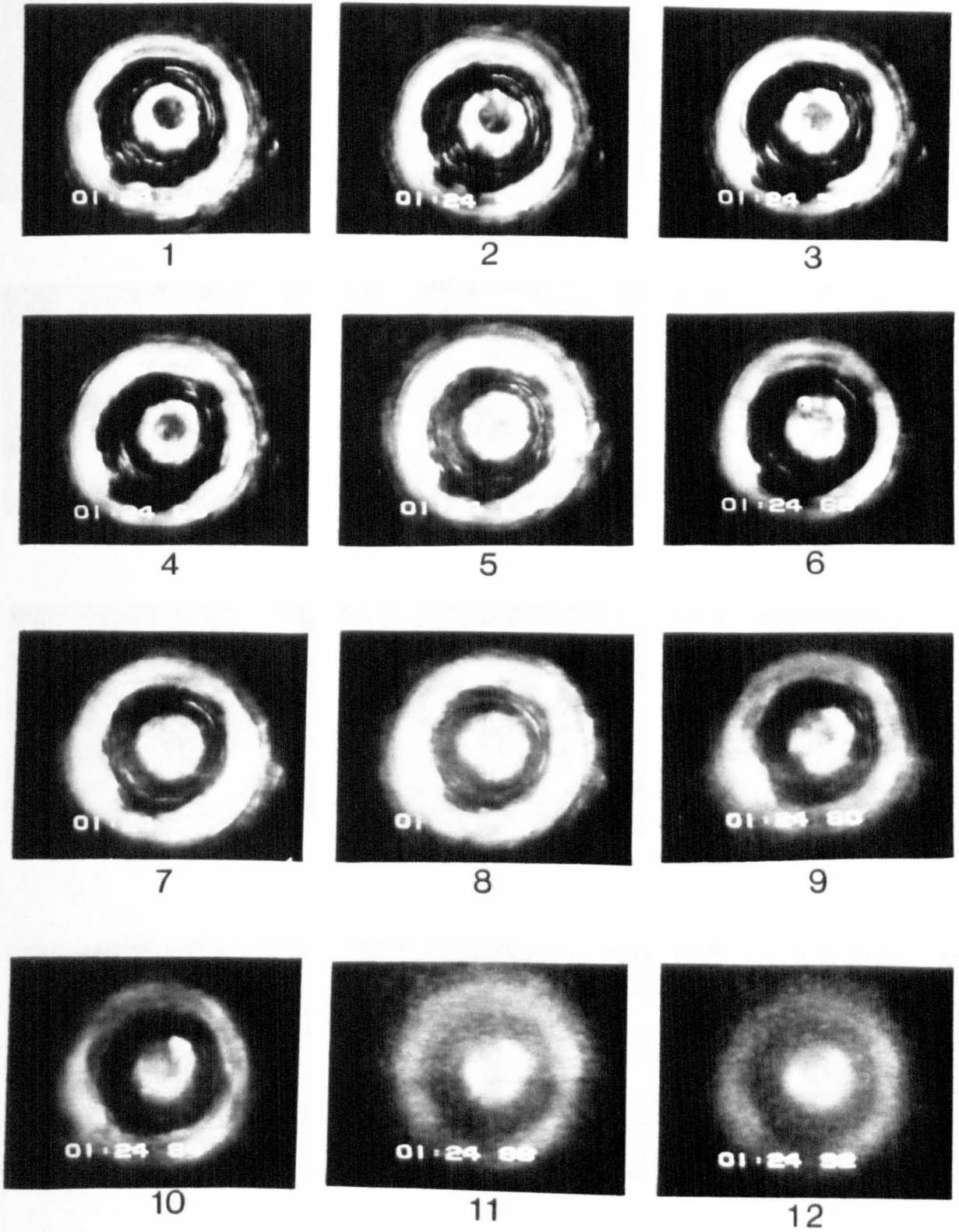


Figure 8.6b Sequence of Events Showing
Liquid Film Behaviour Before and at Flooding

Air - Water Test

Water Flowrate: 10 l/min

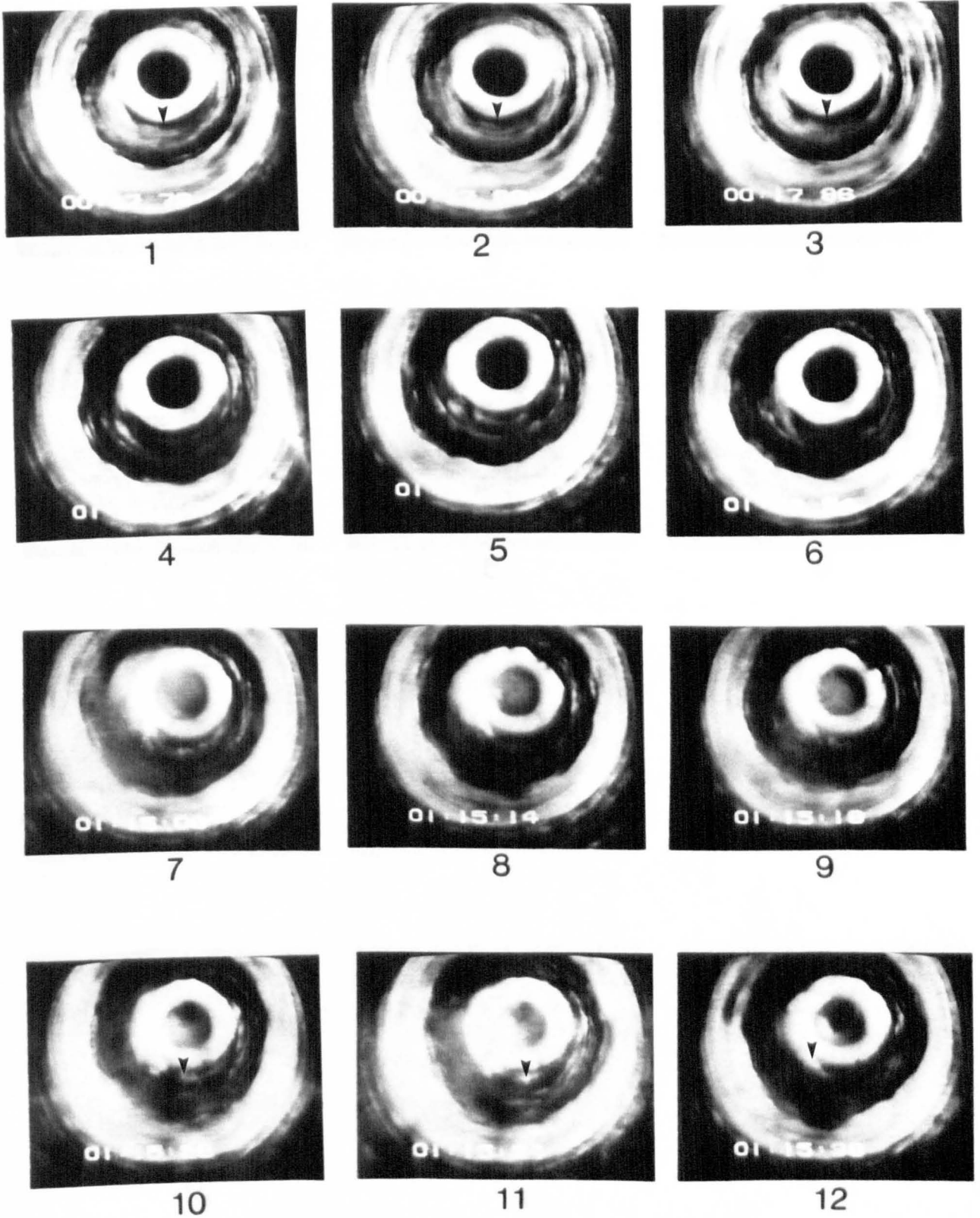


Figure 8.7a Sequence of Events Showing Liquid Film Behaviour Before Flooding

Air - Water Test

Water Flowrate: 10 l/min

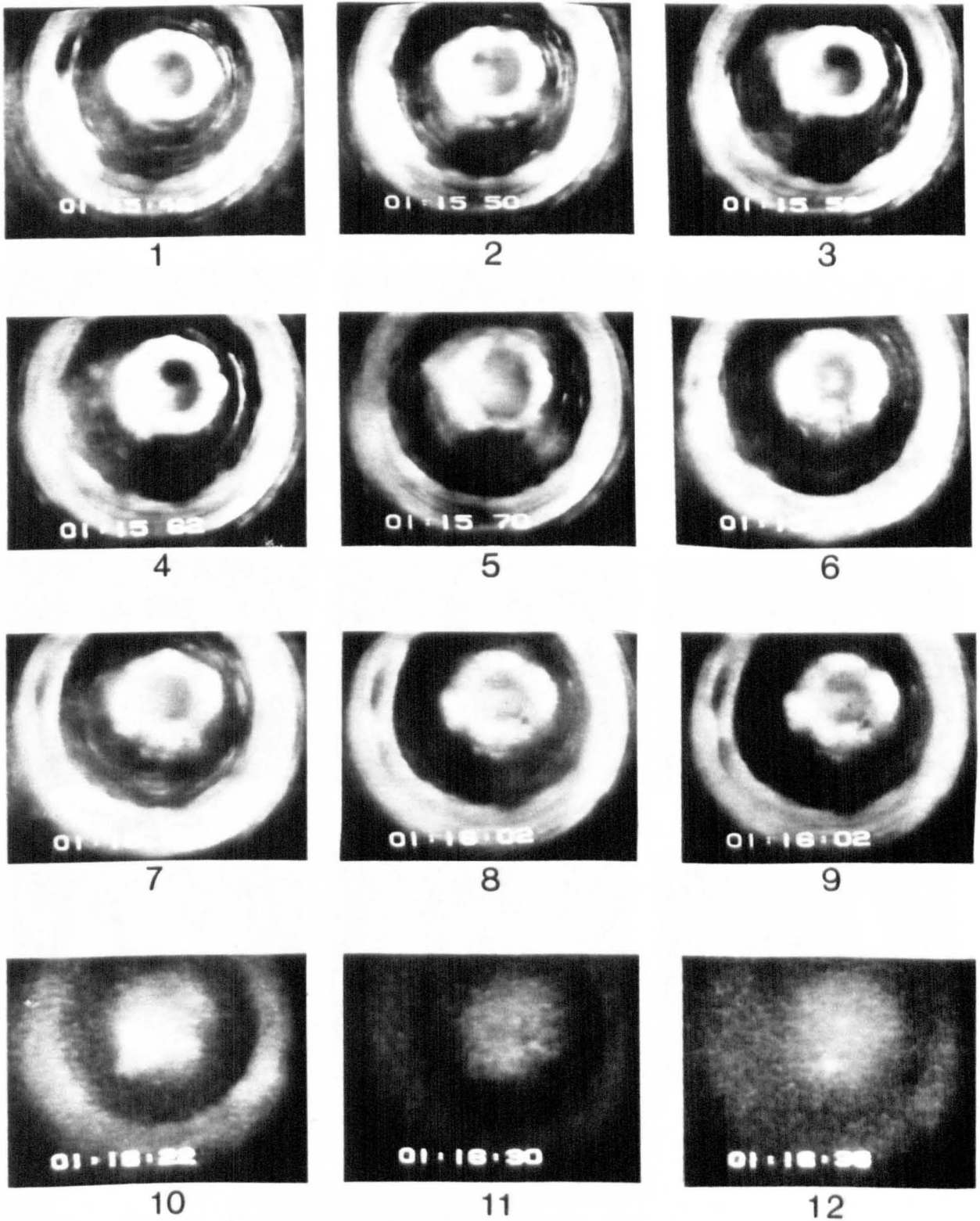


Figure 8.7b Sequence of Events Showing
Liquid Film Behaviour Before and at Flooding

Air - Water Test

Water Flowrate: 10 l/min

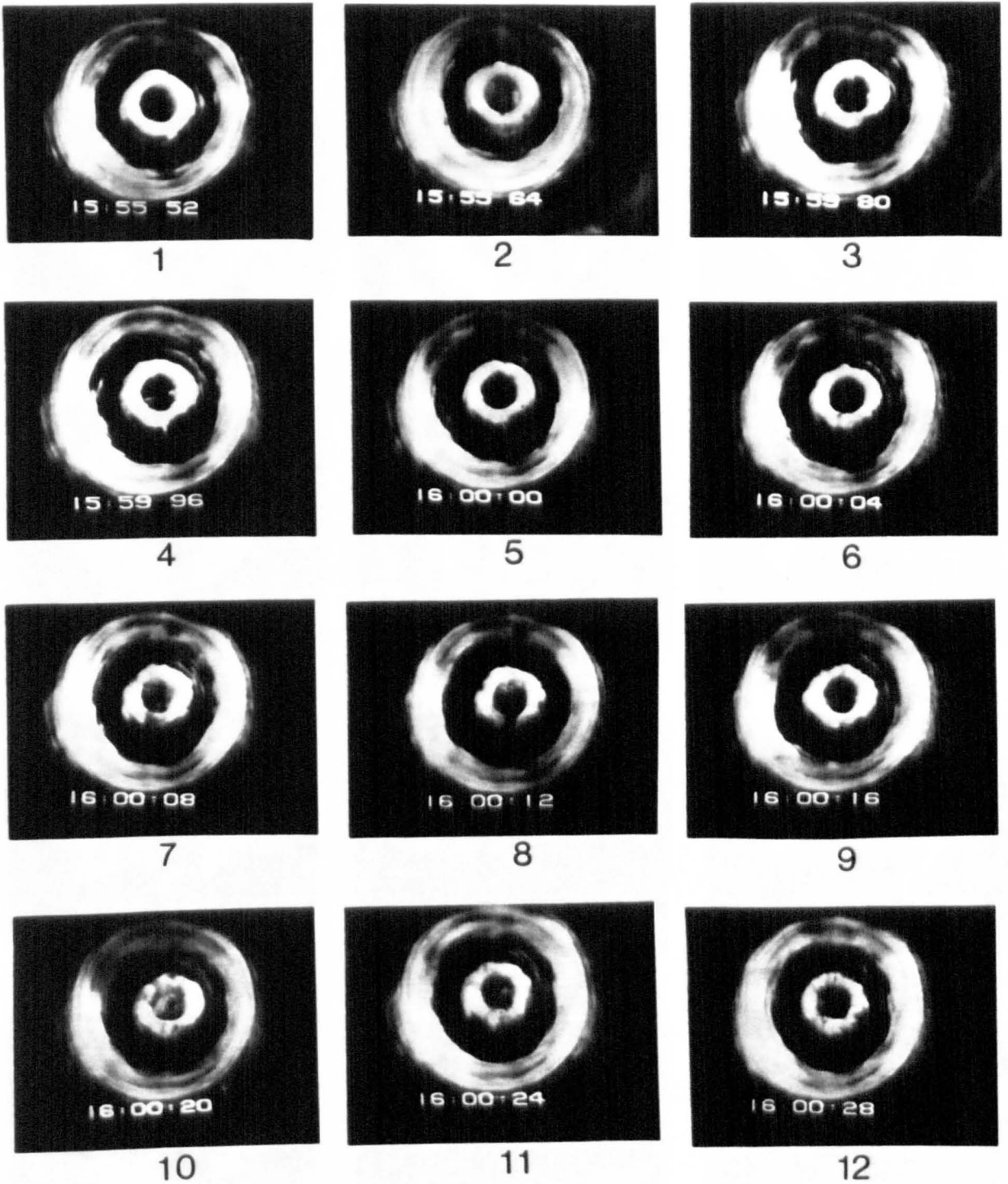


Figure 8.8a Sequence of Events Showing
Liquid Film Behaviour Before Flooding

Air - Water Test

Water Flowrate:16 l/min

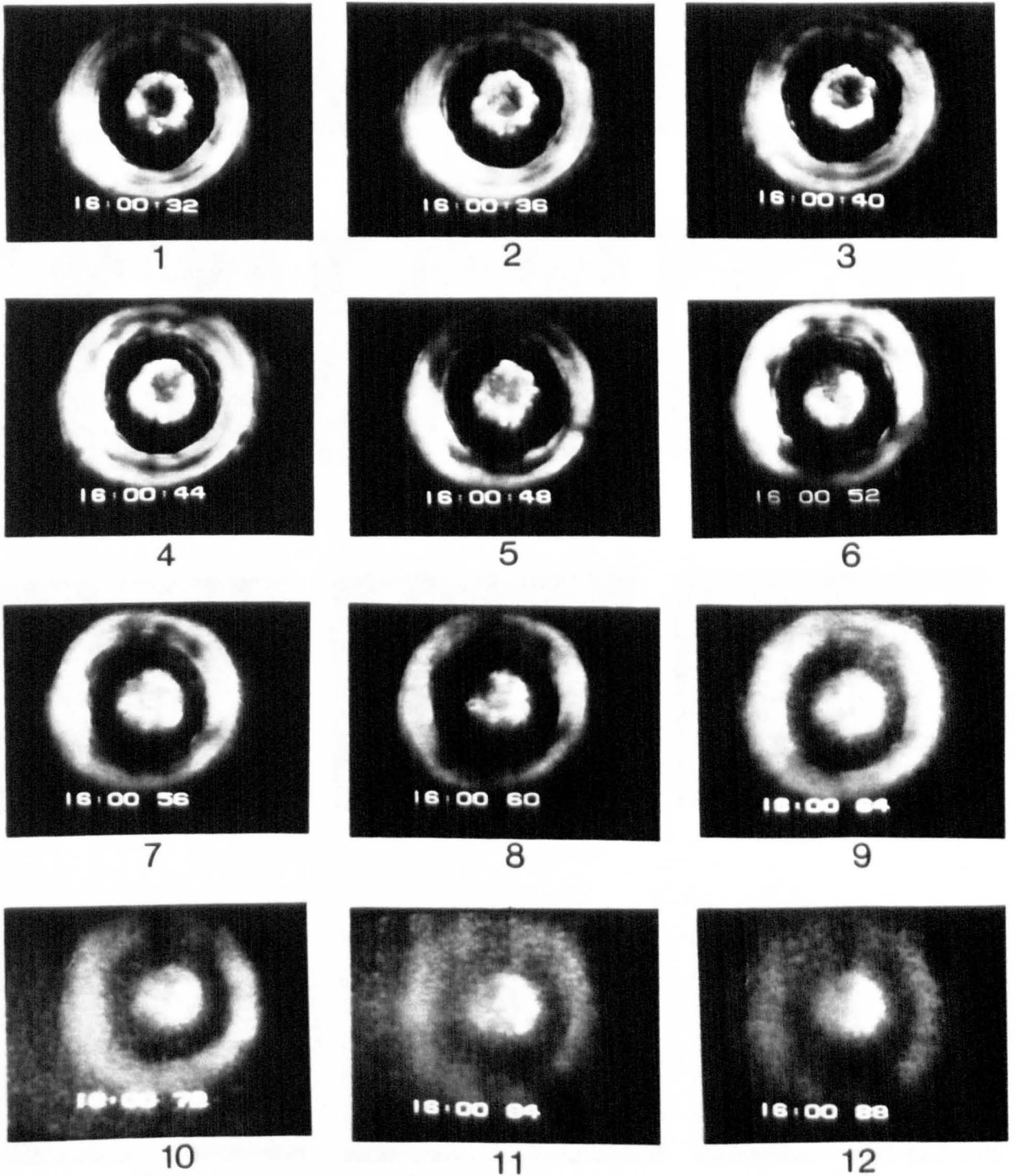


Figure 8.8b Sequence of Events Showing
Liquid Film Behaviour Before and at Flooding

Air - Water Test

Water Flowrate:16 l/min

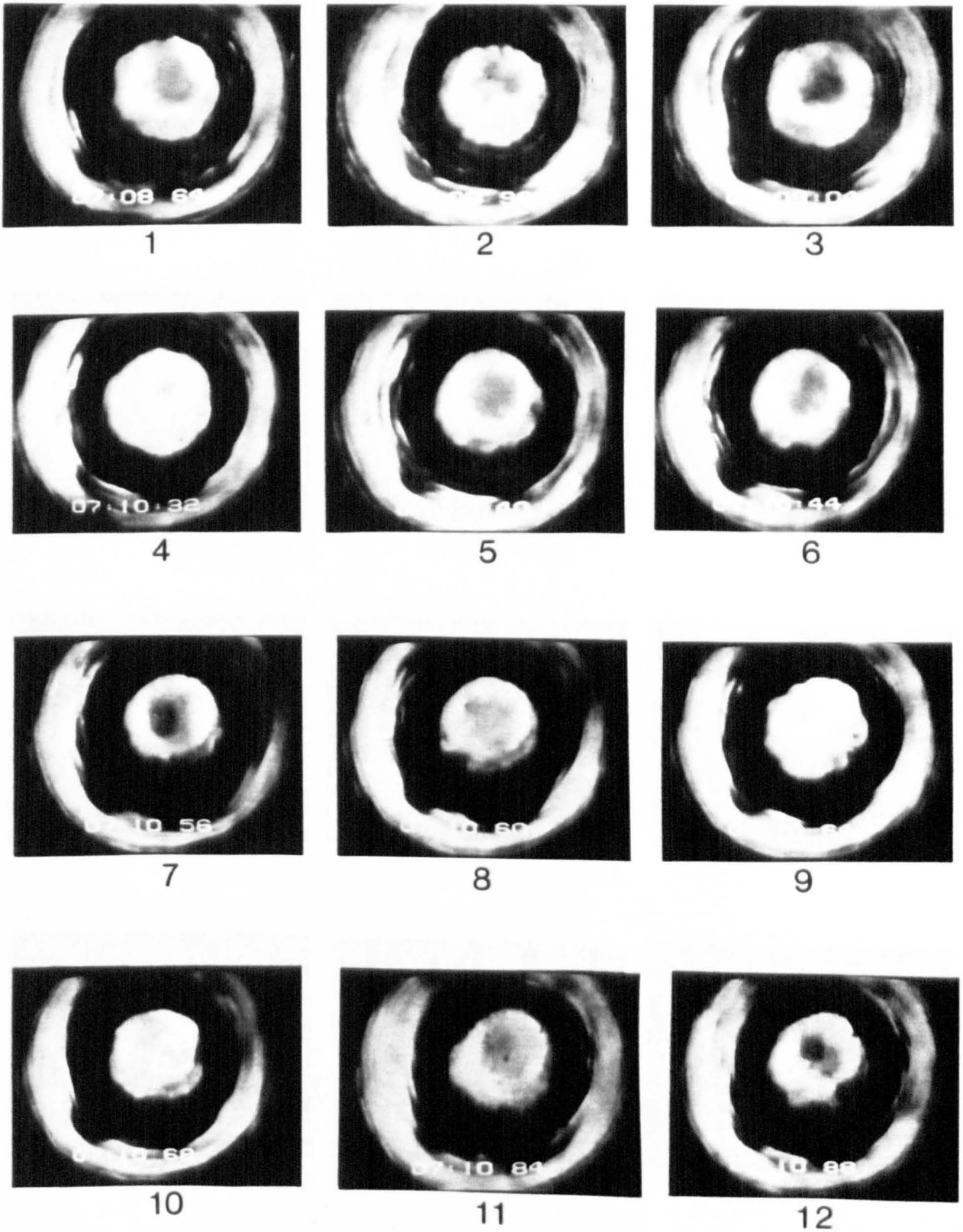


Figure 8.9a Sequence of Events Showing
Liquid Film Behaviour Before Flooding

Air - Water Test

Water Flowrate: 16 l/min

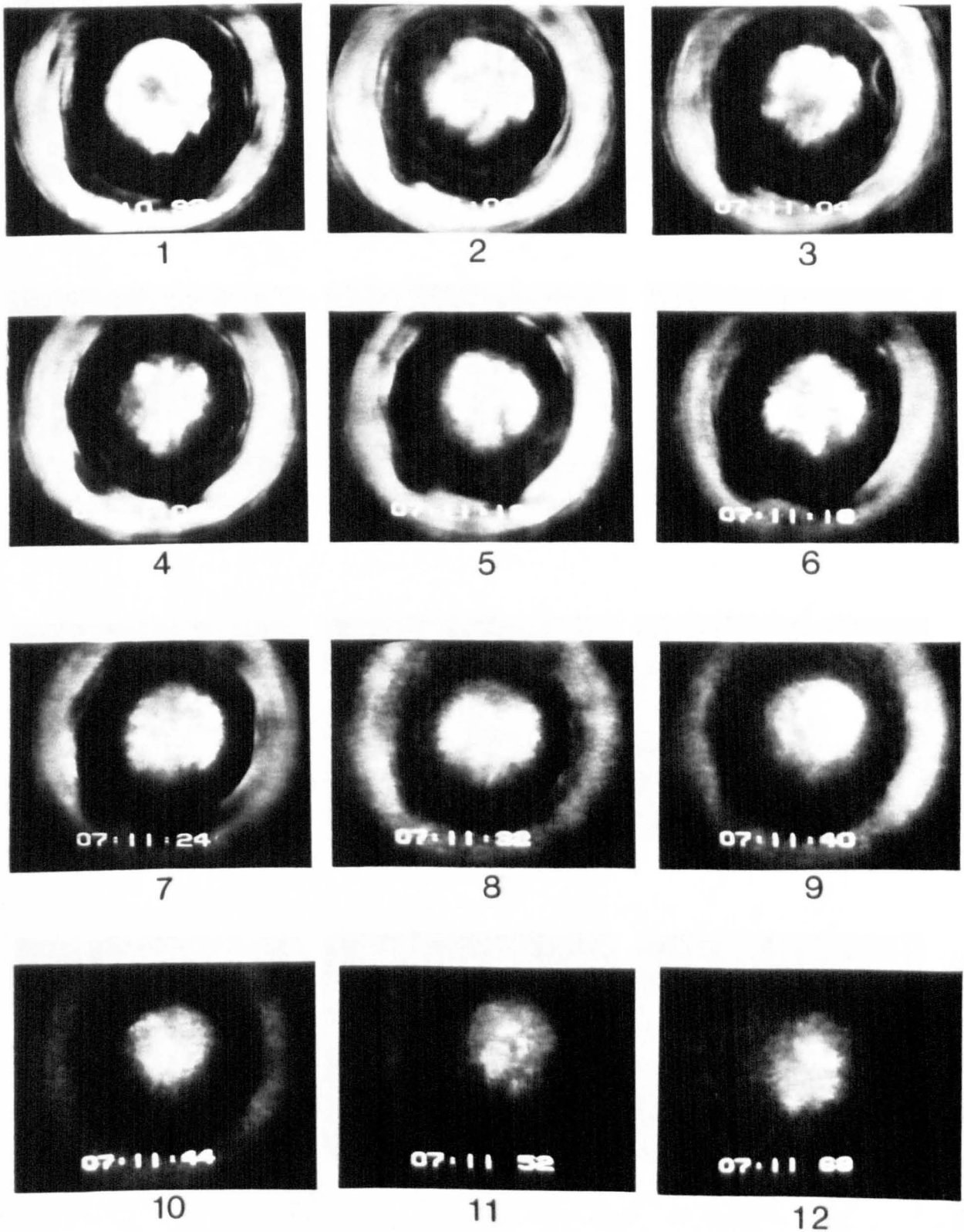


Figure 8.9b Sequence of Events Showing
Liquid Film Behaviour Before and at Flooding

Air - Water Test

Water Flowrate: 16 l/min

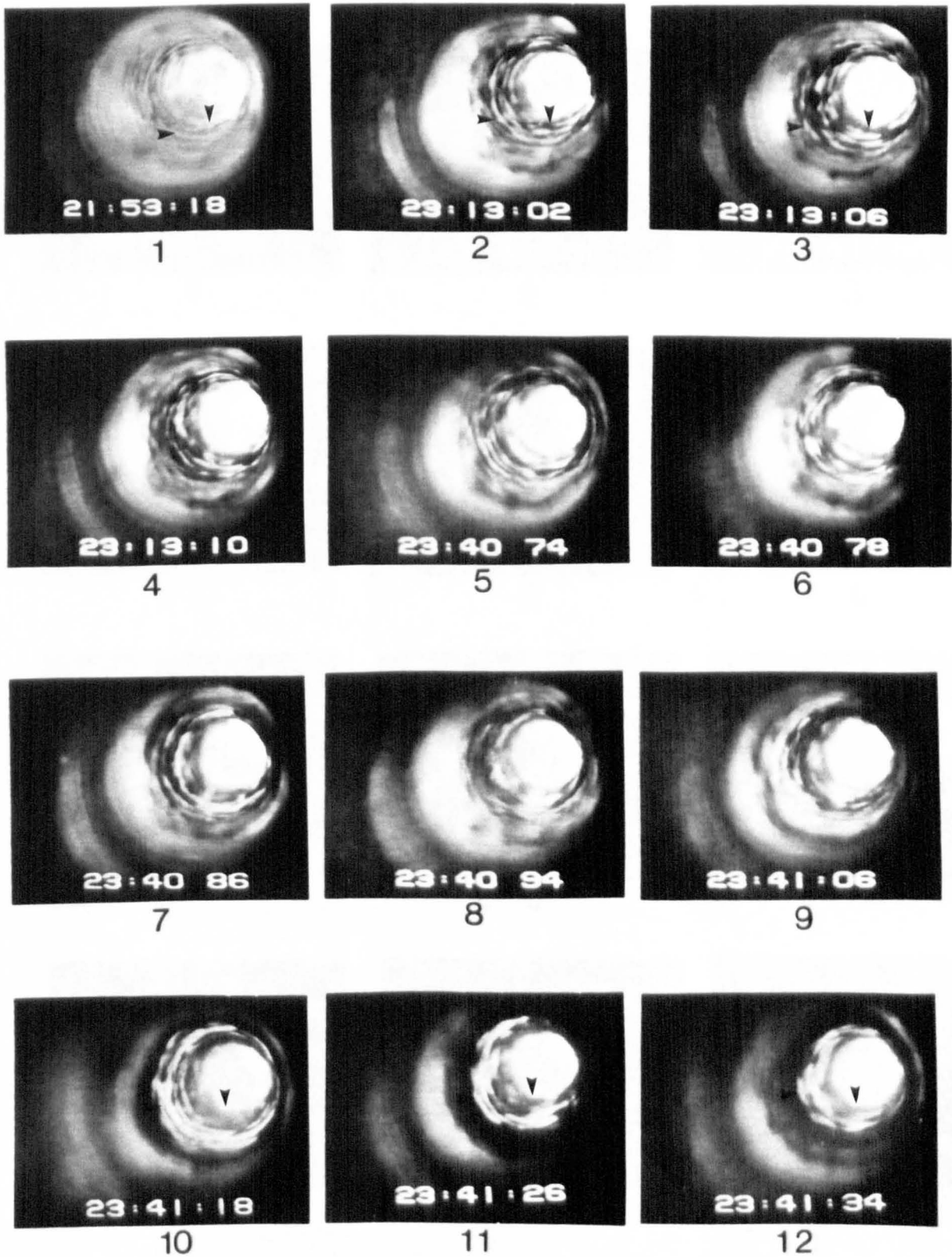


Figure 8.10a Sequence of Events Showing Liquid Film Behaviour at Moderate and High Steam Flowrate

Inlet Water Flowrate : 4 l/min

Inlet Water Subcooling : 30K

Steam - Water Test

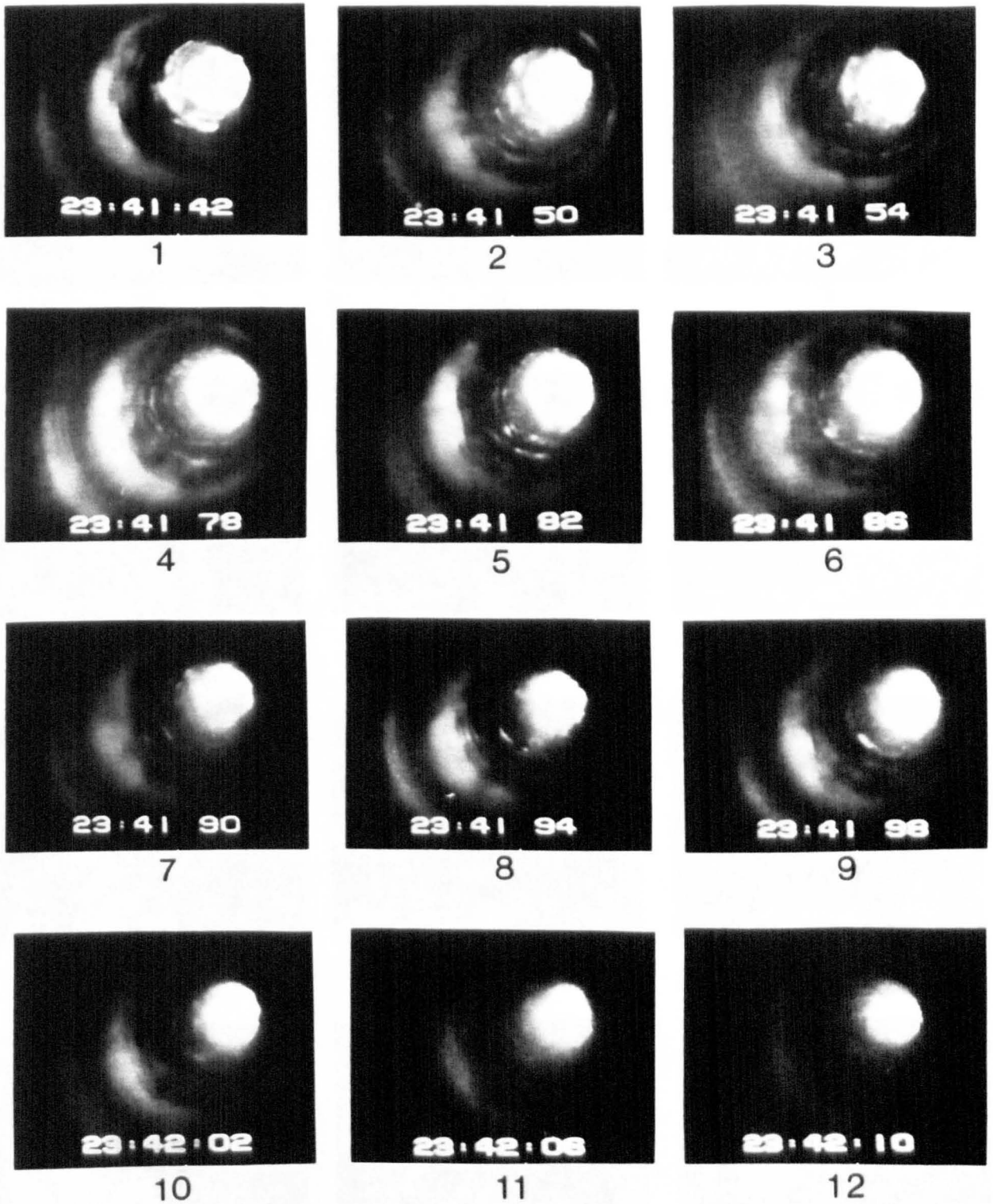


Figure 8.10b Sequence of Events Showing
Liquid Film Behaviour at Flooding

Steam - Water Test Inlet Water Flowrate:4 l/min Inlet Water Subcooling:30K

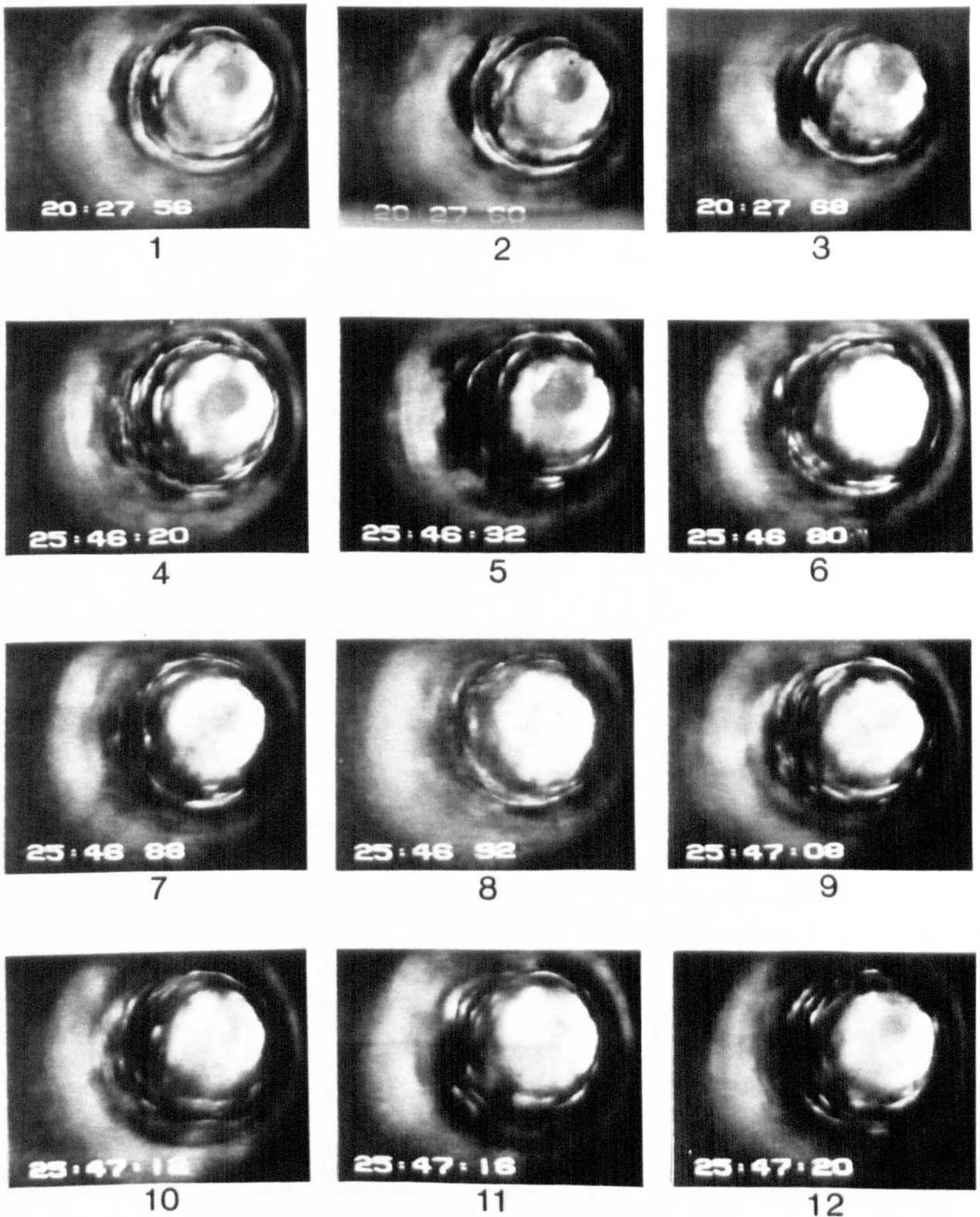


Figure 8.11a Sequence of Events Showing Liquid Film Behaviour at Moderate and High Steam Flowrate

Steam - Water Test Inlet Water Flowrate:4 l/min Inlet Water Subcooling:80K

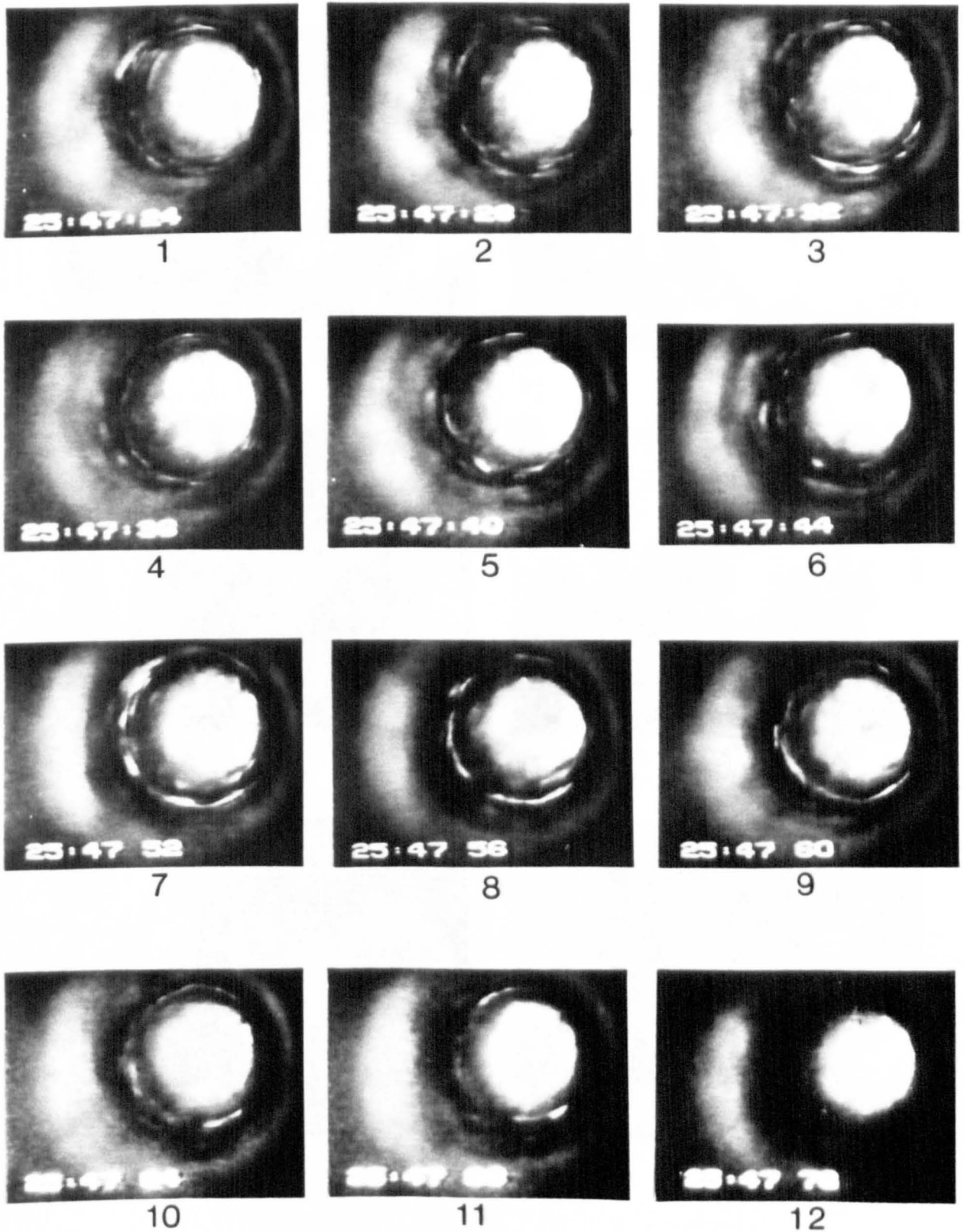


Figure 8.11b Sequence of Events Showing Liquid Film Behaviour at Flooding

Steam - Water Test Inlet Water Flowrate:4 l/min Inlet Water Subcooling:80K

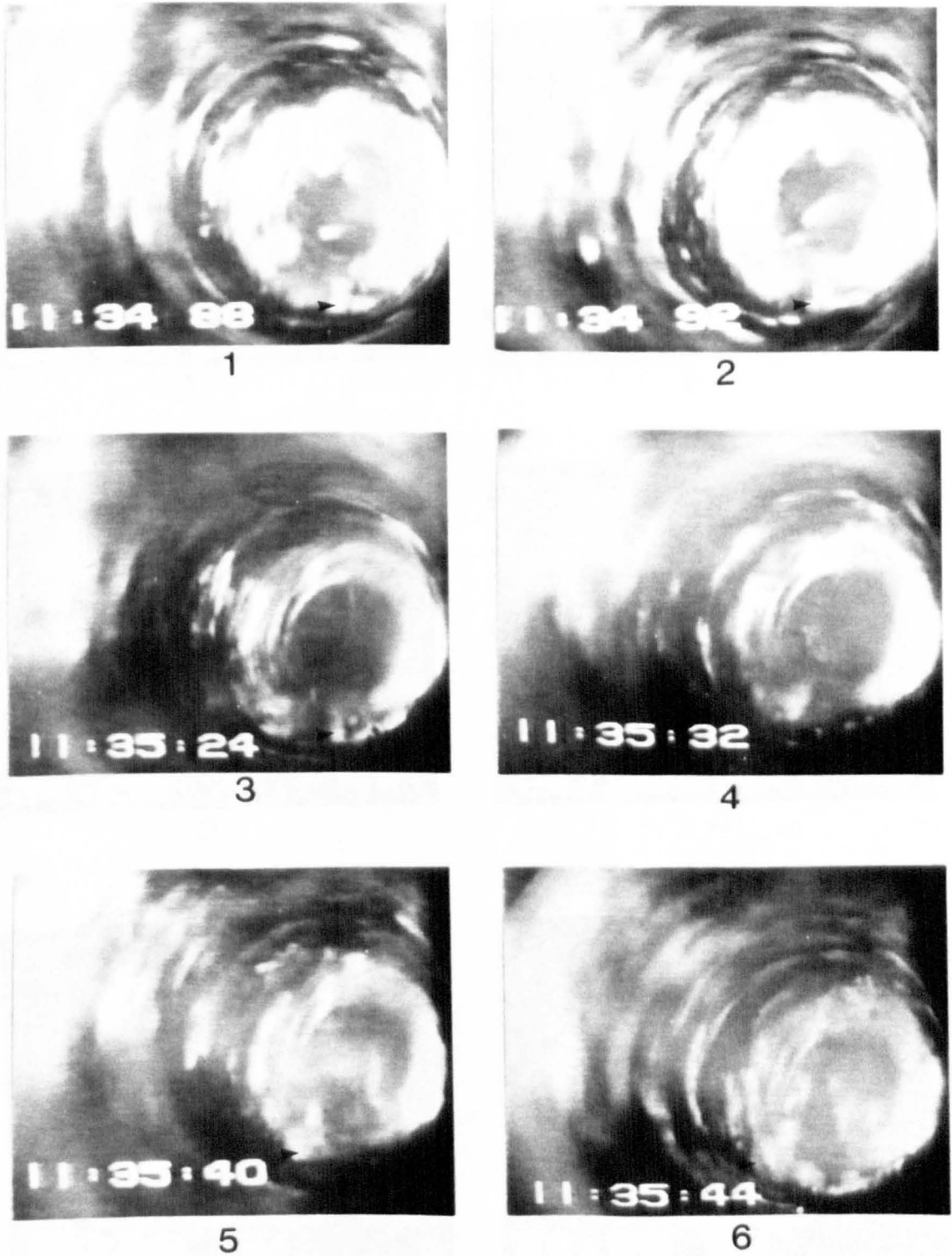


Figure 8.12 Wave Motion Before Flooding

Steam - Water Test Inlet Water Flowrate:4 l/min Inlet Water Subcooling: 20K

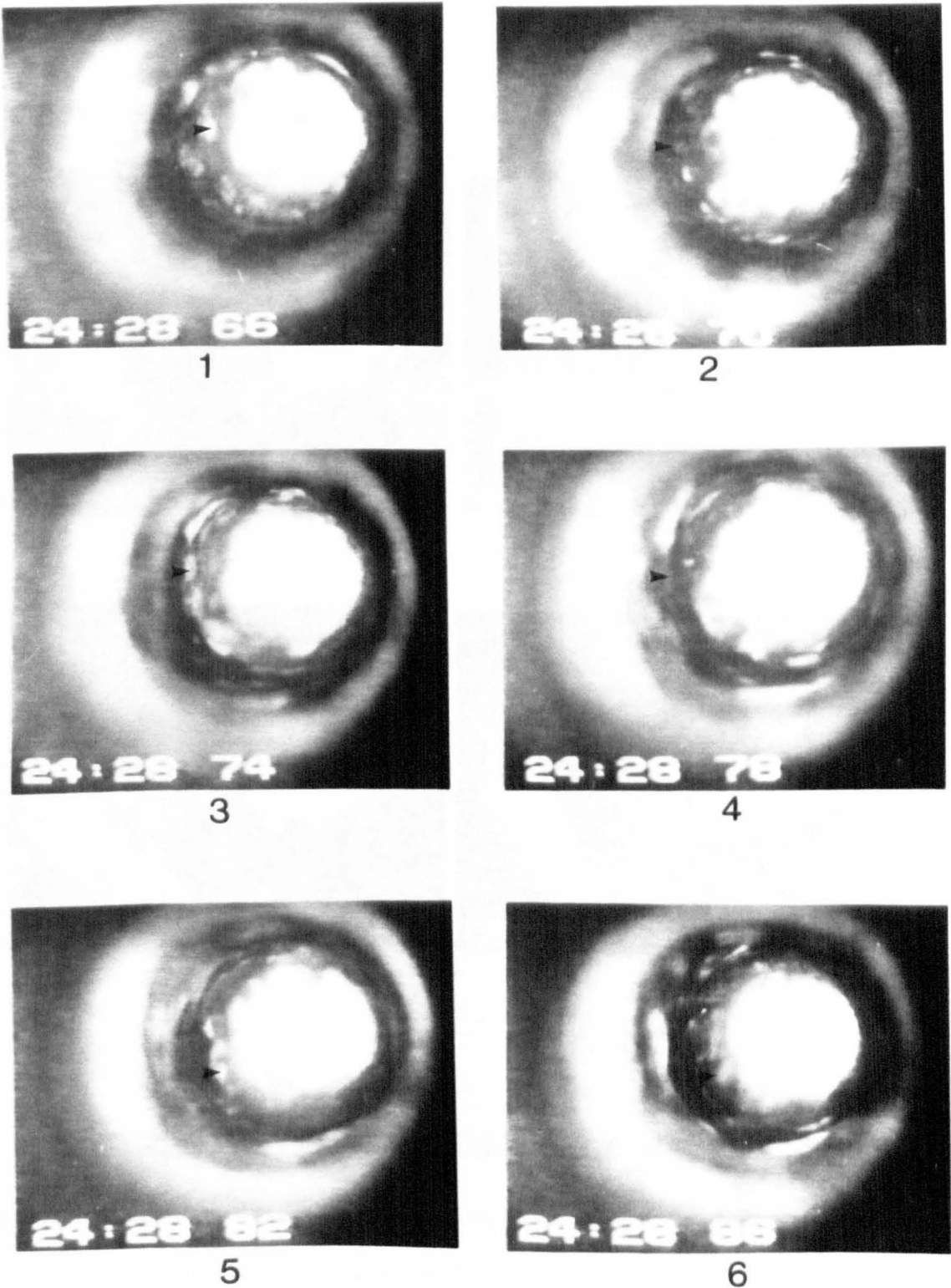


Figure 8.13 Wave Motion Before Flooding

Steam - Water Test Inlet Water Flowrate:4 l/ min Inlet Water Subcooling:30K

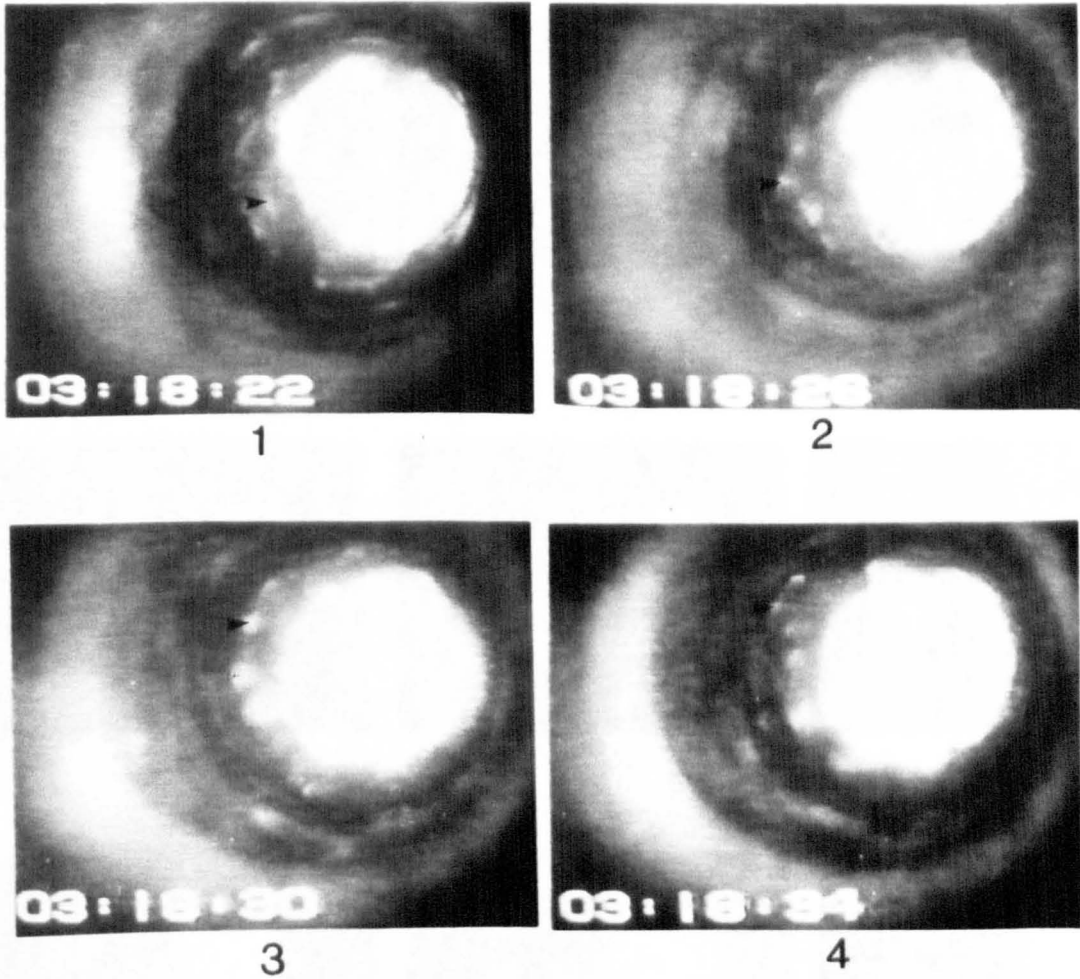


Figure 8.14 Wave Motion Before Flooding

Steam - Water Test Inlet Water Flowrate:4 l/min Inlet Water Subcooling:70K

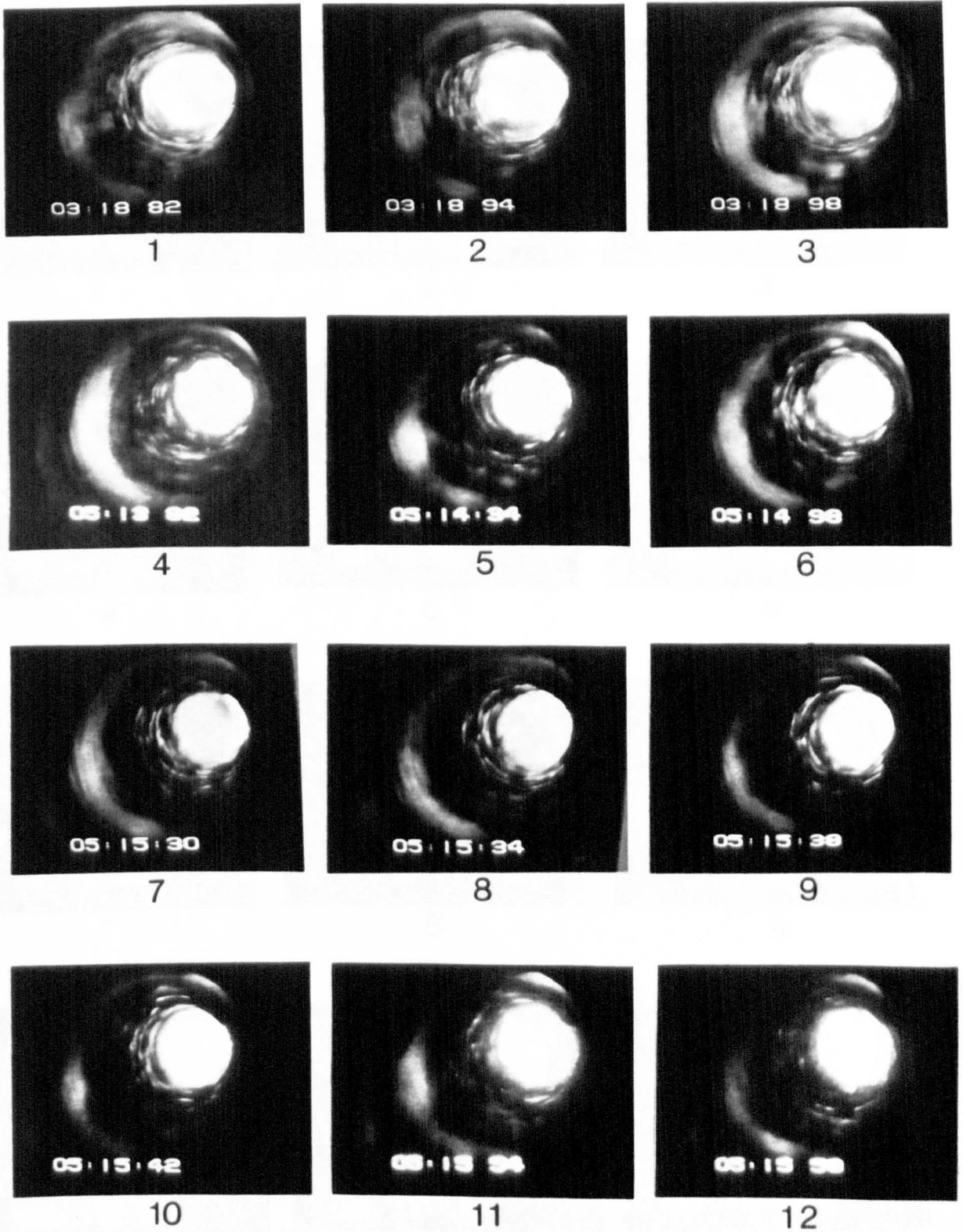
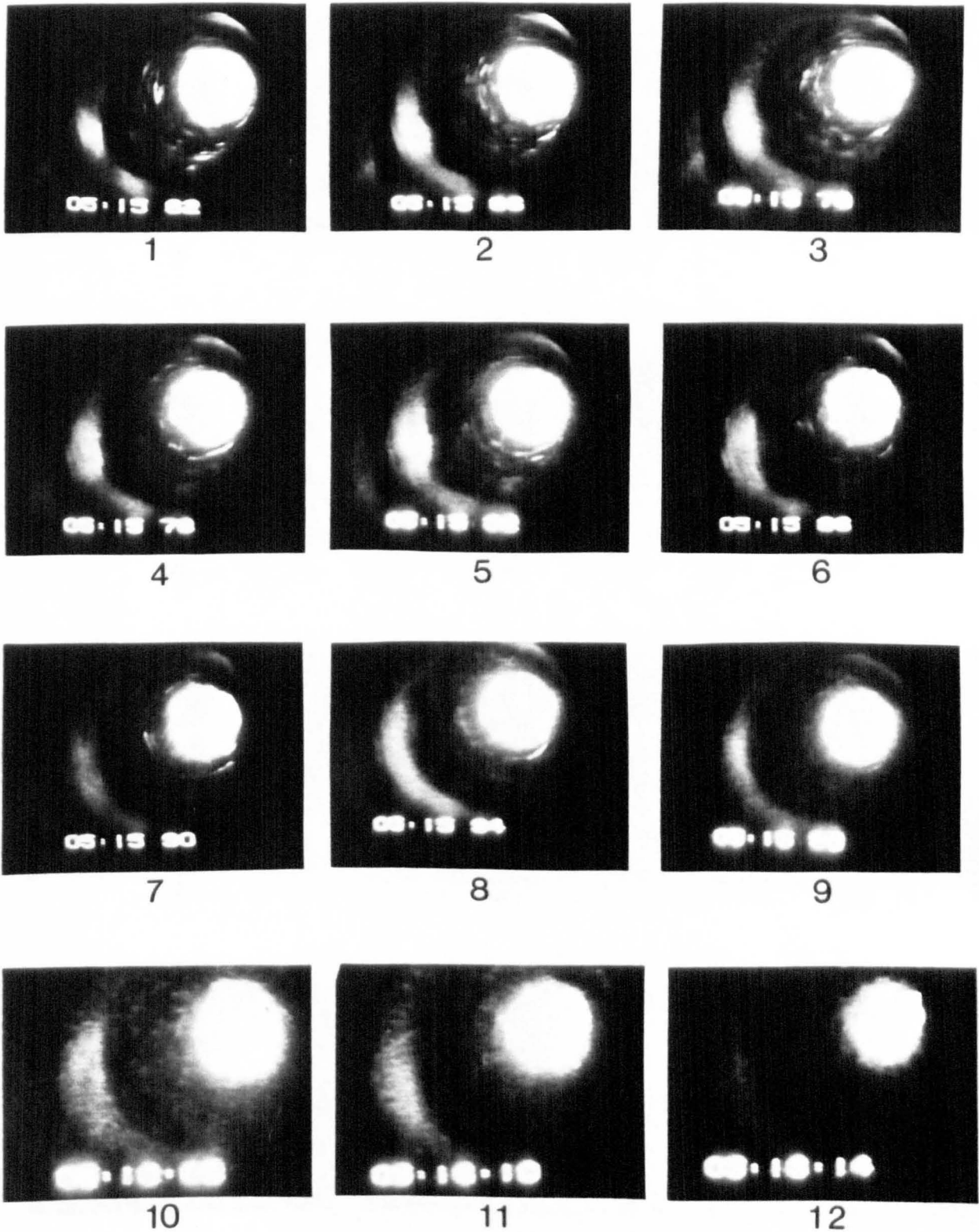


Figure 8.15a Sequence of Events Showing Liquid Film Behaviour at Moderate and High Steam Flowrate

Steam - Water Test Inlet Water Flowrate:10 l/min Inlet Water Subcooling:10K



**Figure 8.15b Sequence of Events Showing
Liquid Film Behaviour Before and at Flooding**

Steam - Water Test Inlet Water Flowrate:10 l/min Inlet Water Subcooling:10K

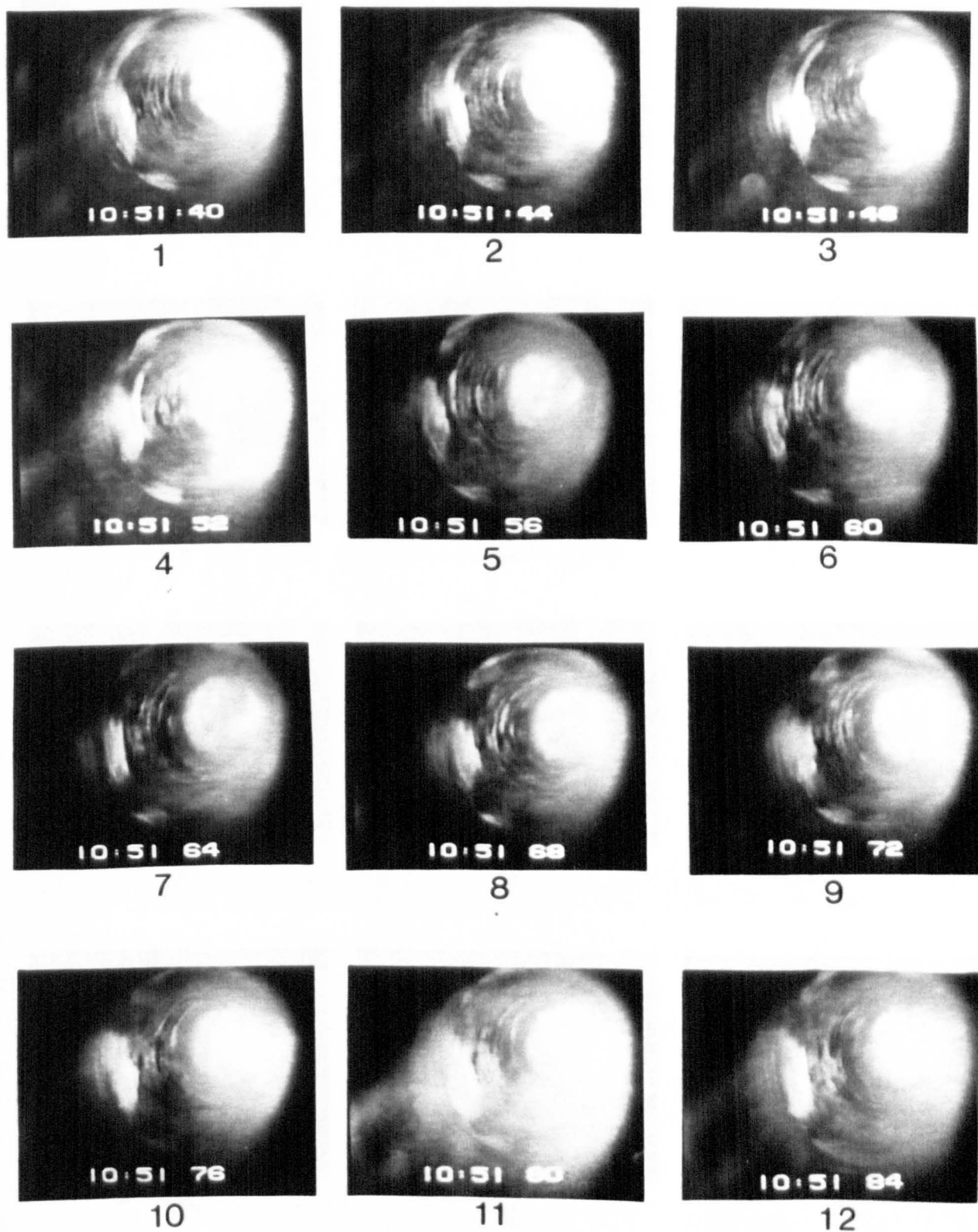


Figure 8.16a Sequence of Events Showing Liquid Film Behaviour Before Flooding

Steam - Water Test

Inlet Water Flowrate:10 l/min

Inlet Water Subcooling:60K

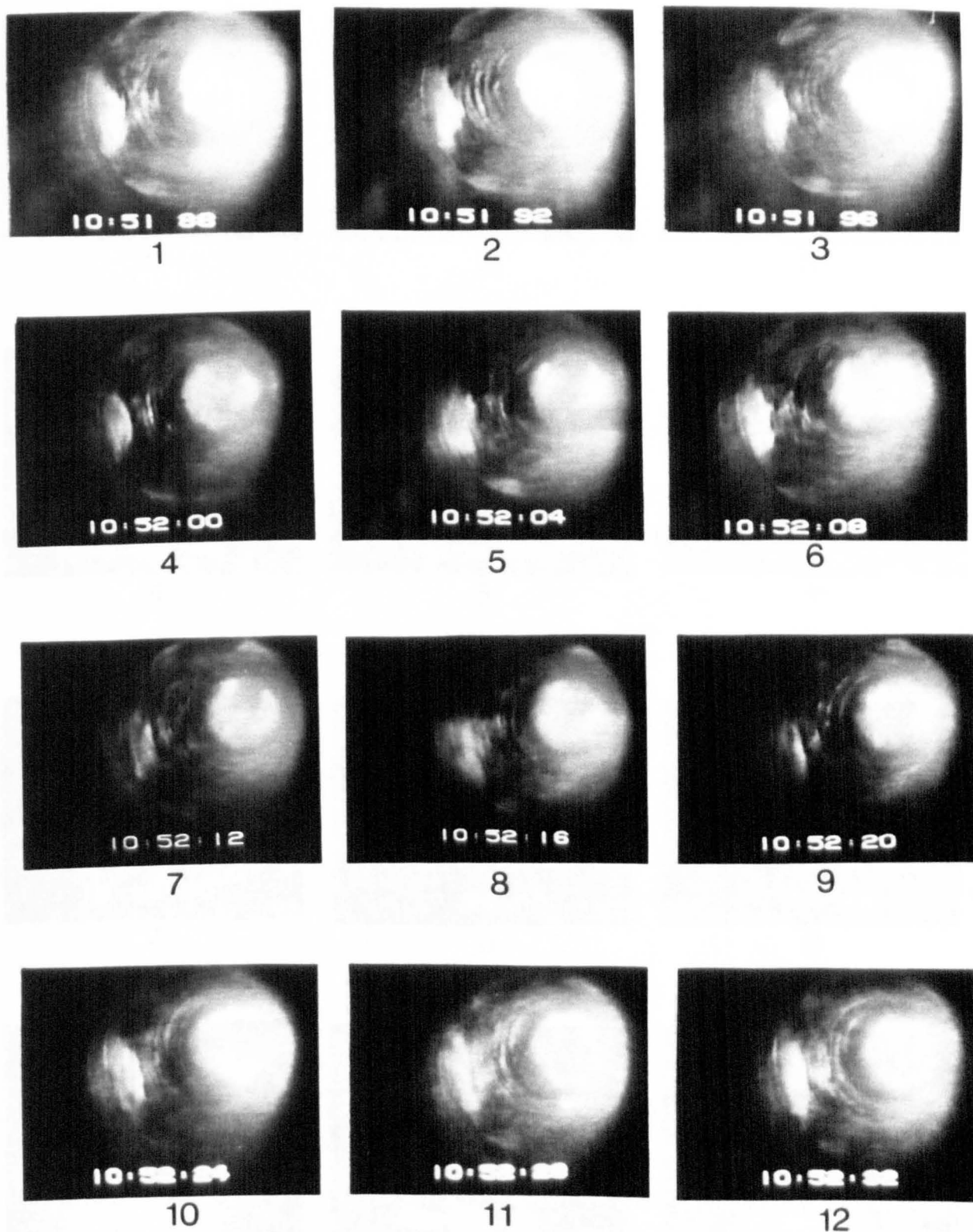


Figure 8.16b Sequence of Events Showing Liquid Film Behaviour Before Flooding

Steam - Water Test Inlet Water Flowrate:10 l/min Inlet Water Subcooling:60K

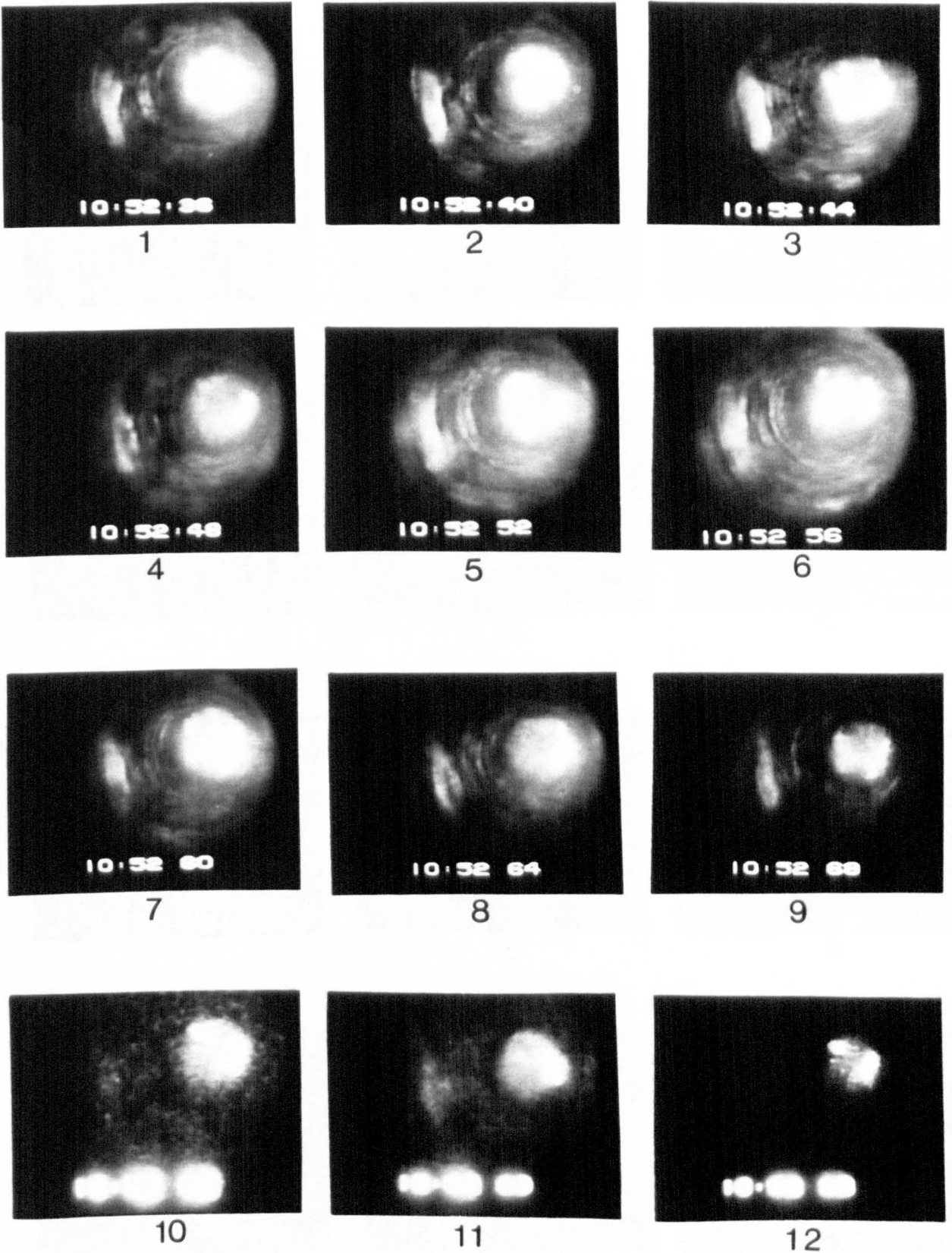
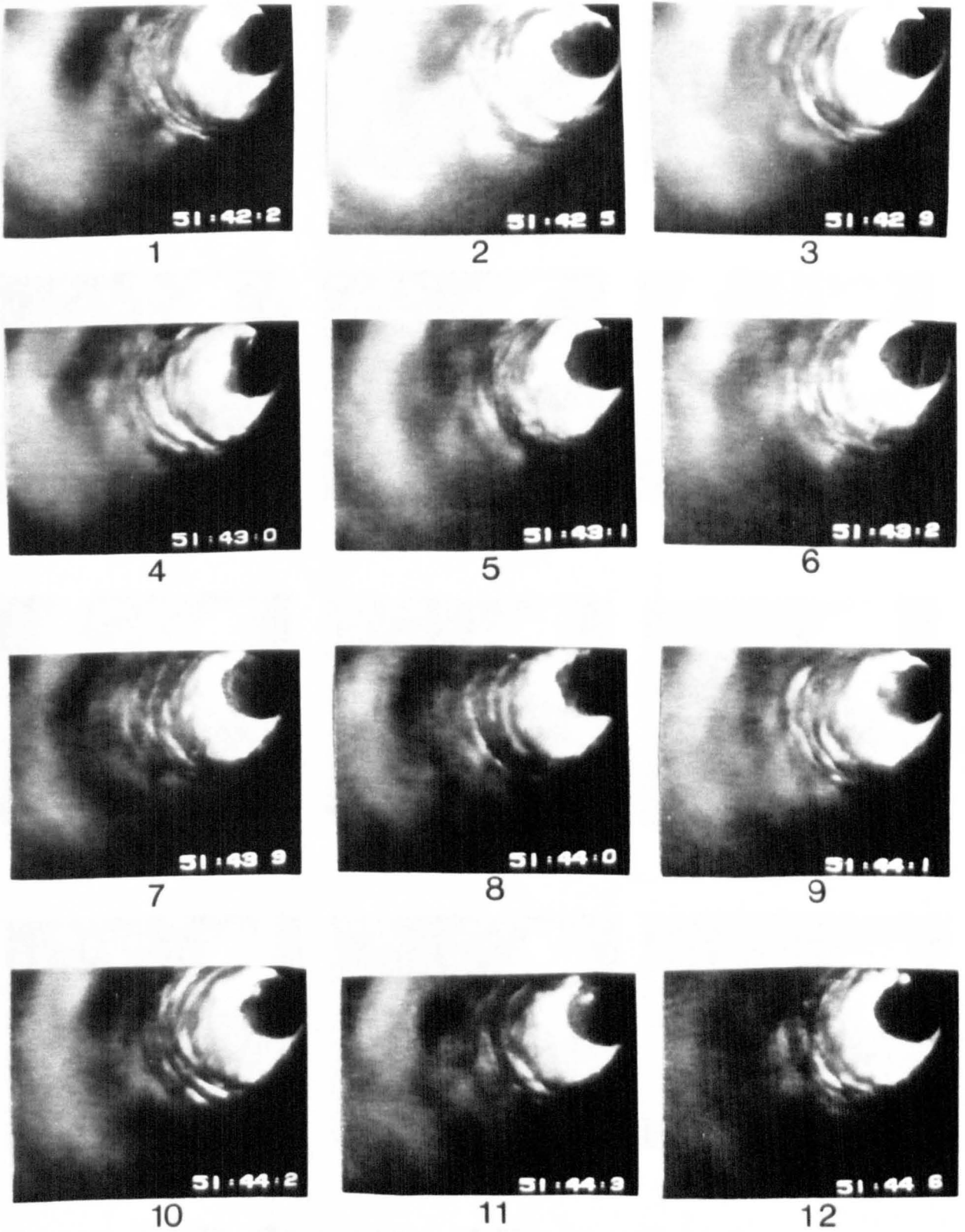


Figure 8.16c Sequence of Events Showing Liquid Film Behaviour Before and at Flooding

Steam - Water Test Inlet Water Flowrate:10 l/min Inlet Water Subcooling:60K



**Figure 8.17a Sequence of Events Showing
Liquid Film Behaviour Before Flooding**

Steam - Water Test Inlet Water Flowrate:16 l/min Inlet Water Subcooling:10K

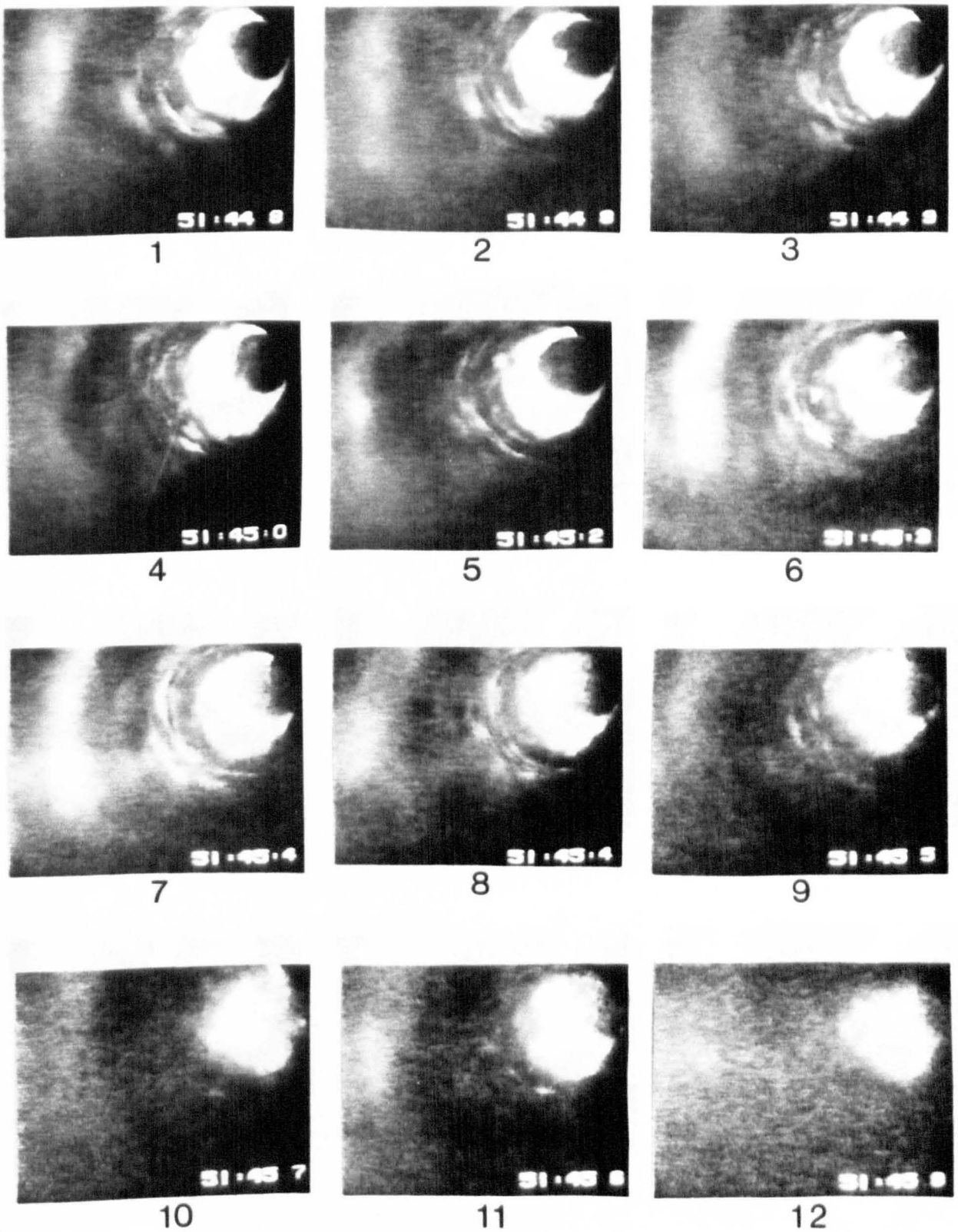


**Figure 8.17b Sequence of Events Showing
Liquid Film Behaviour Before and at Flooding**

Steam - Water Test Inlet Water Flowrate:16 l/min Inlet Water Subcooling:10K

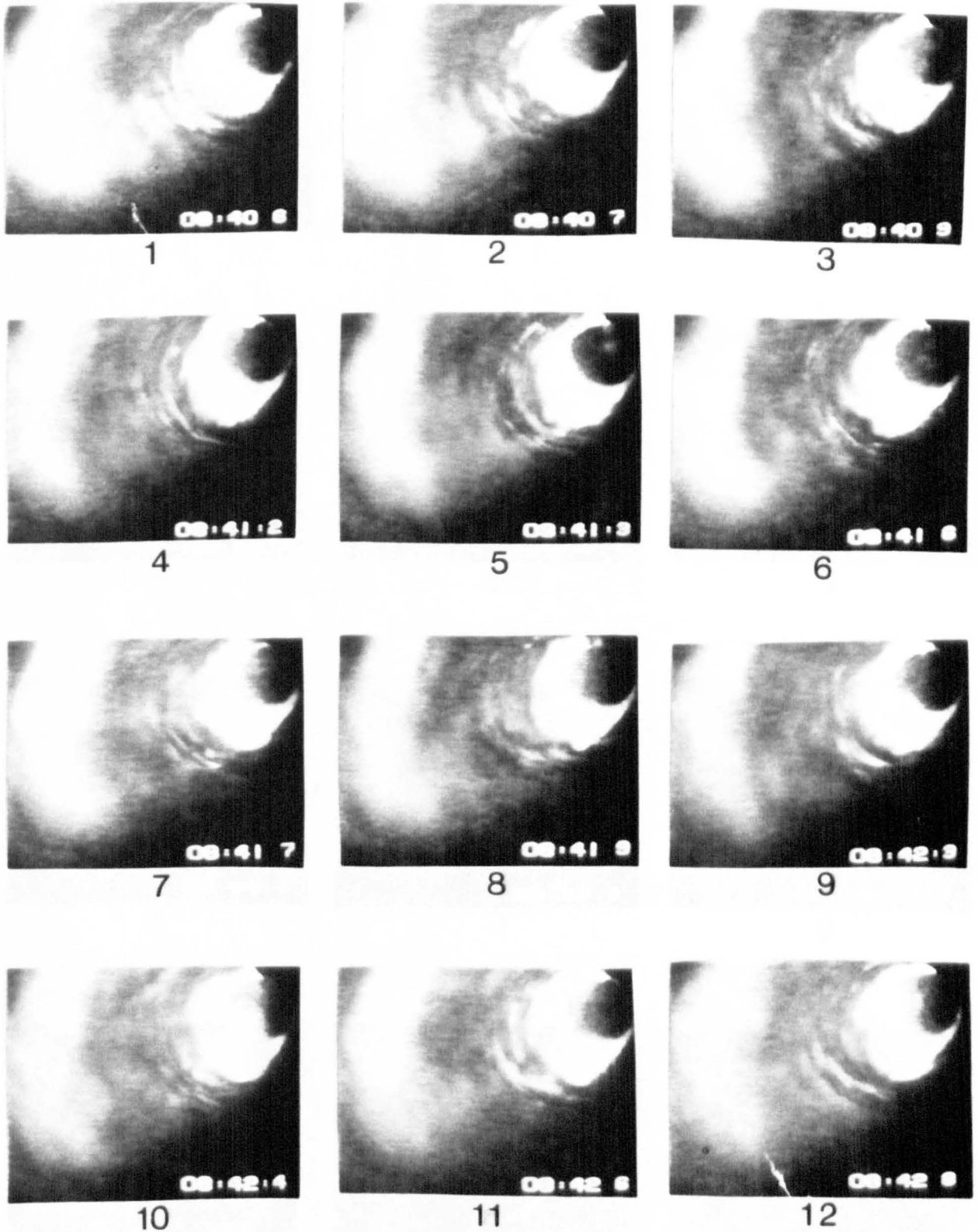


Figure 8.18a Sequence of Events Showing
Liquid Film Behaviour Before Flooding

Steam - Water Test Inlet Water Flowrate:16 l/min Inlet Water Subcooling:50K

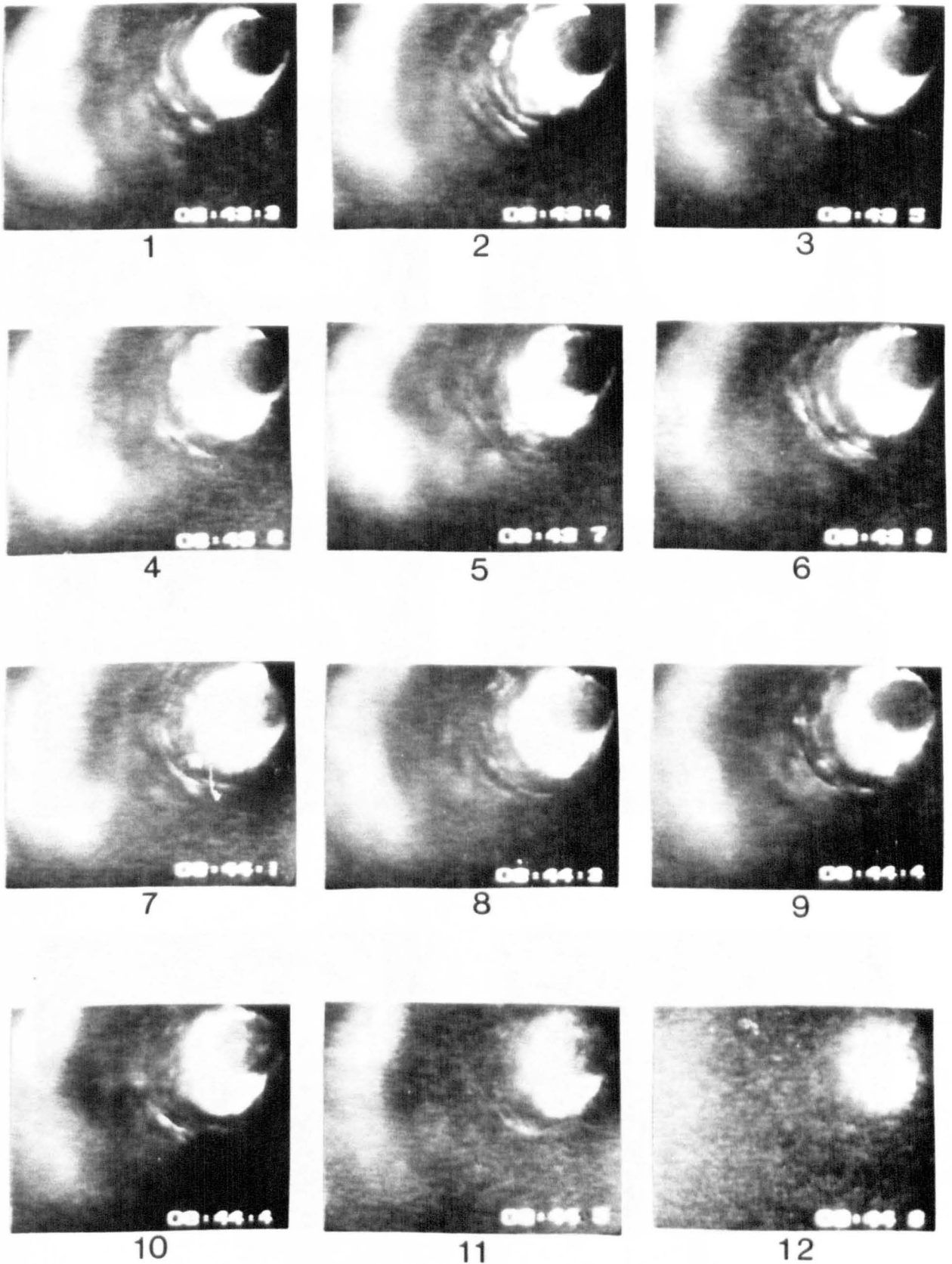


Figure 8.18b Sequence of Events Showing Liquid Film Behaviour Before and at Flooding

Steam - Water Test Inlet Water Flowrate:16 l/min Inlet Water Subcooling:50K

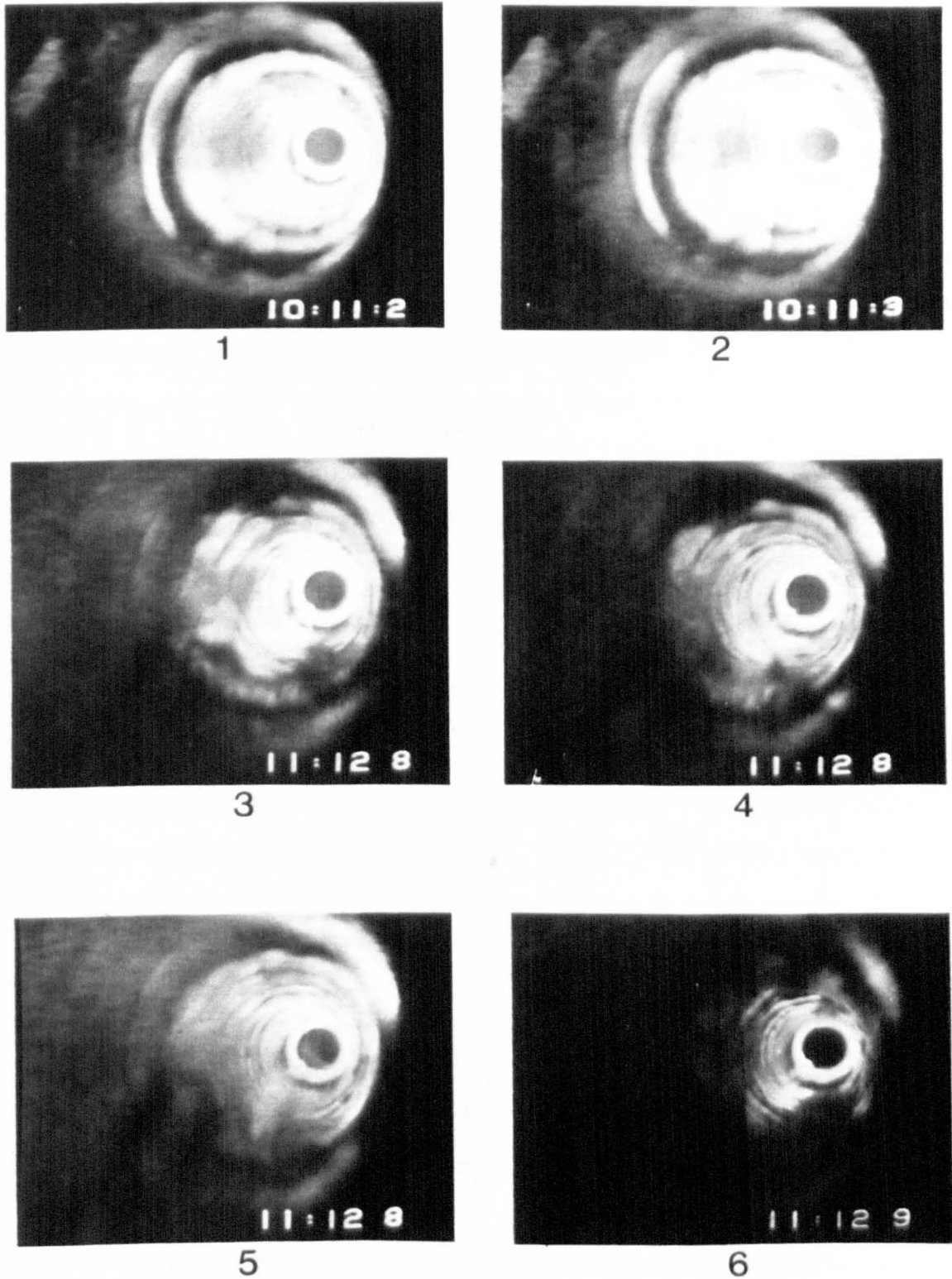


Figure 8.19 Simulated Top Flooding

Steam - Water Test Inlet Water Flowrate:4 l/min Inlet Water Subcooling:10K

CHAPTER 9

ANALYSIS AND DISCUSSION OF RESULTS

CHAPTER 9ANALYSIS AND DISCUSSION OF RESULTS

The experimental results presented in Chapter 7 and the investigations into the effect of air or steam extraction rate on the onset of flooding, are discussed and analysed in this Chapter. The experimental work is also related to the theoretical analysis of liquid film thickness and temperature and to the flooding model.

Before discussing the present results, it should be pointed out that this work represents a continuation of previous research carried out at Strathclyde University. Some of the analysis is based on findings previously discussed and analysed, and where no contradiction arose there was no reason to repeat them. Those findings (which required validation) were tested and compared with the present data. Two of the findings adopted and used here are as follows.

- a) The ranges of laminar, transient or turbulent flow suggested by D.McNeil (1986) were:
 - i) The departure from laminar flow occurred at $Re > 860$
 - ii) The onset of turbulent flow occurred at $Re > 1156$

iii) Transition flow occurred at $860 < Re < 1156$.

These findings are accepted and adopted in the present analysis since the above results were based on liquid film thickness measurements, which were repeated with very good agreement, Figure 9.1. Therefore, if the previous data gave an indication of the limits of laminar, transient, turbulent flow, then the present data should verify them.

b) The liquid film thickness model presented in Chapter 6, was a one dimensional, two-phase, counter-current flow analysis which predicted liquid film thickness along the test tube only. However the two dimensional, single phase analysis by McNeil for the porous injector tube is used to predict the liquid film thickness variation in that part of the test section. That is, the previous analysis is used as the first stage of the present analysis to predict liquid film thickness at the bottom edge of the porous injector which is then used as the initial value for the integration of the liquid film thickness along the test tube. The formulae and equations used are

$$(i) \quad \left(\frac{d\delta^+}{dz^+}\right)_{\text{LAM}} = \frac{2\delta^+}{z^+} + \frac{5}{2Re z^+} - \frac{5\delta^{+3}}{6Fr_f^2 z^{+2}} \quad (9.1)$$

For $Re z^+ < 860$, i.e. laminar flow

$$(ii) \quad \left(\frac{d\delta^+}{dz^+}\right)_{\text{TURB}} = \frac{2\delta^+}{z^+} + \frac{0.1082}{(Re z^+)^{0.449}} - \frac{0.95\delta^+}{(Fr_f z^+)^2} \quad (9.2)$$

For $Re z^+ > 1156$, i.e. turbulent flow

$$(iii) \left(\frac{d\delta^+}{dz^+}\right)_{\text{TRAN}} = \frac{1156 - \text{Re}z^+}{296} \left(\frac{d\delta^+}{dz^+}\right)_{\text{LAM}} + \frac{\text{Re}z^+ - 866}{296} \left(\frac{d\delta^+}{dz^+}\right)_{\text{TURB}} \quad (9.3)$$

For $860 < \text{Re}z^+ < 1156$ i.e. transient flow

where z is the distance from the top of the porous sinter with the boundary conditions

$$\delta_0^+ = 1.342 \text{ Fr } z_0^{+1/2} \quad (9.4)$$

and

$$z_0^+ = 0.01 \quad (9.5)$$

where δ_0^+ is the initial value of the liquid film thickness at the top of the porous sinter and z_0^+ is some small distance down the porous wall (any value less than 0.01 was found to have no effect on the eventual numerical solution).

Discussions on the effect of air and steam extraction rates are presented in Sections 9.1 and 9.2 respectively. The deduction of compatible air-water and steam-water flooding characteristics are presented in Section 9.3. Pressure drop results for both air-water and steam-water systems are discussed in Section 9.4. The visualisation technique results are discussed in Section 9.5. The theoretical analysis, presented in Chapter 6, on the liquid film thickness and temperature, and the flooding model are discussed in Sections 9.6, 9.7 and 9.8 respectively, and finally comparison with some of the

other work in the literature is presented and discussed in Section 9.9.

9.1 Effect of Air Extraction Rate on Air-Water Data

Air-water tests were first performed on the test facility in such a way that care was taken to ensure that the minimum possible air flow was removed with the extracted water flow, and also that all the water flow was extracted through the porous sinter. These tests were carried out with the air flow being increased in small steps from very low rate (in which the liquid film was considered as a free falling film), until the flooding condition was achieved. In order to determine the effect of the air extraction rate on the onset of flooding, another set of tests, where only the flooding data were collected, were performed such that the highest possible extraction flowrate of air passed through the porous sinter with the extracted water flow. The air extraction rates, for both sets of data at the flooding situation, are shown plotted in Figure 9.2. It can be seen that the difference between the two extraction rates is not as high as desired to show the clearest effects. This is attributed to the small type of vacuum pump used. However the difference is sufficient to give a good indication of the air extraction rate effect on the onset of flooding and this can be seen in Figure 9.3, where the two curves characterising the flooding data under both

conditions are plotted in terms of Wallis dimensionless parameters. It clearly indicates that the higher the air extraction rate, the lower the flooding characteristic curve and vice versa.

The effect of air extraction can be explained by considering the control volumes shown on Figure 9.4. For the same water flowrate, the higher air extraction rate occupies a larger extraction area of the porous sinter (Figure 9.4a), than that occupied at low air extraction rates, (Figure 9.4b). Thus when the air extraction flow occupies a larger area of the porous sinter, it forces the water flow to pass through a smaller area, resulting in a more abrupt profile of the water flow at the porous sinter for high extraction rates than at low extraction rates. It has been widely reported that a more abrupt liquid flow profile requires less gas flow to initiate flooding than that of smoother profile. The importance of the water flow profile at the extraction porous sinter is emphasised even more when it is related to the findings of the visual studies, Chapter 8, which indicates that the onset of flooding is started at the flow removal sinter.

Bharathan (1979) reported that alteration of the inlet and outlet conditions of the liquid film flow produced parallel curves on a plot of $j_f^{*1/2}$ versus $j_a^{*1/2}$ with the position of the intersect on the $j_a^{*1/2}$ coordinate decreasing the more abrupt the inlet or outlet conditions become.

The experimental data obtained at flooding, for the two conditions represented by Wallis type equations, are

$$j_a^{*1/2} + 0.59 j_f^{*1/2} = 0.8 \quad (9.6)$$

$$j_a^{*1/2} + 0.55 j_f^{*1/2} = 0.76 \quad (9.7)$$

which confirm Bharathan's reports. Figure 9.3 clearly indicates two approximately parallel flooding characteristics.

9.2 Effect of Steam Extraction Rate on Steam-Water Data

Two types of steam-water tests were performed on the test facility. The first ensured that high steam flows were extracted with the water through the porous sinter. These tests were carried out with the supply steam flowrate being increased in small increments until the flooding condition occurred. This was performed for eight different subcoolings. (The subcooling is the difference between the saturation temperature and the bulk water temperature at the liquid inlet section). In order to determine the effect of varying the steam extraction rate, the second set of tests were performed at low steam extraction rate for the same eight subcoolings. Again the steam supply flow was increased incrementally until the flooding situation occurred. As mentioned in Chapter 7, the steam extraction rate was controlled by varying the

rate of cooling water through the condenser which, in turn, controlled (by condensation), the vacuum pressure created in the condenser. Therefore the vacuum pressure created in those tests performed with high steam extraction flow (high cooling water flowrate) was much higher than those tests with low steam extraction flow (low cooling water flowrate). The effects of varying the steam extraction rate on the onset of flooding are obtained by comparing the two sets of flooding data, for each subcooling shown in Figures 9.5 and 9.6. The same conclusions as those obtained by varying the air extraction rate can be observed from either of these plots, i.e. the higher the steam extraction rate, the lower the flooding curve characteristic and vice versa. The difference in extracted water flow profile, described as rough and smooth, implied by the high and low steam extraction rates respectively, is also regarded as a reasonable explanation for the effect of varying steam extraction rate on the onset of flooding, Figure 9.4. The corresponding steam flow rates extracted at the onset of flooding under both conditions are shown on Figures 9.7 and 9.8 for the two subcoolings. The two sets of data performed under high and low steam extraction rate represent two extreme conditions. Therefore in an attempt to obtain a clearer picture of the effect of varying the steam extraction rate, two further tests were performed. In these tests, two middle range values of condenser cooling water flowrates were used which consequently led to two medium rates of steam flow

extracted with water flow. These were carried out with the inlet water subcoolings fixed at an average value of 10 k. Previously at this subcooling, the high extraction rate was obtained with an average condenser cooling flowrate of 28.9 kg/min, and the low steam extraction rate by an average cooling water flowrate of 5.1 kg/min. Therefore in order to obtain a consistent data, the two medium extraction rate tests were performed with an average condenser cooling water flowrate of 11.2 kg/min and 18.7 kg/min respectively, and consequently low-medium and high-medium steam extraction rates were obtained. The steam flowrate extracted with water flow for all four conditions (low, low-medium, high-medium, and high) are plotted on Figure 9.9, as a function of the inlet water flowrate, while the data marking the onset of flooding are shown in Figure 9.10, in the form of Wallis dimensionless parameters. It can be seen that the flooding characteristic curves are higher as the steam extraction rate decreases or, generally, tests performed under conditions of higher gas extraction rate require less gas flow to initiate flooding.

It was noted that at high inlet water flowrates, the difference in the flooding data, taken at the same inlet water subcooling, for both sets (low and high steam extraction rates) tended to become less, and sometimes even coincided with each other, Figure 9.10. This arose because, during the experimental tests, it was not always possible to maintain the rate of steam extraction constant

as it tended to decrease at high inlet water flowrates and become less affected by the rate of condenser cooling water. The explanation for this could be that at high water flowrates, the vacuum created inside the condenser was not sufficient to extract all the water and the same level of steam. In fact in these tests, a small amount of water was found to overshoot the extractor system.

The optimum situation is represented during the steam-water tests, when no steam is extracted through the porous sinter; however there were many difficulties in attaining this condition as will be explained later in this section. Since steam water tests performed at low steam extraction rates are nearer the optimum condition, this set of data are used in the illustration and discussion presented in this Chapter and in the analysis in the next Chapter. The condenser cooling water flowrate (or the steam extraction rate through the porous sinter) was found to affect the range of inlet water flowrates that could be covered in each subcooling. The general trend was that, for the same subcooling, higher inlet water flowrates could be obtained with higher steam extraction rates than with low steam extraction rates. For example, in tests carried out with inlet water subcooling of 80 K, the range of the inlet water flowrate covered at high steam extraction rate varied up to 15.755 l/min, while at low steam extraction rate it was found to be very difficult to perform any steam-water tests with the inlet water flowrate higher than 10 l/min. A

possible explanation of this effect is that, at high inlet water flowrate and subcoolings, the water flowrate did not reach the saturation temperature at the bottom end of the test section; in fact in some cases the water temperature at the extraction sinter was found to be well below the saturation temperature even though there was substantial steam condensation taking place on the water film along the test tube. However, when this high subcooled water flowrate was forced to pass to the condenser along with the same steam flowrate, with a low condenser cooling water flowrate, the energy removed by the cooling water was small and consequently the vacuum pressure created was small and insufficient to extract further water and steam through the porous sinter. Thus the water flow overshot the extractor bringing the test to an end. If the same amount of subcooled water passed to the condenser with high cooling water flowrate, the energy removed was high, resulting in a high vacuum pressure and consequently not only extracted all of the water flow but also more steam, thus sustaining the process and bringing the extraction rates to an equilibrium and steady state. The existence of steam with the extracted water flow was desirable to create the necessary vacuum pressure in the condenser and make the performance of any steam-water test easier. However although tests with no steam extraction could be performed with difficulty, the ranges of inlet water flowrate and subcooling, were seriously limited. This is the reason for allowing some steam to be extracted with the water in the second set of data as it provided an

acceptable steam extraction percentage and a wide range of inlet water subcoolings of flowrates.

It should be noted that the maximum inlet water flowrate used in any steam-water test was only just over half the water flowrate range covered during the corresponding air-water test. Although this could be explained in terms of steam extraction rates and inlet water subcoolings, another possible effect that limited the extension of the inlet water flowrate was the small amount of water flow that was found to overshoot the extraction section, at high inlet water flowrates. It should be pointed out that 100% water extraction was obtained in all low and medium water flowrates, and only at very high water flowrates was overshooting detected and measured in the secondary separator. Although this amount of water was very small and never exceeded 2% in any steam-water recorded test, its presence was sensitive in the steam-water system while its effect was much smaller in the air-water system. Hence it was possible to perform a complete air-water test up to the flooding point, with some waterflow passing the extraction section (no more than 5%), while it was not possible to do so in the steam-water tests. In fact some steam-water tests were performed at the inlet water subcooling of 10 K with the inlet water flowrates range extended up to 26 l/min. These data are not included in the experimental results since the amount of water flow passing the porous section exceeded the acceptable limit of 2%. The effect of this

amount of water is very important in the steam-water test because at very high inlet water flowrate the water film did not reach the saturation temperature at the bottom of the tube, therefore, if a considerable amount of water overshot the porous section, the condensation process shifted to the settling length tube disturbing the supply steam flow and possibly initiating flooding prematurely in the settling length.

In some experimental tests, with low inlet water subcoolings and flowrates, the experimental wall temperature did not correspond to the inlet steam temperature at the bottom of the test tube, because the suction pressure at the extractor system reduced the system pressure and hence the saturation temperature at this location. However evaluation of the effect on the flooding data proved to be small in general and of negligible effect in low steam extraction data in particular.

9.3 Compatible Flooding Data

Since the air and steam extraction rates were found to have a substantial influence on the flooding characteristics, any comparison between the two modes should be carried out with data taken at the same extraction rate. However, as explained previously, it was not possible to perform air-water and steam-water

tests at the same extraction rates. Since the air-water flooding data were more consistent and covered a wider range of water flows, they were extrapolated to match those of the steam-water. In addition the steam-water data were taken for nine subcoolings, each covering different ranges of inlet water flowrate. The extrapolation of the air-water flooding data was carried out as follows:

- (i) The percentage average steam extraction rate, (the second set of steam-water flooding data), at an inlet water flowrate of 4 l/min for all nine inlet subcoolings, was 30.69%.
- (ii) The air extraction rates for air-water flooding data (first set) for the smallest and largest inlet water flowrate, of 4 l/min and 39.6 l/min were 15.16% and 32.71% respectively.
- (iii) The air extraction rates for air-water flooding data (second set) were 20.17% and 35.37% for the smallest and largest inlet water flowrates respectively.
- (iv) These rates of air extractions were extrapolated to the steam extraction rate of 30.69% and the air flow rates to the test section were obtained at the smallest and the largest water flowrates respectively.

(v) A line was drawn between the two points to represent the air-water flooding characteristic at the same average extraction rate for the steam-water flooding data. This line was fitted into a Wallis type correlation to give

$$j_a^{*1/2} + 0.43 j_f^{*1/2} = 0.71 \quad (9.8)$$

Figure 9.11 shows the measured air-water flooding data with the extrapolated flooding characteristics; while Figure 9.12 shows steam-water flooding data for all nine subcoolings with the compatible (extrapolated) air-water flooding characteristics.

When straight lines are drawn through the flooding data (calculated at the top of the tube), for each subcooling, Figure 9.13, it is seen that the slope of the flooding characteristics becomes steeper as the subcooling increases while the intercept on the $j_s^{*1/2}$ axis is independent of the water subcooling, and is around 0.8. This confirms Wallis' (1961) suggestion that the coefficient C in his correlation is geometry dependent and also that m is a function of the physical properties of the fluids.

It should be pointed out that, before the visualisation technique was implemented, an attempt was made in both air-water and steam-water systems to determine the location of the start of the flooding (i.e. whether it was at the top or the bottom of the test

section). A u.v. recorder was coupled to the conductance probes used for measurements of the liquid film thickness, in the hope that the recorder chart would determine which probe first showed deflections at the point of flooding. This proved difficult to determine from the chart as most of the traces gave a rather indistinct result but, from the few that provided a clear enough trace, it was decided that flooding started at the bottom of the test tube.

9.4 Pressure Drop

Pressure drop effects were taken for both air-water and steam-water systems.

9.4.1 Air-Water System:

In the air-water tests, it was found that, for constant inlet water flowrate, the pressure drop was rather small before flooding. As flooding was approached, the pressure drop increased sharply over a narrow range of air flowrates. Pressure drop measurements are plotted as a function of air flowrates for various inlet water flowrates in Figure 9.14. It can be seen that the pressure drop increases only slightly with increase in the injected water flowrate for the conditions of air flowrate below the flooding point and at the onset of flooding. These pressure drop

characteristics are in agreement and very similar to the characteristics obtained by Bharathan et al (1978), Ostrogorsky (1981), and Howley and Wallis (1982), in adiabatic vertical counter-current flow. During the experimental tests, it was noted that the sudden rise in the pressure drop took place just before, and increased at, the onset of flooding. It was also observed that the onset of flooding, accompanied by the formation of liquid slugs and bridging within the tube, took place at the point where maximum pressure drop was attained. However any further increase in air flowrate decreased the pressure drop, probably because the climbing liquid film formed a co-current annular flow.

9.4.2 Steam-Water System:

In the steam-water tests, it was found that, at the start, the pressure drop fluctuated around zero and decreased in the low steam flow region as steam flowrate increased. This was attributed to an increase in the pressure due to the loss of steam phase momentum by condensation. As the steam flowrate approached the flooding velocity, the pressure drop became steady or exhibited a slight increase near the flooding point becoming strongly positive at the onset of flooding. This was attributed to the considerable augmentation of the interfacial friction stress and to the slug formation, as in the air-water tests.

The pressure drop characteristics were found to be affected by the extracted steamrate, as the vacuum pressure created inside the condenser influenced the pressure drop developed inside the test tube. This resulted in a general trend of the negative pressure drop along the test tube decreasing as the steam extraction rate (or the condenser vacuum pressure) increased. This can clearly be seen in Figure 9.15 for four different steam extraction rates. The pressure drop characteristics in the steam-water tests were also found to be affected by the rate at which the water flow was increased. At low inlet water flowrates, the pressure drop was in some tests, found to be just slightly negative. This 'negative' pressure drop generally decreased as the water injection rate increased. This can be seen by investigating tables C.1a to C.1k in Appendix C. At high water injection rates, the pressure drop became positive throughout the test. This was believed to be caused by either the effect of decreasing steam extraction rate or by a deficiency in the pressure drop measurement system, because at high inlet water flowrates the probability of some water overshooting the extractor system increased, with some of this water possibly entering the lower pressure tapping point situated below the extraction system in the settling length. This may also explain why pressure drop characteristics obtained in the air-water system were more consistent than in the steam-water system where the

possibility of condensation and hence a two-phase mixture existing between the pressure tapping point and the separation chamber. The effect of the inlet water subcooling was found to be small, in comparison to other effects, and was only noticeable with pressure drop data taken at high inlet water subcooling. It could be concluded from the experimental results that the general trend was for the pressure drop to decrease slightly as the inlet water subcooling increased.

However, in general, the pressure drop characteristics obtained in the steam-water system were similar to those obtained by Lee and Bankoff (1982) in counter-current flow in inclined rectangular channels.

9.5 Visualisation Technique

Photographic techniques have provided useful qualitative and quantitative information on a wide variety of aspects of two-phase flow systems being studied at Strathclyde. In this project, photography was considered an integral part of the experiments and the results obtained from the visualisation were very useful in determining the position at which the flooding process started. In addition, monitoring the growth and the propagation of the disturbance waves could be followed along the test tube as the gas flowrate was gradually increased.

Photography of two-phase flow presents considerable problems in illumination, optics and recording, and, in this case, the major problem was illuminating the non-transparent test section. This problem was partially overcome when the video camera technique was used and reasonably good and useful results obtained. The illumination problem restricted the endoscope technique and limited it to observation with the naked eye. However, this problem could probably be overcome by using a transparent test section. The other problem facing the endoscope technique was that the endoscope lens was unprotected from the entrained liquid droplets which increased sharply in number near the flooding situation. No doubt this method could be developed to give better results by blowing gas or vapour across the endoscope lens similar to the technique used with the Video Camera. This would require the endoscope to be inserted from the bottom of the tube, thus producing the least disturbance to the local gas or vapour phase.

As mentioned previously, the main observation was that flooding always occurred at the bottom of the tube, in both air and steam flows. This was probably partly due to the influence of an exit effect since the extraction method used resulted in a relatively large percentage of the air or steam supply passing through the extraction sinter with the liquid. In the literature, it is reported that the location of the inception of flooding

could be the top or the bottom of the tube depending mainly on the nature of the entrance and exit effects. However, eliminating these two important effects proved to be very difficult.

9.6 Liquid Film Thickness Analysis

The liquid film thickness analysis presented in Chapter 6 could predict the liquid film thickness at any position along the test tube, for any liquid flowrate with different steam flowrates up to the flooding point. The analysis required an estimation of the mean liquid film temperature. This was obtained from the film temperature analysis which predicted the liquid film temperature across the film at any position along the test tube. The liquid film thickness variation along the test tube was obtained from

(i) For Laminar Flow

$$\left(\frac{d\delta^+}{dz^+}\right)_{\text{LAM}} = \left\{ \frac{1}{2\delta^+} f_1 \rho^+ (Fr_g - Fr_f)^2 + \frac{8Fr_f^2}{\delta^+ Re_f} - (1 - \rho^+) + \left[\frac{Fr_f - Fr_g}{\delta^+ D^+} + \frac{4 Fr_g}{(D^+ - 2\delta^+)^2} \right] \frac{\delta^+ D^+ Fr_f}{HC_p^+ (T_s^+ - T^+)} \frac{dT^+}{dz^+} \right\} / \left\{ \frac{Fr_f^2}{\delta^+} - \frac{4\rho^+ Fr_g}{(D^+ - 2\delta^+)} \right\} \quad (9.9)$$

For $Re_f < 860$

(ii) For Turbulent Flow

$$\frac{d\delta^+}{dz^+}_{\text{TURB}} = \frac{1}{2\delta^+} f_i \rho^+ Fr_g - Fr_f^2 + \frac{0.0395 Fr_f^2}{Re_f^{0.25}} (1 - \rho^+) + \left[\frac{Fr_g - Fr_f}{\delta^+ - D^+} \right]$$

$$\frac{4 Fr_g}{(D^+ - 2\delta^+)^2} \left[\frac{\delta^+ D^+ Fr_f}{HC_p^+ + (T_s^+ - T^+) dz^+} \frac{dT^+}{dz^+} \right] / \left[\frac{Fr_f^2}{\delta^+} - \frac{4\rho^+ Fr_g}{(D^+ - 2\delta^+)} \right] \quad (9.10)$$

For $Re_f > 1156.0$

(iii) For Transition Flow

$$\left(\frac{d\delta^+}{dz^+} \right)_{\text{TRAN}} = \frac{1156 - Re_f}{296} \left(\frac{d\delta^+}{dz^+} \right)_{\text{LAM}} + \frac{Re_f - 860}{296} \left(\frac{d\delta^+}{dz^+} \right)_{\text{TURB}} \quad (9.11)$$

$$\text{For } 860 < Re_f < 1156$$

The integrations of the above equations were carried out while the variation in the liquid film flowrate, due to condensation, was evaluated at every step by integrating equations (6.8).

$$\frac{d}{dz} (M_f) = \frac{M_f Cp_f}{h_{fg} + Cp_f (T_s - \bar{T}_f)} \frac{d}{dz} (\bar{T}_f) \quad (9.12)$$

The variation in the liquid film mean temperature was also evaluated at every step as described in the next section of this Chapter.

The predicted and measured liquid film thicknesses at flooding along the test tube are listed in Tables 9.1 to 9.4 for four different inlet water flowrates and

subcoolings and plotted in Figures 9.16 to 9.19. The liquid film thickness was measured at only two positions along the test tube, each 128 mm from the test tube edge and referred to as top (upper) and bottom (lower) film thickness. It can be seen that the agreement between the predicted and measured film thickness is reasonably good for the upper liquid film thickness; for the lower liquid film thickness the agreement between prediction and measurements is quite good at the high subcoolings (low inlet water flowrates) and is fair at low and medium subcoolings.

However, it can be concluded that for the lower probe position, the theoretical analysis slightly over-predicted the film thickness. This may have been expected since the analysis treated the flow as one-dimensional which involved some degree of approximations. For the experimental data, it should be pointed out that the performance of the lower probe would not be very satisfactory at the flooding situation since visual observations showed the existence of a highly disturbed and agitated liquid film at the bottom of the test tube. Furthermore the high temperature of the liquid film, which existed in most of the tests at the bottom of the test tube may also have affected the performance of the lower probe. At the upper probe, more disturbance proved (by visual observation) to be much less than that at the bottom of the tube. Also the liquid temperature at the top of the tube was dependent mainly on

the liquid film inlet temperature and not on steam condensation. Therefore the performance of the upper probe was relatively less affected by film temperature or the existence of wave disturbances.

It was found that there were three main effects which influenced the liquid film thickness in any liquid-vapour test. These were:

(i) Viscosity: As the temperature of the liquid film increased due to low inlet water subcooling, or the condensation of steam on the liquid film, then the viscosity of the liquid decreased resulting in an increase in the liquid film Reynolds number. Since the wall friction factor is a function of Reynolds number, the wall shear stress τ_w decreased.

$$\tau_w = f_w \frac{1}{2} \rho_f U_f^2 \quad (9.13)$$

where

$$f_w = \frac{C}{(Re_f)^n} \quad (9.14)$$

Therefore decreasing the liquid viscosity resulted in a thinner liquid film.

(ii) Condensation: As the vapour condensed on the liquid film, the local liquid film flowrate increased resulting in a thicker film.

(iii) Interfacial Shear Stress: The interfacial shear stress depends on the two-phase flowrates, such that any increase in either phase flowrate, results in a higher friction stress and consequently a thicker film.

As can be seen, these effects give a mixture of trends, with lower viscosity thinning the liquid film; condensation and interfacial friction effects thickening the liquid film. In order to project these effects further and give an indication of the degree of each effect, the theoretical film thicknesses were calculated along the test tube for four different cases, with the inlet water flow and temperatures held constant.

Case (a) No steam flowrate. Constant liquid film flowrate and temperature profile along the test tube, this representing the situation of a falling liquid film with no heat or mass transfer. The liquid film thickness for 80 K and 10 K subcooling, is represented by curve (a) in Figures 9.20 and 9.21.

Case (b) No steam flowrate. Constant liquid flowrate along the test tube; no condensation; no interfacial shear stress and variable temperature profile (flooding temperature profile used). Curve (b) on Figures 9.20 and 9.21 represents the liquid film obtained from this case. As the liquid film temperature was the only variable along the test tube, the difference between curves (b) and (a)

represents the effect of liquid viscosity on liquid film thickness.

Case (c) Flooding steam flowrate with condensation. Variable liquid flowrate; interfacial shear stress neglected giving curve (c); on Figures 9.20 and 9.21. The difference between curve (c) and curve (b) represents the effect of thickening the liquid film due to the variation in the liquid film due to condensation.

Case (d) Flooding steam flowrate with condensation. Variable liquid flowrate and interfacial shear stress giving curve (d) on Figures 9.20 and 9.21. The difference between curves (d) and (c) represents the effects of interfacial shear stress on the liquid film thickness.

It can be seen that the interfacial shear stress effect in Figure 9.20 is higher at the bottom of the test tube and decreases substantially at the top of the test section because the steam flowrate is high at the bottom of the test tube and condenses rapidly as it moves towards the top of the tube due to the high subcoolings. Also, in the high-subcooling tests, the effects of viscosity and condensation are very clear and important. This is not the case in low subcooling tests as shown in Figure 9.21 where the viscosity and condensation are very small whilst the effect of interfacial shear stress dominates along the test tube.

Since increasing the liquid film temperature results in a thinner liquid film due to the viscosity effect, then, for the same inlet liquid flowrate with an air-water test performed at standard conditions of 15°C and steam-water test performed at saturated temperature, a thinner film would be expected in the steam-water test. Therefore a higher steam flowrate than that of the air is required to cause flooding. This theoretical argument applied very well when the air-water flooding data was compared with the flooding data at the lowest subcooling tests performed (3 K). As the condensation on the liquid film was very small in the steam-water tests, it was found that a slightly higher steam flowrate was required to cause flooding compared to that of the air. The same trend would be expected if two air-water tests are performed at two different inlet water temperatures.

9.7 Liquid Film Temperature Analysis

Experimental tests were carried out to ascertain the flooding condition in steam-water counter-current flow for different inlet water flowrates. The main experimental parameter here is the tube wall temperature which was measured at eleven locations along the test tube. In order to process or analyse the steam-water data, a knowledge of the liquid film temperature across and along the film is essential. To obtain these two

dimensional analyses the turbulent thermal diffusivity is required and is determined using equation (6.46) in a trial and error process,

$$\frac{T_w - T_s}{T_t - T_s} = \frac{4}{\pi} \sum_{i=0}^{\infty} \frac{(-1)^i}{(2i+1)} \exp\left\{-\frac{(2i+1)\pi^2}{4\delta^2} \left[a_0 z + \frac{a_1}{2} z^2 + \dots + \frac{a_n}{n+1} z^{n+1} \right]\right\} \quad (9.15)$$

It was found that two terms of Fourier series were sufficient to predict the thermal diffusivity, namely the

first ($a_0 z$) and the ultimate ($\frac{a_n}{n+1} z^{n+1}$) terms, and

equation (9.15) thus became

$$\frac{T_w - T_s}{T_t - T_s} = \frac{4}{\pi} \sum_{i=0}^{\infty} \frac{(-1)^i}{(2i+1)} \exp\left\{-\frac{(2i+1)\pi^2}{4\delta^2} [a_0 z + a_N z^{n+1}]\right\} \quad (9.16)$$

and equation (6.45) becomes

$$\zeta = z (a_0 + a_N z^n) \quad (9.17)$$

Fitting equation (9.16) to experimental data with

$T_w = T_{wexp}$, enabled a_0 , a_N and the index n to be evaluated in terms of inlet water subcooling and flowrate.

From equation (9.17)

$$\alpha(z) = \frac{d\zeta}{dz} = a_0 + (n+1)a_N z^n \quad (9.18)$$

equation (9.18) can be written in dimensionless form as

$$\alpha(z) = a_0 + (n+1) a_N L^n (z^+)^n \quad (9.19)$$

$$\text{or } \alpha(z) = a_0 + a_\epsilon (z^+)^n \quad (9.20)$$

on the other hand as:

$$\alpha(z) = \frac{\overline{\epsilon_H + K}}{U_f} \quad (9.21)$$

Then, a_0 was taken to be equal to K/U_f , where

$$K = \frac{k_f}{\rho_f C P_f} \quad (9.22)$$

In all tests, the numerical value of K was found to vary between $1.5 \times 10^{-7} \text{ m}^2/\text{s}$ and $1.7 \times 10^{-7} \text{ m}^2/\text{s}$, and since a_0 is a constant, its value was fixed at the average value of $1.6 \times 10^{-7} \text{ m}$ since U_f was taken to have a mean value of 1.0 m/s down the film.

The second term $a_\epsilon (z^+)^n$ was considered equivalent to ϵ_H/U_f and numerical values for a_ϵ and n were chosen and varied until equation (9.16) satisfied the experimental data with the condition $T_w = T_{w\text{exp}}$. In the Fourier series, the value of the index n was taken as an integer, but in fitting equation (9.16) to the experimental data, it was found that better results could be achieved when non-integer values were taken. The selected values of a_0 , a_ϵ and n were substituted into equation (6.47) to give

$$\frac{\bar{T}_f - T_s}{T_t - T_s} = \frac{4}{\pi} \sum_{i=0}^{\infty} \frac{(-1)^i}{(2i+1)} \exp\left\{-\frac{(2i+1)\pi^2}{4\delta^2} z^+ L [a_0 + a_\epsilon (z^+)^n]\right\} \quad (9.23)$$

which, in turn, gave the liquid film mean temperature at any position along the test tube. The i value within the summation was taken as seven.

The range of inlet film flows in the experimental tests was mainly within the turbulent flow region. Flowrates lying in the laminar or transient flow regions were found to change rapidly to the turbulent region as condensation raised the water temperature quickly.

A comparison between experimental and calculated temperature and calculated liquid film mean temperature are plotted versus dimensionless position along the test section, for various liquid flowrates and two levels of subcooling, in Figures 9.22 and 9.23. It should be pointed out that an exact match between experimental and calculated wall temperature was not possible; there were many options and the best was chosen. From Figures 9.22 and 9.23, it can be seen, in some tests, that the calculated wall temperature at the bottom of the test section, is slightly higher than the liquid film mean temperature. The reason for this is that the experimental wall temperature near the bottom of the test section did not correspond to the inlet steam temperature

due to either experimental error or (which is more likely) the suction pressure in the extractor system slightly reducing the system pressure and hence the saturation temperature at this location.

The variations in n and a_e values were found to be functions of the inlet water subcooling and flowrate, Figure 9.24. The complexity of these variations is obvious but shows a common trend, which for n indicates that its value increased from 1.0 as both water flowrate and subcooling increased; and for a_e tend to decrease from 0.54×10^{-6} m as water flowrate and subcooling increase.

The turbulent diffusivity ratio α/U_f is higher at the bottom of the test tube as ϵ_H increases with distance down the test section. Since K and U_f are relatively constant compared with ϵ_H in equation (9.21), then ϵ_H increases substantially down the tube. This effect may be expected, since visual observation shows that the liquid film increases in turbulence down the tube, and the wave formation prior to flooding is substantially greater at the bottom of the tube than that at the top. Furthermore, increasing the liquid film temperature down the tube due to condensation, would decrease its viscosity, resulting in a higher liquid film Reynolds number and consequently a more turbulent film as it moves towards the bottom of the tube.

The effect of inlet water subcooling and flowrate

on α is even more complex. The numbers on which Figure 9.24 is based are listed in Table 9.5; also presented are values of $a_{\epsilon}(z^+)^n$ at top and bottom of the tube where z^+ is 1.0 and 16.67 respectively. It can be seen, for example, that at an inlet subcooling of 80 K, the effect of Q_f ranging from 4 to 10 l/min is to decrease $a_{\epsilon}(z^+)^n = \epsilon_H/U_f$ from 7.20×10^{-6} to 4.69×10^{-6} m; whilst for a constant value of inlet water flowrate of 8 l/min, the effect of increasing the subcooling from 3 K to 80 K is to decrease $a_{\epsilon}(z^+)^n$ from 9.00×10^{-6} to 4.62×10^{-6} . These are not large effects and all of their contributions are much larger than $a_o = K/U_f \sim 1.6 \times 10^{-7}$ m. Thus the turbulent contribution is 30 to 60 times the laminar contribution, which seems reasonable.

9.8 Flooding Model Analysis

The flooding model derived in Chapter 6 was compared with the air-water flooding characteristics obtained from the test facility operating at design conditions, Figure 9.25. The comparison was made with the air-water characteristics since the flooding model accounted for condensation effects. This is detailed below. The data are reasonably predicted and any scatter in the prediction is mainly due to the flooding model being semi-empirical.

The procedure used in calculating the predicted

flooding data is as follows -

(a) The complex component of the wave speed was determined from equation (6.89)

$$c_i = \left(\frac{k\delta+2}{6} \right) \frac{\rho_g}{\rho_f} v_g + \left[\frac{\sigma\delta}{3\rho_f} \left(k^2 + \frac{1}{(R-\delta)^2} \right) - \frac{1}{3} \frac{\rho_g v_g^2}{\rho_f} \right]^{1/2} \quad (9.24)$$

with δ determined using equations, (9.9) and (9.10) at $z^+ = 1$, and the initial values of steam condensation velocity, v_g , were used.

(b) For a uniform stream, at the maximum wave growth condition, the flooding conditions was determined from equation (6.88)

$$U_{sp} + U_f = \left[\frac{2v_g^2}{3k\delta} - \frac{(2k\delta+1)}{3k\delta} c_i v_g + \frac{4\sigma}{3\rho_f k} \left(k^2 - \frac{1}{2(R-\delta)^2} \right) \right]^{1/2} \quad (9.25)$$

(c) Allowing for acceleration effects the flooding condition was calculated using equation (6.108)

$$\frac{U_s}{U_{sp}} = \exp \left[k \frac{c_i}{2c_r} \left(\frac{\delta_m}{\delta_\infty} - 1 \right) \right] \quad (9.26)$$

where $c_r = U_f$, the liquid mean film thickness, δ_m was determined from equation (6.107) and δ_∞ determined from equation (6.109).

$$(\delta_{\infty})_{\text{LAM}} = \frac{1}{2} \rho^{+} f_i (Fr_g - Fr_f)^2 + \frac{8Fr_f^2}{Re_f} \quad (9.27)$$

for laminar flow

and

$$(\delta_{\infty})_{\text{TURB}} = \frac{1}{2} \rho^{+} f_i (Fr_g - Fr_f)^2 + \frac{0.0395Fr_f^2}{(Re_f)^{0.25}} \quad (9.28)$$

for turbulent flow.

However this still required a knowledge of the wave number (k) which was determined for each point by an iterative procedure using equations (9.24), (9.25) and (9.26). A relationship exists between k and δ which is also a function of water subcooling and because of this complexity, k was determined for each data point at the flooding condition. For the present data k values were found to vary from 534 m^{-1} for a liquid flowrate of 10 l/min and subcooling of 80 K to 202 m^{-1} for liquid flowrate of 21.9 l/min and 3K subcooling.

In air-water systems, $V_g = 0$, equation (9.24) becomes

$$c_{i0} = \left[\frac{\sigma\delta}{3\rho_f} (k^2 + \frac{1}{(R-\delta)^2}) \right]^{1/2} \quad (9.29)$$

Equations (9.24) and (9.29) give a measure of the rate of perturbed wave growth in terms of air/steam and liquid

velocities, the film thickness and the wave number for both steam-water and air-water systems. However if similar conditions were assumed under both flows, then c_i would be slightly smaller than c_{i0} , confirming the above concept that, for accelerating liquid flows under the same rate of air or steam flow, the growth of the perturbation is smaller in the steam-water system due to the effect of condensation. Consequently the wave amplitude at the bottom of the test tube is smaller in the steam-water system than in the air-water system and so more steam would be required to make the wave unstable and cause flooding as was observed experimentally.

As shown in Chapter 8 flooding appeared (by visual observations) to start at the bottom of test tube. The effect of condensation on the wave growth at the bottom of test tube is very small and could be negligible as the liquid film reached the saturation temperature, it is postulated that the effect of condensation is much higher at the top of the test tube. A mechanism showing how the growth of the waves is inhibited by V_g is described in Chapter 6 but this effect is very small even when the high condensation rates at the top are used. However, it is possible that the initiation of the waves at the top of the tube is inhibited by the condensation rate there and this effect may be described by the empirical correlation in Chapter 10. However the inhibition process may be a random one and equipment specific and it is difficult to build the effect of condensation on this into a

theoretical model.

The initial values of steam condensation velocity were used in the predicted flooding data. The condensation velocity, however, could be evaluated along the tube as described in Chapter 6 using equations (6.96) and (6.103) for the test tube and porous sinter respectively.

$$\left(\frac{v_g}{U_f}\right)_{\text{tube}} = \frac{\rho_f}{\rho_g} \text{Ja} \frac{\zeta}{\delta} \sum_{i=0}^{\infty} e^{-\frac{(2i+1)\pi^2}{4\delta^2} \zeta} \zeta \quad (9.30)$$

and

$$\left(\frac{v_g}{U_f}\right)_{\text{por}} = \left(\frac{K+\epsilon_H}{U_f}\right) \frac{\text{Ja}}{\sqrt{\pi\zeta}} \frac{\rho_f}{\rho_g} \quad (9.31)$$

Using equations (9.30) and (9.31), v_g/U_f was plotted versus dimensionless length z^+ in Figure 9.26 showing that v_g/U_f is highest at the top of the tube and decreases with length down the tube. This trend might have been expected as the degree of subcooling between the steam and liquid film is greatest at the top of the porous sinter and as steam condenses on the liquid film, the film temperature (mainly near the interface) increases resulting in less condensation as the film moves downwards. It is emphasised that this process has a strong dependence on the inlet water subcooling, Figure 9.26. This same figure, shows that at $z^+ \rightarrow 0$, $v_g/U_f \rightarrow \infty$

because at $z^+ = 0$, where the liquid film is introduced to the steam there is an infinite temperature gradient.

The initial wave amplitude at the top of the test section when flooding occurred was evaluated from equation (6.105)

$$A_i = \frac{2\sigma}{\rho_s U_s^2} \exp\left(-k \frac{c_i}{c_r} l\right) \quad (9.32)$$

and was found to be less than 1×10^{-5} m for the range of flowrates investigated. The wave grows as it moves down the tube and at the bottom of the test section its amplitude was found from equation (6.104).

$$A_c = \frac{2\sigma}{\rho_s U_s^2} \quad (9.33)$$

to be, on average, about 5 times the liquid film thickness. This is in accordance with the findings of Hewitt and Nicholls (1969).

9.9 Comparison with other data

A comparison with other data for air-water results is presented in Section 9.9.1 and for steam-water results in Section 9.9.2.

9.9.1 Air-Water results

The present air-water data were compared with several of the correlations and semi-empirical methods presented in Chapter 2. These comparisons are shown in Figures 9.27 (correlations) and 9.28 (semi-empirical methods). It can be seen that all the present data points lie just below the Bharathan (1979) predictions. This is an interesting result since Bharathan argued that this was the maximum possible flooding rate and could only be achieved by the elimination of end effects, a condition which was aimed for in the present work but fell just short of fulfilling.

9.9.2 Steam-Water results

The data available in the literature giving the limits of annular counter-current two-phase flow in a vertical tube with heat and mass transfer are few. However Wallis et al (1980) collected such data using a test facility with square tube entries for water and air flows. The tube diameter was 50.8 mm and the inlet water temperature was about 96.0°C. Therefore the results obtained from the inlet water temperature of 97.0°C are compared with those of Wallis, Figure 9.29. The present data are shown to be well above the Bharathan data. This is expected since end effects are much

smaller with the present data. It is also interesting to note that both sets of data tend to curve upwards at higher $j_f^{*1/2}$ as the condensation effect increases.

Test Rig Performance

The test rig, described in Chapter 3, functioned satisfactorily although there are two points worth considering for development, these are

- (i) the injector length chosen led to a thickening of the liquid film at the water inlet which could cause the suppression of the wave growth. This effect could be eliminated by increasing the length of the porous section.

- (ii) The extraction method used resulted in a relatively large percentage of the air or steam supply flow passing through the sinter with the liquid. Developing an extraction system eliminating air or steam extraction with the liquid film is an important step in obtaining the ideal flooding situation. This requires more investigation and again could be associated with the length of the porous sinter.

Instrumentation Performance

Most of the instrumentation used, described in Chapter 4, performed satisfactorily. The percentage error in each parameter measurement is given in Appendix A. However, the largest percentage error occurred in the

conductance probe liquid film thickness measurements in the steam-water system. To measure the liquid film conductivity which was used to calculate the liquid film thickness at the top and bottom of the test tube, a conductivity cell was used. Here the sample for the conductivity cell was taken at inlet water temperature, whereas in fact the temperature and hence the conductivity would vary along the test section due to the steam condensation.

M_{fTop} (kg/min)	δ^+_{Top}	M_{fBot}	δ^+_{Bot}
4.2918	0.10969E-01	4.5849	0.87932E-02
5.2732	0.11940E-01	5.7251	0.10153E-01
6.2268	0.12697E-01	6.8599	0.11470E-01
7.1868	0.13537E-01	7.8923	0.13322E-01
8.2049	0.14575E-01	8.8032	0.14679E-01
9.2147	0.15947E-01	9.8216	0.15845E-01
10.2004	0.17041E-01	10.8204	0.16586E-01

Table 9.1 Predicted Liquid Film Thickness ($\Delta T_{sub} = 80K$)

M_{fTop} (kg/min)	δ^+_{Top}	M_{fBot}	δ^+_{Bot}
4.2436	0.10152E-01	4.4467	0.88255E-02
5.2700	0.11436E-01	5.5442	0.10011E-01
6.2921	0.12737E-01	6.6541	0.11176E-01
8.1945	0.14155E-01	8.8460	0.13585E-01
7.2358	0.13192E-01	7.7696	0.12226E-01
9.1870	0.15317E-01	9.8895	0.14852E-01
10.1964	0.16462E-01	10.8417	0.15916E-01
11.3985	0.18115E-01	12.0311	0.17190E-01
12.9029	0.20041E-01	13.6356	0.19075E-01

Table 9.2 Predicted Liquid Film Thickness ($\Delta T_{sub} = 60K$)

M_{fTop} (kg/min)	δ^+_{Top}	M_{fBot}	δ^+_{Bot}
4.1839	0.96984E-02	4.2929	0.85790E-02
5.2048	0.11224E-01	5.3524	0.97356E-02
6.2317	0.12714E-01	6.4258	0.10859E-01
7.2318	0.13955E-01	7.4895	0.11894E-01
8.2327	0.14993E-01	8.5824	0.12935E-01
9.1967	0.15711E-01	9.6446	0.13866E-01
10.1587	0.16532E-01	10.7231	0.14917E-01
11.3466	0.17908E-01	11.9983	0.16455E-01
12.8538	0.19641E-01	13.4377	0.17781E-01
14.3839	0.21512E-01	14.9861	0.19079E-01
15.9208	0.23385E-01	16.5416	0.20195E-01
17.4618	0.25380E-01	18.1625	0.21897E-01
18.9908	0.27367E-01	19.6717	0.22926E-01
20.5342	0.29494E-01	21.2029	0.24151E-01

Table 9.3 Predicted Liquid Film Thickness ($\Delta T_{sub} = 40K$)

M_{fTop} (kg/min)	δ^+_{Top}	M_{fBot}	δ^+_{Bot}
4.1077	0.90185E-02	4.1497	0.83813E-02
5.1172	0.10549E-01	5.1788	0.95540E-02
6.1357	0.11892E-01	6.2147	0.10568E-01
7.1475	0.13279E-01	7.2425	0.11562E-01
8.1536	0.14745E-01	8.2728	0.12579E-01
9.1711	0.16137E-01	9.3083	0.13494E-01
10.1714	0.17296E-01	10.3584	0.14344E-01
11.3799	0.18955E-01	11.5936	0.15442E-01
12.8883	0.20861E-01	13.1564	0.16764E-01
14.4086	0.22634E-01	14.7502	0.18111E-01
15.9432	0.24418E-01	16.3165	0.19234E-01
17.4194	0.25949E-01	17.8945	0.20690E-01
18.9522	0.27944E-01	19.4266	0.22041E-01
20.4825	0.29800E-01	20.9954	0.23275E-01

Table 9.4 Predicted Liquid Film Thickness ($\Delta T_{sub} = 20K$)

Table 9.5 Estimated Exchange Coefficients

Q_{fin} (1/min)	ΔT_{sub} (K)	K/U_F (m)	a	n	$\epsilon H/U_F$ (m)	
					$z^+=1.0$	$z^+=16.67$
4.0	80.0	0.16E-06	0.432E-06	1.0	0.432E-06	0.720E-05
5.0	80.0	0.16E-06	0.184E-06	1.3	0.184E-06	0.713E-05
6.0	80.0	0.16E-06	0.177E-07	2.2	0.177E-07	0.864E-05
7.0	80.0	0.16E-06	0.190E-09	3.5	0.190E-09	0.360E-05
8.0	80.0	0.16E-06	0.379E-12	5.8	0.379E-12	0.462E-05
9.0	80.0	0.16E-06	0.540E-13	6.5	0.540E-13	0.473E-05
10.0	80.0	0.16E-06	0.449E-15	8.2	0.449E-15	0.469E-05
4.0	70.0	0.16E-06	0.432E-06	1.0	0.432E-06	0.720E-05
5.0	70.0	0.16E-06	0.256E-06	1.2	0.256E-06	0.748E-05
6.0	70.0	0.16E-06	0.114E-06	1.5	0.114E-06	0.775E-05
7.0	70.0	0.16E-06	0.623E-08	2.2	0.623E-08	0.304E-05
8.0	70.0	0.16E-06	0.439E-09	3.2	0.439E-09	0.357E-05
9.0	70.0	0.16E-06	0.236E-10	4.3	0.236E-10	0.424E-05
10.0	70.0	0.16E-06	0.582E-12	5.7	0.582E-12	0.536E-05
11.2	70.0	0.16E-06	0.677E-13	6.5	0.677E-13	0.593E-05
12.7	70.0	0.16E-06	0.175E-13	7.0	0.175E-13	0.624E-05
4.0	60.0	0.16E-06	0.480E-06	1.0	0.480E-06	0.800E-05
5.0	60.0	0.16E-06	0.432E-06	1.0	0.432E-06	0.720E-05
6.0	60.0	0.16E-06	0.263E-06	1.2	0.263E-06	0.770E-05
7.0	60.0	0.16E-06	0.661E-07	1.5	0.661E-07	0.450E-05
8.0	60.0	0.16E-06	0.151E-07	2.0	0.151E-07	0.420E-05
9.0	60.0	0.16E-06	0.223E-08	2.7	0.223E-08	0.444E-05
10.0	60.0	0.16E-06	0.174E-09	3.5	0.174E-09	0.329E-05
11.2	60.0	0.16E-06	0.150E-11	5.3	0.150E-11	0.447E-05
12.7	60.0	0.16E-06	0.600E-13	6.5	0.600E-13	0.525E-05
4.0	50.0	0.16E-06	0.480E-06	1.0	0.480E-06	0.800E-05
5.0	50.0	0.16E-06	0.444E-06	1.0	0.444E-06	0.740E-05
6.0	50.0	0.16E-06	0.342E-06	1.1	0.342E-06	0.756E-05
7.0	50.0	0.16E-06	0.248E-06	1.2	0.248E-06	0.726E-05
8.0	50.0	0.16E-06	0.136E-06	1.4	0.136E-06	0.696E-05
9.0	50.0	0.16E-06	0.249E-07	1.9	0.249E-07	0.522E-05
10.0	50.0	0.16E-06	0.240E-08	2.6	0.240E-08	0.360E-05
11.2	50.0	0.16E-06	0.874E-10	3.8	0.874E-10	0.384E-05
12.7	50.0	0.16E-06	0.468E-11	4.9	0.468E-11	0.454E-05
14.2	50.0	0.16E-06	0.245E-12	6.0	0.245E-12	0.525E-05
15.7	50.0	0.16E-06	0.699E-14	7.3	0.699E-14	0.581E-05

Table 9.5 (cont.) Estimated Exchange Coefficients

Q_{fin} (1/min)	ΔT_{sub} (K)	K/U_F (m)	a	n	$\epsilon H/U_F$ (m)	
					$z^+=1.0$	$z^+=16.67$
4.0	40.0	0.16E-06	0.480E-06	1.0	0.480E-06	0.800E-05
5.0	40.0	0.16E-06	0.456E-06	1.0	0.456E-06	0.760E-05
6.0	40.0	0.16E-06	0.444E-06	1.0	0.444E-06	0.740E-05
7.0	40.0	0.16E-06	0.420E-06	1.0	0.420E-06	0.700E-05
8.0	40.0	0.16E-06	0.285E-06	1.1	0.285E-06	0.630E-05
9.0	40.0	0.16E-06	0.142E-06	1.3	0.142E-06	0.552E-05
10.0	40.0	0.16E-06	0.490E-07	1.6	0.490E-07	0.442E-05
11.2	40.0	0.16E-06	0.140E-07	2.0	0.140E-07	0.390E-05
12.7	40.0	0.16E-06	0.144E-08	2.8	0.144E-08	0.380E-05
14.2	40.0	0.16E-06	0.217E-09	3.5	0.217E-09	0.41E-05
15.7	40.0	0.16E-06	0.204E-10	4.4	0.204E-10	0.486E-05
17.3	40.0	0.16E-06	0.415E-11	5.0	0.415E-11	0.534E-05
18.8	40.0	0.16E-06	0.105E-11	5.5	0.105E-11	0.553E-05
20.3	40.0	0.16E-06	0.261E-12	6.0	0.261E-12	0.560E-05
4.0	30.0	0.16E-06	0.516E-06	1.0	0.516E-06	0.860E-05
5.0	30.0	0.16E-06	0.480E-06	1.0	0.480E-06	0.800E-05
6.0	30.0	0.16E-06	0.456E-06	1.0	0.456E-06	0.760E-05
7.0	30.0	0.16E-06	0.444E-06	1.0	0.444E-06	0.740E-05
8.0	30.0	0.16E-06	0.432E-06	1.0	0.432E-06	0.720E-05
9.0	30.0	0.16E-06	0.408E-06	1.0	0.408E-06	0.680E-05
10.0	30.0	0.16E-06	0.372E-06	1.0	0.372E-06	0.620E-05
11.2	30.0	0.16E-06	0.247E-06	1.1	0.247E-06	0.546E-05
12.7	30.0	0.16E-06	0.113E-06	1.3	0.113E-06	0.437E-05
14.2	30.0	0.16E-06	0.490E-07	1.6	0.490E-07	0.442E-05
15.7	30.0	0.16E-06	0.126E-07	2.1	0.126E-07	0.465E-05
17.3	30.0	0.16E-06	0.335E-08	2.6	0.335E-08	0.504E-05
18.8	30.0	0.16E-06	0.519E-09	3.3	0.519E-09	0.559E-05
20.3	30.0	0.16E-06	0.778E-10	4.0	0.778E-10	0.600E-05
4.0	20.0	0.16E-06	0.540E-06	1.0	0.540E-06	0.900E-05
5.0	20.0	0.16E-06	0.540E-06	1.0	0.540E-06	0.900E-05
6.0	20.0	0.16E-06	0.540E-06	1.0	0.540E-06	0.900E-05
7.0	20.0	0.16E-06	0.540E-06	1.0	0.540E-06	0.900E-05
8.0	20.0	0.16E-06	0.528E-06	1.0	0.528E-06	0.880E-05
9.0	20.0	0.16E-06	0.516E-06	1.0	0.516E-06	0.860E-05
10.0	20.0	0.16E-06	0.480E-06	1.0	0.480E-06	0.800E-05
11.2	20.0	0.16E-06	0.468E-06	1.0	0.468E-06	0.780E-05
12.7	20.0	0.16E-06	0.432E-06	1.0	0.432E-06	0.720E-05
14.2	20.0	0.16E-06	0.384E-06	1.0	0.384E-06	0.640E-05
15.7	20.0	0.16E-06	0.336E-06	1.0	0.336E-06	0.560E-05
17.2	20.0	0.16E-06	0.276E-06	1.0	0.276E-06	0.460E-05
18.8	20.0	0.16E-06	0.162E-06	1.1	0.162E-06	0.357E-05
20.3	20.0	0.16E-06	0.514E-07	1.5	0.514E-07	0.350E-05

Table 9.5 (cont.) Estimated Exchange Coefficients

Q_{fin} (1/min)	ΔT_{sub} (K)	K/U_F (m)	a	n	$\epsilon H/U_F$ (m)	
					$z^+=1.0$	$z^+=16.67$
4.0	10.0	0.16E-06	0.540E-06	1.0	0.540E-06	0.900E-05
5.0	10.0	0.16E-06	0.540E-06	1.0	0.540E-06	0.900E-05
6.0	10.0	0.16E-06	0.540E-06	1.0	0.540E-06	0.900E-05
7.0	10.0	0.16E-06	0.540E-06	1.0	0.540E-06	0.900E-05
8.0	10.0	0.16E-06	0.540E-06	1.0	0.540E-06	0.900E-05
9.0	10.0	0.16E-06	0.540E-06	1.0	0.540E-06	0.900E-05
10.0	10.0	0.16E-06	0.540E-06	1.0	0.540E-06	0.900E-05
11.2	10.0	0.16E-06	0.540E-06	1.0	0.540E-06	0.900E-05
12.7	10.0	0.16E-06	0.540E-06	1.0	0.540E-06	0.900E-05
14.2	10.0	0.16E-06	0.540E-06	1.0	0.540E-06	0.900E-05
15.7	10.0	0.16E-06	0.528E-06	1.0	0.528E-06	0.880E-05
17.2	10.0	0.16E-06	0.504E-06	1.0	0.504E-06	0.840E-05
18.8	10.0	0.16E-06	0.456E-06	1.0	0.456E-06	0.760E-05
20.3	10.0	0.16E-06	0.360E-06	1.0	0.360E-06	0.600E-05
21.9	10.0	0.16E-06	0.288E-06	1.0	0.288E-06	0.480E-05
4.0	3.0	0.16E-06	0.540E-06	1.0	0.540E-06	0.900E-05
5.0	3.0	0.16E-06	0.540E-06	1.0	0.540E-06	0.900E-05
6.0	3.0	0.16E-06	0.540E-06	1.0	0.540E-06	0.900E-05
7.0	3.0	0.16E-06	0.540E-06	1.0	0.540E-06	0.900E-05
8.0	3.0	0.16E-06	0.540E-06	1.0	0.540E-06	0.900E-05
9.0	3.0	0.16E-06	0.540E-06	1.0	0.540E-06	0.900E-05
10.0	3.0	0.16E-06	0.540E-06	1.0	0.540E-06	0.900E-05
11.2	3.0	0.16E-06	0.540E-06	1.0	0.540E-06	0.900E-05
12.7	3.0	0.16E-06	0.540E-06	1.0	0.540E-06	0.900E-05
14.2	3.0	0.16E-06	0.540E-06	1.0	0.540E-06	0.900E-05
15.7	3.0	0.16E-06	0.540E-06	1.0	0.540E-06	0.900E-05
17.2	3.0	0.16E-06	0.540E-06	1.0	0.540E-06	0.900E-05
18.8	3.0	0.16E-06	0.540E-06	1.0	0.540E-06	0.900E-05
20.3	3.0	0.16E-06	0.540E-06	1.0	0.540E-06	0.900E-05
21.9	3.0	0.16E-06	0.528E-06	1.0	0.528E-06	0.880E-05

Air-Water Tests

Present Data	}	x	Upper Probe
		o	Lower Probe

McNeil Data	}	∇	Upper Probe
		◊	Lower Probe

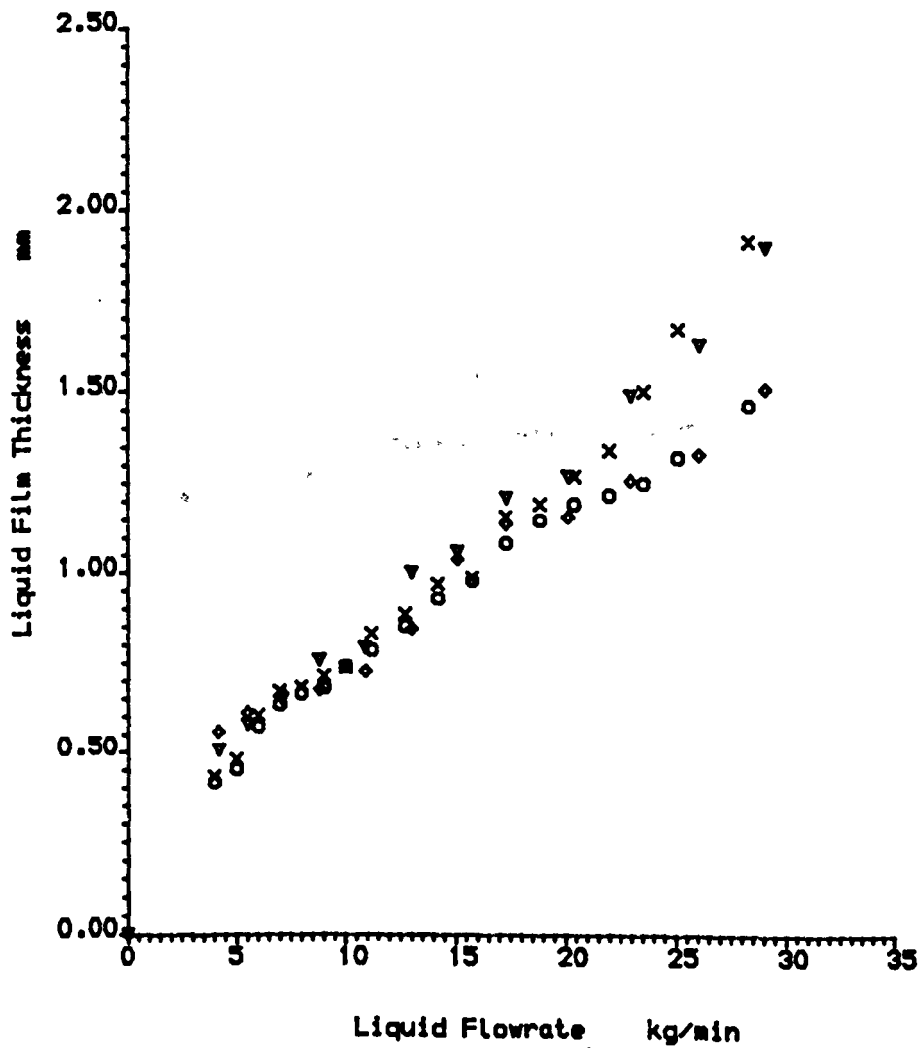


Figure 9.1 Comparison of Liquid Film Thickness Measurements with McNeil (1986).

Air-Water Tests

- o Low Air Extraction Rate Data
- x High Air Extraction Rate Data

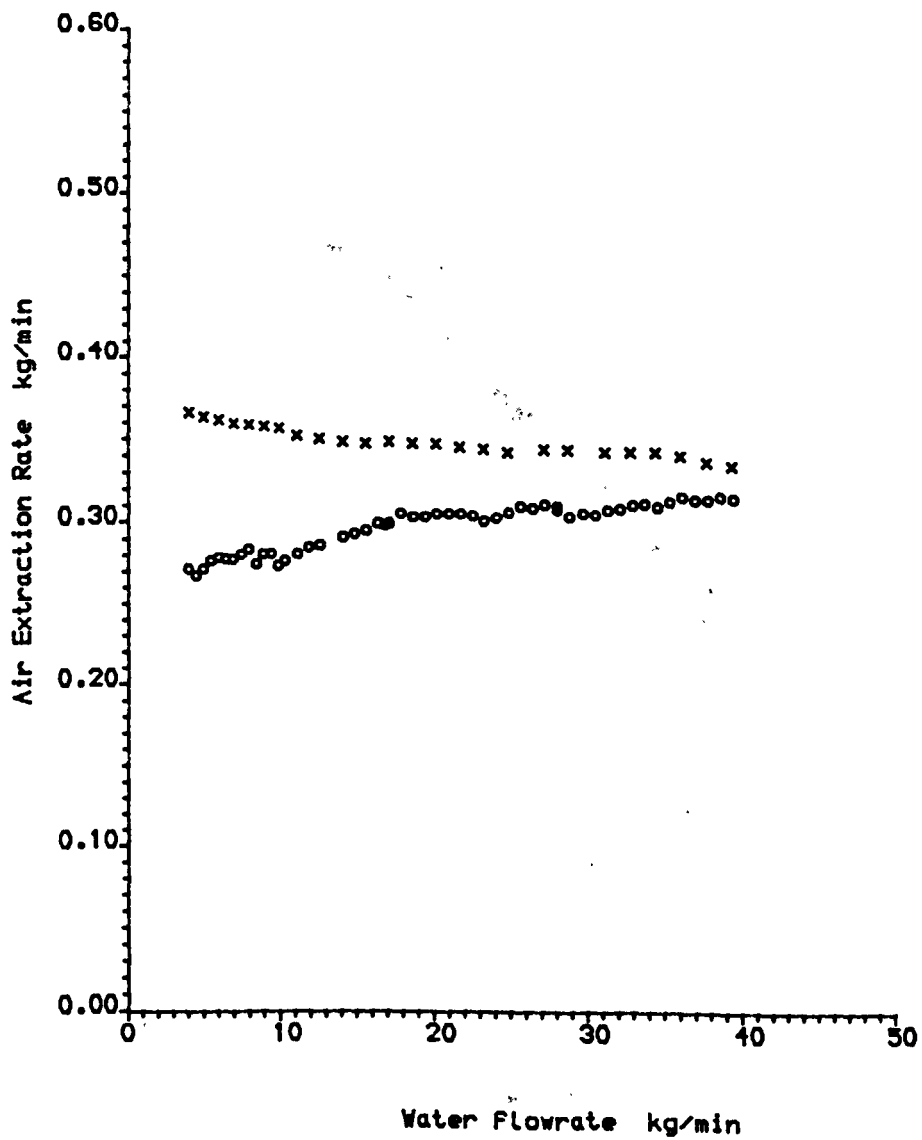
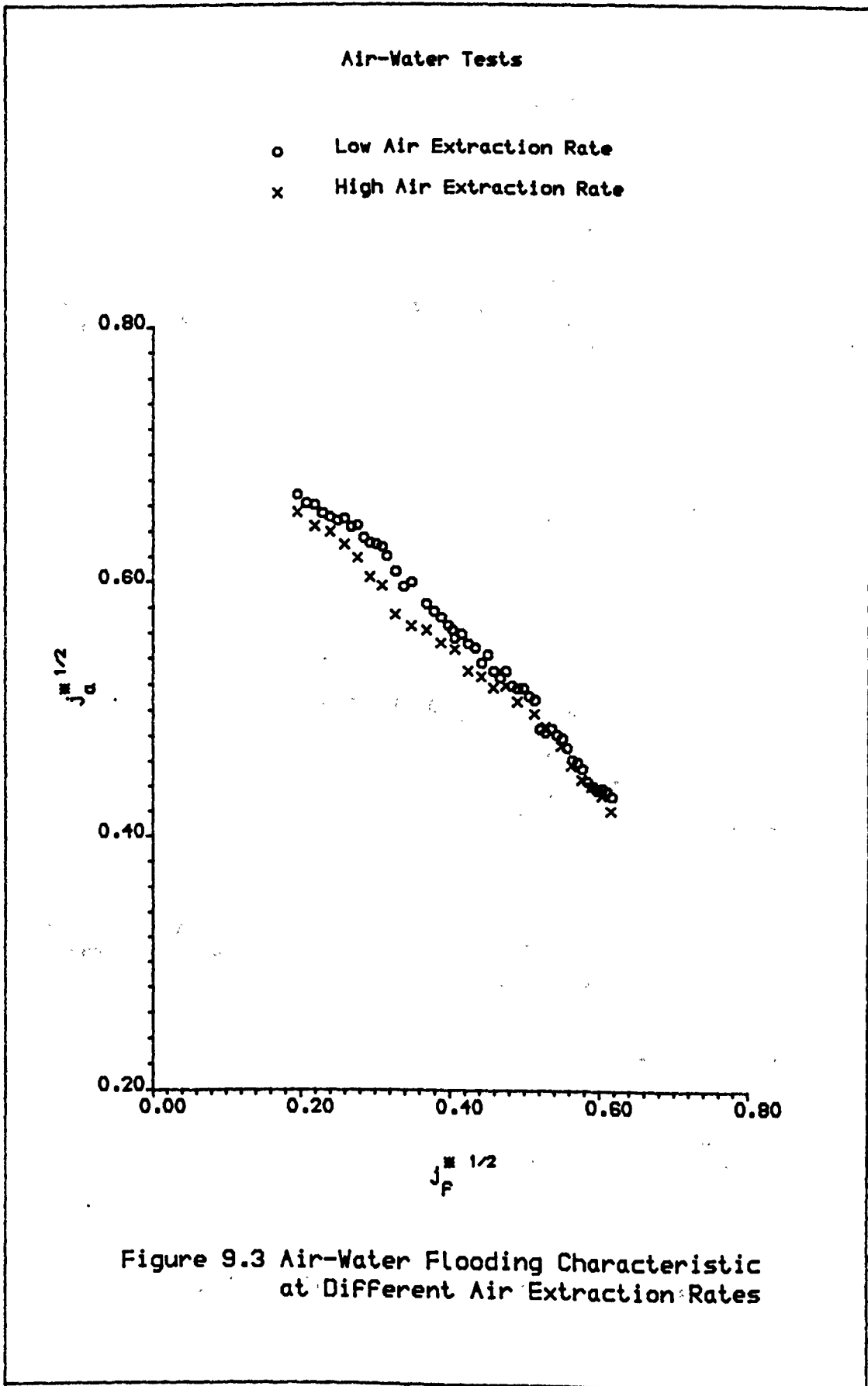


Figure 9.2 Air Extraction Rates at Flooding



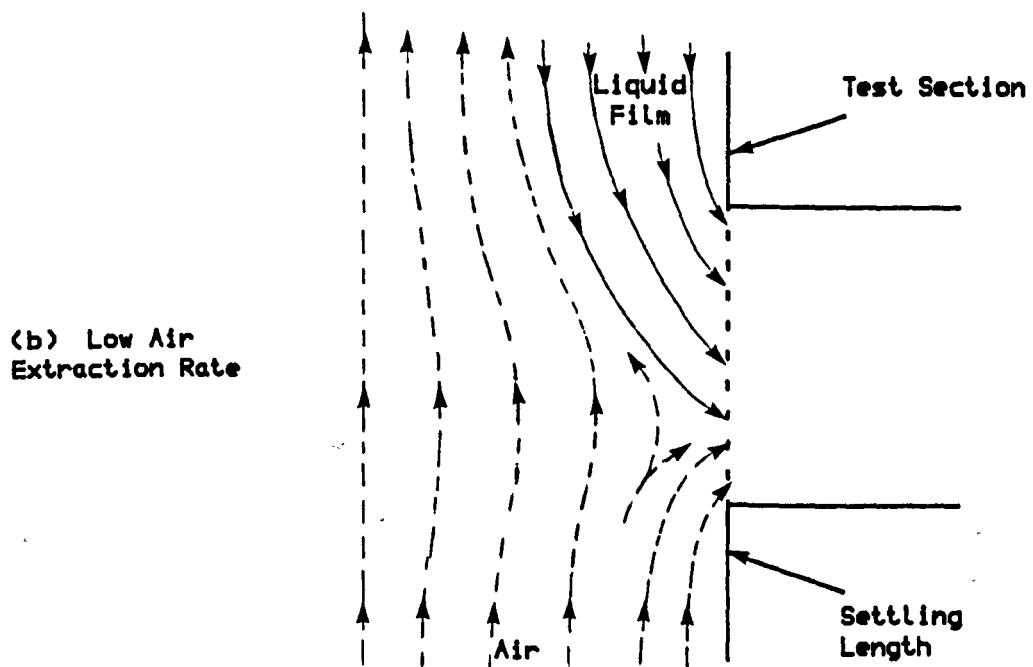
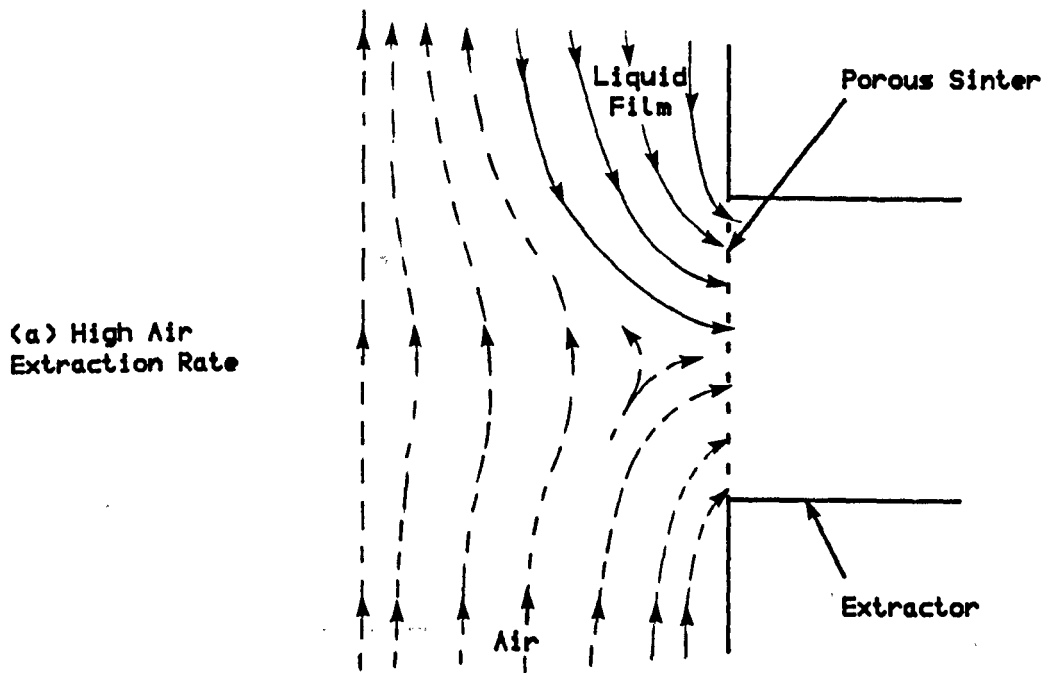
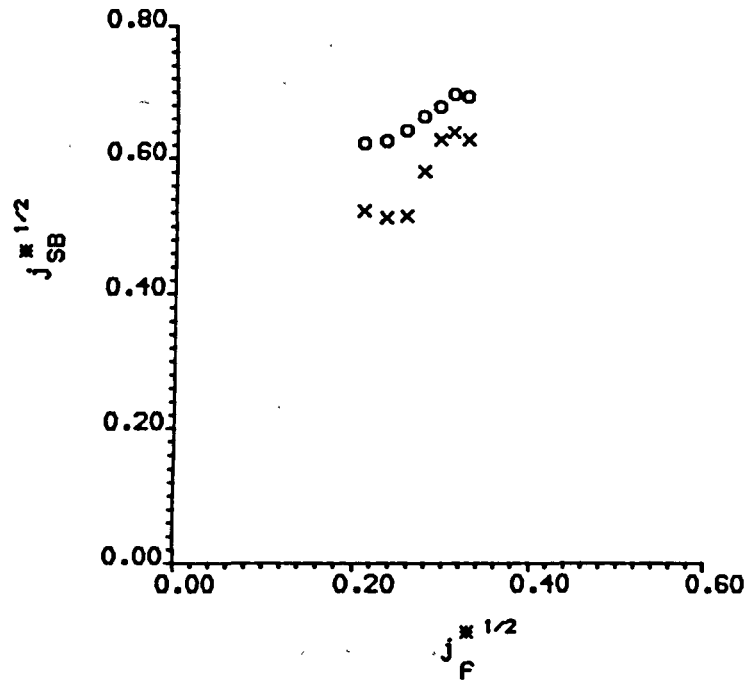


Figure 9.4 Air Extraction Rate Profile

Steam-Water Tests

$\Delta T_{sub} = 80 \text{ K}$

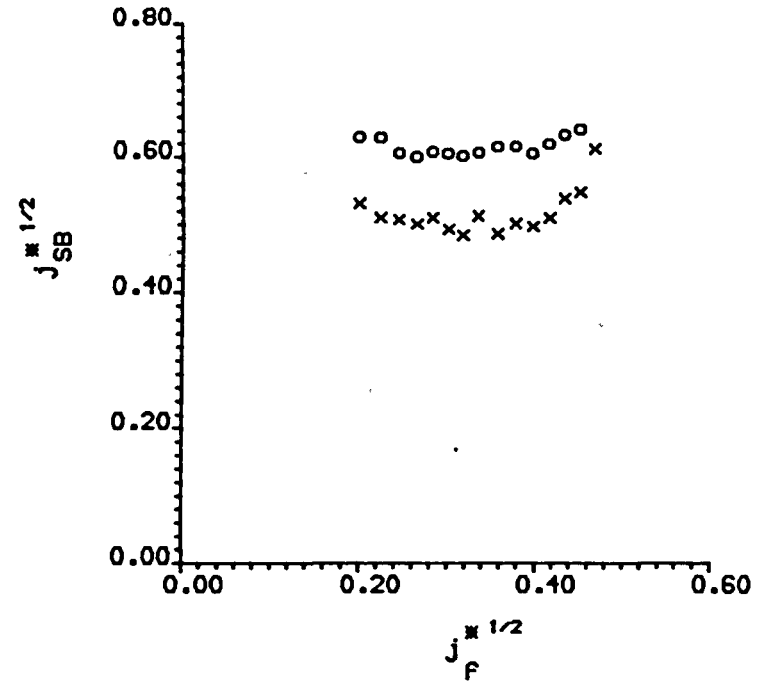
- o Low Steam Extraction Rate Data
- x High Steam Extraction Rate Data



Steam - Water Flooding Data at
Different Steam Extraction Rates
Figure 9.5

$\Delta T_{sub} = 20 \text{ K}$

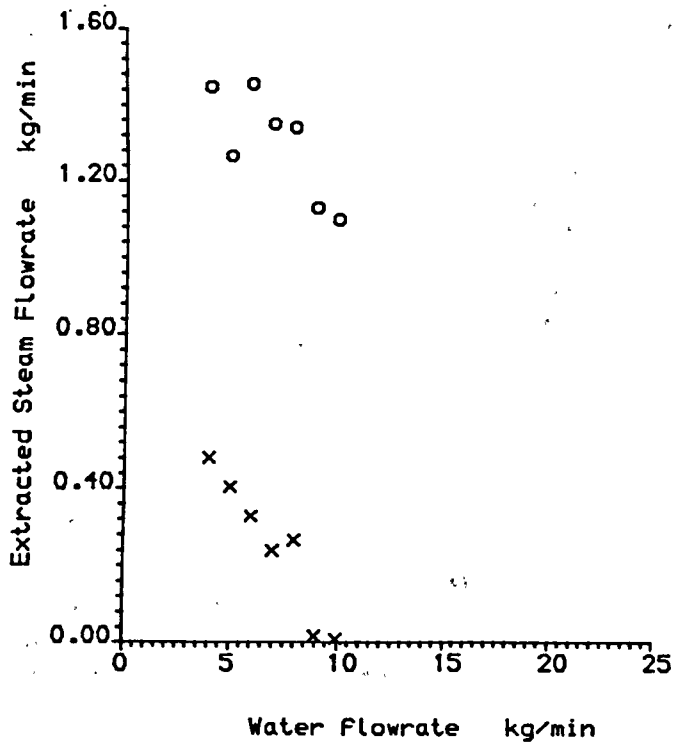
- o Low Steam Extraction Rate Data
- x High Steam Extraction Rate Data



Steam - Water Flooding Data at
Different Steam Extraction Rates
Figure 9.6

Steam-Water tests

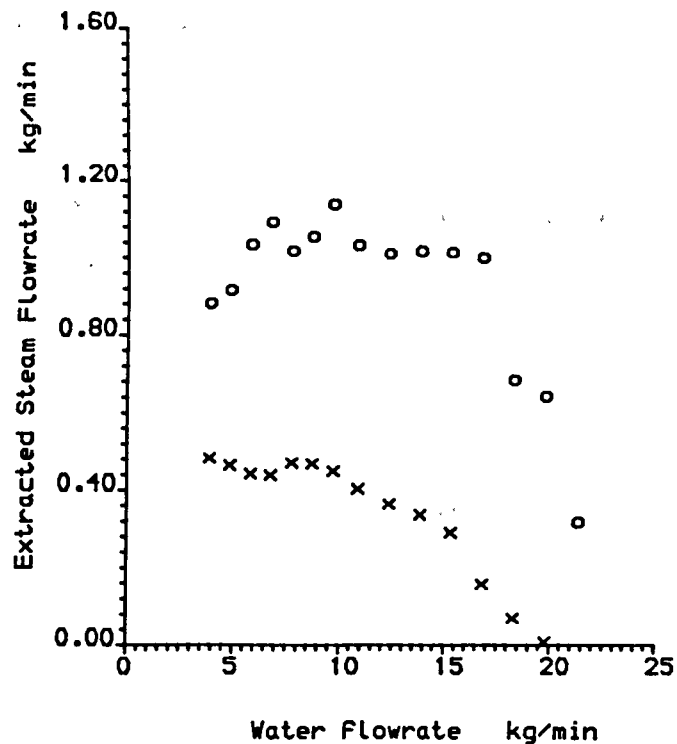
- x Low Steam Extraction Rate Data
- o High Steam Extraction Rate Data



Steam Extraction Rates.($\Delta T_{sub} = 80 \text{ K}$)

Figure 9.7

- x Low Steam Extraction Rate Data
- o High Steam Extraction Rate Data



Steam Extraction Rates.($\Delta T_{sub} = 20 \text{ K}$)

Figure 9.8

Steam-Water Tests

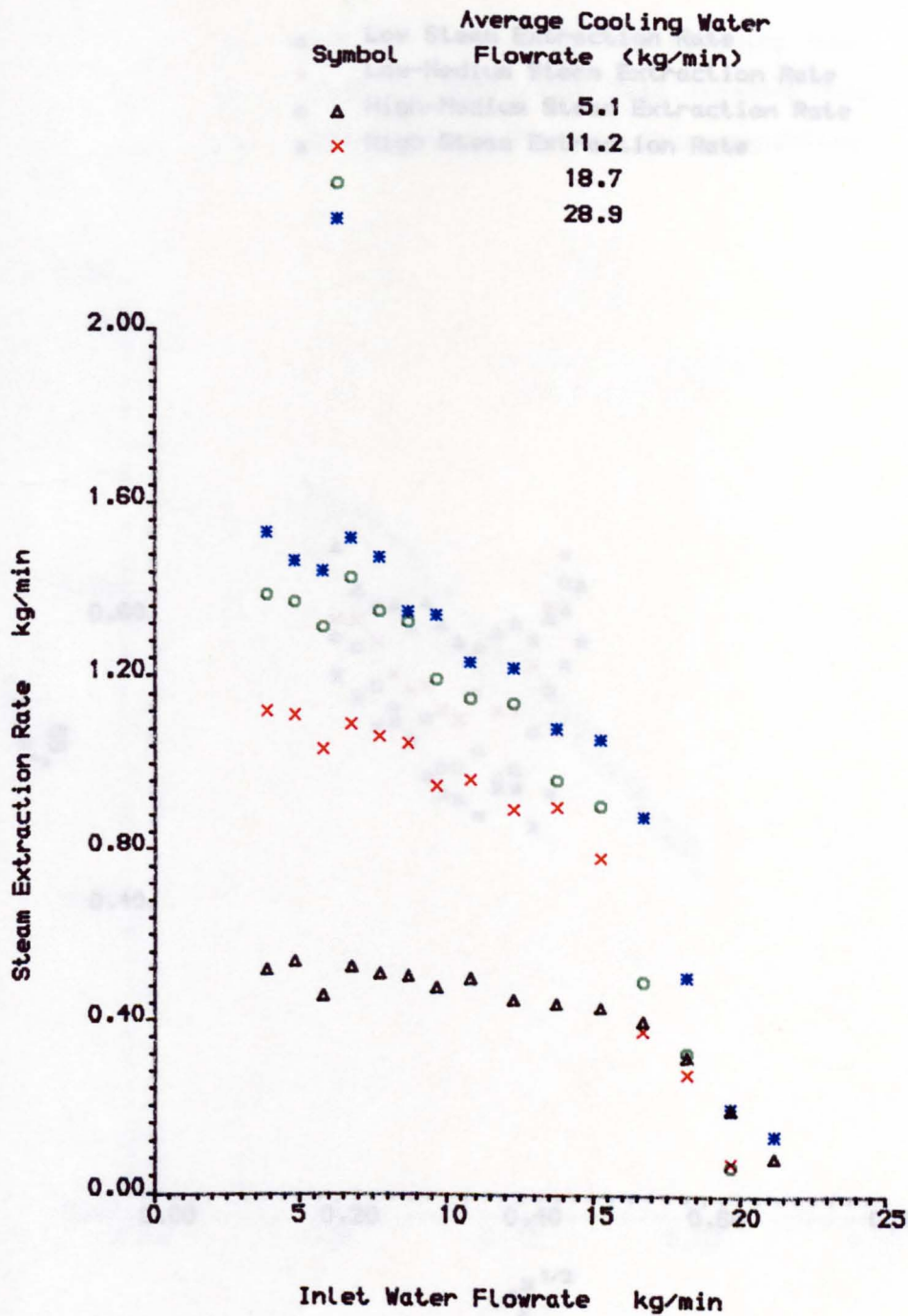


Figure 9.9 Steam Extraction Rates at Different Cooling Water Flowrates. ($\Delta T_{sub} = 10$ K)

Steam-Water Tests

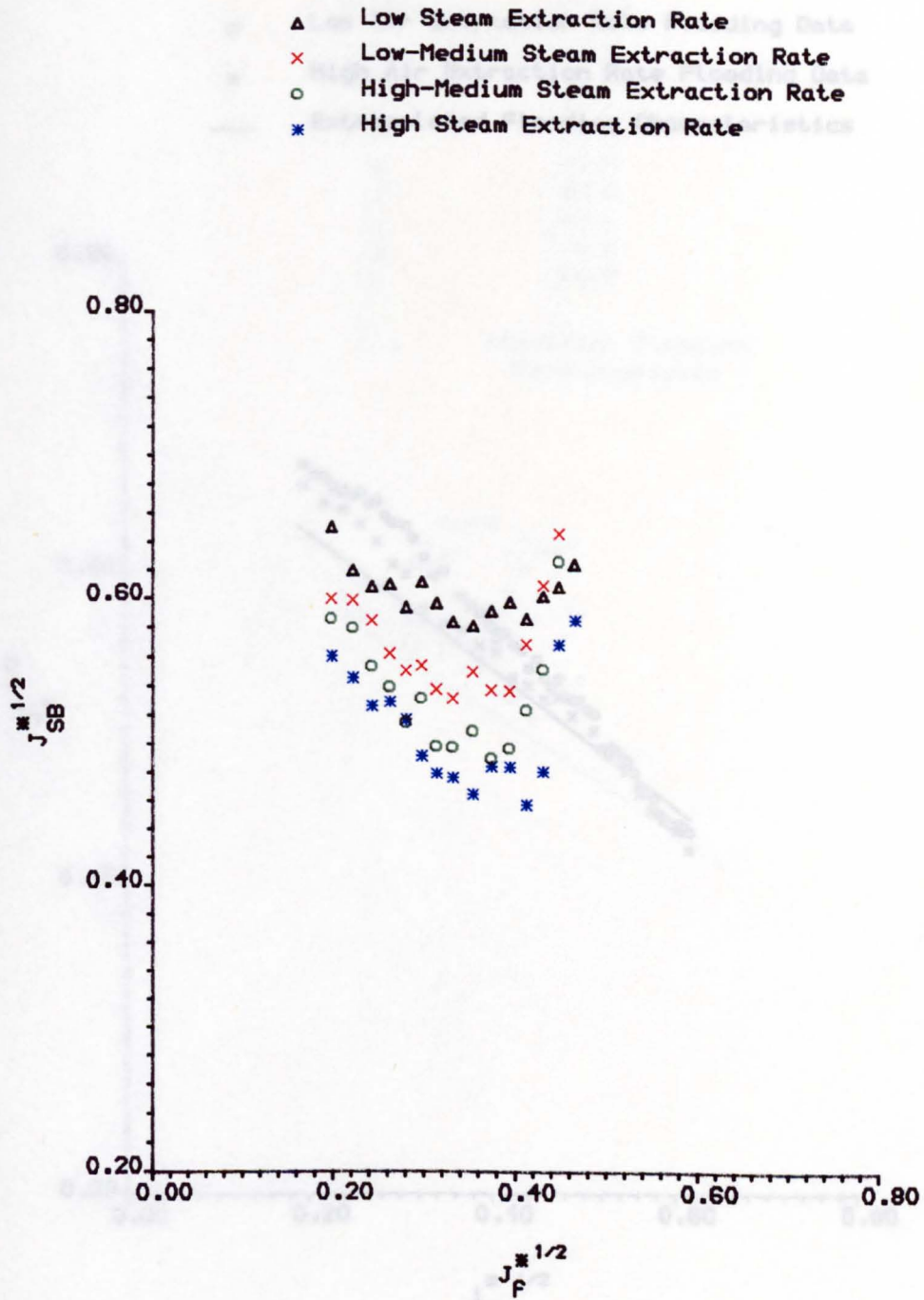
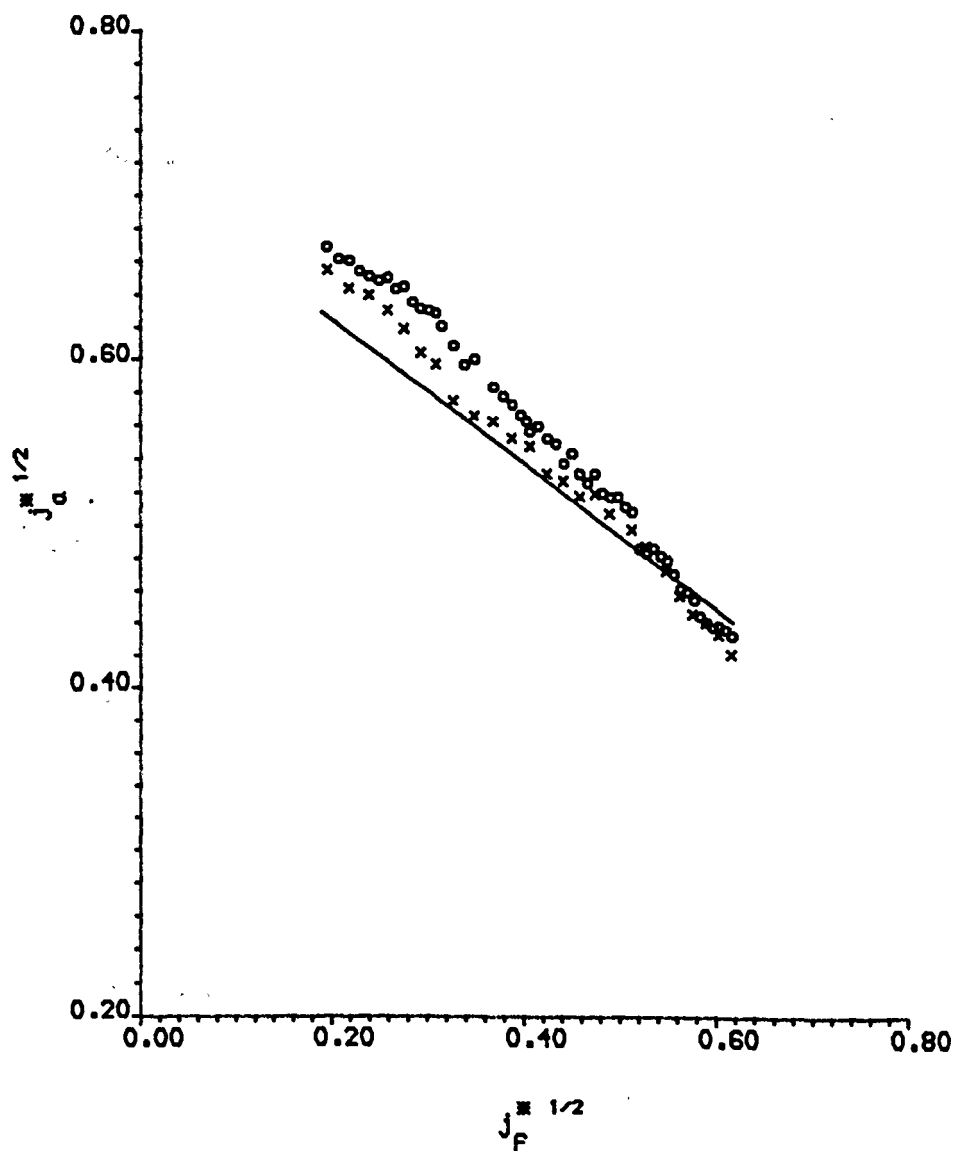


Figure 9.10 Steam-Water Flooding Data at Different Steam Extraction Rates. ($\Delta T_{sub} = 10 \text{ K}$)

Air-Water Tests

- o Low Air Extraction Rate Flooding Data
- x High Air Extraction Rate Flooding Data
- Extrapolated Flooding Characteristics



Figuer 9.11 Air-Water Flooding Data with Extrapolated Flooding Characteristic.

Steam-Water data based on steam Flowrate
at the bottom of the test tube

Steam-Water Tests

Symbol	ΔT_{sub}
○	3 K
▽	10 K
×	20 K
◇	30 K
✱	40 K
△	50 K
+	60 K
□	70 K
○	80 K

— Air-Water Flooding
Characteristic

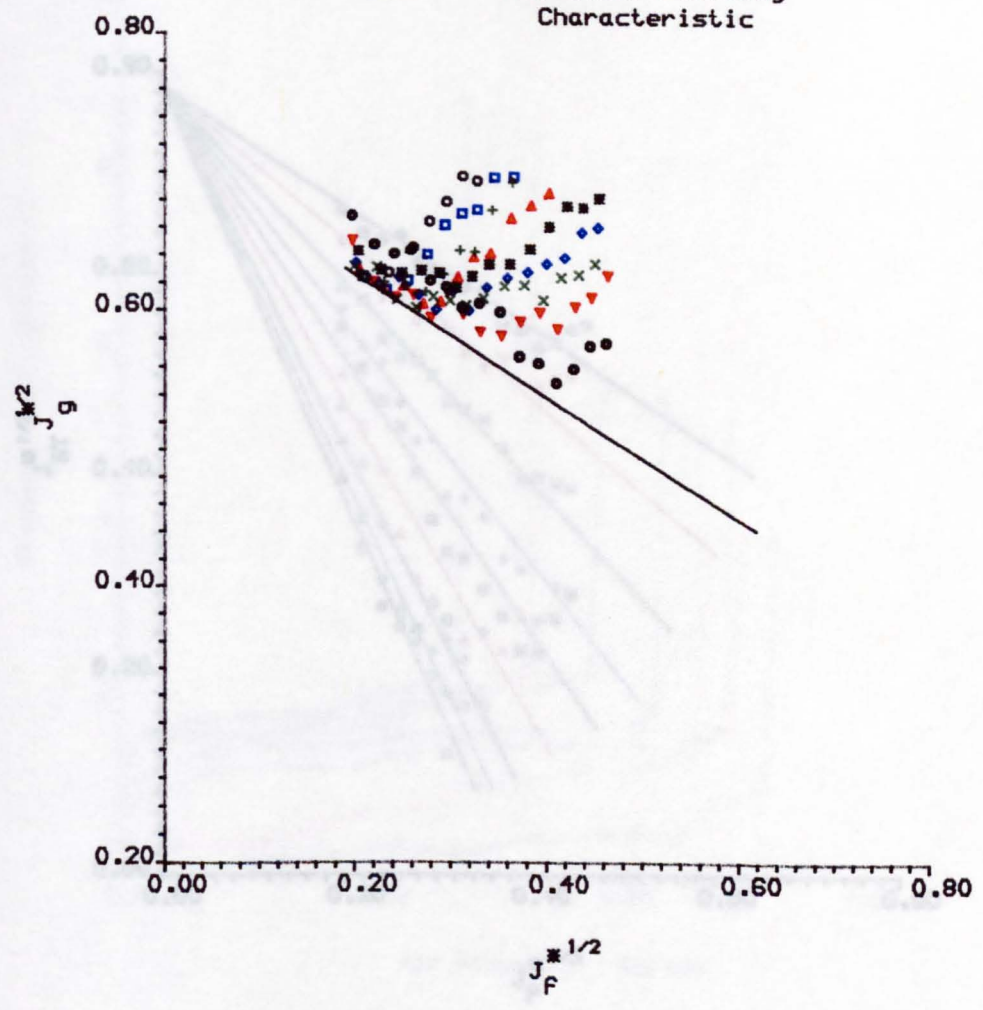


Figure 9.12 Compatible Air-Water and
Steam-Water Flooding Data

Steam-Water Tests

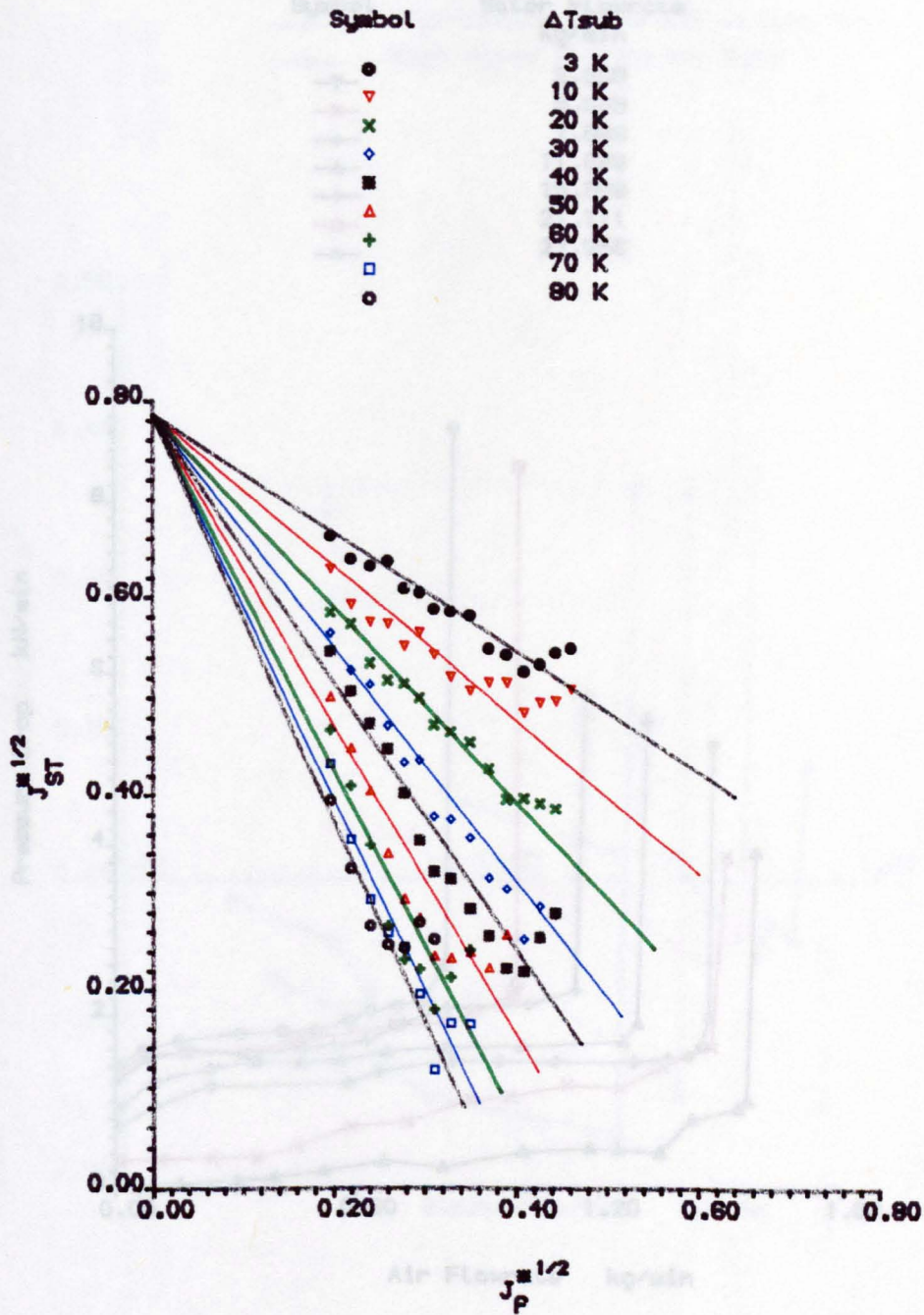


Figure 9.13 Steam-Water Flooding Data at the Top of the Test Tube

Air-Water Tests

Symbol	Water Flowrate kg/min
▼	3.959
×	5.939
◆	7.898
▲	11.098
+	15.598
□	21.711
○	27.956

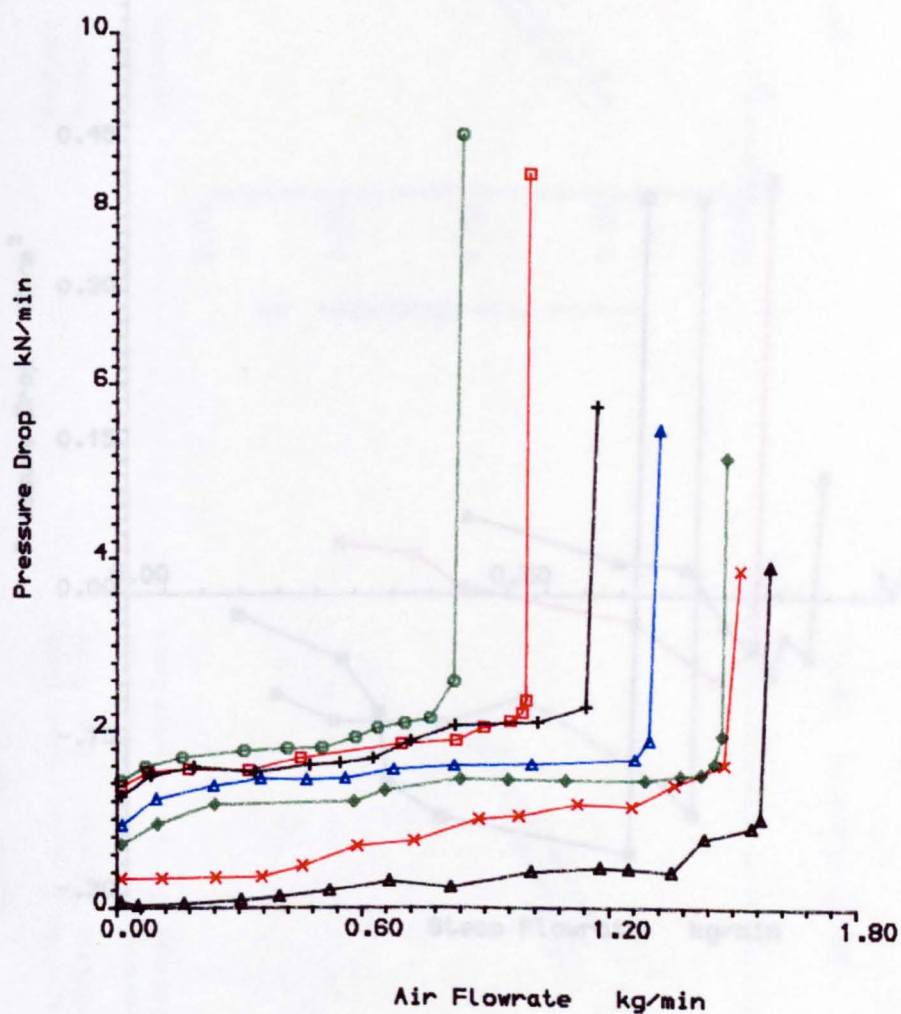


Figure 9.14 Pressure Drop Characteristics at Different Liquid Injection Rates

Steam-Water Tests

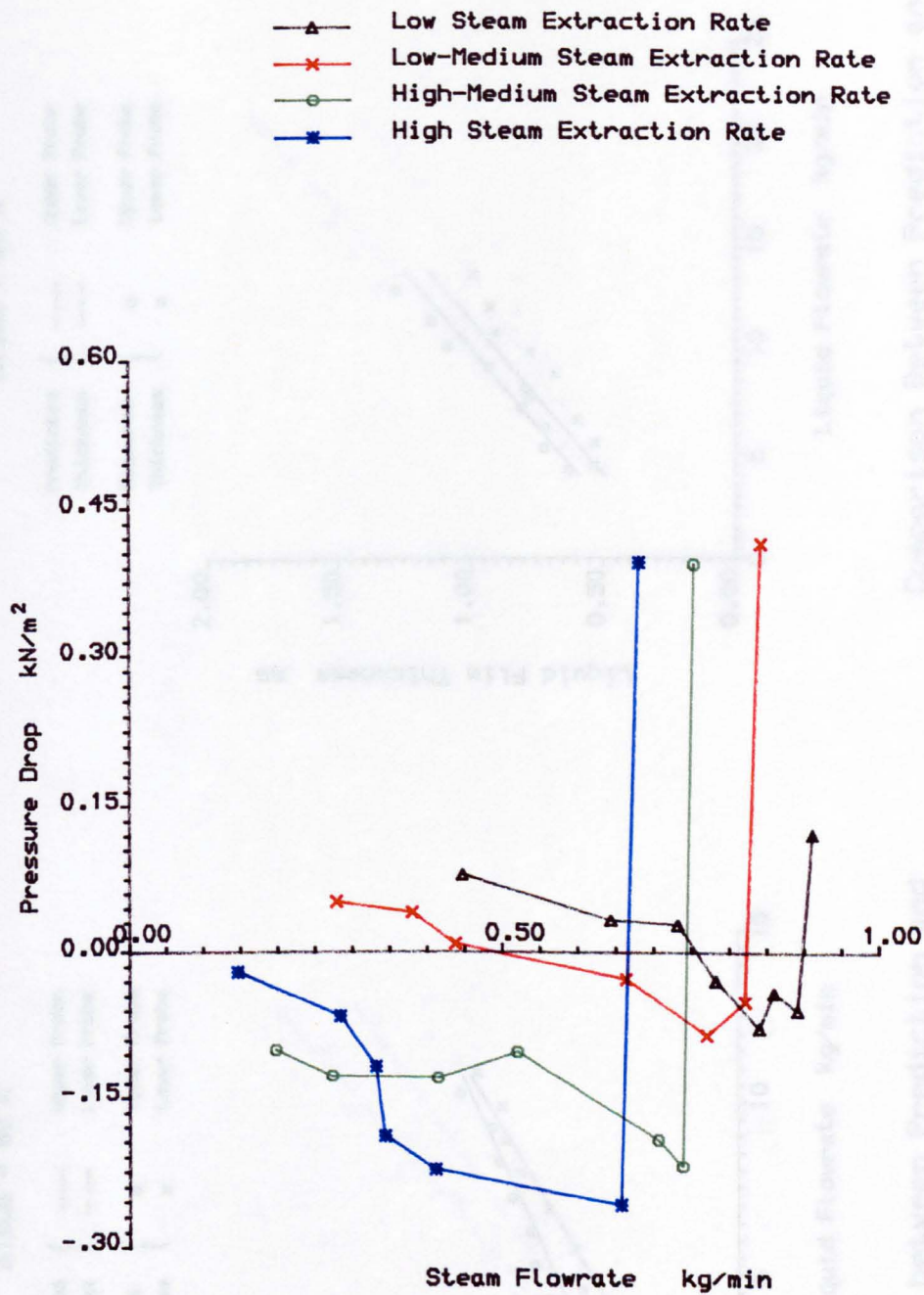
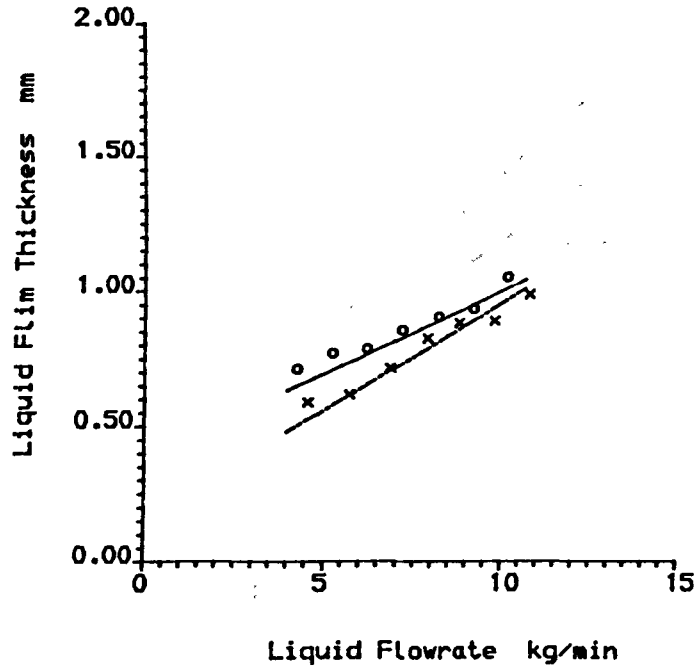


Figure 9.15 Effect of Steam Extraction Rates on Pressure Drop Characteristic. ($\Delta T_{sub} = 10$ k).

Steam-Water Tests

$\Delta T_{sub} = 80 \text{ K}$

Predicted Thickness	{	—	Upper Probe
		- - -	Lower Probe
Measured Thickness	{	o	Upper Probe
		x	Lower Probe

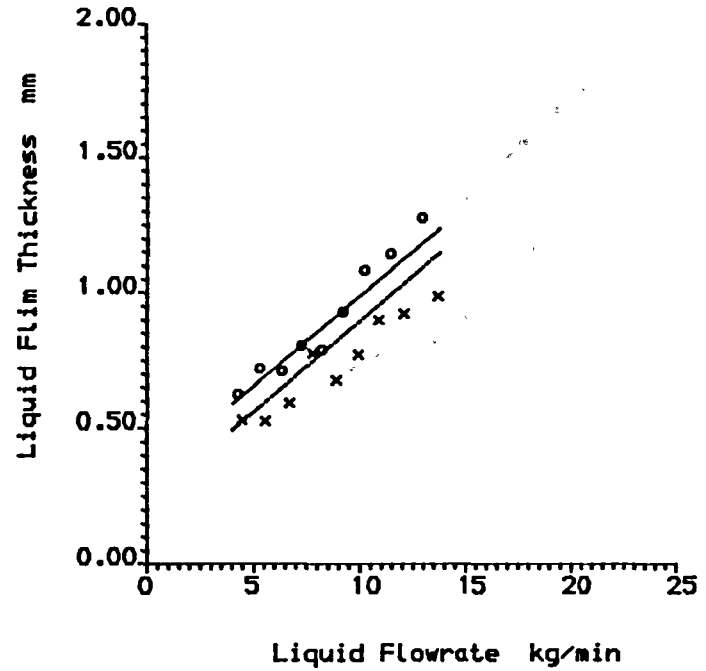


Comparison between Prediction and Measured Film Thickness at Flooding

Figure 9.16

$\Delta T_{sub} = 60 \text{ K}$

Predicted Thickness	{	—	Upper Probe
		- - -	Lower Probe
Measured Thickness	{	o	Upper Probe
		x	Lower Probe



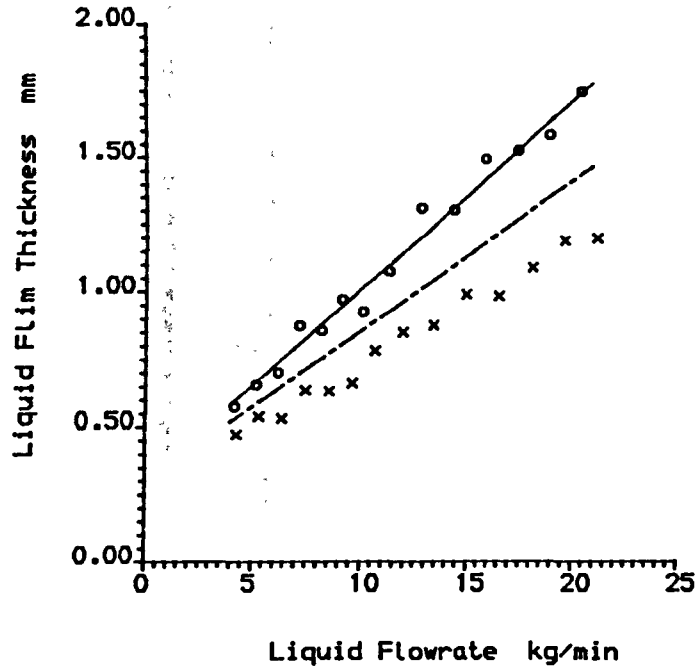
Comparison Between Prediction and Measured Film Thickness at Flooding

Figure 9.17

Steam-Water Tests

$\Delta T_{sub} = 40 \text{ K}$

Predicted Thickness	{	—	Upper Probe
		- - -	Lower Probe
Measured Thickness	{	o	Upper Probe
		x	Lower Probe

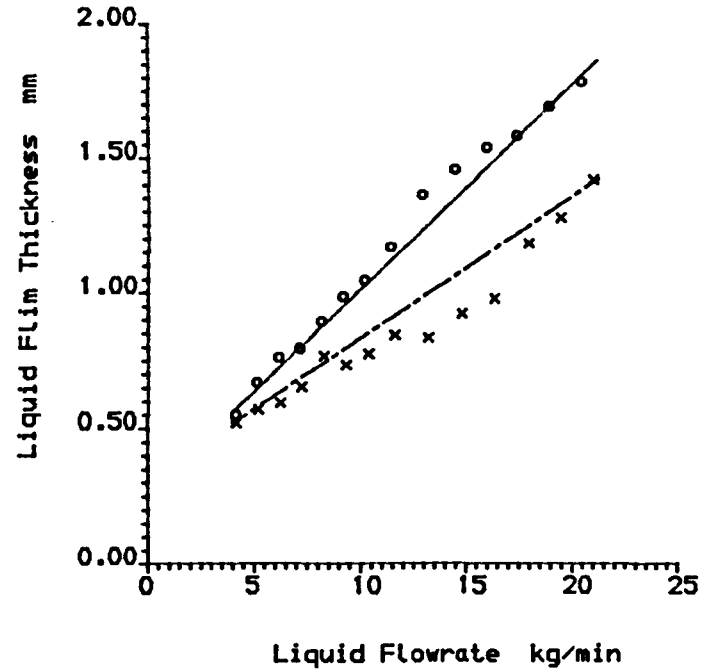


Comparison between Prediction and Measured Film Thickness at Flooding

Figure 9.18

$\Delta T_{sub} = 20 \text{ K}$

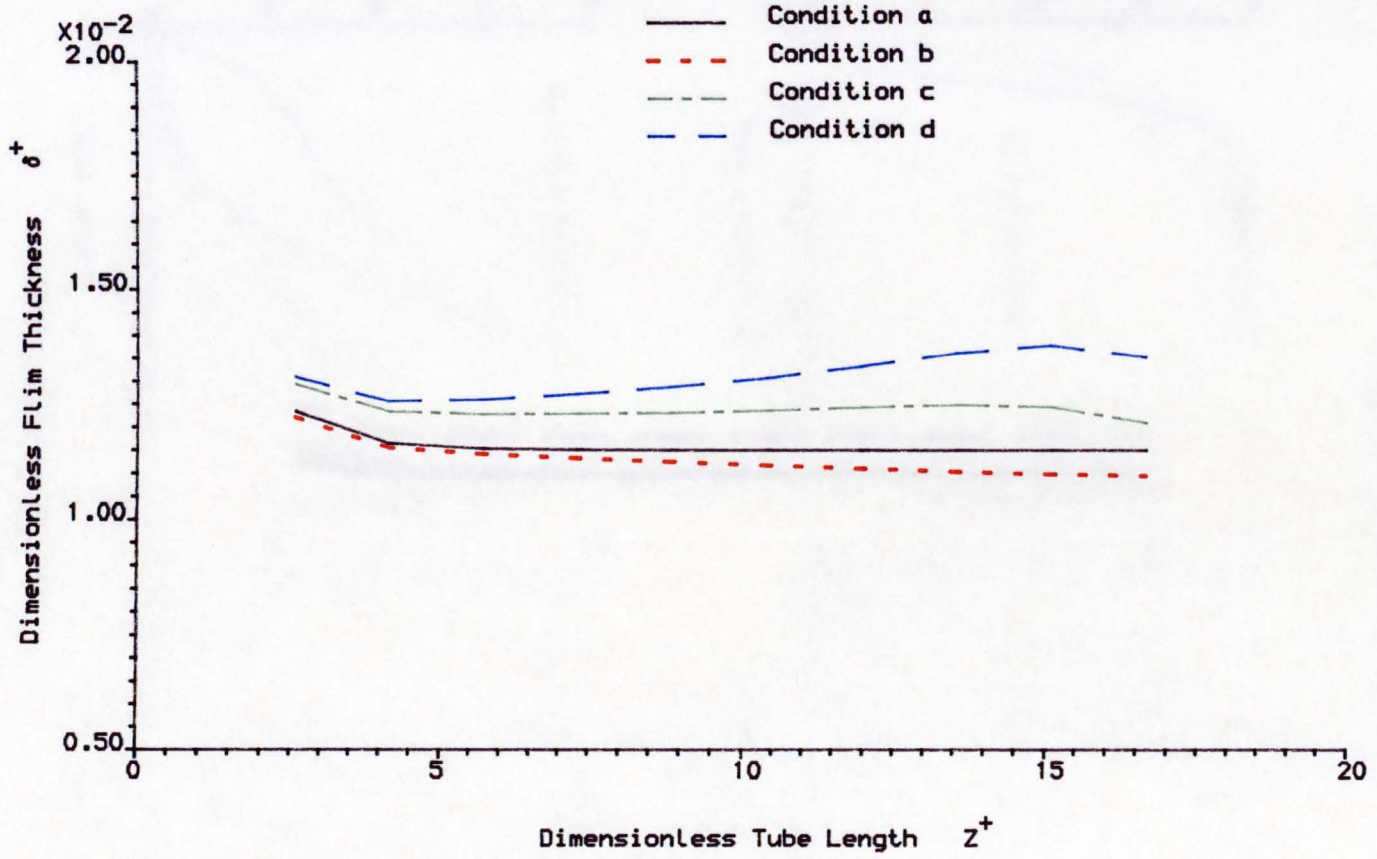
Predicted Thickness	{	—	Upper Probe
		- - -	Lower Probe
Measured Thickness	{	o	Upper Probe
		x	Lower Probe



Comparison Between Prediction and Measured Film Thickness at Flooding

Figure 9.19

Steam-Water Tests



Liquid Film Thickness Prediction at Different Conditions. ($\Delta T_{sub} = 80 \text{ K}$)

Figure 9.20

Steam-Water Tests

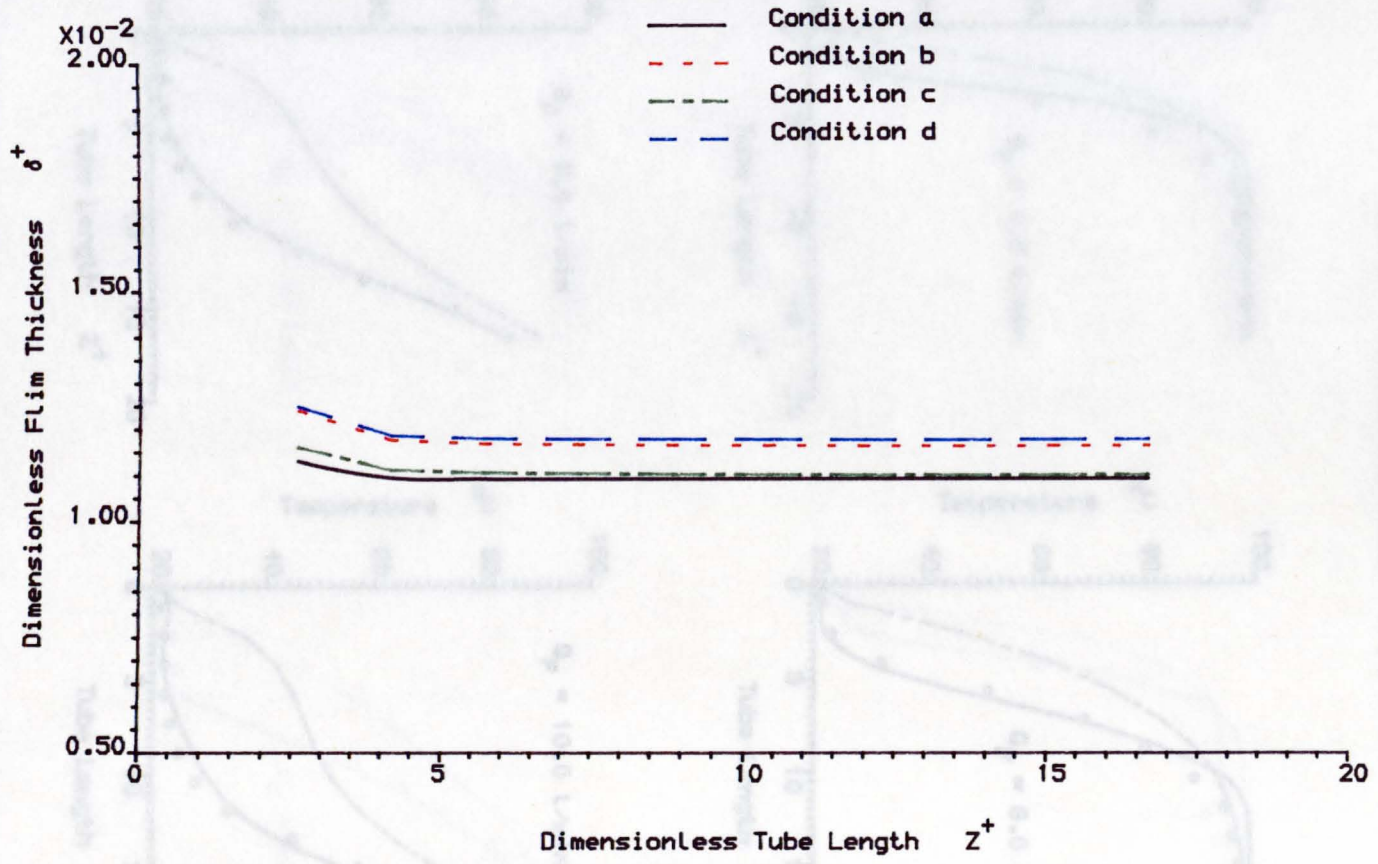
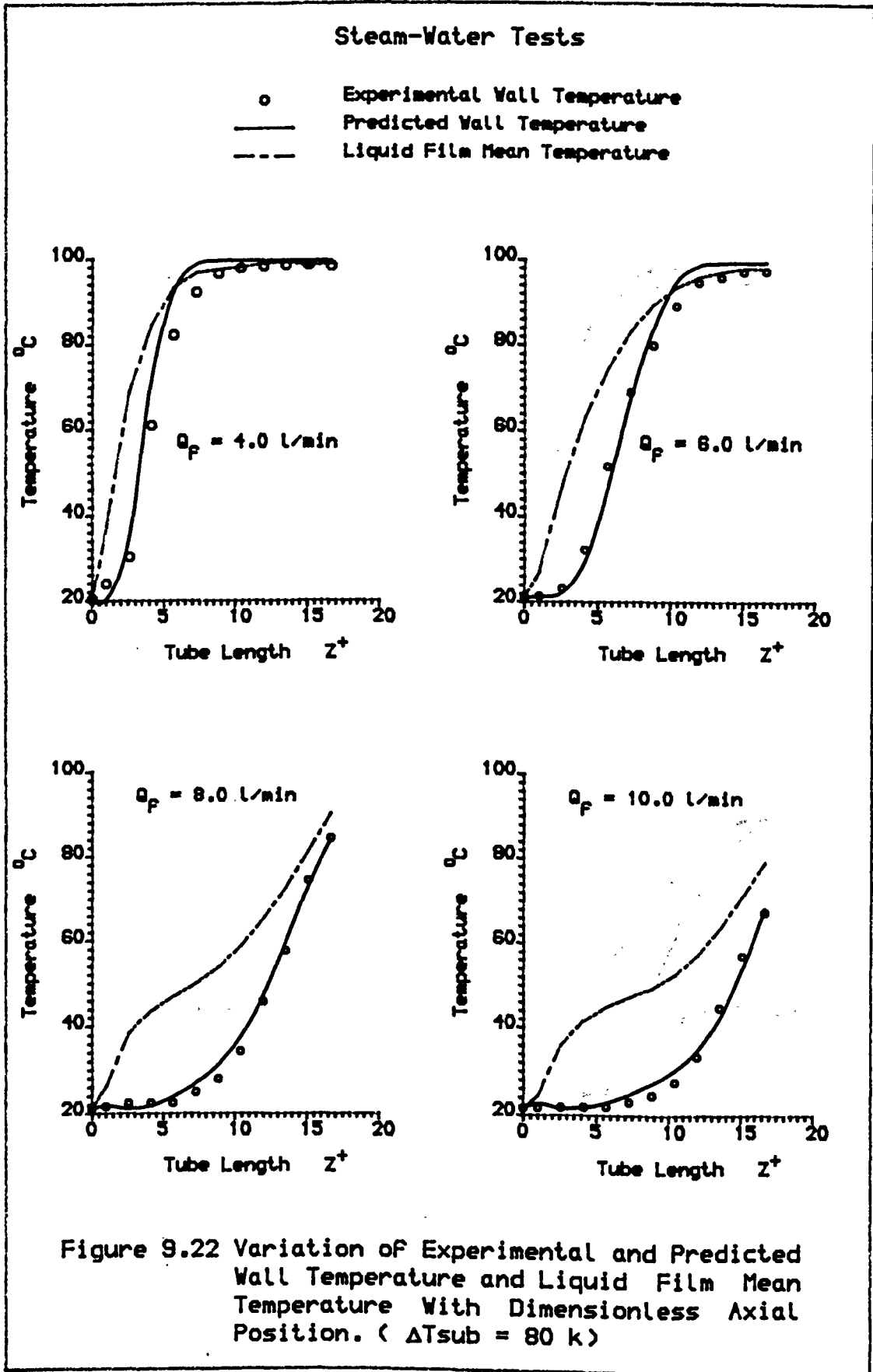


Figure 9.21 Prediction of Experimental and Predicted Wall Temperature and Liquid Film Mean Temperature With Dimensionless Axial Position, ($\Delta T_{sub} = 10 \text{ K}$)

Liquid Film Thickness Prediction at Different Conditions. ($\Delta T_{sub} = 10 \text{ K}$)

Figure 9.21



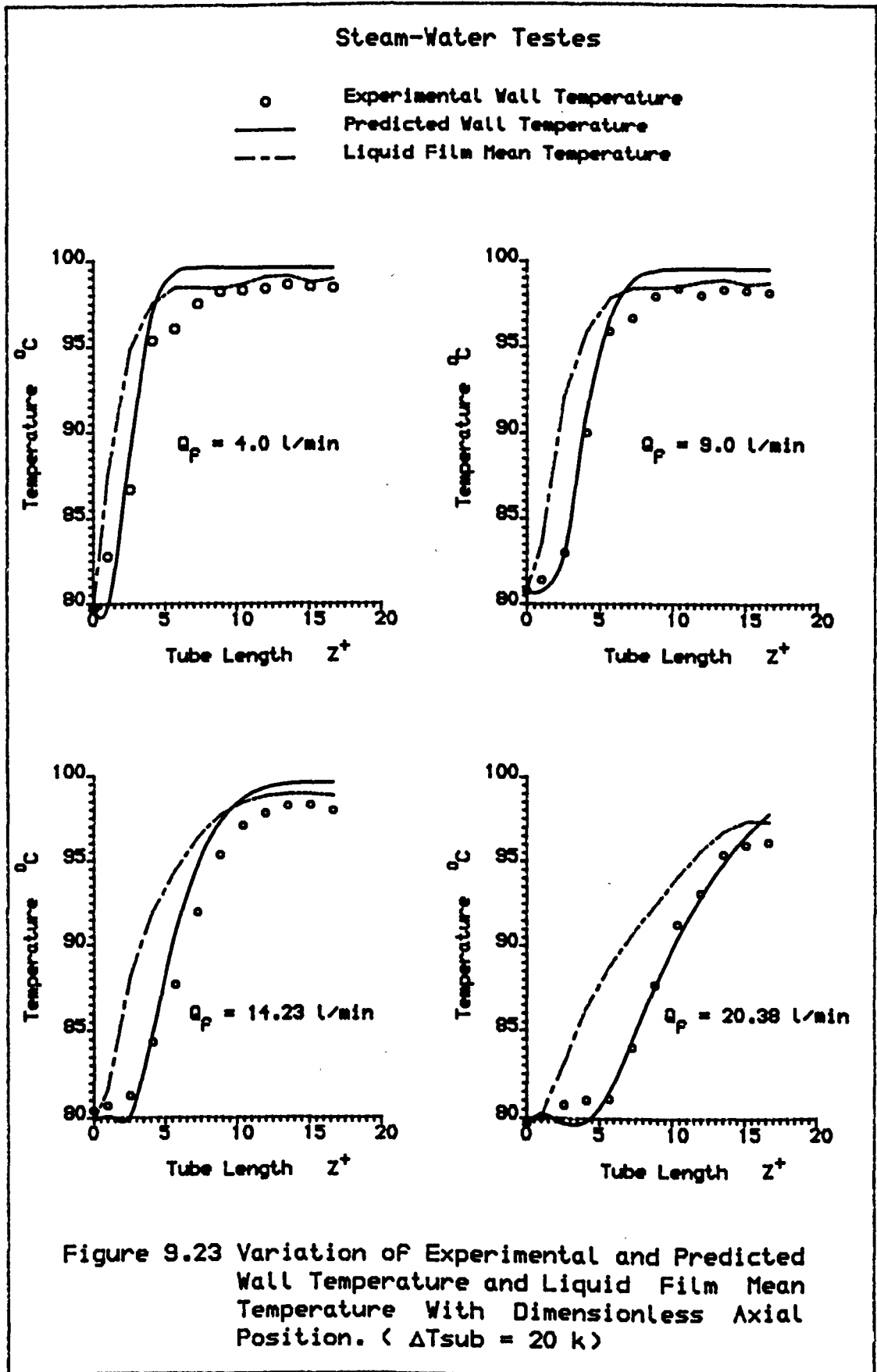


Figure 9.23 Variation of Experimental and Predicted Wall Temperature and Liquid Film Mean Temperature With Dimensionless Axial Position. ($\Delta T_{\text{sub}} = 20 \text{ K}$)

Steam-Water Tests

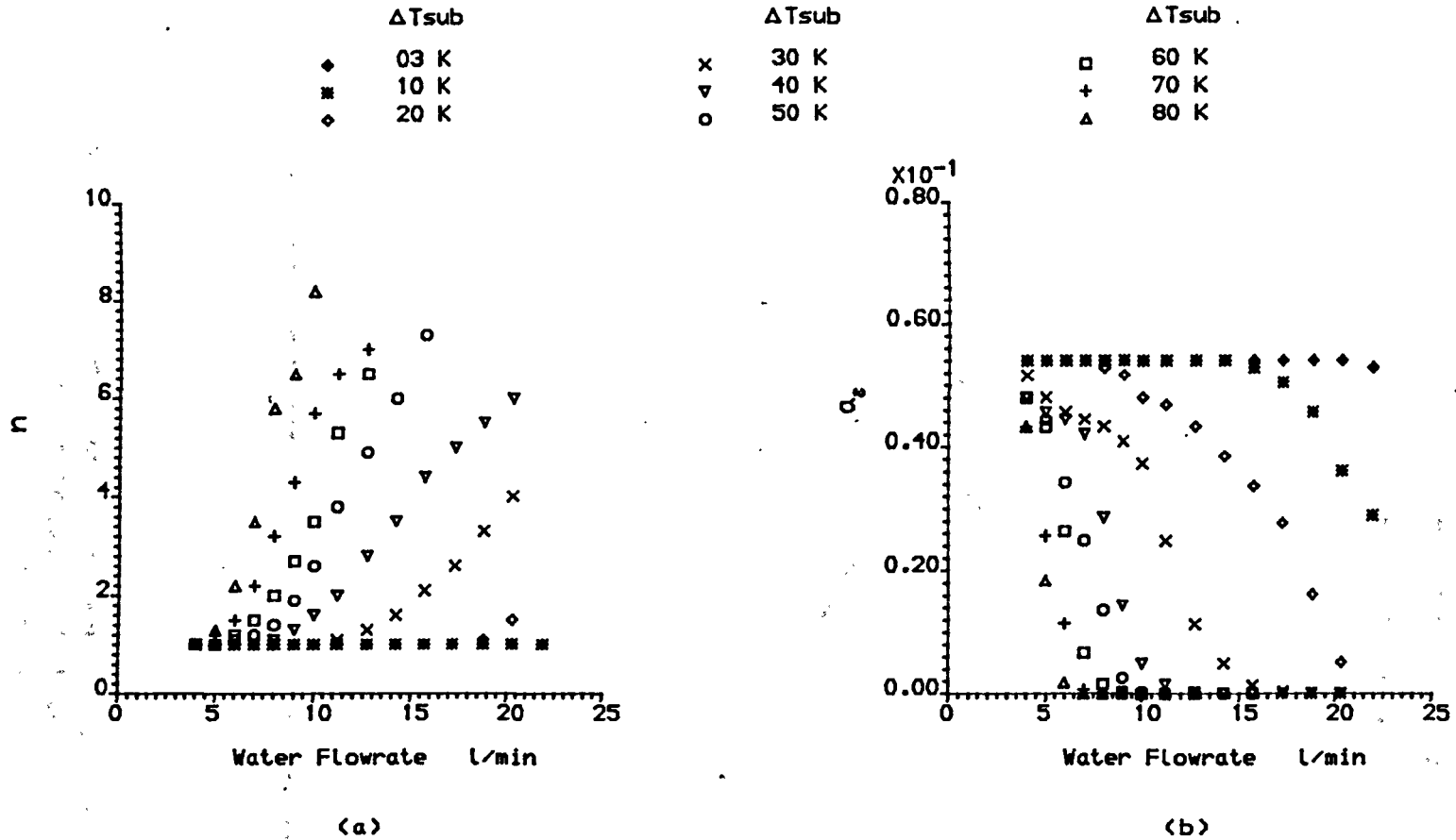


Figure 9.24 Variation of n and a_e in Equation (9.20) with Inlet Water Flowrate and Subcooling

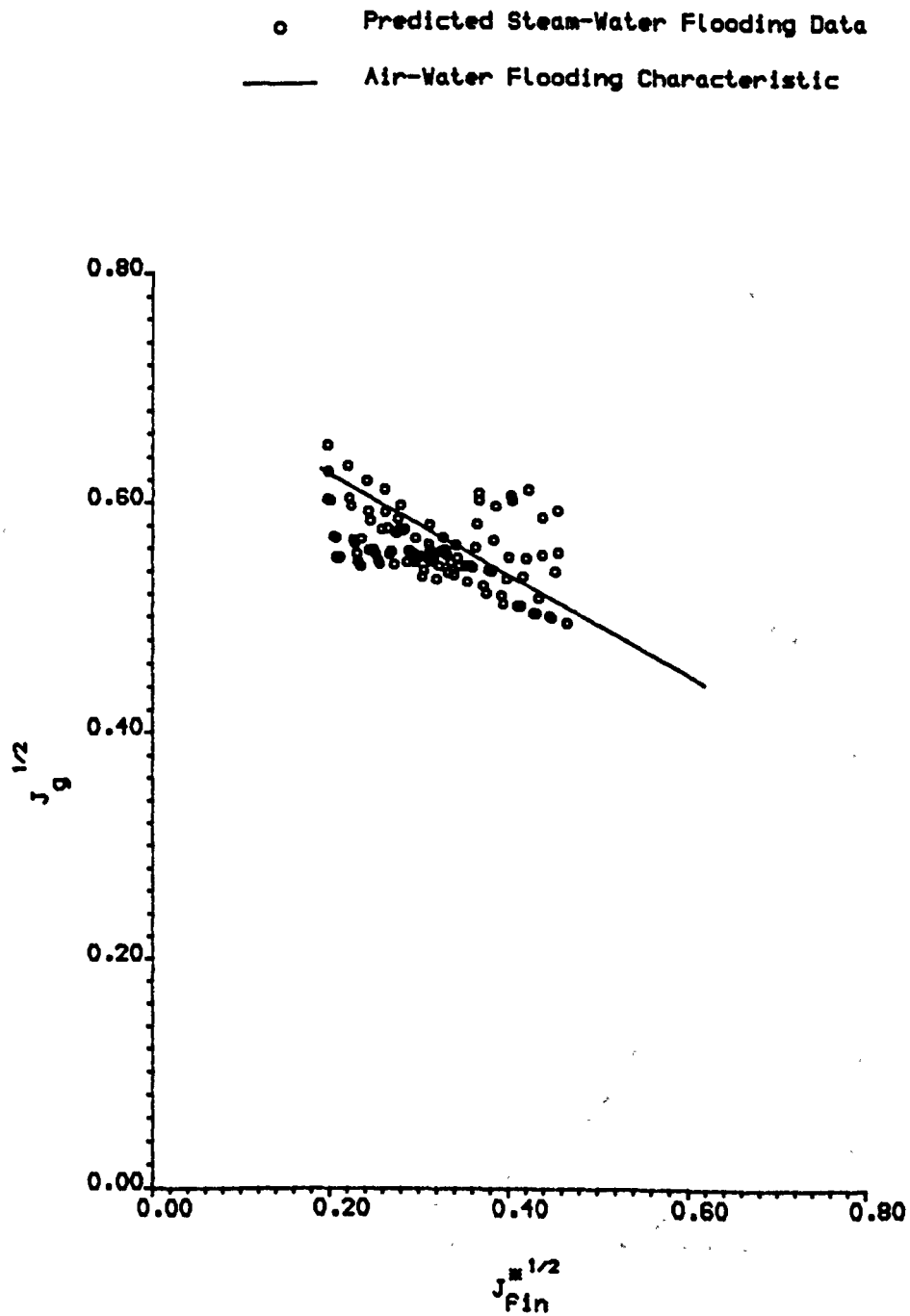
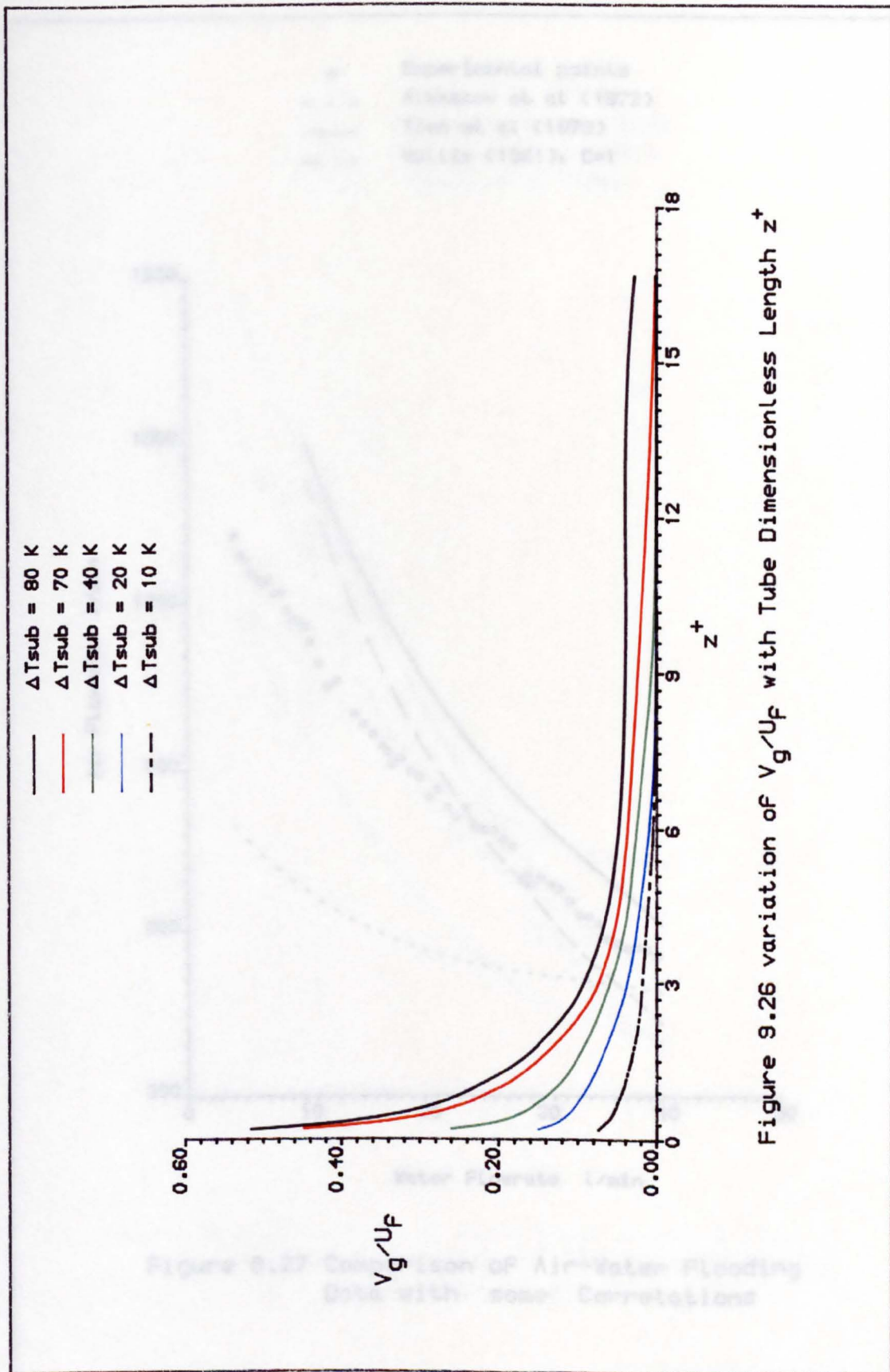


Figure 9.25 Comparison between Proposed Flooding Model with the Air-Water Flooding Characteristic



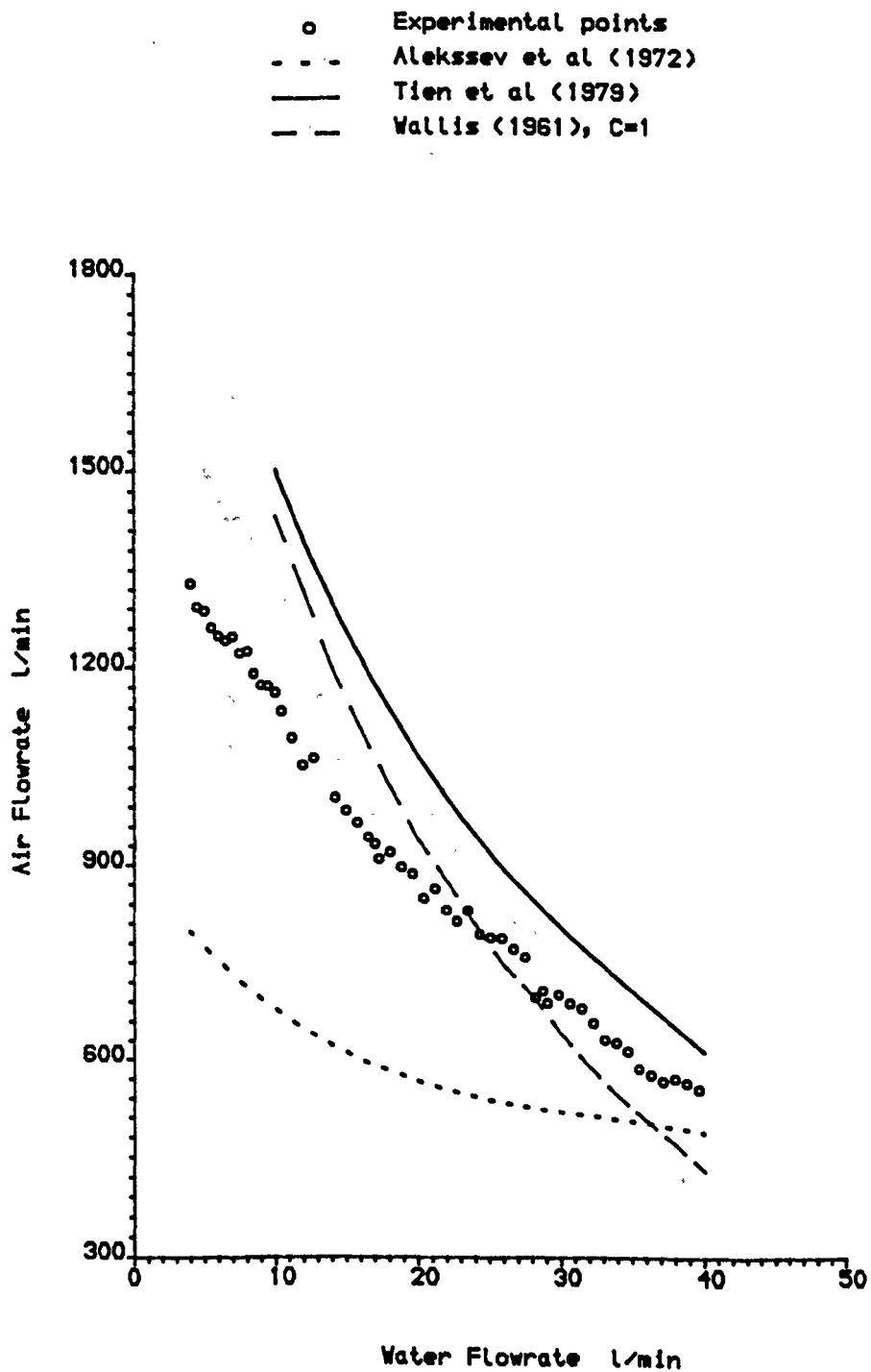


Figure 9.27 Comparison of Air-Water Flooding Data with some Correlations

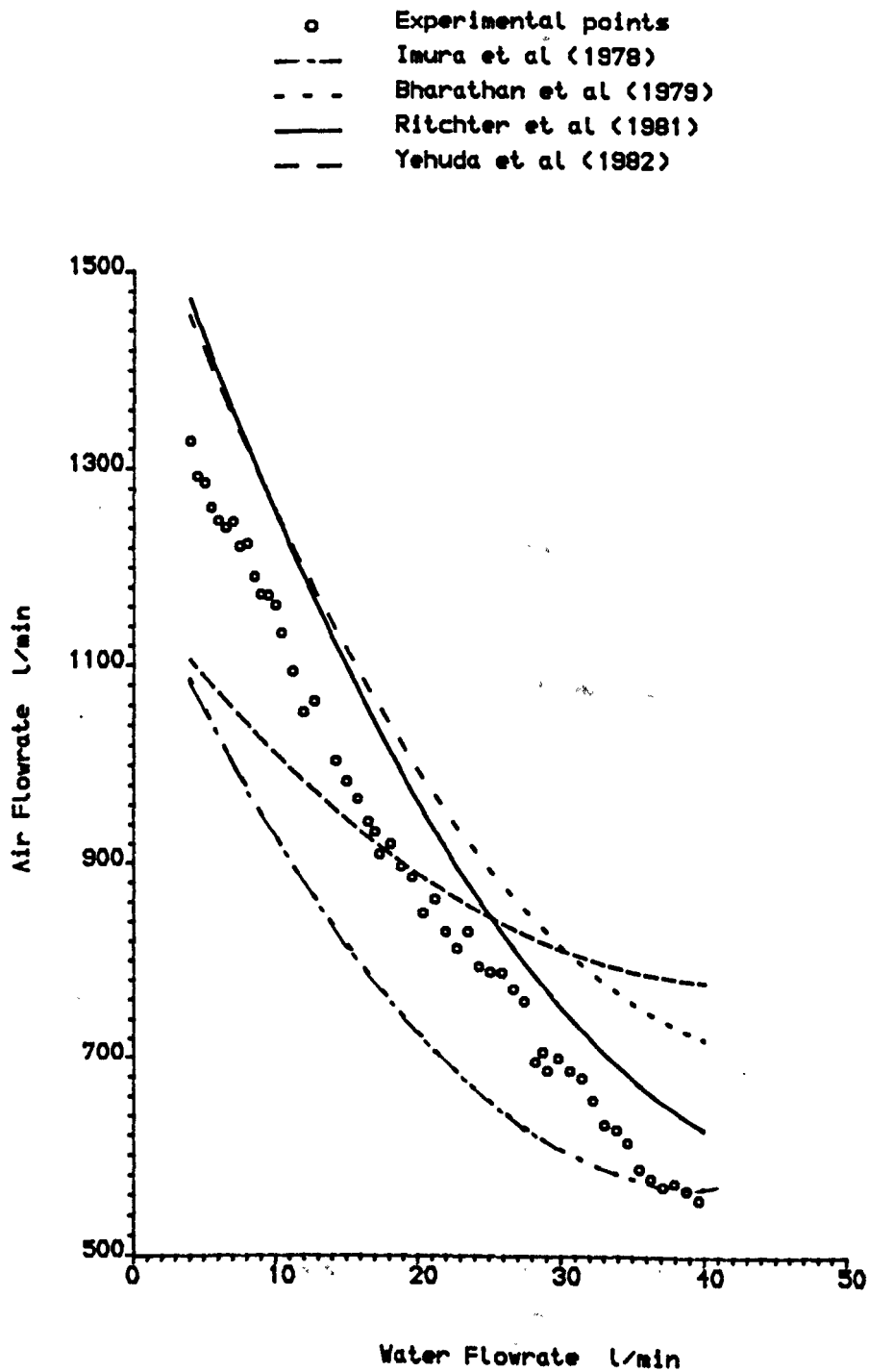


Figure 9.28 Comparison of Air-Water Flooding Data with some Models

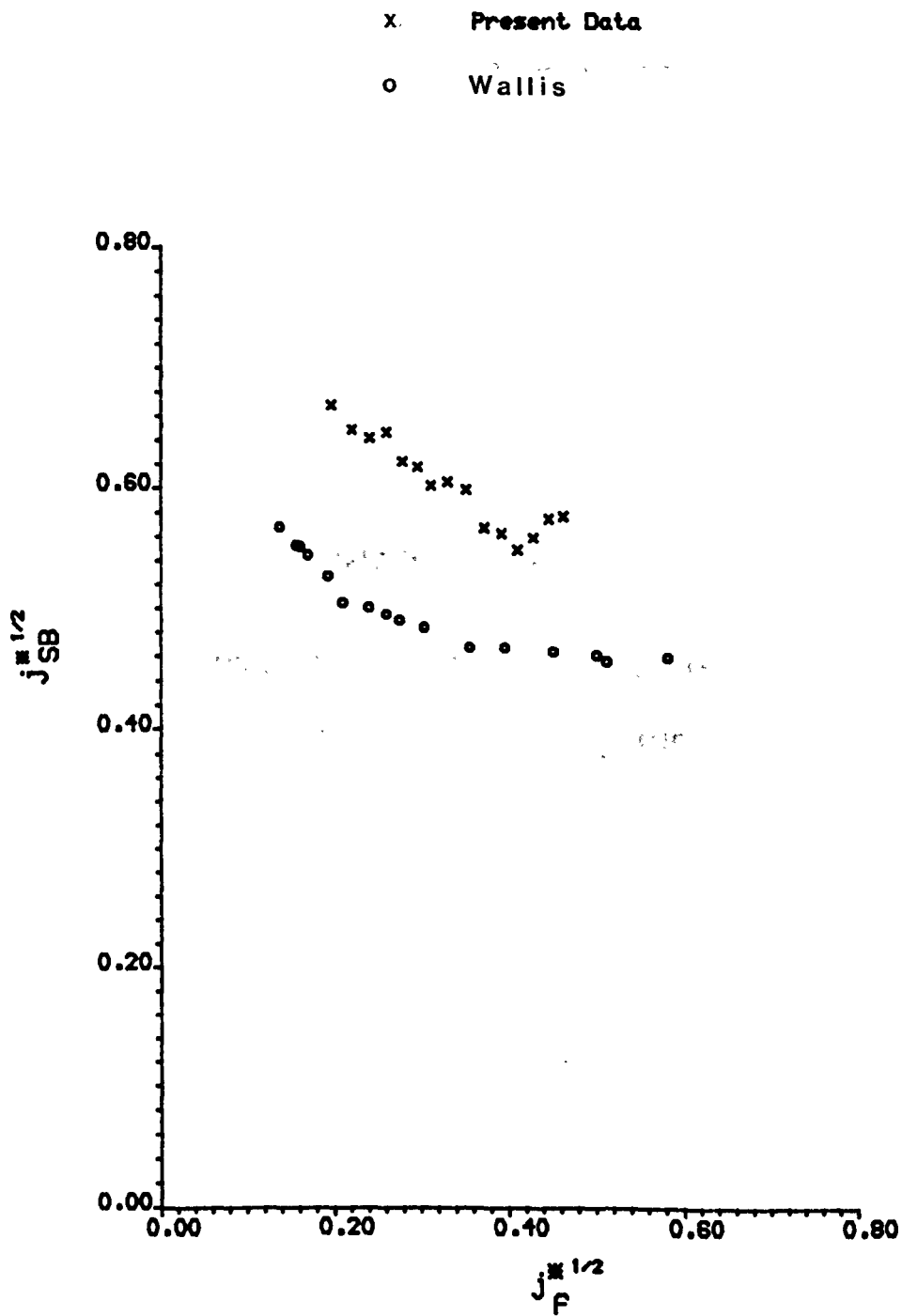


Figure 9.29 Comparison of Steam-Water Flooding Data with that of Bharathan et al (1980). (50.0 mm. Tube with Square Ends).

CHAPTER 10

NON-EQUILIBRIUM EFFECTS

AND EMPIRICAL ANALYSIS

CHAPTER 10NON-EQUILIBRIUM EFFECTS AND EMPIRICAL ANALYSIS

The difference between gas-liquid and vapour-liquid counter-current interactions can often be attributed to heat and mass transfer (or condensation) effects which can be significant (and even overwhelming), depending on the temperature difference between the vapour (steam) and the liquid (water). Thus, in order to correlate the flooding conditions for steam-water, the condensation effects must be separated and allowed for.

It has been reported by many investigators of tests on other geometries, for example TIEN (1977) and MEGAHERD (1981), that air-water and steam-subcooled water flooding data lie on the same curve if the amount of condensed steam is allowed for. A comparison between the air-water and the steam-water flooding data (with condensed steam allowed for) clearly shows that this is not the case here, Figure 10.1.

Visual observation proved that flooding took place at the bottom of the test tube, therefore any comparison between air-water and steam-water flooding data should always be made on the basis of total steam flowrate (at the bottom of the tube). Such a comparison is shown in Figure 10.2 and indicates, as most investigators agree,

including TIEN (1977) and MEGAHED (1981), that for the same inlet water flowrate, more steam flow is required for the onset of flooding in steam-subcooled water conditions than the air required in the corresponding air-water situation. Also the steam flowrate increases as the inlet water subcooling is increased. This may appear contradictory to a simple understanding that higher subcoolings will produce more condensation leading to a thicker liquid film and so requiring less steam flow for flooding. However, the steam condensation will produce a rougher steam-water interface and thus less steam may be required to initiate flooding compared with air over a smooth film, for a constant water injection rate. A possible further explanation for this behaviour (in addition to the postulation described in Section 9.8) is that, although the steam flowrate is higher at the bottom of the test tube than that of air flow, the steam flowrate at the top of the test tube (allowing for condensation) is less than that of air, dependent on the inlet subcooling.

The wave formation, which is responsible for the onset of flooding, is initiated at the top of the test tube and grows as it moves downwards, its growth being affected by the air or steam flowrate existing along the whole length of the test tube. Therefore, for the same flowrate of air and steam at the bottom of the tube the wave growth is higher in the liquid-air situation than in the subcooled liquid-steam case, since the condensation

decreases the steam flowrate. This may also explain why a greater steam flow is required to cause flooding when the inlet water subcooling is increased, as the higher the inlet water subcooling the greater the condensation and so the opportunity for wave growth is reduced.

The subcooling effect obtained from the experimental results supports strongly the explanation that the wave growth is affected by the gas flowrate along the whole length of the test tube and also suggests that this effect is greater than the shear momentum effects.

As mentioned above, the difference between steam-water and air-water results is considered to be isolated and represented by an equilibrium factor k , such that

$$k = j_{SB}^* - j_a^* \quad (10.1)$$

There is some scatter in the experimental data, as might be expected in this type of experiment. Hence, a line was drawn for each subcooling to represent the experimental data reasonably well and specimens can be seen in Figures 10.3 and 10.4 for two different subcoolings.

The amount of condensation at thermal equilibrium conditions was determined from the energy (heat) transfer

necessary to raise the liquid temperature to that of the steam i.e.

$$M_{SC} = \frac{M_f C_{pf} \Delta T_{sub}}{h_{fg}} = M_f Ja \quad (10.2)$$

$$Ja = \text{Jakob Number} = \frac{C_{pf} \Delta T_{sub}}{h_{fg}} \quad (10.3)$$

A plot of k versus $j_{fin} * Ja(\rho_f/\rho_s)^{1/2}$ gives an indication of the non-equilibrium effect represented by the factor k for all data, Figure 10.5. As can be seen, k is very small at low inlet water flowrates and subcoolings indicating a small non-equilibrium effect. Although in about 80% of the flooding data, the inlet water flowrates almost reach the saturation temperature at the bottom of the test tube (the extractor), the non-equilibrium effect is regarded to exist in the liquid film, along the whole test tube such that $k > 0$ and increases as the inlet water flowrates and subcoolings increase. In other words, the non-equilibrium effect does not depend on whether the inlet water flowrate reaches the saturation temperature at the bottom of the tube or not. It depends on non-equilibrium existing along the whole tube. At low inlet water flowrates, the inlet water temperature reaches the saturation temperature at a relatively short distance from the tube entrance, (depending on the inlet water subcooling) and therefore would be very small. For higher inlet water flowrates the inlet water temperature takes longer to

reach the saturation temperature (again depending on inlet subcooling), and the non-equilibrium effect would be greater and consequently k values higher, despite the fact that the liquid film reaches saturation at the bottom of the tube under both conditions.

However, the non-equilibrium data which incorporate a wide range of experimental conditions are represented by a single correlation in terms of an equilibrium factor, of the form:

$$k = \{0.19 - 0.66 [j_{fin}^* Ja(\rho_f/\rho_s)^{1/2}]^{1/2}\}^{2.0} + 0.0037 (Ja)^{-1.86} [j_{fin}^* Ja \frac{\rho_f}{\rho_s}]^{2.16} \quad (10.4)$$

Equation (10.4) is an empirical correlation characterising the effect of condensation on flooding and suggests that k is mainly a function of inlet water flowrate and subcooling. It was established on the basis of j_{fin}^* to allow for fluid physical properties and geometry effects.

To check the non-equilibrium correlation, values of k were computed from equation (10.4) and compared with experimental data (i.e. k values from reduced experimental data), Figure 10.6. To incorporate the effect of steam condensation and non-equilibrium effects, the effective steam flowrate, j_{seff}^* , was obtained by subtracting the condensation effect from the total steam flowrate entering the test tube. That is

$$j_{\text{seff}}^* = j_{\text{SB}}^* - k \quad (10.5)$$

Substituting j_{seff}^* for j_s^* in the Wallis correlation, gave the modified flooding equation

$$(j_{\text{SB}}^* - k)^{1/2} + j_f^{*1/2} = C \quad (10.6)$$

A better check on the non-equilibrium correlation (10.4) was made when the modified flooding correlation, which includes non-equilibrium effects, was plotted against the air-water flooding correlation, which represents the limiting case of $\Delta T_{\text{sub}} = 0$, Figure 10.7. As can be seen from this plot, the steam-water data allowing for non-equilibrium effects, for all subcoolings, have collapsed very successfully on to the air-water flooding line. Although the non-equilibrium expression incorporates the condensation effect and correlates the present experimental data very well, it has some limitation since it does not represent $\Delta T_{\text{sub}} = 0$ conditions as well as higher subcoolings. The non-equilibrium correlation was derived from a range of experimental data. Extrapolation of the correlation equation curves produced minimum turning points with particular minimum values of k at particular values of ΔT_{sub} and j_{fin}^* . Beyond these points, the correlation gave k values which increased as $j_{\text{fin}}^* \text{Ja}(\rho_f/\rho_s)^{1/2}$ tended to zero, with a k intercept value of 0.0361. This is physically unreal as k should be zero at $j_{\text{fin}}^* \text{Ja}(\frac{\rho_f}{\rho_s})^{1/2} = 0$.

The turning points for all 9 subcoolings involved in the test are tabulated in Table 10.1, in terms of k , $j_{fin}^* Ja(\rho_f/\rho_s)^{1/2}$ and j_{fin}^* , and are plotted in Figures 10.8 and 10.9 for two different subcoolings. The part of the non-equilibrium correlation with values of

$j_{fin}^* Ja(\rho_f/\rho_s)^{1/2}$ below the turning points can best be represented by straight lines through the origin, tangential to the correlation curves.

Assuming that

$$x = j_{fin}^* Ja(\rho_f/\rho_s)^{1/2} \quad (10.7)$$

The k values represented by the correlation curves, up to the turning points are functions of x (for a particular subcooling) i.e.

$$k = f(x) \quad (10.8)$$

The straight lines, which predict k values for x values between zero and the tangential points, can be represented (again for particular subcooling) by

$$k_1 = mx \quad (10.9)$$

where m is the gradient of the line.

At the common point, $k = k_1$

$$f(x) = mx \quad (10.10)$$

and

$$m = \frac{d}{dx}(f(x)) \quad (10.11)$$

where

$$\frac{d}{dx}(f(x)) = \frac{dk}{dx} = 0.1254 x^{-0.5} + 0.4356 + 756(\Delta T_{\text{sub}})^{-1.86} x^{1.16} \quad (10.12)$$

Hence, by an iterative procedure, the common points for each ΔT_{sub} curve were determined. These common points for all 9 subcoolings involved in the tests are tabulated in Table 10.2, in terms of k , x and j_{fin}^* . The tangential lines to the correlation curves at these points are shown in Figures 10.8 and 10.9 for two different subcoolings. Figures 10.10 and 10.11 show a combination of the straight lines which are valid up to the tangency points together with the curves from the correlation equation (10.4) which is valid from the common point onwards. In order to determine precisely these common points a correlation was obtained between j_{fin}^* and Ja of the form

$$j_{\text{fin}}^* = 2.0077 \times 10^{-2} + 3.05 \times 10^{-3} \ln(Ja) \quad (10.13)$$

This relationship is plotted in Figure 10.12.

Summary

The non-equilibrium effect is isolated and represented by the equilibrium factor k , correlation (10.4), which incorporates the condensation effect. This correlation has some limitation since its characteristic produced minimum turning points with k values increasing instead of $\rightarrow 0$ as $\Delta T_{\text{sub}} \rightarrow 0$. Beyond these points the correlation was found physically invalid, and therefore replaced by tangential lines from $k = 0$, $x = 0$ to the correlation curves. The common points between the correlation curves and tangential lines are determined and correlated in equation (10.13) as a function of j_{fin}^* and Ja .

ΔT_{sub}	k	j_{fin}^*	$J_a(\rho_f/\rho_s)^{1/2}$	j_{fin}^*
80K	0.00052		0.07810	0.0131
70K	0.00065		0.07677	0.0147
60K	0.00084		0.07521	0.0168
50K	0.00113		0.07272	0.0196
40K	0.00165		0.06910	0.0233
30K	0.00242		0.06327	0.0285
20K	0.00438		0.05327	0.0362
10K	0.00822		0.03493	0.0485
3K	0.01717		0.01303	0.0667

Table 10.1 Turning Points for Equation (10.4)

ΔT_{sub}	k	j_{fin}^*	$J_a(\rho_f/\rho_s)^{1/2}$	j_{fin}^*	J_a
80K	0.00053		0.08017	0.0135	0.1462
70K	0.00066		0.07946	0.0133	0.1282
60K	0.00086		0.07848	0.0132	0.1107
50K	0.00116		0.07704	0.0129	0.0921
40K	0.00167		0.07472	0.0125	0.0721
30K	0.00256		0.07081	0.0119	0.0552
20K	0.00445		0.06345	0.0107	0.0365
10K	0.00968		0.04852	0.0081	0.0178
3K	0.02236		0.02361	0.0041	0.0067

Table 10.2 Minimum Condition for Equation (10.4)

Steam-Water Data Based on Steam Flowrate
at the Top of the Test Tube

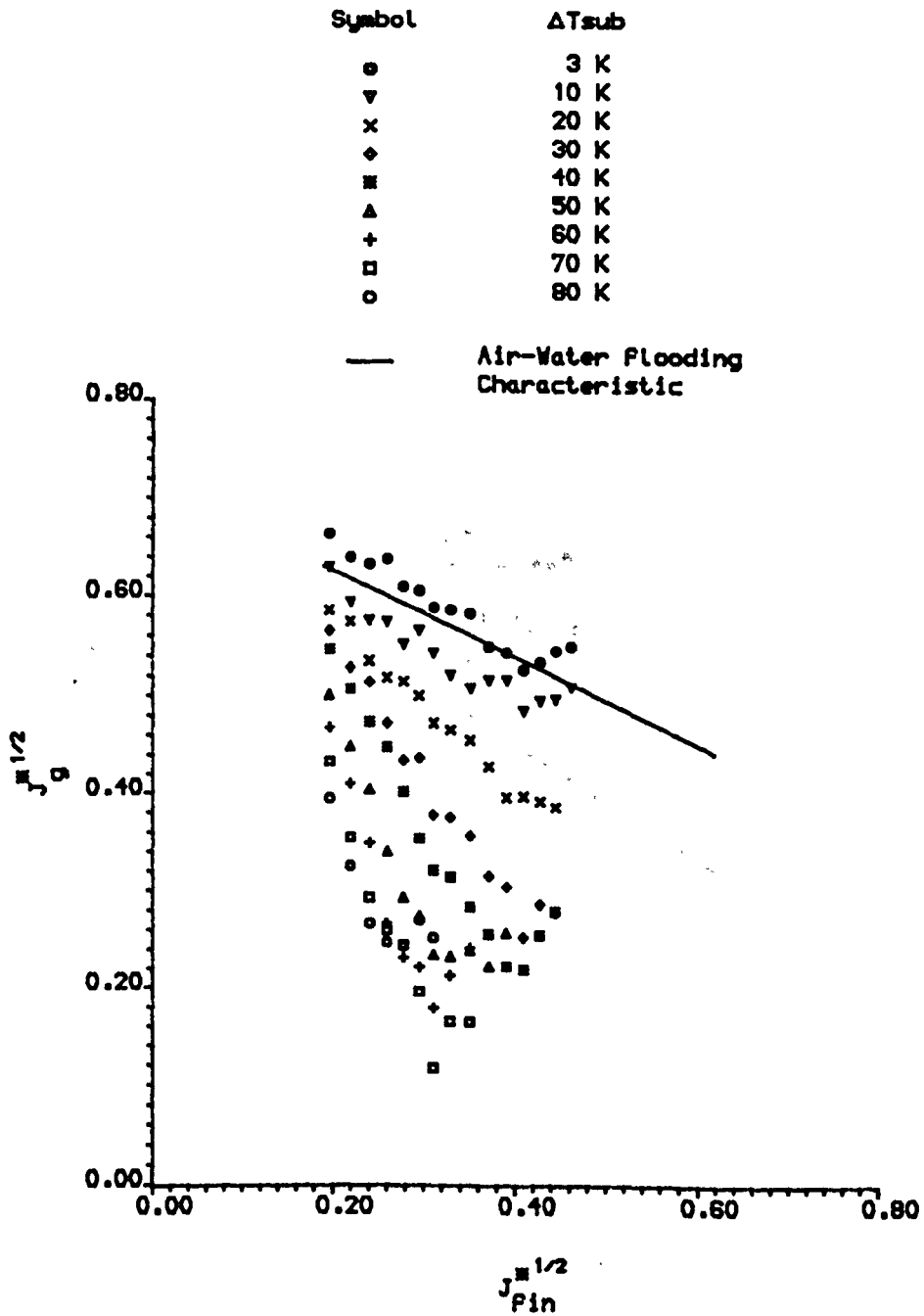


Figure 10.1 Comparison between Air-Water
and Steam-Water Flooding Data

Steam-Water data based on steam Flowrate
at the bottom of the test tube

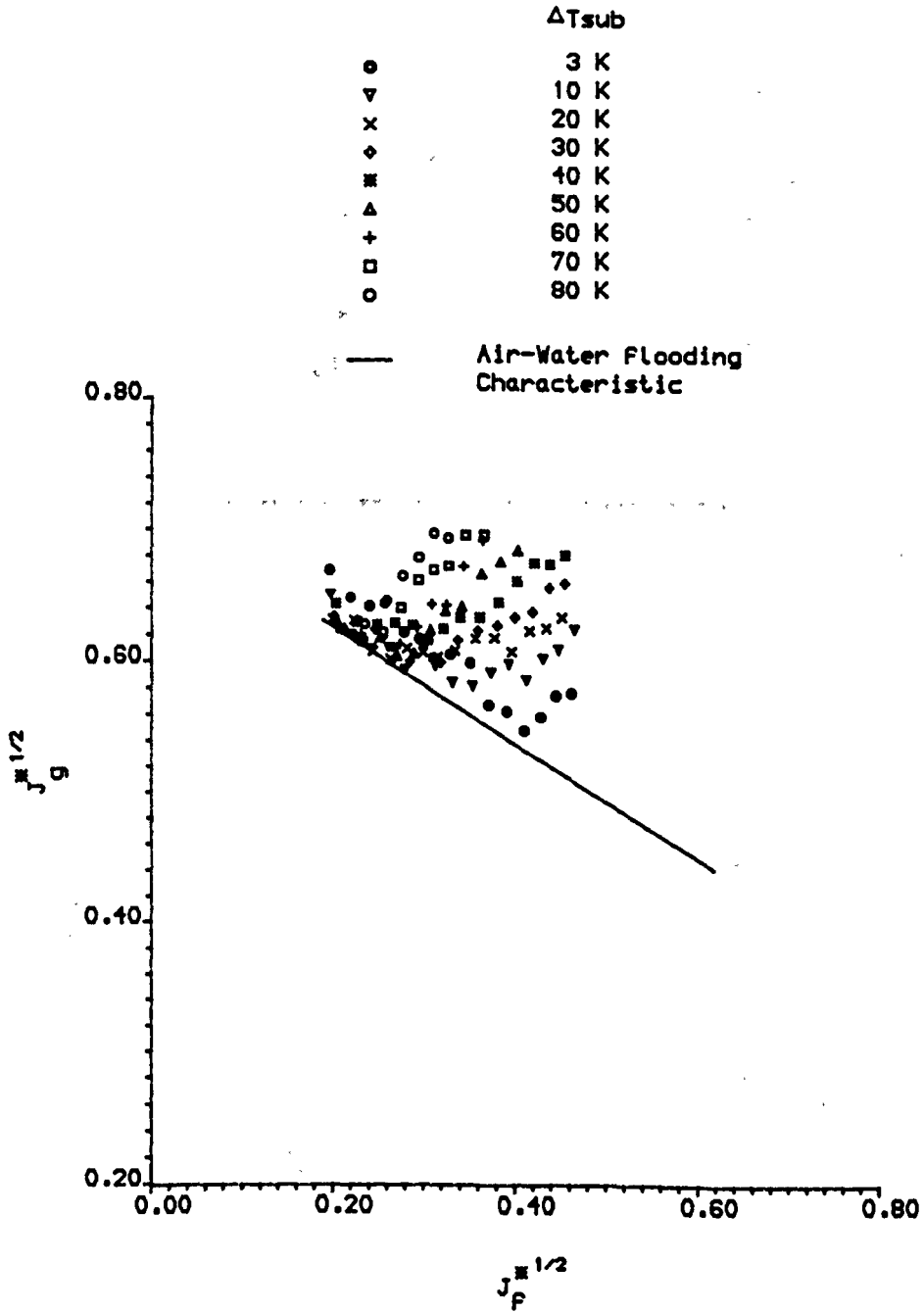
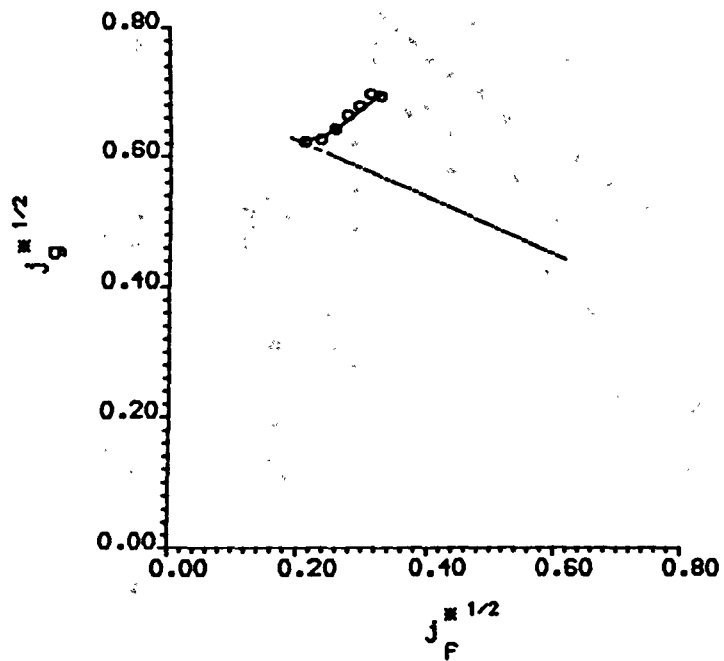


Figure 10.2 Comparison between Air-Water
and Steam-Water Flooding Data

$\Delta T_{sub} = 80 \text{ K}$

- Steam-Water Flooding Data
- Steam-Water Flooding Characteristic
- - - Air-Water Flooding Characteristic

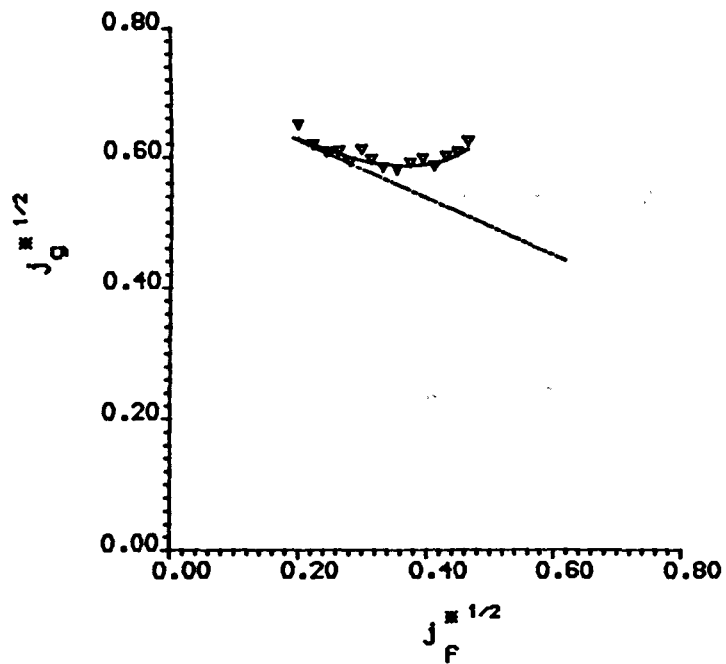


Steam-Water Flooding characteristic

Figure 10.3

$\Delta T_{sub} = 10 \text{ K}$

- ▽ Steam-Water Flooding Data
- Steam-Water Flooding characteristic
- - - Air-Water Flooding characteristic



Steam-Water Flooding characteristic

Figure 10.4

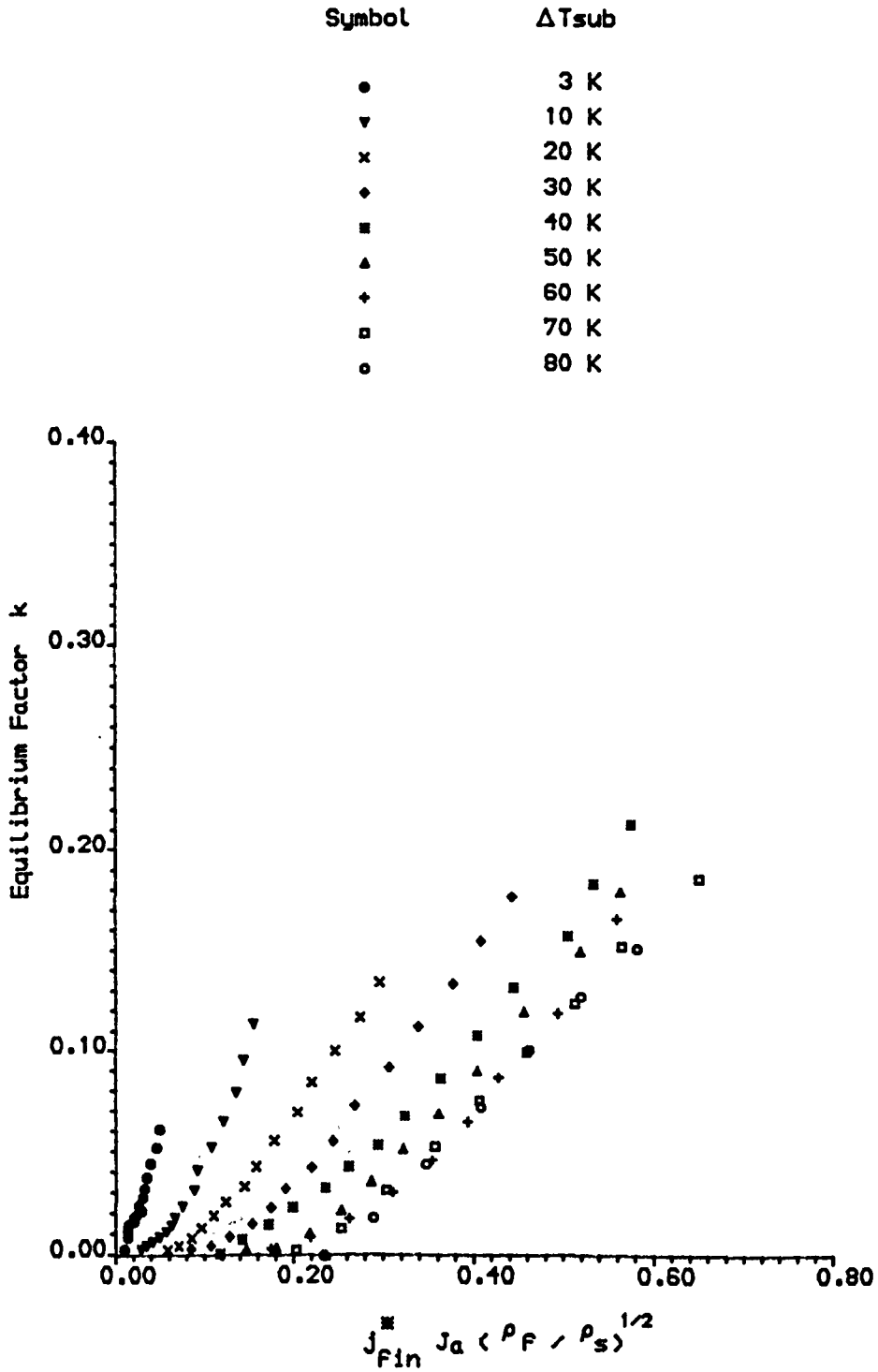


Figure 10.5: Non-Equilibrium Steam-Water Data For all Subcoolings

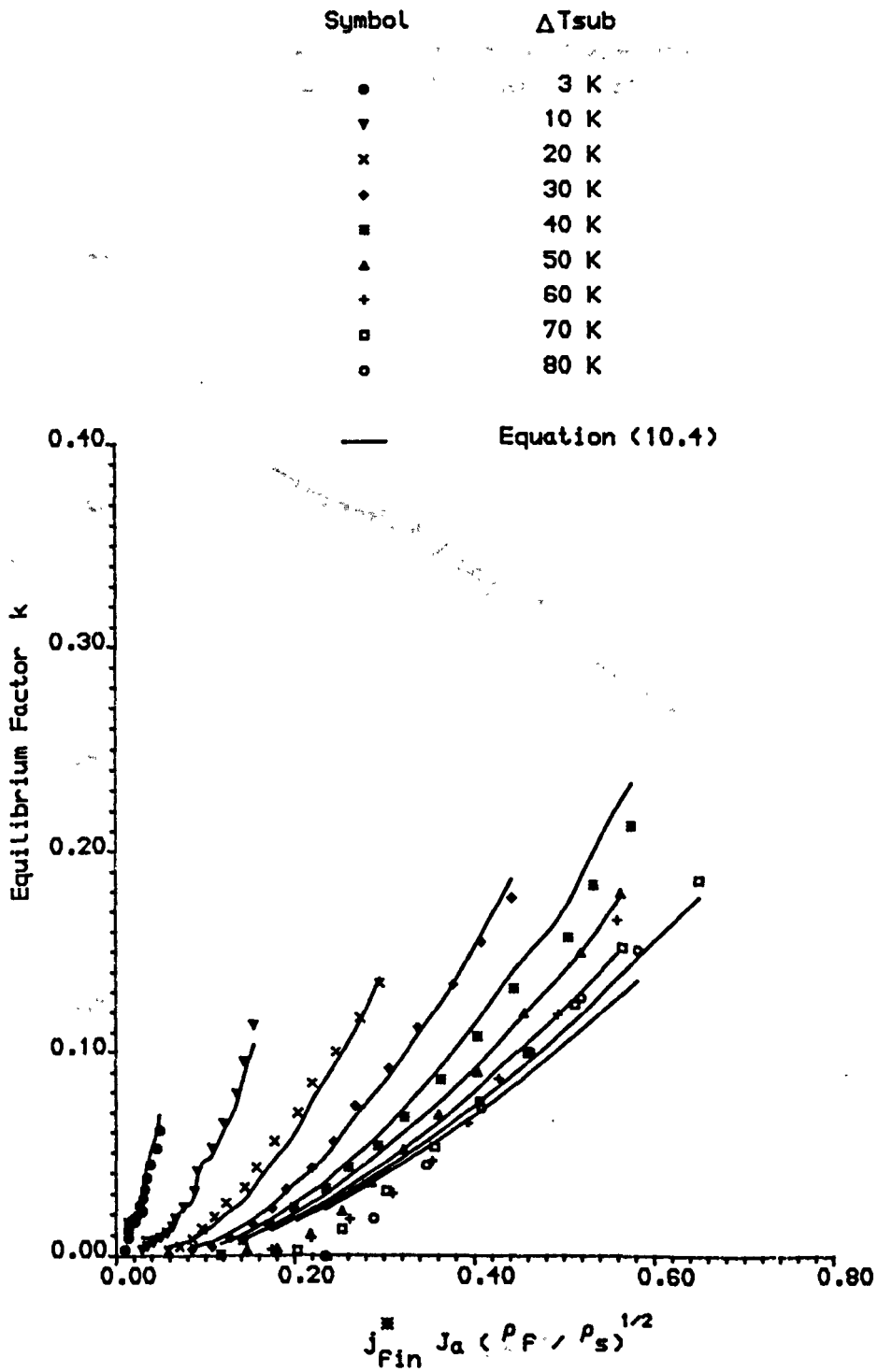


Figure 10.6 Comparison between Non-Equilibrium Data and Correlation

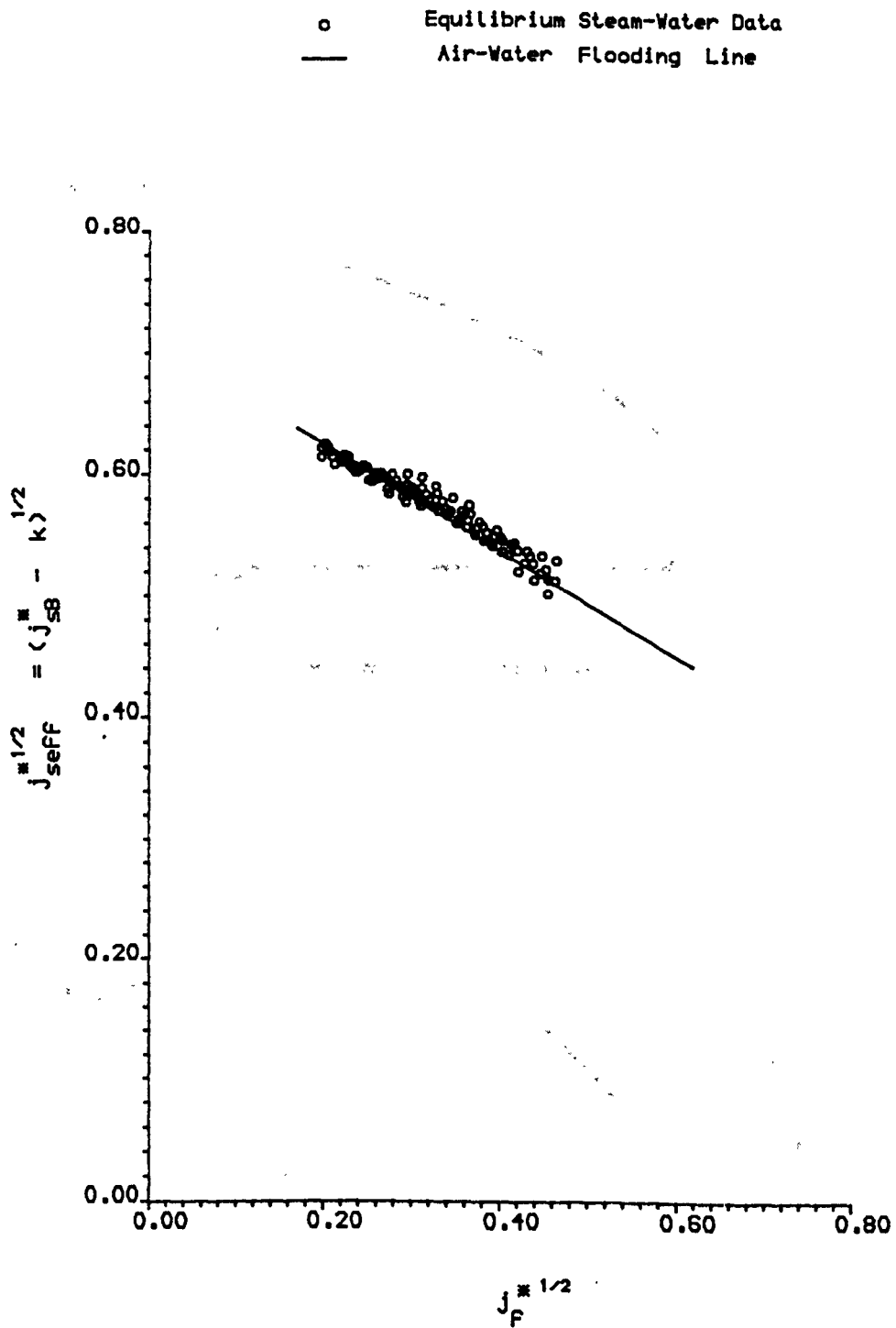
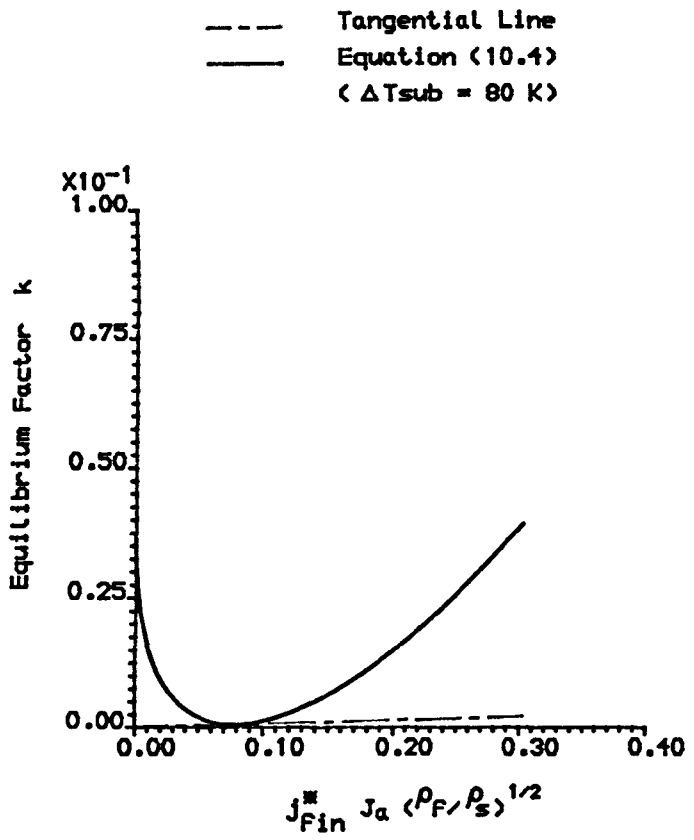
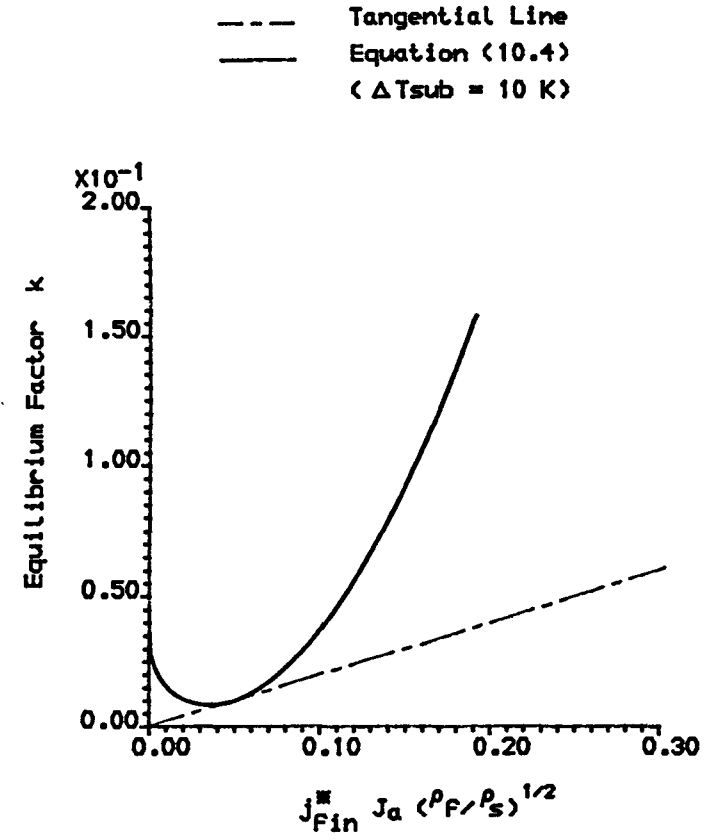


Figure 10.7 Comparison between Equilibrium Steam-Water and Air-Water Data



Minimum Condition For the Non-Equilibrium Correlation . ($\Delta T_{sub} = 80 \text{ k}$)

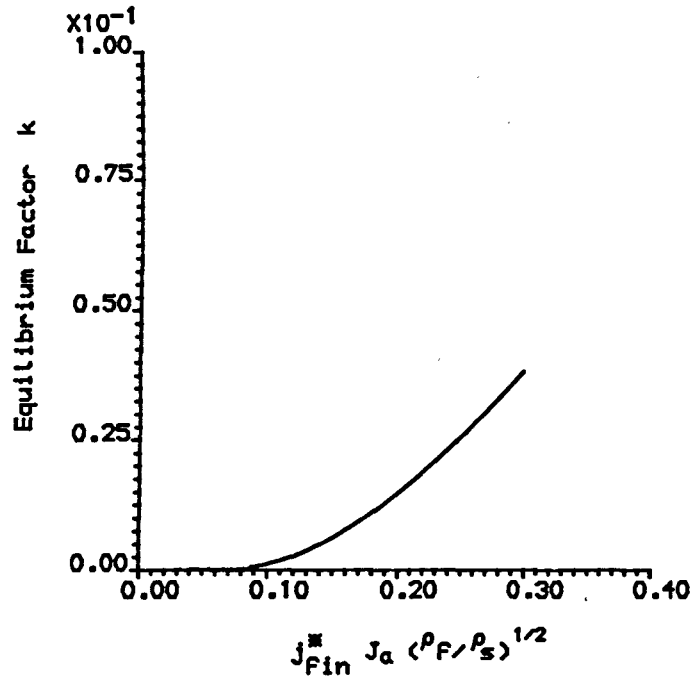
Figure 10.8



Minimum Condition For the Non-Equilibrium Correlation . ($\Delta T_{sub} = 10 \text{ k}$)

Figure 10.9

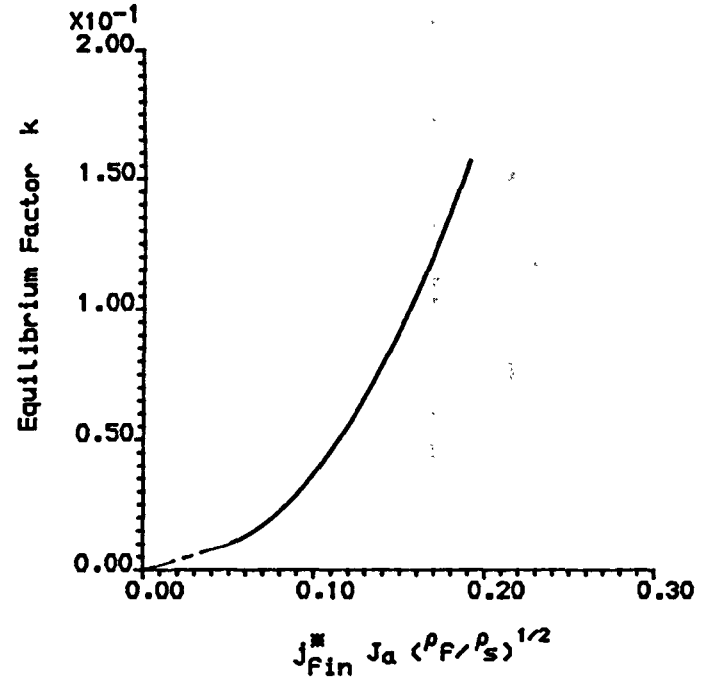
- - - Tangential Line
 — Equation (10.4)
 ($\Delta T_{sub} = 80 \text{ K}$)



Final Non-Equilibrium Relation. ($\Delta T_{sub} = 80 \text{ K}$)

Figure 10.10

- - - Tangential Line
 — Equation (10.4)
 ($\Delta T_{sub} = 10 \text{ K}$)



Final Non-Equilibrium Relation. ($\Delta T_{sub} = 10 \text{ K}$)

Figure 10.11

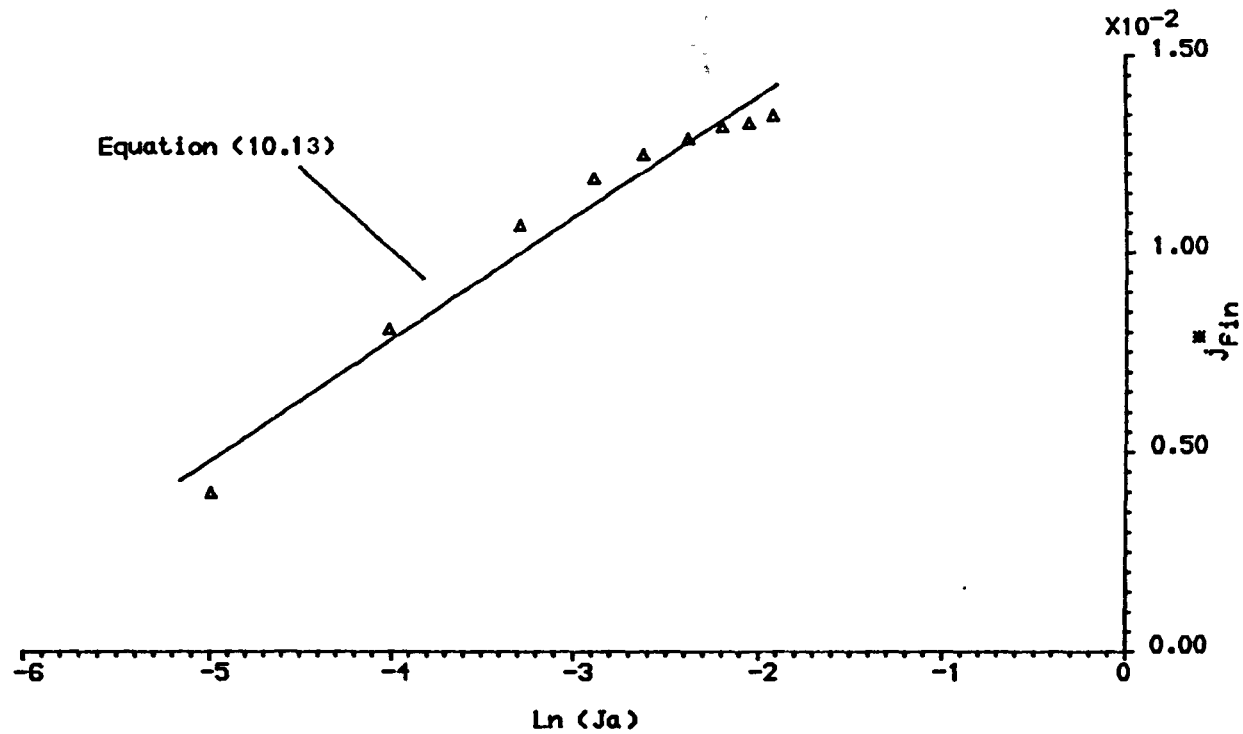


Figure 10.12 Minimum Condition For the the Non-Equilibrium Correlation as a Function of j_{fin}^* and $\ln(Ja)$

CHAPTER 11

CONCLUSIONS AND RECOMMENDATIONS

CHAPTER ELEVEN

CONCLUSIONS AND RECOMMENDATIONS

The conclusions from the research work carried out are presented in Section 11.1 and recommendations for future work in Section 11.2.

11.1 Conclusions

1. Visual observation of the counter-current flow and flooding process were developed and quantitative and qualitative information obtained, but further development is needed. The observations revealed that, for the range of flowrates involved in the tests, the flooding process was always initiated at or near the flow removal sinter in both air-water and steam-water systems.

2. The extraction method of the liquid film used proved satisfactory (for the range of flowrates tested) as it extracted about 95% to 100% of the water in air-water tests, and about 98% to 100% of the water in the steam-water tests. However, the extraction process could be developed further in order to reduce and eliminate the amount of air or steam extracted with the water.

3. The rate of air or steam extracted with the water was found to influence the flooding process in such a way that, for the same amount of inlet water flowrate and subcooling, the higher the air or steam extraction rate the lower the air or steam flow required to initiate flooding. In other words, the flooding process in both air-water and steam-water systems had a strong dependence on the inlet and outlet condition of the liquid film.

4. In the air-water tests, increasing the inlet water flowrate lowered the air flowrate to initiate flooding. In the steam-water tests, a higher steam flowrate was generally required to initiate flooding as the inlet water flowrate increased. This apparent conflict between air-water and steam-water tests can be explained in terms of condensation and non-equilibrium effects.

5. In steam-subcooled water tests, a non-equilibrium effect existed along the whole test tube, and was affected by, but not dependent on, whether or not the liquid film reached the saturation temperature at the bottom of the test section tube.

6. Vapour condensation on the liquid film had the effect of inhibiting the wave growth and formation.

7. It is suggested that the flooding is triggered by a wave starting at the top and travelling to the bottom to initiate flooding.

8. Air-water flooding data in a 54.75 mm diameter stainless tube using 60 mm long porous wall injector and extractor were well correlated, for high extraction rates,

by

$$j_a^{*1/2} + 0.59 j_f^{*1/2} = 0.8 \quad (11.1)$$

and for low extraction rates, by

$$j_a^{*1/2} + 0.55 j_f^{*1/2} = 0.76 \quad (11.2)$$

The extrapolated air-water flooding characteristic to match the extraction rate of steam-water data, was found to conform to

$$j_a^{*1/2} + 0.41 j_f^* = 0.74 \quad (11.3)$$

9. The non-equilibrium effects existing during the counter-current steam-water situation were isolated and found to depend on the water flowrate and the degree of inlet subcooling.

10. An empirical analysis was presented for counter-current steam-water data which yielded an expression for the equilibrium factor given by

$$k = [0.19 - 0.66(x)^{1/2}]^{2.0} + 350(\Delta T_{\text{sub}})^{-1.86}(x)^{2.16}$$

where

$$x = j_{\text{fin}} \left(\frac{\rho_f}{\rho_s} \right)^{1/2}$$

11. A diabatic counter-current liquid film model presented gave reasonably good prediction of the film thickness and proved that the liquid film thickness was dependent on three main parameters (i) liquid viscosity (ii) interfacial shear stress and (iii) steam condensation on the liquid film.

12. The tube wall experimental temperature measurements near the flooding conditions were used to estimate the effective heat transfer exchange coefficients in the liquid film for a series of different water rates and subcoolings and provided information about the turbulence in the liquid film under wavy conditions prior to flooding. It also enabled the liquid film temperature to be evaluated at any position along the tube and at any thickness across the liquid film.

11.2 Recommendations

1. The endoscope optical system should be further developed to provide high speed video recordings of the liquid film interface and the flooding process.

2. The extractor system should be further developed to greatly reduce or even eliminate the quantity of air or steam being removed with the water and thus minimise the exit effects on the flooding process.

3. The pressure difference measurement technique in the steam-water system should be further developed to remove the presence of the two-phase mixture in the system pipes and connections.

REFERENCES

REFERENCES

AHMED, S.Y.

"Axial Distribution of Bulk Temperature and Void Fraction in a Heated Channel with Inlet Subcooling". Transactions of the ASME, Journal of Heat Transfer, Vol. 92, pp. 595 - 609, Nov. 1970.

AKERS, W.W. and ROSSON, H.F.

"Condensation Inside a Horizontal Tube". Chemical Engineering Progress Symposium Series, No. 30, Vol. 56, 1960.

ALEKSEEV, V.P., POBEREZKIN, A.E. and GERAMSIMOV, P.V.

"Determination of Flooding Rates in Regular Packings". Heat Transfer - - Soviet Research, Vol. 4, pp. 159-163, 1972.

ANDREUSSI, P., SANDRONI, G., MINERVINI, A., BATTARRA, V., MARIANI, O. and NICOLAI, H.

"Countercurrent Gas-Liquid Flow in Inclined Pipes". 3rd. International Conference on Multi-Phase Flow, The Hague, Netherlands, paper K1, 18-20th May 1987.

ARNOLD, C.R. and HEWITT, G.F.

"Further Developments in the Photography of Two-Phase Gas-Liquid Flow". UKAEA Report, AERE - R 5318, Jan. 1967.

AZZOPARDI, B.J. and WHALLEY, P.B.

"Artificial Waves in Annular Two-Phase Flow". Basic Mechanisms in Two-Phase Flow and Heat Transfer, ASME, pp. 1 - 8, 1980.

BACH, P. and VILLADSEN, J.

"Simulation of the Vertical Flow of a Thin, Wavy Film using a Finite-Element Method". International Journal of Heat and Mass Transfer, Vol. 27, No. 6, pp. 815 - 827, 1984.

BANKOFF, S.G.

"Some Condensation Studies Pertinent to LWR Safety". International Journal of Multiphase Flow, Vol. 6, pp. 51-67, 1980.

BANKOFF, S.G. and KIM, H.J.

"Local Condensation Rates in Nearly Horizontal Stratified Countercurrent Flow of Steam and Cold Water". AIChE Symposium Series, No. 225, Vol. 79, pp. 209 - 223, 1983.

BANKOFF, S.G. and LEE, S.C.

"Comparison of Flooding Models for Air-Water and Steam-Water Flow". Advances in Two-Phase Flow and Heat Transfer, Vol. II, pp. 745-780. Edited by Kakac, S. and Ishii, M., 1982.

BANKOFF, S.G. and LEE, S.C.

"A Critical Review of the Flooding Literature". NUREG/CR-3060 R2, July 1983.

BANKOFF, S.G., TANKIN, R.S. and YUEN, M.C.

"Steam-Water Condensation Studies". NUREG/CR-1898, 1981.

BASHFORTH, E.Q., FRASER, J.B.P., HUTCHISON, H.P. and NEDDERMAN, R.M.

"Two-Phase Flow in a Vertical Tube". Chemical Engineering Science, Vol. 18, p. 41, 1963.

BELKIN, H.H., MacLEOD, A.A., MONRAD, C.C. and ROTHFUS, R.R.

"Turbulent Liquid Flow Down Vertical Walls". AIChE. Journal, Vol. 5, No. 2, pp. 245 - 248, 1959.

BENJAMIN, T.B.

"Wave Formation in Laminar Flow down an Inclined Plan". Journal of Fluid Mechanics, Vol. 4, pp. 554 -574, 1957.

BENJAMIN, T.B.

"Shearing Flow Over a Wavy Boundary". Journal of Fluid Mechanics, Vol. 6, pp. 161-205, 1959.

BHARATHAN, D., WALLIS, G.B. and RICHTER, H.J.

"Air-Water Countercurrent Annular Flow in Vertical Tubes". EPRI NP-786, 1978.

BHARATHAN, D., WALLIS, G.B. and RICHTER, H.J.

"Air-Water Countercurrent Annular Flow". EPRI NP-1165, 1979.

BLAGETTI, F. and SCHLUNDER, E.U.

"Local Heat Transfer Coefficients on Condensation in a Vertical Tube". in Proc. 6th. International Heat Transfer Conference, Vol. 2, pp. 437 - 442, Hemisphere, New York, 1978.

BLOCK, J.A.

"Condensation-Driven Fluid Motions". International Journal of Multiphase Flow, Vol. 6, pp. 113 - 129, 1980.

BLOCK, J.A. and WALLIS, G.B.

"Heat Transfer and Fluid Flows Limited by Flooding". AIChE Symposium Series, No. 174, Vol. 74, p. 73 - 82, 1978.

BROWN, D.J., JENSEN, A. and WHALLEY, P.B.

"Non-Equilibrium Effects in Heated and Unheated Annular Two-Phase Flow". ASME, paper No. 75-WA/HT7, 1975.

BUTTERWORTH, D. and HEWITT, G.F.

"Two-Phase Flow and Heat Transfer". Oxford University Press, 1977.

CAMPBELL, T.

"Nuclear Reactor Safety, PWR Refill Studies". Ph.D. Thesis, University of Strathclyde, Scotland, 1979.

CARSLAW, H.S. and JAEGER

"Conduction of Heat in Solids". Oxford University Press, 1950.

CELATA, G.P., CUMO, M., FARELLO, G.E. and FOCARDI, G.

"Direct Contact Condensation of Steam on Slowly Moving Water". Nuclear Engineering and Design, Vol. 96, pp.21-31, 1986.

CETINBUDAKLAR, A.G. and JAMESON, G.J.

"The Mechanism of Flooding in Vertical Countercurrent Two-Phase Flow". Chemical Engineering Science, Vol. 24, pp. 1669 - 1680, 1969.

CHAUDRY, A.B.

"A Study of the Flow of Air and Water in a Vertical Tube". Ph.D. Thesis, University of Edinburgh, Scotland, 1967.

CHIEN, S.F. and IBELE, W.

"Pressure Drop and Liquid Film Thickness of Two-Phase Annular and Annular-Mist Flows". Transactions of the ASME, Journal of Heat Transfer, Vol. 86, No. 1, pp. 89 -

96, 1964.

CHUNG, K.S.

"Flooding Phenomena in Countercurrent Two-Phase Flow Systems". Ph.D. Thesis, University of California, Berkeley, 1978.

CHUNG, K.S., LIU, C.P. and TIEN, C.L.

"Flooding in Two-Phase Countercurrent Flows - II. Experimental Investigation". Physicochemical Hydrodynamics, Vol. 1, pp. 209 - 220, 1980.

CLIFT, R., PRITCHARD, C.L. and NEDDERMAN, R.M.

"The Effect of Viscosity on the Flooding Conditions in Wetted Wall Columns". Chemical Engineering Science, Vol. 21, pp. 87 - 95, 1966.

COLLIER, J.G. and HEWITT, G.F.

"Film Thickness Measurements". UKAEA Report, AERE - R 4684, 1964.

CONDER, J.R., GUNN, D.J. and SHAIKH, M.A.

"Heat and Mass Transfer in Two-Phase Flow - A Mathematical Model for Laminar Film Flow and its Experimental Validation". International Journal of Heat Transfer, Vol. 25, No. 8, pp. 1113 - 1126, 1982.

COOPER, K.D., HEWITT, G.F. and PINCHIN, B.

"Photography of Two-Phase Gas - Liquid Flow". UKAEA Report, AERE - R 4301, 1963.

COOK, D., BANKOFF, S.G., TANKIN, R.S. and YUEN, M.C.

"Countercurrent Steam - Water Flow in a Vertical Channel". NUREG/CR-2056, 1981.

COUSINS, L.B., DENTON, W.H. and HEWITT, G.F.

"Liquid Mass Transfer in Annular Two-Phase Flow". UKAEA

Report, AERE - R 4926, May 1965.

DAVIDSON, S., JENSEN, R.J., BANKOFF, S.G., TANKIN, R.S.
and YUEN, M.C.

"Measurements of Condensation Rates in Steam - Water
Flow". Transient Two-Phase Flow proc. 2nd. CSNI
Specialists Meeting, Paris, June 1978.

DEAKIN, A.W., PULLING, D.J. and BROGAN, R.

"Flooding in Reflux Condensers". Harwell Report, HTFS -
R5249, August 1978.

DIEHL, J.C. and KOPPANY, C.R.

"Flooding Velocity Correlation for Gas - Liquid
Counterflow in Vertical Tubes". Chemical Engineering
Progress Symposium Series, No. 92, Vol. 65, pp. 77 - 83,
1969.

DOBRAN, F.

"Condensation Heat Transfer and Flooding in a Counter-
Current Subcooled Liquid and Saturated Vapour Flow".
Paper presented at the 20th. Annual Heat Transfer
Conference, Milwaukee, Wisconsin, 1981.

DOBRAN, F.

"Hydrodynamic and Heat Transfer Analysis of Two-Phase
Annular Flow with a New Liquid Film Model of Turbulence".
International Journal of Heat and Mass Transfer, Vol. 26,
No. 8, pp. 1159 - 1171, 1983.

DOBRAN, F.

"Heat Transfer in Annular Two-Phase Flow". Transactions
of the ASME, Journal of Heat Transfer, Vol. 107, No. 2,
pp. 472 - 481, May 1985.

DUKLER, A.E.

"Fluid Mechanics and Heat Transfer in Vertical Falling-Film Systems". Chemical Engineering Progress Symposium Series, No. 30, Vol. 56, pp. 1 - 10, 1960.

DUKLER, A.E.

"Characterisation Effects and Modelling of the Wavy Gas - Liquid Interface". Progress in Heat and Mass Transfer, Vol. 6, pp. 207 - 234, 1972.

DUKLER, A.E., CHOPRA, A., MOALIM MARON, D. and SIMIAT, R.

"Two-Phase Interaction in Counter Current Flow

I - Studies of the Flooding Mechanism

II - Motion and Size of Drops During Upward Annular Flow

III - Upward Film Flow: Interfacial Structure and Momentum Interactions". Department of Chemical Engineering, University of Houston, Report No. HTFS30453, Dec. 1978.

DUKLER, A.E. and SMITH, L.

"Two-Phase Interactions in Countercurrent Flow, Studies of the Flooding Mechanism". Department of Chemical Engineering, University of Houston, Dec. 1977.

DUKLER, A.E. and SMITH, L.

"Two-Phase Interactions in Countercurrent Flow: Studies of the Flooding Mechanism". NUREG/CR-0617, January 1979.

EICHHORN, R.

"Dimensionless Correlation of the Hanging Film Phenomenon". Transactions of the ASME, Journal of Fluid Engineering, Vol. 102, pp. 372 - 375, Sept. 1980.

EIFLEL, W.

"Condensation of Countercurrent and Cocurrent Steam on the Free Surface of Subcooled Stratified Water Flows".

Commission of the European Communities Joint Research Centre - Ispra, Italy, presented at the 1987 European Two Phase Flow Group Meeting, 1-4th June 1987.

ELIAS, E. and YADIAGAROGLU, G.

"Rewetting and Liquid Entrainment during Reflooding". EPRI NP-435, 1977.

ELLIS, J.E. and LLOYD JONES, E.

"Vertical Gas-Liquid Flow Problems". Symposium on Two-Phase Flow, Exeter, paper B1, 21-23 June 1963.

ENGLISH, K.G., JONES, W.T., SPILLERS, R.C. and ORR, V.

"Flooding in a Vertical Updraft Partial Condenser". Chemical Engineering Progress, Vol. 59, pp. 51 - 54, 1963.

FAN. C.K.

"Phenomena of Flooding with Condensation". Ph.D. Thesis, University of California, Berkley, 1979.

FAN, C.K. and SCHROCK, V.

"Flooding Phenomena with Condensation". Transactions of ANS, Vol. 32, pp. 380 - 381, Nov. 1978.

FEIND, F.

"Falling Liquid Films with Counter Current Air Flow in Vertical Tubes". VDI-Forschungsheft, Vol. 481, p. 26, 1960.

FREA, W.J.

"Two-Phase Heat Transfer and Flooding in Counter Current Flow". Michigan Technological University Proceedings of the International Heat Transfer Conference, Vol. 5, paper B5.10, 1970.

GREIF, R.

"An Experimental and Theoretical Study of Heat Transfer in Vertical Tube Flows". Transactions of the ASME, Journal of Heat Transfer, Vol. 100, pp. 86 - 91, Feb. 1978.

GROLMES, M.A., LAMBERT, G.A. and FAUSKE, H.K.

"Flooding in Vertical Tubes". AIChE Symposium on Multiphase Flow Systems, Glasgow, Scotland, 1974.

HAGI, Y.

"Air-Water Flooding for Parallel Channel Flows Based on the Results for Single Path Flow". M.Sc. Thesis, Dartmouth College, Sept. 1976.

HALL-TAYLOR, N., HEWITT, G.E. and LACEY, P.M.C.

"The Motion and Frequency of Large Disturbance Waves in Annular Two-Phase Flow of Air-Water Mixtures". UKAEA Report, AERE - R 3952, 1962.

HAWLEY, D.L. and WALLIS, G.B.

"Experimental Study of Liquid Film Fraction and Pressure Drop Characteristics in Vertical Countercurrent Annular Flow". EPRI NP-2280, 1982.

HEWITT, G.F.

Influence of End Conditions, Tube Inclination and Physical Properties on Flooding in Gas-Liquid Flows". Harwell Report, HTFS - RS222, Aug. 1977.

HEWITT, G.F.

"Photographic and Entrainment Studies in Two-Phase Flow Systems". UKAEA Report, AERE - R 4683, 1964.

HEWITT, G.F.

"Liquid Mass Transport in Annular Two-Phase Flow".

International Seminar on Momentum, Heat and Mass Transfer in Two-Phase Energy and Chemical Systems, Dubrovnik, Yugoslavia, 1978.

HEWITT, G.F.

"Disturbance Waves in Annular Two-Phase Flow". Proc. Inst. Mech. Engrs., Vol. 184, No. 3c, p. 142, 1970.

HEWITT, G.F. and HALL-TAYLOR, N.S.

"Annular Two-Phase Flow". Pergamon Press, Oxford, 1970.

HEWITT, G.F., KING, R.D. and LOVEGROVE, P.C.

"Techniques for Liquid Film and Pressure Drop Studies in Annular Two-Phase Flow". UKAEA Report, AERE - R 3921, 1962.

HEWITT, G.F. and LACEY, P.M.C.

"The Breakdown of the Liquid Film in Annular Two-Phase Flow". UKAEA Report, AERE - R 4303, 1963.

HEWITT, G.F. LACEY, P.M.C. and NICHOLLS, B.

"Transitions in Film Flow in a Vertical Tube". UKAEA Report, AERE - R 4614, 1965.

HEWITT, G.F., LOVEGROVE, P.C. and NICHOLLS, B.

"Film Thickness Measurements using a Fluorescence Technique. Part I : Description of the Method". UKAEA Report, AERE - R 4478, 1964.

HEWITT, G.F. and NICHOLLS, B.

"Film Thickness Measurements in Annular Two-Phase Flow using a Fluorescence Spectrometer Technique - Part II. Studies of the Shape of Disturbance Waves". UKAEA Report, AERE - R 4506, 1969.

HEWITT, G.F. and ROBERTS, D.N.

"Investigation of Interfacial Phenomena in Annular Two-Phase Flow by Means of the Axial View Technique". UKAEA Report, AERE - R 6070 , 1969.

HEWITT, G.F. and WALLIS, G.B.

"Flooding and associated Phenomena in Falling Film Flow in a Tube". UKAEA Report, AERE - R 4022, 1963.

HUTCHINSON, P. and WHALLEY, P.B.

"A Possible Characterisation of Entrainment in Annular Flow". UKAEA Report, AERE - R 7126, 1972.

HSIEH, C.L, BANKOFF, S.G., TANKIN, R.S. and YUEN, M.C.

"Counter-current Air/Water and Steam/Water Flow above a Perforated Plate". NUREG/CR-1808, R1, R2, R4, Nov. 1980.

IMURA, H., KUSUDA, H. and FUNATSU, S.

"Flooding Velocity in a Counter-Current Annular Two-Phase Flow". Chemical Engineering Science, Vol. 32, pp. 79 - 87, 1977.

JONES, D.D.

"Subcooled Counter-Current Flow Limiting Characteristics of the Upper Region of a BWR Fuel Bundle". NEDG-NUREG-23549, July 1977.

KAMEI, S., OISHI, J. and OKASE, T.

"Flooding in Wetted Wall Tower". Chemical Engineering (Japanese), Vol. 18, pp. 364 - 368, 1954.

KIM, H.J., and BANKOFF, S.G.

"Local Heat Transfer Coefficients for Condensation in Stratified Counter Current Flows". Transactions of the ASME, Journal of Heat Transfer, Vol. 105, No.4, p. 706 - 712, Nov. 1983.

KUSUDA, H. and IMURA, H.

"Stability of Liquid Film in a Counter-Current Annular Two-Phase Flow". TRANS. JAP. SOC. MECH. ENGRS., Vol. 40, pp. 1082 - 1088, 1974.

KUTATELAZE, S.S.

"Elements of the Hydrdynamics of Gas-Liquid Systems". Fluid Mechanics Soviet Research, Vol. 1, No. 4, pp. 29 - 50, 1972.

LEE, S.C. and BANKOFF, S.G.

Stability of Steam-Water Countercurrent Flow in an Inclined Channel". ASME 82-WA/HT-6, 1982.

LEVY, S.

"Prediction of Two-Phase Annular Flow with Liquid Entrainment". International Journal of Heat and Mass Transfer, Vol. 9, pp. 171 - 188, 1966.

LINEHAN, J.H., PETRICK, M. and EL-WAKIL, M.M.

"The Condensation of a Saturated Vapour on a Subcooled Film during Stratified Flow". Chemical Engineering Progress Symposium Series, No. 102, Vol. 66, pp. 11 - 20, 1970.

LIU, J.S.K. and COLLIER, R.P.

"Heat Transfer in Vertical Counter-Current Steam-Water Flooding Flows". Basic Mechanisms in Two-Phase Flow and Heat Transfer, ASME, New York, pp. 123 - 129, 1980.

LIU, J.S.K., COLLIER, R.P. and CUDNIK, R.A.

"Flooding of Counter-Current Steam-Water Flow in an Annulus". ASME meeting, San Fransisco, California, Dec. 10 - 15, 1978.

LIU, J.S.K. and TIEN, C.L.

"Flooding in Vertical Gas-Liquid Counter-Current Flow through Parallel Paths". Final Report, EPRI NP-2262, 1982.

LOVELL, T.W.

"The Effect of Scale on Two-Phase Counter-Current Flow Flooding in Vertical Tubes". M.Sc. Thesis, Dartmouth College, 1977.

MACHEJ, K. and SOKOL, W.

"Determination of the Parameters which Affect the Flooding of a Tube". International Chemical Engineering, Vol. 19, pp. 696 - 700, 1979.

McCARTHY, G.E. and LEE, H.M.

"Review of Entrainment Phenomena and Application to Vertical Two-Phase Counter-Current Flooding". EPRI NP-1284, 1979.

McQUILLAN, K.W. and WHALLEY, P.B.

"A Comparison between Flooding Correlations and Experimental Flooding Data for Gas-Liquid Flow in Vertical Circular Tubes". Chemical Engineering Science, Vol. 40, No. 8, pp. 1425 - 1440, 1985.

McNEIL, D.A.

"Flooding in a Vertical Tube", PhD Thesis, Department of Thermodynamics and Fluid Mechanics, University of Strathclyde, June 1986.

MEGAHED, M.M.

"Flooding and Non-Equilibrium with Reference to Pressurised Water Reactor". Ph.D. Thesis, University of Strathclyde, 1981.

MEGAHED, M.M.

"Interfacial Heat Transfer in Countercurrent Flows of Steam and Water". Idaho National Engineering Laboratory, DOE-ID-10161, April 1987.

MILLS, A.F.

"Condensation Heat Transfer : Comments on Non-Equilibrium Temperature Profiles and Engineering Calculation of Mass Transfer". International Journal of Multiphase Flow, Vol. 6, pp. 41 - 50, 1980.

MOALEM MARON, D. and DUKLER, A.E.

"The Flooding Process : An Analysis of Film Flow Mechanism in Two-Phase Interaction in Counter-Current Flow". NUREG/CR-0669, 1979.

MOALEM MARON, D. and DUKLER, A.E.

"New Concepts on the Mechanisms of Flooding and Flow Reversal Phenomena". Letters in Heat and Mass Transfer, Vol. 8, No. 16, pp. 453 - 463, 1981.

NICKLIN, D.J. and KOCH, B.E.

"A Model of Two-Phase Annular Flow". published in Countercurrent Gas-Liquid Flow, Edited by Rhodes and Scott, 1969.

NORMAN, W.S. and McINTYRE, V.

"Heat Transfer to Liquid Film on a Vertical Surface". Transactions Institute of Chemical Engineers, Vol. 38, pp. 301 - 307, 1960.

NUSSELT, W.

"Surface Condensation of Water Vapour". VDI(Z), Vol. 60, pp. 541 - 546, 1916.

OSTRACH, S. and KOESTEL, A.

"Film Instabilities in Two-Phase Flows". AIChE Journal, Vol. 11, No. 2, pp. 294 - 303, March 1965.

OSTROGORSKY, A.G., GAY, R.R. and LAHEY, R.T.

"The Analysis of Counter Current Two-Phase Flow Pressure Drop and CCFL Breakdown in Diabatic and Adiabatic Conduits". NUREG/CR-2386, 1981.

OWEN, D.G. and HEWITT, G.F.

"Data and Analysis of Pressure Gradient and Liquid Entrainment in a Vertical Annular Gas-Liquid Flow". European Two-Phase Flow Group Meeting, 4 - 7th. June 1985.

OWEN, D.G. and HEWITT, G.F.

"An Improved Annular Two-phase Flow Model". 3rd International Conference on Multi-Phase Flow, The Hague, Netherlands, paper C1, 18-20th May 1987.

PUSHKINA, O.L and SOROKIN, Y.L.

"Breakdown of Liquid Film Motion in Vertical Tubes". Heat Transfer - - Soviet Research, Vol. 1, pp. 56 - 64, 1969.

RAGLAND, W.A. and GANIC, E.N.

"Flooding in Counter-Current Two-Phase Flow". Advances in Two-Phase Flow and Heat Transfer, Vol. II, pp. 505 - 538, Edited by Kakac, K. and Ishii, M., 1983.

RICHTER, H.J.

"Flooding in Tubes and Annuli". International Journal of Multiphase Flow, Vol. 7, pp. 647 - 658, 1981.

RICHTER, H.J. and LOVELL, T.W.

"The Effect of Scale on Two-Phase Countercurrent Flow

Flooding in Vertical Tubes". NRC Contract AT(49-24)-0329, August 1977.

RICHTER, H.J. and WALLIS, G.B.

"ECC Bypass Scaling". NUREG/CR-0850, May 1979.

RICHTER, H.J., WALLIS, G.B. and SPEERS, M.S.

"Effect of Scale on Two-Phase Countercurrent Flow Flooding". Final Report, NUREG/CR-0312 R2, 1978.

ROHSENOW, W.M. and CHOI, H.Y.

"Heat, Mass and Momentum Transfer". Prentice-Hall, London, 1961.

ROONEY, D.H., SIMPSON, H.C., BRADFORD, A.M. and BESSADA, E.W.

"Non-Equilibrium Effects in Direct Contact Condensation under Countercurrent Flow". European Two-Phase Flow Group Meeting, Eindhoven, 2 - 5th. June 1981.

ROONEY, D.H., SIMPSON, H.C. and MEGAHED, M.M.

"Non-Equilibrium Effects in Direct Contact Condensation during Refill in a Pressurized Water Reactor". European Two-Phase Flow Meeting, Paris, 2 - 4th. June 1982, and I. Mech. E. Conference on Heat and Fluid Flow in Nuclear and Process Plant Safety, London, May 1983.

ROTHER, P.H. and CROWLEY, C.J.

"Scaling of Pressure and Subcooling for Countercurrent Flow". NUREG/CR-0464, 1978.

SCHLICHTING, H.

"Boundary Layer Theory, 6th. ed., New York, McGraw-Hill, 1960.

SCHUTT, J.B.

"A Theoretical Study of the Phenomenon of Bridging in Wetted-Wall Columns". Ph.D. Thesis, University of Rochester, New York, 1959.

SEGEV, A. and COLLIER, R.P.

"Condensation and Vapourisation Effects on Counter-Current Steam-Water Flow in an Annulus". Non-Equilibrium Interfacial Transport Processes, ASME, New York, 1979.

SEGEV, A. and COLLIER, R.P.

"A Mechanistic Model for Countercurrent Steam-Water Flow". Transactions of the ASME, Journal of Heat Transfer, Vol. 102, p. 688 - 693, Nov. 1980.

SEGEV, A., FLANIGAN, L.J., KURTH, R.E. and COLLIER, R.P.

"Experimental Study of Countercurrent Steam Condensation". Transactions of the ASME, Journal of Heat Transfer, Vol. 103, pp. 307 - 311, May 1981.

SHEARER, C.J. and DAVIDSON, J.F.

"The Investigation of a Standing Wave due to Gas Blowing Upwards over a Liquid Film ; Its Relation to Flooding in Wetted-Wall Columns". Journal of Fluid Mechanics, Vol. 22, pp. 321 - 336, 1965.

SHIRES, G.L. and PICKERING, A.R.

"The Flooding Phenomena in Counter-Current Two-Phase Flow". Symposium on Two-Phase Flow, paper B5, Exeter, England, 1965.

SHIRES, G.L., PICKERING, A.R. and BLACKER, P.T.

"Film Cooling of Vertical Fuel Rods". UKAEA Report, AEEW - R 343, 1964.

SIMPSON, H.C. and ROONEY, D.H.

"Further Studies of Non-Equilibrium during Refill in a Pressurized Water Reactor". Paper No. 3, Session D2, European Two-Phase Flow Group Meeting, Zurich, Switzerland, June 1983.

SMITH, L., CHOPRA, A. and DUKLER, A.E.

"Flooding and Upwards Film Flow in Tubes - I. Experimental Studies". International Journal of Multiphase Flow, Vol. 10, pp. 585 - 597, 1984.

STAINTHORP, F.P. and BATT, R.S.W.

"The Wave Properties of Falling Liquid Films with Counter-Current Air Flow". Symposium on Two-Phase Flow, Paper B3, Exeter, England, 1965.

SUZUKI, S. and UEDA, T.

"Behaviour of Liquid Films and Flooding in Counter-Current Two-Phase Flow -Part 1. Flow in Circular Tubes". International Journal of Multiphase Flow, Vol. 3, pp. 517 - 532, June 1977.

TAITEL, Y., BARNEA, D. and DUKLER, A.E.

"A Film Model for the Prediction of Flooding and Flow Reversal for Gas-Liquid Flow in Vertical Tubes". International Journal of Multiphase Flow, Vol. 8, pp. 1 - 22, 1982.

THOMAS, R.M.

"Condensation of Steam on Water in Turbulent Motion". International Journal of Multiphase Flow, Vol. 5, pp. 1-15, 1979.

TIEN, C.L.

"A Simple Analytical Model for Counter-Current Flow 15, 1979.

TIEN, C.L.

"A Simple Analytical Model for Counter-Current Flow Limiting Phenomena with Vapour Condensation". Letters in Heat and Mass Transfer, Vol. 4, pp. 231 - 237, 1977.

TIEN, C.L., CHUNG, K.S. and LIU, C.P.

"Flooding in Two-Phase Countercurrent Flows --- I. Analytical Modeling". Physicochemical Hydrdynamics, Vol. 1, pp. 195 - 207, 1980.

TIEN, C.L., CHUNG, K.S. and LIU, C.P.

"Flooding in Two-Phase Countercurrent Flows". EPRI NP-1283, Dec. 1979.

TIEN, C.L. and LIU, C.P.

"Survey on Two-Phase Countercurrent Flooding". EPRI NP-984, Feb. 1979.

TIEN, C.L., LIU, C.P. and CHUNG, K.S.

"A Review of Vertical Two-Phase Countercurrent Flooding". Heat and Mass Transfer in Metallic. Proceedings of the International Centre for Heat and Mass Transfer No. 11, pp. 579 - 596, 1981.

TOBILEVICH, N.Y., SAGAN, I.I. and PORZHEZIHSKII, Y.G.

"The Downward Motion of a Liquid Film in Vertical Tubes in an Air-Vapour Counter Flow". Journal of Engineering Physics, Vol. 15, pp. 1071 - 1076, 1968.

UEDA, T., KUBO, T. and INOUE, M.

"Heat Transfer for Steam Condensing inside a Vertical Tube". In Proc. 5th. International Heat Conference, Vol. 3, pp. 304 - 308, Hemisphere, New York, 1978.

UEDA, T. and SUZUKI, S.

"Behaviour of Liquid Film and Flooding in Counter-Current Two-Phase Flow - Part II. Flow in Annular Rod Bundles". International Journal of Multiphase Flow, Vol. 4, pp. 157 - 170, 1978.

UEDA, T. and TANAKA, T.

"Studies of Liquid Film Flow in Two-Phase Annular and Annular-Mist Flow Regions - Part I. Downflow in a Vertical Tube". Bulletin JSME, Vol. 17, pp. 603 - 613, 1974.

WALLIS, G.B.

"Flooding Velocities for Air and Water in Vertical Tubes". AEEW - R 123, Dec. 1961.

WALLIS, G.B.

"The Influence of Liquid Viscosity on Flooding in a Vertical Tube". General Electric Company Report No. 62GL132, 1962.

WALLIS, G.B.

"The Transition from Flooding to Upwards Cocurrent Annular Flow in Vertical Pipe". AEEW - R 142, Feb. 1962.

WALLIS, G.B.

"One Dimensional Two-Phase Flow". McGraw-Hill, New York, 1969.

WALLIS, G.B.

"Annular Two-Phase Flow. Part I : A Simple Theory". Transactions of the ASME, Journal of Basic Engineering, pp. 59 - 72, March 1970.

WALLIS, G.B.

"Annular Two-Phase Flow. Part II : Additional Effects".

Transactions of ASME, Journal of Basic Engineering, pp. 73 - 82, March 1970.

WALLIS, G.B., CRAWLEY, C.J. and BLOCK, J.
"EEC Bypass Studies". Paper presented at the AIChE Symposium on Light Water Reactor Safety, Boston, U.S.A., 1975.

WALLIS, G.B., DESIEYES, D.C., ROSSELLI, R.J. and LACOMBE, J.

"Countercurrent Annular Flow Regimes for Steam and Subcooled Water in a Vertical Tube". EPRI NP-1336, 1980.

WALLIS, G.B. and KUO, J.T.

"The Behaviour of Gas-Liquid Interfaces in Vertical Tubes". International Journal of Multiphase Flow, Vol. 2, pp. 521 - 536, 1976.

WALLIS, G.B. and MAKKENCHERY, S.

"The Hanging Film Phenomenon in Vertical Annular Two-Phase Flow". Transactions of the ASME, Journal of Fluid Engineering, Vol. 96, pp. 297 - 298, 1974.

WHALLEY, P.B., AZZOPARDI, B.J., PSHYK, L. and HEWITT, G.F.

"Axial View Photography of Waves in annular Two-Phase Flow". UKAEA Report, AERE - R 8987, 1977.

WHALLEY, P.B., HEWITT, G.F. and HUTCHINSON, P.

"Experimental Wave and Entrainment Measurements in Vertical Annular Two-Phase Flow". UKAEA Report, AEAE - R 7521, Sept. 1973.

WHALLEY, P.B., HEWITT, G.F. and TERRY, J.W.

"Photographic Studies of Two-Phase Flow using a Parallel

Light Technique". UKAEA Report, AERE - R 9389, March 1979.

WHALLEY, P.B. and MCQUILLAN, K.W.

"Flooding in Two-Phase Flow : The Effect of Tube Length and Artificial Wave Injection". UKAEA Report, AERE - R 10883, April 1983.

YAO, L.S. and SUN, K.H.

"On the Prediction of the Hydrodynamic Flooding Criterion". Paper presented at the 20th. National Heat Transfer Conference, Milwaukee, Wisconsin, 2 - 5th. August, 1981.

YEHUDA, T., BARNEA, D. and DUKLER, A.E.

"A Film Model for the Prediction of Flooding and Flow Reversal for Gas-Liquid Flow in Vertical Tubes". International Journal of Multiphase Flow, Vol. 8, No. 1, pp. 1-10, 1182

ZVIRIN, Y., DUFFEY, R.B. and SUN, K.H.

"On the Derivation of a Countercurrent Flooding Theory". Symposium on Fluid Flow and Heat Transfer over Rod or Tube Bundles, ASME, New York, pp. 111 - 119, 1979.

ACKNOWLEDGMENT

I always assumed that acknowledging all the help I received carrying out this project would be one of the easier tasks when the time came to write my thesis. However, I now find that I have neither the space nor the literary talent to do justice to my deep feelings of gratitude to all concerned. However there are certain individuals that I would like to thank, particularly Professor Hugh C. Simpson, BSc, SM, DSc, FIMechE, FRSE, Head of Thermodynamics and Fluid Mechanics Department, for his suggestions, criticisms and very helpful advice.

I am also extremely grateful to Dr David H. Rooney, BSc, ARCST, PhD, CEng, FIMechE, MIED, for his valuable help, criticisms, suggestions and collaboration in this investigation.

I would also like to thank Mr A.M. Bradford, BSc, ARCST, CEng, MIMechE, who, as my supervisor, gave continued assistance, guidance and support during this work.

Thanks are due to the technical staff of the Thermodynamics Laboratory who helped with the construction and testing of the experimental plant.

A special word of thanks to Lorraine Nelson for her help and encouragement and to Liz Harvey for considerable assistance in the production of the Figures.

Finally I gratefully acknowledge the Iraqi Government for the financial support received throughout the period of this project.

APPENDICES

APPENDIX A

CALIBRATION METHODS AND RESULTS

APPENDIX A

This appendix contains the calibration details for most of the instrumentation used in the test facility.

A1 AIR ROTAMETER CALIBRATIONS

The rotameters used for air flowrate measurements were calibrated in accordance with "Calibration Data for Metric Series Rotameters", provided by rotameters manufacturing company. The rotameter calibrations are obtained from the following equations:

$$I = \log \left[k_1 v \left(\frac{\sigma \rho}{\omega(\sigma - \rho)} \right)^{1/2} \times 10^4 \right] \quad (\text{A.1})$$

$$F_T = k_2 \left(\frac{\omega(\sigma - \rho)}{\sigma \rho} \right)^{1/2} \quad (\text{A.2})$$

and

$$F = f \cdot F_T \quad (\text{A.3})$$

where f is a value selected from a chart applied at constant I to produce R_A mm on the rotameter scale. Manufacturers Notations are:

k_1 and k_2 are instrument constants which vary with tube size

ω = weight of float (g)

σ = mean density of float (g/cm^3)

ρ = density of fluid at working temperature and pressure (g/cm^3)

ν = kinematic viscosity of fluid at working conditions (m^2/s)

F_T = Theoretical flowrate (l/min)

F = Actual flowrate at working conditions (l/min)

From Air Table, the properties of air at 1 bar and 15°C are

$$\rho = 1.21 \times 10^{-3} \text{ g/cm}^3$$

$$\mu = 0.1478 \text{ st}$$

Four types of rotameters were used to measure air flowrates during the experimental tests. The density of duralumin in all cases was 2.8 g/cm^3 . The relevant float weights and tube constants for each rotameter are given in Table A.1, whilst tables A.2 to A.5 give the values of f against R_A values for each tube. Applying the least squares fit through the data for each tube, the following equations were obtained:

Tube 47G

$$F = 96.42 + 26.16R_A + 0.6424R_A^2 - 0.02468R_A^3 + 0.0004849R_A^4 \quad (\text{A.4})$$

Tube 35G

$$F = 48.03 + 14.28R_A + 0.1167R_A^2 + 0.0001306R_A^3 + 0.00000351R_A^4 \quad (\text{A.5})$$

Tube 35XG

$$F = 28.72 + 8.623R_A + 0.1252R_A^2 - 0.004121R_A^3 + 0.00007225R_A^4 \quad (A.6)$$

TUBE 24XG

$$F = 13.59 + 4.153R_A + 0.08786R_A^2 - 0.003392R_A^3 + 0.0000662R_A^4 \quad (A.7)$$

where R_A is in mm and F is in l/min.

A2 WATER ROTAMETER CALIBRATIONS

As mentioned previously in Chapter 4, two types of water rotameter were used. The 47 metric series tube was used to measure the supply water at relatively high flow rates. The rotameter was calibrated in situ using times collection in a weighing device. For every flow rate the reading of the rotameter was related to the average volume flowrate collected. The measurements listed in table A.6 giving the following correlation:

$$Q_f = 9.691 + 3.007H + 0.01184H^2 + 0.000328H^3 \quad (A.8)$$

where Q_f is the water volume flowrate in l/min and H is the rotameter reading in cm. The subsequent calibration curve is shown in Figure A.1.

The flowrate can be read directly in l/min on the

0 - 10 l.min rotameter therefore no calibration equation was required, although it was checked using the method adopted in the calibration of the other rotameter.

A3 SECONDARY SEPARATOR CALIBRATION

The secondary separator was calibrated by filling it with water to a number of different levels and the water then being drained off into a measuring cylinder. The measurements obtained are listed in Table A.7 and a least squares line gave:

$$v = 0.186475H + 1.388231 \quad (A.9)$$

where v is the volume in litres and H is the liquid height in cm. The calibration curve is shown in Figure A.2.

A4 CONDUCTANCE MEASURING CIRCUIT CALIBRATION

The principle of the conductance measuring circuit, shown in Figure 4.3, is that by applying an oscillating voltage to two elements in series, one a known resistance and the other the unknown liquid film conductance, a measurement of the potential difference across each element will allow the liquid film

conductance to be determined by Ohms Law,

i.e.

$$c = \frac{I}{R_L} \frac{V_L}{V_P} \quad (\text{A.10})$$

In the calibration of the conductance measuring circuit, allowance was made for amplification (A) and offset (B) in the conditioning elements so that equation (A.10) became

$$c = \frac{1}{R_L} \frac{A_L B_L}{A_P V_{PO} B_P} \quad (\text{A.11})$$

The liquid film was then simulated by inserting known resistors in its place, these resistors (R) and the fixed resistor (R_L) being measured by a Wayne-Kerr automatic component bridge (B 605). The oscillator supply voltage (V_S) was measured by a Solartron (7051) digital voltmeter as was the circuit output voltages (V_{LO} , V_{PO}). The voltages across the resistor (R_L) and simulated liquid film was calculated from Ohms Law,

$$V_L = \frac{R_L}{R_L + R} V_S \quad (\text{A.12})$$

and

$$V_P = \frac{R}{R_L + R} V_S \quad (\text{A.13})$$

These voltages were correlated with the output voltages V_{LO} and V_{PO} respectively. A least square line

fit method was then applied to the data in order to determine A_L , A_P , B_L , B_P . The calibration data is shown in table A.8 and the best fit line gives

$$V_P = 0.3490V_{PO} - 0.01060 \quad (\text{A.14})$$

$$V_L = 0.3517V_{LO} + 0.01606 \quad (\text{A.15})$$

hence

$$A_L = 0.3517V^{-1} \quad (\text{A.16})$$

$$A_P = 0.3490V^{-1} \quad (\text{A.17})$$

$$B_L = 0.1606V \quad (\text{A.18})$$

$$B_P = -0.01060V \quad (\text{A.19})$$

Then

$$c = 19.86 \frac{(0.3517V_{LO} + 0.01606)}{(0.3490V_{PO} - 0.0106)} \quad (\text{A.20})$$

where the conductance C is in μs and voltages V_{LO} and V_{PO} are in volts.

To check the validity of the calibration, known resistors were again used to replace the liquid film and the measurement circuit used to calculate those resistors. The comparison between known and measured values is listed in Table A.9.

A5 FILM THICKNESS PROBE CALIBRATIONS

The probes and gap thickness were calibrated in situ by inserting plugs of known diameter into the tube section containing the probe, as shown in Figure A.3. The test section was then filled with water and the

liquid conductivity and probe conductance measured through the data acquisition system by an Applesoft Basic programme specially written for this reason.

The calibration data for the upper and lower probes are shown in Tables A.10 and A.11 respectively. The calibration equation for the upper probe was

$$\delta = 6.137 - [37.64 - 3.906\left(\frac{C}{r} - 0.495\right)]^{1/2} \quad (\text{A.20})$$

and for the lower probe

$$\delta = 5.986 - [35.83 - 3.546\left(\frac{C}{r} - 0.063\right)]^{1/2} \quad (\text{A.21})$$

where δ in mm, C in μs and v in $\mu\text{s}/\text{mm}$.

A6 PRESSURE TRANSDUCER CALIBRATION

The differential pressure transducer was calibrated using a mercury manometer, which was connected in parallel, to indicate the pressure. The connection lines were filled with water which was maintained at a certain level in the two volume chambers. Different pressure forces were applied by changing the level of one volume chamber with respect to the other. Accordingly, the transmitter connected to the pressure transducer produced different signals, which were collected through the data acquisition system by an Applesoft Basic programme which had been written for this purpose. Every voltage reading collected was related to the

corresponding pressure indicated by the mercury manometer reading. The numerical details of the data collected are given in Table A.12. A least squares line fitted to the data gave the calibration characteristic shown in Figure A.4 and the calibration equation is

$$P = 20.6230125V - 7.310256 \quad (A.23)$$

where P is the pressure in mm Hg

and V is the pressure transducer output voltage in volts.

A7 STEAM ORIFICE PLATE CALIBRATION

The supply steam flow was passed through the orifice plate to the test facility. By shutting off the water extraction system and the draining valve, the supply steam was passed directly to the steam discharge condenser where it condensed and a weighed collection was made. The upstream pressure and temperature along with the transducer voltage were noted over the period of the timed collection. The averages of the measured quantities are listed on table A.13 and a least squares fit through the data gave,

$$m = 11.3857 \frac{PV}{T} - 0.057195 \quad (A.24)$$

where P is the upstream pressure (PSI)

V is the pressure transducer's output voltage (V)

and T is the upstream temperature (K)

The calibration curve is shown in Figure A.5.

A8 WATER TURBINE FLOWMETER CALIBRATIONS

There were two turbine flowmeters used in the test rig. The first was used to measure the cooling inlet water flowrate to the extractor system condenser, and the other to measure the discharge water flowrate from the extractor system. The calibration of each turbine flowmeter was carried out by passing different water flows through the meter and collecting and weighing these over a time period. At the same time, the output pulses produced by the turbine flowmeter were monitored by the data acquisition system using an Applesoft programme which had been written for this purpose. For each flowrate, the average of the voltage readings was associated with the corresponding average volume flowrate. The averages of the collected data are listed in tables A.14 and A.15, and a least square fit produced the following equations for the two turbines respectively.

(i) cooling water turbine flowmeter

$$Q_f = 2.899112V + 0.206657 \quad (\text{A.25})$$

(ii) discharge water turbine flowmeter

$$Q_f = 5.2504613V + 0.1193941 \quad (\text{A.26})$$

where Q_f is the volumetric water flowrate
and V is the turbine flowmeter output voltage

The two calibration curves are shown in Figures (A.6) and
(A.7) respectively.

A9 THERMOCOUPLE CALIBRATIONS

The thermocouples used on the test facility and connected to the data acquisition system were constructed in two parts (i) the hot junction approximately 1m in length, connected to a plug and (ii) a longer length, containing a socket which was connected to the input terminals of the conditioning circuits. The plugs and sockets were of the same material as the thermocouple wire. The cold junctions were independently insulated and contained within an oil filled flask surrounded by an ice filled vacuum flask.

All the thermocouples were calibrated by inserting

the hot junction into a controlled temperature water bath. The temperature of the water bath was measured by a calibrated mercury thermometer. For the thermocouples which could be removed from their location, the calibration was carried out by inserting the thermocouple into the water bath, noting the temperature on the mercury thermometer and then recording the thermocouple output voltage by the computer. A similar system was used for the thermocouples fixed to the tube wall except that temperature variations were accomplished by steam heating of the tube wall. A computer programme was written to accept and tabulate the calibration data, then to fit it with a least square curve. The calibration results are listed in Tables A.16 to A.33 and some calibration characteristics are shown in Figures A.8 and A.9. The calibration equations of all the thermocouples are listed in Table A.34.

TABLE A.1AIR ROTAMETER FLOAT WEIGHTS AND TUBE CONSTANTS

TUBE TYPE (-)	FLOAT WEIGHT (g)	K ₁ TUBE CONSTANT (-)	K ₂ TUBE CONSTANT (-)
47G	61.48	2.30	4.355
35G	27.71	1.50	3.330
35XG	27.71	1.50	1.997
24XG	8.96	0.865	1.735

TABLE A.2CALIBRATION RESULTS FOR TUBE 47G

SCALE READING (mm.)	f VALUE (-)	FLOW RATE (l/min)
0.7	0.1	98.1
35.3	0.2	196.0
67.0	0.3	294.0
97.3	0.4	393.0
126.0	0.5	491.0
154.0	0.6	589.0
181.0	0.7	687.0
208.0	0.8	785.0
232.0	0.9	883.0
256.0	1.0	981.0

TABLE A.3
CALIBRATION RESULTS FOR TUBE 35G

SCALE READING (mm.)	f VALUE (-)	FLOW RATE (l/min)
1.67	0.1	50.4
36.0	0.2	101.0
68.3	0.3	151.0
99.7	0.4	202.0
129.0	0.5	252.0
157.0	0.6	302.0
185.0	0.7	353.0
211.0	0.8	403.0
236.0	0.9	453.0
261.0	1.0	504.0

TABLE A.4
CALIBRATION RESULTS FOR TUBE 35XG

SCALE READING (mm.)	f VALUE (-)	FLOW RATE (l/min)
1.88	0.1	30.2
34.7	0.2	60.4
66.7	0.3	90.6
97.3	0.4	121.0
126.0	0.5	151.0
155.0	0.6	181.0
183.0	0.7	212.0
211.0	0.8	242.0
238.0	0.9	272.0
263.0	1.0	302.0

TABLE A.5
CALIBRATION RESULTS FOR TUBE 24XG

SCALE READING (mm.)	f VALUE (-)	FLOW RATE (l/min)
3.1	0.1	14.9
36.9	0.2	29.9
67.5	0.3	44.8
97.2	0.4	59.7
126.0	0.5	74.6
153.0	0.6	89.6
181.0	0.7	104.0
206.0	0.8	119.0
232.0	0.9	134.0
256.0	1.0	149.0

TABLE A.6
CALIBRATION CURVE OF WATER TUBE 47

SCALE READING (cm.)	MEASURED FLOWRATE (l/min)	CALCULATED FLOWRATE (l/min)	PERCENTAGE DIFFERENCE (%)
0.75	11.85	11.86	0.05
4.20	22.19	22.18	0.06
6.4	29.21	29.19	0.05
9.5	39.40	39.47	0.17
12.4	49.35	49.28	0.14
14.5	56.37	56.40	0.05

TABLE A.7

CALIBRATION RESULTS FOR SECONDARY SEPARATOR

LIQUID HEIGHT IN SEPARATOR (cm.)	VOLUME OF LIQUID IN SEPARATOR (L)	CALCULATED VOLUME (L)	PERCENTAGE DIFFERENCE (%)
0.0	1.388	1.388	0.072
3.0	1.953	1.947	0.308
5.0	2.317	2.320	-0.087
6.9	2.637	2.674	-1.347
10.0	3.277	3.252	0.768
15.0	4.157	4.185	-0.670
20.0	5.149	5.117	0.625
25.0	6.050	6.050	0.016
30.0	6.992	6.982	0.143
35.0	7.942	7.914	0.353
40.0	8.874	8.847	0.305
43.5	9.442	9.499	-0.601

TABLE A.8
RESISTANCE CALIBRATION RESULTS

MEASURED RESISTANCE	PROBE OUTPUT VOLTAGE	LOAD OUTPUT VOLTAGE	CALCULATED RESISTANCE	PERCENTAGE DIFFERENCE
(R) (k)	(V_{po}) (V)	(V_{Lo}) (V)	(R_c) (k)	(D) (%)
5.01	0.928	8.933	4.995	-0.2170
47.06	4.839	5.062	47.040	-0.0384
89.45	6.407	3.515	89.520	0.0783
184.80	7.865	2.077	184.400	-0.2150
339.40	8.720	1.234	339.400	0.0000
380.20	8.843	1.112	380.500	0.0707
541.30	9.163	0.798	540.600	-0.1290

TABLE A.9
CALIBRATION DATA FOR CONDUCTANCE MEASURING CIRCUIT

MEASURED RESISTANCE	PROBE OUTPUT	LOAD OUTPUT	CALCULATED RESISTANCE	PERCENTAGE DIFFERENCE
(R) (k)	(V_{po}) (V)	(V_{Lo}) (V)	(R_c) (k)	(D) (%)
5.00	0.927	8.935	3.1580	0.313
47.11	4.844	5.061	1.7960	1.680
89.51	6.411	3.514	1.2520	2.227
184.90	7.872	2.071	0.7444	2.770
339.60	8.723	1.233	0.4497	3.034
380.60	8.845	1.113	0.4075	3.076
342.40	9.164	0.7997	0.2973	3.188

TABLE A.10
CALIBRATION DATA FOR THE TOP PROBE

FILM THICKNESS (mm.)	SPECIFIC CONDUCTIVITY (mm.)	CALC. SPEC. CONDUCTIVITY (mm.)	PERCENTAGE DIFFERENCE (%)
0.205	1.296	1.128	14.900
0.465	1.739	1.900	-8.500
0.935	3.165	3.209	-1.360
1.275	4.048	4.084	-0.889
1.690	5.063	5.073	-0.198
2.000	5.801	5.754	0.815
2.490	6.756	6.730	0.294
2.895	7.537	7.444	1.250
3.400	8.213	8.217	-0.046
3.665	8.474	8.570	-1.120
4.085	9.080	9.056	0.264

TABLE A.11
CALIBRATION DATA FOR THE LOWER PROBE

FILM THICKNESS (mm.)	SPECIFIC CONDUCTIVITY (mm.)	CALC. SPEC. CONDUCTIVITY (mm.)	PERCENTAGE DIFFERENCE (%)
0.205	0.776	0.743	4.390
0.465	1.543	1.572	-1.830
0.935	2.992	2.973	0.630
1.275	3.823	3.909	-2.210
2.000	5.760	5.688	1.270
2.490	6.800	6.722	1.160
2.895	7.386	7.474	-1.180
3.400	8.273	8.283	-0.167
3.665	8.643	8.649	-0.075
4.085	9.167	9.150	0.190

TABLE A.12PRESSURE TRANSDUCER CALIBRATION RESULTS

LIQUID HEIGHT IN SEPARATOR (cm.)	VOLUME OF LIQUID IN SEPARATOR (L)	CALCULATED VOLUME (L)	PERCENTAGE DIFFERENCE (%)
0.495	3	2.918	2.810
0.637	6	5.847	2.616
0.941	12	12.095	-0.786
1.336	20	20.242	-1.196
1.785	30	29.501	1.691
2.303	40	40.184	-0.458
2.752	50	49.444	1.124
3.477	64	64.395	-0.614
3.945	74	74.047	-0.640
4.517	84	85.864	-2.171
4.912	94	93.989	0.011
5.297	102	101.929	0.069
5.562	108	107.394	0.564
6.059	118	117.644	0.302
6.269	122	121.975	0.020
6.643	130	129.688	0.240
7.069	139	138.473	0.380
7.368	145	144.640	0.248
7.856	155	154.704	0.191
8.453	166	167.016	-0.609

TABLE A.13

STEAM ORIFICE PLATE CALIBRATION DATA

UPSTREAM PRESSURE (P.S.I.)	UPSTREAM TEMPERATURE (K)	PRESSURE TRANSDUCER VOLTAGE (V)	MEASURED FLOWRATE (kg/min)
9.8	141.4	0.088	0.766
10.0	141.6	0.107	0.853
10.4	142.1	0.137	0.986
9.9	142.3	0.177	1.121
10.1	142.5	0.224	1.269
10.7	143.1	0.258	1.386
11.6	143.9	0.288	1.488
14.9	144.0	0.325	1.691
14.6	146.0	0.444	1.973
10.1	146.0	0.623	2.151
13.0	148.0	0.731	2.466
15.6	148.4	0.813	2.732
16.0	148.4	0.922	2.928
16.3	148.5	0.957	3.002
16.5	148.6	1.056	3.165

TABLE A.14

COOLING WATER TURBINE METER CALIBRATION RESULTS

MEASURED VOLTAGE (V)	MEASURED FLOWRATE (l/min)	CALCULATED FLOWRATE (l/min)	PERCENTAGE DIFFERENCE (%)
0.297	1.054	1.067	-0.219
0.651	2.076	2.093	-0.813
1.768	5.304	5.330	-0.488
2.226	6.621	6.657	-0.526
2.854	8.477	8.477	0.000
3.157	9.359	9.358	0.010
3.711	10.963	10.961	0.018
4.146	12.208	12.222	-0.115
4.871	14.348	14.323	0.174
5.552	16.313	16.296	0.110
6.095	17.885	17.870	0.083
6.717	19.876	19.673	1.031
7.442	21.853	21.774	0.362
7.917	23.148	23.151	-0.013
8.331	24.160	24.350	-0.781
8.868	25.956	25.910	0.177
9.175	26.813	26.796	0.063
9.423	27.524	27.515	0.032
9.763	28.498	28.500	0.000
9.993	29.063	29.167	-0.357

TABLE A.15

DISCHARGE WATER TURBINE METER CALIBRATION RESULTS

MEASURED VOLTAGE (V)	MEASURED FLOWRATE (l/min)	CALCULATED FLOWRATE (l/min)	PERCENTAGE DIFFERENCE (%)
0.503	2.731	2.760	-0.051
0.982	5.297	5.275	0.417
1.373	7.228	7.328	-1.365
1.606	8.565	8.551	0.163
1.973	10.484	10.478	0.057
2.117	11.279	11.234	0.400
2.413	12.810	12.788	0.172
2.792	14.888	14.778	0.744
3.172	16.578	16.773	-1.163
3.547	18.804	18.742	0.330
3.862	20.399	20.396	0.014
4.206	22.387	22.202	0.837
4.684	24.561	24.712	-0.612
4.940	26.049	26.056	-0.027
5.444	28.668	28.702	-0.119
5.870	31.225	30.944	0.908
6.342	33.212	33.417	-0.611
6.905	36.376	36.373	0.000
7.609	40.038	40.070	-0.080
8.502	44.768	44.758	0.024

TABLE A.16
CALIBRATION DATA FOR THERMOCOUPLE T₁

MEASURED VOLTAGE (V)	MEASURED TEMPERATURE (°C)	CALCULATED TEMPERATURE (°C)	PERCENTAGE DIFFERENCE (%)
1.083	12.8	12.7	0.787
1.746	20.3	20.3	0.000
2.617	30.2	30.1	0.332
3.587	40.9	40.8	0.245
4.525	51.1	51.0	0.196
5.471	61.1	61.1	0.000
6.269	69.4	69.4	0.000
7.255	79.4	79.4	0.000
8.291	89.9	89.8	0.111
9.217	98.8	98.8	0.000

TABLE A.17
CALIBRATION DATA FOR THERMOCOUPLE T₂

MEASURED VOLTAGE (V)	MEASURED TEMPERATURE (°C)	CALCULATED TEMPERATURE (°C)	PERCENTAGE DIFFERENCE (%)
0.645	13.9	13.9	0.000
1.421	23.1	23.0	0.434
2.301	33.1	33.1	0.000
3.271	44.1	44.0	0.227
3.847	50.5	50.4	0.198
4.347	56.1	55.9	0.357
5.632	69.7	69.8	-0.144
6.171	75.5	75.5	0.000
7.138	85.5	85.6	-0.117
8,271	97.3	97.1	0.205

TABLE A.18
CALIBRATION DATA FOR THERMOCOUPLE T₃

MEASURED VOLTAGE (V)	MEASURED TEMPERATURE (°C)	CALCULATED TEMPERATURE (°C)	PERCENTAGE DIFFERENCE (%)
0.664	13.0	13.0	0.000
1.413	21.9	21.9	0.000
2.273	32.1	32.0	0.312
3.243	43.3	43.2	0.231
3.757	49.3	49.0	0.612
4.665	59.3	59.2	0.168
5.341	66.6	66.7	-0.150
6.008	74.0	74.0	0.000
7.129	86.1	86.1	0.000
8.432	99.9	99.8	0.100

TABLE A.19
CALIBRATION DATA FOR THERMOCOUPLE T₄

MEASURED VOLTAGE (V)	MEASURED TEMPERATURE (°C)	CALCULATED TEMPERATURE (°C)	PERCENTAGE DIFFERENCE (%)
0.634	12.0	12.0	0.000
1.418	21.4	21.3	0.469
2.250	31.1	31.0	0.322
3.251	42.4	42.4	0.000
3.753	48.1	48.1	0.000
4.251	53.6	53.6	0.000
5.459	66.9	66.7	0.299
6.096	73.5	73.5	0.000
7.365	86.7	86.7	0.000
8.671	99.9	99.8	0.100

TABLE A.20
CALIBRATION DATA FOR THERMOCOUPLE T₅

MEASURED VOLTAGE (V)	MEASURED TEMPERATURE (°C)	CALCULATED TEMPERATURE (°C)	PERCENTAGE DIFFERENCE (%)
0.655	12.2	12.2	0.000
1.451	21.7	21.6	0.462
2.273	31.1	31.1	0.000
3.286	42.7	42.7	0.000
3.772	48.2	48.1	0.207
4.290	53.9	53.8	0.185
5.410	66.1	66.0	0.151
6.152	73.8	73.8	0.000
7.250	85.1	85.1	0.000
8.720	99.9	99.8	0.100

TABLE A.21
CALIBRATION DATA FOR THERMOCOUPLE T₆

MEASURED VOLTAGE (V)	MEASURED TEMPERATURE (°C)	CALCULATED TEMPERATURE (°C)	PERCENTAGE DIFFERENCE (%)
0.666	12.1	12.1	0.000
1.427	20.5	20.6	-0.486
2.235	29.5	29.5	0.000
3.307	41.6	41.2	0.970
3.781	46.5	46.3	0.431
4.327	52.3	52.2	0.191
5.427	63.9	63.8	0.156
6.245	72.3	72.3	0.000
7.399	83.7	84.2	-0.594
8.914	99.8	99.4	0.402

TABLE A.22
CALIBRATION DATA FOR THERMOCOUPLE T₇

MEASURED VOLTAGE (V)	MEASURED TEMPERATURE (°C)	CALCULATED TEMPERATURE (°C)	PERCENTAGE DIFFERENCE (%)
0.501	11.8	11.8	0.000
1.334	21.5	21.4	0.467
2.106	30.3	30.2	0.331
3.154	41.9	41.8	0.239
3.632	47.1	47.1	0.000
4.166	52.8	52.9	-0.190
5.179	63.9	63.7	0.313
6.052	72.9	72.9	0.000
7.190	84.6	84.5	0.118
8.720	99.8	99.8	0.000

TABLE A.23
CALIBRATION DATA FOR THERMOCOUPLE T₈

MEASURED VOLTAGE (V)	MEASURED TEMPERATURE (°C)	CALCULATED TEMPERATURE (°C)	PERCENTAGE DIFFERENCE (%)
0.544	12.3	12.3	0.000
1.366	21.8	21.7	0.460
2.168	30.8	30.7	0.325
3.228	42.3	42.3	0.000
3.698	47.5	47.4	0.210
4.242	53.3	53.2	0.187
5.253	63.9	63.9	0.000
6.142	73.2	73.1	0.136
7.307	85.0	84.9	0.177
8.852	100.2	100.1	0.099

TABLE A.24
CALIBRATION DATA FOR THERMOCOUPLE T₉

MEASURED VOLTAGE (V)	MEASURED TEMPERATURE (°C)	CALCULATED TEMPERATURE (°C)	PERCENTAGE DIFFERENCE (%)
0.659	12.4	12.4	0.000
1.468	21.9	21.7	0.921
3.301	42.3	42.3	0.000
3.754	47.2	47.2	0.000
4.287	53.2	53.0	0.377
5.280	63.7	63.7	0.000
6.152	73.0	72.9	0.137
7.302	84.9	84.8	0.177
8.814	100.1	100.1	0.000

TABLE A.25
CALIBRATION DATA FOR THERMOCOUPLE T₁₀

MEASURED VOLTAGE (V)	MEASURED TEMPERATURE (°C)	CALCULATED TEMPERATURE (°C)	PERCENTAGE DIFFERENCE (%)
0.625	12.5	12.5	0.000
1.402	21.8	21.7	0.460
2.146	30.3	30.4	-0.329
3.176	42.3	42.2	0.236
3.621	47.2	47.2	0.000
4.143	53.2	53.1	0.188
5.107	63.7	63.7	0.000
5.952	72.9	72.9	0.000
7.077	84.9	84.8	0.177
8.564	100.2	100.2	0.000

TABLE A.26
CALIBRATION DATA FOR THERMOCOUPLE T₁₁

MEASURED VOLTAGE (V)	MEASURED TEMPERATURE (°C)	CALCULATED TEMPERATURE (°C)	PERCENTAGE DIFFERENCE (%)
0.567	12.7	12.7	0.000
1.395	22.4	22.5	0.448
2.131	30.9	30.8	0.324
3.012	40.9	40.8	0.245
3.641	47.8	47.9	-0.209
4.166	53.8	53.7	0.186
5.149	64.5	64.4	0.155
5.996	73.5	73.5	0.000
7.145	85.5	85.5	0.000
8.568	100.1	100.0	0.100

TABLE A.27
CALIBRATION DATA FOR THERMOCOUPLE T₁₂

MEASURED VOLTAGE (V)	MEASURED TEMPERATURE (°C)	CALCULATED TEMPERATURE (°C)	PERCENTAGE DIFFERENCE (%)
0.527	12.3	12.2	0.819
1.376	22.2	22.3	-0.449
2.025	30.1	29.9	0.668
2.985	41.2	41.1	0.243
3.547	47.6	47.6	0.000
4.217	55.2	55.2	0.000
4.903	62.9	62.9	0.000
5.721	72.1	72.1	0.000
6.817	84.3	84.1	0.237
8.262	99.6	99.6	0.000

TABLE A.28
CALIBRATION DATA FOR THERMOCOUPLE T₁₃

MEASURED VOLTAGE (V)	MEASURED TEMPERATURE (°C)	CALCULATED TEMPERATURE (°C)	PERCENTAGE DIFFERENCE (%)
0.871	12.6	12.6	0.000
1.511	20.3	20.3	0.000
2.361	30.7	30.5	0.655
3.233	40.9	40.7	0.491
4.128	50.9	51.0	-0.197
4.982	60.9	60.8	0.164
5.850	70.2	70.3	-0.426
6.593	78.7	78.7	0.000
7.204	85.8	85.4	0.468
8.497	99.2	99.2	0.000

TABLE A.29
CALIBRATION DATA FOR THERMOCOUPLE T₁₄

MEASURED VOLTAGE (V)	MEASURED TEMPERATURE (°C)	CALCULATED TEMPERATURE (°C)	PERCENTAGE DIFFERENCE (%)
1.131	12.5	12.5	0.000
1.726	19.6	19.6	0.000
2.588	29.9	29.8	0.335
3.627	42.1	41.8	0.717
4.463	51.3	51.3	0.000
5.341	60.9	61.1	-0.328
6.128	70.4	70.3	0.142
7.168	80.9	80.9	0.000
7.970	89.4	89.4	0.000
8.855	98.6	98.5	0.101

TABLE A.30
CALIBRATION DATA FOR THERMOCOUPLE T₁₅

MEASURED VOLTAGE (V)	MEASURED TEMPERATURE (°C)	CALCULATED TEMPERATURE (°C)	PERCENTAGE DIFFERENCE (%)
0.956	11.1	11.1	0.000
1.834	21.7	21.7	0.000
2.533	30.1	30.0	0.333
3.537	41.7	41.7	0.000
4.191	49.2	49.2	0.000
5.412	62.9	62.8	0.159
6.116	70.6	70.5	0.141
6.959	79.6	79.6	0.000
7.737	87.8	87.8	0.000
8.845	99.3	99.2	0.100

TABLE A.31
CALIBRATION DATA FOR THERMOCOUPLE T₁₆

MEASURED VOLTAGE (V)	MEASURED TEMPERATURE (°C)	CALCULATED TEMPERATURE (°C)	PERCENTAGE DIFFERENCE (%)
0.675	11.1	11.1	0.000
1.371	19.0	18.9	0.529
2.195	27.9	27.9	0.000
3.321	39.8	39.8	0.000
4.210	48.9	48.8	0.204
5.110	57.8	57.7	0.173
5.952	65.8	65.8	0.000
6.956	75.1	75.0	0.133
8.284	86.7	86.7	0.000
9.781	99.2	99.1	0.100

TABLE A.32
CALIBRATION DATA FOR THERMOCOUPLE T₁₇

MEASURED VOLTAGE (V)	MEASURED TEMPERATURE (°C)	CALCULATED TEMPERATURE (°C)	PERCENTAGE DIFFERENCE (%)
0.776	11.2	11.1	0.900
1.561	20.4	20.4	0.000
2.602	32.6	32.5	0.307
3.446	42.2	42.2	0.000
4.562	54.8	54.7	0.182
5.495	65.0	65.0	0.000
5.970	70.2	70.2	0.000
7.014	81.4	81.3	0.123
7.844	90.1	90.0	0.111
8.799	99.8	99.8	0.000

TABLE A.33
CALIBRATION DATA FOR THERMOCOUPLE T₁₈

MEASURED VOLTAGE (V)	MEASURED TEMPERATURE (°C)	CALCULATED TEMPERATURE (°C)	PERCENTAGE DIFFERENCE (%)
1.009	14.7	14.7	0.000
1.431	19.2	19.2	0.000
2.156	27.0	26.9	0.371
3.077	36.8	36.5	0.821
3.715	42.9	43.1	-0.465
5.175	57.9	57.9	0.000
6.729	73.5	73.2	0.409
7.479	80.5	80.5	0.000
8.565	90.8	90.8	0.000
9.477	99.3	99.3	0.000

TABLE A.34
THERMOCOUPLE CALIBRATION EQUATIONS

T_1	=	0.146191	+	11.776490V	-	0.1160658V ²
T_2	=	6.362958	+	11.882968V	-	0.1092592V ²
T_3	=	5.045472	+	12.113481V	-	0.1038098V ²
T_4	=	4.407498	+	12.128836V	-	0.1290816V ²
T_5	=	4.324521	+	12.125987V	-	0.1342778V ²
T_6	=	4.596831	+	11.352337V	-	0.0795628V ²
T_7	=	5.984857	+	11.738862V	-	0.1123962V ²
T_8	=	6.106876	+	11.580003V	-	0.1074142V ²
T_9	=	4.784898	+	11.697097V	-	0.0999316V ²
T_{10}	=	5.002559	+	12.073867V	-	0.1116786V ²
T_{11}	=	5.991961	+	11.909365V	-	0.1085042V ²
T_{12}	=	5.911193	+	12.065597V	-	0.0867634V ²
T_{13}	=	2.011159	+	12.303742V	-	0.1007002V ²
T_{14}	=	-1.195715	+	12.283726V	-	0.1151167V ²
T_{15}	=	-0.666289	+	12.438887V	-	0.1292127V ²
T_{16}	=	3.419812	+	11.561740V	-	0.1812599V ²
T_{17}	=	1.819366	+	12.107838V	-	0.1097483V ²
T_{18}	=	3.744495	+	10.995479V	-	0.0919899V ²

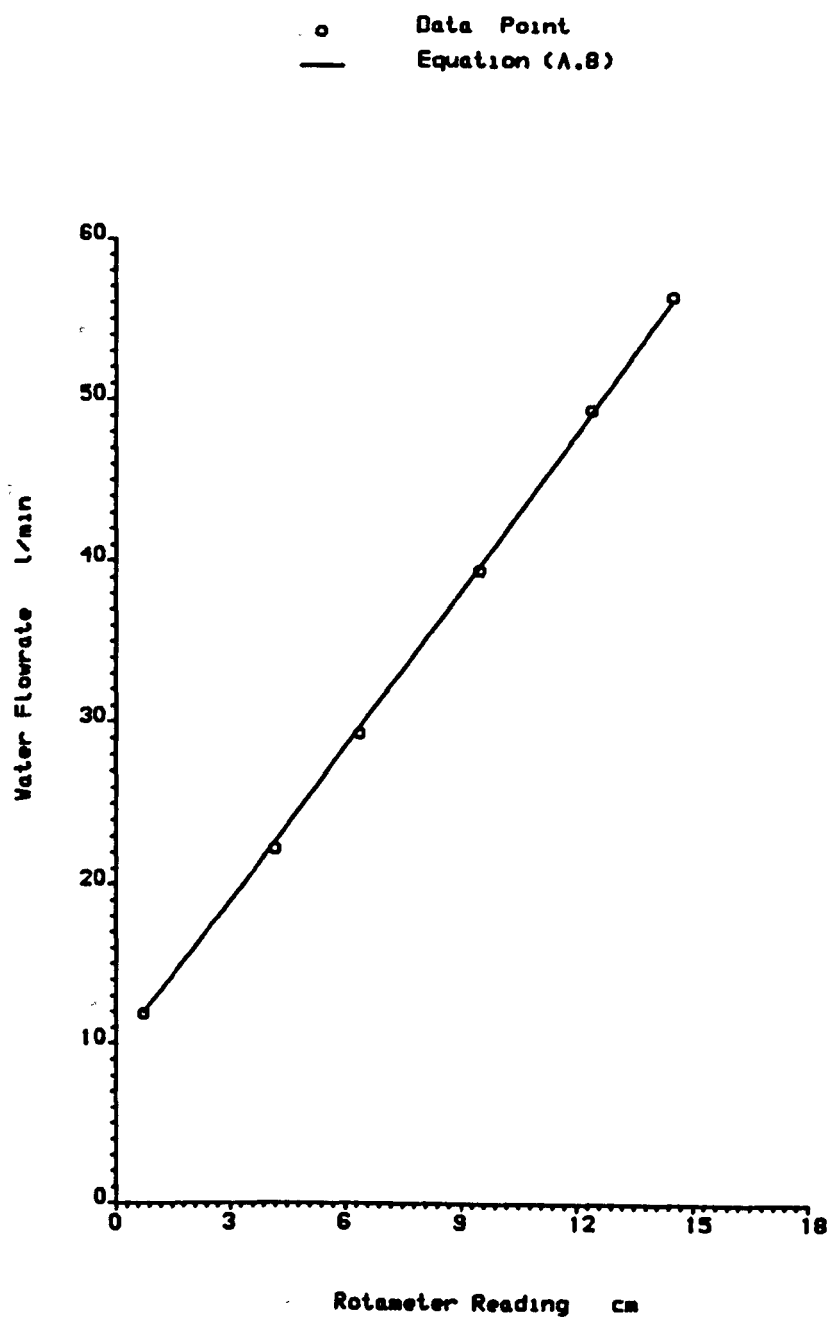
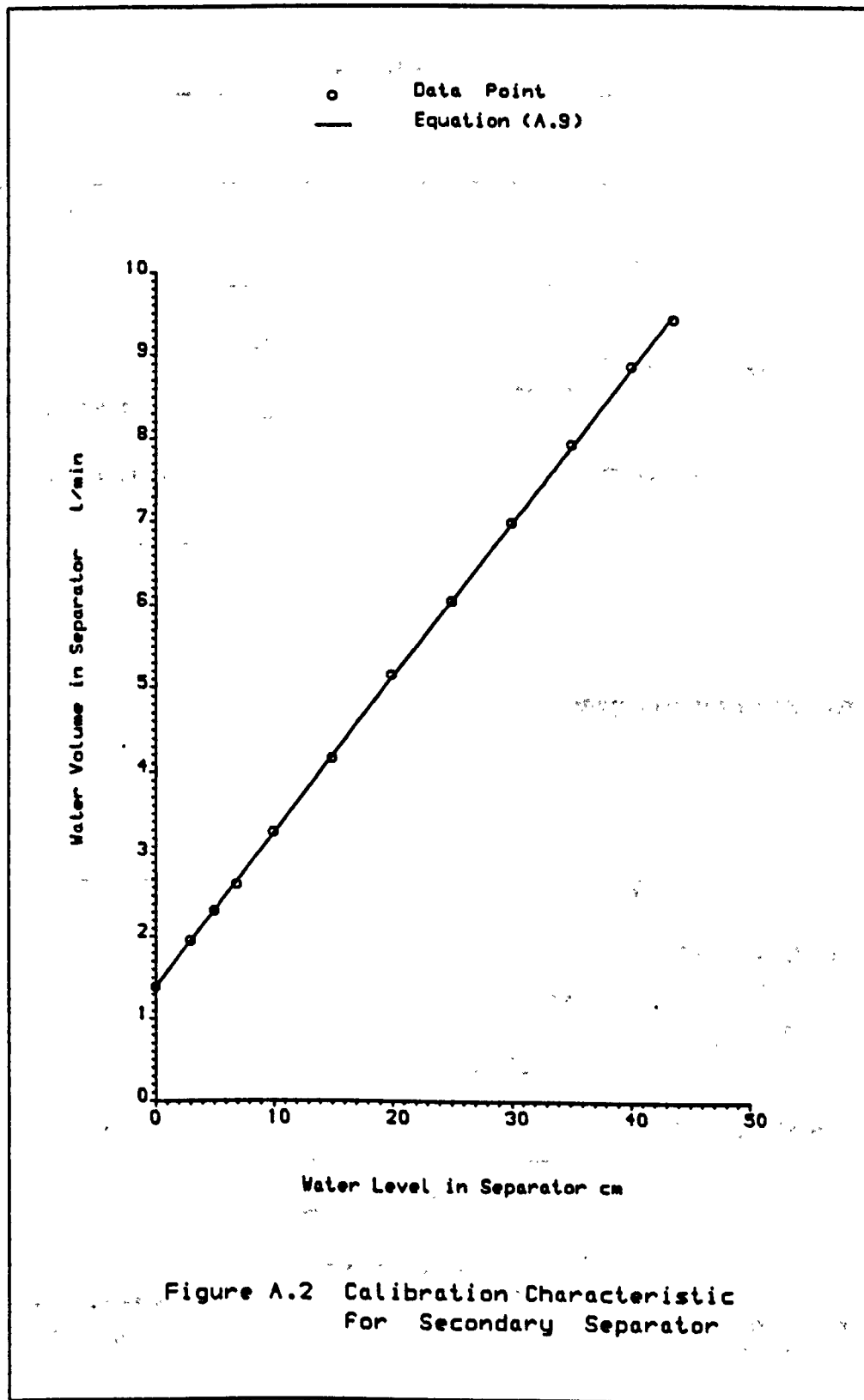


Figure A.1 Calibration Characteristic
For Water Rotameter



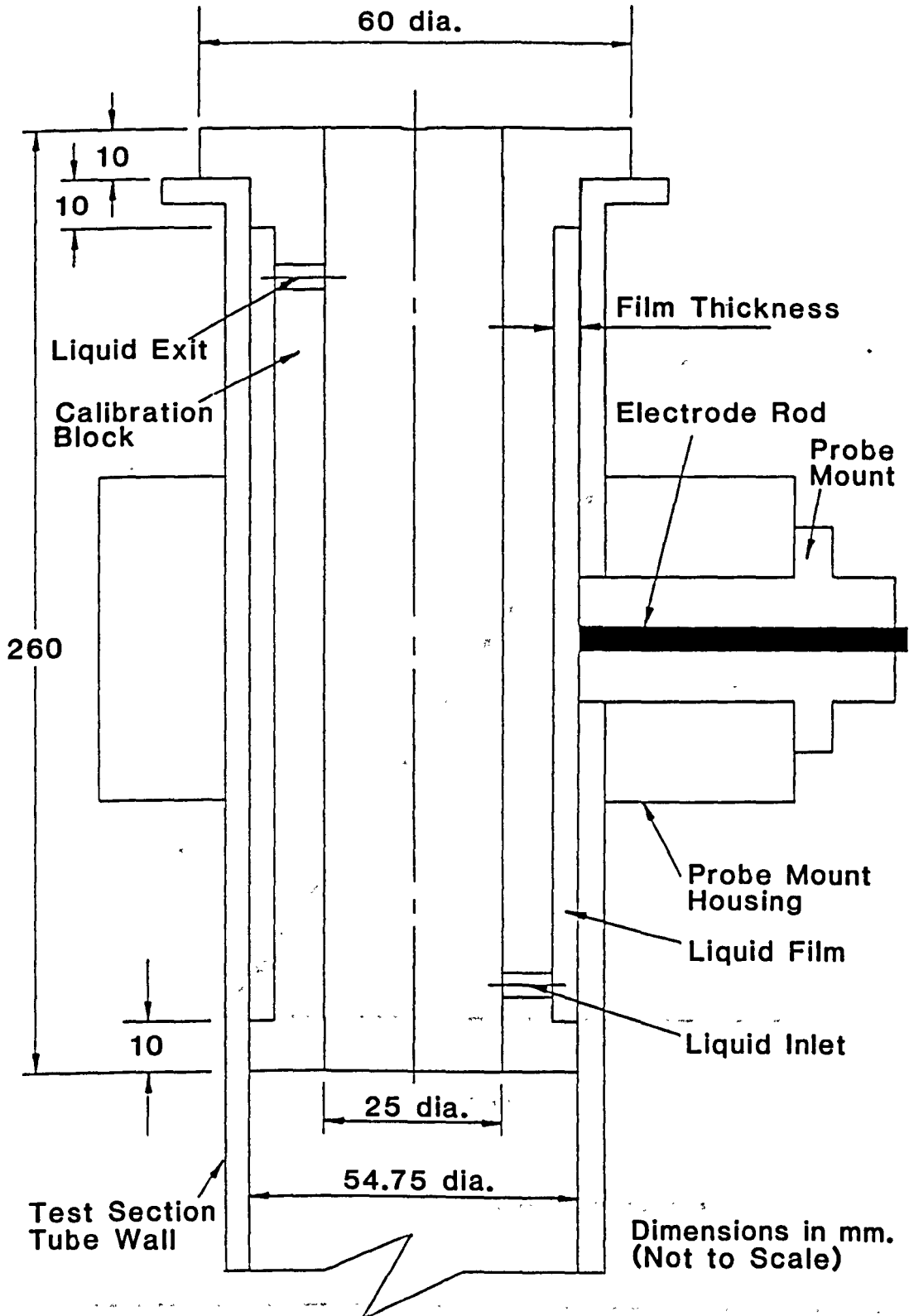
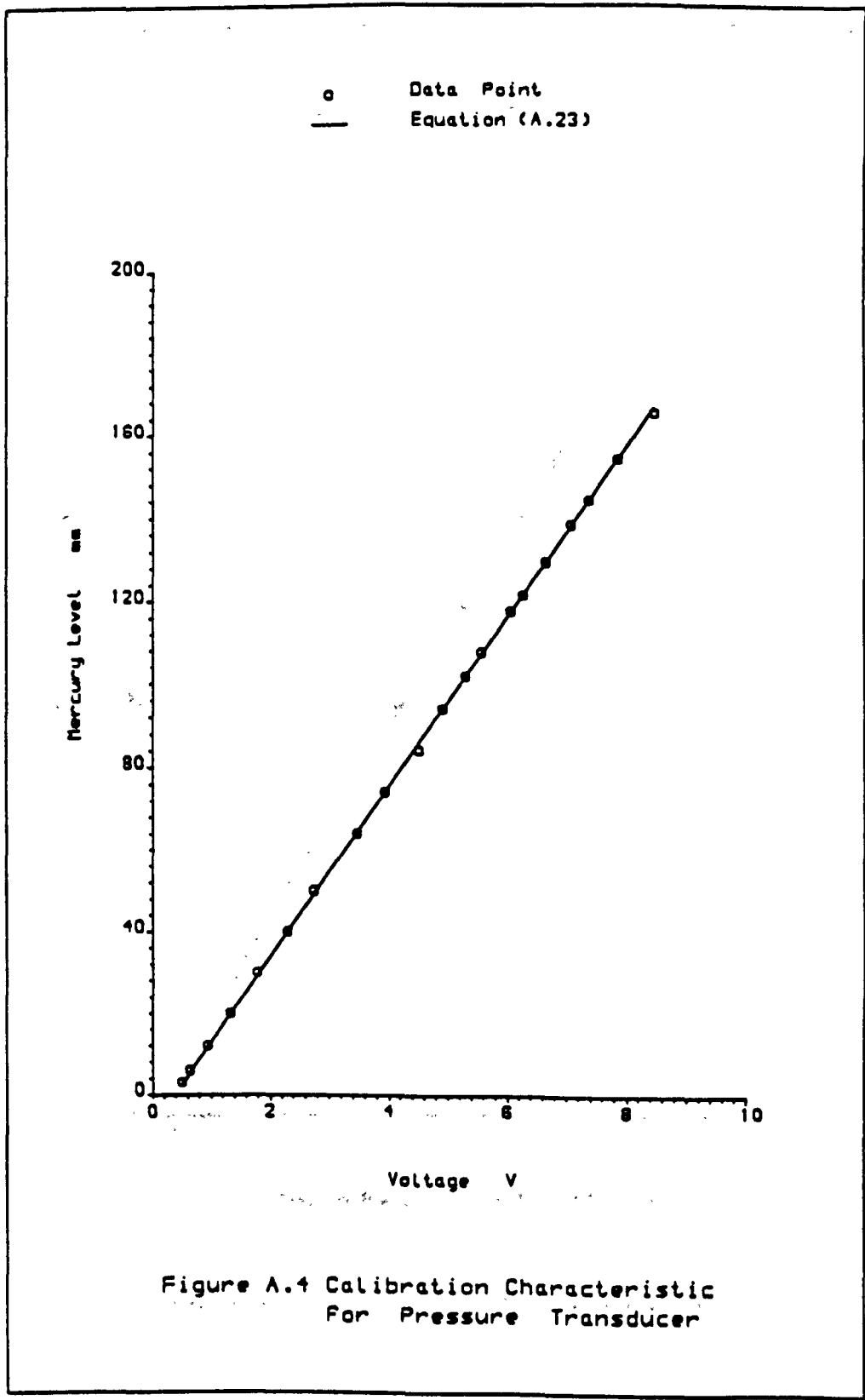
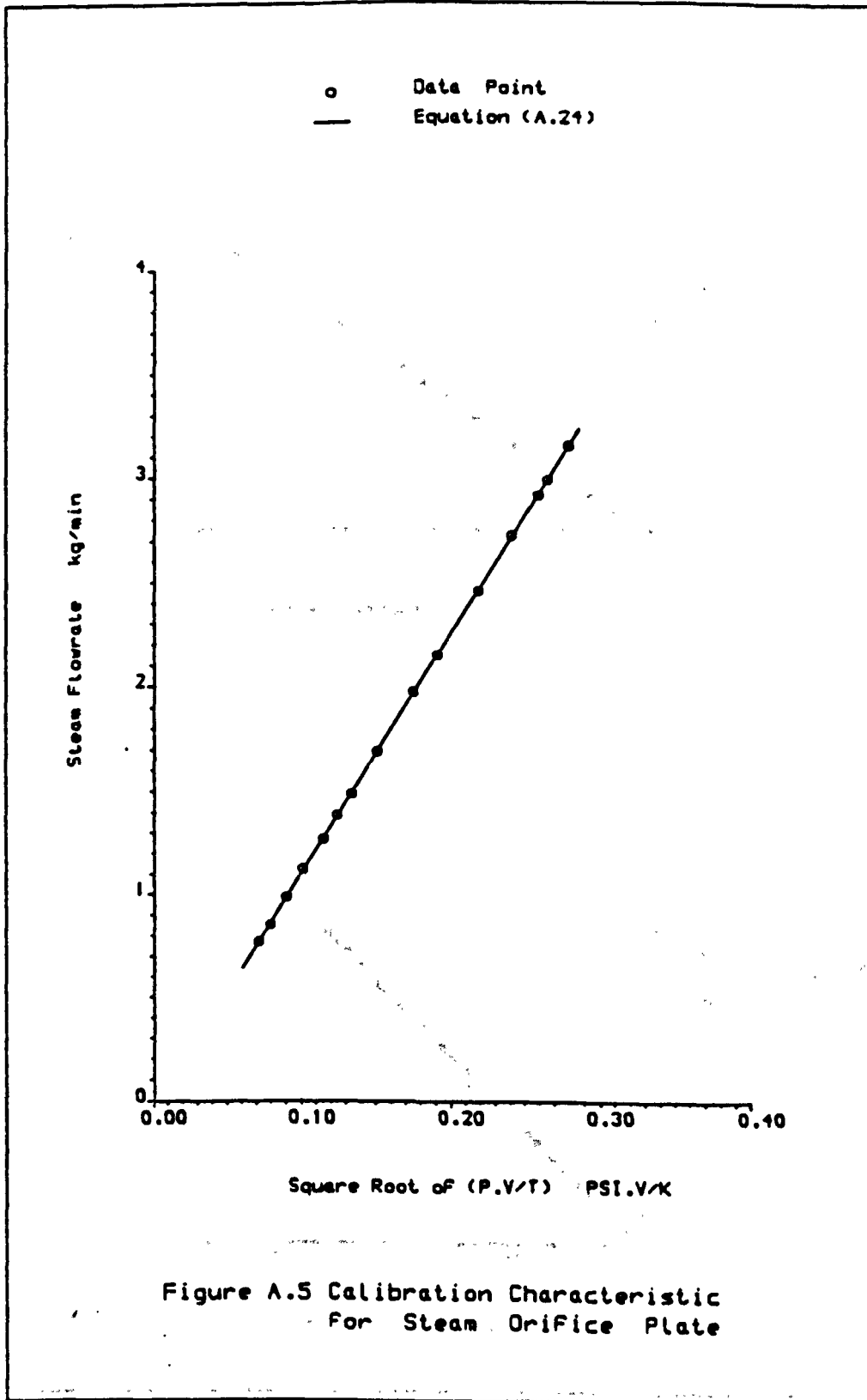
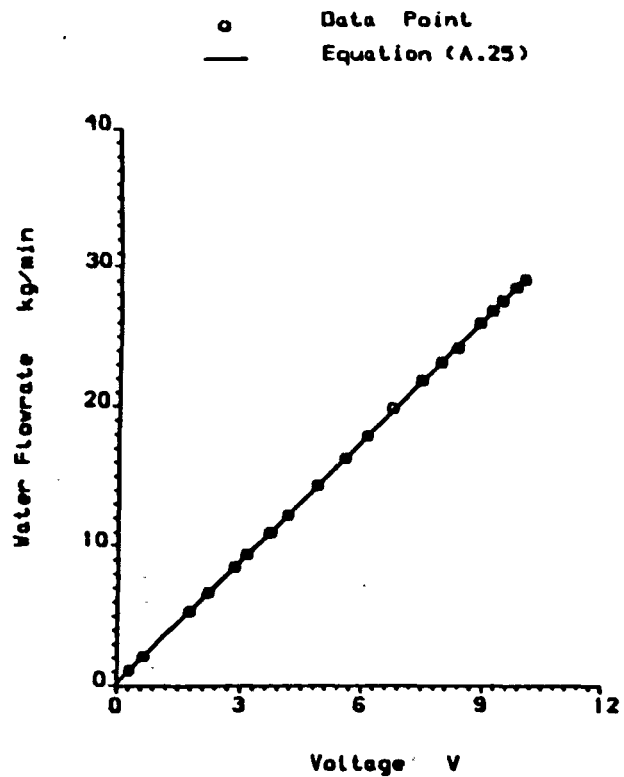


Figure A.3 Liquid Film Thickness Calibration Block in Location

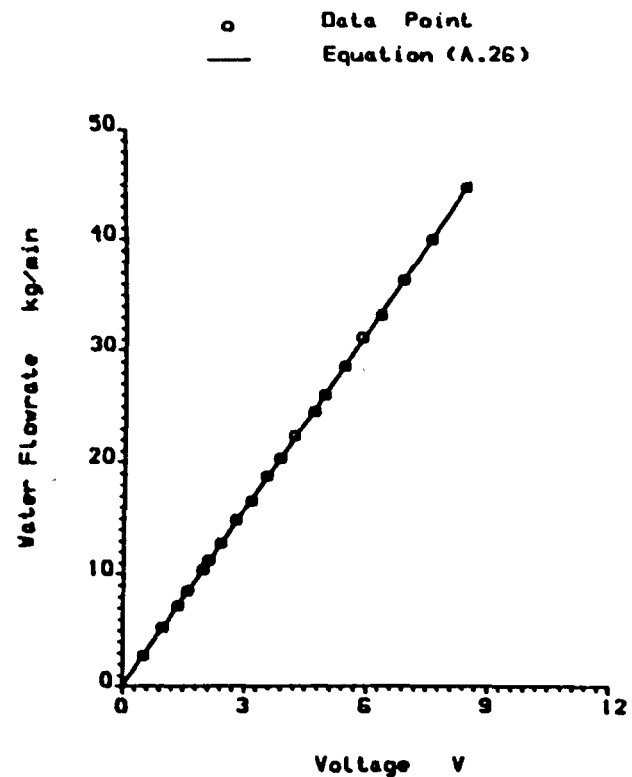






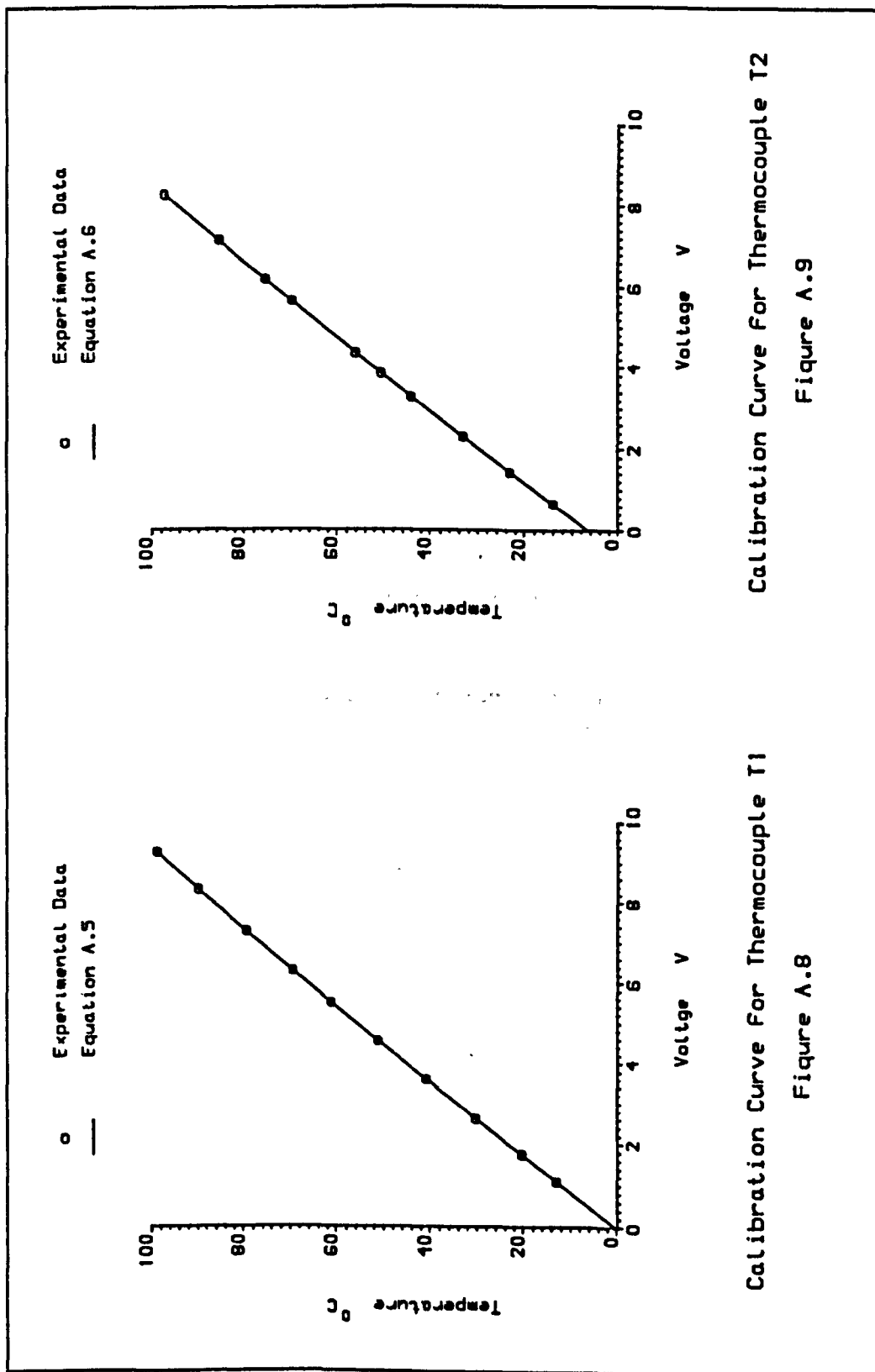
Calibration Characteristic For Cooling Water Turbine Flow Meter

Figure A.6



Calibration Characteristic For Discharge Water Turbine Flow Meter

Figure A.7



Calibration Curve for Thermocouple T1

Figure A.8

Calibration Curve for Thermocouple T2

Figure A.9

APPENDIX B

AIR-WATER DATA

APPENDIX B

In air-water tests, each particular test is given a reference number consisting of 10 digits. The first three pairs of digits correspond to the day, month and year respectively on which the test was carried out. The fourth pair refer to the inlet water flow whilst the last pair of digits correspond to the inlet air flow. The definition of symbols used in the tables are:-

Test No.	Test number
Q_f	Water Volumetric flowrate, l/min.
P_{atm}	Atmospheric pressure, bar.
T_{fin}	Inlet water temperature, °C.
WC	Water conductivity, MSiEM/mm.
Q_{asup}	Supply air volumetric flowrate, l/min.
Q_{atst}	Test section air volumetric flowrate, l/min.
T_{atst}	Test section air temperature, °C.
Q_{aL}	Extracted (leaked) air volumetric flowrate, l/min.
T_{aL}	Extracted (leaked) air temperature, °C.
PD	Pressure difference, KN/m ² .
TT	Top (upper) film thickness, mm.
TL	Bottom (lower) film thickness, mm.
M_f	Water mass flowrate, kg/min.
M_{asup}	Supply air mass flowrate, kg/min.
M_{atst}	Test section air mass flowrate, kg/min.
M_{aL}	Extracted (leaked) air mass flowrate, kg/min.
ρ_{atst}	Test section air density, kg/m ³ .
ρ_{aL}	Extracted (leaked) air density, kg/m ³ .
J_f^*	Wallis liquid parameter.
J_a^*	Wallis air parameter.

TABLE B.1a

Air-Water Data (Low Air Extraction Rate Tests)

Qf = 4.000 l/min Patm = 1.0040 Bar

TEST NO	Tfin	WC	Qasup	Qatst	Tatst	QaL	TaL	PD	TT	TL
1609850401	13.9	3.364	239.81	7.32	16.2	232.49	30.2	0.0699	0.4310	0.4159
1609850402	13.9	3.639	277.72	44.38	18.1	233.34	31.1	0.0318	0.4573	0.4719
1609850403	13.9	3.621	371.12	138.30	18.1	232.82	31.3	0.0539	0.4804	0.5098
1609850404	13.9	3.599	487.49	254.12	18.3	233.37	31.5	0.0942	0.5039	0.4822
1609850405	13.9	3.611	565.45	332.08	18.2	233.37	31.7	0.1323	0.5444	0.4723
1609850406	13.9	3.611	667.32	433.95	18.3	233.37	32.1	0.1982	0.5450	0.4731
1609850407	13.9	3.612	790.08	556.59	18.3	233.49	32.4	0.3037	0.5476	0.4751
1609850408	13.8	3.625	915.20	680.89	18.3	234.31	32.8	0.2349	0.5385	0.5071
1609850409	13.8	3.653	1076.95	842.46	18.4	234.49	32.9	0.4132	0.5349	0.4986
1609850410	13.8	3.651	1216.97	981.66	18.4	235.31	32.9	0.4557	0.5364	0.5213
1609850411	13.8	3.665	1276.29	1040.11	18.5	236.18	33.1	0.4433	0.5499	0.4761
1609850412	13.9	3.653	1363.67	1127.49	18.5	236.18	33.2	0.4091	0.5440	0.4704
1609850413	13.9	3.643	1431.55	1194.72	18.8	236.83	33.3	0.7857	0.5524	0.4721
1609850414	13.9	3.652	1528.07	1290.89	18.9	237.18	33.5	0.9153	0.5531	0.4802
1609850415	13.9	3.655	1547.12	1309.80	19.1	237.32	33.5	1.0154	0.5612	0.5028
1609850416	13.9	3.671	1565.26	1327.94	19.2	237.32	33.6	3.9330	0.5875	0.5237

TABLE B.1b

Air-Water Data (Low Air Extraction Rate Tests)

Qf = 5.000 l/min Patm = 1.0080 Bar

TEST NO	Tfin	WC	Qasup	Qatst	Tatst	QaL	TaL	PD	TT	TL
1709850501	14.0	3.541	240.37	8.98	14.0	231.39	26.0	0.2138	0.4789	0.4521
1709850502	14.0	3.553	301.77	69.70	14.4	232.07	26.4	0.1893	0.4782	0.4587
1709850503	14.0	3.550	389.65	156.83	14.6	232.82	27.0	0.2639	0.4829	0.4606
1709850504	14.0	3.551	451.56	218.19	14.8	233.37	27.5	0.3012	0.4856	0.4552
1709850505	14.0	3.553	512.97	279.48	15.0	233.49	27.8	0.2973	0.4855	0.4632
1709850506	14.0	3.550	580.39	346.58	15.2	233.81	28.2	0.3241	0.4884	0.4655
1709850507	14.0	3.551	678.77	444.58	15.6	234.19	28.6	0.4277	0.4893	0.4611
1709850508	14.0	3.552	794.56	560.64	15.8	233.92	29.2	0.4961	0.4910	0.4765
1709850509	14.0	3.550	862.02	628.53	15.9	233.49	29.8	0.4858	0.4949	0.4756
1709850510	14.0	3.552	977.84	744.09	15.9	233.75	30.3	0.5044	0.5013	0.4832
1709850511	14.0	3.523	1078.02	843.72	16.0	234.30	30.5	0.4539	0.5012	0.4801
1709850512	14.0	3.553	1119.30	884.81	16.0	234.49	30.9	0.4643	0.5007	0.4922
1709850513	14.0	3.557	1180.19	945.70	16.2	234.49	31.0	0.4318	0.5059	0.5103
1709850514	14.0	3.560	1331.03	1096.32	16.2	234.71	31.2	0.5012	0.5129	0.5179
1709850515	14.0	3.564	1380.29	1145.34	16.2	234.95	31.4	0.8714	0.5086	0.5231
1709850516	14.0	3.565	1463.98	1228.97	16.2	235.01	31.5	0.9626	0.5145	0.5256
1709850517	14.0	3.567	1511.56	1276.44	16.3	235.12	31.6	1.2604	0.5207	0.5367
1709850518	14.0	3.571	1520.54	1285.42	16.3	235.12	31.6	4.2686	0.5661	0.5829

TABLE B.1c

Air-Water Data (Low Air Extraction Rate Tests)

Qf = 6.000 l/min Pata = 1.0080 Bar

TEST NO	Tfin	WC	Qasup	Qatst	Tatst	QaL	TaL	PD	TT	TL
1709850601	14.0	3.563	244.75	9.04	15.0	235.71	27.0	0.3319	0.6035	0.5719
1709850602	14.0	3.567	327.98	92.16	14.8	235.82	28.0	0.3341	0.6170	0.5931
1709850603	14.0	3.569	436.89	199.87	14.8	237.02	28.7	0.3470	0.6173	0.5913
1709850604	14.0	3.569	528.84	291.82	14.8	237.02	29.1	0.3558	0.6201	0.5862
1709850605	14.0	3.569	611.39	374.09	14.9	237.30	29.6	0.4738	0.6218	0.5849
1709850606	14.0	3.572	722.24	483.69	14.7	238.55	30.3	0.6972	0.6269	0.5856
1709850607	14.0	3.576	835.51	596.28	14.6	239.23	30.8	0.7552	0.6326	0.6005
1709850608	14.0	3.568	965.66	726.24	14.6	239.42	31.3	0.9967	0.6318	0.6073
1709850609	14.0	3.583	1046.03	805.80	14.6	240.23	31.5	1.0352	0.6379	0.5959
1709850610	14.0	3.584	1161.62	921.23	14.7	240.39	31.7	1.1809	0.6416	0.5941
1709850611	14.0	3.585	1270.22	1029.67	14.7	240.55	31.8	1.1516	0.6440	0.5936
1709850612	14.0	3.590	1356.80	1115.49	14.9	241.31	32.0	1.4037	0.6432	0.5983
1709850613	14.0	3.592	1456.45	1215.14	15.1	241.31	32.1	1.6385	0.6488	0.5915
1709850614	13.9	3.592	1488.46	1247.02	15.4	241.44	32.2	3.8864	0.6453	0.6263

TABLE B.1d

Air-Water Data (Low Air Extraction Rate Tests)

Qf = 7.000 l/min Pata = 1.0080 Bar

TEST NO	Tfin	WC	Qasup	Qatst	Tatst	QaL	TaL	PD	TT	TL
1709850701	13.8	3.664	243.51	7.34	14.5	236.17	25.0	0.5433	0.6695	0.6332
1709850702	13.8	3.654	315.23	78.74	14.5	236.49	26.5	0.5857	0.6785	0.6419
1709850703	13.8	3.652	406.83	170.01	14.3	236.82	27.7	0.8465	0.6801	0.6395
1709850704	13.8	3.650	493.57	255.38	14.3	238.19	28.0	0.8966	0.6797	0.6344
1709850705	13.8	3.648	562.93	324.38	14.3	238.55	28.6	0.9305	0.6728	0.6324
1709850706	13.8	3.650	704.84	465.92	14.2	238.92	29.0	1.0973	0.6785	0.6334
1709850707	13.8	3.648	861.82	622.79	15.0	239.03	29.3	1.1677	0.6707	0.6395
1709850708	13.8	3.647	949.09	710.06	15.3	239.03	29.5	1.1147	0.6711	0.6355
1709850709	13.9	3.647	1092.30	853.27	15.7	239.03	29.8	1.0932	0.6696	0.6316
1709850710	13.9	3.645	1195.68	956.56	15.8	239.12	30.1	1.2819	0.6723	0.6327
1709850711	13.9	3.643	1267.44	1028.32	16.0	239.12	30.4	1.3720	0.6727	0.6341
1709850712	13.9	3.642	1439.34	1200.12	16.4	239.22	30.4	1.6611	0.6739	0.6315
1709850713	13.9	3.645	1467.77	1228.55	16.6	239.22	30.5	1.8104	0.6749	0.6418
1709850714	13.9	3.643	1484.77	1245.55	16.6	239.22	30.5	5.1642	0.6864	0.6530

TABLE B.1e

Air-Water Data (Low Air Extraction Rate Tests)

Qf = 8.000 l/min Pata = 1.0080 Bar

TEST NO	Tfin	WC	Qasup	Qatst	Tatst	QaL	TaL	PD	TT	TL
1709850801	15.0	3.659	240.94	8.33	17.0	232.61	29.0	0.7138	0.6816	0.6646
1709850802	15.0	3.632	325.63	82.61	15.7	243.02	29.4	0.9456	0.6852	0.6628
1709850803	15.0	3.637	439.15	195.86	15.0	243.29	29.7	1.1664	0.6834	0.6712
1709850804	15.1	3.637	718.88	475.51	15.0	243.37	29.8	1.1948	0.6882	0.6775
1709850805	15.1	3.637	782.68	539.03	15.4	243.65	30.3	1.3233	0.6899	0.6735
1709850806	15.0	3.638	933.51	689.63	15.5	243.88	30.7	1.4539	0.6897	0.6725
1709850807	15.0	3.638	1030.17	786.29	15.6	243.88	30.8	1.4521	0.6872	0.6701
1709850808	15.0	3.639	1144.84	900.28	15.8	244.56	30.9	1.4519	0.6826	0.6488
1709850809	15.0	3.638	1304.05	1058.87	16.0	245.18	31.0	1.4549	0.6900	0.6559
1709850810	15.0	3.638	1375.51	1130.18	16.2	245.33	31.2	1.5062	0.6929	0.6503
1709850811	15.0	3.639	1417.28	1171.95	16.2	245.33	31.6	1.5254	0.6885	0.6594
1709850812	15.0	3.638	1446.47	1200.48	16.6	245.99	31.9	1.6577	0.6936	0.6685
1709850813	15.0	3.637	1461.48	1215.41	16.6	246.07	32.3	1.9832	0.6964	0.6701
1709850814	15.0	3.639	1470.21	1223.90	16.6	246.31	32.4	5.1772	0.6931	0.6802

TABLE B.1f

Air-Water Data (Low Air Extraction Rate Tests)

Qf = 9.000 l/min Pata = 1.0079 Bar

TEST NO	Tfin	WC	Qasup	Qatst	Tatst	QaL	TaL	PD	TT	TL
1809850901	15.3	3.632	249.09	9.08	16.0	240.01	28.0	0.8652	0.7129	0.6801
1809850902	15.3	3.633	311.99	71.43	15.8	240.56	30.3	1.3431	0.7184	0.6874
1809850903	15.3	3.633	398.71	158.32	15.2	240.39	30.8	1.4111	0.7166	0.6845
1809850904	15.3	3.633	545.40	304.30	15.1	241.10	31.1	1.4431	0.7134	0.6771
1809850905	15.3	3.633	663.27	421.90	15.1	241.37	31.3	1.4661	0.7174	0.6768
1809850906	15.2	3.634	760.78	518.87	15.0	241.91	31.6	1.5596	0.7169	0.6742
1809850907	15.3	3.633	941.47	699.06	14.8	242.41	31.8	1.5327	0.7132	0.6784
1809850908	15.3	3.634	1100.03	857.12	14.7	242.91	32.2	1.4332	0.6984	0.6832
1809850909	15.3	3.635	1207.66	965.38	15.6	242.28	32.3	1.5876	0.7052	0.6793
1809850910	15.3	3.635	1300.85	1057.56	15.6	243.29	32.7	1.5555	0.7190	0.6824
1809850911	15.2	3.636	1382.10	1138.08	16.5	244.02	32.9	1.7255	0.7223	0.6829
1809850912	15.3	3.634	1416.22	1172.20	16.6	244.02	33.0	4.8574	0.7251	0.6955

TABLE B.1g

Air-Water Data (Low Air Extraction Rate Tests)

Qf = 10.000 l/min Patm = 1.0081 Bar

TEST NO	Tfin	WC	Qasup	Qatst	Tatst	QaL	TaL	PD	TT	TL
1809851001	15.0	3.633	245.76	9.56	15.0	236.20	29.0	0.8900	0.7371	0.7396
1809851002	15.0	3.636	298.94	62.28	15.8	236.66	29.6	1.1906	0.7385	0.7331
1809851003	15.0	3.637	406.40	169.54	15.2	236.86	30.3	1.3503	0.7382	0.7353
1809851004	15.0	3.629	585.26	348.34	15.3	236.92	30.6	1.3731	0.7381	0.7380
1809851005	15.0	3.612	730.84	493.92	15.4	236.92	31.1	1.4279	0.7392	0.7394
1809851006	14.9	3.588	929.59	692.57	15.7	237.02	31.8	1.4778	0.7418	0.7369
1809851007	14.9	3.577	1072.31	835.29	15.8	237.02	32.0	1.6239	0.7414	0.7404
1809851008	14.9	3.567	1206.65	969.46	16.0	237.19	32.3	1.7006	0.7387	0.7386
1809851009	14.9	3.562	1301.41	1064.22	16.0	237.19	32.5	1.8851	0.7434	0.7381
1809851010	14.9	3.557	1327.75	1090.56	16.0	237.19	32.6	1.9841	0.7449	0.7423
1809851011	14.9	3.556	1366.75	1129.43	16.0	237.32	32.7	2.1799	0.7495	0.7499
1809851012	14.9	3.548	1397.82	1160.50	16.0	237.32	32.7	5.0177	0.7527	0.7714

TABLE B.1h

Air-Water Data (Low Air Extraction Rate Tests)

Qf = 11.197 l/min Patm = 1.0067 Bar

TEST NO	Tfin	WC	Qasup	Qatst	Tatst	QaL	TaL	PD	TT	TL
1909851101	13.3	3.581	250.30	10.18	14.0	240.12	28.5	0.9308	0.8301	0.7844
1909851102	13.3	3.575	319.80	79.58	15.2	240.22	29.0	1.2235	0.8383	0.8088
1909851103	13.3	3.573	436.72	195.86	15.0	240.86	29.3	1.3739	0.8269	0.8081
1909851104	13.3	3.568	529.31	288.76	14.9	240.55	29.5	1.4549	0.8345	0.8044
1909851105	13.3	3.566	623.57	382.55	15.5	241.02	29.7	1.4415	0.8443	0.8042
1909851106	13.3	3.565	701.48	460.14	15.7	241.34	29.8	1.4584	0.8499	0.8037
1909851107	13.3	3.565	800.54	559.52	16.2	241.02	29.9	1.5617	0.8558	0.8035
1909851108	13.3	3.563	922.98	681.48	16.5	241.50	30.0	1.6089	0.8416	0.8027
1909851109	13.2	3.562	1078.94	837.22	16.8	241.72	30.1	1.6311	0.8714	0.8181
1909851110	13.2	3.562	1285.51	1043.40	16.8	242.11	30.2	1.6985	0.8922	0.8377
1909851111	13.2	3.565	1315.63	1073.21	17.0	242.42	30.3	1.9209	0.8919	0.8423
1909851112	13.3	3.566	1335.62	1093.20	16.9	242.42	30.3	5.4925	0.9047	0.9022

TABLE B.1i

Air-Water Data (Low Air Extraction Rate Tests)

Qf = 12.710 l/min Patm = 1.0083 Bar

TEST NO	Tfin	WC	Qasup	Qatst	Tatst	QaL	TaL	PD	TT	TL
2009851201	13.5	3.586	256.07	10.95	14.0	245.12	30.0	1.0869	0.8839	0.8516
2009851202	13.5	3.590	301.78	56.30	14.1	245.48	30.2	1.2113	0.8891	0.8573
2009851203	13.5	3.600	418.99	173.17	14.2	245.82	30.3	1.4539	0.8950	0.8651
2009851204	13.5	3.592	595.01	349.68	15.0	245.33	30.5	1.4518	0.9171	0.8759
2009851205	13.5	3.602	657.26	411.59	16.3	245.67	30.8	1.6218	0.8992	0.8834
2009851206	13.6	3.606	752.36	506.43	16.4	245.93	31.4	1.6260	0.8917	0.8689
2009851207	13.6	3.605	845.70	599.77	16.5	245.93	31.6	1.7048	0.8819	0.8776
2009851208	13.6	3.602	942.94	696.39	16.6	246.55	31.7	1.7638	0.9369	0.8818
2009851209	13.6	3.599	1024.46	777.55	16.8	246.91	31.9	1.7772	0.9339	0.8990
2009851210	13.6	3.594	1169.60	922.69	17.0	246.91	32.0	1.8831	0.9278	0.9027
2009851211	13.6	3.584	1249.29	1002.15	17.1	247.14	32.1	2.0369	1.0261	0.8959
2009851212	13.6	3.533	1310.41	1062.64	17.1	247.77	32.1	5.1877	1.0597	0.9175

TABLE B.1j

Air-Water Data (Low Air Extraction Rate Tests)

Qf = 14.229 l/min Patm = 1.0080 Bar

TEST NO	Tfin	WC	Qasup	Qatst	Tatst	QaL	TaL	PD	TT	TL
2009851401	13.7	3.548	256.67	9.29	14.0	247.38	29.1	1.1865	0.9687	0.9283
2009851402	13.7	3.547	319.47	70.56	15.8	248.91	29.4	1.3891	0.9505	0.9467
2009851403	13.7	3.547	413.88	164.97	15.8	248.91	29.7	1.4456	0.9763	0.9469
2009851404	13.8	3.549	550.79	301.61	16.0	249.18	29.9	1.5250	0.9849	0.9574
2009851405	13.8	3.549	672.40	422.91	16.2	249.49	30.3	1.5949	1.0421	0.9405
2009851406	13.8	3.549	761.20	511.71	16.4	249.49	40.5	1.5761	1.0439	0.9484
2009851407	13.7	3.549	822.50	572.79	16.5	249.71	30.8	1.5503	1.0448	0.9523
2009851408	13.8	3.551	999.51	748.51	16.6	251.00	31.0	1.7912	1.0719	0.9308
2009851409	13.8	3.557	1138.04	886.89	16.8	251.15	31.2	1.8686	1.0903	0.9439
2009851410	13.8	3.559	1172.42	920.93	17.0	251.49	31.3	1.9467	1.0689	0.9532
2009851411	13.8	3.559	1211.97	960.24	17.1	251.73	31.3	2.0408	1.0972	0.9558
2009851412	13.8	3.527	1255.21	1003.48	17.1	251.73	31.3	5.9292	1.1406	0.9605

TABLE B.1k

Air-Water Data (Low Air Extraction Rate Tests)

Qf = 15.755 l/min Pats = 1.0085 Bar

TEST NO	Tfin	WC	Qasup	Qatst	Tatst	QaL	TaL	PD	TT	TL
2309851501	13.8	3.562	260.80	8.33	13.8	252.47	29.0	1.2528	0.9867	0.9791
2309851502	13.8	3.566	322.18	69.34	16.0	252.84	29.3	1.4810	1.0210	0.9767
2309851503	13.8	3.564	409.99	156.99	15.8	253.00	29.8	1.5810	1.0242	0.9871
2309851504	13.8	3.561	531.30	278.08	16.0	253.22	30.0	1.5229	1.0119	0.9866
2309851505	13.8	3.557	643.03	389.81	16.4	253.22	30.3	1.6065	1.0159	0.9901
2309851506	13.8	3.553	703.38	449.97	16.4	253.41	30.4	1.6319	1.0216	0.9841
2309851507	13.8	3.552	770.64	517.23	16.5	253.41	30.5	1.6867	1.0274	0.9867
2309851508	13.8	3.550	846.08	592.33	16.5	253.75	31.0	1.8913	1.0607	0.9761
2309851509	13.8	3.547	935.97	681.78	16.5	254.19	31.2	2.0717	1.0985	0.9925
2309851510	13.8	3.545	1101.55	846.83	16.5	254.72	31.3	2.1173	1.1581	0.9894
2309851511	13.8	3.524	1198.38	943.66	16.7	254.72	31.5	2.3016	1.1860	0.9934
2309851512	13.8	3.533	1220.33	965.61	16.7	254.72	31.5	5.7392	1.0086	1.0248

TABLE B.1l

Air-Water Data (Low Air Extraction Rate Tests)

Qf = 17.288 l/min Pats = 1.0120 Bar

TEST NO	Tfin	WC	Qasup	Qatst	Tatst	QaL	TaL	PD	TT	TL
2409851701	14.6	3.586	263.15	7.19	16.6	255.96	27.5	1.2937	1.1584	1.0859
2409851702	14.6	3.571	306.93	50.82	16.3	256.11	28.2	1.3528	1.1808	1.0961
2409851703	14.7	3.560	381.58	125.29	16.5	256.29	28.7	1.4969	1.1892	1.0905
2409851704	14.7	3.550	506.08	249.67	16.5	256.41	29.1	1.4658	1.1892	1.0905
2409851705	14.6	3.541	622.62	366.21	16.4	256.41	29.7	1.6051	1.1749	1.0800
2409851706	14.6	3.546	753.18	496.30	16.4	256.88	30.4	1.7450	1.1832	1.0859
2409851707	14.7	3.527	884.72	627.71	16.4	257.01	30.7	1.8188	1.1884	1.0630
2409851708	14.7	3.526	941.27	684.26	16.4	257.01	30.8	1.8512	1.1883	1.0895
2409851709	14.7	3.522	1051.54	794.53	16.5	257.01	30.9	1.9971	1.1933	1.0878
2409851710	14.6	3.519	1127.03	869.91	16.4	257.12	30.9	2.2717	1.1854	1.0845
2409851711	14.6	3.508	1153.85	896.73	16.5	257.12	31.0	2.3704	1.1817	1.0993
2409851712	14.6	3.498	1167.22	909.73	16.5	257.49	31.0	5.8491	1.1993	1.0936

TABLE B.1a

Air-Water Data (Low Air Extraction Rate Tests)

Qf = 18.827 l/min Patm = 1.0127 Bar

TEST NO	Tfin	WC	Qasup	Qatst	Tatst	QaL	TaL	PD	TT	TL
2409851801	13.9	3.528	269.51	10.18	16.1	259.33	27.9	1.3366	1.1941	1.1507
2409851802	13.9	3.529	314.66	55.22	15.5	259.44	28.5	1.4543	1.2174	1.1491
2409851803	13.9	3.523	379.50	120.06	15.6	259.44	29.3	1.5310	1.2757	1.1400
2409851804	13.9	3.520	542.81	283.30	15.9	259.51	29.7	1.7082	1.2541	1.1516
2409851805	13.9	3.514	647.11	387.44	16.2	259.67	30.3	1.6854	1.2490	1.1526
2409851806	13.9	3.509	787.05	527.02	16.2	260.03	30.5	1.8414	1.1907	1.1601
2409851807	13.9	3.509	874.64	614.61	16.7	260.03	30.9	1.8181	1.2152	1.1594
2409851808	13.9	3.506	947.15	686.97	16.7	260.18	31.1	1.8517	1.2001	1.1603
2409851809	13.9	3.504	1013.60	753.29	16.8	260.31	31.2	1.9761	1.1945	1.1570
2409851810	13.9	3.500	1082.18	821.72	16.7	260.46	31.3	2.1834	1.2347	1.1838
2409851811	13.9	3.499	1125.82	865.17	17.1	260.65	31.4	2.3215	1.2438	1.1927
2409851812	13.9	3.489	1157.61	896.96	17.1	260.65	31.5	7.0819	1.2673	1.2175

TABLE B.1n

Air-Water Data (Low Air Extraction Rate Tests)

Qf = 20.374 l/min Patm = 1.0134 Bar

TEST NO	Tfin	WC	Qasup	Qatst	Tatst	QaL	TaL	PD	TT	TL
2509852001	13.9	3.534	267.60	8.55	15.9	259.05	25.2	1.3563	1.2698	1.1937
2509852002	13.9	3.529	326.38	67.18	15.9	259.20	26.1	1.5227	1.3093	1.1903
2509852003	13.9	3.510	399.72	140.39	16.2	259.33	27.5	1.5626	1.2951	1.1784
2509852004	13.9	3.512	454.03	194.61	16.2	259.42	27.9	1.5992	1.2966	1.1894
2509852005	13.9	3.514	527.95	268.44	16.5	259.51	28.6	1.6891	1.2970	1.1829
2509852006	13.9	3.507	639.20	379.69	16.7	259.51	29.1	1.7056	1.2703	1.1699
2509852007	13.9	3.499	758.73	499.06	16.8	259.67	29.9	1.7055	1.3060	1.1698
2509852008	13.9	3.498	898.67	637.87	17.1	260.80	30.3	1.9185	1.3174	1.1622
2509852009	13.9	3.491	999.26	738.16	17.2	261.10	30.5	1.9963	1.3254	1.1882
2509852010	13.9	3.489	1064.93	803.70	17.2	261.23	30.5	2.0105	1.3044	1.1891
2509852011	13.9	3.481	1096.96	835.73	17.4	261.23	30.6	2.2226	1.3490	1.2100
2509852012	13.9	3.487	1110.02	848.53	17.4	261.49	30.7	7.6999	1.3950	1.2721

TABLE B.1o

Air-Water Data (Low Air Extraction Rate Tests)

Qf = 21.929 l/min Patm = 1.0127 Bar

TEST NO	Tfin	WC	Qasup	Qatst	Tatst	QaL	TaL	PD	TT	TL
2609852101	13.8	3.555	270.05	9.27	14.1	260.78	25.4	1.3694	1.3397	1.2187
2609852102	13.9	3.521	325.94	64.64	14.1	261.30	26.2	1.5222	1.3146	1.2437
2609852103	13.9	3.512	405.78	144.37	14.3	261.41	28.5	1.5616	1.3526	1.2710
2609852104	13.9	3.502	527.82	266.23	16.5	261.59	30.1	1.5517	1.3177	1.2732
2609852105	13.9	3.491	632.54	370.72	17.0	261.82	30.5	1.6952	1.2969	1.2674
2609852106	13.8	3.492	836.51	574.49	17.1	262.02	30.7	1.8642	1.3229	1.1846
2609852107	13.8	3.495	944.95	682.80	17.1	262.15	30.8	1.9034	1.3222	1.1909
2609852108	13.8	3.500	1002.15	739.94	17.2	262.21	30.8	2.0574	1.3260	1.2103
2609852109	13.8	3.500	1054.92	792.71	17.3	262.21	30.9	2.1321	1.3757	1.2272
2609852110	13.8	3.501	1078.35	815.86	17.4	262.49	31.1	2.2297	1.3826	1.1942
2609852111	13.8	3.502	1086.33	823.68	17.4	262.65	31.2	2.3716	1.3955	1.2505
2609852112	13.8	3.502	1092.37	829.72	17.4	262.65	31.3	8.3839	1.4325	1.3691

TABLE B.1p

Air-Water Data (Low Air Extraction Rate Tests)

Qf = 23.492 l/min Patm = 1.0128 Bar

TEST NO	Tfin	WC	Qasup	Qatst	Tatst	QaL	TaL	PD	TT	TL
2609852301	13.9	3.520	264.36	6.03	14.1	258.33	29.0	1.3855	1.5001	1.2519
2609852302	13.9	3.520	312.44	53.88	16.4	258.56	30.1	1.4693	1.5029	1.2596
2609852303	13.9	3.512	409.23	150.34	16.4	258.89	30.7	1.6641	1.5082	1.2592
2609852304	13.9	3.510	523.93	264.82	16.6	259.11	31.3	1.6508	1.4693	1.3177
2609852305	13.9	3.506	685.47	426.15	16.7	259.32	31.8	1.7093	1.4522	1.3226
2609852306	13.9	3.503	762.55	503.15	16.8	259.40	31.9	1.7330	1.4942	1.3209
2609852307	13.9	3.502	874.14	614.63	16.9	259.51	32.1	1.7719	1.5097	1.3263
2609852328	13.9	3.500	977.39	717.88	16.9	259.51	32.5	1.9368	1.4931	1.2721
2609852309	13.9	3.490	1041.46	781.95	17.2	259.51	32.6	2.1111	1.5025	1.2597
2609852310	13.9	3.488	1066.28	806.65	17.4	259.63	32.6	2.3174	1.5191	1.2922
2609852311	13.9	3.481	1075.51	815.71	17.4	259.80	32.7	2.5033	1.5754	1.3096
2609852312	13.9	3.480	1090.17	830.24	17.4	259.93	32.7	8.9988	1.5744	1.3860

TABLE B.1q

Air-Water Data (Low Air Extraction Rate Tests)

Qf = 25.063 l/min Patm = 1.0117 Bar

TEST NO	Tfin	WC	Qasup	Qatst	Tatst	QaL	TaL	PD	TT	TL
2709852501	13.8	3.555	268.25	7.10	14.5	261.15	25.1	1.4393	1.6731	1.3213
2709852502	13.8	3.550	322.32	60.91	14.2	261.41	26.7	1.5710	1.6959	1.3771
2709852503	13.8	3.544	401.92	140.51	14.1	261.41	27.4	1.6565	1.6881	1.3869
2709852504	13.8	3.529	520.90	259.31	14.0	261.59	28.1	1.7858	1.6596	1.3484
2709852505	13.8	3.503	638.49	376.67	15.2	261.82	28.4	1.7938	1.6831	1.3087
2709852506	13.8	3.511	730.10	468.17	15.3	261.93	28.6	1.8212	1.6906	1.3376
2709852507	13.8	3.512	820.72	558.72	16.3	262.00	28.9	1.9010	1.7378	1.3402
2709852508	13.8	3.517	926.08	663.87	16.3	262.21	29.2	2.0342	1.6958	1.3381
2709852509	13.8	3.510	951.97	689.76	16.9	262.21	29.6	2.0628	1.7469	1.3532
2709852510	13.8	3.500	982.54	720.21	17.5	262.33	29.8	2.1734	1.7433	1.3739
2709852511	13.8	3.500	1032.67	770.18	17.4	262.49	29.9	2.5792	1.7421	1.3932
2709852512	13.8	3.499	1051.32	788.83	17.7	262.49	29.9	8.7917	1.7682	1.4324

TABLE B.1r

Air-Water Data (Low Air Extraction Rate Tests)

Qf = 28.230 l/min Patm = 1.0117 Bar

TEST NO	Tfin	WC	Qasup	Qatst	Tatst	QaL	TaL	PD	TT	TL
2709852801	13.7	3.542	271.24	6.73	14.5	264.51	26.2	1.4288	1.9152	1.4636
2709852802	13.7	3.542	322.03	57.31	14.2	264.72	26.7	1.5859	1.9463	1.4958
2709852803	13.7	3.533	395.26	130.37	14.1	264.89	27.3	1.6971	1.9590	1.4797
2709852804	13.7	3.513	518.71	253.70	14.0	265.01	28.0	1.7782	1.9577	1.4919
2709852805	13.7	3.504	606.34	341.33	15.2	265.01	28.3	1.8052	1.9428	1.5050
2709852806	13.7	3.502	676.16	411.02	15.3	265.14	28.2	1.8129	1.9664	1.5268
2709852807	13.7	3.503	744.75	479.53	16.3	265.22	28.5	1.9319	1.9373	1.5216
2709852808	13.7	3.505	788.80	523.58	16.3	265.22	28.9	2.0438	1.9678	1.5427
2709852809	13.7	3.497	845.01	579.71	16.9	265.30	29.4	2.1019	1.9510	1.5490
2709852810	13.7	3.493	896.69	631.25	17.5	265.44	29.5	2.1641	1.9605	1.5755
2709852811	13.7	3.492	944.63	679.19	17.4	265.44	29.7	2.5887	1.9892	1.6049
2709852812	13.7	3.487	962.23	696.71	17.7	265.52	29.8	8.8299	2.0073	1.6719

TABLE B.2

Air-Water Flooding Data (Low Air Extraction Rate Tests)

TEST NO	Qf	Tfin	WC	Qasup	Qatst	Tatst	QaL	TaL	Pata	PD	TT	TL
1609850416	4.000	13.9	3.671	1563.26	1327.94	19.2	237.32	33.6	1.0040	3.933	0.587	0.524
3009850414	4.500	13.2	3.594	1525.76	1291.95	16.0	233.81	33.5	1.0069	3.388	0.560	0.534
1609850518	5.000	14.0	3.571	1520.54	1285.42	16.3	235.12	31.6	1.0080	4.269	0.566	0.583
0110850414	5.500	13.8	3.604	1499.14	1259.92	16.7	239.22	32.0	1.0120	4.745	0.591	0.599
1709850614	6.000	13.9	3.592	1488.46	1247.02	15.4	241.44	32.2	1.0080	3.886	0.645	0.626
3009850412	6.500	13.4	3.602	1480.48	1239.83	16.3	240.65	31.6	1.0071	4.437	0.664	0.656
1709850714	7.000	13.9	3.643	1484.77	1245.55	16.6	239.22	30.5	1.0080	5.164	0.686	0.653
3009850411	7.500	13.5	3.591	1464.23	1221.22	16.4	243.01	31.1	1.0068	3.882	0.675	0.663
1709850814	8.000	15.0	3.639	1470.21	1223.90	16.6	246.31	32.4	1.0080	5.177	0.693	0.680
3009850815	8.500	13.5	3.604	1429.13	1189.91	16.4	239.22	32.7	1.0067	5.045	0.689	0.680
1809850912	9.000	15.3	3.634	1416.22	1172.20	16.6	244.02	33.0	1.0079	4.857	0.725	0.696
3009850911	9.500	13.5	3.589	1414.83	1170.81	16.6	244.02	32.9	1.0069	5.384	0.729	0.711
1809851012	10.000	14.9	3.548	1397.82	1160.50	16.0	237.32	32.7	1.0081	5.018	0.753	0.771
0110851014	10.443	14.7	3.664	1369.83	1132.51	17.7	237.32	30.9	1.0160	6.233	0.845	0.805
1909851112	11.197	13.3	3.566	1335.62	1093.20	16.9	242.42	30.3	1.0067	5.492	0.905	0.902
1909851110	11.953	13.3	3.559	1298.22	1051.91	17.1	246.31	31.3	1.0067	4.285	0.982	0.809
2009851212	12.710	13.6	3.533	1310.41	1062.64	17.1	247.77	32.1	1.0083	5.188	1.060	0.918
2009851412	14.229	13.8	3.527	1255.21	1003.48	17.1	251.73	31.3	1.0080	5.929	1.141	0.961
2009851410	14.991	13.8	3.545	1236.12	983.07	16.7	253.05	31.0	1.0080	5.794	1.110	0.959
2309851512	15.755	13.8	3.533	1220.33	965.61	16.7	254.72	31.5	1.0085	5.739	1.009	1.025
0110851610	16.520	13.7	3.518	1199.12	942.94	17.3	256.18	31.4	1.0161	6.207	1.155	1.100
0110851610	16.980	13.3	3.482	1188.02	932.53	18.2	255.49	31.6	1.0161	4.595	1.159	1.089
2409851712	17.288	14.6	3.498	1167.22	909.73	16.5	257.49	31.0	1.0120	5.849	1.199	1.094
0110851810	18.056	14.7	3.574	1180.52	919.87	17.8	260.65	30.9	1.0163	6.470	1.189	1.145
2409851812	18.827	13.9	3.489	1157.61	896.96	17.1	260.65	31.5	1.0127	7.082	1.267	1.217
2509851910	19.600	13.7	3.490	1146.14	886.21	16.9	259.93	31.0	1.0134	5.897	1.299	1.203
2509852012	20.374	13.9	3.487	1110.02	848.53	17.4	261.49	30.7	1.0134	7.700	1.395	1.272
2509852110	21.151	13.7	3.510	1124.62	863.13	13.7	261.49	30.8	1.0137	7.465	1.426	1.301
2609852112	21.929	13.8	3.502	1092.37	829.72	17.4	262.65	31.3	1.0127	8.384	1.433	1.369
0210852210	22.709	13.8	3.514	1075.14	813.22	16.9	261.92	31.4	1.0120	5.955	1.541	1.396
2609852312	23.492	13.9	3.480	1090.17	830.24	17.4	259.93	32.7	1.0128	8.999	1.574	1.386
0210852410	24.276	13.9	3.537	1054.73	794.24	16.6	260.49	31.3	1.0120	7.937	1.609	1.434
2709852512	25.063	13.8	3.499	1051.32	788.83	17.7	262.49	29.9	1.0117	8.792	1.768	1.432
0310852510	25.851	13.7	3.506	1053.67	787.85	16.9	265.82	30.1	1.0134	8.207	1.811	1.522
0210852614	26.642	14.1	3.528	1036.41	771.43	18.2	264.98	30.0	1.0120	7.723	1.887	1.593
0310852712	27.435	14.5	3.545	1025.18	759.11	15.8	266.07	29.8	1.0134	5.591	1.931	1.643
2709852812	28.230	13.7	3.487	962.23	696.71	17.7	265.52	29.8	1.0117	8.830	2.007	1.672
0410852811	28.734	14.1	3.502	970.20	706.70	14.4	264.50	30.2	1.0054	7.951	2.014	1.605
0410852910	29.027	14.1	3.499	950.08	688.16	14.7	261.92	30.1	1.0054	6.222	2.064	1.644
0710852911	29.826	12.6	3.476	965.12	701.13	17.5	263.99	29.9	1.0047	9.819	2.034	1.671
0710853012	30.628	12.6	3.470	951.12	687.90	17.5	263.22	29.6	1.0047	8.309	2.082	1.661
0710853112	31.432	12.6	3.468	945.92	680.10	17.7	265.82	29.5	1.0047	8.298	2.069	1.664
0810853212	32.239	12.7	3.471	923.86	657.79	17.2	266.07	29.8	1.0051	7.642	2.131	1.695
0810853310	33.047	12.8	3.471	900.46	632.27	17.2	268.19	29.7	1.0051	8.496	2.205	1.732
0810853311	33.859	12.8	3.472	896.14	627.14	17.4	269.00	30.0	1.0051	9.282	2.194	1.685
0810853410	34.672	12.8	3.480	881.41	614.13	17.7	267.28	29.7	1.0053	8.779	2.331	1.709
0810853510	35.488	12.8	3.490	857.03	587.23	17.7	269.80	29.5	1.0053	8.285	2.411	1.702
0810853612	36.307	12.8	3.501	849.70	577.51	17.7	272.19	29.1	1.0053	9.088	2.440	1.749
0910853710	37.128	13.0	3.519	839.05	568.57	17.4	270.48	29.3	1.0047	7.978	2.592	1.773
0910853711	37.952	13.0	3.511	842.14	572.34	17.3	269.80	29.0	1.0047	9.310	2.625	1.731
1010853810	38.778	12.9	3.493	836.70	565.65	17.2	271.05	28.6	1.0051	8.488	2.678	1.793
1010853910	39.607	12.9	3.486	826.81	556.33	17.5	270.48	28.3	1.0051	9.553	2.634	1.780

TABLE B.3

Air-Water Flooding Data (High Air Extraction Rate Tests)

TEST NO	Qf	Tfin	WC	Qasup	Qatst	Tatst	QaL	TaL	Patm	PD	TT	TL
1507870414	4.000	14.1	3.601	1591.31	1270.36	17.1	320.95	33.3	1.0033	3.529	0.537	0.521
1507870514	5.000	14.1	3.605	1545.75	1227.52	17.2	318.23	33.1	1.0032	4.109	0.560	0.549
1507870615	6.000	14.0	3.593	1526.83	1211.31	17.1	315.52	32.7	1.0032	4.442	0.653	0.612
1507870716	7.000	14.1	3.550	1488.80	1174.35	17.1	314.45	33.0	1.0032	4.319	0.673	0.652
1507870815	8.000	14.3	3.727	1447.67	1134.30	17.2	313.37	33.0	1.0032	4.931	0.710	0.660
1507870914	9.000	14.2	3.529	1392.32	1080.58	17.4	311.74	31.9	1.0032	5.423	0.712	0.708
1607871014	10.000	14.4	3.553	1366.46	1056.35	17.4	310.11	31.5	1.0032	5.332	0.745	0.730
1607871114	11.197	14.4	3.498	1282.42	976.59	17.5	305.83	31.3	1.0032	5.730	0.881	0.873
1607871216	12.710	14.5	3.498	1250.27	946.07	17.5	304.20	31.7	1.0032	5.530	0.995	0.992
1607871415	14.229	14.7	3.492	1238.68	935.29	17.5	303.39	32.4	1.0032	5.621	1.195	0.996
1607871514	15.755	14.7	3.535	1204.04	901.94	17.6	302.10	32.1	1.0032	6.212	1.212	1.018
1707871712	17.288	14.6	3.513	1189.29	887.19	17.7	302.10	31.4	1.0029	6.738	1.254	0.967
1707871811	18.827	14.7	3.619	1134.97	833.58	17.7	301.39	31.3	1.0029	6.616	1.389	1.159
1707872009	20.375	14.7	3.589	1121.54	820.15	17.7	301.39	30.9	1.0029	7.961	1.500	1.301
1707872110	21.929	14.8	3.556	1092.33	793.04	17.6	299.29	30.8	1.0029	7.917	1.498	1.290
1707872312	23.492	14.8	3.540	1097.47	798.18	17.7	299.29	31.4	1.0029	8.501	1.612	1.373
2007872511	25.063	15.0	3.542	1059.22	761.31	17.7	297.91	31.8	1.0030	8.991	1.718	1.552
2007872710	27.435	14.9	3.567	1033.23	733.94	17.8	299.29	31.4	1.0030	9.298	1.884	1.635
2007872914	29.027	15.2	3.585	1002.38	704.47	17.8	297.91	30.8	1.0030	7.640	1.977	1.592
2007873114	31.432	15.1	3.554	959.27	662.22	17.7	297.05	30.3	1.0030	8.439	2.188	1.633
2007873312	33.047	15.0	3.542	916.64	620.36	17.7	296.28	29.9	1.0030	8.745	2.299	1.670
2107873411	34.672	14.7	3.540	886.98	591.03	17.8	295.95	29.3	1.0032	9.351	2.328	1.650
2107873612	36.307	14.7	3.519	869.69	576.17	17.7	293.52	28.9	1.0032	9.288	2.371	1.699
2107873710	37.952	14.3	3.495	848.88	558.01	17.8	290.87	29.0	1.0032	9.660	2.618	1.742
2107873910	39.607	14.3	3.479	815.72	527.19	17.9	288.53	28.7	1.0032	9.153	2.659	1.805

TABLE B.4

Air-Water Flooding Results (Low Air Extraction Rate Tests)

TEST NO	Mf	Tfin	Masup	Matst	Tatst	ρ_{atst}	MaL	TaL	ρ_{aL}	Jf	Ja
1609850416	3.959	13.9	1.873	1.589	19.2	1.196	0.271	33.6	1.140	0.0383	0.4462
3009850414	4.461	13.2	1.851	1.567	16.0	1.213	0.267	33.5	1.144	0.0431	0.4369
1609850518	4.948	14.0	1.845	1.560	16.3	1.213	0.271	31.6	1.152	0.0478	0.4350
0110850414	5.445	13.8	1.824	1.533	16.7	1.216	0.276	32.0	1.155	0.0526	0.4269
1709850614	5.939	13.9	1.812	1.518	15.4	1.217	0.278	32.2	1.150	0.0574	0.4226
3009850412	6.441	13.4	1.795	1.503	16.3	1.212	0.277	31.6	1.151	0.0622	0.4191
1709850714	6.929	13.9	1.800	1.510	16.6	1.212	0.277	30.5	1.157	0.0669	0.4213
3009850411	7.430	13.5	1.774	1.479	16.4	1.211	0.280	31.1	1.153	0.0718	0.4128
1709850814	7.898	15.0	1.782	1.483	16.6	1.212	0.283	32.4	1.149	0.0763	0.4145
3009850815	8.421	13.5	1.731	1.441	16.4	1.211	0.274	32.7	1.147	0.0814	0.4022
1809850912	8.879	15.3	1.716	1.421	16.6	1.212	0.280	33.0	1.147	0.0858	0.3971
3009850911	9.412	13.5	1.713	1.417	16.6	1.211	0.280	32.9	1.146	0.0909	0.3956
1809851012	9.875	14.9	1.698	1.410	16.0	1.215	0.273	32.7	1.148	0.0954	0.3934
0110851014	10.318	14.7	1.667	1.378	17.7	1.217	0.276	30.9	1.164	0.0997	0.3842
1909851112	11.098	13.3	1.615	1.322	16.9	1.209	0.280	30.3	1.156	0.1072	0.3691
1909851110	11.847	13.3	1.569	1.271	17.1	1.208	0.284	31.3	1.152	0.1145	0.3550
2009851212	12.589	13.6	1.586	1.286	17.1	1.210	0.285	32.1	1.151	0.1216	0.3590
2009851412	14.088	13.8	1.519	1.214	17.1	1.210	0.290	31.3	1.153	0.1361	0.3391
2009851410	14.842	13.8	1.498	1.191	16.7	1.212	0.292	31.0	1.155	0.1434	0.3324
2309851512	15.598	13.8	1.479	1.170	16.7	1.212	0.294	31.5	1.153	0.1507	0.3266
0110851610	16.359	13.7	1.461	1.149	17.3	1.219	0.298	31.4	1.162	0.1581	0.3197
0110851610	16.829	13.3	1.443	1.133	18.2	1.215	0.297	31.6	1.162	0.1626	0.3156
2409851712	17.085	14.6	1.421	1.107	16.5	1.217	0.298	31.0	1.159	0.1651	0.3086
0110851810	17.840	14.7	1.437	1.119	17.8	1.217	0.304	30.9	1.165	0.1724	0.3120
2409851812	18.636	13.9	1.407	1.090	17.1	1.216	0.302	31.5	1.158	0.1801	0.3038
2509851910	19.409	13.7	1.395	1.079	16.9	1.217	0.302	31.0	1.161	0.1875	0.3003
2509852012	20.167	13.9	1.349	1.031	17.4	1.215	0.304	30.7	1.162	0.1949	0.2874
2509852110	20.945	13.7	1.385	1.063	13.7	1.231	0.304	30.8	1.162	0.2024	0.2942
2609852112	21.711	13.8	1.326	1.008	17.4	1.214	0.304	31.3	1.159	0.2098	0.2809
0210852210	22.483	13.8	1.307	0.989	16.9	1.216	0.303	31.4	1.158	0.2172	0.2754
2609852312	23.254	13.9	1.324	1.008	17.4	1.214	0.300	32.7	1.154	0.2247	0.2811
0210852410	24.030	13.9	1.283	0.966	16.6	1.217	0.302	31.3	1.158	0.2322	0.2692
2709852512	24.814	13.8	1.274	0.956	17.7	1.212	0.305	29.9	1.163	0.2398	0.2668
0310852510	25.600	13.7	1.283	0.959	16.9	1.217	0.309	30.1	1.164	0.2473	0.2670
0210852614	26.360	14.1	1.254	0.934	18.2	1.210	0.308	30.0	1.163	0.2547	0.2608
0310852712	27.119	14.5	1.253	0.928	15.8	1.222	0.310	29.8	1.165	0.2620	0.2580
2709852812	27.956	13.7	1.166	0.844	17.7	1.212	0.309	29.8	1.163	0.2701	0.2356
0410852811	27.931	14.1	1.172	0.849	14.4	1.218	0.307	30.2	1.155	0.2699	0.2363
0410852910	28.720	14.1	1.156	0.837	14.7	1.217	0.303	30.1	1.155	0.2775	0.2333
0710852911	29.600	12.6	1.162	0.844	17.5	1.204	0.305	29.9	1.155	0.2860	0.2361
0710853012	30.396	12.6	1.145	0.828	17.5	1.204	0.304	29.6	1.156	0.2937	0.2316
0710853112	31.194	12.6	1.138	0.818	17.7	1.203	0.307	29.5	1.157	0.3014	0.2289
0810853212	31.989	12.7	1.114	0.793	17.2	1.206	0.308	29.8	1.156	0.3091	0.2217
0810853310	32.784	12.8	1.086	0.763	17.2	1.206	0.310	29.7	1.156	0.3168	0.2131
0810853311	33.590	12.8	1.080	0.756	17.4	1.205	0.311	30.0	1.155	0.3245	0.2113
0810853410	34.396	12.8	1.061	0.740	17.7	1.204	0.309	29.7	1.156	0.3323	0.2068
0810853510	35.206	12.8	1.032	0.707	17.7	1.204	0.312	29.5	1.157	0.3402	0.1978
0810853612	36.018	12.8	1.023	0.695	17.7	1.204	0.315	29.1	1.159	0.3480	0.1945
0910853710	36.819	13.0	1.011	0.685	17.4	1.205	0.313	29.3	1.157	0.3557	0.1915
0910853711	37.636	13.0	1.015	0.690	17.3	1.205	0.313	29.0	1.158	0.3636	0.1928
1010853810	38.463	12.9	1.009	0.682	17.2	1.206	0.315	28.6	1.160	0.3716	0.1906
1010853910	39.285	12.9	0.996	0.670	17.5	1.205	0.314	28.3	1.162	0.3796	0.1874

TABLE B.5

Air-Water Flooding Results (High Air Extraction Rate Tests)

TEST NO	Mf	Tfin	Masup	Matst	Tatst	P_{atst}	MaL	TaL	P_{aL}	J_f^*	J_a^*
1507870414	3.958	14.1	1.916	1.530	17.1	1.204	0.366	33.3	1.141	0.0382	0.4284
1507870514	4.947	14.1	1.861	1.478	17.2	1.204	0.363	33.1	1.141	0.0478	0.4138
1507870615	5.938	14.0	1.839	1.459	17.1	1.204	0.361	32.7	1.143	0.0574	0.4084
1507870716	6.926	14.1	1.793	1.414	17.1	1.204	0.359	33.0	1.142	0.0669	0.3960
1507870815	7.912	14.3	1.743	1.365	17.2	1.204	0.358	33.0	1.142	0.0764	0.3825
1507870914	8.903	14.2	1.675	1.300	17.4	1.203	0.357	31.9	1.146	0.0860	0.3642
1607871014	9.887	14.4	1.644	1.271	17.4	1.203	0.356	31.5	1.147	0.0955	0.3561
1607871114	11.071	14.4	1.542	1.174	17.5	1.202	0.351	31.3	1.148	0.1070	0.3292
1607871216	12.564	14.5	1.503	1.138	17.5	1.202	0.349	31.7	1.146	0.1214	0.3189
1607871415	14.059	14.7	1.490	1.125	17.5	1.202	0.347	32.4	1.144	0.1358	0.3154
1607871514	15.566	14.7	1.447	1.084	17.6	1.202	0.346	32.1	1.145	0.1504	0.3041
1707871712	17.085	14.6	1.429	1.066	17.7	1.201	0.347	31.4	1.147	0.1651	0.2990
1707871811	18.601	14.7	1.363	1.001	17.7	1.201	0.346	31.3	1.148	0.1797	0.2809
1707872009	20.131	14.7	1.347	0.985	17.7	1.201	0.346	30.9	1.149	0.1945	0.2764
1707872110	21.661	14.8	1.313	0.953	17.6	1.202	0.344	30.8	1.150	0.2093	0.2674
1707872312	23.205	14.8	1.318	0.959	17.7	1.201	0.343	31.4	1.147	0.2242	0.2690
2007872511	24.744	15.0	1.273	0.915	17.7	1.201	0.341	31.8	1.146	0.2391	0.2567
2007872710	27.093	14.9	1.241	0.881	17.8	1.201	0.343	31.4	1.147	0.2618	0.2474
2007872914	28.643	15.2	1.204	0.846	17.8	1.201	0.342	30.8	1.150	0.2767	0.2376
2007873114	31.024	15.1	1.152	0.796	17.7	1.201	0.342	30.3	1.152	0.2998	0.2233
2007873312	32.627	15.0	1.101	0.745	17.7	1.201	0.342	29.9	1.153	0.3152	0.2092
2107873411	34.257	14.7	1.065	0.710	17.8	1.201	0.342	29.3	1.156	0.3310	0.1992
2107873612	35.872	14.7	1.045	0.692	17.7	1.202	0.340	28.9	1.157	0.3466	0.1942
2107873710	37.533	14.3	1.020	0.670	17.8	1.201	0.336	29.0	1.157	0.3626	0.1880
2107873910	39.170	14.3	0.980	0.633	17.9	1.201	0.334	28.7	1.158	0.3785	0.1776

APPENDIX C

STEAM-WATER DATA

APPENDIX C

The steam-water data is given a reference number consisting of 10 digits similar to the air-water tests described in Appendix B. The definition of the symbols used in the tables are:-

Test No.	Test number
Q_{fin}	Inlet water volumetric flowrate, l/min.
WC	Water conductivity, MSIEM/mm.
T_{fin}	Inlet water temperature, °C.
T_{wo}	Wall temperature at water outlet, °C.
M_{cw}	Cooling water flowrate, kg/min.
T_{c1}	Cooling water inlet temperature, °C.
T_{c2}	Cooling water outlet temperature, °C.
TD	Discharge water temperature, °C.
T_s	Steam temperature, °C.
M_{ssup}	Supply steam mass flowrate, kg/min.
V_{p1}	Vacuum pressure before condenser, ins. Hg.
V_{p2}	Vacuum pressure after condenser, ins. Hg.
P_{atm}	Atmospheric pressure, bar.
PD	Pressure difference, KN/m ² .
TT	Top (upper) film thickness, mm.
TL	Bottom (lower) film thickness, mm.
M_{fin}	Inlet water mass flowrate, kg/min.
M_{SB}	Steam flowrate at bottom of test section, kg/min.
M_{SC}	Condensed steam flowrate, kg/min.
M_{ST}	Steam flowrate at top of test section, kg/min.
M_{SL}	Extracted (leaked) steam flowrate, kg/min.
J_{fin}^*	Wallis water parameter (Top).
J_{ST}^*	Wallis steam parameter (Top).
J_f^*	Wallis water parameter (Bottom).
J_{SB}^*	Wallis steam parameter (Bottom).
$T_1 - T_{11}$	Tube wall temperature, °C.

TABLE C.1a

Steam-Water Data (Low Steam Extraction Rate Tests)

Inlet Water Subcooling = 80 K

TEST No	Qfin	WC	Tfin	Two	M _{cm}	Tc1	Tc2	TD	M _{ssup}	Ts	VPI	Patm	PD	TT	TL
0507850401	4.000	3.904	19.82	80.00	4.068	14.01	58.48	51.95	0.5704	99.58	1.5	0.9947	0.020	0.624	0.400
0507850402	4.000	3.917	19.99	87.67	4.120	14.17	71.27	63.26	0.7689	99.57	1.6	0.9947	-0.006	0.653	0.441
0507850403	4.000	3.924	19.97	96.08	4.103	14.26	75.48	67.39	0.8459	99.57	1.7	0.9947	-0.003	0.657	0.451
0507850404	4.000	3.938	20.03	97.66	4.099	14.31	87.45	72.14	0.9857	99.56	1.9	0.9947	-0.098	0.662	0.502
0507850405	4.000	3.951	20.16	97.90	4.127	14.65	91.74	79.13	1.1726	99.58	2.3	0.9947	-0.077	0.688	0.513
0507850406	4.000	3.969	20.35	97.99	4.218	14.75	92.12	82.41	1.2949	99.60	2.8	0.9947	-0.073	0.708	0.542
0507850407	4.000	3.973	20.36	98.09	4.164	14.67	92.25	83.29	1.4056	99.60	3.0	0.9947	0.089	0.697	0.562
0507850408	4.000	3.979	20.34	98.26	4.188	14.44	92.73	83.81	1.4514	99.61	3.1	0.9947	1.125	0.731	0.608
0507850501	5.000	4.222	20.76	75.58	4.172	15.06	56.80	54.96	0.6077	99.69	1.0	0.9947	0.061	0.748	0.529
0507850502	5.000	4.267	20.90	80.79	4.044	15.25	76.06	66.71	0.8979	99.67	2.8	0.9947	-0.118	0.757	0.520
0507850503	5.000	4.231	20.77	90.30	4.235	15.85	87.01	73.19	1.0703	99.65	2.8	0.9947	-0.135	0.755	0.581
0507850504	5.000	4.221	20.79	96.89	4.192	15.90	89.02	78.77	1.1707	99.66	2.9	0.9947	-0.167	0.756	0.584
0507850505	5.000	4.236	20.81	97.78	4.162	15.92	90.32	80.94	1.2625	99.67	2.9	0.9947	-0.151	0.759	0.584
0507850506	5.000	4.269	20.97	97.76	4.172	15.92	91.75	81.87	1.3323	99.68	2.9	0.9947	-0.148	0.764	0.589
0507850507	5.000	4.287	21.00	98.17	4.099	15.94	91.94	82.47	1.3876	99.68	2.9	0.9947	1.016	0.792	0.638
0507850601	6.000	4.261	20.93	80.91	4.004	15.61	62.81	55.91	0.7121	99.74	1.0	0.9947	-0.046	0.753	0.656
0507850602	6.000	4.255	20.90	86.04	4.095	15.65	70.19	65.23	0.8864	99.76	2.0	0.9947	-0.198	0.740	0.634
0507850603	6.000	4.253	20.90	94.71	4.128	15.71	76.02	69.17	0.9944	99.75	2.7	0.9447	-0.176	0.741	0.635
0507850604	6.000	4.251	20.89	96.53	4.259	15.77	83.99	72.67	1.1454	99.76	2.8	0.9947	-0.161	0.745	0.638
0507850605	6.000	4.259	21.92	97.33	4.198	15.87	87.71	76.98	1.2419	99.75	2.8	0.9947	-0.145	0.749	0.673
0507850606	6.000	4.290	21.05	97.45	4.117	15.98	89.62	78.69	1.3209	99.78	2.8	0.9947	-0.098	0.750	0.660
0507850607	6.000	4.297	21.07	97.58	4.121	15.99	91.42	79.08	1.3646	99.79	2.8	0.9947	2.134	0.807	0.735
0807850701	7.000	4.270	20.98	48.78	4.093	16.23	64.62	52.71	0.7223	99.64	1.0	0.9987	0.001	0.829	0.772
0807850702	7.000	4.296	21.06	62.10	4.134	17.40	68.61	61.56	0.8843	99.64	1.3	0.9987	0.000	0.834	0.786
0807850703	7.000	4.283	20.91	66.39	4.152	17.54	72.66	65.77	1.0112	99.65	1.7	0.9987	-0.031	0.824	0.784
0807850704	7.000	4.271	20.88	74.50	4.149	17.59	78.11	68.56	1.1261	99.64	1.9	0.9987	-0.013	0.838	0.804
0807850705	7.000	4.257	20.78	82.22	4.172	17.59	82.61	71.47	1.2263	99.65	2.8	0.9987	-0.005	0.841	0.788
0807850706	7.000	4.223	20.52	88.81	4.297	17.60	85.58	72.42	1.3018	99.66	3.0	0.9987	-0.045	0.838	0.796
0807850707	7.000	4.140	20.47	91.88	4.338	17.65	86.08	73.56	1.3423	99.66	3.0	0.9987	2.567	0.875	0.845
0807850801	8.000	4.277	20.83	40.29	4.096	17.36	54.40	48.89	0.7001	99.64	0.0	1.0000	0.020	0.886	0.824
0807850802	8.000	4.261	20.88	47.50	4.019	17.44	62.69	58.45	0.8693	99.64	0.0	1.0000	0.023	0.884	0.802
0807850803	8.000	4.272	20.92	51.57	4.010	17.47	66.49	61.20	0.9371	99.65	0.0	1.0000	-0.092	0.884	0.815
0807850804	8.000	4.283	20.95	54.74	4.007	17.56	71.24	65.54	1.0816	99.67	0.0	1.0000	-0.051	0.892	0.840
0807850805	8.000	4.289	20.98	68.86	4.009	17.81	78.36	72.08	1.2372	99.65	0.0	1.0000	-0.014	0.885	0.857
0807850806	8.000	4.302	21.05	79.10	3.989	18.01	83.96	73.90	1.3094	99.67	0.0	1.0000	-0.011	0.890	0.843
0807850807	8.000	4.311	21.16	82.30	3.971	18.10	86.57	74.90	1.3647	99.67	0.0	1.0000	-0.005	0.897	0.856
0807850808	8.000	4.238	21.24	84.45	3.978	18.18	87.41	75.82	1.4175	99.67	0.0	1.0000	3.169	0.925	0.902
0907850901	9.000	4.278	20.92	43.27	4.465	16.41	48.43	46.72	0.7115	99.72	0.0	0.9987	0.065	0.922	0.834
0907850902	9.000	4.281	20.95	48.15	4.389	17.08	55.27	56.00	0.8612	99.72	0.0	0.9987	0.045	0.936	0.818
0907850903	9.000	4.275	20.92	53.06	4.367	17.13	62.40	59.86	0.9753	99.71	0.0	0.9987	-0.020	0.929	0.846
0907850904	9.000	4.295	21.06	58.81	4.387	17.22	62.23	61.91	1.0439	99.70	0.0	0.9987	-0.049	0.918	0.837
0907850905	9.000	4.324	21.17	65.96	4.370	17.26	63.13	63.05	1.1107	99.70	0.0	0.9987	-0.080	0.913	0.845
0907850906	9.000	4.347	21.26	70.77	4.362	17.27	65.54	64.50	1.1683	99.69	0.0	0.9987	0.116	0.898	0.853
0907850907	9.000	4.602	21.37	74.90	4.239	17.27	66.62	65.23	1.2339	99.73	0.0	0.9987	4.299	0.955	0.910
1107851001	10.000	4.034	20.02	44.79	5.784	17.80	47.54	46.44	0.7447	99.65	0.0	1.0067	0.063	1.008	0.919
1107851002	10.000	4.058	20.14	48.39	5.805	17.72	52.05	55.12	0.9424	99.66	0.0	1.0067	0.020	1.012	0.913
1107851003	10.000	4.239	20.67	51.94	5.807	17.73	52.22	56.34	1.0143	99.68	0.0	1.0067	0.014	1.021	0.937
1107851004	10.000	4.103	20.12	55.88	5.739	17.71	53.99	58.03	1.0830	99.68	0.0	1.0067	-0.020	1.013	0.937
1107851005	10.000	4.269	20.70	59.66	5.815	17.71	54.62	58.28	1.1634	99.69	0.0	1.0067	-0.004	1.020	0.927
1107851006	10.000	4.241	20.61	62.13	5.895	17.63	55.54	58.52	1.2104	99.71	0.0	1.0067	-0.011	1.013	0.949
1107851007	10.000	4.262	20.69	66.60	5.960	17.60	56.10	58.91	1.2128	99.71	0.0	1.0067	4.751	1.073	1.007

TABLE C.1b

Steam-Water Data (Low Steam Extraction Rate Tests)

Inlet Water Subcooling = 70 K

TEST No	Bfin	WC	Tfin	Two	Hcw	Tc1	Tc2	TD	Mssup	Ts	VPI	Pata	PD	TT	TL
1807850401	4.000	5.233	30.67	89.14	3.378	15.81	81.28	72.16	0.7011	99.67	3.8	0.9960	-0.012	0.520	0.371
1807850402	4.000	5.239	30.75	94.36	3.353	15.91	83.80	74.12	0.7711	99.70	3.8	0.9960	-0.100	0.512	0.334
1807850403	4.000	5.235	30.64	97.00	3.258	15.86	84.54	75.82	0.8334	99.71	3.9	0.9960	-0.059	0.640	0.394
1807850404	4.000	5.240	30.64	97.89	3.271	15.91	87.63	77.91	0.9359	99.71	3.9	0.9960	-0.017	0.680	0.382
1807850405	4.000	5.289	30.77	98.05	3.310	15.94	90.59	79.18	0.9932	99.72	3.9	0.9960	-0.018	0.694	0.392
1807850406	4.000	5.303	30.72	98.19	3.289	15.89	91.78	80.38	1.0701	99.74	3.9	0.9660	-0.024	0.714	0.380
1807850407	4.000	5.311	30.74	98.25	3.274	15.90	92.29	81.98	1.1382	99.74	4.0	0.9960	-0.010	0.738	0.399
1807850408	4.000	5.297	30.71	98.19	3.266	15.92	92.33	83.00	1.1991	99.75	4.1	0.9960	0.011	0.720	0.397
1807850409	4.000	5.289	30.70	98.26	3.253	15.94	92.40	83.87	1.2459	99.75	4.1	0.9960	0.072	0.728	0.416
1807850410	4.000	5.275	30.64	98.71	3.212	15.96	93.20	84.93	1.3159	99.78	4.2	0.9960	0.967	0.781	0.489
1807850501	5.000	5.252	30.55	91.92	3.699	15.26	75.12	69.21	0.7719	99.61	3.9	0.9960	0.027	0.587	0.424
1807850502	5.000	5.258	30.56	94.54	3.729	15.45	79.29	70.32	0.8549	99.61	3.9	0.9960	0.024	0.589	0.424
1807850503	5.000	5.271	30.59	97.65	3.812	15.56	83.55	71.65	0.9613	99.65	3.9	0.9960	-0.062	0.593	0.433
1807850504	5.000	5.296	30.64	97.71	3.709	15.99	87.75	73.72	1.0512	99.65	4.0	0.9960	-0.138	0.661	0.437
1807850505	5.000	5.302	30.65	97.81	3.757	15.80	88.66	75.51	1.1255	99.66	4.0	0.9660	-0.131	0.697	0.423
1807850506	5.000	5.308	30.67	97.89	3.829	16.16	89.74	78.95	1.1977	99.67	4.1	0.9660	0.110	0.737	0.418
1807850507	5.000	5.312	30.67	98.05	3.847	16.23	90.80	79.21	1.2704	99.67	4.2	0.9960	0.970	0.789	0.486
1807850601	6.000	5.366	30.80	82.42	3.843	16.02	65.46	64.46	0.7472	99.69	3.4	0.9960	0.057	0.617	0.475
1807850602	6.000	5.315	30.58	88.09	3.820	16.11	69.72	66.82	0.8039	99.69	3.5	0.9960	-0.001	0.641	0.544
1807850603	6.000	5.321	30.63	93.29	3.815	16.15	73.69	68.11	0.8620	99.68	3.6	0.9960	-0.006	0.604	0.507
1807850604	6.000	5.378	30.83	93.29	3.810	16.18	74.37	69.85	0.9129	99.69	3.7	0.9960	-0.002	0.676	0.498
1807850605	6.000	5.382	30.80	96.08	3.819	16.21	77.48	70.58	0.9581	99.70	3.7	0.9960	-0.009	0.774	0.502
1807850606	6.000	5.391	30.88	97.24	3.834	16.29	80.71	71.49	0.9936	99.72	3.9	0.9960	-0.093	0.778	0.492
1807850607	6.000	5.405	30.90	97.77	3.787	16.39	85.38	73.20	1.0594	99.72	4.0	0.9960	-0.092	0.801	0.537
1807850608	6.000	5.414	30.93	97.81	3.694	16.32	87.70	76.06	1.1224	99.76	4.0	0.9960	0.071	0.861	0.617
1807850609	6.000	5.423	30.95	97.95	3.667	16.49	90.60	78.20	1.2014	99.76	4.1	0.9960	1.244	0.697	0.576
2207850701	7.000	5.105	30.24	65.58	3.951	16.18	68.26	67.02	0.8175	99.64	0.0	1.0000	0.050	0.676	0.551
2207850702	7.000	5.118	30.36	75.50	3.983	16.30	75.38	69.94	0.9593	99.68	0.0	1.0000	-0.067	0.734	0.571
2207850703	7.000	5.213	30.34	79.62	3.927	16.36	80.94	70.44	1.0381	99.69	0.0	1.0000	-0.033	0.777	0.613
2207850704	7.000	5.227	30.35	84.95	3.995	16.22	85.88	72.78	1.1039	99.67	0.0	1.0000	-0.063	0.793	0.637
2207850705	7.000	5.261	30.41	89.10	4.171	16.24	86.39	73.32	1.1693	99.67	0.3	1.0000	-0.061	0.823	0.657
2207850706	7.000	5.272	30.40	92.79	4.009	16.25	88.43	75.44	1.2384	99.69	0.4	1.0000	0.096	0.880	0.729
2207850707	7.000	5.279	30.42	96.67	4.108	16.20	90.13	76.49	1.2882	99.69	0.5	1.0000	6.388	0.782	0.672
2207850801	8.000	5.287	30.43	56.04	3.492	16.67	67.96	62.81	0.8300	99.61	0.0	1.0000	0.039	0.778	0.656
2207850802	8.000	5.292	30.45	60.06	3.467	16.53	72.55	65.59	0.9443	99.59	0.1	1.0000	-0.060	0.825	0.666
2207850803	8.000	5.311	30.50	67.99	3.417	16.38	77.00	70.33	1.0600	99.63	0.1	1.0000	-0.038	0.847	0.711
2207850804	8.000	5.317	30.54	74.95	3.398	16.38	80.56	73.97	1.1593	99.64	0.0	1.0000	-0.031	0.874	0.684
2207850805	8.000	5.329	30.58	80.04	3.387	16.32	85.89	75.63	1.2286	99.66	0.0	1.0000	-0.049	0.873	0.703
2207850806	8.000	5.336	30.59	87.09	3.303	16.38	88.20	78.81	1.2822	99.67	0.0	1.0000	-0.043	0.894	0.696
2207850807	8.000	5.349	30.59	92.63	3.470	16.23	90.18	80.42	1.3250	99.67	0.0	1.0000	3.701	0.958	0.772

TABLE C.1b (Continue)

Steam-Water Data (Low Steam Extraction Rate Tests)

Inlet Water Subcooling = 70 K

TEST No	Qfin	WC	Tfin	Two	Mcw	Tc1	Tc2	TD	Mssup	Ts	VPI	Pata	PD	TT	TL
2207850901	9.000	5.096	30.10	48.09	3.520	17.34	63.58	60.89	0.8079	99.58	0.0	1.0000	-0.011	0.867	0.715
2207850902	9.000	5.110	30.18	53.98	3.525	17.24	65.32	64.21	0.9132	99.58	0.0	1.0000	-0.019	0.868	0.734
2207850903	9.000	5.144	30.25	58.27	3.516	17.08	70.10	69.43	1.0428	99.59	0.0	1.0000	-0.013	0.872	0.711
2207850904	9.000	5.158	30.29	62.48	3.307	16.86	73.76	71.76	1.1551	99.61	0.0	1.0000	-0.024	0.861	0.770
2207850905	9.000	5.179	30.29	68.12	3.527	16.45	78.73	73.63	1.2438	99.60	0.0	1.0000	-0.024	0.857	0.804
2207850906	9.000	5.185	30.31	77.71	3.700	16.03	86.34	75.92	1.3542	99.60	0.0	1.0000	-0.242	0.883	0.834
2207850907	9.000	5.189	30.32	87.88	3.951	15.73	89.40	79.43	1.4096	99.61	0.0	1.0000	5.114	0.989	0.909
2207851001	10.000	5.021	30.07	49.02	5.989	15.65	52.04	50.55	0.8033	99.57	0.0	1.0000	0.109	0.884	0.765
2207851002	10.000	5.065	30.10	56.60	5.945	15.64	57.91	53.90	0.9875	99.59	0.0	1.0000	0.041	0.894	0.775
2207851003	10.000	5.073	30.12	59.96	6.051	15.57	65.72	61.92	1.1043	99.60	0.0	1.0000	-0.013	0.904	0.775
2207851004	10.000	5.062	30.09	65.16	6.262	15.50	68.59	64.29	1.2136	99.61	0.0	1.0000	-0.017	0.925	0.828
2207851005	10.000	5.034	30.02	71.08	6.274	15.45	72.71	66.99	1.3159	99.61	0.0	1.0000	-0.301	0.936	0.845
2207851006	10.000	5.021	30.03	77.33	6.301	15.42	76.93	68.72	1.3902	99.64	0.0	1.0000	-0.294	0.961	0.865
2207851007	10.000	5.010	30.03	84.76	6.361	15.41	79.38	69.54	1.4516	99.64	0.0	1.0000	3.586	1.055	0.956
1908851101	11.197	5.374	30.75	46.10	4.730	16.39	50.71	49.39	0.6756	99.59	0.0	0.9973	0.024	1.014	0.774
1908851102	11.197	5.382	30.76	51.33	4.724	16.56	54.19	54.23	0.7955	99.58	0.0	0.9973	-0.044	0.978	0.755
1908851103	11.197	5.399	30.81	57.36	4.737	16.76	58.35	55.67	0.8716	99.61	0.1	0.9973	-0.024	1.010	0.794
1908851104	11.197	5.428	30.91	63.93	4.771	16.82	61.07	57.33	0.9505	99.60	0.0	0.9973	-0.025	1.057	0.776
1908851105	11.197	5.441	30.96	69.66	4.885	16.92	63.58	60.44	1.0693	99.61	0.0	0.9973	-0.028	1.063	0.818
1908851106	11.197	5.462	31.02	75.68	4.892	17.03	64.15	61.78	1.1873	99.63	0.0	0.9973	0.058	1.075	0.877
1908851107	11.197	5.480	31.14	79.55	4.886	17.03	65.71	62.48	1.2092	99.62	0.0	0.9973	2.707	1.235	1.015
1908851201	12.710	5.216	30.23	43.97	4.946	17.83	51.68	48.96	0.6958	99.67	0.0	0.9973	0.109	1.067	0.869
1908851202	12.710	5.231	30.18	48.78	4.976	17.92	54.08	51.50	0.8191	99.68	0.0	0.9973	0.068	1.082	0.853
1908851203	12.710	5.237	30.20	51.48	4.980	18.04	55.34	53.18	0.9163	99.68	0.0	0.9973	-0.099	1.067	0.877
1908851204	12.710	5.241	30.22	54.02	4.966	18.08	56.82	54.64	0.9801	99.69	0.0	0.9973	-0.026	1.109	0.938
1908851205	12.710	5.249	30.20	59.60	4.955	18.13	57.85	56.16	1.0948	99.70	0.0	0.9973	-0.079	1.121	0.912
1908851206	12.710	5.266	30.30	64.31	4.947	18.20	59.50	58.97	1.1547	99.73	0.0	0.9973	0.118	1.143	0.926
1908851207	12.710	5.261	30.23	69.61	4.905	18.23	61.20	60.68	1.2137	99.73	0.0	0.9973	4.879	1.239	1.064

TABLE C.1c

Steam-Water Data (Low Steam Extraction Rate Tests)

Inlet Water Subcooling = 60 K

TEST No	Qfin	WC	Tfin	Two	Mcw	Tc1	Tc2	TD	Mssup	Ts	VPI	Patm	PD	TT	TL
2307850401	4.000	6.223	40.24	89.90	4.122	16.73	79.84	65.80	0.7910	99.64	1.0	1.0133	-0.005	0.596	0.409
2307850402	4.000	6.220	40.21	94.73	4.104	16.78	82.59	67.04	0.9271	99.66	1.5	1.0133	-0.007	0.654	0.436
2307850403	4.000	6.228	40.23	97.38	4.087	16.85	87.23	69.54	1.0134	99.67	2.2	1.0133	-0.049	0.666	0.428
2307850404	4.000	6.233	40.29	97.67	4.089	16.55	91.22	75.08	1.2125	99.67	2.5	1.0133	-0.041	0.656	0.430
2307850405	4.000	6.241	40.30	97.73	4.220	16.63	92.48	79.63	1.3220	99.67	2.8	1.0133	-0.007	0.659	0.442
2307850406	4.000	6.245	40.31	97.99	4.217	16.69	92.79	81.14	1.3850	99.70	3.0	1.0133	-0.034	0.628	0.454
2307850407	4.000	6.242	40.31	98.04	4.231	16.87	93.08	82.74	1.4307	99.71	3.2	1.0133	0.012	0.638	0.492
2307850408	4.000	6.251	40.34	98.25	4.203	16.40	93.31	83.93	1.4523	99.71	3.2	1.0133	0.420	0.625	0.530
2307850501	5.000	6.112	39.96	90.76	4.488	15.99	80.58	69.15	0.8113	99.64	2.0	1.0133	0.048	0.576	0.472
2307850502	5.000	6.182	39.92	93.92	4.479	16.08	82.49	69.90	0.8653	99.64	2.1	1.0133	-0.035	0.633	0.483
2307850503	5.000	6.185	39.96	96.91	4.455	16.12	84.90	70.71	0.9218	99.65	2.3	1.0133	-0.034	0.686	0.459
2307850504	5.000	6.197	39.98	97.47	4.446	16.30	87.43	71.23	1.0420	99.66	2.5	1.0133	-0.075	0.690	0.451
2307850505	5.000	6.203	40.00	97.73	4.349	16.33	89.59	73.71	1.1575	99.66	2.9	1.0133	-0.006	0.685	0.460
2307850506	5.000	6.211	40.05	97.73	4.458	16.57	91.93	80.50	1.2969	99.68	3.4	1.0133	-0.030	0.689	0.474
2307850507	5.000	6.210	40.06	97.74	4.452	16.59	92.39	82.04	1.3444	99.69	4.6	1.0133	-0.025	0.715	0.468
2307850508	5.000	6.214	40.06	97.90	4.488	16.67	92.71	83.06	1.4304	99.72	3.8	1.0133	0.741	0.720	0.526
2307850601	6.000	6.226	40.26	91.99	4.352	16.00	76.73	64.67	0.7788	99.87	2.0	1.0133	0.052	0.653	0.501
2307850602	6.000	6.232	40.35	96.04	4.359	16.11	85.82	71.07	0.9488	99.89	2.8	1.0133	-0.003	0.688	0.542
2307850603	6.000	6.236	40.35	97.01	4.364	16.28	90.99	79.88	1.1166	99.87	3.6	1.0133	-0.005	0.715	0.528
2307850604	6.000	6.237	40.31	97.56	4.323	16.07	91.61	81.08	1.1905	99.86	3.9	1.0133	-0.015	0.687	0.531
2307850605	6.000	6.231	40.30	97.60	4.368	16.10	92.29	84.49	1.2735	99.88	4.3	1.0133	-0.121	0.696	0.491
2307850606	6.000	6.219	40.21	97.46	4.351	16.14	92.78	85.77	1.3556	99.88	3.2	1.0133	-0.014	0.713	0.502
2307850607	6.000	6.203	40.13	97.88	4.366	16.50	92.60	85.98	1.4098	99.90	3.2	1.0133	0.750	0.711	0.592
2307850701	7.000	6.193	39.95	76.71	4.335	15.38	72.35	67.05	0.7934	99.73	0.0	1.0133	-0.017	0.662	0.563
2307850702	7.000	6.150	39.70	81.88	4.342	15.39	80.11	72.76	0.9283	99.75	0.0	1.0133	-0.063	0.703	0.568
2307850703	7.000	6.129	39.58	88.72	4.349	15.32	89.32	77.94	1.1011	99.76	0.0	1.0133	-0.070	0.691	0.572
2307850704	7.000	6.131	39.59	93.72	4.341	15.35	90.89	79.75	1.1984	99.77	0.0	1.0133	-0.102	0.695	0.590
2307850705	7.000	6.148	39.61	95.95	4.356	15.31	91.14	82.22	1.2783	99.78	0.8	1.0133	-0.106	0.721	0.588
2307850706	7.000	6.151	39.52	96.71	4.343	15.32	92.00	84.93	1.3303	99.79	0.2	1.0133	-0.095	0.722	0.600
2307850707	7.000	6.136	39.41	97.41	4.382	15.41	92.23	85.94	1.3802	99.80	0.0	1.0133	2.948	0.788	0.676
2407850801	8.000	6.144	39.59	60.40	4.777	15.20	59.91	61.59	0.7110	99.60	0.0	1.0133	-0.076	0.778	0.633
2407850802	8.000	6.152	39.59	69.41	4.779	15.18	65.91	65.83	0.8478	99.61	0.0	1.0133	-0.095	0.790	0.716
2407850803	8.000	6.151	39.59	74.30	4.788	15.16	73.98	67.98	0.9551	99.60	0.0	1.0133	-0.106	0.778	0.672
2407850804	8.000	6.145	39.54	84.72	4.821	15.13	82.02	71.63	1.1230	99.61	0.0	1.0133	-0.092	0.786	0.642
2407850805	8.000	6.189	39.64	90.44	4.857	15.19	87.58	76.32	1.2668	99.63	0.0	1.0133	-0.030	0.721	0.681
2407850806	8.000	6.183	39.61	92.44	4.787	15.13	88.28	80.04	1.3469	99.64	0.0	1.0133	0.011	0.729	0.690
2407850807	8.000	6.172	39.51	94.52	4.830	15.20	89.36	82.07	1.3947	99.66	0.0	1.0133	2.948	0.803	0.776

TABLE C.1c (Continue)

Steam-Water Data (Low Steam Extraction Rate Tests)

Inlet Water Subcooling = 60 K

TEST No	Qfin	WC	Tfin	Two	Mcw	Tc1	Tc2	TD	Mssup	Ts	VPI	Pata	PD	TT	TL
2407850901	9.000	6.235	40.27	67.66	4.886	16.38	62.46	61.32	0.7709	99.59	0.0	1.0133	0.053	0.840	0.660
2407850902	9.000	6.231	40.25	77.02	4.937	16.35	73.58	67.76	0.9988	99.61	0.0	1.0133	0.005	0.836	0.656
2407850903	9.000	6.227	40.21	83.05	4.912	16.33	82.05	71.32	1.1293	99.59	0.0	1.0133	-0.014	0.830	0.655
2407850904	9.000	6.221	40.20	85.63	4.911	16.38	87.61	77.51	1.2988	99.61	0.0	1.0133	-0.051	0.839	0.680
2407850905	9.000	6.214	40.17	89.16	4.884	15.21	89.05	79.44	1.3845	99.63	0.0	1.0133	-0.043	0.842	0.703
2407850906	9.000	6.210	40.15	91.59	4.917	16.59	90.39	81.69	1.4403	99.65	0.0	1.0133	-0.198	0.847	0.701
2407850907	9.000	6.205	40.15	93.72	4.898	16.43	90.91	82.67	1.4705	99.65	0.0	1.0133	4.844	0.929	0.770
2707851001	10.000	6.311	41.26	65.13	4.759	18.10	62.21	61.95	0.7348	99.67	0.0	1.0053	-0.054	1.052	0.750
2707851002	10.000	6.318	41.26	68.76	4.741	18.27	68.20	67.52	0.8941	99.68	0.0	1.0053	-0.114	1.026	0.748
2707851003	10.000	6.330	41.41	72.67	4.730	18.24	73.62	70.46	1.0084	99.69	0.0	1.0053	-0.120	0.978	0.768
2707851004	10.000	6.339	41.44	78.51	4.726	18.54	83.71	73.70	1.1528	99.70	0.0	1.0053	-0.189	1.005	0.778
2707851005	10.000	6.360	41.38	83.37	4.698	18.53	87.10	76.27	1.2333	99.70	0.0	1.0053	-0.165	1.035	0.772
2707851006	10.000	6.377	41.40	88.71	4.703	18.67	88.11	77.71	1.2907	99.71	0.0	1.0053	-0.126	1.045	0.790
2707851007	10.000	6.380	41.40	90.48	4.712	18.85	89.25	78.23	1.3316	99.72	0.0	1.0053	3.879	1.083	0.898
2808851101	11.197	6.183	39.95	61.09	5.120	15.87	59.63	58.46	0.7558	99.59	0.0	1.0087	0.359	1.065	0.776
2808851102	11.197	6.174	39.92	67.38	5.334	15.91	62.99	60.56	0.8699	99.61	0.0	1.0087	-0.025	1.045	0.768
2808851103	11.197	6.168	39.84	71.81	5.365	16.16	65.48	61.94	0.9486	99.58	0.0	1.0087	-0.089	1.023	0.787
2808851104	11.197	6.161	39.80	73.64	5.551	16.07	68.45	64.14	1.0234	99.60	0.0	1.0087	-0.076	1.042	0.780
2808851105	11.197	6.155	39.79	77.00	5.552	16.18	70.20	65.36	1.1092	99.60	0.0	1.0087	-0.018	1.059	0.796
2808851106	11.197	6.129	39.57	79.61	5.690	16.18	70.11	66.21	1.1572	99.61	0.0	1.0087	0.035	1.071	0.830
2808851107	11.197	6.137	39.66	83.84	5.678	16.20	71.49	66.77	1.1910	99.62	0.0	1.0087	3.790	1.142	0.921
2808851201	12.710	6.161	39.70	51.54	5.659	16.28	54.87	50.04	0.7057	99.69	0.0	1.0080	0.073	1.236	0.838
2808851202	12.710	6.166	39.72	56.63	5.628	16.37	57.63	55.51	0.8509	99.71	0.0	1.0080	0.059	1.220	0.869
2808851203	12.701	6.172	39.74	60.87	5.617	16.43	60.85	59.23	0.9691	99.74	0.0	1.0080	0.008	1.208	0.906
2808851204	12.710	6.181	39.81	62.34	5.650	16.44	62.34	61.82	1.0448	99.75	0.0	1.0080	0.029	1.214	0.890
2808851205	12.710	6.190	39.82	65.96	5.631	16.44	64.03	63.07	1.1063	99.75	0.0	1.0080	-0.002	1.202	0.903

TABLE C.1d

Steam-Water Data (Low Steam Extraction Rate Tests)

Inlet Water Subcooling = 50 K

TEST No	Qfin	WC	Tfin	Two	M _{cw}	Tc1	Tc2	TD	M _{ssup}	Ts	VPI	Patm	PD	TT	TL
2507850401	4.000	7.163	50.09	97.36	4.634	22.35	79.54	71.80	0.7345	99.87	2.0	1.0133	0.038	0.514	0.445
2507850402	4.000	7.162	50.08	98.70	4.770	22.33	91.25	76.06	0.9923	99.88	2.4	1.0133	0.026	0.503	0.420
2507850403	4.000	7.154	50.00	98.78	4.763	22.34	92.01	77.91	1.0519	99.87	3.0	1.0133	0.000	0.491	0.417
2507850404	4.000	7.147	49.93	98.76	4.757	22.36	92.24	80.21	1.1856	99.88	3.1	1.0133	-0.006	0.507	0.428
2507850405	4.000	7.149	49.93	98.65	4.755	22.29	92.44	82.09	1.2547	99.89	3.2	1.0133	-0.024	0.482	0.416
2507850406	4.000	7.141	49.87	98.71	4.743	22.26	92.66	83.66	1.3487	99.90	3.3	1.0133	-0.032	0.495	0.431
2507850407	4.000	7.140	49.91	98.79	4.781	22.43	92.60	84.46	1.4008	99.89	3.4	1.0133	-0.025	0.525	0.453
2507850408	4.000	7.121	49.87	98.82	4.771	22.49	92.56	85.25	1.4527	99.89	3.4	1.0133	0.126	0.537	0.431
2507850409	4.000	7.119	49.88	98.99	4.762	22.59	92.87	86.00	1.5008	99.90	3.4	1.0133	0.779	0.595	0.470
2507850501	5.000	7.335	50.44	93.68	4.907	22.05	73.34	67.68	0.6999	99.78	1.9	1.0120	0.038	0.442	0.430
2507850503	5.000	7.275	50.37	97.99	4.912	22.69	86.58	72.31	0.9239	99.80	2.4	1.0120	-0.097	0.452	0.450
2507850502	5.000	7.277	50.35	98.01	4.837	22.92	87.85	73.91	0.9783	99.78	2.5	1.0120	-0.096	0.522	0.425
2507850504	5.000	7.253	50.32	98.29	4.738	23.04	89.94	75.69	1.0460	99.77	2.8	1.0120	-0.082	0.512	0.437
2507850505	5.000	7.266	50.37	98.67	4.901	23.03	91.93	81.51	1.1376	99.77	3.0	1.0120	0.047	0.505	0.429
2507850506	5.000	7.276	50.38	98.69	4.894	23.09	91.99	82.04	1.2270	99.76	3.2	1.0120	-0.033	0.506	0.447
2507850507	5.000	7.290	50.39	98.63	4.888	23.11	92.30	83.85	1.3417	99.76	3.3	1.0120	0.020	0.539	0.449
2507850508	5.000	7.312	50.40	98.70	4.788	23.18	92.73	84.94	1.4221	99.78	3.3	1.0120	0.833	0.726	0.538
2507850601	6.000	7.036	49.80	88.54	4.477	22.41	71.76	67.40	0.7065	99.74	2.2	1.0120	-0.010	0.498	0.435
2507850602	6.000	7.058	49.83	92.81	4.355	22.49	82.02	70.92	0.8230	99.73	2.6	1.0120	-0.078	0.501	0.430
2507850603	6.000	7.071	49.89	96.43	4.308	23.51	87.17	73.89	0.9456	99.72	2.8	1.0120	-0.087	0.537	0.451
2507850604	6.000	7.143	49.95	97.64	4.293	23.63	88.98	75.34	0.9844	99.74	2.8	1.0120	-0.089	0.525	0.439
2507850605	6.000	7.151	49.97	98.72	4.287	23.73	91.40	79.84	1.1018	99.75	2.9	1.0120	0.005	0.557	0.451
2507850606	6.000	7.179	50.00	98.71	4.309	23.58	92.31	82.52	1.2469	99.73	3.1	1.0120	-0.032	0.545	0.450
2507850607	6.000	7.182	50.02	98.74	4.304	23.91	92.67	84.54	1.3063	99.76	3.1	1.0120	0.124	0.660	0.463
2507850608	6.000	7.195	50.07	98.93	4.312	23.75	92.93	85.56	1.3366	99.76	3.1	1.0120	0.812	0.752	0.548
2607850701	7.000	7.380	50.36	85.00	4.478	20.48	70.60	67.84	0.6849	99.79	2.0	1.0040	0.113	0.596	0.478
2607850702	7.000	7.381	50.35	91.94	4.399	19.54	84.82	72.82	0.8744	99.77	2.3	1.0040	0.013	0.599	0.478
2607850703	7.000	7.366	50.34	95.83	4.378	19.14	86.51	75.47	0.9765	99.79	2.3	1.0040	0.018	0.581	0.480
2607850704	7.000	7.318	50.26	97.86	4.485	19.42	89.09	83.20	1.1252	99.82	0.0	1.0040	-0.045	0.598	0.490
2607850705	7.000	7.304	50.23	97.67	4.473	18.94	91.73	86.66	1.2340	99.82	0.0	1.0040	-0.050	0.611	0.496
2607850706	7.000	7.259	50.26	97.84	4.513	18.79	91.83	87.46	1.2855	99.83	1.0	1.0040	0.051	0.636	0.538
2607850707	7.000	7.244	50.26	97.79	4.395	19.18	91.92	87.49	1.3435	99.84	2.0	1.0040	1.089	0.761	0.630
2607850801	8.000	7.376	50.49	83.81	4.279	20.78	68.61	65.81	0.6430	99.60	1.3	1.0040	0.069	0.691	0.529
2607850802	8.000	7.367	50.49	88.31	4.282	20.72	75.54	69.35	0.7658	99.61	1.4	1.0040	0.073	0.687	0.518
2607850803	8.000	7.382	50.54	92.11	4.237	20.50	81.45	73.65	0.9302	99.60	1.4	1.0040	-0.005	0.701	0.499
2607850804	8.000	7.410	50.66	94.33	4.221	19.71	87.56	78.68	1.0591	99.62	1.5	1.0040	-0.047	0.699	0.510
2607850805	8.000	7.421	50.73	95.79	4.203	19.60	91.30	85.04	1.1668	99.61	2.0	1.0040	0.028	0.723	0.523
2607850806	8.000	7.419	50.77	97.48	4.166	20.43	91.83	88.30	1.2327	99.61	2.0	1.0040	0.016	0.736	0.504
2607850807	8.000	7.429	50.79	97.50	4.203	20.51	91.89	88.20	1.3019	99.61	2.0	1.0040	1.272	0.844	0.728

TABLE C.1d (Continue)

Steam-Water Data (Low Steam Extraction Rate Tests)

Inlet Water Subcooling = 50 K

TEST No	Qfin	WC	Tfin	Two	Mcw	Tc1	Tc2	TD	Mssup	Ts	VPI	Patm	PD	TT	TL
2607850901	9.000	7.458	50.96	76.29	4.539	20.67	69.84	64.84	0.6459	99.62	0.0	1.0040	0.083	0.809	0.638
2607850902	9.000	7.447	50.84	82.71	4.549	20.73	75.75	69.93	0.8058	99.61	0.0	1.0040	0.099	0.795	0.664
2607850903	9.000	7.451	50.85	88.19	4.413	20.77	82.40	77.39	0.9929	99.60	0.0	1.0040	0.048	0.805	0.683
2607850904	9.000	7.501	50.81	93.77	4.439	20.81	86.59	82.56	1.1487	99.63	0.0	1.0040	-0.068	0.812	0.692
2607850905	9.000	7.426	50.79	95.69	4.566	20.80	87.49	85.26	1.2294	99.63	0.0	1.0040	0.015	0.835	0.700
2607850906	9.000	7.403	50.78	96.20	4.545	20.78	88.45	87.32	1.2914	99.64	0.0	1.0040	0.011	0.854	0.748
2608850907	9.000	7.470	50.90	96.71	4.639	20.94	90.06	86.32	1.3452	99.65	0.0	1.0040	2.925	0.930	0.847
2608850901	10.000	7.262	50.32	68.62	4.591	21.52	74.39	65.51	0.7293	99.73	0.0	1.0027	0.025	0.873	0.645
2608851002	10.000	7.268	50.37	73.35	4.571	21.88	84.52	74.82	0.9697	99.72	0.0	1.0027	-0.168	0.862	0.615
2608851003	10.000	7.339	50.56	79.75	4.566	21.69	88.54	79.64	1.1179	99.73	0.0	1.0027	-0.088	0.860	0.655
2608851004	10.000	7.312	50.48	86.45	4.564	21.40	89.82	84.08	1.2265	99.74	0.0	1.0027	-0.043	0.879	0.661
2608851005	10.000	7.314	50.47	90.73	4.564	21.13	90.43	85.86	1.2813	99.73	0.0	1.0027	-0.103	0.890	0.684
2608851006	10.000	7.319	50.47	93.92	4.566	21.10	90.43	86.61	1.3338	99.73	0.0	1.0027	-0.059	0.901	0.741
2608851007	10.000	7.322	50.47	95.85	4.555	21.11	90.42	87.78	1.3861	99.73	0.0	1.0027	1.615	0.981	0.858
2608851101	11.197	7.190	50.22	67.67	4.856	16.73	67.22	64.67	0.7227	99.75	0.0	1.0093	-0.096	0.896	0.752
2508851102	11.197	7.319	50.43	73.09	4.884	16.77	73.38	69.09	0.8815	99.73	0.0	1.0093	-0.210	0.917	0.745
2508851103	11.197	7.465	50.62	77.00	4.837	16.67	79.21	72.44	1.0114	99.73	0.0	1.0093	-0.215	0.915	0.685
2507851104	11.197	7.397	50.54	81.80	4.842	16.57	88.68	77.14	1.1922	99.73	0.0	1.0093	-0.264	0.923	0.786
2507851105	11.197	7.514	50.78	85.02	4.849	16.73	89.22	82.89	1.3392	99.73	0.0	1.0093	-0.125	0.915	0.785
2507851106	11.197	7.463	50.50	88.12	4.844	16.85	89.41	84.32	1.4209	99.73	0.0	1.0093	-0.078	0.942	0.856
2507851107	11.197	7.431	50.43	90.96	4.833	16.99	89.41	85.59	1.4776	99.74	0.0	1.0093	4.225	1.062	0.962
2507851201	12.710	7.429	50.41	60.71	4.809	18.52	61.90	59.82	0.6094	99.59	0.0	1.0093	0.019	0.967	0.802
2507851202	12.710	7.507	50.51	65.89	4.812	18.53	66.72	63.91	0.7544	99.60	0.0	1.0093	-0.072	0.973	0.835
2507851203	12.710	7.524	50.67	69.27	4.866	18.59	70.23	68.11	0.8932	99.51	0.0	1.0093	-0.105	0.968	0.828
2507851204	12.710	7.498	50.54	74.30	4.788	18.84	78.47	72.55	1.0743	99.57	0.0	1.0093	-0.126	0.970	0.858
2507851205	12.710	7.516	50.75	80.92	4.859	18.57	83.43	74.00	1.1859	99.59	0.0	1.0093	-0.160	0.983	0.835
2507851206	12.710	7.523	50.76	85.52	4.866	18.63	86.41	75.64	1.2729	99.60	0.0	1.0093	0.776	1.003	0.835
2507851207	12.710	7.535	50.77	88.49	4.862	18.69	87.59	76.38	1.3157	99.61	0.0	1.0093	4.991	1.163	0.957
2507851401	14.229	7.210	50.04	59.98	4.828	13.33	62.43	58.62	0.6754	99.70	0.0	1.0053	-0.110	1.144	0.873
2507851402	14.229	7.127	49.90	66.14	4.702	13.71	67.44	68.11	0.9426	99.73	0.0	1.0053	-0.040	1.160	0.866
2507851403	14.229	7.120	49.91	70.58	4.683	13.60	73.05	70.92	1.0747	99.74	0.0	1.0053	-0.218	1.171	0.955
2507851404	14.229	7.173	50.05	74.88	4.715	13.40	77.43	72.09	1.1573	99.76	0.0	1.0053	-0.188	1.172	0.958
2507851405	14.229	7.169	50.05	78.83	4.743	13.76	79.03	73.27	1.2160	99.76	0.0	1.0053	-0.197	1.188	0.960
2507851406	14.229	7.165	50.04	83.67	4.504	13.58	82.57	74.31	1.2699	99.77	0.0	1.0053	-0.089	1.207	0.967
2507851407	14.229	7.159	50.03	86.47	4.471	13.54	83.09	74.87	1.2983	99.78	0.0	1.0053	5.805	1.297	1.071
2507851501	15.755	7.567	50.98	57.26	4.861	16.14	58.47	57.99	0.6084	99.69	0.0	1.0053	0.033	1.261	1.001
2507851502	15.755	7.573	50.99	61.17	4.845	16.13	64.56	62.15	0.7829	99.71	0.0	0.0000	0.005	1.297	1.030
2507851503	15.755	7.630	51.00	65.13	4.860	16.21	71.11	65.74	0.9522	99.70	0.0	1.0053	0.051	1.267	1.009
2507851504	15.755	7.651	51.09	68.37	4.877	16.31	74.97	68.26	1.0855	99.69	0.0	1.0053	0.056	1.268	1.028
2507851505	15.755	7.664	51.04	72.21	4.807	16.45	76.37	70.37	1.1577	99.70	0.0	1.0053	-0.002	1.307	1.053
2507851506	15.755	7.703	51.08	75.43	4.817	16.32	77.64	70.43	1.2034	99.72	0.0	1.0053	0.101	1.349	1.092
2507851507	15.755	7.672	51.00	78.25	4.813	16.25	78.37	70.99	1.2406	99.72	0.0	1.0053	3.578	1.421	1.206

TABLE C.1a

Steam-Water Data (Low Steam Extraction Rate Tests)

Inlet Water Subcooling = 40 K

TEST NO	Dfin	WC	Tfin	Two	Mcw	Tc1	Tc2	TD	Mssup	Ts	VPI	Patm	PD	TT	TL
2907850401	4.000	7.995	59.48	92.30	4.292	21.42	86.89	71.73	0.6787	99.62	2.1	0.9960	-0.016	0.471	0.400
2907850402	4.000	8.005	59.56	97.61	4.270	21.52	92.55	80.14	0.8959	99.62	2.3	0.9960	0.137	0.472	0.410
2907850403	4.000	8.011	59.60	97.63	4.203	21.44	92.90	81.24	0.9587	99.64	2.5	0.9960	0.128	0.466	0.401
2907850404	4.000	8.115	59.69	97.59	4.199	21.27	93.11	83.84	1.0972	99.64	2.6	0.9960	0.055	0.458	0.418
2907850405	4.000	8.121	59.69	97.77	4.160	21.03	93.15	85.73	1.2012	99.66	2.6	0.9960	0.163	0.470	0.409
2907850406	4.000	8.001	59.43	97.82	4.001	21.19	93.27	86.14	1.3486	99.69	2.7	0.9960	0.079	0.453	0.402
2907850407	4.000	8.004	59.48	97.98	4.077	21.31	93.13	89.53	1.4524	99.69	2.9	0.9960	0.135	0.460	0.414
2907850408	4.000	8.012	59.54	98.08	4.162	21.25	93.37	89.98	1.5138	99.70	3.0	0.9960	0.721	0.575	0.473
2907850501	5.000	8.247	60.54	95.32	4.300	20.28	78.45	71.83	0.6109	99.75	2.3	0.9960	0.303	0.472	0.446
2907850502	5.000	8.258	60.62	97.31	4.305	20.50	87.61	75.56	0.7343	99.75	3.1	0.9960	-0.066	0.478	0.441
2907850503	5.000	8.270	60.72	97.94	4.312	21.36	90.11	77.56	0.8494	99.76	3.2	0.9960	-0.049	0.488	0.430
2907850504	5.000	8.296	60.79	98.07	4.299	20.92	90.56	80.64	0.9945	99.74	3.3	0.9960	-0.045	0.531	0.439
2907850505	5.000	8.289	60.80	98.08	4.246	20.54	90.86	84.27	1.2662	99.75	3.4	0.9960	-0.046	0.547	0.460
2907850506	5.000	8.296	60.81	97.98	4.261	20.21	91.97	85.67	1.3897	99.74	3.4	0.9960	-0.019	0.541	0.445
2907850507	5.000	8.308	60.84	98.24	4.247	20.20	92.64	86.86	1.4353	99.79	3.4	0.9960	0.672	0.657	0.540
2907850601	6.000	8.175	60.39	93.04	4.545	18.44	77.95	71.71	0.6651	99.68	2.1	0.9960	0.080	0.540	0.439
2907850602	6.000	8.165	60.43	96.32	4.530	18.63	87.22	76.05	0.8366	99.74	2.3	0.9960	0.059	0.537	0.411
2907850603	6.000	8.134	60.40	97.16	4.431	18.48	89.77	79.81	1.0100	99.75	2.9	0.9960	0.119	0.487	0.428
2907850604	6.000	8.157	60.33	97.26	4.287	18.76	90.65	81.46	1.1263	99.76	3.0	0.9960	0.168	0.573	0.451
2907850605	6.000	8.163	60.40	97.87	4.331	18.79	92.34	83.29	1.3118	99.76	3.0	0.9960	0.162	0.564	0.448
2907850606	6.000	8.167	60.35	97.92	4.330	18.93	92.26	86.60	1.3803	99.76	3.0	0.9960	0.227	0.635	0.464
2907850607	6.000	8.179	60.46	98.07	4.304	18.85	92.19	87.83	1.4317	99.77	3.0	0.9960	1.243	0.701	0.532
2907850701	7.000	8.214	60.59	89.80	4.236	20.77	80.58	71.86	0.6553	99.71	2.0	0.9960	0.230	0.720	0.535
2907850702	7.000	8.225	60.67	92.06	4.225	20.91	86.63	73.84	0.7705	99.71	2.0	0.9960	0.131	0.726	0.574
2907850703	7.000	8.231	60.67	95.22	4.258	20.97	88.37	75.04	0.8352	99.70	2.0	0.9960	0.133	0.744	0.576
2907850704	7.000	8.237	60.72	95.64	4.297	21.01	90.50	77.95	0.9138	99.70	2.0	0.9960	0.129	0.746	0.577
2907850705	7.000	8.238	60.62	96.93	4.097	21.10	91.23	86.22	1.0753	99.69	1.0	0.9960	0.120	0.768	0.576
2907850706	7.000	8.235	60.66	97.25	4.230	21.24	91.53	88.00	1.2528	99.69	2.0	0.9960	0.109	0.780	0.570
2907850707	7.000	8.241	60.67	97.25	4.237	21.04	91.82	88.20	1.3376	99.73	2.0	0.9960	0.071	0.790	0.570
2907850708	7.000	8.253	60.69	97.71	4.186	21.09	91.90	88.89	1.3966	99.74	2.0	0.9960	1.841	0.874	0.636
3007850801	8.000	7.882	59.45	85.86	4.449	18.34	79.86	71.13	0.6812	99.63	0.0	1.0013	0.017	0.705	0.507
3007850802	8.000	7.937	59.57	89.09	4.438	18.40	84.16	76.04	0.8431	99.63	0.0	1.0013	0.021	0.736	0.534
3007850803	8.000	7.941	59.54	93.63	4.397	18.57	86.92	80.13	1.0003	99.62	0.0	1.0013	0.104	0.724	0.501
3007850804	8.000	8.001	59.64	96.47	4.450	18.44	90.43	82.43	1.1401	99.64	2.0	1.0013	0.024	0.725	0.504
3007850805	8.000	7.984	59.57	97.07	4.478	18.44	90.96	86.90	1.3060	99.66	2.9	1.0013	0.141	0.795	0.534
3007850806	8.000	7.973	59.51	97.72	4.435	18.13	91.19	88.00	1.3753	99.66	3.0	1.0013	-0.014	0.776	0.555
3007850807	8.000	7.944	59.44	98.03	4.444	18.20	91.72	89.06	1.4280	99.67	3.5	1.0013	1.259	0.856	0.632
3007850901	9.000	8.072	59.87	84.30	4.419	20.07	75.23	70.81	0.6762	99.63	0.0	1.0000	-0.069	0.879	0.525
3007850902	9.000	8.081	59.87	91.23	4.497	20.21	79.71	73.93	0.7905	99.67	0.0	1.0000	0.022	0.846	0.592
3007850903	9.000	8.087	59.85	95.53	4.533	20.66	82.32	77.44	1.0199	99.67	0.0	1.0000	0.058	0.897	0.610
3007850904	9.000	8.093	59.91	97.03	4.445	18.62	90.42	84.46	1.1499	99.64	0.0	1.0000	0.088	0.890	0.564
3007850905	9.000	8.096	59.90	97.23	4.416	19.54	90.89	87.22	1.2570	99.67	0.0	1.0000	0.060	0.897	0.583
3007850906	9.000	8.121	59.95	97.40	4.431	19.48	91.32	88.06	1.3187	99.66	0.0	1.0000	0.070	0.904	0.593
3007850907	9.000	8.129	59.98	97.50	4.429	19.49	91.99	89.20	1.3724	99.68	0.0	1.0000	2.093	0.970	0.662
3007851001	10.000	8.044	59.78	80.65	4.411	20.54	71.06	68.44	0.6550	99.74	0.0	1.0000	0.045	0.868	0.577
3007851002	10.000	8.031	59.62	88.67	4.431	20.97	78.79	72.77	0.8076	99.74	0.0	1.0000	0.011	0.871	0.588
3007851003	10.000	8.017	59.53	93.31	4.435	21.14	85.29	75.11	0.9563	99.73	0.0	1.0000	0.004	0.875	0.628
3007851004	10.000	7.994	59.43	95.82	4.423	20.12	90.05	82.58	1.1494	99.74	0.0	1.0000	0.002	0.876	0.605
30.0785105	10.000	7.991	59.45	95.87	4.411	20.65	90.36	83.46	1.1801	99.73	0.0	1.0000	0.003	0.868	0.637
3007851005	10.000	8.003	59.56	96.07	4.401	21.21	90.72	84.85	1.2206	99.72	0.0	1.0000	0.126	0.863	0.661
3007851006	10.000	7.997	59.51	97.03	4.441	21.32	91.00	86.44	1.2646	99.72	0.0	1.0000	-0.023	0.850	0.709

TABLE C.1e (Continue)

Steam-Water Data (Low Steam Extraction Rate Tests)

Inlet Water Subcooling = 40 K

TEST NO	Qfin	WC	Tfin	Two	Mcw	Tc1	Tc2	TD	Mssup	Ts	VPI	Patm	PD	TT	TL
3007851007	10.000	7.989	59.51	97.57	4.399	20.40	91.37	87.43	1.3283	99.75	0.0	1.0000	1.227	0.924	0.782
3007851101	11.197	8.115	60.07	75.06	4.427	20.77	73.50	68.42	0.6559	99.59	0.0	1.0000	0.066	0.963	0.580
3007851102	11.197	8.131	60.10	82.00	4.387	21.15	79.85	74.05	0.8337	99.57	0.0	1.0000	-0.020	0.989	0.646
3007851103	11.197	8.149	60.20	88.76	4.432	20.27	89.91	79.19	1.0374	99.63	0.0	1.0000	0.070	0.970	0.653
3007851104	11.197	8.139	60.11	93.58	4.417	20.07	90.57	83.80	1.1573	99.60	0.0	1.0000	0.088	1.016	0.731
3007851105	11.197	8.142	60.14	95.45	4.417	20.83	90.89	88.50	1.2714	99.60	1.0	1.0000	0.057	1.016	0.735
3007851106	11.197	8.132	60.12	96.33	4.410	20.76	90.60	88.10	1.3309	99.61	1.2	1.0000	0.102	1.025	0.732
3076851107	11.197	8.125	60.13	96.85	4.403	20.83	90.72	88.77	1.3839	99.63	1.3	1.0000	3.157	1.076	0.851
3007851201	12.710	8.214	60.57	72.63	4.959	16.12	72.00	66.41	0.6623	99.60	0.0	0.9973	-0.187	1.121	0.688
2008851202	12.710	8.221	60.53	80.79	4.853	16.86	77.07	71.55	0.8568	99.63	0.0	0.9973	0.041	1.114	0.724
2008851203	12.710	8.259	60.72	84.13	4.830	16.87	84.55	75.83	1.0242	99.60	0.0	0.9973	-0.005	1.085	0.739
2008851204	12.710	8.243	60.55	86.11	4.781	16.97	89.78	80.41	1.2101	99.60	0.0	0.9973	0.038	1.116	0.784
2008851205	12.710	8.238	60.53	89.64	4.930	16.63	90.81	83.01	1.3173	99.63	0.0	0.9973	0.059	1.106	0.797
2008851206	12.710	8.228	60.56	92.71	4.953	16.95	91.30	86.10	1.4070	99.65	0.0	0.9973	-0.028	1.140	0.782
2008851207	12.710	8.233	60.57	93.33	4.953	16.84	92.23	86.65	1.4733	99.65	0.0	0.9973	1.768	1.310	0.876
2008851401	14.229	8.176	60.22	69.54	5.001	16.76	69.86	64.39	0.6028	99.61	0.0	0.9973	-0.083	1.182	0.798
2008851402	14.229	8.183	60.27	74.13	4.802	17.09	77.18	69.39	0.8274	99.59	0.0	0.9973	0.156	1.200	0.802
2008851403	14.229	8.202	60.35	78.50	4.816	17.29	81.45	74.15	0.9987	99.63	0.0	0.9973	0.140	1.152	0.837
2008851404	14.229	8.210	60.37	82.70	4.953	17.10	86.40	77.47	1.1562	99.64	0.0	0.9973	-0.037	1.215	0.816
2008851405	14.229	8.254	60.65	86.02	4.912	17.66	89.19	78.67	1.2209	99.63	0.0	0.9973	0.121	1.202	0.821
2008851406	14.229	8.283	60.77	90.23	4.898	17.78	90.01	79.83	1.2773	99.64	0.0	0.9973	0.157	1.215	0.841
2008851407	14.229	8.295	60.85	91.19	4.887	17.78	90.72	80.75	1.3065	99.66	0.0	0.9973	2.384	1.302	0.989
2008851501	15.755	8.290	60.82	75.69	4.909	17.93	71.96	63.67	0.6183	99.69	0.0	0.9960	0.194	1.312	0.828
2008851502	15.755	8.312	60.97	77.60	4.911	17.93	73.55	65.97	0.6970	99.69	0.0	0.9960	0.187	1.286	0.809
2008851503	15.755	8.319	60.96	84.80	4.914	17.94	77.26	68.30	0.8512	99.70	0.0	0.9960	0.183	1.326	0.854
2008851504	15.755	8.321	60.96	86.29	4.924	17.97	79.88	71.57	0.9343	99.69	0.0	0.9960	0.161	1.301	0.881
2008851505	15.755	8.336	61.01	89.42	4.920	17.91	83.58	74.23	1.0706	99.69	0.0	0.9960	0.073	1.318	0.874
2008851506	15.755	8.342	61.11	90.02	4.912	17.77	85.92	76.46	1.1266	99.68	0.0	0.9960	0.147	1.361	0.896
2008851507	15.755	8.357	61.15	91.22	4.921	17.78	86.02	77.19	1.1659	99.69	0.0	0.9960	2.984	1.493	0.982
2108851701	17.287	8.082	59.86	70.15	4.875	15.52	67.10	62.06	0.6011	99.61	0.0	1.0067	0.080	1.370	0.840
2108851702	17.287	8.054	59.71	74.74	4.881	15.50	70.72	64.54	0.7130	99.61	0.0	1.0067	0.004	1.383	0.874
2108851703	17.287	8.041	59.65	77.55	4.918	15.50	73.41	66.80	0.8224	99.62	0.0	1.0067	-0.005	1.400	0.889
2108851704	17.287	8.053	59.74	80.32	4.888	15.49	75.76	68.96	0.9273	99.60	0.0	1.0067	0.014	1.379	0.926
2108851705	17.287	8.079	59.81	83.12	4.864	15.51	77.26	70.00	1.0172	99.60	0.0	1.0067	0.017	1.389	0.914
2108851706	17.287	8.063	59.74	85.87	4.999	15.37	78.76	70.32	1.0967	99.61	0.0	1.0067	0.165	1.397	0.958
2108851707	17.287	8.059	59.75	87.34	4.923	15.33	79.12	71.06	1.1331	99.62	0.0	1.0067	3.766	1.525	1.088
2208851801	18.827	8.294	60.92	67.89	5.068	16.28	66.17	61.26	0.5829	99.60	0.0	1.0053	0.002	1.435	0.904
2208851802	18.827	8.288	60.91	71.77	5.046	16.26	68.71	63.71	0.6919	99.61	0.0	1.0053	0.091	1.445	0.874
2208851803	18.827	8.278	60.90	76.31	5.022	16.24	72.25	66.12	0.8708	99.64	0.0	1.0053	0.107	1.449	0.933
2208851804	18.827	8.275	60.91	77.67	4.984	16.16	74.88	68.42	0.9510	99.62	0.0	1.0053	0.113	1.444	0.922
2208851805	18.827	8.285	60.95	78.93	4.978	16.20	75.35	69.24	1.0207	99.64	0.0	1.0053	0.149	1.464	0.975
2208851806	18.827	8.295	60.96	80.91	4.982	16.22	76.63	69.61	1.0968	99.65	0.0	1.0053	0.298	1.466	0.997
2208851807	18.827	8.319	61.01	83.45	4.950	16.23	77.25	70.23	1.1299	99.66	0.0	1.0053	3.006	1.582	1.187
2208852001	20.374	8.325	61.00	63.91	5.090	16.40	64.51	60.82	0.5909	99.61	0.0	1.0053	0.057	1.536	0.950
2208852002	20.374	8.338	61.09	69.78	5.088	16.38	67.68	62.43	0.7160	99.61	0.0	1.0053	0.059	1.559	0.959
2208852003	20.374	8.335	61.03	71.46	4.989	16.22	70.78	64.27	0.7883	99.63	0.0	1.0053	0.172	1.576	0.990
2208852004	20.374	8.347	61.11	73.22	4.996	16.20	71.85	65.81	0.8983	99.62	0.0	1.0053	0.122	1.569	1.039
2208852005	20.374	8.359	61.15	74.24	5.067	16.16	72.01	66.90	1.0365	99.66	0.0	1.0053	0.118	1.596	1.035
2208852006	20.374	8.333	61.08	76.33	4.951	16.17	74.50	68.74	1.1092	99.66	0.0	1.0053	0.111	1.587	1.071
2208852007	20.374	8.342	61.12	79.81	4.917	16.18	75.17	68.98	1.1532	99.65	0.0	1.0053	3.950	1.743	1.194

TABLE C.1f

Steam-Water Data (Low Steam Extraction Rate Tests)

Inlet Water Subcooling = 30 K

TEST No	Qfin	WC	Tfin	Two	Mcw	Tc1	Tc2	TD	Mssup	Ts	VPI	Pata	PD	TT	TL
3107850401	4.000	8.938	69.78	96.68	4.211	18.97	79.85	74.85	0.7123	99.67	2.8	1.0100	0.042	0.451	0.394
3107850402	4.000	8.966	69.90	97.57	4.210	18.77	90.74	79.41	0.8861	99.69	3.0	1.0100	0.096	0.454	0.391
3107850403	4.000	9.046	70.33	97.75	4.177	18.55	91.78	81.11	0.9658	99.69	3.0	1.0100	0.009	0.467	0.418
3107850404	4.000	9.093	70.52	97.89	4.218	18.64	92.14	84.92	1.0975	99.69	3.0	1.0100	0.079	0.440	0.428
3107850405	4.000	9.115	70.63	97.98	4.250	18.33	92.54	85.86	1.3110	99.68	3.0	1.0100	0.087	0.471	0.424
3107850406	4.000	9.122	70.65	98.07	4.228	18.55	92.40	86.43	1.4215	99.71	3.1	1.0100	0.132	0.469	0.446
3107850407	4.000	9.129	70.68	98.13	4.254	18.63	92.76	86.43	1.4549	98.64	3.1	1.0100	0.176	0.489	0.450
3107850408	4.000	9.141	70.67	98.27	4.237	18.90	92.53	86.88	1.4811	99.78	3.1	1.0100	0.528	0.572	0.501
3107850501	5.000	8.977	69.84	97.08	4.260	20.72	84.04	73.90	0.7088	99.78	2.8	1.0100	0.043	0.496	0.427
3107850502	5.000	8.991	69.96	97.90	4.219	20.96	91.37	79.27	0.9393	99.76	2.9	1.0100	0.047	0.486	0.435
3107850503	5.000	9.037	70.15	97.93	4.236	20.93	92.45	81.02	1.0944	99.76	3.0	1.0100	0.095	0.495	0.437
3107850504	5.000	9.042	70.19	98.06	4.233	20.58	92.62	83.79	1.2434	99.79	3.0	1.0100	0.003	0.506	0.470
3107850505	5.000	9.065	70.24	98.00	4.253	20.92	92.69	84.89	1.2996	99.78	3.0	1.0100	0.020	0.491	0.469
3107850506	5.000	9.072	70.26	98.18	4.233	20.96	92.52	85.76	1.3593	99.79	3.1	1.0100	0.121	0.566	0.495
3107850507	5.000	9.079	70.32	98.31	4.217	21.09	92.49	86.48	1.3879	99.83	3.1	1.0100	0.855	0.576	0.533
3107850601	6.000	8.983	69.81	97.38	4.293	21.14	78.85	70.20	0.6416	99.68	2.7	1.0100	0.156	0.550	0.516
3107850602	6.000	9.007	70.04	97.75	4.279	21.37	89.04	76.17	0.8811	99.78	2.8	1.0100	0.043	0.556	0.506
3107850603	6.000	9.012	70.10	97.78	4.246	21.66	91.92	82.67	1.0301	99.80	2.9	1.0100	0.004	0.548	0.522
3107850604	6.000	9.029	70.33	97.83	4.267	21.55	92.21	84.72	1.1826	99.78	3.0	1.0100	0.071	0.532	0.514
3107850605	6.000	9.036	70.38	97.96	4.267	21.16	92.43	86.46	1.2596	99.78	3.0	1.0100	0.011	0.569	0.549
3107850606	6.000	9.041	70.35	98.13	4.255	21.32	92.32	86.94	1.3193	99.80	3.1	1.0100	0.115	0.586	0.536
3107850607	6.000	9.044	70.39	98.29	4.249	21.69	92.03	87.09	1.3812	99.81	3.1	1.0100	0.744	0.668	0.605
3107850701	7.000	8.925	69.57	96.66	4.293	21.64	90.37	74.03	0.6875	99.65	2.2	1.0100	0.025	0.581	0.505
3107850702	7.000	8.929	69.57	97.97	4.277	21.41	90.87	76.00	0.7503	99.66	2.3	1.0100	0.026	0.582	0.509
3107850703	7.000	8.948	69.66	97.93	4.262	21.36	91.70	79.87	0.8921	99.66	2.5	1.0100	0.031	0.561	0.538
3107850704	7.000	8.943	69.61	97.99	4.262	21.36	91.70	84.30	1.0615	99.65	2.0	1.0100	0.051	0.571	0.558
3107850705	7.000	8.954	69.64	98.00	4.286	21.49	84.61	87.54	1.1896	99.65	2.9	1.0100	0.034	0.581	0.568
3107850706	7.000	8.956	69.60	97.91	4.250	21.28	91.85	89.47	1.2587	99.67	3.0	1.0100	0.005	0.614	0.603
3107850707	7.000	8.948	69.59	97.89	4.258	20.93	92.10	89.29	1.3344	99.68	3.0	1.0100	0.027	0.627	0.580
3107850708	7.000	8.933	69.57	98.10	4.257	20.95	92.11	90.04	1.3655	99.70	3.0	1.0100	0.695	0.703	0.658
3107850801	8.000	8.969	69.71	91.61	4.280	20.94	81.37	76.04	0.6801	99.73	0.0	1.0100	0.034	0.696	0.621
3107850802	8.000	8.986	69.88	95.63	4.307	21.54	90.61	80.69	0.8835	99.75	0.0	1.0100	0.022	0.696	0.643
3107850803	8.000	8.973	69.71	97.71	4.244	21.44	91.64	84.61	1.0433	99.74	0.0	1.0100	0.031	0.696	0.631
3107850804	8.000	8.980	69.80	97.95	4.223	21.42	91.54	87.51	1.1095	99.76	0.0	1.0100	0.010	0.708	0.656
3107850805	8.000	8.977	69.75	97.95	4.220	21.41	91.53	89.04	1.1855	99.79	0.0	1.0100	0.012	0.712	0.660
3107850806	8.000	8.982	69.75	97.96	4.229	21.44	91.55	89.24	1.2437	99.76	0.0	1.0100	0.019	0.742	0.650
3107850807	8.000	8.973	69.78	98.39	4.238	21.45	91.76	90.32	1.3099	99.77	0.0	1.0100	0.001	0.838	0.720
3107850901	9.000	9.116	70.54	92.82	4.239	21.00	79.79	72.84	0.6178	98.73	0.0	1.0100	0.159	0.800	0.675
3107850902	9.000	9.121	70.54	96.32	4.246	21.65	90.69	79.84	0.8628	99.78	0.0	1.0100	0.007	0.813	0.666
3107850903	9.000	9.137	70.59	97.70	4.255	21.60	90.94	84.50	1.0036	99.79	0.0	1.0100	0.002	0.815	0.653
3107850904	9.000	9.140	70.61	97.73	4.261	21.59	91.18	86.71	1.1001	99.79	0.0	1.0100	0.032	0.811	0.653
3107850905	9.000	9.150	70.66	97.74	4.267	21.61	91.49	89.91	1.1793	99.79	2.2	1.0100	0.072	0.829	0.665
3107850906	9.000	9.153	70.63	97.84	4.249	21.42	91.48	89.44	1.2862	99.79	2.6	1.0100	0.040	0.816	0.678
3107850907	9.000	9.165	70.67	97.98	4.238	21.76	91.65	89.90	1.3269	99.81	2.9	1.0100	0.122	0.910	0.766
0107851001	10.000	8.905	69.45	86.18	4.089	18.33	77.13	76.50	0.6530	99.76	0.0	1.0100	0.001	0.904	0.687
0108851002	10.000	8.912	69.47	93.01	4.105	18.50	89.53	82.42	0.7980	99.74	0.0	1.0100	0.005	0.914	0.671
0108851003	10.000	8.898	69.43	97.67	4.104	18.71	90.69	86.77	1.0191	99.73	0.0	1.0100	0.064	0.926	0.684
2508851004	10.000	8.887	69.43	97.73	4.180	18.66	91.13	87.96	1.1242	99.79	3.0	1.0100	0.039	0.956	0.694
2508851005	10.000	8.901	69.43	97.71	4.222	18.83	90.96	88.93	1.2043	99.78	3.3	1.0100	0.059	0.966	0.702
2508851006	10.000	8.915	69.48	97.77	4.231	18.94	90.99	88.93	1.2541	99.77	3.5	1.0100	0.169	0.970	0.711
2508851007	10.000	8.929	69.59	98.51	4.233	19.05	91.26	89.28	1.2685	99.79	3.4	1.0100	0.560	1.079	0.797

TABLE C.1f (Continue)

Steam-Water Data (Low Steam Extraction Rate Tests)

Inlet Water Subcooling = 30 K

TEST No	Qfin	WC	Tfin	Two	Mcw	Tc1	Tc2	TD	Mssup	Ts	vPl	Patm	PD	TT	TL
2508851101	11.197	8.974	69.81	88.54	4.223	19.21	77.65	73.97	0.6518	98.68	0.0	1.0100	0.020	1.000	0.713
2508851102	11.197	8.974	69.84	91.44	4.111	19.75	89.03	79.58	0.8008	99.69	0.0	1.0100	0.098	0.981	0.735
2508851103	11.197	8.981	69.88	93.57	4.116	19.01	90.86	87.92	1.0175	99.69	0.0	1.0100	0.062	0.996	0.743
2508851104	11.197	8.993	69.87	96.64	4.115	19.21	90.88	88.01	1.0493	99.72	2.0	1.0100	0.069	1.008	0.728
2508851105	11.197	9.002	69.92	97.18	4.116	19.30	90.99	88.37	1.0997	99.74	3.4	1.0100	0.072	0.997	0.707
2508851106	11.197	8.990	69.82	97.53	4.118	19.45	91.09	89.00	1.1540	99.73	3.6	1.0100	0.053	1.011	0.780
2508851107	11.197	8.994	69.91	97.91	4.192	19.76	91.14	89.11	1.2348	99.73	3.6	1.0100	0.009	1.054	0.793
2508851108	11.197	8.982	69.82	98.12	4.170	19.58	91.28	89.25	1.2869	99.73	3.5	1.0100	0.743	1.191	0.860
2508851201	12.710	9.055	70.36	85.55	4.859	16.12	76.94	74.31	0.6759	99.60	0.0	1.0100	0.002	1.129	0.732
2508851202	12.710	9.063	70.41	90.38	4.849	16.21	80.60	79.31	0.8024	99.58	0.0	1.0100	0.002	1.172	0.754
2508851203	12.710	9.069	70.46	93.99	4.833	16.13	83.60	82.66	0.9413	99.58	0.0	1.0100	0.001	1.193	0.729
2508851204	12.710	9.076	70.46	96.00	4.867	16.03	87.60	85.33	1.1354	99.61	0.0	1.0100	0.010	1.163	0.740
2508851205	12.710	9.079	70.44	97.56	4.869	16.00	90.47	86.05	1.2516	99.64	0.0	1.0100	0.010	1.171	0.761
2508851206	12.710	9.093	70.44	97.89	4.847	16.01	91.71	87.23	1.3372	99.66	0.0	1.0100	0.012	1.186	0.800
2508851207	12.710	9.149	70.75	98.03	4.852	16.03	92.62	88.51	1.3991	99.68	0.0	1.0100	0.536	1.263	0.870
2508851401	14.229	9.010	70.02	80.70	4.843	15.99	74.78	75.01	0.6753	99.70	0.0	1.0100	0.044	1.298	0.755
2508851402	14.229	9.028	70.10	84.77	4.863	16.28	83.97	78.86	0.8094	99.71	0.0	1.0100	0.037	1.277	0.794
2508851403	14.229	9.033	70.20	91.51	4.802	16.31	89.25	83.86	1.0495	99.70	0.0	1.0100	0.023	1.291	0.816
2508851404	14.229	9.037	70.13	95.79	4.799	16.17	91.57	86.92	1.1676	99.69	0.0	1.0100	0.066	1.414	0.797
2508851405	14.229	9.041	70.17	96.47	4.774	16.11	92.01	87.85	1.2717	99.69	0.0	1.0100	0.096	1.270	0.796
2508851406	14.229	9.031	70.09	96.85	4.781	16.04	92.11	88.17	1.3325	99.70	0.0	1.0100	0.296	1.314	0.800
2508851407	14.229	9.025	70.10	96.95	4.784	16.04	92.29	88.34	1.3776	99.59	0.0	1.0100	0.796	1.407	0.898
2508851501	15.754	9.059	70.34	78.82	4.606	16.35	74.66	74.76	0.6761	99.59	0.0	1.0100	0.055	1.412	0.889
2508851502	15.754	9.066	70.32	84.72	4.617	16.54	79.91	76.98	0.8181	99.60	0.0	1.0100	0.081	1.397	0.910
2508851503	15.754	9.053	70.25	92.50	4.626	16.61	82.24	79.21	0.9025	99.61	0.0	1.0100	0.004	1.410	0.885
2508851504	15.754	9.034	70.15	93.13	4.606	16.77	85.71	82.60	0.9944	99.61	0.0	1.0100	0.032	1.427	0.893
2508851505	15.754	9.028	70.15	95.43	4.609	16.06	87.81	84.02	1.1434	99.59	0.0	1.0100	0.009	1.435	0.880
2508851506	15.754	9.015	70.01	95.55	4.610	17.06	89.52	84.93	1.2114	99.60	0.0	1.0100	0.180	1.435	0.897
2508851507	15.754	9.033	70.18	96.11	4.594	17.10	91.51	85.12	1.2683	99.62	0.0	1.0100	0.640	1.506	0.974
2508851701	17.287	8.977	69.68	88.23	4.858	15.77	72.46	69.81	0.6543	99.62	0.0	1.0100	0.107	1.517	0.925
2508851702	17.287	8.965	69.63	90.60	5.001	16.04	78.99	76.32	0.7795	99.67	0.0	1.0100	0.088	1.489	0.924
2508851703	17.287	8.981	69.77	92.67	5.029	16.15	86.88	77.56	0.8869	99.67	0.0	1.0100	0.083	1.490	0.897
2508851704	17.287	8.975	69.73	93.77	5.046	16.46	89.82	79.27	1.0314	99.66	0.0	1.0100	0.058	1.467	0.911
2508851705	17.287	8.963	69.69	94.67	5.023	16.63	91.00	81.87	1.1122	99.67	0.0	1.0100	0.283	1.506	0.950
2508851706	17.287	8.980	69.78	95.07	5.025	16.70	91.34	82.66	1.1923	99.69	0.0	1.0100	0.249	1.510	0.967
2508851707	17.287	8.987	69.78	95.89	5.019	16.71	91.46	82.96	1.2401	99.69	0.0	1.0100	0.966	1.597	1.051
2508851801	18.827	8.969	69.71	77.53	4.789	16.29	75.54	70.25	0.6311	99.57	0.0	1.0100	0.118	1.622	0.975
2508851802	18.827	8.983	69.86	83.78	4.883	16.32	76.87	72.82	0.7938	99.63	0.0	1.0100	0.147	1.634	0.969
2508851803	18.827	8.992	69.90	88.48	4.875	16.39	78.77	75.52	0.8845	99.65	0.0	1.0100	0.115	1.630	0.972
2508851804	18.827	8.998	69.93	91.21	4.877	16.44	79.94	77.36	0.9877	99.66	0.0	1.0100	0.113	1.648	0.959
2508851805	18.827	8.994	69.91	92.39	4.876	16.46	81.89	78.02	1.0319	99.67	0.0	1.0100	0.182	1.651	0.974
2508851806	18.827	8.998	69.94	93.53	4.821	16.52	83.01	79.83	1.1094	99.66	0.0	1.0100	0.236	1.667	0.989
2508851807	18.827	9.009	69.96	93.90	4.831	16.50	83.11	80.86	1.1422	99.67	0.0	1.0100	0.136	1.739	1.120
2508852001	20.374	8.994	70.04	77.43	4.825	16.00	70.18	70.25	0.6632	99.57	0.0	1.0100	0.171	1.718	1.012
2508852002	20.374	9.011	70.07	83.43	4.833	16.12	72.52	71.16	0.7321	99.58	0.0	1.0100	0.151	1.728	1.026
2508852003	20.374	8.995	70.02	86.53	4.867	16.24	73.51	71.98	0.8721	99.61	0.0	1.0100	0.135	1.794	1.074
2508852004	20.374	8.987	69.98	87.56	4.876	16.32	73.72	73.76	0.9110	98.62	0.0	1.0100	0.275	1.766	1.101
2508852005	20.374	9.017	70.10	89.32	4.871	16.30	75.85	75.38	0.9870	96.62	0.0	1.0100	0.240	1.795	1.073
2508852006	20.374	9.004	70.07	90.57	4.862	16.25	76.93	76.93	1.0319	99.66	0.0	1.0100	0.356	1.820	1.164
2508852007	20.374	8.987	69.97	91.62	4.861	16.30	77.89	77.39	1.0784	99.69	0.0	1.0101	0.051	1.894	1.274

TABLE C.1g

Steam-Water Data (Low Steam Extraction Rate Tests)

TEST No	Qfin	WC	Tfin	Two	Mcw	Tc1	Tc2	TD	Mssup	Ts	Inlet Water Subcooling = 20 K				
											VP1	Patn	PD	TT	TL
2506850401	4.000	10.156	79.80	97.49	4.177	20.56	84.76	79.08	0.6124	99.59	2.2	1.0107	0.054	0.428	0.363
2506850402	4.000	10.148	79.72	97.79	4.109	20.48	92.45	88.28	0.7951	99.65	3.0	1.0107	0.080	0.429	0.363
2506850403	4.000	10.182	79.80	97.96	4.119	19.93	92.70	88.65	0.8733	99.64	3.1	1.0107	-0.006	0.449	0.422
2506850404	4.000	10.185	79.80	98.10	4.117	19.92	92.71	88.67	1.0243	99.64	3.1	1.0107	0.098	0.492	0.411
2506850405	4.000	10.179	79.80	98.17	4.117	20.14	92.75	88.77	1.2316	99.64	3.1	1.0107	0.132	0.483	0.362
2506850406	4.000	10.174	79.75	98.26	4.113	20.08	93.06	89.07	1.4032	99.65	3.1	1.0107	0.181	0.465	0.432
2506850407	4.000	10.170	79.75	98.42	4.112	20.32	93.16	89.38	1.4666	99.64	3.2	1.0107	0.675	0.549	0.520
2506850501	5.000	10.214	80.13	94.74	4.113	19.95	83.98	75.76	0.5704	99.60	2.0	1.0107	-0.039	0.580	0.453
2506850502	5.000	10.229	80.15	97.93	4.109	19.87	91.67	86.09	0.8540	99.59	2.0	1.0107	-0.004	0.589	0.469
2506850503	5.000	10.223	80.10	98.03	4.103	19.84	91.95	86.77	0.9027	99.61	2.5	1.0107	-0.005	0.601	0.473
2506850504	5.000	10.216	80.15	98.25	4.102	19.83	92.12	87.00	1.0746	99.60	3.8	1.0107	-0.029	0.601	0.473
2506850505	5.000	10.210	80.17	98.32	4.060	19.95	92.44	87.58	1.2692	99.62	3.3	1.0107	0.027	0.594	0.467
2506850506	5.000	10.201	80.07	98.29	4.066	19.93	92.67	88.17	1.3854	99.64	3.3	1.0107	0.250	0.555	0.452
2506850507	5.000	10.212	80.11	98.35	4.105	19.84	92.76	88.72	1.4312	99.63	3.3	1.0107	0.050	0.542	0.507
2506850508	5.000	10.217	80.10	98.45	4.089	19.65	93.14	89.04	1.4442	99.62	3.3	1.0107	0.549	0.669	0.570
2506850601	6.000	10.180	79.88	97.35	4.112	19.83	84.58	73.84	0.5733	99.59	2.5	1.0107	0.059	0.648	0.507
2506850602	6.000	10.187	79.91	97.18	4.100	19.77	88.54	83.40	0.7533	99.58	2.9	1.0107	0.045	0.664	0.511
2506850603	6.000	10.193	79.91	98.16	4.090	19.68	91.68	85.36	0.9014	99.58	3.0	1.0107	0.020	0.673	0.501
2506850604	6.000	10.190	79.90	98.14	4.114	19.62	92.56	86.87	1.0762	99.59	3.0	1.0107	-0.019	0.680	0.495
2506850605	6.000	10.197	79.93	98.22	4.112	19.61	92.56	87.44	1.1593	99.60	3.1	1.0107	0.034	0.695	0.491
2506850606	6.000	10.206	79.93	98.36	4.111	19.58	92.60	88.10	1.2912	99.63	3.0	1.0107	0.086	0.664	0.511
2506850607	6.000	10.215	80.00	98.43	4.093	19.80	92.44	89.28	1.3501	99.62	3.0	1.0107	0.704	0.762	0.594
2506850701	7.000	10.353	80.70	97.95	4.121	19.53	83.47	73.91	0.6185	99.67	1.9	1.0107	0.079	0.769	0.536
2506850702	7.000	10.369	80.82	98.00	4.122	19.53	89.40	78.75	0.7647	99.65	2.8	1.0107	0.023	0.783	0.536
2506850703	7.000	10.380	80.86	98.03	4.124	19.54	91.47	80.97	0.8719	99.63	3.2	1.0107	-0.020	0.763	0.531
2506850704	7.000	10.376	80.81	98.15	4.143	19.32	92.07	83.93	1.0672	99.66	3.0	1.0107	0.046	0.792	0.576
2506850705	7.000	10.365	80.78	98.38	4.116	19.34	92.46	85.07	1.2645	99.70	3.0	1.0107	0.095	0.828	0.598
2506850706	7.000	10.355	80.74	98.55	4.138	19.17	92.50	87.50	1.3009	99.70	3.1	1.0107	0.104	0.742	0.582
2506850707	7.000	10.339	80.73	98.77	4.130	19.40	92.56	89.93	1.3315	99.71	3.1	1.0107	0.677	0.794	0.652
2506850801	8.000	10.311	80.60	92.81	4.446	17.91	85.92	75.49	0.5747	99.60	0.0	0.9960	0.079	0.824	0.594
2506850802	8.000	10.298	80.59	96.08	4.497	17.91	88.71	87.92	0.8922	99.63	0.0	0.9960	0.061	0.799	0.608
2506850803	8.000	10.292	80.57	97.45	4.503	17.98	88.90	88.21	0.9475	99.62	2.0	0.9960	0.044	0.853	0.596
2506850804	8.000	10.290	80.62	97.71	4.503	18.11	89.09	88.67	1.0682	99.62	3.0	0.9960	0.047	0.835	0.623
2506850805	8.000	10.289	80.59	97.93	4.523	18.31	89.68	89.29	1.2015	99.60	3.0	0.9960	-0.013	0.819	0.654
2506850806	8.000	10.287	80.60	98.18	4.493	18.42	90.07	89.77	1.2887	99.64	3.2	0.9960	-0.041	0.779	0.654
2506850807	8.000	10.290	80.60	98.31	4.489	18.41	90.17	89.78	1.3311	99.64	3.5	0.9960	-0.041	0.793	0.673
2506850808	8.000	10.997	80.65	98.46	4.545	18.29	90.75	89.71	1.3859	99.64	3.2	0.9960	0.975	0.894	0.767
2506850901	9.000	10.377	80.87	91.87	4.322	18.07	85.78	76.83	0.5928	99.61	0.0	0.9960	0.071	0.900	0.568
2506850902	9.000	10.354	80.76	96.55	4.500	18.10	89.14	87.97	0.9191	99.63	1.0	0.9960	0.043	0.904	0.602
2506850903	9.000	10.342	80.76	97.69	4.509	18.22	90.90	88.71	1.0851	99.63	2.0	0.9960	0.028	0.923	0.619
2506850904	9.000	10.331	80.65	97.86	4.499	18.13	90.47	89.73	1.1738	99.65	3.5	0.9960	0.011	0.942	0.623
2506850905	9.000	10.338	80.68	97.97	4.510	18.33	90.93	89.86	1.3176	99.65	3.7	0.9960	-0.014	0.931	0.654
2506850906	9.000	10.366	80.79	97.96	4.516	18.62	91.03	89.83	1.3442	99.67	3.8	0.9960	0.097	0.948	0.671
2506850907	9.000	10.376	80.80	98.18	4.483	18.25	91.63	90.54	1.3762	99.68	3.8	0.9960	1.279	0.985	0.733
2506851001	10.000	10.193	79.96	93.46	4.551	18.40	85.31	77.81	0.5761	99.63	0.0	0.9973	0.050	0.974	0.639
2506851002	10.000	10.188	79.93	95.55	4.498	18.47	87.72	84.74	0.7729	99.65	3.0	0.9973	0.010	1.005	0.650
2506851003	10.000	10.175	79.90	97.63	4.462	18.53	89.80	86.40	0.9139	99.66	3.7	0.9973	-0.010	1.007	0.654
2506851004	10.000	10.159	79.78	97.72	4.486	18.12	90.23	89.17	1.0641	99.68	3.0	0.9973	0.060	1.023	0.662
2506851005	10.000	10.150	79.75	97.97	4.462	18.18	90.74	90.04	1.1720	99.68	3.7	0.9973	0.004	1.023	0.706
2506851006	10.000	10.168	79.80	98.36	4.482	18.29	90.87	90.25	1.2972	99.69	3.9	0.9973	0.071	1.038	0.693
2506851007	10.000	10.175	79.84	98.58	4.467	18.30	91.09	90.94	1.3473	99.71	3.9	0.9973	1.062	1.047	0.774

TABLE C.1g (Continue)

Steam-Water Data (Low Steam Extraction Rate Tests)

Inlet Water Subcooling = 20 K

TEST No	Qfin	WC	Tfin	Two	CW	Tc1	Tc2	TD	Mssup	Ts	VP1	Pata	PD	TT	TL
2506851101	11.19710.254	80.32	90.66	4.198	17.45	85.72	79.59	0.5846	99.59	0.0	0.9973	0.091	1.004	0.731	
2506851102	11.19710.264	80.40	97.28	4.195	17.63	87.77	85.77	0.7441	99.60	3.0	0.9973	0.086	0.954	0.751	
2506851103	11.19710.268	80.41	97.50	4.198	17.61	89.00	88.13	0.8301	99.63	3.0	0.9973	0.001	1.003	0.745	
2506851104	11.19710.273	80.43	97.75	4.177	17.70	89.54	89.00	0.9548	99.64	3.5	0.9973	-0.003	1.016	0.768	
2506851105	11.19710.281	80.42	97.91	4.163	17.74	89.97	89.26	1.0769	99.66	3.6	0.9973	-0.005	1.108	0.772	
2506851106	11.19710.291	80.47	98.21	4.209	17.43	91.17	89.67	1.2411	99.68	3.6	0.9973	0.163	1.096	0.790	
2506851107	11.19710.277	80.31	98.53	4.149	17.68	90.94	91.47	1.3167	99.71	3.7	0.9973	1.513	1.168	0.843	
2506851201	12.71010.297	80.40	89.54	4.172	17.41	85.22	80.42	0.5635	99.64	0.0	0.9973	0.068	1.182	0.763	
2506851202	12.71010.289	80.42	92.88	4.140	17.54	88.82	87.73	0.7471	99.63	0.0	0.9973	0.030	1.182	0.763	
2506851203	12.71010.266	80.31	95.76	4.133	17.68	89.59	88.57	0.9248	99.65	2.0	0.9973	0.016	1.210	0.750	
2506851204	12.71010.251	80.29	96.72	4.123	17.60	89.79	88.54	0.9881	99.65	2.0	0.9973	0.015	1.255	0.730	
2506851205	12.71010.273	80.43	96.89	4.150	17.53	89.91	89.58	1.0531	99.67	2.0	0.9973	0.002	1.275	0.758	
2506851206	12.71010.286	80.45	97.70	4.104	17.73	90.09	89.64	1.1640	99.67	2.3	0.9973	0.016	1.275	0.778	
2506851207	12.71010.299	80.47	98.29	4.042	17.68	90.45	89.75	1.2443	99.69	2.4	0.9973	0.164	1.325	0.805	
2506851208	12.71010.294	80.44	98.78	3.992	17.70	91.01	91.71	1.3044	99.72	2.5	0.9973	1.507	1.362	0.832	
2506851401	14.22910.157	79.79	94.09	3.996	17.40	85.48	81.04	0.6428	99.69	0.0	0.9973	-0.018	1.350	0.788	
2506851402	14.22910.162	79.80	96.56	4.001	17.45	87.73	84.71	0.7833	99.68	0.0	0.9973	-0.004	1.350	0.793	
2506851403	14.22910.176	79.87	97.46	4.006	17.56	89.10	87.38	0.8843	99.66	0.0	0.9973	0.004	1.350	0.811	
2506851404	14.22910.185	79.89	97.64	3.991	17.50	89.51	88.66	0.9901	99.64	0.0	0.9973	0.011	1.350	0.836	
2506851405	14.22910.197	80.00	97.93	3.992	17.47	89.96	89.09	1.0913	99.67	0.0	0.9973	0.045	1.337	0.878	
2506851406	14.22910.209	79.99	98.14	3.921	17.73	90.56	90.25	1.1768	99.68	0.0	0.9973	0.083	1.387	0.852	
2506851407	14.22910.201	79.91	98.38	3.910	17.80	91.07	91.70	1.2783	99.70	0.0	0.9973	1.388	1.455	0.922	
2506851501	15.75510.327	80.65	89.00	4.591	16.75	85.36	79.42	0.6507	99.68	0.0	1.0080	0.117	1.327	0.832	
2506851502	15.75510.313	80.58	90.06	4.661	17.12	89.45	81.52	0.8567	99.68	0.0	1.0080	0.082	1.363	0.876	
2506851503	15.75510.297	80.46	91.26	4.662	17.16	91.22	83.96	0.9467	99.67	0.0	1.0080	-0.008	1.384	0.871	
2506851504	15.75510.294	80.49	94.54	4.629	17.31	91.21	84.50	0.9948	99.66	0.0	1.0080	0.087	1.404	0.887	
2506851505	15.75510.290	80.46	96.74	4.650	17.25	91.60	85.20	1.0361	99.68	0.0	1.0080	0.119	1.407	0.900	
2506851506	15.75510.270	80.40	97.69	4.622	17.31	91.72	86.27	1.1613	99.65	0.0	1.0080	0.142	1.399	0.881	
2506851507	15.75510.285	80.43	97.93	4.660	17.23	91.82	86.76	1.1998	99.67	0.0	1.0080	1.109	1.538	0.978	
2506851701	17.28710.220	80.12	86.11	4.593	16.90	83.04	76.83	0.5975	99.60	0.0	1.0080	0.096	1.423	0.919	
2506851702	17.28710.244	80.23	91.71	4.610	16.98	85.75	79.04	0.7147	99.62	0.0	1.0080	0.100	1.373	0.976	
2506851703	17.28710.254	80.23	93.88	4.675	17.20	87.51	80.52	0.8829	99.61	0.0	1.0080	0.213	1.440	0.974	
2506851704	17.28710.260	80.22	95.58	4.646	17.21	88.54	81.31	0.9775	99.66	0.0	1.0080	0.224	1.453	0.964	
2506851705	17.28710.241	80.14	96.01	4.652	17.22	89.60	82.09	1.0224	99.69	0.0	1.0080	0.233	1.453	0.984	
2506851706	17.28710.229	80.11	96.32	4.649	17.21	89.95	82.84	1.0746	99.69	0.0	1.0080	0.266	1.544	1.031	
2506851707	17.28710.214	80.07	96.64	4.624	17.36	90.65	83.57	1.1116	99.69	0.0	1.0080	4.349	1.581	1.181	
2506851801	18.82710.093	79.50	89.51	4.800	17.00	81.46	75.99	0.6529	99.65	0.0	1.0080	0.127	1.427	0.954	
2506851802	18.82710.110	79.58	93.76	4.826	17.11	84.94	76.97	0.7572	99.68	0.0	1.0080	0.124	1.630	0.972	
2506851803	18.82710.138	79.74	94.86	4.676	17.21	87.75	78.13	0.8326	99.71	0.0	1.0080	0.193	1.605	0.959	
2506851804	18.82710.129	79.72	95.22	4.689	17.48	89.04	79.85	0.9136	99.73	0.0	1.0080	0.193	1.578	1.021	
2506851805	18.82710.121	79.68	95.12	4.664	17.67	89.46	80.53	0.9723	99.68	0.0	1.0080	0.221	1.600	1.057	
2506851806	18.82710.216	79.68	95.71	4.672	17.72	90.18	81.77	1.0227	99.69	0.0	1.0080	0.284	1.633	1.170	
2506851807	18.82710.211	79.68	96.02	4.650	17.66	90.50	81.95	1.0668	99.70	0.0	1.0080	5.503	1.690	1.274	
2506852001	20.37410.267	79.71	88.20	4.886	16.50	80.52	74.94	0.5984	99.66	0.0	1.0053	0.096	1.528	1.014	
2506852002	20.37410.260	79.67	93.85	4.858	16.65	83.77	75.55	0.6938	99.65	0.0	1.0053	0.085	1.545	1.074	
2506852003	20.37410.277	79.79	94.64	4.689	17.17	85.11	76.25	0.8158	99.67	0.0	1.0053	0.221	1.564	1.064	
2506852004	20.37410.289	79.86	94.43	4.689	17.12	88.63	78.92	0.8683	99.67	0.0	1.0053	0.323	1.587	1.184	
2506852005	20.37410.268	79.71	94.50	4.674	17.32	88.69	80.07	0.9074	99.66	0.0	1.0053	0.308	1.695	1.236	
2506852006	20.37410.253	79.69	94.83	4.630	17.37	88.69	80.55	0.9841	99.68	0.0	1.0053	0.333	1.706	1.297	
2506852007	20.37410.247	79.69	95.18	4.660	17.40	88.78	81.38	1.0288	99.68	0.0	1.0053	6.676	1.780	1.414	

TABLE C.1h

Steam-Water Data (Low Steam Extraction Rate Tests)

Inlet Water Subcooling = 10 K

TEST No	Qfin	WC	Tfin	Two	Mcw	Tc1	Tc2	TD	Mssup	Ts	VPI	Pata	PD	TT	TL
0306850401	4.000	11.170	89.74	97.05	4.796	17.12	75.36	68.40	0.5178	99.71	2.0	1.0147	0.058	0.387	0.371
0306850402	4.000	11.174	89.86	97.46	4.587	17.47	77.80	70.41	0.7176	99.72	2.3	1.0147	0.034	0.379	0.366
0306850403	4.000	11.168	89.76	97.83	4.602	17.53	79.56	72.87	0.8122	99.75	2.5	1.0147	0.024	0.376	0.364
0306850404	4.000	11.173	89.86	97.99	4.632	17.63	82.12	75.72	1.0073	99.75	4.0	1.0117	0.005	0.391	0.369
0306850405	4.000	11.176	89.86	97.94	4.683	17.88	86.54	78.15	1.2586	99.73	4.5	1.0147	-0.039	0.456	0.351
0306850406	4.000	11.177	89.85	98.05	4.724	18.14	88.30	80.54	1.4331	99.75	4.0	1.0147	-0.058	0.468	0.346
0306850407	4.000	11.178	89.82	98.15	4.781	18.22	89.31	81.47	1.4947	99.76	4.0	1.0147	-0.037	0.482	0.367
0306850408	4.000	11.180	89.87	98.18	4.715	18.27	89.75	82.54	1.5281	99.77	4.0	1.0147	0.131	0.479	0.395
0306850409	4.000	11.182	89.86	98.26	4.719	18.34	90.55	83.49	1.5601	99.78	4.0	1.0147	0.500	0.532	0.468
0506850501	5.000	11.219	90.08	97.99	5.575	22.72	69.14	62.63	0.7338	99.77	3.0	1.0120	-0.005	0.411	0.416
0506850502	5.000	11.210	90.03	98.06	5.559	22.79	70.67	66.56	0.9024	99.77	3.1	1.0120	0.011	0.425	0.402
0506850503	5.000	11.214	90.03	98.19	5.571	22.86	73.69	67.90	0.9839	99.77	3.3	1.0120	-0.033	0.421	0.406
0506850504	5.000	11.216	90.06	98.21	5.583	23.06	77.15	69.75	1.0934	99.79	3.5	1.0120	-0.074	0.416	0.408
0506850505	5.000	11.220	90.10	98.17	5.579	23.06	83.23	76.00	1.2657	99.80	3.6	1.0120	-0.080	0.421	0.389
0506850506	5.000	11.231	90.16	98.28	5.393	22.99	88.42	82.23	1.3851	99.84	3.7	1.0120	-0.101	0.424	0.400
0506850507	5.000	11.226	90.13	98.40	5.531	23.17	89.85	82.55	1.4657	99.86	3.8	1.0120	0.010	0.400	0.444
0506850508	5.000	11.222	90.18	98.48	5.499	23.15	90.59	82.78	1.4858	99.86	4.0	1.0120	0.500	0.464	0.493
0506850601	6.000	11.223	90.15	98.57	5.364	24.23	69.96	62.83	0.5063	99.59	2.0	1.0120	0.079	0.503	0.455
0506850602	6.000	11.219	90.14	98.61	5.411	24.24	71.71	65.65	0.7543	99.60	3.0	1.0120	0.032	0.504	0.460
0506850603	6.000	11.227	90.14	98.71	5.443	24.25	74.89	68.43	0.9073	99.66	3.3	1.0120	0.027	0.509	0.456
0506850604	6.000	11.218	90.03	98.77	5.425	24.31	78.61	70.34	1.0132	99.64	4.0	1.0120	-0.030	0.490	0.442
0506000605	6.000	11.212	90.05	98.75	5.397	24.34	79.93	73.80	1.1169	99.66	4.3	1.0120	-0.078	0.507	0.433
0506850606	6.000	11.209	90.03	98.72	5.362	24.99	86.02	77.88	1.2330	99.67	4.8	1.0120	-0.042	0.481	0.436
0506850607	6.000	11.211	90.16	98.70	5.224	24.89	89.58	81.89	1.3286	99.68	4.9	1.0120	-0.060	0.498	0.433
0506850608	6.000	11.208	90.07	98.80	5.252	24.88	90.44	82.79	1.3694	99.71	5.0	1.0120	0.121	0.526	0.486
0706850701	7.000	11.161	89.78	97.19	5.214	20.27	72.19	63.56	0.5096	99.68	3.1	1.0173	0.007	0.545	0.469
0706850702	7.000	11.166	89.80	97.16	5.208	20.35	75.30	66.86	0.7640	99.72	3.2	1.0173	0.064	0.526	0.452
0706850703	7.000	11.176	89.88	97.19	5.366	20.32	80.49	71.69	0.9093	99.72	3.3	1.0173	0.012	0.560	0.474
0706850704	7.000	11.187	89.94	97.36	5.220	20.31	85.02	73.49	1.0019	99.73	3.8	1.0173	0.041	0.554	0.460
0706850705	7.000	11.188	89.91	97.56	5.184	20.53	86.11	81.68	1.1279	99.72	4.0	1.0173	-0.006	0.597	0.476
0706850706	7.000	11.192	89.94	97.65	5.252	20.50	87.14	86.40	1.2921	99.74	4.1	1.0173	0.022	0.575	0.476
0706850707	7.000	11.197	89.98	97.67	5.243	20.48	89.03	87.70	1.4422	99.75	4.0	1.0173	0.770	0.648	0.552
0706850801	8.000	11.152	89.61	96.60	5.134	18.11	75.41	73.08	0.6304	99.69	0.0	1.0173	0.034	0.609	0.472
0706850802	8.000	11.159	89.68	96.63	5.137	18.58	80.11	78.08	0.8007	99.66	0.0	1.0173	-0.007	0.583	0.480
0706851823	8.000	11.163	89.66	96.72	5.080	18.47	85.29	83.32	0.9311	99.67	0.0	1.0173	0.036	0.603	0.481
0706850804	8.000	11.169	89.74	96.53	5.060	18.59	87.46	86.53	1.1137	99.69	0.0	1.0173	-0.064	0.639	0.482
0706850805	8.000	11.171	89.74	96.63	5.009	18.35	88.06	87.51	1.2593	99.70	2.0	1.0173	-0.053	0.623	0.496
0706850806	8.000	11.175	89.73	96.72	5.033	18.33	88.58	87.64	1.3281	99.73	3.0	1.0173	0.000	0.658	0.521
0706850807	8.000	11.184	89.88	97.10	5.048	18.31	88.79	88.19	1.3783	99.75	3.0	1.0173	0.597	0.747	0.562
1006850901	9.000	11.225	90.12	96.50	4.956	16.61	79.91	75.31	0.7174	99.60	0.0	1.0146	0.101	0.699	0.554
1006000902	9.000	11.222	90.10	96.77	4.953	16.65	82.09	77.16	0.8595	99.61	0.0	1.0146	0.032	0.736	0.539
1006850903	9.000	11.219	90.11	96.98	4.950	16.68	84.59	79.04	0.9377	99.60	0.0	1.0146	0.006	0.722	0.528
1006850904	9.000	11.214	90.08	97.04	4.936	16.87	87.52	84.92	1.1024	99.59	0.0	1.0146	-0.043	0.733	0.538
1006850905	9.000	11.206	90.05	97.20	4.930	17.25	89.15	88.00	1.2213	99.60	3.0	1.0146	0.023	0.721	0.541
1006850906	9.000	11.198	90.02	97.19	4.934	17.25	89.63	88.75	1.3042	99.62	4.0	1.0146	-0.071	0.746	0.516
1006850907	9.000	11.195	90.01	97.25	4.941	17.29	89.69	88.42	1.3592	99.63	4.1	1.0146	0.010	0.769	0.510
1006850908	9.000	11.191	90.00	97.55	4.972	17.24	89.87	88.56	1.4257	99.67	4.2	1.0146	0.592	0.832	0.598
1106851001	10.000	11.257	90.57	97.07	5.193	17.37	85.01	80.66	0.7909	99.71	0.0	1.0160	0.060	0.731	0.533
1106851002	10.000	11.253	90.57	96.71	5.171	16.39	86.27	82.80	0.8767	99.71	2.0	1.0160	0.054	0.711	0.552
1106851003	10.000	11.249	90.57	97.44	5.200	17.48	86.50	86.82	1.0235	99.74	3.0	1.0160	0.074	0.739	0.553
1106851004	10.000	11.244	90.48	97.66	5.206	17.47	86.97	87.76	1.0999	99.74	3.8	1.0160	0.035	0.746	0.577
1106851005	10.000	11.242	90.48	97.69	5.202	17.69	87.21	87.99	1.2209	99.73	4.0	1.0160	0.068	0.750	0.604
1106851006	10.000	11.245	90.49	98.04	5.192	17.69	87.43	88.18	1.3167	99.75	4.2	1.0160	0.100	0.777	0.614
1106851007	10.000	11.248	90.52	98.58	5.175	17.33	87.68	88.34	1.3550	99.75	4.2	1.0160	1.543	0.882	0.710

TABLE C.1h (Continue)

Steam-Water Data (Low Steam Extraction Rate Tests)

Inlet Water Subcooling = 10 K

TEST No	Qfin	WC	Tfin	Two	Mcw	Tc1	Tc2	TD	Mssup	Ts	VP1	Patm	PD	TT	TL
1006851001	11.19711.269	90.57	98.31	5.170	18.10	79.55	76.32	0.7037	99.68	0.0	1.0153	0.074	0.881	0.625	
1006851102	11.19711.258	90.45	98.16	5.312	17.91	86.47	78.67	0.9141	99.69	3.0	1.0153	0.068	0.882	0.613	
1006851103	11.19711.254	90.45	97.92	5.151	18.16	88.77	85.67	1.0748	99.69	3.5	1.0153	0.052	0.882	0.632	
1006851104	11.19711.247	90.33	98.11	5.311	18.12	89.93	86.78	1.1766	99.72	4.5	1.0153	0.055	0.875	0.615	
1006851105	11.19711.239	90.34	98.21	5.343	18.09	90.10	86.50	1.2318	99.70	4.5	1.0153	0.020	0.889	0.608	
1006851106	11.19711.236	90.36	98.25	5.337	18.07	90.12	87.06	1.2954	99.71	4.4	1.0153	0.006	0.898	0.624	
1006851107	11.19711.230	90.38	98.42	5.329	17.86	90.82	88.19	1.3383	99.71	4.5	1.0153	1.876	0.988	0.670	
1106851201	12.71011.256	90.47	98.03	4.901	19.05	82.74	79.18	0.5379	99.72	0.0	1.0160	0.216	0.954	0.658	
1106851202	12.71011.250	90.42	97.91	4.883	19.27	87.73	82.75	0.7014	99.74	2.0	1.0160	0.100	0.960	0.677	
1106851203	12.71011.253	90.46	97.48	4.846	19.46	87.97	88.51	0.8811	99.77	3.0	1.0160	-0.008	0.963	0.676	
1106851204	12.71011.238	90.25	97.89	4.856	19.52	89.01	89.46	0.9702	99.79	4.3	1.0160	0.051	0.962	0.676	
1106851205	12.71011.234	90.26	98.04	4.824	19.43	89.23	89.78	1.0594	99.83	4.4	1.0160	0.197	0.976	0.672	
1106851206	12.71011.222	90.20	98.04	4.842	19.65	89.23	89.83	1.2329	99.82	4.5	1.0160	0.274	0.959	0.680	
1106851207	12.71011.217	90.21	98.32	4.934	19.24	89.80	90.67	1.2841	99.83	4.5	1.0160	1.597	1.002	0.759	
1106851401	14.22911.282	90.74	97.38	4.798	19.42	88.95	80.64	0.6530	99.59	0.0	1.0160	-0.044	1.008	0.696	
1106851402	14.22911.277	90.72	97.35	4.786	19.53	90.00	85.67	0.8321	99.61	0.0	1.0160	-0.077	1.021	0.681	
1106851403	14.22911.265	90.65	97.83	4.784	19.07	90.77	89.61	1.0136	99.57	1.0	1.0160	-0.043	1.049	0.669	
1106851404	14.22911.264	90.69	97.88	4.802	19.59	90.83	89.56	1.0753	99.60	2.1	1.0160	-0.060	1.046	0.677	
1106851405	14.22911.269	90.69	97.86	4.758	19.41	90.61	89.97	1.1398	99.61	2.9	1.0160	-0.049	1.069	0.677	
1106851406	14.22911.279	90.74	98.09	4.709	19.50	90.68	90.43	1.2068	99.62	3.1	1.0160	0.063	1.089	0.664	
1106851407	14.22911.287	90.74	98.31	4.751	19.50	92.71	91.13	1.3021	99.63	3.5	1.0160	1.649	1.153	0.732	
1206851501	15.75511.225	90.37	95.85	5.331	14.64	83.11	80.75	0.6413	99.65	3.9	1.0053	0.110	1.140	0.766	
1206851502	15.75511.221	90.37	96.11	5.311	14.95	87.29	84.54	0.8061	99.64	0.0	1.0053	-0.013	1.158	0.747	
1206851503	15.75511.212	90.29	96.27	5.331	15.12	87.21	85.46	0.9010	99.66	2.0	1.0053	0.047	1.179	0.759	
1206851504	15.75511.228	90.34	96.34	5.298	15.19	87.18	86.89	1.0051	99.68	2.9	1.0053	0.011	1.162	0.750	
1206851505	15.75511.237	90.33	96.77	5.141	16.49	87.28	87.36	1.1942	99.67	3.8	1.0053	0.092	1.177	0.762	
1206851506	15.75511.239	90.32	96.97	5.102	16.79	87.16	88.84	1.2294	99.68	3.5	1.0053	0.162	1.187	0.802	
1206851507	15.77511.228	90.27	97.01	5.142	16.80	88.36	89.68	1.3127	99.70	4.1	1.0053	1.197	1.287	0.872	
1406851701	17.28711.176	89.87	96.95	5.549	19.07	85.27	82.79	0.6473	99.62	0.0	1.0067	0.123	1.202	0.741	
1406851702	17.28711.183	89.88	97.14	5.532	19.00	86.09	83.12	0.7531	99.63	0.0	1.0067	0.119	1.225	0.762	
1406851703	17.28711.186	89.88	97.27	5.516	18.99	86.84	83.90	0.8521	99.63	0.0	1.0067	0.119	1.249	0.782	
1406851704	17.28711.192	89.89	97.26	5.502	19.00	86.44	84.77	0.9932	99.63	1.0	1.0067	0.044	1.233	0.771	
1406851705	17.28711.196	89.90	97.37	5.495	19.07	89.27	85.69	1.1399	99.65	2.3	1.0067	0.019	1.269	0.845	
1406851706	17.28711.201	89.97	97.56	5.480	18.88	89.43	87.74	1.2099	99.67	2.5	1.0067	0.053	1.303	0.819	
1406851707	17.28711.209	89.98	97.67	5.505	18.95	89.47	88.56	1.2473	99.68	3.0	1.0067	1.256	1.392	0.972	
1406851801	18.82711.223	89.99	96.31	5.790	14.80	83.40	80.88	0.5755	99.60	0.0	1.0067	0.127	1.225	0.767	
1406851802	18.82711.211	89.95	96.45	5.744	14.88	85.39	82.15	0.7054	99.60	0.0	1.0067	0.179	1.238	0.779	
1406851803	18.82711.203	89.90	96.66	5.751	14.89	86.52	82.94	0.7896	99.60	0.0	1.0067	0.052	1.257	0.804	
1406851804	18.82711.199	89.96	96.63	5.758	14.91	87.59	83.28	0.8960	99.63	0.0	1.0067	0.061	1.279	0.825	
1406851805	18.82711.195	89.89	96.53	5.735	14.91	88.07	83.56	1.0857	99.63	0.0	1.0067	-0.037	1.307	0.824	
1406851806	18.82711.188	89.89	96.72	5.739	14.58	88.29	84.06	1.1631	99.66	0.0	1.0067	0.127	1.347	0.844	
1406851807	18.82711.176	89.73	97.05	5.746	14.95	88.34	84.85	1.2109	99.67	0.0	1.0067	1.648	1.470	0.911	
1706852001	20.37411.183	89.82	95.61	4.861	15.68	83.42	81.35	0.6099	99.67	0.0	1.0027	0.026	1.309	0.835	
1706852002	20.37411.194	89.88	96.28	4.855	15.72	84.65	82.52	0.7986	99.70	0.0	1.0027	0.055	1.328	0.860	
1706852003	20.37411.197	89.90	96.30	4.846	15.82	86.73	83.45	0.8797	99.71	0.0	1.0027	0.132	1.349	0.873	
1706852004	20.37411.201	89.90	96.69	4.873	15.94	88.73	84.72	0.9829	99.70	0.0	1.0027	0.227	1.330	0.906	
1706852005	20.37411.208	89.91	96.85	4.874	16.17	89.69	85.01	1.0300	99.69	0.0	1.0027	0.303	1.389	0.914	
1706852006	20.37411.215	89.96	99.55	4.855	15.50	91.74	85.34	1.0889	99.68	0.0	1.0027	0.359	1.393	0.946	
1706852007	20.37411.219	89.97	97.05	4.854	15.50	92.20	85.06	1.1097	99.71	0.0	1.0027	1.804	1.535	1.061	
1706852101	21.92911.169	89.77	95.05	4.854	16.66	85.17	74.87	0.6299	99.60	0.0	1.0027	0.035	1.361	0.876	
1706852102	21.92911.177	89.87	96.15	4.855	16.67	88.17	78.71	0.7699	99.58	0.0	1.0027	0.057	1.409	0.916	
1706852103	21.92911.196	89.99	96.29	4.844	16.52	89.85	80.68	0.8384	99.61	0.0	1.0027	0.260	1.417	0.920	
1706852104	21.92911.207	90.02	96.20	4.869	16.45	89.51	81.38	0.9272	99.61	0.0	1.0027	0.277	1.466	0.917	
1706852105	21.92911.216	90.08	96.31	4.856	16.21	91.47	82.53	0.9856	99.62	0.0	1.0027	0.303	1.496	0.914	
1706852106	21.92911.203	89.92	96.56	4.870	16.19	91.90	82.88	1.0217	99.64	0.0	1.0027	0.375	1.502	0.930	
1706852107	21.92911.207	89.93	96.78	4.858	16.32	92.22	83.21	1.0458	99.66	0.0	1.0027	2.092	1.656	1.054	

TABLE C.2a

Steam-Water Data (Low-Medium Steam Extraction Rate Tests)

Inlet Water Subcooling = 10 K

TEST No	Bfin	Tfin	Two	Mcm	Tc1	Tc2	TD	Mssup	Ts	VP1	VP2	Pata	PD
0306850401	4.000	90.03	95.16	12.155	21.56	59.90	50.72	0.7406	99.70	5.1	0.2	1.015	0.137
0306850402	4.000	90.09	97.07	12.163	21.68	64.62	54.63	0.8982	99.70	6.0	1.0	1.015	0.037
0306850403	4.000	90.18	97.38	12.179	21.84	69.08	58.69	1.0507	99.71	6.2	1.1	1.015	0.024
0306850404	4.000	90.20	97.64	12.195	22.01	75.30	62.37	1.2748	99.73	7.0	1.5	1.015	-0.079
0306850405	4.000	90.12	97.61	12.331	22.21	78.45	66.87	1.4837	99.72	7.3	2.0	1.015	-0.124
0306850406	4.000	90.23	97.78	12.155	22.28	79.34	69.51	1.6749	99.73	7.3	2.0	1.015	-0.147
0306850407	4.000	90.14	97.81	12.141	22.34	80.09	71.98	1.9771	99.76	7.4	2.2	1.015	0.074
0306850408	4.000	90.08	97.83	12.177	22.40	80.40	72.60	2.0041	99.76	7.5	2.4	1.015	0.342
0706850501	5.000	90.40	97.66	12.382	22.86	60.51	60.51	0.6881	99.75	4.1	0.3	1.012	-0.016
0706850502	5.000	90.33	97.98	12.385	22.89	63.51	61.06	0.7989	99.75	4.3	0.8	1.012	-0.030
0706850503	5.000	90.32	98.08	12.385	22.94	65.91	62.95	1.0027	99.78	4.9	1.5	1.012	-0.035
0706850504	5.000	90.28	98.09	12.371	22.96	68.69	63.49	1.2960	99.78	5.3	2.3	1.012	-0.096
0706850505	5.000	90.28	98.10	12.339	23.02	75.94	64.66	1.5810	99.77	6.0	2.8	1.012	-0.126
0706850506	5.000	90.30	98.09	12.315	23.07	80.03	67.24	1.8074	99.76	6.5	3.0	1.012	-0.167
0706850507	5.000	90.29	98.15	12.336	23.08	81.64	69.94	1.9199	99.80	7.1	3.2	1.012	-0.122
0706850508	5.000	90.30	98.21	12.325	23.13	82.25	72.37	1.9914	99.80	8.0	3.3	1.012	0.107
0706850601	6.000	90.45	98.19	12.917	23.91	60.06	60.52	0.7245	99.62	3.2	1.0	1.012	0.051
0706850602	6.000	90.39	98.70	12.892	23.94	62.23	60.90	0.8768	99.66	4.9	1.5	1.012	0.040
0706850603	6.000	90.35	98.71	12.888	23.99	64.91	61.97	1.0080	99.69	6.0	2.3	1.012	0.008
0706850604	6.000	90.29	98.61	12.848	24.33	66.54	63.97	1.2842	99.70	6.9	3.2	1.012	-0.028
0706850605	6.000	90.15	98.72	12.816	23.91	73.58	66.94	1.5972	99.71	7.7	4.8	1.012	-0.085
0706850606	6.000	90.06	98.78	12.843	24.29	78.54	69.50	1.7873	99.72	8.3	5.2	1.012	-0.051
0706850607	6.000	90.01	98.99	12.799	24.27	79.47	73.71	1.8711	99.72	8.7	5.3	1.012	0.414
0906850701	7.000	89.89	93.77	11.863	14.13	58.33	57.61	0.6589	99.70	5.2	1.0	1.017	-0.082
0906850702	7.000	89.92	96.22	11.869	14.30	60.11	58.08	0.7612	99.69	5.9	1.6	1.017	-0.096
0906850703	7.000	89.93	97.07	11.855	14.31	63.55	59.98	0.8891	99.70	6.5	2.7	1.017	-0.099
0906850704	7.000	89.93	97.06	11.844	15.49	65.38	61.36	1.0554	99.70	7.4	4.1	1.017	-0.100
0906850705	7.000	89.97	97.18	11.846	15.19	74.92	67.18	1.3778	99.67	8.0	4.9	1.017	-0.111
0906850706	7.000	90.08	97.13	11.951	15.46	78.20	71.92	1.6681	99.69	8.5	5.0	1.017	-0.105
0906850707	7.000	90.11	97.08	11.927	15.51	78.49	74.54	1.8638	99.70	8.9	5.1	1.017	0.029
0906850801	8.000	90.47	97.09	11.865	17.37	62.50	55.50	0.7269	99.60	3.0	0.5	1.017	0.077
0906850802	8.000	90.49	97.42	11.899	17.52	64.17	55.95	0.8012	99.60	3.5	0.8	1.017	-0.003
0906850803	8.000	90.52	97.54	11.901	17.78	66.34	56.27	0.9129	99.58	4.0	1.5	1.017	-0.101
0906850804	8.000	90.54	97.54	11.908	17.84	68.74	57.43	1.0291	99.60	6.0	2.5	1.017	-0.126
0906850805	8.000	90.57	97.91	11.793	17.92	73.12	61.41	1.2731	99.61	7.3	3.4	1.017	-0.146
0906850806	8.000	90.53	97.77	11.853	17.98	79.01	69.82	1.5285	99.62	8.5	4.5	1.017	-0.123
0906850807	8.000	90.53	97.93	11.877	17.93	79.83	77.90	1.8025	99.64	9.7	5.3	1.017	0.636
1006850901	9.000	90.16	95.16	12.255	17.51	66.34	61.05	0.6409	99.64	1.0	0.0	1.015	0.066
1006850902	9.000	90.12	96.26	12.187	17.63	68.59	64.18	0.7852	99.66	3.0	0.5	1.015	0.003
1006850903	9.000	90.09	96.17	12.121	17.58	72.16	68.09	0.9644	99.66	6.0	3.0	1.015	-0.001
1006850904	9.000	90.08	96.29	12.004	17.47	75.72	73.80	1.2608	99.66	8.0	4.0	1.015	-0.032
1006850905	9.000	90.14	96.31	11.941	17.54	77.94	79.09	1.4934	99.70	8.4	4.5	1.015	-0.161
1006850906	9.000	90.16	96.49	11.918	17.59	78.10	79.46	1.7242	99.71	9.0	5.2	1.015	-0.209
1006850907	9.000	90.26	97.00	11.909	17.66	78.53	80.04	1.7974	99.72	9.8	5.5	1.015	1.182
1106851001	10.000	90.43	97.35	11.271	21.70	71.36	68.36	0.7078	99.68	4.4	1.0	1.016	0.085
1106851002	10.000	90.42	97.43	11.361	21.60	73.72	71.09	0.8325	99.69	5.7	2.6	1.016	0.034
1106851003	10.000	90.41	97.68	11.433	20.56	77.31	74.02	1.0777	99.70	6.9	3.0	1.016	0.024
1006851004	10.000	90.47	97.74	11.589	21.34	79.77	78.38	1.2704	99.70	8.3	4.0	1.016	-0.123
1106851005	10.000	90.46	97.83	11.413	21.17	80.49	81.26	1.4805	99.71	9.0	4.3	1.016	-0.130
1106851006	10.000	90.51	97.89	11.387	21.24	80.83	81.05	1.5786	99.71	9.4	4.5	1.016	-0.136
1106851007	10.000	90.54	97.96	11.357	21.28	80.98	81.74	1.6568	99.72	9.8	4.7	1.016	0.630

TABLE C.2a (Continue)

Steam-Water Data (Low-Medium Steam Extraction Rate Tests)

Inlet Water Subcooling = 10 K

TEST NO	Qfin	Tfin	Two	Mcw	Tc1	Tc2	TD	Mssup	Ts	VP1	VP2	Pata	PD
1006851101	11.197	90.41	97.43	11.790	18.14	71.33	68.02	0.7394	99.71	1.0	0.0	1.015	0.140
1006851102	11.197	90.42	97.50	11.788	18.13	73.52	70.67	0.8428	99.70	3.3	1.2	1.015	0.082
1006851103	11.197	90.47	97.81	11.764	18.12	75.04	73.80	1.0621	99.71	5.2	1.5	1.015	0.060
1006851104	11.197	90.49	97.75	11.693	18.08	78.73	79.18	1.3416	99.71	6.5	2.5	1.015	-0.008
1006851105	11.197	90.48	97.99	11.664	18.07	78.72	80.30	1.4371	99.71	7.7	4.3	1.015	-0.112
1006851116	11.197	90.48	97.98	11.655	18.05	78.62	80.34	1.5664	99.73	8.7	5.0	1.015	-0.140
1006851107	11.197	90.42	98.07	11.635	17.63	79.08	80.99	1.6554	99.73	9.9	5.2	1.015	1.003
1106851201	12.710	90.56	96.10	11.755	18.09	70.07	68.46	0.8085	99.66	0.0	0.0	1.016	0.068
1106851202	12.710	90.50	97.28	11.753	18.12	72.01	69.73	0.9134	99.66	2.8	0.0	1.016	0.000
1106851203	12.710	90.45	97.37	11.751	18.13	74.35	71.72	1.0202	99.67	3.5	1.7	1.016	-0.082
1106851204	12.710	90.56	97.72	11.737	18.12	77.47	73.32	1.1544	99.68	5.6	3.0	1.016	-0.075
1106851205	12.710	90.83	97.73	11.754	18.15	78.57	77.53	1.4071	99.67	8.7	4.1	1.016	-0.102
1106851206	12.710	90.61	97.79	11.714	18.25	78.64	80.14	1.5492	99.68	9.0	5.1	1.016	-0.115
1106851207	12.710	90.69	98.12	11.659	18.27	78.95	80.81	1.6363	99.68	9.7	5.2	1.016	0.919
1106851401	14.229	90.53	98.03	11.865	17.89	70.97	69.64	0.6835	99.73	0.0	0.0	1.016	0.079
1106851402	14.229	90.54	97.83	11.871	17.90	71.62	70.23	0.7918	99.72	1.0	0.0	1.016	0.046
1106851403	14.229	90.56	97.89	11.875	17.91	73.72	72.09	0.8954	99.75	3.0	1.8	1.016	0.011
1106851404	14.229	90.67	97.86	11.832	18.01	78.85	74.18	1.1718	99.77	4.5	3.0	1.016	-0.056
1106851405	14.229	90.61	97.89	11.807	17.99	80.23	78.96	1.3323	99.79	5.5	4.3	1.016	-0.116
1106851406	14.229	90.71	97.75	11.800	18.02	79.28	79.84	1.5497	99.80	7.9	4.7	1.016	-0.135
1106851407	14.229	90.75	97.80	11.749	18.00	81.01	80.54	1.6111	99.81	9.7	5.0	1.016	1.219
1206851501	15.755	90.01	95.50	11.561	15.88	72.15	70.56	0.8062	99.72	0.0	0.0	1.005	-0.044
1206851502	15.755	90.03	95.80	11.545	15.87	74.02	72.49	0.9233	99.72	0.8	0.0	1.005	-0.058
1206851503	15.755	90.06	96.04	11.535	15.84	76.57	75.51	1.0985	99.76	1.1	0.2	1.005	-0.088
1206851504	15.755	89.93	96.03	11.507	15.74	77.00	78.86	1.2877	99.79	1.8	0.8	1.005	-0.030
1206851505	15.755	89.81	96.71	11.494	15.85	77.54	79.54	1.3747	99.80	2.9	1.9	1.005	-0.034
1206851506	15.755	89.81	97.86	11.480	15.90	78.42	79.42	1.4350	99.79	3.6	2.8	1.005	0.038
1206851507	15.755	89.75	97.06	11.468	15.95	78.86	79.06	1.4909	99.79	5.8	3.5	1.005	1.859
1406851701	17.287	90.20	97.33	11.699	17.97	69.92	65.26	0.5879	99.80	0.0	0.0	1.007	-0.001
1406851702	17.287	90.20	97.28	11.709	17.97	70.35	66.43	0.6662	99.80	0.0	0.0	1.007	-0.002
1406851703	17.287	90.19	97.25	11.716	17.98	70.69	67.06	0.7273	99.81	0.0	0.5	1.007	-0.005
1406851704	17.287	90.26	97.28	11.653	17.97	71.92	67.29	0.8048	99.81	0.5	2.5	1.007	-0.029
1406851705	17.287	90.14	97.22	11.654	17.89	73.89	68.86	0.9194	99.82	1.9	3.1	1.007	-0.018
1406851706	17.287	90.28	97.26	11.832	17.89	75.06	69.73	1.1032	99.81	2.3	3.4	1.007	-0.002
1406851707	17.287	90.32	97.33	11.853	17.90	76.02	69.93	1.1744	99.81	3.0	3.0	1.007	2.398
1406851801	18.827	89.10	96.59	12.857	16.18	67.00	63.92	0.5576	99.62	0.0	0.0	1.007	0.118
1406851802	18.827	89.08	96.79	12.898	16.18	68.39	64.00	0.6186	99.63	0.0	0.0	1.007	0.213
1406851803	18.827	89.11	96.73	12.902	16.17	69.99	65.03	0.7012	99.67	0.0	0.0	1.007	0.231
1406851804	18.827	89.12	96.90	12.906	16.17	71.12	66.03	0.7967	99.68	0.0	0.0	1.007	0.255
1406851805	18.827	89.15	97.15	12.915	16.16	71.97	66.52	0.9935	99.70	0.8	0.0	1.007	0.275
1406851806	18.827	89.20	97.42	12.908	16.13	72.93	67.01	1.1190	99.70	1.0	0.0	1.007	0.320
1406851807	18.827	89.34	97.93	12.905	16.13	73.16	67.12	1.1937	99.69	1.6	0.0	1.007	2.278
1706852001	20.374	89.39	95.34	12.849	15.93	70.93	60.63	1.1009	99.70	0.0	0.0	1.003	0.169
1706852002	20.374	89.43	96.04	12.853	16.96	70.93	61.69	1.1009	99.73	0.0	0.0	1.003	0.145
1706852003	20.374	89.46	96.93	12.857	16.97	70.93	63.48	1.1009	99.72	0.0	0.0	1.003	0.175
1706852004	20.374	89.50	97.28	12.864	16.01	70.93	64.73	1.1009	99.74	0.0	0.0	1.003	0.503
1706852005	20.374	89.49	97.59	12.869	16.02	70.93	65.27	1.1009	99.75	0.0	0.0	1.003	3.047

TABLE C.2b

Steam-Water Data (High-Medium Steam Extraction Rate Tests)

Inlet Water Subcooling = 10 K

TEST No	Bfin	Tfin	Two	Mcm	Tc1	Tc2	TD	Mssup	Ts	VP1	VP2	Patm	PD
0306850401	4.000	90.05	97.48	19.863	22.46	47.78	51.32	0.7781	99.60	3.5	0.3	1.015	0.171
0306850402	4.000	90.04	97.79	19.911	22.49	50.79	53.91	0.9973	99.60	6.0	0.9	1.015	0.022
0306850403	4.000	90.00	97.67	19.953	22.54	55.81	56.69	1.3078	99.62	7.5	1.3	1.015	0.006
0306850404	4.000	90.18	97.65	19.914	22.57	60.50	56.84	1.6245	99.64	9.8	3.5	1.015	-0.102
0306850405	4.000	90.13	97.57	19.819	22.53	65.39	58.12	1.8571	99.64	10.5	3.9	1.015	-0.104
0306850406	4.000	90.11	97.59	19.796	22.56	67.03	60.09	2.0257	99.66	10.9	4.5	1.015	-0.215
0306850407	4.000	90.07	97.59	19.762	22.60	67.74	60.98	2.1473	99.68	11.0	4.8	1.015	-0.049
0306850408	4.000	90.05	97.61	19.775	22.63	67.91	61.07	2.2297	99.69	11.1	5.0	1.015	0.260
0706850501	5.000	90.18	98.34	20.045	23.09	49.76	50.10	0.7479	99.70	2.0	0.0	1.012	0.053
0706850502	5.000	90.15	98.15	20.031	23.11	51.56	51.44	0.9143	99.68	5.0	0.7	1.012	0.003
0706850503	5.000	90.12	99.19	20.023	23.33	53.54	52.90	1.1064	99.70	7.1	2.5	1.012	0.000
0706850504	5.000	90.02	99.15	20.022	23.40	57.79	55.69	1.3958	99.70	9.8	3.9	1.012	-0.001
0706850505	5.000	90.09	99.24	19.966	23.45	63.69	57.76	1.7051	99.69	10.2	4.7	1.012	-0.042
0706850506	5.000	90.02	99.21	19.981	23.46	67.63	59.08	1.9310	99.69	11.4	5.5	1.012	-0.123
0706850507	5.000	89.99	99.21	19.970	23.50	69.77	61.49	2.1934	99.69	12.9	6.1	1.012	0.510
0706850601	6.000	89.85	97.08	20.179	23.66	52.50	51.09	0.7582	99.60	3.0	0.0	1.012	-0.101
0706850602	6.000	89.86	97.95	20.101	23.69	54.02	53.57	0.9074	99.59	3.3	0.9	1.012	-0.128
0706850603	6.000	89.87	98.51	20.007	23.78	55.41	54.13	1.0954	99.58	5.7	1.7	1.012	-0.130
0706850604	6.000	89.87	98.46	20.053	23.88	61.09	57.96	1.4532	99.60	7.5	2.3	1.012	-0.103
0706850605	6.000	89.72	98.29	19.985	23.82	65.33	58.90	1.8047	99.63	9.8	3.2	1.012	-0.193
0706850606	6.000	89.69	98.26	19.979	23.72	68.40	60.60	1.9726	99.65	11.5	4.7	1.012	-0.220
0706850607	6.000	89.56	98.37	19.924	23.08	69.50	61.92	2.0603	99.66	12.8	5.8	1.012	0.393
0906850701	7.000	89.54	94.29	20.585	15.36	49.10	47.63	0.8032	99.63	3.1	0.0	1.017	0.093
0906850702	7.000	89.54	95.39	20.513	15.28	51.09	48.66	0.9387	99.64	3.5	0.0	1.017	0.065
0906850703	7.000	89.54	96.00	20.411	15.26	52.94	50.65	1.0854	99.65	4.9	2.2	1.017	0.017
0906850704	7.000	89.54	96.04	20.340	15.35	57.96	53.11	1.3825	99.64	5.9	2.9	1.017	-0.024
0906850705	7.000	89.58	96.55	20.291	15.51	63.25	58.51	1.7125	99.65	8.4	5.6	1.017	-0.039
0906850706	7.000	89.61	96.86	20.267	15.61	63.37	65.86	2.0021	99.66	12.0	8.1	1.017	-0.112
0906850707	7.000	89.64	97.11	20.248	15.70	63.75	68.74	2.1379	99.68	15.5	9.0	1.017	0.540
0906850801	8.000	90.06	96.55	20.304	16.68	50.11	50.30	0.8147	99.68	1.5	0.0	1.017	0.093
0906850802	8.000	90.08	96.81	20.277	16.69	51.24	51.17	0.9513	99.68	2.0	0.0	1.017	0.057
0906850803	8.000	90.09	97.09	20.225	16.78	53.54	52.38	1.1766	99.67	5.6	2.0	1.017	0.037
0906850804	8.000	90.10	97.27	20.064	16.80	56.95	55.53	1.4053	99.68	8.1	3.9	1.017	-0.053
0906850805	8.000	90.06	97.05	20.022	16.86	60.42	60.10	1.6593	99.69	11.7	6.2	1.012	-0.130
0906850806	8.000	90.07	96.63	20.098	16.87	63.79	66.59	1.8917	99.69	15.1	8.5	1.017	-0.134
0906850907	8.000	90.06	96.77	20.191	17.10	64.33	69.37	1.9967	99.70	17.2	9.5	1.017	0.330
1006850901	9.000	90.59	96.42	19.988	17.78	52.25	53.41	0.7388	99.63	2.0	0.0	1.015	0.080
1006850902	9.000	90.59	96.30	19.986	17.84	53.98	54.61	0.8902	99.64	3.5	2.1	1.015	0.033
1006850903	9.000	90.59	96.33	19.980	17.86	56.60	56.42	1.0283	99.66	6.7	4.5	1.015	0.008
1006850904	9.000	90.49	96.54	19.995	18.05	62.99	63.53	1.3367	99.64	8.5	6.9	1.015	-0.058
1006850905	9.000	90.54	96.51	19.991	18.13	65.33	69.26	1.5649	99.65	12.6	8.8	1.015	-0.128
1006850906	9.000	90.67	96.61	19.974	18.30	63.64	70.48	1.9341	99.63	18.1	9.2	1.015	-0.154
1006850907	9.000	90.68	96.87	19.962	18.34	66.29	70.64	2.0149	99.65	19.6	9.8	1.015	0.964
1106851101	10.000	90.28	97.46	20.013	21.22	55.14	53.10	0.7261	99.71	3.0	0.0	1.016	-0.015
1106851102	10.000	90.28	97.48	19.996	21.21	58.65	57.91	0.9554	99.70	5.6	3.7	1.016	-0.011
1106851103	10.000	90.27	97.58	19.977	21.20	60.65	64.59	1.2165	99.71	8.0	5.3	1.016	-0.099
1106851104	10.000	90.35	97.76	20.075	21.23	62.92	69.17	1.4296	99.73	9.9	6.1	1.016	-0.087
1106851105	10.000	90.43	97.73	20.132	21.26	63.78	70.36	1.5356	99.74	12.1	7.3	1.016	-0.145
1106851106	10.000	90.31	97.62	20.122	20.59	64.74	71.08	1.6748	99.73	15.2	8.3	1.016	-0.071
1106851107	10.000	90.28	97.92	20.114	20.50	65.66	71.61	1.7992	99.75	17.3	8.7	1.016	1.355

TABLE C.2b (Continue)

Steam-Water Data (High-Medium Steam Extraction Rate Tests)

TEST NO	Qfin	Tfin	Two	CW	Tc1	Tc2	TD	Mssup	Ts	Inlet Water Subcooling = 10 K			
										VP1	VP2	Pata	PD
1006851101	11.197	90.75	96.89	20.628	17.78	53.57	54.84	0.7935	99.64	0.0	0.0	1.015	-0.057
1006851102	11.197	90.71	99.23	20.519	17.80	54.66	57.62	0.8771	99.64	2.3	1.5	1.015	-0.799
1006851103	11.197	90.68	96.95	20.417	17.87	56.96	61.93	1.0655	99.63	6.5	4.2	1.015	-0.176
1006851104	11.197	90.63	97.50	20.381	17.86	60.08	66.99	1.3742	99.63	8.9	5.3	1.015	-0.157
1006851105	11.197	90.61	97.60	20.363	17.95	62.46	69.29	1.5543	99.66	10.2	6.5	1.015	-0.129
1006851106	11.197	90.60	97.59	20.305	17.99	63.49	69.76	1.6785	99.66	14.8	7.1	1.015	-0.045
1006851107	11.197	90.56	97.67	20.279	18.08	63.83	70.49	1.7547	99.67	15.3	8.5	1.015	0.941
1106851201	12.710	90.54	96.48	20.222	18.16	55.76	57.26	0.7637	99.68	2.2	0.8	1.016	-0.047
1106851202	12.710	90.50	96.51	20.202	18.11	58.03	58.54	0.8327	99.70	2.9	1.0	1.016	-0.040
1106851203	12.710	90.48	96.99	20.194	18.07	59.97	60.53	0.9965	99.72	3.9	2.1	1.016	-0.088
1106851204	12.710	90.43	97.25	20.069	18.03	62.79	63.79	1.1328	99.71	7.0	3.8	1.016	-0.078
1106851205	12.710	90.59	97.68	20.011	18.33	64.65	67.21	1.4383	99.71	9.7	7.1	1.016	-0.099
1106851206	12.710	90.49	97.89	20.005	18.35	65.14	69.05	1.6168	99.69	11.3	7.9	1.016	-0.155
1106851207	12.710	90.44	98.03	20.008	18.38	66.17	71.29	1.7724	99.70	17.6	8.3	1.016	1.588
1106851401	14.229	90.19	96.24	19.819	17.39	55.23	57.01	0.7384	99.61	2.0	0.4	1.011	-0.065
1106851402	14.229	90.11	96.91	19.814	17.40	56.80	59.00	0.8132	99.62	3.5	1.1	1.011	-0.066
1106851403	14.229	90.09	97.02	19.802	17.44	58.43	60.88	0.9055	99.63	5.6	3.2	1.011	-0.067
1106851404	14.229	90.06	97.20	19.766	17.45	60.51	63.07	1.0344	99.62	8.5	5.3	1.011	-0.089
1106851405	14.229	90.00	97.21	19.703	17.53	63.13	66.92	1.2754	99.64	9.7	6.1	1.011	-0.122
1106851406	14.229	89.99	97.31	19.660	17.64	65.09	68.08	1.4454	99.65	11.4	7.3	1.011	-0.155
1106851407	14.229	89.91	97.67	19.505	17.71	65.29	69.38	1.5522	99.65	12.9	8.1	1.017	1.510
1206851501	15.755	90.23	96.61	20.393	16.36	56.28	57.55	0.7113	99.66	0.0	0.0	1.005	0.005
1206851502	15.755	90.25	96.56	20.388	16.40	58.00	58.78	0.8554	99.69	1.4	0.0	1.005	0.000
1206851503	15.755	90.28	96.46	20.383	16.43	60.09	59.78	0.9073	99.67	2.6	1.9	1.005	-0.004
1206851504	15.755	90.12	96.48	20.406	16.43	61.34	61.71	1.0524	99.69	2.9	2.0	1.005	-0.034
1206851505	15.755	90.20	96.56	20.374	16.42	63.14	63.24	1.2941	99.69	4.3	3.5	1.005	-0.169
1206851506	15.755	90.19	96.76	20.351	16.43	64.66	64.64	1.4151	99.70	5.3	4.7	1.005	-0.146
1206851507	15.755	90.20	97.09	20.416	16.49	65.02	65.86	1.5124	99.70	6.7	6.0	1.005	0.915
1406851701	17.287	90.02	96.56	19.929	17.77	57.19	59.70	0.6625	99.59	0.0	0.0	1.007	0.184
1406851702	17.287	90.02	97.06	19.927	17.63	58.23	59.95	0.7196	99.58	0.0	0.0	1.007	0.168
1406851703	17.287	90.01	97.38	19.910	17.55	59.10	60.98	0.7957	99.58	0.0	0.0	1.007	0.154
1406851704	17.287	90.00	97.39	19.906	17.49	60.16	60.98	0.8713	99.60	0.5	0.0	1.007	0.131
1406851705	17.287	90.10	97.38	19.864	17.81	61.31	60.85	1.0001	99.59	0.8	0.0	1.007	0.035
1406851706	17.287	89.99	97.35	19.857	17.82	62.26	60.84	1.0492	99.61	1.0	0.0	1.007	0.058
1406851707	17.287	89.97	97.59	19.846	17.90	63.10	61.38	1.1659	99.61	1.7	0.0	1.007	1.354
1406851801	18.827	89.87	95.90	19.999	15.49	54.57	57.49	0.6073	99.73	0.0	0.0	1.007	0.213
1406851802	18.827	89.83	96.15	20.082	15.50	55.77	57.98	0.6729	99.73	0.0	0.0	1.007	0.213
1406851803	18.927	89.83	96.64	20.089	15.50	55.98	58.09	0.7579	99.74	0.0	0.0	1.007	0.213
1406851804	18.927	89.88	96.80	20.102	15.50	56.57	58.77	0.8333	99.73	0.0	0.0	1.007	0.219
1406851805	18.927	89.81	96.86	20.111	15.60	57.99	59.01	0.9088	99.75	0.0	0.0	1.007	0.219
1406851806	18.827	89.73	96.87	20.147	15.56	59.31	59.39	0.9958	99.75	0.0	0.0	1.007	0.229
1406851807	18.827	89.57	97.08	20.186	15.63	59.77	59.78	1.0770	99.74	0.0	0.0	1.007	2.919
1706852001	20.374	89.27	95.53	20.245	15.12	52.99	53.53	1.0308	99.67	0.0	0.0	1.003	0.265
1706852002	20.374	89.29	95.96	20.251	15.19	53.63	54.80	1.0308	99.67	0.0	0.0	1.003	0.222
1706852003	20.374	89.30	96.04	20.266	15.28	55.84	55.68	1.0308	99.68	0.0	0.0	1.003	0.217
1706852004	20.374	89.33	96.48	20.270	15.34	57.05	56.27	1.0308	99.68	0.0	0.0	1.003	0.384
1706852005	20.374	89.34	96.74	20.273	15.43	57.93	56.85	1.0308	99.69	0.0	0.0	1.003	3.528

TABLE C.2c

Steam-Water Data (High Steam Extraction Rate Tests)

Inlet Water Subcooling = 10 K

TEST No	Qfin	Tfin	Two	M _{cm}	Tc1	Tc2	TD	M _{ssup}	Ts	VP1	VP2	P _{ata}	PD
0306850401	4.000	89.51	97.17	27.781	22.62	39.80	50.80	0.8311	99.65	3.5	0.0	1.015	0.073
0306850402	4.000	89.60	97.44	27.758	22.63	44.51	51.13	0.9762	99.67	6.0	0.5	1.015	0.057
0306850403	4.000	89.64	97.82	27.706	22.65	47.37	51.78	1.3055	99.67	7.5	1.3	1.015	0.011
0306850404	4.000	89.59	97.66	27.743	22.90	53.44	52.88	1.7527	99.69	9.8	3.5	1.015	-0.144
0306850405	4.000	89.63	97.67	27.676	23.01	58.78	53.66	2.0822	99.69	10.5	3.9	1.015	-0.133
0306850406	4.000	89.60	97.68	27.678	23.05	58.86	54.11	2.1908	99.70	10.9	4.5	1.015	-0.056
0306850407	4.000	89.61	97.68	27.668	23.06	59.18	54.61	2.3021	99.71	11.1	5.0	1.015	0.301
0706850501	5.000	90.03	98.31	28.759	23.59	40.10	46.03	0.8004	99.68	2.0	0.0	1.012	0.116
0706850502	5.000	90.05	98.37	28.716	23.61	43.60	48.76	0.9813	99.68	3.3	0.0	1.012	0.043
0706850503	5.000	90.08	98.36	28.627	23.69	45.40	51.45	1.2939	99.69	5.5	1.5	1.012	-0.082
0706850504	5.000	90.16	98.32	28.592	23.71	49.73	52.18	1.6151	99.68	7.8	2.9	1.012	-0.102
0706850505	5.000	90.10	98.29	28.617	23.74	54.30	53.36	1.8658	99.69	9.5	4.0	1.012	-0.124
0706850506	5.000	90.04	98.27	28.566	23.81	57.28	54.06	2.1295	99.69	10.6	4.6	1.012	-0.087
0706850507	5.000	90.01	98.29	28.513	23.85	59.13	54.86	2.1935	99.69	12.1	5.1	1.012	0.370
0706850601	6.000	90.09	97.68	28.854	22.28	42.77	52.07	0.7323	99.66	3.1	0.0	1.012	-0.021
0706850602	6.000	90.09	98.00	28.855	22.28	44.03	52.55	0.9405	99.67	5.3	0.9	1.012	-0.066
0706850603	6.000	90.09	98.34	28.855	22.28	45.59	52.88	1.0734	99.68	8.5	3.9	1.012	-0.118
0706850604	6.000	90.09	98.35	28.852	22.27	49.48	53.20	1.2975	99.68	10.0	4.2	1.012	-0.190
0706850605	6.000	90.01	98.11	28.850	22.15	56.75	54.55	1.7757	99.69	11.8	5.8	1.012	-0.224
0706850606	6.000	90.07	98.09	28.832	22.44	57.19	54.71	2.0305	99.70	12.5	6.3	1.012	-0.259
0706850607	6.000	89.96	98.29	28.854	22.53	58.26	55.84	2.1193	99.70	12.9	6.6	1.012	0.395
0906850701	7.000	89.69	96.30	29.235	15.79	37.82	41.04	0.7383	99.74	1.5	0.0	1.017	0.052
0906850702	7.000	89.67	96.63	29.235	15.80	38.66	43.76	0.9587	99.73	3.2	0.0	1.017	0.002
0906850703	7.000	89.60	96.59	29.233	15.82	39.73	45.06	0.9188	99.75	4.5	2.1	1.002	-0.006
0906850704	7.000	89.57	96.57	29.236	15.85	40.13	50.26	1.2796	99.74	6.3	3.5	1.017	-0.023
0906850705	7.000	89.63	96.76	29.196	16.02	45.36	53.70	1.7144	99.77	8.4	5.5	1.017	-0.186
0906850706	7.000	89.59	96.81	29.236	16.07	50.54	57.56	2.0279	99.76	12.0	7.1	1.017	-0.185
0906850707	7.000	89.60	96.95	29.150	15.91	52.61	61.85	2.2043	99.76	18.0	9.9	1.017	0.668
0906850701	8.000	90.06	96.61	29.182	16.33	40.46	45.00	0.7593	99.71	1.3	0.0	1.017	0.038
0906850802	8.000	90.06	96.49	29.174	16.39	41.87	45.64	0.9021	99.71	2.0	0.0	1.017	0.005
0906850803	8.000	90.08	96.66	29.160	16.39	42.71	46.84	1.0251	99.73	6.7	4.0	1.017	-0.005
0906850804	8.000	90.08	96.57	29.156	16.48	47.23	49.22	1.3401	99.75	9.1	5.1	1.017	-0.049
0906850805	8.000	90.18	96.66	29.193	16.46	52.44	52.98	1.7076	99.74	14.2	7.8	1.017	-0.202
0906850806	8.000	90.26	96.53	29.157	16.53	53.24	61.50	1.9576	99.76	17.0	9.1	1.017	-0.250
0906850807	8.000	90.26	96.65	29.192	16.33	53.42	61.44	2.1273	99.75	22.3	9.9	1.017	0.871
1006850901	9.000	89.68	96.36	29.143	18.52	43.57	51.77	0.7537	99.70	0.0	0.0	1.015	0.003
1006850902	9.000	89.69	96.63	29.144	18.52	45.62	53.03	0.9231	99.71	2.5	1.9	1.015	-0.056
1006850903	9.000	89.78	96.51	29.147	18.51	47.40	54.35	1.0846	99.72	5.3	4.1	1.015	-0.199
1006850904	9.000	89.74	96.72	29.114	18.56	49.84	56.15	1.2627	99.72	8.5	6.9	1.015	-0.070
1006850905	9.000	89.79	96.93	29.236	18.68	51.95	60.37	1.5386	99.70	12.5	8.3	1.015	-0.140
1006850906	9.000	89.88	96.93	29.236	18.74	54.13	63.26	1.8597	99.74	18.1	9.3	1.015	-0.251
1006850007	9.000	89.97	96.95	29.104	18.86	54.76	62.31	1.9398	99.73	20.8	9.8	1.015	0.245
1106851001	10.000	90.01	96.45	28.083	15.73	45.37	52.75	0.6899	99.61	1.5	0.0	1.016	0.015
1106851002	10.000	90.02	96.70	28.054	15.80	47.45	54.17	0.8144	99.61	3.2	2.7	1.016	-0.001
1106851003	10.000	90.02	97.61	28.030	15.88	49.46	55.18	0.9761	99.63	6.5	4.9	1.016	-0.004
1106851004	10.000	89.95	97.58	28.064	15.98	52.81	55.88	1.2777	99.63	8.1	6.8	1.016	-0.128
1106851005	10.000	90.01	97.59	28.046	15.98	54.81	57.10	1.5774	99.64	16.9	8.3	1.016	-0.164
1106851006	10.000	90.03	97.49	28.036	16.05	55.19	58.00	1.8145	99.65	17.1	9.1	1.016	-0.194
1106851007	10.000	90.00	97.63	28.086	16.10	55.97	58.14	1.9028	99.66	19.7	9.7	1.016	0.427

TABLE C.2c (Continue)

Steam-Water Data (High Steam Extraction Rate Tests)

TEST NO	Q _{fin}	T _{fin}	T _{wo}	C _N	T _{c1}	T _{c2}	T _D	M _{ssup}	T _s	Inlet Water Subcooling = 10 K			
										VP1	VP2	P _{atm}	PD
1006851101	11.197	90.24	97.38	29.215	16.93	43.53	52.81	0.6706	99.68	0.6	0.0	1.015	-0.061
1006851102	11.197	90.30	97.39	29.201	17.07	45.10	52.99	0.7934	99.68	3.0	0.6	1.015	-0.070
1006851103	11.197	90.30	96.50	29.110	17.02	46.86	53.08	0.9055	99.70	5.5	4.2	1.015	-0.076
1006851104	11.197	90.34	97.55	29.099	17.14	49.78	53.55	1.0846	99.71	8.1	5.7	1.015	-0.088
1006851105	11.197	90.50	97.52	29.084	17.20	51.08	58.08	1.2991	99.70	11.7	6.9	1.015	-0.145
1006851106	11.197	90.39	97.66	29.059	17.29	53.52	62.00	1.6042	99.69	17.1	8.9	1.015	-0.245
1006851107	11.197	90.28	97.78	29.066	17.33	53.93	62.27	1.7874	99.72	19.1	9.3	1.015	0.981
1106851201	12.710	89.75	96.19	28.723	16.71	43.96	52.52	0.6309	99.61	0.0	0.0	1.009	0.316
1106851202	12.710	89.76	96.27	28.806	16.88	45.97	53.43	0.7588	99.61	2.9	1.5	1.009	-0.095
1106851203	12.710	89.73	96.49	28.849	16.92	48.11	55.70	0.8983	99.60	5.5	4.8	1.009	-0.178
1106851204	12.710	89.77	96.49	28.891	16.92	50.99	57.39	1.1163	99.62	8.5	6.3	1.009	-0.249
1106851205	12.710	89.72	96.55	28.864	16.99	52.53	59.37	1.3409	99.64	12.3	8.1	1.009	-0.350
1106851206	12.710	89.77	96.82	28.901	17.03	54.60	61.51	1.6127	99.64	14.2	8.8	1.009	-0.332
1106851207	12.710	89.74	97.06	28.867	16.95	55.15	62.59	1.7471	99.63	18.1	9.1	1.009	1.297
1106851401	14.229	90.61	96.01	28.734	17.22	48.89	52.02	0.7233	99.69	0.0	0.0	1.011	0.000
1106851402	14.229	90.57	96.50	28.735	17.23	49.56	53.52	0.8348	99.68	3.2	2.8	1.011	0.056
1106851403	14.229	90.59	96.60	28.733	17.23	50.90	54.01	0.9101	99.69	4.4	3.1	1.011	0.129
1106851404	14.229	90.59	96.70	28.728	17.22	52.79	55.85	1.1221	99.69	9.1	6.7	1.011	-0.211
1106851405	14.229	90.70	96.86	28.720	17.28	54.82	58.47	1.3681	99.71	10.8	7.7	1.011	-0.208
1106851406	14.229	90.67	97.06	28.782	17.34	55.02	60.46	1.5786	99.71	11.2	8.1	1.011	-0.231
1106851407	14.229	90.53	97.36	28.779	17.36	55.15	62.36	1.6582	99.71	14.5	8.9	1.011	1.704
1206851501	15.755	90.22	96.74	29.234	16.78	47.37	54.42	0.7053	99.65	0.0	0.0	1.011	0.080
1206851502	15.755	90.11	96.78	29.235	16.78	47.99	54.91	0.8323	99.67	2.0	1.5	1.011	0.033
1206851503	15.755	90.09	97.04	29.236	16.77	49.91	55.29	0.9389	99.67	2.9	2.1	1.011	-0.042
1206851504	15.755	90.00	97.09	29.235	16.80	52.02	57.05	1.1541	99.66	4.2	3.8	1.011	-0.112
1206851505	15.755	89.94	97.24	29.236	16.85	54.31	59.04	1.3482	99.68	5.3	4.1	1.011	-0.149
1206851506	15.755	90.02	96.45	29.234	16.89	55.82	59.93	1.5132	99.68	5.7	4.9	1.011	-0.199
1206851507	15.755	90.04	97.59	29.236	16.96	56.71	60.32	1.6328	99.69	5.8	5.1	1.011	1.829
1406851701	17.287	90.22	96.48	29.237	16.97	48.14	55.57	0.6269	99.66	0.0	0.0	1.007	0.030
1406851702	17.287	90.40	97.01	29.231	17.00	49.02	55.78	0.7011	99.66	0.0	0.0	1.007	0.005
1406851703	17.287	90.42	97.29	29.233	17.01	51.98	55.99	0.7904	99.67	0.0	0.0	1.007	0.002
1406851704	17.287	90.44	97.47	29.236	17.02	53.46	56.81	0.9228	99.68	0.0	0.0	1.007	0.004
1406851705	17.287	90.47	97.45	29.234	17.15	55.19	57.12	1.1468	99.70	1.1	0.0	1.007	-0.020
1406851706	17.287	90.49	97.48	29.240	17.17	56.11	57.76	1.2669	99.69	2.3	0.0	1.007	-0.098
1406851707	17.287	90.51	97.75	29.245	17.17	56.88	58.19	1.3953	99.70	3.2	0.0	1.007	1.215
1406851801	18.827	90.33	96.50	29.133	14.79	43.93	54.90	0.6288	99.58	0.0	0.0	1.007	0.082
1406851802	18.827	90.35	96.60	29.131	14.80	45.09	55.00	0.6909	99.59	0.0	0.0	1.007	0.099
1406851803	18.827	90.37	96.80	29.130	14.80	45.76	56.10	0.7794	99.61	0.0	0.0	1.007	0.124
1406851804	18.827	90.38	97.07	29.129	14.86	46.46	56.99	0.8912	99.60	0.0	0.0	1.007	0.261
1406851805	18.927	90.39	97.21	29.119	14.88	47.98	57.31	0.9876	99.59	0.0	0.0	1.007	0.299
1406851806	18.827	90.40	97.54	29.144	14.89	49.03	57.91	1.0145	99.59	0.0	0.0	1.007	0.352
1406851807	18.827	90.38	97.76	29.134	14.70	49.42	58.60	1.0733	99.60	0.0	0.0	1.007	1.269
1906852001	20.374	90.06	95.10	28.152	14.18	40.97	53.51	0.6028	99.70	0.0	0.0	1.006	0.187
1906852002	20.374	90.06	96.20	28.222	14.20	42.65	53.78	0.6552	99.69	0.0	0.0	1.006	0.190
1906852003	20.374	90.06	96.26	28.329	14.21	43.87	53.94	0.7047	99.68	0.0	0.0	1.006	0.198
1906852004	20.374	90.04	96.20	28.331	14.27	45.53	54.07	0.7831	99.67	0.0	0.0	1.006	0.209
1906852005	20.374	90.07	96.27	28.311	14.44	46.90	54.99	0.8532	99.69	0.0	0.0	1.006	0.234
1906852006	20.376	90.10	96.36	28.263	14.64	47.07	55.76	0.9224	99.69	0.0	0.0	1.006	0.307
1906852007	20.376	90.09	96.59	28.952	14.77	47.38	56.26	0.9963	99.71	0.0	0.0	1.006	2.481
1906852107	21.929	89.74	99.15	29.205	12.14	46.87	55.83	0.9828	99.83	0.0	0.0	1.006	2.753

TABLE C.3a

Steam-Water Data, Wall Temperature Measurements (Low Steam Extraction Rate Tests)

TEST NO	Q _{fin}	T _{fin}	Inlet Water Subcooling = 80 K										
			T1	T2	T3	T4	T5	T6	T7	T8	T9	T10	T11
0507850401	4.000	19.82	20.18	20.56	20.97	21.15	21.77	22.71	23.29	34.67	58.86	70.96	79.99
0507850402	4.000	19.99	20.15	21.04	21.21	21.09	23.78	27.06	42.50	66.66	74.31	85.61	87.66
0507850403	4.000	19.97	20.14	20.47	20.92	23.79	31.59	43.61	58.49	73.17	84.59	94.09	96.08
0507850404	4.000	20.03	20.18	21.61	33.72	53.56	70.87	79.96	87.07	93.39	95.09	96.44	97.66
0507850405	4.000	20.16	20.93	21.74	44.02	76.65	75.52	86.84	93.41	96.51	97.21	97.93	97.89
0507850406	4.000	20.35	21.54	23.21	52.60	79.14	88.17	95.77	97.37	97.51	98.02	98.04	97.99
0507850407	4.000	20.36	21.87	26.03	55.75	80.11	90.37	95.81	97.34	97.49	98.10	98.18	98.09
0507850408	4.000	20.33	23.92	30.26	61.07	82.12	92.03	96.42	97.69	98.03	98.35	98.44	98.26
0507850501	5.000	20.76	20.97	21.18	21.20	21.07	22.41	23.41	27.30	32.37	40.57	64.31	75.58
0507850502	5.000	20.89	21.06	21.29	21.49	21.70	24.39	27.56	31.35	43.82	66.13	78.43	80.78
0507850503	5.000	20.77	20.87	21.59	24.46	28.16	33.44	39.68	50.48	64.61	76.04	87.01	90.88
0507850504	5.000	20.79	20.93	21.06	27.87	41.60	49.87	65.76	79.09	87.43	92.96	95.08	96.80
0507850505	5.000	20.81	21.12	22.23	37.06	52.20	73.35	85.56	92.44	95.03	96.65	97.11	97.77
0507850506	5.000	20.97	21.48	22.24	41.73	60.44	79.91	88.40	93.04	96.06	96.82	97.61	97.76
0507850507	5.000	20.99	22.89	24.70	43.92	65.29	81.72	90.22	94.82	96.84	97.23	98.14	98.16
0507850601	6.000	20.93	20.96	21.05	21.33	22.42	24.01	26.88	29.47	39.99	60.19	75.00	80.91
0507850602	6.000	20.90	20.91	21.01	21.73	22.90	25.82	29.97	41.58	65.33	73.62	83.04	86.04
0507850603	6.000	20.90	21.11	21.05	23.44	31.01	44.76	56.60	68.81	77.65	88.95	92.78	94.71
0507850604	6.000	20.89	21.19	22.03	25.75	39.94	55.71	66.09	81.44	92.76	94.11	96.49	96.53
0507850605	6.000	20.92	21.14	22.54	27.45	44.52	62.34	74.84	86.07	93.44	95.03	96.98	97.33
0507850606	6.000	21.05	21.45	22.91	30.64	48.57	66.27	78.60	88.97	93.91	95.77	97.11	97.45
0507850607	6.000	21.07	21.38	22.20	32.24	51.71	69.12	80.02	89.13	94.77	96.03	97.41	97.57
0807850701	7.000	20.98	21.07	21.06	21.13	21.52	21.58	22.95	25.08	26.54	29.10	34.38	48.78
0807850702	7.000	21.06	20.98	21.15	21.24	21.22	21.62	22.10	26.55	28.96	34.89	47.54	62.10
0807850703	7.000	29.91	20.93	20.98	21.39	21.31	21.77	22.29	27.57	30.80	40.60	54.54	66.39
0807850704	7.000	20.88	20.97	20.01	20.01	21.31	23.72	23.22	28.51	34.00	48.39	59.81	74.49
0807850705	7.000	20.78	21.08	21.00	21.74	22.73	24.32	27.00	33.65	41.11	57.11	70.57	82.21
0807850706	7.000	20.52	20.13	21.12	22.55	24.70	27.37	32.82	43.86	55.18	67.10	78.86	88.81
0807850707	7.000	20.47	20.96	21.72	23.90	29.47	39.63	48.50	59.02	69.97	81.35	87.59	91.88
0807850801	8.000	20.82	20.80	21.08	21.49	21.36	21.57	21.57	22.07	22.68	23.67	25.68	40.29
0807850802	8.000	20.88	20.92	21.66	21.59	21.48	21.84	21.94	22.85	24.16	26.39	32.00	47.50
0807850803	8.000	20.92	20.97	21.47	21.69	21.73	21.86	21.93	22.91	24.56	26.90	35.29	51.57
0807850804	8.000	20.95	21.00	21.74	21.67	21.57	21.94	22.09	23.07	24.56	27.27	38.59	54.73
0807850805	8.000	20.97	21.09	21.61	21.52	22.03	22.79	23.14	24.53	26.34	33.43	49.57	68.85
0807850806	8.000	21.05	21.27	21.67	21.68	22.14	23.00	23.40	26.16	31.02	47.73	67.53	79.10
0807850807	8.000	21.16	21.42	21.63	21.75	22.15	23.96	25.12	29.51	36.93	50.83	70.43	82.29
0807850808	8.000	21.23	21.66	22.48	22.49	22.52	24.98	28.03	34.38	45.83	57.79	74.56	84.44
0907850901	9.000	20.91	21.03	21.09	21.27	21.17	21.67	21.52	22.36	22.96	25.63	29.79	43.26
0907850902	9.000	20.95	21.09	21.01	20.96	20.92	21.01	21.14	21.77	22.35	24.62	33.38	48.15
0907850903	9.000	20.91	21.06	20.93	20.98	20.93	21.08	21.29	22.25	23.24	27.64	38.35	53.05
0907850904	9.000	21.05	21.09	21.37	21.34	21.41	21.57	21.91	22.93	25.38	33.93	42.08	58.81
0907850905	9.000	21.17	21.12	21.50	21.49	21.95	21.94	22.42	23.19	26.89	36.09	48.30	65.95
0907850906	9.000	21.25	21.44	21.73	21.95	22.00	22.69	23.23	24.75	30.21	40.66	57.60	70.76
0907850907	9.000	21.37	21.49	22.12	22.64	23.24	25.09	27.91	29.20	37.42	51.05	67.44	74.90
1107851001	10.000	21.01	21.19	21.20	21.32	21.42	21.64	21.65	22.24	24.13	26.84	33.06	44.78
1107851002	10.000	21.13	21.35	21.36	21.24	21.53	21.75	21.92	22.92	24.90	26.96	35.29	48.39
1107851003	10.000	21.66	21.88	21.71	21.72	21.55	21.85	21.89	22.40	24.44	27.14	47.71	51.93
1107851004	10.000	21.62	21.66	21.72	21.98	21.84	22.16	22.79	23.65	25.34	30.51	46.41	55.87
1107851005	10.000	21.70	21.76	21.70	21.87	21.75	22.09	22.58	23.61	25.57	32.98	48.92	59.65
1107851006	10.000	21.60	21.70	21.62	21.67	21.48	22.82	23.48	25.50	27.81	37.16	53.50	62.13
1107851007	10.000	21.69	21.74	21.85	21.97	22.07	23.09	24.67	27.62	33.50	45.00	59.34	66.60

TABLE C.3b

Steam-Water Data, Wall Temperature Measurements (Low Steam Extraction Rate Tests)

Inlet Water Subcooling = 70 K

TEST NO	Q _{fin}	T _{fin}	T ₁	T ₂	T ₃	T ₄	T ₅	T ₆	T ₇	T ₈	T ₉	T ₁₀	T ₁₁
1807850401	4.000	30.66	30.88	30.90	31.85	32.04	33.03	36.99	47.89	59.75	74.17	85.28	89.14
1807850402	4.000	30.75	30.75	31.53	31.57	32.72	35.85	41.46	52.45	67.38	78.68	90.06	94.35
1807850403	4.000	30.64	30.75	32.22	35.43	42.80	51.64	62.31	75.98	82.22	87.94	94.43	97.00
1807850404	4.000	30.63	30.92	32.89	40.94	58.02	68.02	77.52	86.69	92.21	97.97	97.84	97.88
1807850405	4.000	30.77	31.22	32.97	43.96	60.36	80.51	91.10	95.53	97.19	98.04	98.13	98.05
1807850406	4.000	30.71	31.97	33.42	45.17	66.58	87.84	93.43	96.62	97.20	98.11	98.17	98.18
1807850407	4.000	30.73	31.72	33.31	46.74	73.66	88.22	93.38	96.53	97.15	98.21	98.29	98.25
1807850408	4.000	30.71	31.89	34.11	50.05	76.72	89.43	93.86	96.76	97.29	98.25	98.25	98.18
1807850409	4.000	30.70	31.94	36.59	59.33	83.21	91.85	95.58	97.42	97.59	98.21	98.41	98.25
1807850410	4.000	30.64	32.91	44.83	68.15	88.52	94.43	97.73	97.97	98.58	98.74	98.88	98.71
1807850501	5.000	30.58	30.72	31.06	31.72	31.90	31.95	33.90	34.64	45.45	66.64	84.77	91.92
1807850502	5.000	30.56	30.72	31.14	32.05	33.39	36.09	42.66	63.74	79.38	87.58	92.49	94.54
1807850503	5.000	30.59	30.77	31.08	33.65	37.74	44.09	58.76	73.87	85.05	90.05	96.00	97.65
1807850504	5.000	30.63	30.86	32.14	36.79	44.94	56.88	69.68	82.05	90.75	94.67	97.10	97.71
1807850505	5.000	30.65	30.89	32.12	39.99	54.47	73.54	85.08	93.23	95.59	97.59	97.88	97.80
1807850506	5.000	30.66	31.21	34.28	44.60	64.41	82.44	90.98	95.20	96.57	97.56	98.03	97.89
1807850507	5.000	30.67	32.37	38.96	53.02	78.61	88.93	94.93	96.84	97.43	97.92	98.18	98.05
1807850601	6.000	30.79	30.95	31.14	31.20	31.37	31.95	33.26	36.35	43.86	56.55	73.37	82.42
1807850602	6.000	30.58	30.72	31.16	31.72	32.90	33.95	35.99	38.65	49.45	66.06	80.05	88.09
1807850603	6.000	30.63	30.77	30.98	31.79	33.31	34.74	37.49	44.79	56.39	71.49	82.90	91.28
1807850604	6.000	30.83	31.07	31.21	32.37	34.39	36.71	42.65	50.34	63.12	77.71	87.11	93.29
1807850605	6.000	30.80	31.20	31.23	33.50	38.16	46.50	53.29	67.39	78.21	86.33	93.39	96.08
1807850606	6.000	30.88	31.29	32.31	36.82	48.33	58.85	70.56	89.08	95.24	97.38	97.93	97.24
1807850607	6.000	30.89	31.45	32.12	39.36	50.61	76.32	87.96	93.46	96.58	97.53	97.66	97.77
1807850608	6.000	30.93	31.31	33.93	41.34	67.24	82.59	90.58	95.34	96.45	97.75	97.90	97.81
1807850609	6.000	30.95	32.00	35.84	45.82	70.48	84.04	92.34	96.80	97.19	97.98	98.05	97.94
2207850701	7.000	30.24	30.33	30.67	30.85	31.79	31.92	32.84	36.43	41.34	51.40	59.37	65.58
2207850702	7.000	30.36	30.64	30.48	30.95	31.05	31.08	32.20	37.24	45.27	59.82	71.52	75.49
2207850703	7.000	30.33	30.63	30.97	31.22	31.34	31.78	33.33	39.39	48.80	65.73	73.56	79.61
2207850704	7.000	30.34	30.83	30.82	30.88	31.15	31.70	34.82	42.25	53.54	69.56	77.52	84.94
2207850705	7.000	30.41	30.87	30.98	31.07	32.19	32.89	37.83	46.88	57.52	75.52	85.76	89.09
2207850706	7.000	30.40	30.72	31.53	32.77	34.95	40.91	49.23	60.34	71.05	82.60	88.83	92.79
2207850707	7.000	30.41	31.81	32.81	35.01	39.15	49.66	61.70	74.42	84.60	90.91	94.26	96.67
2207850801	8.000	30.43	30.42	30.54	30.42	30.27	30.59	31.31	32.05	32.75	34.59	40.50	56.04
2207850802	8.000	30.45	30.46	30.50	30.36	30.26	30.57	31.45	32.27	32.91	34.82	42.70	60.05
2207850803	8.000	30.50	30.57	30.54	30.36	30.27	30.61	31.42	32.25	32.94	36.73	50.62	67.99
2207850804	8.000	30.54	30.66	30.59	30.75	30.45	30.81	31.90	33.04	34.95	41.94	59.34	74.95
2207850805	8.000	30.57	30.74	30.67	30.74	30.66	31.03	32.31	34.52	38.38	45.80	64.18	80.04
2207850806	8.000	30.59	30.75	30.95	31.29	31.46	32.48	34.03	37.16	49.48	62.21	80.66	87.09
2207850807	8.000	30.59	30.85	31.85	32.81	33.73	36.99	42.69	53.67	65.67	78.57	87.38	92.63

TABLE C.3b (Continue)

Steam-Water Data, Wall Temperature Measurements (Low Steam Extraction Rate Tests)

Average Inlet Water Subcooling = 70 K

TEST NO	Q _{fin}	T _{fin}	T1	T2	T3	T4	T5	T6	T7	T8	T9	T10	T11
2207850901	9.000	30.10	30.11	30.08	29.97	29.96	30.09	30.29	30.66	30.98	31.85	34.10	48.08
2207850902	9.000	30.18	30.14	30.09	30.14	30.22	30.55	31.08	31.98	32.98	34.65	43.76	53.98
2207850903	9.000	30.29	30.33	30.57	30.43	30.57	30.96	31.49	31.92	33.26	36.68	47.32	58.27
2207850904	9.000	30.29	30.41	30.54	30.39	30.53	30.85	31.32	32.91	35.60	38.80	52.90	62.47
2207850905	9.000	30.30	30.49	30.47	30.37	30.52	31.88	32.04	33.23	37.28	44.88	56.31	68.12
2207850906	9.000	30.31	30.37	30.51	30.38	30.99	31.87	34.80	37.09	43.62	50.20	64.47	77.71
2207850907	9.000	30.24	30.52	30.55	31.74	32.17	33.93	38.53	46.43	59.15	71.84	82.34	87.87
2207851001	10.000	30.10	30.18	30.29	30.58	30.39	30.68	31.32	31.95	32.48	34.81	40.66	49.02
2207851002	10.000	30.07	30.13	30.29	30.51	30.38	30.82	31.51	32.15	32.85	35.42	43.05	56.60
2207851003	10.000	30.11	30.05	30.41	30.76	30.65	30.96	31.77	32.44	32.03	37.77	47.47	59.96
2207851004	10.000	30.09	30.13	30.48	30.81	30.74	30.99	31.58	32.71	33.67	42.26	53.31	65.16
2207851005	10.000	30.01	30.15	30.49	30.88	30.93	31.29	31.98	32.93	35.24	45.27	59.24	71.08
2207851006	10.000	30.03	30.23	30.43	30.15	30.10	31.29	32.66	34.21	37.21	50.14	69.47	77.33
2207851007	10.000	30.03	30.35	30.45	31.13	31.91	32.75	35.48	41.71	52.00	63.90	77.17	84.76
1908851101	11.197	30.75	30.84	30.75	30.92	31.15	31.37	31.85	32.44	33.89	35.53	38.95	46.09
1908851102	11.197	30.76	30.80	30.87	31.00	31.57	31.71	32.28	33.81	34.86	37.21	42.73	51.32
1908851103	11.197	30.80	30.95	30.98	31.08	31.78	31.69	32.05	34.24	36.12	41.28	53.91	57.35
1908851104	11.197	30.90	30.98	31.02	31.11	31.86	31.71	32.75	34.41	35.84	39.73	52.71	63.93
1908851105	11.197	30.96	30.91	31.17	31.28	31.72	31.94	32.96	35.28	36.77	41.54	54.72	69.66
1908851106	11.197	31.01	31.02	31.37	31.31	32.04	32.53	33.49	37.18	39.25	45.74	58.93	75.67
1908851107	11.197	31.14	31.28	32.42	32.91	33.09	33.56	35.52	40.02	48.44	59.31	72.73	79.54
1908851201	12.170	30.22	30.38	30.65	30.71	30.78	30.75	30.98	31.15	31.72	33.06	36.75	43.97
1908851202	12.710	30.17	30.28	30.43	30.32	30.18	30.25	31.45	31.25	32.34	34.26	40.87	48.78
1908851203	12.710	30.19	30.23	30.30	30.31	30.39	30.59	31.02	31.43	32.93	35.45	42.37	51.48
1908851204	12.710	30.22	30.43	30.42	30.42	30.52	30.66	31.16	31.22	32.89	36.71	43.91	54.02
1908851205	12.710	30.20	30.35	30.84	30.84	30.89	31.03	31.55	32.92	34.70	38.61	46.76	59.60
1908851206	12.710	30.29	30.41	30.55	30.49	30.47	30.51	32.60	34.01	36.03	41.27	50.72	64.30
1908851207	12.710	30.23	30.57	30.62	30.72	30.85	31.92	33.03	38.15	44.21	53.99	62.38	69.61

TABLE C.3c

 Steam-Water Data, Wall Temperature Measurements (Low Steam Extraction Rate Tests)

Inlet Water Subcooling = 60 K

TEST NO	Q _{fin}	T _{fin}	T1	T2	T3	T4	T5	T6	T7	T8	T9	T10	T11
2307850401	4.000	40.24	40.29	40.51	41.09	42.20	44.54	49.36	55.32	61.29	70.72	86.29	89.90
2307850402	4.000	40.21	40.36	40.64	41.95	45.38	51.58	60.19	72.50	82.59	87.39	92.17	94.73
2307850403	4.000	40.22	40.47	40.64	47.86	63.80	80.35	87.57	92.18	94.91	96.27	97.41	97.38
2307850404	4.000	40.28	40.55	40.78	55.18	75.09	92.52	95.96	97.66	98.19	98.52	98.53	97.67
2307850405	4.000	40.29	40.66	41.13	59.97	82.61	94.37	96.29	97.85	98.21	98.49	98.61	97.73
2307850406	4.000	40.30	40.72	41.83	64.88	85.91	94.46	96.68	97.97	98.29	98.55	98.60	97.98
2307850407	4.000	40.31	41.03	45.02	68.02	87.33	95.84	96.78	98.03	98.29	98.54	98.71	98.03
2307850408	4.000	40.33	41.31	49.94	76.55	90.21	96.59	98.06	98.28	98.54	98.79	98.82	98.24
2307850501	5.000	39.96	40.37	40.50	40.84	41.86	41.07	44.96	48.18	53.64	66.83	79.42	90.75
2307850502	5.000	39.92	40.44	40.50	41.08	42.19	45.49	51.30	59.33	70.29	83.30	89.32	93.92
2307850503	5.000	39.96	40.51	40.53	44.81	53.64	74.49	88.66	95.10	96.96	97.96	97.82	96.91
2307850504	5.000	39.98	40.48	40.66	48.18	59.77	81.99	91.88	96.10	97.46	98.21	98.27	97.46
2307850505	5.000	40.00	40.59	40.94	49.43	60.94	84.53	92.76	96.25	97.53	98.24	98.43	97.73
2307850506	5.000	40.04	40.64	41.05	52.88	66.67	87.18	93.60	96.51	97.64	98.23	98.45	97.73
2307850507	5.000	40.06	41.64	42.05	57.78	72.75	89.08	94.50	96.93	97.94	98.24	98.49	97.73
2307850508	5.000	40.06	42.31	45.73	67.03	87.82	95.97	97.44	97.88	98.26	98.48	98.55	97.90
2307850601	6.000	40.25	40.87	40.10	40.71	40.78	41.48	43.09	46.00	50.75	64.85	81.18	91.98
2307850602	6.000	40.35	40.93	40.50	42.27	45.27	52.45	67.71	81.50	90.59	94.65	96.38	96.03
2307850603	6.000	40.35	40.33	40.63	46.04	57.75	71.97	84.67	92.06	95.14	96.48	97.16	97.05
2307850604	6.000	40.31	40.50	40.55	48.12	59.98	75.77	89.07	94.44	95.22	96.45	97.45	97.55
2307850605	6.000	40.29	40.63	41.13	52.12	61.95	80.76	90.06	95.32	96.89	97.88	98.32	97.59
2307850606	6.000	40.21	40.82	41.86	56.23	64.01	86.93	92.78	96.53	97.83	97.91	98.24	97.46
2307850607	6.000	40.13	41.30	43.99	62.85	82.71	91.88	94.86	96.94	98.07	98.16	98.38	97.88
2307850701	7.000	39.95	40.29	40.19	40.21	40.15	40.38	40.88	42.04	45.20	54.96	65.99	76.71
2307850702	7.000	39.70	40.36	40.22	40.32	40.36	41.73	42.38	44.12	49.19	58.16	74.40	81.87
2307850703	7.000	39.48	40.05	40.52	40.94	41.43	42.81	44.43	46.28	53.53	66.63	80.15	88.72
2307850704	7.000	39.41	41.94	40.69	42.20	43.19	44.14	47.65	52.40	63.45	75.43	87.42	93.72
2307850705	7.000	39.41	40.56	40.84	43.34	44.78	47.30	58.92	67.60	77.59	87.49	95.55	95.94
2307850706	7.000	39.41	40.59	41.04	45.09	49.76	53.09	66.54	77.66	89.66	94.65	97.39	96.70
2307850707	7.000	39.41	40.31	41.16	54.73	59.42	71.84	81.82	90.84	95.39	97.05	97.77	97.41
2407850801	8.000	39.59	39.58	39.59	39.88	39.94	40.72	41.79	43.71	45.08	49.46	57.63	60.39
2407850802	8.000	39.59	39.58	39.67	40.13	40.24	42.09	43.49	46.58	48.82	53.05	65.66	69.41
2407850803	8.000	39.58	39.60	39.78	40.65	41.79	42.70	44.15	48.50	52.30	60.04	69.49	74.30
2407850804	8.000	89.54	39.74	39.79	40.82	41.99	43.81	46.50	63.35	58.61	67.48	78.72	84.72
2407850805	8.000	39.64	39.68	40.06	41.73	42.05	44.94	49.77	54.79	66.11	77.41	86.69	90.44
2407850806	8.000	39.60	40.00	40.42	42.66	45.91	52.74	55.69	66.07	74.22	87.70	90.64	92.44
2407850807	8.000	39.51	40.79	40.53	46.56	51.61	60.07	71.13	79.00	87.92	91.68	93.21	94.52

TABLE C.3c (Continue)

 Steam-Water Data, Wall Temperature Measurements (Low Steam Extraction Rate Tests)

Inlet Water Subcooling = 60 K

TEST NO	Qfin	Tfin	T1	T2	T3	T4	T5	T6	T7	T8	T9	T10	T11
2407850901	9.000	40.27	40.53	40.61	40.61	40.89	41.42	42.03	43.06	44.72	47.88	54.88	67.65
2407850902	9.000	40.25	40.38	40.37	40.74	41.14	41.70	42.41	43.99	46.95	58.27	67.99	77.02
2407850903	9.000	40.21	40.64	40.50	40.84	41.17	41.71	42.99	44.91	48.13	60.66	76.19	83.04
2407850904	9.000	40.19	40.38	40.43	40.75	41.19	41.69	43.30	45.86	49.50	63.91	79.02	85.63
2407850905	9.000	40.16	40.30	40.43	40.79	41.40	42.19	43.26	49.91	63.26	77.43	84.35	89.16
2407850906	9.000	40.17	41.46	41.16	41.73	42.51	45.30	49.66	56.95	71.41	82.86	87.56	91.58
2407850907	9.000	40.14	41.07	42.11	44.60	47.49	51.42	62.87	72.03	80.81	86.93	91.55	93.72
2707851001	10.000	41.26	41.35	41.43	41.66	41.42	41.66	42.03	42.30	43.88	44.17	48.99	65.12
2707851002	10.000	41.26	41.59	41.80	41.72	41.44	41.51	42.77	42.22	43.54	45.05	51.06	68.75
2707851003	10.000	41.41	41.66	41.57	41.18	41.30	41.50	41.82	42.65	43.88	48.22	58.61	72.66
2707851004	10.000	41.44	41.66	41.60	41.26	41.41	41.69	42.08	42.95	44.23	49.18	62.72	78.50
2707851005	10.000	41.38	41.50	41.00	41.65	41.82	42.14	42.80	45.30	49.24	58.80	72.82	83.36
2707851006	10.000	41.39	41.98	41.93	42.74	42.86	44.13	47.53	51.45	61.18	68.71	79.97	88.71
2707851007	10.000	41.40	41.98	42.75	43.28	44.19	47.39	53.32	61.62	69.93	77.85	86.45	90.48
2808851101	11.197	39.95	39.92	40.10	40.61	40.30	40.74	40.88	41.21	44.12	50.80	57.42	61.09
2808851102	11.197	39.91	40.07	40.16	40.65	40.40	40.81	41.15	42.58	45.18	53.53	62.95	67.38
2808851103	11.197	39.84	40.06	40.24	40.89	40.94	41.47	41.95	42.95	46.92	55.78	67.80	71.81
2808851104	11.197	39.80	40.14	40.47	40.73	41.34	41.64	42.22	43.13	48.57	57.76	69.84	73.63
2808851105	11.197	39.78	39.99	40.68	40.70	41.60	41.87	43.44	47.23	53.94	62.52	73.53	76.99
2808851106	11.197	39.56	40.15	40.66	40.78	41.33	42.93	45.45	51.51	58.03	65.82	75.38	79.61
2808851107	11.197	39.66	40.65	40.95	41.02	41.84	44.94	48.90	54.43	62.55	69.91	78.31	83.84
2808851201	12.710	39.70	39.79	40.04	40.56	40.55	40.65	40.95	41.48	41.81	42.92	45.35	51.53
2808851202	12.710	39.71	39.97	40.05	40.90	40.92	40.95	41.27	41.69	42.01	43.90	47.58	56.62
2808851203	12.701	39.73	40.02	40.07	40.14	40.66	40.69	41.74	41.62	42.87	45.51	51.60	60.86
2808851204	12.710	39.81	39.80	40.82	40.67	40.69	40.75	41.92	41.49	43.99	47.79	54.78	62.34
2808851205	12.710	39.81	40.21	40.81	40.63	40.64	40.94	41.96	42.17	46.04	51.83	57.81	65.96

TABLE C.3d

 Steam-Water Data, Wall Temperature Measurements (Low Steam Extraction Rate Tests)

Inlet Water Subcooling = 50 K

TEST NO	Qfin	Tfin	T1	T2	T3	T4	T5	T6	T7	T8	T9	T10	T11
2507850401	4.000	50.09	50.16	50.88	55.74	58.51	72.35	80.92	87.58	95.84	96.20	97.02	97.35
2507850402	4.000	50.07	50.03	51.47	58.64	69.05	88.90	93.70	95.69	96.97	97.84	98.03	98.70
2507850403	4.000	50.00	50.23	52.39	60.29	76.93	90.64	95.13	97.70	97.76	98.18	98.24	98.78
2507850404	4.000	49.93	49.97	52.72	63.54	80.65	92.01	95.47	97.88	97.92	98.28	98.44	98.76
2507850405	4.000	49.92	50.73	53.09	64.80	83.62	94.50	95.74	98.02	97.94	98.12	98.24	98.64
2507850406	4.000	49.87	50.81	53.40	67.86	85.55	95.12	95.92	97.99	97.98	98.36	98.22	98.70
2507850407	4.000	49.90	51.13	54.36	70.67	88.25	96.11	96.74	98.13	98.14	98.43	98.40	98.79
2507850408	4.000	49.86	52.72	56.11	75.42	90.41	96.30	97.06	98.40	98.41	98.55	98.58	98.81
2507850409	4.000	49.88	54.85	66.42	80.28	92.26	96.78	97.23	98.42	98.44	98.68	98.66	98.98
2507850501	5.000	50.44	49.49	49.23	50.28	50.78	51.92	53.88	56.71	62.94	77.48	89.92	93.68
2507850503	5.000	50.37	50.24	50.99	51.71	55.01	71.53	82.32	89.31	94.45	96.46	97.61	97.98
2507850502	5.000	50.35	50.39	51.32	53.79	58.69	76.69	87.20	92.96	96.49	97.97	97.95	98.01
2507850504	5.000	50.38	50.52	51.47	59.44	75.43	89.53	94.94	97.25	97.55	98.02	98.00	98.29
2507850505	5.000	50.32	50.46	52.57	62.34	78.43	91.14	95.11	97.36	97.42	98.13	98.11	98.66
2507850506	5.000	50.36	50.84	53.31	66.33	80.65	92.53	96.03	97.64	97.58	98.31	98.17	98.69
2507850507	5.000	50.37	51.95	55.50	69.09	83.03	93.65	96.33	97.99	98.01	98.46	98.29	98.63
2507850508	5.000	50.40	53.24	64.91	77.52	88.93	94.97	97.81	98.14	98.12	98.50	98.39	98.69
2507850601	6.000	49.80	50.98	50.50	52.37	53.05	54.08	55.26	57.91	62.39	70.70	82.23	88.54
2507850602	6.000	49.83	50.97	50.45	53.26	54.51	57.25	60.23	68.58	75.26	82.25	88.92	92.81
2507850603	6.000	49.89	50.31	51.99	54.30	58.00	65.90	76.20	85.98	91.41	94.14	95.19	96.42
2507850604	6.000	49.95	50.00	52.03	55.99	66.73	74.55	83.34	90.58	94.56	97.37	97.37	97.64
2507850605	6.000	49.97	50.04	52.26	64.08	82.31	89.02	94.60	97.06	97.39	98.12	98.05	98.71
2507850606	6.000	50.00	51.31	52.99	67.30	84.11	91.70	95.26	96.98	97.41	98.24	98.19	98.70
2507850607	6.000	50.02	52.90	53.78	72.00	86.75	93.70	96.76	97.85	97.79	98.30	98.28	98.74
2507850608	6.000	50.07	53.48	62.03	75.94	88.06	94.40	97.79	98.02	98.73	99.14	99.30	98.93
2607850701	7.000	50.34	50.65	51.00	51.39	51.17	51.50	52.02	53.54	55.02	60.06	78.21	85.00
2607850702	7.000	50.36	50.35	50.89	51.29	51.33	52.80	55.28	61.00	71.91	80.25	86.62	91.93
2607850703	7.000	50.35	50.44	50.93	51.84	54.65	58.70	66.72	75.76	80.09	87.33	92.87	95.82
2607850704	7.000	50.26	50.47	51.77	55.57	62.29	73.96	85.18	92.22	95.64	96.55	97.80	97.86
2607850705	7.000	50.22	50.55	51.99	65.87	72.76	82.76	90.09	94.65	96.96	97.50	97.78	97.67
2607850706	7.000	50.26	50.77	53.13	69.64	78.24	90.12	93.73	95.83	96.36	97.50	97.76	97.84
2607850707	7.000	50.26	52.91	59.93	72.52	83.13	93.20	96.39	97.33	97.07	97.75	97.86	97.79
2607850801	8.000	50.48	50.80	51.04	51.37	50.51	51.42	51.80	52.28	54.76	60.52	71.83	83.33
2607850802	8.000	50.49	50.83	51.15	51.07	51.82	53.27	54.73	57.41	62.21	71.64	83.78	88.31
2607850803	8.000	50.53	50.72	50.89	51.84	51.89	55.71	66.70	72.69	74.67	81.72	88.59	92.11
2607850804	8.000	50.66	50.68	50.92	52.61	53.01	62.90	72.81	79.96	84.95	89.03	92.76	93.33
2607850805	8.000	50.72	50.77	51.86	52.04	55.21	64.54	75.52	81.26	87.09	92.33	94.66	95.79
2607850806	8.000	50.77	50.95	53.48	58.68	67.32	78.50	89.55	94.14	95.04	97.09	97.48	97.47
2607850807	8.000	50.78	52.03	54.02	63.32	75.96	88.55	93.05	95.95	96.89	97.45	97.62	97.49

TABLE C.3d (Continue)

Steam-Water Data, Wall Temperature Measurements (Low Steam Extraction Rate Tests)

TEST NO	Q _{fin}	T _{fin}	Inlet Water Subcooling = 50 K										
			T ₁	T ₂	T ₃	T ₄	T ₅	T ₆	T ₇	T ₈	T ₉	T ₁₀	T ₁₁
2607850901	9.000	50.95	51.15	51.50	51.91	51.80	51.72	51.94	52.53	54.54	59.56	65.97	76.28
2607850902	9.000	50.83	51.29	51.32	51.52	51.64	51.20	52.20	54.28	59.30	66.61	76.13	82.71
2607850903	9.000	50.84	51.00	51.97	51.91	51.04	52.48	55.06	59.39	65.32	75.55	84.92	88.19
2607850904	9.000	50.81	51.10	51.41	51.37	51.87	53.17	57.68	64.78	74.98	83.55	89.13	93.76
2607850905	9.000	50.79	51.04	52.71	53.99	54.62	57.35	63.97	71.10	82.85	91.45	94.05	95.68
2607850906	9.000	50.77	51.26	52.73	54.67	57.28	62.96	68.49	80.20	92.25	96.05	96.38	96.20
2608850907	9.000	50.90	52.67	53.49	57.19	66.53	74.49	86.87	92.53	95.77	96.84	96.88	96.70
2608850901	10.000	50.12	50.80	50.73	50.65	50.45	50.60	51.21	52.01	53.04	60.58	65.02	68.61
2608851002	10.000	50.37	50.80	50.66	50.79	50.77	50.87	51.26	52.80	54.08	62.48	69.89	73.35
2608851003	10.000	50.56	50.11	50.96	51.16	51.11	51.24	51.67	52.89	55.34	64.69	75.11	79.75
2608851004	10.000	50.48	50.01	50.98	51.38	51.43	51.78	52.97	55.35	59.73	70.56	81.96	86.44
2608851005	10.000	50.46	50.00	50.95	51.28	51.98	52.77	56.50	59.61	65.21	77.44	85.34	90.72
2608851006	10.000	50.47	50.01	50.73	51.97	53.45	55.45	60.68	66.18	77.87	84.96	91.48	93.91
2608851007	10.000	50.46	50.81	51.70	53.93	57.44	61.90	69.10	78.77	85.84	90.89	94.77	95.84
2608851101	11.197	50.21	50.39	50.36	50.27	50.24	50.42	51.46	51.56	52.92	55.20	61.72	67.67
2508851102	11.197	50.43	50.17	50.17	50.80	50.33	50.87	51.27	51.96	54.61	57.26	67.40	73.08
2508851103	11.197	50.62	50.21	50.63	51.22	51.07	51.59	52.19	54.78	58.59	65.10	72.50	77.00
2507851104	11.197	50.54	50.24	50.71	51.16	50.90	52.22	53.63	56.97	61.04	69.29	76.29	81.79
2507851105	11.197	50.77	50.21	50.63	51.22	51.07	52.59	54.19	57.78	63.59	74.10	80.50	84.02
2507851106	11.197	50.50	50.40	51.05	51.60	52.53	53.99	56.59	62.59	68.73	79.86	84.63	88.11
2507851107	11.197	50.43	50.42	50.80	52.07	53.81	56.13	60.28	67.92	75.24	83.17	88.15	90.95
2507851201	12.710	50.41	50.92	51.35	51.74	51.62	51.72	52.03	52.44	52.55	53.72	56.47	60.71
2507851202	12.710	50.50	50.46	50.69	51.04	51.15	51.28	51.67	52.21	52.63	54.77	60.74	65.89
2507851203	12.710	50.66	50.78	51.23	51.55	51.46	51.58	51.78	52.33	53.30	56.31	64.49	69.26
2507851204	12.710	50.54	50.87	51.20	51.50	51.38	51.45	52.60	52.84	54.91	59.70	67.82	74.29
2507851205	12.710	50.75	50.46	50.99	51.19	51.14	51.27	51.58	53.31	56.63	63.77	73.74	80.91
2507851206	12.710	50.50	50.85	51.05	51.49	51.14	51.27	52.89	55.74	60.85	67.73	79.74	85.51
2507851207	12.710	50.77	50.88	51.65	52.05	51.98	53.09	55.42	59.68	67.84	75.97	83.87	88.49
2507851401	14.229	49.94	49.99	49.66	50.58	50.08	50.57	50.58	50.93	51.46	53.34	55.20	59.97
2507851402	14.229	49.91	50.58	50.51	51.34	51.14	51.29	51.64	51.91	52.06	54.36	59.13	66.13
2507851403	14.229	50.01	50.37	50.84	50.57	51.20	51.14	52.01	52.33	52.94	55.19	62.76	70.57
2507851404	14.229	49.94	50.05	50.65	50.43	50.62	50.89	51.76	51.99	53.86	57.76	65.83	74.87
2507851405	14.229	49.98	50.05	50.56	50.65	50.93	51.34	51.89	52.11	54.95	60.72	70.56	78.83
2507851406	14.229	49.91	50.12	50.56	50.98	50.99	51.33	52.00	53.42	57.06	63.89	73.78	83.66
2507851407	14.229	50.04	50.55	51.01	51.23	51.98	52.76	53.79	56.68	60.90	69.72	79.65	86.47
2507851501	15.755	50.98	51.11	51.39	51.42	51.33	51.63	51.78	51.88	51.99	52.62	53.77	57.25
2507851502	15.755	50.99	51.23	51.48	51.50	51.29	51.86	51.88	51.81	52.23	53.45	55.02	61.17
2507851503	15.755	50.99	51.38	51.44	51.28	51.26	51.89	52.09	52.78	52.98	53.40	56.59	65.13
2507851504	15.755	51.09	51.48	51.56	51.65	51.18	51.70	52.72	52.04	52.32	53.43	58.82	68.36
2507851505	15.755	51.04	51.32	51.77	51.58	51.14	51.77	52.00	52.85	53.17	54.88	61.92	72.21
2507851506	15.755	51.07	51.21	51.68	51.81	51.32	51.83	52.85	53.19	54.66	57.57	63.99	75.42
2507851507	15.755	51.00	51.84	51.97	51.94	51.42	52.79	53.12	54.39	56.06	61.61	71.51	78.25

TABLE C.3e

Steam-Water Data, Wall Temperature Measurements (Low Steam Extraction Rate Tests)

Inlet Water Subcooling = 40 K

TEST NO	Q _{fin}	T _{fin}	T ₁	T ₂	T ₃	T ₄	T ₅	T ₆	T ₇	T ₈	T ₉	T ₁₀	T ₁₁
2907850401	4.000	59.48	59.83	59.95	60.01	61.01	62.30	64.22	67.62	75.49	84.72	90.74	92.30
2907850402	4.000	59.56	59.85	60.01	61.65	63.54	65.60	70.76	79.95	89.76	93.87	96.08	97.60
2907850403	4.000	59.60	59.85	60.21	62.49	66.40	72.11	80.09	89.34	93.89	96.32	96.37	97.63
2907850404	4.000	59.69	59.72	60.33	70.48	81.05	92.98	95.39	96.26	97.06	97.58	97.69	97.59
2907850405	4.000	59.68	59.92	61.04	72.31	86.63	95.09	96.76	97.33	97.39	97.62	97.85	97.77
2907850406	4.000	59.43	60.17	61.83	72.83	87.66	95.43	96.81	97.47	97.42	97.99	98.03	97.82
2907850407	4.000	59.48	60.60	62.49	77.23	90.84	96.45	97.13	97.44	97.41	98.01	98.12	97.98
2907850408	4.000	59.54	62.21	62.84	85.89	94.80	97.21	97.32	97.83	97.85	98.25	98.29	98.08
2907850501	5.000	60.54	60.81	60.90	61.76	64.13	66.99	70.73	77.67	85.87	91.42	94.96	95.32
2907850502	5.000	60.62	60.66	60.90	63.76	69.16	76.64	85.27	90.98	95.11	97.47	97.58	97.31
2907850503	5.000	60.72	60.62	60.84	70.99	80.68	91.19	95.33	96.82	96.95	97.66	97.96	97.94
2907850504	5.000	60.79	58.80	61.95	71.09	84.96	92.48	96.39	97.69	97.52	98.12	98.21	98.07
2907850505	5.000	60.80	60.77	62.08	73.08	85.22	93.64	96.69	97.47	97.64	98.05	98.19	98.08
2907850506	5.000	60.81	60.86	61.92	78.13	90.99	94.73	97.37	97.51	97.55	98.10	98.27	97.98
2907850507	5.000	60.83	61.09	62.14	83.96	94.66	97.39	97.67	98.37	98.42	98.46	98.52	98.23
2907850601	6.000	60.39	60.39	60.68	61.38	61.25	61.55	63.11	68.70	74.49	83.91	91.84	93.04
2907850602	6.000	60.42	60.49	60.77	63.55	68.76	76.76	85.22	90.08	95.05	97.03	97.46	96.31
2907850603	6.000	60.40	60.62	60.84	70.99	80.60	91.56	94.33	96.32	96.68	97.44	97.52	97.16
2907850604	6.000	60.32	60.79	60.95	73.87	85.42	93.99	96.49	97.36	97.34	97.76	97.74	97.26
2907850605	6.000	60.39	60.43	61.21	74.17	87.95	94.06	95.84	97.45	97.30	98.03	98.10	97.87
2907850606	6.000	60.35	60.93	62.17	77.66	88.54	93.87	95.97	97.57	97.49	98.05	98.20	97.91
2907850607	6.000	60.45	61.87	63.00	80.27	91.44	95.95	97.39	97.84	97.81	98.16	98.31	98.07
2907850701	7.000	60.59	60.15	60.07	60.46	60.49	60.84	61.01	64.68	69.36	74.20	80.55	89.79
2907850702	7.000	60.66	60.70	60.55	60.95	60.97	62.32	63.63	67.29	72.18	78.06	85.77	92.05
2907850703	7.000	60.67	60.69	60.98	61.87	64.49	68.89	75.29	83.54	89.00	93.50	94.01	95.22
2907850704	7.000	60.72	60.57	60.51	69.53	79.35	85.45	91.28	94.89	95.94	96.78	96.95	95.63
2907850705	7.000	60.62	60.95	60.73	71.87	81.42	88.68	92.56	95.84	96.61	97.12	97.36	96.93
2907850706	7.000	60.65	60.03	60.91	72.94	83.60	90.98	93.99	95.82	96.60	97.41	97.59	97.25
2907850707	7.000	60.67	60.87	61.90	73.83	84.76	91.78	94.92	96.21	97.74	97.62	97.71	97.25
2907850708	7.000	60.69	61.15	63.07	75.12	87.11	94.78	97.87	97.92	97.81	98.04	98.06	97.70
3007850801	8.000	59.45	59.70	60.04	61.31	60.98	61.18	62.10	63.17	67.12	73.26	79.59	85.86
3007850802	8.000	59.57	59.79	59.94	60.81	60.37	62.13	66.09	72.59	83.48	87.36	88.79	89.09
3007850803	8.000	59.53	60.03	60.24	61.20	62.00	65.87	72.20	77.16	87.42	92.51	93.91	93.63
3007850804	8.000	59.63	59.77	60.34	61.30	66.34	80.67	90.09	95.77	96.52	97.05	97.12	96.47
3007850805	8.000	59.57	59.85	60.46	63.84	75.24	85.68	92.66	96.28	96.70	97.54	97.46	97.07
3007850806	8.000	59.51	60.58	61.12	65.71	80.61	90.28	93.45	96.00	97.40	97.71	97.83	97.71
3007850807	8.000	59.43	60.88	61.21	70.65	80.08	92.70	94.66	96.27	97.78	98.01	98.16	98.03
3007850901	9.000	59.87	59.90	60.27	61.47	61.52	62.16	62.66	64.59	69.68	75.91	83.39	84.29
3007850902	9.000	59.86	59.85	60.00	62.00	62.16	63.73	67.48	72.58	77.56	83.08	87.61	91.23
3007850903	9.000	59.85	60.09	60.61	61.64	64.69	69.57	77.06	83.26	88.77	91.23	94.36	95.52
3007850904	9.000	59.90	60.34	60.55	62.38	70.82	80.30	88.97	92.97	94.90	96.03	97.14	97.03
3007850905	9.000	59.90	60.51	60.70	64.31	73.03	83.31	89.02	92.98	95.45	96.42	97.42	97.23
3007850906	9.000	59.95	60.62	60.77	65.82	73.22	84.53	91.18	95.01	96.63	97.25	97.68	97.39
3007850907	9.000	59.97	60.66	60.94	67.81	75.25	85.56	92.08	95.08	96.93	97.54	97.79	97.50
3007851001	10.000	59.78	59.28	60.35	60.58	60.73	60.97	61.25	62.91	68.42	73.93	77.71	80.65
3007851002	10.000	59.61	60.05	60.22	60.48	61.54	61.71	62.03	65.53	70.99	82.34	87.96	88.67
3007851003	10.000	59.52	60.11	60.33	60.53	60.96	62.51	66.10	76.59	84.77	90.25	93.07	93.30
3007851004	10.000	59.43	59.77	60.25	60.56	60.64	64.94	71.31	80.95	89.81	93.76	95.17	95.81
30.0785105	10.000	59.45	59.87	60.21	61.60	63.79	67.81	76.09	88.39	91.32	94.76	95.80	95.87
3007851005	10.000	59.56	59.90	60.19	62.10	67.53	77.87	83.02	91.40	94.39	95.82	96.27	96.07
3007851006	10.000	59.51	60.27	60.45	62.09	69.56	77.99	83.27	92.01	94.76	96.32	97.25	97.02

TABLE C.3e (Continue)

Steam-Water Data, Wall Temperature Measurements (Low Steam Extraction Rate Tests)

Inlet Water Subcooling = 40 K

TEST NO	G _{fin}	T _{fin}	T1	T2	T3	T4	T5	T6	T7	T8	T9	T10	T11
3007851007	10.000	59.51	60.57	60.65	63.64	70.16	79.84	88.10	93.82	95.29	97.01	97.76	97.56
3007851101	11.197	60.07	60.07	59.98	60.16	60.15	60.19	60.44	60.86	62.17	67.27	73.17	75.06
3007851102	11.197	60.10	60.36	60.79	61.04	61.09	61.27	61.55	62.15	64.75	70.03	77.00	82.00
3007851103	11.197	60.19	60.28	60.71	60.76	60.72	60.86	62.58	67.33	76.75	81.03	85.24	88.75
3007851104	11.197	60.11	60.48	61.14	61.65	61.90	65.27	73.88	82.83	86.05	89.15	90.91	93.58
3007851105	11.197	60.14	60.66	61.02	61.28	63.26	67.46	76.85	85.28	89.80	92.83	95.30	95.44
3007851106	11.197	60.11	60.54	60.87	61.92	64.18	70.50	77.54	88.82	91.68	94.19	96.59	96.32
3076851107	11.197	60.12	60.78	61.19	64.74	66.02	72.16	78.98	89.62	93.14	95.76	96.99	96.84
3007851201	12.710	60.56	60.17	60.07	60.28	60.73	60.91	61.18	61.69	62.40	64.08	68.38	72.62
2008851202	12.710	60.52	60.11	60.59	60.84	60.90	61.08	61.55	62.90	65.41	70.92	76.69	80.79
2008851203	12.710	60.72	60.32	60.74	60.86	60.88	61.04	61.15	62.67	65.37	73.79	81.01	84.12
2008851204	12.710	60.55	60.55	60.86	60.69	61.28	61.79	62.38	64.60	70.07	77.64	84.16	86.10
2008851205	12.710	60.53	60.45	60.78	61.21	61.00	61.66	63.90	67.70	74.40	80.08	87.65	89.64
2008851206	12.710	60.55	60.60	60.93	61.78	61.42	62.47	64.94	70.41	78.41	83.65	91.58	92.71
2008851207	12.710	60.57	60.64	60.88	62.13	61.95	63.06	66.90	74.70	82.90	88.08	92.65	93.33
2008851401	14.229	60.22	60.27	60.31	60.36	60.32	60.63	60.99	61.47	61.90	63.40	67.41	69.54
2008851402	14.229	60.26	60.26	60.77	61.02	61.01	61.68	61.66	62.05	62.44	65.50	70.18	74.12
2008851403	14.229	60.35	60.43	60.55	60.82	60.97	60.93	61.60	61.91	63.07	69.89	75.74	78.50
2008851404	14.229	60.36	60.53	60.53	61.13	61.08	61.36	62.48	63.07	63.30	74.87	80.18	82.70
2008851405	14.229	60.65	60.44	60.96	62.00	61.71	62.49	62.79	63.94	67.63	77.97	84.32	86.01
2008851406	14.229	60.76	60.90	61.11	61.85	61.65	61.69	62.02	65.81	70.07	80.05	87.05	90.23
2008851407	14.229	60.84	60.99	61.37	61.90	61.91	62.69	63.68	67.78	74.50	82.67	88.63	91.19
2008851501	15.755	60.81	61.03	61.77	62.09	62.31	62.67	62.88	63.63	64.19	66.00	70.39	75.69
2008851502	15.755	60.96	60.86	61.47	62.08	62.07	62.39	62.57	63.26	63.97	68.38	73.29	77.60
2008851503	15.755	60.95	61.11	61.87	62.13	62.47	62.41	62.48	63.03	64.04	70.09	80.80	84.80
2008851504	15.755	60.96	61.07	61.79	62.23	62.50	62.42	63.09	63.83	64.92	73.27	81.77	86.28
2008851505	15.755	61.00	61.21	61.96	62.15	62.53	62.67	63.08	62.96	66.56	73.03	83.74	89.41
2008851506	15.755	61.11	61.16	61.80	62.06	62.77	62.75	64.16	64.60	68.51	76.27	86.45	90.22
2008851507	15.755	61.15	61.80	62.09	62.15	62.77	62.91	64.03	65.94	71.54	78.92	87.34	91.22
2108851701	17.287	59.85	59.92	60.07	60.38	60.47	60.34	60.86	61.27	62.51	63.35	65.65	70.14
2108851702	17.287	59.70	59.91	59.98	60.76	60.70	60.65	61.18	61.91	63.63	65.63	71.21	74.74
2108851703	17.287	59.65	59.85	60.08	60.33	60.83	60.97	61.37	62.09	64.06	70.81	74.97	77.55
2108851704	17.287	59.74	59.73	60.17	60.54	60.79	60.39	60.66	61.38	64.38	71.26	76.76	80.32
2108851705	17.287	59.81	59.84	60.13	60.86	60.77	60.74	61.01	61.93	65.65	72.41	78.89	83.12
2108851706	17.287	59.74	59.77	60.26	60.78	60.80	60.75	60.91	62.86	66.97	74.38	82.96	85.86
2108851707	17.287	59.74	59.93	60.57	60.54	60.89	60.89	61.26	63.88	70.38	78.26	84.76	87.34
2208851801	18.827	66.91	60.95	60.90	61.14	61.13	61.21	61.25	61.51	61.72	63.05	65.63	67.88
2208851802	18.827	66.91	60.97	61.00	61.11	61.14	61.37	61.33	61.88	63.63	64.69	68.63	71.77
2208851803	18.827	66.90	61.01	60.94	61.27	61.25	61.53	61.65	62.32	64.37	67.12	72.48	76.31
2208851804	18.827	66.90	61.04	61.29	61.32	61.42	61.73	61.67	62.20	64.93	70.19	75.07	77.66
2208851805	18.827	60.95	60.91	61.10	61.05	62.10	61.53	61.83	61.95	65.83	72.66	76.20	78.93
2208851806	18.827	60.96	60.99	61.42	61.51	61.43	61.60	61.85	62.18	66.51	74.41	78.32	80.90
2208851807	18.827	61.00	61.13	61.47	61.53	61.54	61.67	61.91	63.63	68.39	77.52	81.54	83.45
2208852001	20.374	61.02	60.97	61.07	61.21	61.15	61.32	61.39	61.85	61.99	62.01	63.44	65.91
2208852002	20.374	61.08	61.04	61.15	61.39	61.42	61.46	61.44	61.49	62.41	64.21	67.04	69.78
2208852003	20.374	61.02	60.99	61.17	61.20	61.33	61.38	61.45	61.53	63.08	64.26	68.21	71.46
2208852004	20.374	61.11	61.04	61.25	61.23	61.29	61.46	61.47	61.46	63.66	66.03	71.49	73.22
2208852005	20.374	61.14	61.08	61.07	61.34	61.48	61.57	61.69	61.72	64.17	68.90	73.05	74.04
2208852006	20.374	61.08	61.17	61.21	61.68	61.66	61.74	61.94	62.34	65.20	70.24	74.95	76.33
2208852007	20.374	61.12	61.40	61.53	61.60	61.74	61.93	62.28	63.12	67.62	72.60	77.53	79.81

TABLE C.3f

Steam-Water Data, Wall Temperature Measurements (Low Steam Extraction Rate Tests)

TEST NO	Qfin	Tfin	Inlet Water Subcooling = 30 K										
			T1	T2	T3	T4	T5	T6	T7	T8	T9	T10	T11
3107850401	4.000	69.77	69.62	70.28	74.33	85.05	94.23	95.22	96.18	96.36	96.41	96.45	96.67
3107850402	4.000	69.90	70.01	71.00	77.47	86.56	95.95	96.74	97.15	97.35	97.24	97.57	97.56
3107850403	4.000	70.32	70.14	71.12	77.11	88.68	96.73	97.12	97.23	97.78	97.36	97.83	97.74
3107850404	4.000	70.52	70.63	71.08	77.48	87.27	96.16	97.03	97.36	97.82	97.79	98.95	97.88
3107850405	4.000	70.62	70.81	71.18	77.67	88.95	96.41	97.16	97.51	97.66	97.92	98.04	97.97
3107850406	4.000	70.65	70.86	72.01	80.73	91.98	97.07	97.57	97.73	97.92	97.94	98.14	98.07
3107850407	4.000	70.68	70.99	72.37	84.44	93.84	97.21	97.65	97.85	97.98	98.11	98.23	98.12
3107850408	4.000	70.66	71.27	73.55	87.72	95.15	97.82	98.09	98.12	98.28	98.22	98.34	98.27
3107850501	5.000	69.83	69.96	70.11	73.17	80.05	91.00	94.40	96.51	96.91	97.10	97.09	97.07
3107850502	5.000	69.96	70.10	71.73	76.53	84.44	94.96	96.06	97.33	97.88	98.06	98.00	97.89
3107850503	5.000	70.15	70.57	72.17	77.02	86.06	95.01	96.49	97.73	97.87	98.16	98.03	97.93
3107850504	5.000	70.18	70.65	72.07	76.77	85.98	94.84	96.50	97.78	97.86	98.26	98.17	98.05
3107850505	5.000	70.24	71.15	72.24	78.86	88.64	95.27	96.64	97.80	97.89	98.35	98.21	97.99
3107850506	5.000	70.26	71.00	72.63	82.05	91.63	95.77	96.90	97.83	98.08	98.38	98.30	98.17
3107850507	5.000	70.32	71.23	74.79	86.12	95.02	96.39	97.56	98.03	98.36	98.39	98.44	98.31
3107850601	6.000	69.80	69.84	69.95	70.38	75.51	82.15	90.52	95.61	96.65	97.11	97.33	97.37
3107850602	6.000	70.04	70.09	70.11	72.90	80.44	91.23	94.07	96.54	97.00	97.09	97.72	97.74
3107850603	6.000	70.10	70.27	70.64	74.07	83.07	93.04	95.79	97.36	97.45	97.93	97.83	97.77
3107850604	6.000	70.32	70.60	72.97	75.84	83.98	93.49	95.72	97.43	97.47	97.95	97.03	97.82
3107850605	6.000	70.37	70.89	73.16	77.09	85.57	94.12	95.90	97.48	97.50	97.97	98.01	97.96
3107850606	6.000	70.34	70.89	72.07	79.97	88.83	94.52	96.00	97.69	97.83	98.04	98.20	98.12
3107850607	6.000	70.38	70.60	73.27	83.91	91.77	95.32	97.51	97.90	98.08	98.26	98.33	98.29
3107850701	7.000	69.56	69.83	69.92	70.59	70.80	72.53	77.05	83.38	92.68	94.60	95.62	96.65
3107850702	7.000	69.57	69.77	69.99	71.48	74.10	79.01	87.69	91.38	94.22	95.90	96.28	96.97
3107850703	7.000	69.66	69.74	70.17	75.27	83.04	90.42	94.47	96.01	97.42	97.89	98.06	97.93
3107850704	7.000	69.60	69.81	71.30	80.34	85.48	93.29	95.50	97.09	97.37	97.95	98.07	97.98
3107850705	7.000	69.63	69.86	73.20	83.34	88.00	94.43	96.10	97.60	97.67	98.03	98.07	97.99
3107850706	7.000	69.60	69.87	72.44	83.78	88.07	94.97	96.28	97.57	97.66	98.10	98.09	97.91
3107850707	7.000	69.58	70.29	72.48	83.62	89.74	94.78	96.45	97.79	97.81	98.14	98.12	97.89
3107850708	7.000	69.57	70.44	73.15	84.05	89.97	95.75	97.15	97.95	97.93	98.23	98.20	98.09
3107850801	8.000	69.70	68.46	69.81	70.25	70.20	71.82	72.02	77.74	83.94	88.68	90.12	91.60
3107850802	8.000	69.87	70.06	70.20	71.55	74.27	78.68	82.83	87.18	90.34	94.87	95.65	95.63
3107850803	8.000	69.70	69.92	70.89	74.51	79.61	83.84	87.72	91.00	94.03	96.99	97.78	97.71
3107850804	8.000	69.79	69.99	72.33	80.59	86.22	90.18	92.62	94.07	96.90	98.03	98.01	97.95
3107850805	8.000	69.74	69.84	73.27	81.39	88.98	93.73	95.06	96.81	96.97	98.02	98.46	97.95
3107850806	8.000	69.74	69.93	73.33	81.89	88.98	94.09	95.60	97.75	97.72	98.04	98.10	97.95
3107850807	8.000	69.77	71.45	74.01	83.32	89.33	94.89	97.39	98.07	97.99	98.51	98.50	98.39
3107850901	9.000	70.54	70.55	70.53	71.24	72.51	73.79	77.60	80.63	83.44	87.67	91.13	92.82
3107850902	9.000	70.53	70.69	71.23	77.33	83.66	90.10	93.81	95.50	96.29	96.70	96.76	96.32
3107850903	9.000	70.59	70.77	71.32	79.53	84.29	91.62	94.71	96.17	96.46	97.45	97.80	97.69
3107850904	9.000	70.61	70.89	72.01	80.91	85.47	91.76	94.84	96.30	96.94	97.54	97.72	97.72
3107850905	9.000	70.66	70.72	72.47	81.64	86.05	92.00	95.11	96.41	96.94	97.73	97.82	97.73
3107850906	9.000	70.63	71.00	72.60	81.99	86.14	92.07	95.21	96.52	97.22	97.76	97.84	97.83
3107850907	9.000	70.67	71.78	72.69	80.09	86.82	92.12	95.77	96.79	97.93	98.16	98.19	97.98
0107851001	10.000	69.45	69.55	69.55	70.89	73.04	77.12	81.28	84.08	88.18	90.51	92.09	93.01
0108851002	10.000	69.46	69.45	69.94	70.89	73.04	77.12	81.28	84.08	88.18	90.51	92.09	93.01
0108851003	10.000	69.42	69.58	70.62	72.99	80.97	89.61	92.12	94.67	96.14	97.27	97.75	97.66
2508851004	10.000	69.42	69.58	70.83	74.92	81.97	90.12	94.06	95.91	96.50	97.56	97.81	97.72
2508851005	10.000	69.42	69.66	71.08	75.54	82.25	90.86	94.70	96.53	97.64	97.79	97.94	97.75
2508851006	10.000	69.48	69.78	71.84	75.57	82.58	90.96	95.02	97.04	97.96	97.92	98.24	97.76
2508851007	10.000	69.59	70.21	71.92	76.49	83.03	91.31	95.52	97.10	98.55	98.62	98.66	98.50

TABLE C.3f (Continue)

Steam-Water Data, Wall Temperature Measurements (Low Steam Extraction Rate Tests)

Inlet Water Subcooling = 30 K

TEST NO	Q _{fin}	T _{fin}	T ₁	T ₂	T ₃	T ₄	T ₅	T ₆	T ₇	T ₈	T ₉	T ₁₀	T ₁₁
2508851101	11.197	69.81	69.84	69.88	71.20	70.82	71.37	72.08	73.88	76.29	82.76	86.19	88.53
2508851102	11.197	69.83	69.93	70.47	70.96	71.74	72.79	73.95	76.91	80.58	85.80	88.38	91.43
2508851103	11.197	69.88	69.92	70.90	71.94	72.50	75.81	78.25	82.66	86.50	89.61	91.84	93.57
2508851104	11.197	69.87	69.89	70.98	71.88	74.69	79.21	84.69	89.49	93.92	94.78	96.01	96.64
2508851105	11.197	69.91	70.21	71.06	72.45	77.69	85.21	91.17	95.55	96.44	97.35	97.52	97.17
2508851106	11.197	69.82	70.66	70.84	73.62	79.43	87.67	92.12	96.11	96.86	97.55	97.72	97.52
2508851107	11.197	69.90	71.07	71.29	74.03	79.78	88.27	92.28	96.23	97.71	98.07	98.19	97.91
2508851108	11.197	69.81	70.02	71.64	74.90	80.28	88.91	93.05	96.51	98.02	98.25	98.32	98.12
2508851201	12.710	70.36	70.45	70.46	70.39	70.82	71.04	72.47	75.59	80.36	86.93	93.58	85.55
2508851202	12.710	70.40	70.42	70.83	70.46	71.00	72.07	74.52	80.54	87.72	92.05	95.03	90.38
2508851203	12.710	70.46	70.43	70.61	70.72	71.40	74.35	79.21	86.35	90.11	93.48	95.67	93.98
2508851204	12.710	70.45	70.54	70.63	71.26	73.51	78.07	83.52	89.16	93.37	95.30	96.02	96.00
2508851205	12.710	70.44	70.64	70.64	71.90	74.14	80.84	86.73	92.96	95.95	97.47	97.63	97.56
2508851206	12.710	70.44	70.86	70.94	72.06	75.51	81.71	88.39	93.73	96.83	97.80	97.95	97.89
2508851207	12.710	70.75	70.88	71.93	72.26	76.66	82.07	89.52	94.16	97.37	98.08	98.12	98.02
2508851401	14.229	70.01	70.25	70.57	70.57	70.62	70.87	72.11	74.29	78.20	80.35	81.58	80.70
2508851402	14.229	70.09	70.34	70.45	70.51	70.78	70.96	72.30	77.57	82.75	84.15	85.06	84.77
2508851403	14.229	70.19	70.24	70.63	70.77	70.74	71.39	76.08	83.13	90.90	91.99	92.26	91.51
2508851404	14.229	70.12	70.39	70.69	71.11	71.65	72.72	77.44	84.40	91.72	94.51	96.14	95.79
2508851405	14.229	70.16	70.67	70.64	71.11	71.58	75.54	82.11	86.68	92.65	95.02	96.62	96.47
2508851406	14.229	70.09	70.40	70.66	71.00	71.68	75.86	82.72	87.64	92.72	95.00	96.77	96.85
2508851407	14.229	70.10	70.42	70.93	72.08	74.95	78.57	84.90	89.86	94.38	96.92	97.16	96.95
2508851501	15.754	70.34	70.42	70.74	70.27	70.25	70.54	70.49	71.07	72.24	73.99	76.57	78.82
2508851502	15.754	70.31	70.48	70.45	70.94	70.96	71.41	71.43	72.19	73.85	77.20	81.73	84.71
2508851503	15.754	70.25	70.37	65.85	70.94	70.80	71.34	71.80	76.21	81.31	87.95	91.70	92.49
2508851504	15.754	70.15	70.92	70.39	71.21	71.14	72.56	75.24	83.06	88.75	92.72	93.35	93.12
2508851505	15.754	70.14	70.45	70.52	70.50	70.99	73.55	77.42	85.41	90.20	93.97	95.55	95.43
2508851506	15.754	70.00	70.03	70.13	70.86	71.45	74.56	80.35	86.87	91.50	94.26	96.04	95.55
2508851507	15.754	70.18	70.71	70.93	71.95	72.70	75.94	82.03	87.81	92.14	94.96	96.21	96.11
2508851701	17.287	69.67	69.66	69.80	70.00	69.97	70.81	71.79	72.56	74.25	78.74	84.45	88.23
2508851702	17.287	69.63	69.71	70.01	70.78	71.03	71.91	72.40	76.99	81.92	84.97	88.97	90.60
2508851703	17.287	69.77	69.79	69.86	70.79	70.80	71.40	72.37	78.05	83.14	87.04	91.92	92.67
2508851704	17.287	69.72	69.89	69.73	70.57	71.74	72.51	75.27	80.10	86.36	88.09	92.86	93.77
2508851705	17.287	69.69	69.76	69.97	70.38	71.82	72.30	76.69	82.02	89.99	92.97	94.43	94.67
2508851706	17.287	69.77	70.22	70.45	70.74	72.05	72.56	77.53	84.11	90.52	93.84	95.02	95.07
2508851707	17.287	69.77	70.38	70.94	71.02	72.03	74.65	80.48	85.22	90.96	94.01	95.77	95.89
2508851801	18.827	69.71	69.86	70.05	70.15	70.77	70.79	71.00	71.52	71.93	73.26	75.76	77.53
2508851802	18.827	69.86	69.85	69.96	70.44	70.51	70.62	71.95	73.06	76.81	79.12	81.29	83.77
2508851803	18.827	69.91	70.00	70.12	70.48	70.55	70.52	71.65	75.40	80.68	83.35	86.69	88.48
2508851804	18.827	69.90	69.94	69.95	70.22	70.34	70.62	71.95	77.03	85.67	88.16	90.38	91.21
2508851805	18.827	69.90	69.95	70.33	70.43	70.89	71.12	72.74	79.03	86.89	89.34	91.87	92.38
2508851806	18.827	69.96	69.89	70.20	70.30	71.02	71.93	74.87	82.16	88.79	91.02	93.19	93.52
2508851807	18.827	69.97	70.33	70.56	70.85	71.08	73.38	77.64	84.25	89.45	92.37	93.57	93.89
2508852001	20.374	70.04	70.06	70.25	70.74	70.74	71.58	71.59	71.84	72.17	73.33	75.22	77.42
2508852002	20.374	70.07	70.12	70.37	70.91	71.02	71.92	71.88	72.77	75.96	79.55	82.01	83.42
2508852003	20.374	70.02	70.12	70.14	70.75	70.84	71.03	72.01	73.31	76.94	82.08	85.11	86.52
2508852004	20.374	69.98	69.99	70.10	70.70	70.13	70.64	71.85	74.29	79.05	84.63	86.41	87.57
2508852005	20.374	70.10	70.12	70.21	70.88	71.00	71.98	72.32	75.96	81.54	86.51	87.56	89.31
2508852006	20.374	70.07	70.07	70.38	70.86	70.87	71.86	73.18	77.35	83.66	88.01	89.23	90.56
2508852007	20.374	69.97	70.32	70.64	70.95	70.94	72.03	74.81	79.96	85.04	90.54	91.10	91.61

TABLE C.3g

Steam-Water Data, Wall Temperature Measurements (Low Steam Extraction Rate Tests)

Inlet Water Subcooling = 20 K

TEST NO	Qfin	Tfin	T1	T2	T3	T4	T5	T6	T7	T8	T9	T10	T11
2506850401	4.000	79.79	79.76	80.77	80.88	82.16	91.21	94.41	95.79	97.66	97.44	97.56	97.49
2506850402	4.000	79.71	80.04	80.07	87.89	92.04	95.90	97.00	97.33	97.79	97.79	98.00	97.78
2506850403	4.000	79.80	79.93	81.03	86.13	92.47	95.94	97.27	97.60	97.84	97.87	98.03	97.95
2506850404	4.000	79.80	79.96	81.96	87.99	93.90	96.13	97.78	97.97	98.09	98.32	98.12	98.10
2506850405	4.000	79.79	81.49	82.45	87.59	93.69	96.72	97.73	97.77	98.14	98.19	98.23	98.17
2506850406	4.000	79.75	81.61	84.15	91.20	94.39	96.92	97.83	98.15	98.21	98.51	98.38	98.26
2506850407	4.000	79.74	82.76	86.66	95.34	96.03	97.47	98.17	98.26	98.35	98.59	98.47	98.41
2506850501	5.000	80.12	80.00	79.87	80.04	80.31	81.25	81.85	83.91	86.35	89.02	92.23	94.73
2506850502	5.000	80.15	80.22	80.88	82.98	86.76	92.87	95.87	97.76	97.96	98.12	98.10	97.93
2506850503	5.000	80.10	80.12	80.86	83.69	88.50	93.56	96.07	97.05	97.96	98.14	98.14	98.03
2506850504	5.000	80.15	80.10	80.74	89.83	91.47	94.89	96.80	97.88	98.09	98.29	98.25	98.24
2506850505	5.000	80.17	80.23	81.42	91.31	95.46	96.01	97.02	97.99	98.12	98.30	98.25	98.31
2506850506	5.000	80.07	80.61	82.78	91.18	94.53	97.66	97.70	97.87	98.13	98.40	98.36	98.28
2506850507	5.000	80.11	80.31	82.94	92.03	95.32	98.12	97.85	97.98	98.23	98.46	99.41	98.35
2506850508	5.000	80.10	80.74	83.71	93.90	96.95	98.37	98.55	98.41	98.57	98.67	98.53	98.44
2506850601	6.000	79.87	79.87	79.85	80.74	82.10	83.20	85.66	88.52	90.92	93.18	95.06	97.35
2506850602	6.000	79.91	79.90	80.08	85.37	94.16	97.43	97.58	97.79	98.14	98.45	98.42	98.18
2506850603	6.000	79.90	80.11	80.31	90.23	94.56	97.45	97.56	97.68	98.07	98.33	98.33	98.15
2506850604	6.000	79.90	80.10	80.20	91.38	94.73	97.63	97.60	97.72	98.10	98.35	98.37	98.13
2506850605	6.000	79.93	79.98	81.57	90.93	94.41	97.44	97.59	97.73	98.12	98.44	98.41	98.22
2506850606	6.000	79.92	80.05	81.98	90.37	94.16	97.43	97.58	97.79	98.14	98.45	98.42	98.36
2506850607	6.000	79.99	80.14	83.89	92.19	96.90	98.16	98.44	98.40	98.49	98.75	98.68	98.43
2506850701	7.000	80.70	80.19	80.59	82.71	83.86	86.90	90.95	93.98	95.86	96.84	97.59	97.95
2506850702	7.000	80.82	80.80	80.62	85.08	90.52	94.60	96.91	97.14	97.65	98.06	98.08	98.00
2506850703	7.000	80.85	80.51	80.83	87.63	90.84	96.02	97.18	97.43	97.91	98.25	98.29	98.03
2506850704	7.000	80.81	80.00	80.52	90.35	93.73	96.97	97.27	97.55	97.98	98.44	98.36	98.15
2506850705	7.000	80.77	80.34	81.10	90.30	95.13	96.65	98.08	98.32	98.08	98.46	98.16	98.38
2506850706	7.000	80.74	80.77	81.00	90.11	95.95	96.46	98.23	98.50	98.29	98.56	98.73	98.54
2506850707	7.000	80.73	81.54	82.69	92.28	96.65	97.86	98.53	98.65	98.70	98.66	98.86	98.78
2506850801	8.000	80.60	80.73	80.75	80.99	81.19	82.88	83.72	87.47	90.96	86.45	90.83	92.80
2506850802	8.000	80.59	80.49	80.53	81.86	83.82	85.86	87.40	89.70	91.04	93.77	94.95	96.08
2506850803	8.000	80.57	80.59	80.77	82.90	85.59	89.19	93.59	95.09	96.49	97.15	97.33	97.45
2506850804	8.000	80.62	80.84	80.92	88.96	92.28	95.89	96.53	97.35	97.39	97.98	97.93	97.70
2506850805	8.000	80.59	80.65	80.86	88.90	92.34	95.86	96.61	97.39	97.41	98.02	98.01	97.93
2506850806	8.000	80.59	80.61	80.12	88.54	92.18	95.83	96.59	97.44	97.71	98.13	98.23	98.18
2506850807	8.000	80.65	80.89	81.33	90.88	95.05	97.55	97.93	98.08	98.25	98.40	98.41	98.31
2506850808	8.000	80.87	81.52	82.95	92.48	96.69	97.95	98.11	98.39	98.47	98.57	98.62	98.45
2506850901	9.000	80.87	80.80	80.85	80.99	81.62	81.59	81.88	82.47	84.53	87.43	90.35	91.86
2506850902	9.000	80.76	80.71	80.78	81.66	82.06	82.49	85.17	88.86	91.74	93.50	95.97	96.54
2506850903	9.000	80.76	80.67	80.95	88.13	91.33	95.22	95.99	97.00	97.17	97.86	97.74	97.69
2506850904	9.000	80.65	81.10	81.15	88.15	91.49	95.16	95.99	97.08	97.22	97.87	97.95	97.86
2506850905	9.000	80.68	81.10	81.00	87.98	91.45	95.20	96.12	97.19	97.25	97.94	97.97	97.97
2506850906	9.000	80.78	81.06	81.16	88.84	92.23	95.69	96.48	97.34	97.31	97.93	98.04	97.95
2506850907	9.000	80.79	81.41	83.01	90.01	95.90	96.63	97.97	98.40	98.00	98.34	98.31	98.18
2506851001	10.000	79.96	79.95	79.80	80.33	80.52	81.61	82.20	83.40	85.37	90.60	93.97	93.45
2506851002	10.000	79.93	80.03	80.58	82.07	82.60	84.34	85.91	90.53	93.34	95.47	96.38	95.55
2506851003	10.000	79.89	79.88	80.55	83.39	88.34	93.44	95.76	96.90	97.07	97.53	97.69	97.62
2506851004	10.000	79.78	79.48	80.99	84.92	92.00	95.29	96.09	97.05	97.11	97.73	97.85	97.72
2506851005	10.000	79.75	79.94	80.99	86.77	92.07	95.36	96.16	97.11	97.39	97.81	97.87	97.97
2506851006	10.000	79.80	80.77	81.15	86.90	92.00	95.32	96.44	97.48	97.59	98.29	98.40	98.36
2506851007	10.000	79.83	80.03	81.54	87.26	93.02	96.37	97.85	98.08	98.22	98.61	98.79	98.58

TABLE C.3g (Continue)

Steam-Water Data, Wall Temperature Measurements (Low Steam Extraction Rate Tests)

Inlet Water Subcooling = 20 K

TEST NO	Q _{fin}	T _{fin}	T ₁	T ₂	T ₃	T ₄	T ₅	T ₆	T ₇	T ₈	T ₉	T ₁₀	T ₁₁
2506851101	11.197	80.31	80.37	80.44	81.47	81.77	81.63	82.08	82.66	83.79	85.18	88.24	90.65
2506851102	11.197	80.39	80.35	80.53	82.37	82.40	84.43	87.56	90.61	93.38	95.39	96.94	97.27
2506851103	11.197	80.41	80.49	80.61	83.65	86.44	87.14	91.33	94.59	96.45	97.21	97.54	97.49
2506851104	11.197	80.43	80.55	81.77	83.81	87.51	89.10	94.09	96.90	97.29	97.57	97.83	97.75
2506851105	11.197	80.42	80.49	82.65	85.80	90.81	93.12	95.07	97.09	97.50	98.09	98.10	97.91
2506851106	11.197	80.46	80.57	82.58	87.03	90.25	93.80	95.94	97.28	97.67	98.34	98.44	98.20
2506851107	11.197	80.31	80.73	82.18	88.07	92.73	94.90	97.58	98.32	98.56	98.75	98.70	98.53
2506851201	12.710	80.39	79.89	80.01	80.49	80.83	81.36	81.26	82.11	82.94	84.03	87.27	89.53
2506851202	12.710	80.41	80.33	80.34	80.77	80.84	81.67	82.09	83.99	86.06	88.56	91.19	92.88
2506851203	12.710	80.31	80.59	80.63	80.98	81.08	83.75	85.95	87.77	90.78	93.62	95.72	95.76
2506851204	12.710	80.29	80.58	80.77	81.04	82.90	85.39	89.39	92.80	94.17	95.74	96.48	96.72
2506851205	12.710	80.43	80.59	80.79	83.26	86.11	90.48	94.54	95.93	96.30	97.07	97.15	96.88
2506851206	12.710	80.45	80.47	80.89	84.04	87.12	92.07	95.65	96.44	96.94	97.35	97.75	97.69
2506851207	12.710	80.46	80.78	80.91	85.50	88.26	93.74	96.47	97.07	97.57	98.20	98.35	98.29
2506851208	12.710	80.44	81.20	81.24	87.45	90.39	94.31	97.22	97.58	97.94	98.84	98.82	98.78
2506851401	14.229	79.79	79.77	79.81	80.17	80.57	80.79	81.02	83.39	87.74	90.47	92.29	94.08
2506851402	14.229	79.80	79.82	79.88	80.15	81.93	82.29	84.34	89.29	92.04	94.74	95.44	96.56
2506851403	14.229	79.86	79.89	80.37	80.45	81.29	84.73	87.28	92.56	94.93	96.90	97.19	97.45
2506851404	14.229	79.89	79.92	80.54	81.99	89.64	87.89	92.17	95.70	96.22	97.01	97.26	97.63
2506851405	14.229	80.00	80.11	83.40	82.11	85.00	88.82	93.01	96.49	97.09	97.91	98.79	97.92
2506851406	14.229	79.98	80.55	83.57	82.60	87.64	91.89	94.17	96.70	97.82	99.21	98.26	98.13
2506851407	14.229	79.90	80.79	80.88	84.90	88.92	93.53	95.79	97.75	98.31	98.52	98.51	98.37
2506851501	15.755	80.64	80.66	80.66	80.61	80.51	80.58	81.21	81.80	82.02	84.64	86.59	89.00
2506851502	15.755	80.58	80.55	80.69	80.50	81.08	81.12	81.65	82.51	83.63	86.91	89.91	90.06
2506851503	15.755	80.46	80.68	80.98	81.09	80.94	81.57	81.53	82.57	84.29	87.93	91.03	91.26
2506851504	15.755	80.48	80.56	80.74	81.67	83.76	86.39	90.74	92.65	94.72	95.45	96.06	94.54
2506851505	15.755	80.46	80.64	81.02	82.71	86.77	89.39	92.75	94.68	95.63	96.50	97.11	96.73
2506851506	15.755	80.40	80.69	81.19	83.99	87.05	90.66	92.90	94.86	95.77	97.65	98.01	97.69
2506851507	15.755	80.42	80.69	81.26	84.34	87.65	91.93	95.31	97.05	97.76	98.22	98.24	97.93
2506851701	17.287	80.12	79.88	79.96	80.45	80.65	88.76	81.04	80.97	81.41	82.40	84.42	86.11
2506851702	17.287	80.22	80.24	80.73	81.05	81.44	81.33	84.01	88.50	90.67	91.04	91.76	91.71
2506851703	17.287	80.22	80.23	80.63	80.99	81.85	82.63	85.61	90.10	92.76	93.37	94.38	93.88
2506851704	17.287	80.21	80.67	80.77	81.16	82.68	84.41	87.01	92.31	94.05	95.47	96.15	95.58
2506851705	17.287	80.14	80.77	80.89	82.24	83.57	85.08	89.77	93.88	94.54	95.59	96.17	96.01
2506851706	17.287	80.11	80.66	80.80	82.27	85.09	87.11	90.05	94.04	95.00	95.90	96.38	96.32
2506851707	17.287	80.07	80.52	80.96	82.47	85.38	88.70	91.63	94.55	95.77	96.41	96.75	96.64
2506851801	18.827	79.49	79.52	79.55	80.05	81.48	81.73	81.89	82.60	83.08	85.65	87.59	89.51
2506851802	18.827	79.58	79.75	79.82	80.77	81.06	82.56	82.91	85.03	88.89	91.10	93.81	93.75
2506851803	18.827	79.74	79.85	79.93	80.51	81.35	83.90	87.00	90.37	92.20	94.31	94.99	94.85
2506851804	18.827	79.72	79.91	79.92	80.74	82.22	85.01	88.61	92.30	94.16	95.26	96.01	95.22
2506851805	18.827	79.68	79.84	80.05	80.83	83.03	85.59	89.62	92.51	95.16	96.14	96.44	95.12
2506851806	18.827	79.68	79.77	80.40	81.03	83.37	86.03	90.71	92.90	95.77	96.32	96.61	95.70
2506851807	18.827	79.66	79.94	80.38	81.93	83.66	86.96	90.80	93.39	95.99	96.52	96.82	96.01
2506852001	20.374	79.71	79.66	79.69	79.88	79.83	80.16	81.57	82.86	83.60	85.33	86.08	88.19
2506852002	20.374	79.66	79.75	79.92	79.99	80.06	81.49	82.67	87.55	91.11	93.35	93.57	93.85
2506852003	20.374	79.79	79.85	80.02	80.22	81.77	82.09	85.88	91.81	93.25	94.53	94.82	94.64
2506852004	20.374	79.86	79.91	80.30	80.30	82.06	82.93	85.91	91.96	93.39	94.68	95.01	94.42
2506852005	20.374	79.71	79.91	80.29	80.77	81.00	83.69	86.11	92.45	93.74	94.82	95.37	94.50
2506852006	20.374	79.68	79.95	80.46	80.45	81.08	83.86	87.10	93.04	93.93	95.01	95.65	94.82
2506852007	20.374	79.69	80.08	80.76	81.04	81.12	84.07	87.75	93.33	94.16	95.43	95.91	95.17

TABLE C.3h

Steam-Water Data, Wall Temperature Measurements (Low Steam Extraction Rate Tests)

TEST NO	Bfin	Tfin	Inlet Water Subcooling = 10 K										
			T1	T2	T3	T4	T5	T6	T7	T8	T9	T10	T11
0306850401	4.000	89.74	89.75	89.95	90.76	93.91	94.58	95.36	96.24	96.95	97.02	96.90	97.04
0306850402	4.000	89.85	89.97	90.53	91.59	93.21	97.12	95.95	97.04	97.25	97.63	97.55	97.45
0306850403	4.000	89.76	89.90	90.48	91.49	94.25	97.04	96.87	97.15	97.32	98.18	98.05	97.83
0306850404	4.000	89.85	90.19	90.49	92.88	94.73	97.24	96.99	97.06	97.33	98.23	98.17	97.98
0306850405	4.000	89.86	90.00	90.39	93.01	94.42	97.13	97.04	97.11	97.88	98.29	98.23	97.94
0306850406	4.000	89.85	90.45	90.31	92.41	93.97	96.91	97.06	97.20	97.82	98.43	98.35	98.04
0306850407	4.000	89.82	90.92	90.91	92.49	94.41	97.18	97.17	97.30	97.96	98.41	98.38	98.15
0306850408	4.000	89.87	90.94	91.73	93.10	94.53	97.62	97.74	98.31	98.25	98.59	98.60	98.17
0306850409	4.000	89.86	91.38	93.41	95.49	96.33	98.03	98.38	98.40	98.45	98.74	98.59	98.26
0506850501	5.000	90.07	90.16	90.38	92.89	95.76	96.17	97.61	97.94	97.83	98.07	97.70	97.99
0506850502	5.000	90.03	90.25	90.97	93.01	95.90	96.74	97.70	98.01	97.95	98.16	97.83	98.05
0506850503	5.000	90.03	90.23	90.87	93.21	95.89	96.79	97.76	98.00	97.98	98.21	97.97	98.19
0506850504	5.000	90.05	90.19	90.85	93.26	95.92	96.89	97.76	98.09	98.01	98.24	98.02	98.20
0506850505	5.000	90.10	90.21	90.57	93.07	95.68	96.81	97.75	98.12	98.05	98.30	98.07	98.16
0506850506	5.000	90.15	90.47	90.87	93.05	95.76	97.22	97.83	98.14	98.01	98.30	98.16	98.27
0506850507	5.000	90.13	90.81	91.27	93.74	96.17	98.43	98.02	98.28	98.19	98.43	98.28	98.40
0506850508	5.000	90.18	90.90	92.49	95.54	97.29	98.19	98.38	98.41	98.26	98.52	98.38	98.48
0506850601	6.000	90.14	90.24	90.38	93.45	95.01	96.52	97.64	98.08	98.02	98.24	98.10	98.57
0506850602	6.000	90.11	90.11	90.12	93.55	95.36	96.83	97.63	98.18	98.14	98.24	98.11	98.61
0506850603	6.000	90.13	90.12	90.26	93.60	95.79	97.28	97.79	98.21	98.16	98.39	98.20	98.70
0506850604	6.000	90.02	90.25	90.80	93.55	95.87	97.16	97.86	98.28	98.24	98.45	98.31	98.76
0506000605	6.000	90.05	90.32	90.88	93.73	95.89	97.21	97.89	98.29	98.26	98.48	98.33	98.77
0506850606	6.000	90.02	90.47	90.91	93.95	96.02	97.21	97.91	98.33	98.21	98.47	98.31	98.71
0506850607	6.000	90.15	90.35	91.63	93.62	96.00	97.85	97.97	98.38	98.29	98.53	98.40	98.70
0506850608	6.000	90.07	90.82	92.08	95.21	97.29	98.24	98.46	98.60	98.40	98.64	98.51	98.79
0706850701	7.000	89.78	89.77	89.93	90.87	91.07	94.46	96.01	96.39	96.68	97.02	97.16	97.19
0706850702	7.000	89.80	89.97	90.43	90.95	91.24	95.04	96.27	97.10	97.02	97.16	97.17	97.15
0706850703	7.000	89.88	89.94	90.41	91.35	92.13	95.39	96.12	97.14	97.09	97.30	97.26	97.18
0706850704	7.000	89.94	90.31	90.44	91.74	92.38	95.65	96.28	97.36	97.25	97.48	97.36	97.36
0706850705	7.000	89.91	90.02	90.98	92.05	92.81	95.65	96.59	97.44	97.35	97.63	97.60	97.56
0706850706	7.000	89.94	90.25	91.89	92.22	93.18	96.06	96.93	97.52	97.47	97.73	97.64	97.65
0706850707	7.000	89.98	90.86	92.83	94.41	95.43	97.05	97.46	97.64	97.52	97.86	97.72	97.66
0706850801	8.000	89.60	89.77	90.08	91.07	92.59	93.98	94.78	95.17	96.54	96.79	96.53	96.58
0706850802	8.000	89.67	89.82	90.30	91.70	92.97	93.99	95.10	95.60	96.64	96.75	96.71	96.63
0706851823	8.000	89.66	89.92	90.30	92.31	93.71	95.52	95.00	95.69	96.26	96.82	96.73	96.72
0706850804	8.000	89.74	89.96	90.49	92.84	94.16	95.56	95.43	95.82	96.61	96.95	96.80	96.53
0706850805	8.000	89.73	90.08	91.33	93.51	94.83	95.77	95.69	96.05	96.83	97.19	96.81	96.63
0706850806	8.000	89.73	90.44	91.58	93.63	94.87	96.20	95.90	96.02	96.99	97.39	96.96	96.72
0706850807	8.000	89.88	91.03	92.35	94.55	95.88	96.72	96.53	96.77	97.42	97.53	97.38	97.10
1006850901	9.000	90.12	90.11	90.57	93.13	94.28	95.51	95.40	95.57	96.66	97.15	97.35	96.50
1006000902	9.000	90.10	90.15	90.64	93.49	94.55	95.60	95.69	95.92	96.77	97.35	97.31	96.89
1006850903	9.000	90.10	90.14	90.85	93.65	94.77	96.07	95.72	96.07	97.15	97.52	97.05	96.97
1006850904	9.000	90.08	90.12	90.88	93.68	94.86	96.15	95.99	96.16	97.21	97.58	97.09	97.03
1006850905	9.000	90.04	90.04	90.93	93.81	94.94	96.30	96.07	96.22	97.28	97.79	97.25	97.20
1006850906	9.000	90.02	90.39	90.87	93.82	94.98	96.44	96.20	96.33	97.37	97.89	97.31	97.19
1006850907	9.000	90.01	90.57	91.18	93.82	95.09	96.53	96.26	96.41	97.41	97.94	97.28	97.24
1006850908	9.000	89.99	90.82	92.93	95.05	96.83	97.89	97.11	96.93	97.83	98.03	97.67	97.54
1106851001	10.000	90.57	90.55	90.71	90.92	92.68	94.50	95.03	96.14	96.82	97.59	97.12	97.07
1106851002	10.000	90.57	90.60	90.65	91.19	93.56	94.34	95.28	96.40	96.94	97.71	97.38	97.71
1106851003	10.000	90.56	90.64	90.89	91.70	93.91	95.13	95.47	96.46	96.95	97.74	97.36	97.44
1106851004	10.000	90.48	90.53	90.77	92.78	93.77	95.76	95.95	96.85	97.18	97.80	97.59	97.66
1106851005	10.000	90.47	90.53	90.93	93.04	94.28	96.17	96.28	97.11	97.37	98.05	97.69	97.69
1106851006	10.000	90.49	90.66	91.21	93.82	95.27	97.40	97.81	98.12	98.08	98.31	98.17	98.03
1106851007	10.000	90.52	91.32	92.90	94.87	96.93	98.37	98.55	98.64	98.57	98.86	98.69	98.58

TABLE C.3h (Continue)

Steam-Water Data, Wall Temperature Measurements (Low Steam Extraction Rate Tests)

Inlet Water Subcooling = 10 K

TEST NO	Q _{fin}	T _{fin}	T ₁	T ₂	T ₃	T ₄	T ₅	T ₆	T ₇	T ₈	T ₉	T ₁₀	T ₁₁
1006851001	11.197	90.56	90.08	90.37	93.02	94.36	96.76	96.83	97.50	97.49	98.19	98.09	98.31
1006851102	11.197	90.45	90.47	90.49	93.06	94.36	96.73	96.78	97.44	97.43	98.10	98.03	98.15
1006851103	11.197	90.44	90.30	90.48	92.81	94.07	96.43	96.53	97.18	97.40	98.02	97.96	97.92
1006851104	11.197	90.33	90.96	90.85	92.75	94.26	96.75	96.80	97.49	97.50	98.23	98.15	98.11
1006851105	11.197	90.33	90.94	90.82	92.77	94.34	96.81	96.84	97.59	97.54	98.25	98.18	98.21
1006851106	11.197	90.36	91.04	91.33	92.73	94.88	96.93	96.94	97.64	97.62	98.28	98.21	98.24
1006851107	11.197	90.37	91.34	92.99	94.53	96.21	97.71	98.06	98.02	98.11	98.59	98.50	98.42
1106851201	12.710	90.49	90.49	90.71	92.25	93.78	96.04	96.25	97.14	97.31	97.78	97.87	98.03
1106851202	12.710	90.42	90.45	90.83	92.30	93.86	96.10	96.56	97.07	97.26	97.79	97.83	97.90
1106851203	12.710	90.45	90.43	90.82	92.19	93.63	96.07	96.24	96.73	96.87	97.40	97.42	97.47
1106851204	12.710	90.24	90.38	90.87	92.86	94.29	96.46	96.52	97.32	97.46	97.96	97.99	97.88
1106851205	12.710	90.25	90.63	91.30	93.15	94.54	96.72	96.75	97.51	97.60	98.09	98.10	98.04
1106851206	12.710	90.20	90.97	91.27	93.22	94.62	96.86	96.90	97.62	97.68	98.20	98.18	98.03
1106851207	12.710	90.20	90.81	92.56	94.73	96.05	96.90	97.15	97.84	97.86	98.54	98.41	98.31
1106851401	14.229	90.74	90.75	90.80	91.65	92.16	94.42	95.69	96.52	96.75	97.36	97.47	97.38
1106851402	14.229	90.72	90.77	90.93	91.46	92.76	94.95	96.29	96.62	96.88	97.10	97.23	97.35
1106851403	14.229	90.65	90.65	90.91	92.15	93.62	95.87	96.09	96.93	97.07	97.71	97.80	97.83
1106851404	14.229	90.69	90.80	91.17	92.17	93.83	96.26	96.35	97.20	97.29	97.91	98.00	97.88
1106851405	14.229	90.69	90.86	91.00	92.11	93.98	96.25	96.39	97.28	97.36	97.93	98.02	97.85
1106851406	14.229	90.73	90.95	91.35	92.37	93.99	96.27	96.42	97.26	97.41	97.99	98.04	98.08
1106851407	14.229	90.74	91.03	92.10	94.12	96.81	97.21	97.74	97.63	98.07	98.39	98.33	98.30
1206851501	15.755	90.36	90.36	90.41	90.92	91.17	92.01	93.33	94.37	95.33	96.40	95.87	95.84
1206851502	15.755	90.36	90.29	90.48	90.93	91.93	93.55	94.03	94.80	95.60	96.60	96.20	96.10
1206851503	15.755	90.29	90.44	90.73	91.40	92.33	93.94	94.78	95.13	95.82	96.78	96.43	96.26
1206851504	15.755	90.33	90.39	90.95	91.62	92.56	94.17	95.03	95.39	95.93	96.86	96.60	96.33
1206851505	15.755	90.32	90.49	90.73	92.08	93.25	95.33	95.88	95.90	96.32	97.03	96.89	96.77
1206851506	15.755	90.31	90.77	90.93	92.31	93.74	95.68	95.93	96.11	96.46	97.21	97.19	96.96
1206851507	15.775	90.26	90.89	91.67	93.82	95.61	96.42	96.57	96.53	96.83	97.41	97.28	97.01
1406851701	17.287	89.87	89.93	90.06	90.07	90.71	92.36	93.82	94.96	95.76	96.54	96.72	96.95
1406851702	17.287	89.87	89.88	89.99	90.75	91.29	93.86	94.18	95.29	96.05	96.76	96.83	97.13
1406851703	17.287	89.88	90.12	89.45	91.75	92.93	94.18	95.16	96.01	96.54	97.10	97.11	97.26
1406851704	17.287	89.89	90.09	90.46	92.16	93.01	94.27	95.35	96.23	96.63	97.15	97.12	97.26
1406851705	17.287	89.89	90.30	90.77	92.20	93.43	95.64	96.55	96.31	96.75	97.31	97.29	97.36
1406851706	17.287	89.97	90.78	91.00	92.39	93.86	95.56	96.77	97.11	97.05	97.54	97.49	97.55
1406851707	17.287	89.98	90.99	91.17	93.53	95.00	96.27	97.05	97.28	97.15	97.71	97.59	97.66
1406851801	18.827	89.99	90.02	90.32	90.54	90.72	92.25	93.96	94.83	95.98	96.98	96.94	96.31
1406851802	18.827	89.94	90.28	90.36	90.75	91.97	93.03	94.30	95.10	96.43	96.98	96.95	96.44
1406851803	18.827	89.90	90.34	90.57	90.94	92.14	93.56	94.46	95.30	96.50	97.08	97.07	96.66
1406851804	18.827	89.96	90.49	90.67	90.95	92.15	93.58	94.49	95.32	96.52	97.23	97.18	96.62
1406851805	18.827	89.88	90.44	90.64	90.93	92.22	93.64	94.50	95.35	96.43	97.31	97.24	96.52
1406851806	18.827	89.88	90.46	90.72	91.22	92.69	94.46	95.80	95.55	96.77	97.33	97.20	96.71
1406851807	18.827	89.72	90.88	90.99	91.94	93.75	95.40	96.51	96.39	97.10	97.50	97.32	97.05
1706852001	20.374	89.81	89.90	90.15	90.24	90.24	90.86	91.55	93.80	94.40	94.89	95.18	95.61
1706852002	20.374	89.88	89.98	90.24	90.21	90.28	92.33	93.42	94.75	96.61	97.30	97.20	96.29
1706852003	20.374	89.90	90.24	90.31	90.25	92.37	94.03	95.08	95.87	96.57	97.25	97.26	96.31
1706852004	20.374	89.90	90.22	90.32	90.45	92.36	94.55	94.90	95.72	96.47	97.20	97.15	96.68
1706852005	20.374	89.91	90.39	90.46	90.84	92.40	94.54	94.93	96.12	96.51	97.28	97.16	96.84
1706852006	20.374	89.95	90.43	90.84	91.03	92.44	93.92	94.94	96.32	96.55	97.19	97.01	96.55
1706852007	20.374	89.97	90.63	90.94	91.44	92.80	94.02	95.66	97.04	96.91	97.38	97.32	97.05
1706852101	21.929	89.76	89.98	90.17	90.76	90.77	90.88	91.39	93.97	94.90	95.10	95.01	95.05
1706852102	21.929	89.87	89.88	90.08	90.37	90.77	91.33	93.29	94.97	95.40	96.21	96.29	96.14
1706852103	21.929	89.99	90.09	90.80	90.96	91.83	93.03	95.82	96.57	96.78	97.12	97.12	96.29
1706852104	21.929	90.02	89.98	90.88	91.59	93.01	94.62	96.11	96.73	96.79	97.09	97.05	96.20
1706852105	21.929	90.07	90.18	90.91	92.11	94.19	94.72	96.22	96.75	96.80	97.19	97.18	96.30
1706852106	21.929	89.91	90.27	91.00	92.47	94.30	94.88	96.39	96.81	97.03	97.26	97.25	96.55
1706852107	21.929	89.92	90.59	91.59	92.89	94.80	95.20	96.72	96.97	97.17	97.38	97.41	96.78

TABLE C.4

Steam-Water Flooding Data (High Steam Extraction Rate Tests)

Inlet Water Subcooling = 10 K

TEST No	Qfin	Tfin	Two	Mcw	Tc1	Tc2	TD	Mssup	Ts	Patm	PD	TT	TL
2304850410	4.000	20.61	98.81	20.668	16.31	65.85	55.17	2.1287	99.64	1.012	0.232	0.610	0.445
2404850510	5.000	20.23	98.61	20.540	18.12	61.64	55.43	1.9232	99.85	1.017	0.655	0.654	0.471
2404850612	6.000	20.81	98.49	22.467	18.64	65.42	60.19	2.0675	99.71	1.017	2.931	0.698	0.607
2504850715	7.000	20.14	93.63	20.787	19.79	68.24	61.09	2.1971	99.89	1.021	1.466	0.776	0.762
2604850816	8.000	20.76	85.20	24.312	15.63	58.92	55.73	2.3290	99.64	1.013	4.620	0.868	0.799
3004850909	9.000	26.69	77.97	22.414	16.47	57.94	56.08	2.1553	99.85	1.020	2.205	0.905	0.860
3004851009	10.000	20.31	68.50	20.882	17.91	58.26	57.97	1.9868	99.66	1.021	9.332	0.888	0.836
0205851114	11.197	20.45	58.77	20.789	17.41	61.47	59.14	2.3111	99.80	1.018	5.784	0.961	0.842
0305851214	12.710	19.79	51.83	20.184	17.78	61.07	60.32	2.3129	99.66	1.012	4.745	0.985	0.833
0305851408	14.229	20.22	46.15	20.998	18.57	40.59	50.61	1.4821	99.61	1.011	3.264	1.093	0.939
0305851507	15.754	20.87	43.62	20.493	20.52	43.37	52.36	1.6628	99.67	1.011	6.030	1.186	0.978
0904850413	4.000	30.03	98.84	24.592	15.41	61.13	60.83	2.4578	99.84	1.025	0.816	0.692	0.474
1004850512	5.000	30.89	98.83	25.399	13.02	57.90	59.98	2.3086	99.84	1.017	0.131	0.776	0.590
1004850614	6.000	30.58	98.67	22.431	14.65	63.09	64.92	2.2227	98.62	1.017	0.907	0.751	0.650
1004850718	7.000	30.79	96.36	26.461	15.19	52.10	53.28	2.1590	99.72	1.018	0.259	0.777	0.758
1204850815	8.000	30.95	89.42	25.926	12.88	55.87	61.48	2.4430	98.35	1.001	0.698	0.874	0.791
1204850914	9.000	30.98	86.49	25.487	11.45	56.81	54.09	2.3245	99.77	1.001	2.844	0.931	0.846
1504851015	10.000	30.14	82.56	25.240	11.55	54.71	55.07	2.3858	99.82	0.995	1.525	0.955	0.951
1604851115	11.197	30.35	75.80	24.517	16.49	56.92	57.75	2.2675	99.86	1.025	5.224	1.171	0.975
2903850415	4.000	40.36	98.90	24.207	15.10	60.36	58.51	2.5518	90.98	0.986	0.682	0.538	0.439
2903850514	5.000	40.63	99.16	24.311	14.10	59.77	62.46	2.3061	99.64	0.986	0.949	0.724	0.515
0103850612	6.000	40.78	98.62	24.608	14.40	58.63	61.84	2.1185	99.74	0.987	1.934	0.586	0.439
0104850712	7.000	41.23	97.88	24.704	12.84	58.66	65.67	2.1479	99.70	0.997	2.309	0.608	0.589
0204850813	8.000	40.70	95.89	21.723	14.12	62.69	69.09	2.1387	99.78	1.007	2.459	0.679	0.579
0204850914	9.000	40.15	91.82	24.777	12.42	56.46	62.56	2.1297	99.71	0.997	2.437	0.695	0.668
0304851012	10.000	40.33	89.18	24.594	13.41	57.58	60.81	2.1640	99.71	0.995	2.522	0.691	0.671
0304851112	11.197	39.95	84.24	24.581	13.80	58.44	58.52	2.2698	99.80	0.994	2.215	0.858	0.778
0304851212	12.710	40.48	75.08	25.455	11.87	52.59	54.10	2.1423	99.73	0.995	1.721	1.207	0.952
0304851412	14.229	40.87	70.67	24.648	14.64	60.59	58.59	2.3609	99.68	0.994	3.618	1.390	0.989
0504851512	15.754	41.08	67.03	25.240	15.35	58.17	59.68	2.3345	99.72	1.004	3.888	1.519	1.054
0504851612	17.287	40.41	65.09	25.144	16.54	59.59	58.73	2.6327	99.72	1.004	5.537	1.714	1.218
0504851810	18.827	39.96	61.44	25.142	17.04	58.68	61.85	2.3834	99.77	1.004	4.561	1.673	1.271
0504852010	20.374	40.64	58.31	25.137	17.58	53.22	55.79	2.4422	99.69	1.004	5.500	1.687	1.312
0803852210	21.929	40.73	54.56	23.863	15.40	58.06	13.80	2.5222	99.85	0.986	9.589	1.889	1.325
1803850418	4.000	49.92	98.60	25.784	12.52	60.98	58.60	2.2334	99.72	0.986	0.723	0.468	0.382
1803850517	5.000	50.03	98.95	24.635	14.74	63.96	66.75	2.3302	99.76	0.986	0.271	0.487	0.497
1803850618	6.000	50.50	98.78	24.673	13.45	60.45	68.21	2.4393	99.65	0.986	0.143	0.554	0.519
1903850718	7.000	50.21	98.61	20.021	9.45	65.65	70.82	2.2272	99.67	1.011	1.511	0.598	0.527
1903850814	8.000	49.98	98.54	24.998	10.39	52.88	50.99	1.7830	99.85	1.007	2.869	0.631	0.584
2003850910	9.000	50.09	98.55	25.078	11.26	47.64	50.85	1.5717	99.81	0.990	4.313	0.800	0.630
2003851014	10.000	50.89	97.10	24.846	11.47	51.55	53.59	1.8867	99.12	0.991	3.935	0.850	0.684
2103851114	11.197	49.98	93.20	24.670	12.64	54.65	55.28	1.6868	99.66	0.992	1.467	0.879	0.691
2103851210	12.710	50.27	90.40	24.664	13.47	53.45	55.96	1.7448	99.10	0.993	0.611	0.968	0.756
2103851416	14.229	50.43	87.23	24.428	13.12	60.86	59.40	2.1671	99.71	0.992	0.904	0.992	0.763
2203851510	15.754	50.75	81.31	26.525	15.19	56.36	59.26	1.9037	99.73	1.010	0.428	1.179	0.880
2203851714	17.287	50.31	75.03	25.935	14.78	56.93	59.01	2.0247	99.67	1.010	1.482	1.258	0.925
2203851814	18.827	50.68	70.13	25.904	15.48	59.14	62.11	2.1540	99.71	1.010	2.857	1.439	0.955
2503852010	20.374	50.49	67.24	25.821	16.07	52.16	58.85	1.9872	99.62	0.997	1.691	1.519	0.993
2603852110	21.929	50.85	60.29	25.893	16.28	50.40	59.00	1.8694	99.65	1.011	2.950	1.646	1.086

TABLE C.4 (Continue)

Steam-Water Flooding Data (High Steam Extraction Rate Tests)

Inlet Water Subcooling = 10 K

TEST No	Qfin	Tfin	Two	Mcw	Tc1	Tc2	TD	Mssup	Ts	Patm	PD	TT	TL
0403850412	4.000	59.80	99.19	21.381	13.00	43.16	46.68	1.6233	99.86	1.017	0.362	0.529	0.428
0403850512	5.000	60.03	98.93	21.364	13.97	46.56	50.69	1.5598	99.85	1.014	0.765	0.659	0.487
0603850612	6.000	59.45	98.87	22.859	13.26	50.83	52.49	1.6779	99.87	1.018	0.972	0.567	0.500
0603850712	7.000	60.12	98.59	21.947	13.15	53.64	53.95	1.6915	99.79	1.016	0.541	0.594	0.550
0703850812	8.000	59.74	98.55	25.826	15.34	53.75	52.58	1.7048	99.67	1.022	0.762	0.680	0.577
0703850914	9.000	60.33	97.56	25.877	16.87	55.33	53.41	1.7114	99.76	1.022	0.949	0.694	0.586
0703851012	10.000	60.03	96.89	25.881	13.39	51.84	54.36	1.6981	99.76	1.024	2.217	0.779	0.620
0803851112	11.197	60.43	96.77	24.047	11.01	51.21	55.32	1.6306	99.63	1.009	1.142	0.851	0.675
0803851214	12.710	60.37	95.21	24.214	12.32	54.59	55.32	1.6928	99.29	1.009	1.186	0.965	0.695
1203851412	14.229	59.86	90.15	24.196	13.65	55.55	56.97	1.6665	99.18	1.007	4.651	0.983	0.847
1203851512	15.754	60.54	89.05	24.005	14.42	56.85	57.46	1.7146	99.26	1.007	3.658	1.199	0.849
1203851716	17.287	60.35	85.47	24.245	14.88	61.42	61.86	1.8746	99.64	1.006	0.929	1.311	0.873
1403851815	18.827	60.33	80.21	24.105	13.21	60.19	64.76	2.1747	99.65	0.998	4.434	1.377	0.936
1403820412	20.374	60.19	76.57	24.059	13.90	62.67	62.95	2.1238	99.70	0.998	1.934	1.410	0.996
1403821412	21.929	60.57	73.72	24.032	13.88	61.51	64.34	2.1175	99.33	0.997	3.089	1.544	1.108
1902850412	4.000	69.20	99.08	26.383	14.84	37.02	44.57	1.5847	99.75	0.987	0.699	0.527	0.492
2002850507	5.000	69.28	98.92	25.342	18.08	43.15	48.10	1.4552	99.86	1.020	3.773	0.480	0.435
2102850609	6.000	70.14	98.89	25.175	17.81	45.49	50.02	1.6112	99.92	1.023	4.395	0.604	0.533
2002850711	7.000	69.77	97.95	28.160	18.23	43.47	48.92	1.6037	99.67	1.021	4.734	0.724	0.554
2202850813	8.000	70.86	96.80	26.009	11.35	46.50	49.47	1.4723	99.71	1.009	2.716	0.772	0.587
2502850915	9.000	69.85	96.37	25.265	17.35	51.26	53.51	1.4573	99.78	1.020	3.381	0.756	0.580
2602851014	10.000	69.51	95.34	24.121	15.19	59.92	56.25	1.5816	99.79	1.007	2.150	0.838	0.697
0702850410	4.000	79.15	99.27	26.395	17.87	41.40	50.51	1.5818	99.68	1.014	0.422	0.495	0.436
0702850510	5.000	79.12	99.14	26.424	17.74	42.27	53.50	1.5634	99.80	1.014	0.553	0.591	0.511
0802850610	6.000	80.26	99.12	27.689	17.37	40.71	52.91	1.6725	99.71	1.016	0.644	0.633	0.629
0802850710	7.000	80.01	98.95	27.375	17.07	50.73	52.47	1.7134	99.68	1.016	0.883	0.729	0.577
0802850810	8.000	80.41	98.72	27.190	17.43	51.65	52.22	1.6647	99.84	1.017	0.908	0.779	0.580
1106850912	9.000	79.46	98.39	25.750	16.64	54.49	54.91	1.6582	99.83	1.021	0.973	0.810	0.631
1206851010	10.000	80.44	98.57	27.280	17.31	55.98	55.85	1.7197	99.61	1.016	1.023	0.772	0.724
1206851110	11.197	81.04	98.70	22.019	11.74	58.25	57.76	1.6865	99.66	1.017	1.844	1.266	0.810
1206851210	12.710	81.43	98.69	22.749	11.72	58.69	58.23	1.5959	99.68	1.016	1.422	1.329	0.851
1206851410	14.229	80.80	98.83	22.915	11.68	61.43	57.91	1.6418	99.73	1.016	2.467	1.366	0.996
1306851512	15.754	79.67	98.53	22.584	11.72	61.39	59.97	1.6272	99.70	1.009	1.150	1.499	0.952
1306851712	17.287	79.18	98.08	22.379	12.02	62.62	61.95	1.6456	99.61	1.008	6.364	1.598	0.991
1306851810	18.827	80.37	96.46	22.506	11.76	60.04	60.18	1.4054	99.75	1.007	5.171	1.760	1.223
1406852008	20.374	80.91	97.07	22.478	11.45	62.17	59.56	1.3861	99.69	1.009	3.642	1.803	1.274
1406852108	21.929	79.90	95.62	21.956	11.60	57.66	59.52	1.2477	99.63	1.007	3.381	1.890	1.331
0306850407	4.000	89.61	97.68	27.668	23.06	59.18	54.61	2.3021	99.71	1.014700.301	0.524	0.327	
0706850507	5.000	90.01	98.29	28.513	23.85	59.13	54.86	2.1935	99.69	1.012	0.370	0.553	0.378
0706850607	6.000	89.96	98.29	28.854	22.53	58.26	55.84	2.1193	99.70	1.012	0.395	0.621	0.391
0906850707	7.000	89.60	96.95	29.150	15.91	52.61	61.85	2.2043	99.76	1.017300.668	0.693	0.496	
0906850807	8.000	90.26	96.65	29.192	16.33	53.42	61.44	2.1273	99.75	1.017300.871	0.685	0.463	
1006850007	9.000	89.97	96.95	29.104	18.86	54.76	62.31	1.8698	99.73	1.014700.245	0.765	0.502	
1106851107	10.000	90.00	97.63	28.086	16.10	55.97	58.14	1.8528	99.66	1.016	0.427	0.803	0.561
1006851107	11.197	90.28	97.78	29.066	17.33	53.93	62.27	1.7374	99.72	1.015300.981	0.884	0.664	
1106851207	12.710	89.74	97.06	28.867	16.95	55.15	62.59	1.7271	99.63	1.009301.297	0.975	0.673	
1106851407	14.229	90.53	97.36	28.779	17.36	55.15	62.36	1.5682	99.71	1.010701.704	0.991	0.692	
1206851507	15.755	90.04	97.59	29.236	16.96	56.71	60.32	1.6228	99.69	1.010701.829	1.084	0.703	
1406851707	17.287	90.51	97.75	29.245	17.17	56.88	58.19	1.3953	99.70	1.006701.215	1.296	0.727	
1406851807	18.827	90.38	97.76	29.134	14.70	49.42	58.60	1.0733	99.60	1.006701.269	1.374	0.789	
1906852007	20.376	90.09	96.59	28.952	14.77	47.38	56.26	0.9963	99.71	1.006	2.481	1.480	0.834
1906852107	21.929	89.74	99.15	29.205	12.14	46.87	55.83	0.9828	99.83	1.000	2.753	1.534	0.887

TABLE C.5

Steam-Water Flooding Data (Low Steam Extraction Rate Tests)

TEST No	Qfin	WC	Tfin	Two	Mcw	Tc1	Tc2	TD	Mssup	Ts	VPI	Pata	PD	TT	TL
0507850408	4.000	3.979	20.34	98.26	4.188	14.44	92.73	83.81	1.4514	99.61	3.1	0.9947	1.120	0.731	0.608
0507850507	5.000	4.287	21.00	98.17	4.099	15.94	91.94	82.47	1.3876	99.68	2.9	0.9947	1.010	0.792	0.638
0507850607	6.000	4.297	21.07	97.58	4.121	15.99	91.42	79.08	1.3646	99.79	2.8	0.9947	2.130	0.807	0.735
0807850707	7.000	4.140	20.47	91.88	4.338	17.65	86.08	73.56	1.3423	99.66	3.0	0.9987	2.560	0.875	0.845
0807850808	8.000	4.238	21.24	84.45	3.978	18.18	87.41	75.82	1.4175	99.67	0.0	1.0000	3.160	0.925	0.902
0907850907	9.000	4.602	21.37	74.90	4.239	17.27	66.62	65.23	1.2339	99.73	0.0	0.9987	4.290	0.955	0.910
1107851007	10.000	4.262	20.69	66.60	5.960	17.60	56.10	58.91	1.2128	99.71	0.0	1.0067	4.750	1.073	1.007
1807850410	4.000	5.275	30.64	98.71	3.212	15.96	93.20	84.93	1.3159	99.78	4.2	0.9960	0.960	0.781	0.489
1807850507	5.000	5.312	30.67	98.05	3.847	16.23	90.80	79.21	1.2704	99.67	4.2	0.9960	0.970	0.789	0.486
1807850609	6.000	5.423	30.95	97.95	3.667	16.49	90.60	78.20	1.2014	99.76	4.1	0.9960	1.240	0.861	0.617
2207850707	7.000	5.279	30.42	96.67	4.108	16.20	90.13	76.49	1.2882	99.69	0.5	1.0000	6.380	0.880	0.729
2207850807	8.000	5.349	30.59	92.63	3.470	16.23	90.18	80.42	1.3250	99.67	0.0	1.0000	3.700	0.958	0.772
2207850907	9.000	5.189	30.32	87.88	3.951	15.73	89.40	79.43	1.4096	99.61	0.0	1.0000	5.110	0.989	0.909
2207851007	10.000	5.010	30.03	84.76	6.361	15.41	79.38	69.54	1.4516	99.64	0.0	1.0000	3.580	1.055	0.956
1908851107	11.197	5.480	31.14	79.55	4.886	17.03	65.71	62.48	1.2092	99.62	0.0	0.9973	2.700	1.235	1.015
1908851207	12.710	5.261	30.23	69.61	4.905	18.23	61.20	60.68	1.2137	99.73	0.0	0.9973	4.870	1.239	1.064
2307850408	4.000	6.251	40.34	98.25	4.203	16.40	93.31	83.93	1.4523	99.71	3.2	1.0133	0.420	0.625	0.530
2307850508	5.000	6.214	40.06	97.90	4.488	16.67	92.71	83.06	1.4304	99.72	3.8	1.0133	0.740	0.720	0.526
2307850607	6.000	6.203	40.13	97.88	4.366	16.50	92.60	85.98	1.4098	99.90	3.2	1.0133	0.750	0.711	0.592
2307850707	7.000	6.136	39.41	97.41	4.382	15.41	92.23	85.94	1.3802	99.80	0.0	1.0133	2.940	0.788	0.676
2407850807	8.000	6.172	39.51	94.52	4.830	15.20	89.36	82.07	1.3947	99.66	0.0	1.0133	2.940	0.803	0.776
2407850907	9.000	6.205	40.15	93.72	4.898	16.43	90.91	82.67	1.4705	99.65	0.0	1.0133	4.840	0.929	0.770
2707851007	10.000	6.380	41.40	90.48	4.712	18.85	89.25	78.23	1.3316	99.72	0.0	1.0053	3.870	1.083	0.898
2808851107	11.197	6.137	39.66	83.84	5.678	16.20	71.49	66.77	1.1910	99.62	0.0	1.0087	3.790	1.142	0.921
2808851207	12.710	6.189	39.82	77.62	5.638	16.49	66.62	65.25	1.1984	99.78	0.0	1.0080	2.880	1.275	0.985
2507850409	4.000	7.119	49.88	98.99	4.762	22.59	92.87	86.00	1.5008	99.90	3.4	1.0133	0.770	0.595	0.470
2507850508	5.000	7.312	50.40	98.70	4.788	23.18	92.73	84.94	1.4221	99.78	3.3	1.0120	0.830	0.726	0.538
2507850608	6.000	7.195	50.07	98.93	4.312	23.75	92.93	85.56	1.3366	99.76	3.1	1.0120	0.810	0.752	0.548
2607850707	7.000	7.244	50.26	97.79	4.395	19.18	91.92	87.49	1.3435	99.84	2.0	1.0040	1.080	0.761	0.630
2607850807	8.000	7.429	50.79	97.50	4.203	20.51	91.89	88.20	1.3019	99.61	2.0	1.0040	1.270	0.844	0.728
2608850907	9.000	7.470	50.90	96.71	4.639	20.94	90.06	86.32	1.3452	99.65	0.0	1.0040	2.920	0.930	0.847
2608851007	10.000	7.322	50.47	95.85	4.555	21.11	90.42	87.78	1.3861	99.73	0.0	1.0027	1.610	0.981	0.858
2507851107	11.197	7.431	50.43	90.96	4.833	16.99	89.41	85.59	1.4776	99.74	0.0	1.0093	4.220	1.062	0.962
2507851207	12.710	7.535	50.77	88.49	4.862	18.69	87.59	76.38	1.3157	99.61	0.0	1.0093	4.990	1.163	0.957
2507851407	14.229	7.159	50.03	86.47	4.471	13.54	83.09	74.87	1.2983	99.78	0.0	1.0053	5.800	1.297	1.071
2507851507	15.755	7.672	51.00	78.25	4.813	16.25	78.37	70.99	1.2406	99.72	0.0	1.0053	3.570	1.421	1.206
2907850408	4.000	8.012	59.54	98.08	4.162	21.25	93.37	89.98	1.5138	99.70	3.0	0.9960	0.720	0.575	0.473
2907850507	5.000	8.308	60.84	98.24	4.247	20.20	92.64	86.86	1.4353	99.79	3.4	0.9960	0.670	0.657	0.540
2907850607	6.000	8.179	60.46	98.07	4.304	18.85	92.19	87.83	1.4317	99.77	3.0	0.9960	1.240	0.701	0.532
2907850708	7.000	8.253	60.69	97.71	4.186	21.09	91.90	88.89	1.3966	99.74	2.0	0.9960	1.840	0.874	0.636
3007850807	8.000	7.944	59.44	98.03	4.444	18.20	91.72	89.06	1.4280	99.67	3.5	1.0013	1.250	0.856	0.632
3007850907	9.000	8.129	59.98	97.50	4.429	19.49	91.99	89.20	1.3724	99.68	0.0	1.0000	2.090	0.970	0.662
3007851007	10.000	7.989	59.51	97.57	4.399	20.40	91.37	87.43	1.3283	99.75	0.0	1.0000	1.220	0.924	0.782
3076851107	11.197	8.125	60.13	96.85	4.403	20.83	90.72	88.77	1.3839	99.63	1.3	1.0000	3.150	1.076	0.851
2008851207	12.710	8.233	60.57	93.33	4.953	16.84	92.23	86.65	1.4733	99.65	0.0	0.9973	1.760	1.310	0.876
2008851407	14.229	8.295	60.85	91.19	4.887	17.78	90.72	80.75	1.3065	99.66	0.0	0.9973	2.380	1.302	0.989
2008851507	15.755	8.357	61.15	91.22	4.921	17.78	86.02	77.19	1.1659	99.69	0.0	0.9960	2.980	1.493	0.982
2108851707	17.287	8.059	59.75	87.34	4.923	15.33	79.12	71.06	1.1331	99.62	0.0	1.0067	3.760	1.525	1.088
2208851807	18.827	8.319	61.01	83.45	4.950	16.23	77.25	70.23	1.1299	99.66	0.0	1.0053	3.000	1.582	1.187
2208852007	20.374	8.342	61.12	79.81	4.917	16.18	75.17	68.98	1.1532	99.65	0.0	1.0053	3.950	1.743	1.194
3107850408	4.000	9.141	70.67	98.27	4.237	18.90	92.53	86.88	1.4811	99.78	3.1	1.0100	0.520	0.572	0.501
3107850507	5.000	9.079	70.32	98.31	4.217	21.09	92.49	86.48	1.3879	99.83	3.1	1.0100	0.850	0.576	0.533
3107850607	6.000	9.044	70.39	98.29	4.249	21.69	92.03	87.09	1.3812	99.81	3.1	1.0100	0.740	0.668	0.605
3107850708	7.000	8.933	69.57	98.10	4.257	20.95	92.11	90.04	1.3655	99.70	3.0	1.0100	0.690	0.703	0.658

TABLE C.5 (Continue)

Steam-Water Flooding Data (Low Steam Extraction Rate Tests)

TEST No	Q _{fin}	WC	T _{fin}	T _{wo}	M _{cw}	TC1	Tc2	TD	M _{ssup}	T _s	VPI	P _{ata}	PD	TT	TL
3107850807	8.000	8.973	69.78	98.39	4.238	21.45	91.76	90.32	1.3099	99.77	0.0	1.0100	1.000	0.838	0.720
3107850907	9.000	9.165	70.67	97.98	4.238	21.76	91.65	89.90	1.3269	99.81	2.9	1.0100	1.120	0.910	0.766
2508851007	10.000	8.929	69.59	98.51	4.233	19.05	91.26	89.28	1.2685	99.79	3.4	1.0100	1.560	1.079	0.797
2508851108	11.197	8.982	69.82	98.12	4.170	19.58	91.28	89.25	1.2869	99.73	3.5	1.0100	1.740	1.191	0.860
2508851207	12.710	9.149	70.75	98.03	4.652	16.03	92.62	88.51	1.3991	99.68	0.0	1.0100	4.530	1.263	0.870
2508851407	14.229	9.025	70.10	96.95	4.784	16.04	92.29	88.34	1.3776	99.59	0.0	1.0100	2.790	1.407	0.898
2508851507	15.754	9.033	70.18	96.11	4.594	17.10	91.51	85.12	1.2683	99.62	0.0	1.0100	2.640	1.506	0.974
2508851707	17.287	8.987	69.78	95.89	5.019	16.71	91.46	82.96	1.2401	99.69	0.0	1.0100	0.960	1.597	1.051
2508851807	18.827	9.009	69.96	93.90	4.831	16.50	83.11	80.86	1.1422	99.67	0.0	1.0100	2.130	1.739	1.120
2508852007	20.374	8.987	69.97	91.62	4.861	16.30	77.89	77.39	1.0784	99.69	0.0	1.0100	8.050	1.894	1.274
2506850407	4.000	10.170	79.75	98.42	4.112	20.32	93.16	89.38	1.4666	99.64	3.2	1.0107	0.670	0.549	0.520
2506850508	5.000	10.217	80.10	98.45	4.089	19.65	93.14	89.04	1.4442	99.62	3.3	1.0107	0.540	0.669	0.570
2506850607	6.000	10.215	80.00	98.43	4.093	19.80	92.44	89.28	1.3501	99.62	3.0	1.0107	0.700	0.762	0.594
2506850707	7.000	10.339	80.73	98.77	4.130	19.40	92.56	89.93	1.3315	99.71	3.1	1.0107	0.670	0.794	0.652
2506850808	8.000	10.997	80.65	98.46	4.545	18.29	90.75	89.71	1.3859	99.64	3.2	0.9960	0.970	0.894	0.767
2506850907	9.000	10.376	80.80	98.18	4.483	18.25	91.63	90.54	1.3762	99.68	3.8	0.9960	1.270	0.985	0.733
2506851007	10.000	10.175	79.84	98.58	4.467	18.30	91.09	90.94	1.3473	99.71	3.9	0.9973	1.060	1.047	0.774
2506851107	11.197	10.277	80.31	98.53	4.149	17.68	90.94	91.47	1.3167	99.71	3.7	0.9973	1.510	1.168	0.843
2506851208	12.710	10.294	80.44	98.78	3.992	17.70	91.01	91.71	1.3044	99.72	2.5	0.9973	1.500	1.362	0.832
2506851407	14.229	10.201	79.91	98.38	3.910	17.80	91.07	91.70	1.2783	99.70	0.0	0.9973	1.380	1.455	0.922
2506851507	15.755	10.285	80.43	97.93	4.660	17.23	91.82	86.76	1.1998	99.67	0.0	1.0080	1.100	1.538	0.978
2506851707	17.287	10.214	80.07	96.64	4.624	17.36	90.65	83.57	1.1116	99.69	0.0	1.0080	4.340	1.581	1.181
2506851807	18.827	10.211	79.68	96.02	4.650	17.66	90.50	81.95	1.0668	99.70	0.0	1.0080	5.500	1.690	1.274
2506852007	20.374	10.247	79.69	95.18	4.660	17.40	88.78	81.38	1.0288	99.68	0.0	1.0053	6.670	1.780	1.414
0306850409	4.000	11.182	89.86	98.26	4.719	18.34	90.55	83.49	1.5601	99.78	4.0	1.0147	0.500	0.532	0.468
0506850508	5.000	11.222	90.18	98.48	5.499	23.15	90.59	82.78	1.4858	99.86	4.0	1.0120	0.500	0.464	0.493
0506850608	6.000	11.208	90.07	98.80	5.252	24.88	90.44	82.79	1.3694	99.71	5.0	1.0120	0.120	0.526	0.486
0706850707	7.000	11.197	89.98	97.67	5.243	20.48	89.03	87.70	1.4422	99.75	4.0	1.0173	0.770	0.648	0.552
0706850807	8.000	11.184	89.88	97.10	5.048	18.31	88.79	88.19	1.3783	99.75	3.0	1.0173	0.590	0.747	0.562
1006850908	9.000	11.191	90.00	97.55	4.972	17.24	89.87	88.56	1.4257	99.67	4.2	1.0146	0.590	0.832	0.598
1106851007	10.000	11.248	90.52	98.58	5.175	17.33	87.68	88.34	1.3550	99.75	4.2	1.0160	1.540	0.882	0.710
1006851107	11.197	11.230	90.38	98.42	5.329	17.86	90.82	88.19	1.3383	99.71	4.5	1.0153	1.870	0.988	0.670
1106851207	12.710	11.217	90.21	98.32	4.934	19.24	89.80	90.67	1.2841	99.83	4.5	1.0160	1.590	1.002	0.759
1106851407	14.229	11.287	90.74	98.31	4.751	19.50	92.71	91.13	1.3021	99.63	3.5	1.0160	1.640	1.153	0.732
1206851507	15.775	11.228	90.27	97.01	5.142	16.80	88.36	89.68	1.3127	99.70	4.1	1.0053	1.190	1.287	0.872
1406851707	17.287	11.209	89.98	97.67	5.505	18.95	89.47	88.56	1.2473	99.68	3.0	1.0067	1.250	1.392	0.972
1406851807	18.827	11.176	89.73	97.05	5.746	14.95	88.34	84.85	1.2109	99.67	0.0	1.0067	1.640	1.470	0.911
1706852007	20.374	11.219	89.97	97.05	4.854	15.50	92.20	85.06	1.1097	99.71	0.0	1.0027	1.800	1.535	1.061
1706852107	21.929	11.207	89.93	96.78	4.858	16.32	92.22	83.21	1.0458	99.66	0.0	1.0027	0.620	1.656	1.054

TABLE C.6

 Steam-Water Flooding Data, Wall Temperature Measurements (Low Steam Extraction Rate Tests)

TEST NO	Qfin	Tfin	T1	T2	T3	T4	T5	T6	T7	T8	T9	T10	T11
0507850408	4.000	20.33	23.92	30.26	61.07	82.12	92.03	96.42	97.69	98.03	98.35	98.44	98.26
0507850507	5.000	20.99	22.89	24.70	43.92	65.29	81.72	90.22	94.82	96.84	97.23	98.34	98.16
0507850607	6.000	21.07	21.38	23.20	32.24	51.71	69.12	80.02	89.13	94.77	96.03	97.41	97.57
0807850707	7.000	20.47	20.96	21.72	23.90	29.47	39.63	48.50	59.02	69.97	81.35	87.59	91.88
0807850808	8.000	21.23	21.66	22.48	22.49	22.52	24.98	28.03	34.38	45.83	57.79	74.56	84.44
0907850907	9.000	21.37	21.49	22.12	22.64	23.24	25.09	27.91	29.20	37.42	51.05	67.44	76.90
1107851007	10.000	21.69	21.74	21.85	21.97	22.07	23.09	24.67	27.62	33.50	45.00	57.34	67.60
1807850410	4.000	30.64	32.91	44.83	68.15	88.52	94.43	97.73	97.97	98.58	98.74	98.88	98.71
1807850507	5.000	30.67	32.37	38.96	53.02	78.61	88.93	94.93	96.84	97.43	97.92	98.18	98.05
1807850609	6.000	30.95	32.00	35.84	45.82	70.48	84.04	92.34	96.80	97.19	97.98	98.05	97.94
2207850707	7.000	30.41	31.81	32.81	35.01	39.15	49.66	61.70	74.42	84.60	90.91	94.26	96.67
2207850807	8.000	30.59	30.85	31.85	32.81	33.73	36.99	42.69	53.67	65.67	78.57	87.38	92.63
2207850907	9.000	30.24	30.52	30.55	31.74	32.17	33.93	38.53	46.43	59.15	71.84	82.34	87.87
2207851007	10.000	30.03	30.35	30.45	31.13	31.91	32.75	35.48	41.71	52.00	63.90	77.17	84.76
1908851107	11.197	31.14	31.28	32.42	32.91	33.09	33.56	35.52	40.02	48.44	59.31	72.73	79.54
1908851207	12.710	30.23	30.57	30.62	30.72	30.85	31.92	33.03	38.15	44.21	53.99	62.38	69.61
2307850408	4.000	40.33	41.31	49.94	76.55	90.21	96.59	98.06	98.28	98.54	98.79	98.82	98.24
2307850508	5.000	40.06	42.31	45.73	67.03	87.82	95.97	97.44	97.88	98.26	98.48	98.55	97.90
2307850607	6.000	40.13	41.30	43.99	62.85	82.71	91.88	94.86	96.94	98.07	98.16	98.38	97.88
2307850707	7.000	39.41	40.31	41.16	54.73	59.42	71.84	81.82	90.84	95.39	97.05	97.77	97.41
2407850807	8.000	39.51	40.79	40.53	46.56	51.61	60.07	71.13	79.00	87.92	91.68	93.21	94.52
2407850907	9.000	40.14	41.07	42.11	44.60	47.49	51.42	62.87	72.03	80.81	86.93	91.55	93.72
2707851007	10.000	41.40	41.98	42.75	43.28	44.19	47.39	53.32	61.62	69.93	77.85	86.45	90.48
2808851107	11.197	39.66	40.65	40.95	41.02	41.84	44.94	48.90	54.43	62.55	69.91	78.31	83.84
2808851207	12.710	39.81	39.80	40.11	41.57	41.90	42.83	44.48	49.86	56.38	64.36	73.67	77.62
2507850409	4.000	39.53	40.52	40.86	41.38	41.71	42.05	43.34	47.26	53.97	61.67	69.84	73.76
2507850508	5.000	49.88	54.85	66.42	80.28	92.26	96.78	97.23	98.42	98.44	98.68	98.66	98.98
2507850608	6.000	50.40	53.24	64.91	77.52	88.93	94.97	97.81	98.14	98.12	98.50	98.39	98.69
2607850707	7.000	50.07	53.48	62.03	75.94	88.06	94.40	97.79	98.02	98.73	99.14	99.30	98.93
2607850807	8.000	50.26	52.91	59.93	72.52	83.13	93.20	96.39	97.33	97.07	97.75	97.86	97.79
2608850907	9.000	50.78	52.03	54.02	63.32	75.96	88.55	93.05	95.95	96.89	97.45	97.62	97.49
2608851007	10.000	50.90	52.67	53.49	57.19	66.53	74.49	86.87	92.53	95.77	96.84	96.88	96.70
2507851107	11.197	50.46	50.81	51.70	53.93	57.44	61.90	69.10	78.77	85.84	90.89	94.77	95.84
2507851207	12.710	50.43	50.42	50.80	52.07	53.81	56.13	60.28	67.92	75.24	83.17	88.15	90.95
2507851407	14.229	50.77	50.88	51.65	52.05	51.98	53.09	55.42	59.68	67.84	75.97	83.87	88.49
2507851507	15.755	50.04	50.55	51.01	51.23	51.98	52.76	53.79	56.68	60.90	69.72	79.65	86.47
2907850408	4.000	51.00	51.84	51.97	51.94	51.42	52.79	53.12	54.39	56.06	61.61	71.51	78.25
2907850507	5.000	59.54	62.21	62.84	85.89	94.80	97.21	97.32	97.83	97.85	98.25	98.29	98.08
2907850607	6.000	60.83	61.09	62.14	83.96	94.66	97.39	97.67	98.37	98.42	98.46	98.52	98.23
2907850708	7.000	60.45	61.87	63.00	80.27	91.44	95.95	97.39	97.84	97.81	98.16	98.31	98.07
3007850807	8.000	60.69	61.15	63.07	75.12	87.11	94.78	97.87	97.92	97.81	98.04	98.06	97.70
3007850907	9.000	59.43	60.88	61.21	70.65	80.08	92.70	94.66	96.27	97.78	98.01	98.16	98.03
3007851007	10.000	59.97	60.66	60.94	67.81	75.25	85.56	92.08	95.08	96.93	97.54	97.79	97.50
3076851107	11.197	59.51	60.57	60.65	63.64	70.16	79.84	88.10	93.82	95.29	97.01	97.76	97.56
2008851207	12.710	60.12	60.78	61.19	64.74	66.02	72.16	78.98	89.62	93.14	95.76	96.99	96.84
2008851407	14.229	60.57	60.64	60.88	62.13	61.95	63.06	66.90	74.70	82.90	88.08	92.65	93.33
2008851507	15.755	60.84	60.99	61.37	61.90	61.91	62.69	63.68	67.78	74.50	82.67	88.63	91.19
2108851707	17.287	61.15	61.80	62.09	62.15	62.77	62.91	64.03	65.94	71.54	78.92	87.34	91.22
2208851807	18.827	59.74	59.93	60.57	60.54	60.89	60.89	61.26	63.88	70.38	78.26	84.76	87.34
2208852007	20.374	61.00	61.13	61.47	61.53	61.54	61.67	61.91	63.63	68.39	77.52	81.54	83.45
3107850408	4.000	61.12	61.40	61.53	61.60	61.74	61.93	62.28	63.12	67.62	72.60	77.53	79.81
3107850507	5.000	70.66	71.27	73.55	87.72	95.15	97.82	98.09	98.12	98.28	98.22	98.34	98.27
3107850607	6.000	70.32	71.23	74.79	86.12	95.02	96.39	97.56	98.03	98.36	98.39	98.44	98.31
3107850708	7.000	70.38	70.60	73.27	83.91	91.77	95.32	97.51	97.90	98.08	98.26	98.33	98.29

TABLE C.6 (Continue)

Steam-Water Flooding Data, Wall Temperature Measurements (Low Steam Extraction Rate Tests)

TEST NO	Qfin	Tfin	T1	T2	T3	T4	T5	T6	T7	T8	T9	T10	T11
3107850807	8.000	69.57	70.44	73.15	84.05	89.97	95.75	97.15	97.95	97.93	98.23	98.20	98.09
3107850907	9.000	69.77	71.45	74.01	83.32	89.33	94.89	97.39	98.07	97.99	98.51	98.50	98.39
2508851007	10.000	70.67	71.78	72.69	80.09	86.82	92.12	95.77	96.79	97.93	98.16	98.19	97.98
2508851108	11.197	69.59	70.21	71.92	76.49	83.03	91.31	95.52	97.10	98.55	98.62	98.66	98.50
2508851207	12.710	69.81	70.02	71.64	74.90	80.28	88.91	93.05	96.51	98.02	98.25	98.32	98.12
2508851407	14.229	70.75	70.88	71.93	72.26	76.66	82.07	89.52	94.16	97.37	98.08	98.12	98.02
2508851507	15.754	70.10	70.42	70.93	72.08	74.95	78.57	84.90	89.86	94.38	96.92	97.16	96.95
2508851707	17.287	70.18	70.71	70.93	71.95	72.70	75.94	82.03	87.81	92.14	94.96	96.21	96.11
2508851807	18.827	69.77	70.38	70.94	71.02	72.03	74.65	80.48	85.22	90.96	94.01	95.77	95.89
2508852007	20.374	69.97	70.33	70.56	70.85	71.08	73.38	77.64	84.25	89.45	92.37	93.57	93.89
2506850407	4.000	69.97	70.32	70.64	70.95	70.94	72.03	74.81	79.96	85.04	90.54	91.10	91.61
2506850508	5.000	79.74	82.76	86.66	95.34	96.03	97.47	98.17	98.26	98.35	98.59	98.47	98.41
2506850607	6.000	80.10	80.74	83.71	93.90	96.95	98.37	98.55	98.41	98.57	98.67	98.53	98.44
2506850707	7.000	79.99	80.14	83.89	92.19	96.90	98.16	98.44	98.40	98.49	98.75	98.68	98.43
2506850808	8.000	80.73	81.54	82.69	92.28	96.65	97.86	98.53	98.65	98.70	98.66	98.86	98.77
2506850907	9.000	80.87	81.52	82.95	92.48	96.69	97.95	98.11	98.39	98.47	98.57	98.62	98.45
2506851007	10.000	80.79	81.41	83.01	90.01	95.90	96.63	97.97	98.40	98.00	98.34	98.31	98.18
2506851107	11.197	79.83	80.03	81.54	87.26	93.02	96.37	97.85	98.08	98.22	98.61	98.79	98.58
2506851208	12.710	80.31	80.73	82.18	88.07	92.73	94.90	97.58	98.32	98.56	98.75	98.70	98.53
2506851407	14.229	80.44	81.20	81.24	87.45	90.39	94.31	97.22	97.58	97.94	98.84	98.82	98.78
2506851507	15.755	79.90	80.79	80.88	84.90	88.92	93.53	95.79	97.75	98.31	98.52	98.51	98.37
2506851707	17.287	80.42	80.69	81.26	84.34	87.65	91.93	95.31	97.05	97.76	98.22	98.24	97.93
2506851807	18.827	80.07	80.52	80.96	82.47	85.38	88.70	91.63	94.55	95.77	96.41	96.75	96.64
2506852007	20.374	79.66	79.94	80.38	81.93	83.66	86.96	90.80	93.39	95.99	96.52	96.82	96.01
0306850409	4.000	79.69	80.08	80.76	81.04	81.12	84.07	87.75	91.33	93.16	95.43	95.91	95.17
0506850508	5.000	89.86	91.38	93.41	95.49	96.33	98.03	98.38	98.40	98.45	98.74	98.59	98.26
0506850608	6.000	90.18	90.90	92.49	95.54	97.29	98.19	98.38	98.41	98.26	98.52	98.38	98.48
0706850707	7.000	90.07	90.82	92.08	95.21	97.29	98.24	98.46	98.60	98.40	98.64	98.51	98.79
0706850807	8.000	89.98	90.86	92.83	94.41	95.43	97.05	97.46	97.64	97.52	97.86	97.72	97.66
1006850908	9.000	89.88	91.03	92.35	94.55	95.88	96.72	96.53	96.77	97.42	97.53	97.38	97.10
1106851007	10.000	89.99	90.82	92.93	95.05	96.83	97.89	97.11	96.93	97.83	98.03	97.67	97.54
1006851107	11.197	90.52	91.32	92.90	94.87	96.93	98.37	98.55	98.64	98.57	98.86	98.69	98.58
1106851207	12.710	90.37	91.34	92.99	94.53	96.21	97.71	98.06	98.02	98.11	98.59	98.50	98.42
1106851407	14.229	90.20	90.81	92.56	94.73	96.05	96.90	97.15	97.84	97.86	98.54	98.41	98.31
1206851507	15.775	90.74	91.03	92.10	94.12	96.81	97.21	97.74	97.63	98.07	98.39	98.33	98.30
1406851707	17.287	90.26	90.89	91.67	93.82	95.61	96.42	96.57	96.53	96.83	97.41	97.28	97.01
1406851807	18.827	89.98	90.99	91.17	93.53	95.00	96.27	97.05	97.28	97.15	97.71	97.59	97.66
1706852007	20.374	89.72	90.88	90.99	91.94	93.75	95.40	96.51	96.39	97.10	97.50	97.32	97.05
1706852107	21.929	89.97	90.63	90.94	91.44	92.80	94.02	95.66	97.04	96.91	97.38	97.32	97.05
0312850414	4.000	89.92	90.59	91.59	92.89	94.80	95.20	96.72	96.97	97.17	97.38	97.41	96.78
0312850514	5.000	96.51	96.61	97.19	98.67	98.79	99.01	99.12	99.39	98.90	99.06	98.89	98.08
0312850612	6.000	95.93	95.96	96.65	98.35	98.59	98.79	98.82	98.82	98.84	98.09	98.23	97.88
0312850711	7.000	96.56	96.79	97.42	98.18	98.59	98.87	98.96	98.94	98.95	98.55	98.82	98.38
0312850812	8.000	97.02	97.39	97.70	98.23	98.58	98.79	98.91	98.94	98.99	98.74	98.87	98.25
0312850912	9.000	96.07	96.12	96.66	96.98	97.78	98.03	97.82	97.87	98.02	98.18	97.93	97.74
0312851012	10.000	96.61	96.66	97.01	97.29	97.55	97.94	97.99	98.02	98.19	98.24	98.14	98.01
0312851110	11.197	96.41	96.58	97.66	97.54	97.51	97.71	97.89	98.09	98.18	98.08	97.87	97.66
0512851210	12.710	95.97	95.88	96.05	96.92	97.47	98.16	98.22	98.47	98.63	98.88	98.16	97.95
0512851411	14.229	96.85	95.88	96.32	97.87	97.68	98.58	98.31	98.73	98.70	98.94	98.47	98.28
0512851510	15.754	96.76	96.75	96.96	97.97	97.86	98.67	98.78	98.79	98.58	98.79	98.54	97.90
0512851710	17.287	96.84	96.92	97.31	97.94	97.85	98.41	98.59	98.87	98.53	98.59	98.40	97.91
0512851812	18.827	96.90	97.05	97.19	98.20	97.99	98.61	98.79	99.04	98.83	98.85	98.61	98.05
0512852011	20.374	96.91	97.45	97.87	98.27	98.47	98.72	98.67	98.93	98.85	99.05	98.79	98.16
0512852110	21.929	96.54	96.51	97.08	97.30	97.41	97.84	97.71	98.08	98.19	98.15	98.40	97.94

TABLE C.7

Steam-Water Flooding Results (Low Steam Extraction Rate Tests)

TEST No	Dfin	Tsub	Mssup	MSB	MST	MSC	MSL	* Jfin	* JST	* Jf	* JSB
0507850408	3.991	79.27	1.4514	0.9722	0.3914	0.5808	0.4792	0.1966	0.3949	0.2110	0.6224
0507850507	4.988	78.68	1.3876	0.9846	0.2649	0.7197	0.4030	0.2198	0.3247	0.2357	0.6260
0507850607	5.985	78.72	1.3646	1.0376	0.1779	0.8597	0.3270	0.2408	0.2659	0.2581	0.6421
0807850707	6.983	79.19	1.3423	1.1044	0.1526	0.9517	0.2379	0.2601	0.2465	0.2778	0.6631
0807850808	7.980	78.43	1.4175	1.1528	0.1482	1.0046	0.2647	0.2780	0.2429	0.2956	0.6775
0907850907	8.977	78.36	1.2339	1.2179	0.1825	1.0354	0.0160	0.2949	0.2694	0.3119	0.6960
1107851007	9.976	79.02	1.2128	1.2051	0.1596	1.0455	0.0077	0.3108	0.2520	0.3271	0.6924
1807850410	3.980	69.14	1.3159	0.9752	0.4693	0.5059	0.3407	0.1966	0.4321	0.2092	0.6229
1807850507	4.975	69.00	1.2704	0.9431	0.3149	0.6282	0.3273	0.2198	0.3543	0.2338	0.6131
1807850609	5.970	68.81	1.2114	0.9652	0.2147	0.7505	0.2462	0.2408	0.2923	0.2560	0.6198
2207850707	6.966	69.27	1.2882	1.0234	0.1680	0.8553	0.2648	0.2601	0.2588	0.2761	0.6386
2207850807	7.961	69.08	1.3250	1.0927	0.1493	0.9435	0.2323	0.2780	0.2439	0.2946	0.6600
2207850907	8.956	69.29	1.4096	1.1193	0.0963	1.0230	0.2903	0.2949	0.1960	0.3118	0.6683
2207851007	9.952	69.61	1.4516	1.1299	0.0346	1.0953	0.3217	0.3108	0.1174	0.3280	0.6712
1908851107	11.140	68.48	1.2092	1.2092	0.0688	1.1404	0.0000	0.3289	0.1657	0.3458	0.6946
1908851207	12.649	69.50	1.2137	1.2137	0.0685	1.1452	0.0000	0.3504	0.1651	0.3663	0.6952
2307850408	3.968	59.37	1.4523	0.9763	0.5454	0.4309	0.4760	0.1966	0.4665	0.2074	0.6241
2307850508	4.960	59.66	1.4304	0.9590	0.4195	0.5395	0.4714	0.2198	0.4090	0.2318	0.6185
2307850607	5.952	59.77	1.4098	0.9524	0.3049	0.6475	0.4574	0.2408	0.3482	0.2540	0.6154
2307850707	6.946	60.39	1.3802	0.9379	0.1770	0.7608	0.4423	0.2601	0.2655	0.2744	0.6112
2407850807	7.938	60.15	1.3947	0.9756	0.1336	0.8420	0.4191	0.2780	0.2309	0.2929	0.6241
2407850907	8.928	59.50	1.4705	1.0313	0.1221	0.9091	0.4392	0.2949	0.2209	0.3100	0.6417
2707851007	9.915	58.32	1.3316	1.0289	0.0805	0.9485	0.3027	0.3108	0.1792	0.3258	0.6407
2807851107	11.109	59.96	1.1910	1.1268	0.1134	1.0135	0.0642	0.3289	0.2128	0.3440	0.6709
2807851207	12.610	59.96	1.1984	1.1984	0.1459	1.0525	0.0000	0.3504	0.2411	0.3651	0.6910
2507850409	3.953	50.02	1.5008	0.9881	0.6250	0.3631	0.5127	0.1966	0.4990	0.2057	0.6275
2507850508	4.940	49.38	1.4221	0.9478	0.5009	0.4470	0.4743	0.2198	0.4472	0.2298	0.6152
2507850608	5.928	49.69	1.3366	0.9491	0.4077	0.5413	0.3875	0.2408	0.4036	0.2519	0.6157
2607850707	6.916	49.58	1.3435	0.9097	0.2881	0.6216	0.4338	0.2601	0.3390	0.2719	0.6024
2607850807	7.902	48.82	1.3019	0.9115	0.2130	0.6985	0.3904	0.2780	0.2921	0.2904	0.6042
2607850907	8.889	48.75	1.3452	0.9669	0.1870	0.7799	0.3783	0.2949	0.2735	0.3079	0.6221
2607851007	9.879	49.26	1.3861	1.0144	0.1374	0.8770	0.3717	0.3108	0.2343	0.3248	0.6367
2507851107	11.062	49.31	1.4776	1.0238	0.1352	0.8886	0.4538	0.3289	0.2324	0.3422	0.6396
2507851207	12.555	48.84	1.3157	1.1046	0.1425	0.9620	0.2111	0.3504	0.2389	0.3640	0.6651
2507851407	14.060	49.75	1.2983	1.1392	0.1238	1.0154	0.1591	0.3708	0.2223	0.3843	0.6744
2507851507	15.561	48.72	1.2406	1.1683	0.1645	1.0038	0.0723	0.3902	0.2565	0.4028	0.6834
2907850408	3.935	40.16	1.5138	1.0277	0.7410	0.2867	0.4861	0.1966	0.5449	0.2038	0.6417
2907850507	4.915	38.95	1.4353	0.9840	0.6365	0.3475	0.4513	0.2198	0.5047	0.2276	0.6276
2907850607	5.899	39.31	1.4317	0.9770	0.5569	0.4201	0.4547	0.2408	0.4722	0.2494	0.6254
3007850708	6.882	39.05	1.3966	0.9820	0.4975	0.4845	0.4146	0.2601	0.4464	0.2693	0.6272
3007850807	7.870	40.23	1.4280	0.9761	0.4019	0.5743	0.4519	0.2780	0.4014	0.2883	0.6255
3007850907	8.851	39.70	1.3724	0.9430	0.3105	0.6324	0.4294	0.2949	0.3528	0.3055	0.6148
3007851007	9.837	40.24	1.3283	0.9698	0.2570	0.7128	0.3585	0.3108	0.3208	0.3222	0.6231
3007851107	11.011	39.50	1.3839	0.9947	0.2455	0.7491	0.3892	0.3289	0.3139	0.3402	0.6317
2008851207	12.496	39.08	1.4733	0.9958	0.1997	0.7961	0.4775	0.3504	0.2830	0.3617	0.6320
2008851407	13.988	38.81	1.3065	1.0318	0.1624	0.8694	0.2747	0.3708	0.2552	0.3824	0.6433
2008851507	15.485	38.54	1.1659	1.0853	0.1234	0.9618	0.0806	0.3902	0.2224	0.4024	0.6596
2108851707	17.003	39.87	1.1331	1.1331	0.1203	1.0128	0.0000	0.4087	0.2197	0.4209	0.6743
2208851807	18.506	38.65	1.1299	1.1299	0.1615	0.9684	0.0000	0.4265	0.2545	0.4377	0.6732
2208852007	20.025	38.53	1.1532	1.1532	0.1948	0.9584	0.0000	0.4437	0.2796	0.4544	0.6802
3107850408	3.911	29.11	1.4811	0.9959	0.7905	0.2054	0.4852	0.1966	0.5633	0.2018	0.6323
3107850507	4.890	29.51	1.3879	0.9503	0.6900	0.2604	0.4376	0.2198	0.5260	0.2257	0.6173
3107850607	5.867	29.42	1.3812	0.9645	0.6531	0.3114	0.4167	0.2408	0.5119	0.2472	0.6220
3107850708	6.848	30.13	1.3655	0.9230	0.5511	0.3719	0.4425	0.2601	0.4706	0.2672	0.6090

TABLE C.7 (Continue)

Steam-Water Flooding Results (Low Steam Extraction Rate Tests)

TEST No	Dfin	Tsub	Mssup	MSB	MST	MSC	MSL	* Jfin	* JST	* Jf	* JSB
3107850807	7.826	29.99	1.3099	0.8919	0.4672	0.4247	0.4180	0.2780	0.4330	0.2856	0.5983
3107850907	8.799	29.14	1.3269	0.9327	0.4729	0.4598	0.3942	0.2949	0.4356	0.3027	0.6117
2508851007	9.783	30.20	1.2685	0.8909	0.3552	0.5357	0.3776	0.3108	0.3775	0.3194	0.5979
2508851108	10.953	29.91	1.2869	0.9401	0.3498	0.5903	0.3468	0.3289	0.3748	0.3379	0.6144
2508851207	12.426	28.93	1.3991	0.9614	0.3148	0.6466	0.4377	0.3504	0.3558	0.3596	0.6217
2508851407	13.916	29.49	1.3776	0.9726	0.2467	0.7259	0.4050	0.3708	0.3151	0.3805	0.6257
2508851507	15.407	29.44	1.2683	0.9920	0.2295	0.7625	0.2763	0.3902	0.3039	0.3999	0.6318
2508851707	16.910	29.91	1.2401	1.0076	0.1586	0.8490	0.2325	0.4087	0.2525	0.4190	0.6363
2508851807	18.415	29.71	1.1422	1.0673	0.2040	0.8633	0.0749	0.4265	0.2864	0.4366	0.6550
2508852007	19.928	29.72	1.0784	1.0784	0.1924	0.8860	0.0000	0.4437	0.2781	0.4536	0.6583
2506850407	3.889	19.89	1.4666	0.9838	0.8450	0.1389	0.4828	0.1966	0.5839	0.2001	0.6300
2506850508	4.860	19.52	1.4442	0.9807	0.8103	0.1704	0.4635	0.2198	0.5719	0.2237	0.6292
2506850607	5.832	19.62	1.3501	0.9084	0.7029	0.2055	0.4417	0.2408	0.5326	0.2450	0.6055
2506850707	6.801	18.98	1.3315	0.8930	0.6598	0.2332	0.4385	0.2601	0.5157	0.2646	0.6000
2506850808	7.773	18.99	1.3859	0.9149	0.6500	0.2649	0.4710	0.2780	0.5122	0.2828	0.6077
2506850907	8.743	18.88	1.3762	0.9074	0.6139	0.2935	0.4688	0.2949	0.4976	0.2999	0.6050
2506851007	9.721	19.87	1.3473	0.8980	0.5504	0.3476	0.4493	0.3108	0.4710	0.3164	0.6016
2506851107	10.881	19.40	1.3167	0.9132	0.5341	0.3791	0.4035	0.3289	0.4640	0.3347	0.6067
2506851208	12.350	19.28	1.3044	0.9407	0.5103	0.4304	0.3637	0.3504	0.4535	0.3566	0.6157
2506851407	13.831	19.79	1.2783	0.9424	0.4523	0.4901	0.3359	0.3708	0.4270	0.3774	0.6163
2506851507	15.309	19.24	1.1998	0.9091	0.3885	0.5207	0.2907	0.3902	0.3958	0.3968	0.6056
2506851707	16.802	19.62	1.1116	0.9596	0.3915	0.5681	0.1520	0.4087	0.3973	0.4156	0.6220
2506851807	18.304	20.02	1.0668	0.9664	0.3814	0.5850	0.1004	0.4265	0.3921	0.4334	0.6241
2506852007	19.807	19.99	1.0288	0.9914	0.3712	0.6202	0.0374	0.4437	0.3868	0.4507	0.6322
0306850409	3.861	9.92	1.5601	1.0420	0.9765	0.0655	0.5181	0.1966	0.6281	0.1983	0.6488
0506850508	4.825	9.68	1.4858	0.9478	0.8674	0.0804	0.5380	0.2198	0.5916	0.2216	0.6184
0506850608	5.791	9.64	1.3694	0.9111	0.8125	0.0985	0.4583	0.2408	0.5733	0.2428	0.6070
0706850707	6.756	9.77	1.4422	0.9169	0.8077	0.1092	0.5253	0.2601	0.5714	0.2622	0.6088
0706850807	7.722	9.87	1.3783	0.8686	0.7466	0.1221	0.5097	0.2780	0.5493	0.2802	0.5925
1006850908	8.686	9.67	1.4257	0.9215	0.7831	0.1384	0.5042	0.2949	0.5630	0.2973	0.6107
1106851007	9.648	9.23	1.3550	0.8771	0.7226	0.1545	0.4779	0.3108	0.5405	0.3133	0.5955
1006851107	10.804	9.33	1.3383	0.8393	0.6655	0.1738	0.4990	0.3289	0.5188	0.3316	0.5827
1106851207	12.265	9.62	1.2841	0.8334	0.6320	0.2014	0.4507	0.3504	0.5051	0.3533	0.5800
1106851407	13.726	8.89	1.3021	0.8603	0.6511	0.2092	0.4418	0.3708	0.5136	0.3736	0.5903
1206851507	15.222	9.43	1.3127	0.8800	0.6523	0.2277	0.4327	0.3904	0.5137	0.3933	0.5967
1406851707	16.685	9.70	1.2473	0.8462	0.5776	0.2685	0.4011	0.4087	0.4835	0.4120	0.5851
1406851807	18.175	9.94	1.2109	0.8923	0.6021	0.2901	0.3186	0.4265	0.4936	0.4299	0.6009
1706852007	19.665	9.74	1.1097	0.9131	0.6071	0.3059	0.1966	0.4437	0.4955	0.4472	0.6077
1706852107	21.166	9.73	1.0458	0.9605	0.6359	0.3245	0.0853	0.4603	0.5074	0.4639	0.6235
0312850414	3.841	3.22	1.3295	1.0992	1.0822	0.0170	0.2303	0.1966	0.6623	0.1970	0.6675
0312850514	4.804	3.77	1.2661	1.0308	1.0054	0.0255	0.2353	0.2198	0.6385	0.2204	0.6465
0312850612	5.762	3.15	1.2379	1.0093	0.9827	0.0266	0.2286	0.2408	0.6312	0.2413	0.6397
0312850711	6.720	2.83	1.2785	1.0258	1.0005	0.0253	0.2527	0.2601	0.6363	0.2606	0.6443
0312850812	7.685	3.68	1.3157	0.9494	0.9113	0.0381	0.3663	0.2780	0.6076	0.2787	0.6201
0312850912	8.642	3.13	1.2026	0.9348	0.8984	0.0363	0.2678	0.2949	0.6034	0.2955	0.6155
0312851012	9.604	3.30	1.2533	0.8896	0.8492	0.0404	0.3637	0.3108	0.5868	0.3115	0.6006
0312851110	10.757	3.70	1.2730	0.8983	0.8416	0.0567	0.3747	0.3289	0.5843	0.3298	0.6036
0512851210	12.203	2.85	1.1879	0.8795	0.8311	0.0485	0.3084	0.3504	0.5806	0.3511	0.5973
0512851411	13.662	2.96	1.0689	0.7903	0.7385	0.0519	0.2786	0.3708	0.5472	0.3715	0.5661
0512851510	15.125	2.84	1.0159	0.7770	0.7223	0.0547	0.2389	0.3902	0.5413	0.3909	0.5614
0512851710	16.596	2.81	0.9661	0.7391	0.6783	0.0608	0.2270	0.4087	0.5245	0.4095	0.5475
0512851812	18.074	2.89	0.8749	0.7681	0.6988	0.0693	0.1068	0.4265	0.5319	0.4273	0.5577
0512852011	19.565	3.12	0.8370	0.8108	0.7290	0.0819	0.0262	0.4437	0.5439	0.4446	0.5736
0512852110	21.059	3.12	0.8166	0.8166	0.7408	0.0758	0.0000	0.4603	0.5483	0.4611	0.5757

APPENDIX D

MATHEMATICAL ANALYSIS

APPENDIX D

This Appendix gives the mathematical analysis of Chapter six in more detail.

D.1.1 Mass Balance

Considering the control volume shown in Figure 6.1, the mass balance can be written as:

$$(M_g + \frac{d}{dz}(M_g)dz) - M_g + M_f - (M_f + \frac{d}{dz}(M_f)dz) = 0 \quad (D.1)$$

and hence

$$\frac{d}{dz}(M_f) = \frac{d}{dz}(M_g) \quad (D.2)$$

D.1.2 Momentum Balance

In the momentum balance, the net force acting on each phase in the direction of motion is equal to the rate of change of momentum of that phase. Applying this balance to both liquid and vapour phases, considering the control volume shown on Figure 6.2, yields:

(i) Liquid Phase:

$$\begin{aligned}
& \left[\left(-\frac{\pi}{4} D^2 - \frac{\pi}{4} (D-2\delta)^2 \right) p_f \right] - \left[\left(-\frac{\pi}{4} D^2 - \frac{\pi}{4} \left(D - 2 \left(\delta + \frac{d\delta}{dz} dz \right) \right)^2 \right) \left(p_f + \frac{dp_f}{dz} dz \right) \right] + \\
& \left[\left(-\frac{\pi}{4} D^2 - \frac{\pi}{4} \left(D - 2 \left(\delta + \frac{d\delta}{dz} dz \right) \right)^2 \right) - \left(-\frac{\pi}{4} D^2 - \frac{\pi}{4} (D-2\delta)^2 \right) \right] \left[\frac{1}{2} \left(p_i + \left(p_i + \frac{dp_i}{dz} dz \right) \right) \right] \\
& - \left[\frac{1}{2} \left(\pi(D-2\delta) + \pi \left(D - 2 \left(\delta + \frac{d\delta}{dz} dz \right) \right) \right) dz \tau_{fiz} \right] - \pi D dz \tau_w \Big] + \\
& \left[\rho_f g \frac{1}{2} \left(\left(-\frac{\pi}{4} D^2 - \frac{\pi}{4} (D-2\delta)^2 \right) + \left(-\frac{\pi}{4} D^2 - \frac{\pi}{4} \left(D - 2 \left(\delta + \frac{d\delta}{dz} dz \right) \right)^2 \right) \right) dz \right] = \\
& \left[M_f U_f + \frac{d}{dz} (M_f U_f) dz \right] - M_f U_f - U_g \frac{d}{dz} (M_g) dz \tag{D.3}
\end{aligned}$$

where τ_{fiz} is the vertical component of τ_{fi}

Simplifying, equation D.3, gives

$$\begin{aligned}
& \left[(\pi D \delta - \pi \delta^2) p_f \right] - \left[\left(\pi D \delta + \pi D \frac{d\delta}{dz} dz - \pi \left(\delta + \frac{d\delta}{dz} dz \right)^2 \right) \left(p_f + \frac{dp_f}{dz} dz \right) \right] + \\
& \left[\left(\pi D \delta + \pi D \frac{d\delta}{dz} dz - \pi \left(\delta + \frac{d\delta}{dz} dz \right)^2 \right) - (\pi D \delta - \pi \delta^2) \right] \left[p_i + \frac{1}{2} \frac{dp_i}{dz} dz \right] - \\
& \left[\left(\pi(D-2\delta) - \pi \left(\frac{d\delta}{dz} dz \right) \right) \tau_{fiz} dz \right] - \left[\pi D \tau_w dz \right] + \left[\rho_f g \frac{1}{2} (\pi D \delta - \pi \delta^2) \right. \\
& \left. + (\pi D \delta - \pi \delta^2 - \pi(D-2\delta) \frac{d\delta}{dz} dz - \pi \left(\frac{d\delta}{dz} dz \right)^2) \right] dz =
\end{aligned}$$

$$\frac{d}{dz} (M_f U_f) dz - U_g \frac{dM_g}{dz} dz \tag{D.4}$$

$$-\pi\delta(D-\delta)\frac{dp_f}{dz}dz - \pi(D-2\delta)\left(\frac{d\delta}{dz}\right)p_f + \pi(D-2\delta)\left(\frac{d\delta}{dz}\right)p_i - \pi(D-2\delta)$$

$$\tau_{fiz}dz - \pi D\tau_w dz + \pi\delta(D-\delta)\rho_f g dz = M_f \frac{d}{dz}(U_f)dz +$$

$$U_f \frac{d}{dz}(M_f)dz - U_g \frac{d}{dz}(M_g)dz \quad (D.5)$$

Assuming $p_f = p_g = p_i = p$, equation (D.5) becomes

$$-\pi\delta(D-\delta)\frac{dp}{dz}dz - \pi(D-2\delta)\tau_{fiz}dz - \pi D\tau_w dz + \pi\delta(D-\delta)\rho_f g dz =$$

$$M_f \frac{d}{dz}(U_f)dz + U_f \frac{d}{dz}(M_f)dz - U_g \frac{d}{dz}(M_g)dz \quad (D.6)$$

equation (D.6) can be written as:

$$\frac{dp}{dz} = -\frac{(D-2\delta)}{\delta(D-\delta)}\tau_{fiz} - \frac{D}{\delta(D-\delta)}\tau_w + \rho_f g + \frac{(D-2\delta)\rho_f U_f^2}{\delta(D-\delta)}\frac{d\delta}{dz} -$$

$$\frac{2U_f}{\pi\delta(D-\delta)}\frac{d}{dz}(M_f) + \frac{U_g}{\pi\delta(D-\delta)}\frac{d}{dz}(M_g) \quad (D.7)$$

(ii) Vapour Phase

$$\left[\frac{\pi}{4} (D-2\delta)^2 p_g - \left(\frac{\pi}{4} (D-2(\delta + \frac{d\delta}{dz}))^2 \right) (p_g + \frac{dp_g}{dz} dz) \right] - \left[\frac{1}{2} (p_i + (p_i + \frac{dp_i}{dz} dz)) \right]$$

$$\left(\frac{\pi}{4} (D-2(\delta + \frac{d\delta}{dz}))^2 - \frac{\pi}{4} (D-2\delta)^2 \right) + \left[\frac{1}{2} (\pi(D-2\delta) + \pi(D-2(\delta + \frac{d\delta}{dz}))) \right]$$

$$dz \tau_{giz}] + \left[\rho_g g \left(\frac{1}{2} \frac{\pi}{4} (D-2\delta)^2 + \frac{\pi}{4} (D-2(\delta + \frac{d\delta}{dz}))^2 \right) dz \right] =$$

$$- \left[(M_g U_g \frac{d}{dz} (M_g U_g) dz) - M_g U_g - U_g \frac{dM_g}{dz} dz \right] \quad (D.8)$$

where τ_{giz} is the vertical component of τ_{gi}

Simplifying equation (D.8), gives:

$$\left[\frac{\pi}{4} (D-2\delta)^2 p_g - \left(\frac{\pi}{4} (D-2\delta)^2 - \pi(D-2\delta) \left(\frac{d\delta}{dz} \right) + \pi \left(\frac{d\delta}{dz} \right)^2 \right) (p_g + \frac{dp_g}{dz} dz) \right]$$

$$- \left[\left(\frac{\pi}{4} (D-2\delta)^2 - \pi(D-2\delta) \left(\frac{d\delta}{dz} \right) + \pi \left(\frac{d\delta}{dz} \right)^2 \right) \frac{\pi}{4} (D-2\delta)^2 (p_i + \frac{1}{2} \frac{dp_i}{dz} dz) \right]$$

$$+ \left[\frac{1}{2} (\pi(D-2\delta) - \pi \left(\frac{d\delta}{dz} \right)) dz \tau_{giz} \right] + \left[\rho_g g \left(\frac{1}{2} \frac{\pi}{4} (D-2\delta)^2 + \right. \right.$$

$$\left. \left(\frac{\pi}{4} (D-2\delta)^2 - \pi(D-2\delta) \left(\frac{d\delta}{dz} \right) + \pi \left(\frac{d\delta}{dz} \right)^2 \right) dz \right] =$$

$$- \left[\frac{d}{dz} (M_g U_g) dz - U_g \frac{dM_g}{dz} dz \right] \quad (D.9)$$

neglecting high order terms and simplifying, equation (D.9) yields

$$\begin{aligned} & -\frac{\pi}{4}(D-2\delta)^2 \frac{dp_g}{dz} + \pi(D-2\delta) \left(\frac{d\delta}{dz}\right) p_g - \pi(D-2\delta) \left(\frac{d\delta}{dz}\right) p_i \\ & + \pi(D-2\delta) dz \tau_{giz} + \frac{\pi}{4}(D-2\delta)^2 dz \rho_g g = -M_g \frac{d}{dz}(U_g) dz \\ & -U_g \frac{d}{dz}(M_g) dz + U_g \frac{d}{dz}(M_g) dz \end{aligned} \quad (D.10)$$

Using the assumption of $p_g = p_i = p$ and simplifying equation (D.10) gives

$$\begin{aligned} & -\frac{\pi}{4}(D-2\delta)^2 \frac{dp}{dz} + \pi(D-2\delta) dz \tau_{giz} + \frac{\pi}{4}(D-2\delta)^2 dz \rho_g g = \\ & -M_g \frac{d}{dz}(U_g) dz \end{aligned} \quad (D.11)$$

equation (D.11) can be re-written as

$$\frac{dp}{dz} = \frac{4}{(D-2\delta)} \tau_{giz} + \rho_g g + \frac{4\rho_g U_g^2}{(D-2\delta)} \frac{d\delta}{dz} + \frac{4U_g}{\pi(D-2\delta)^2} \frac{d}{dz}(M_g) \quad (D.12)$$

D.1.3 Energy Conservation

When a saturated vapour moves counter-current to a subcooled liquid film, condensation occurs and energy is

transferred. Considering the control volume shown in Figure 6.3, the energy balance is:

$$[M_f \bar{h}_{fL} + (M_g h_g + \frac{d}{dz}(M_g h_g) dz)] - [M_g \bar{h}_g + (M_f h_{fL} + \frac{d}{dz}(M_f \bar{h}_{fL}) dz) = q_w \quad (D.13)$$

If the liquid film is assumed to flow over an adiabatic surface i.e. no heat losses across the tube wall, then equation (D.13) yields:

$$\frac{d}{dz}(M_f \bar{h}_{fL}) = \frac{d}{dz}(M_g h_g) \quad (D.14)$$

Since it is assumed that the vapour phase is dry saturated and the saturation temperature remains constant, therefore

$$\frac{d}{dz}(M_f \bar{h}_{fL}) = h_g \frac{d}{dz}(M_g) \quad (D.15)$$

or

$$\frac{d}{dz}(M_f C_{pf} \bar{T}_f) = (h_{fg} + h_f) \frac{d}{dz}(M_g) \quad (D.16)$$

Using equation (D.2) and equation (D.16) and simplifying gives

$$C_{pf} \bar{T}_f \frac{dM_f}{dz} + M_f \frac{d}{dz}(C_{pf} \bar{T}_f) = h_{fg} \frac{d(M_f)}{dz} + C_{pf} T_s \frac{d(M_f)}{dz} \quad (D.17)$$

If C_{pf} is assumed constant, then

$$(C_{pf} \bar{T}_f - C_{pf} T_s) \frac{d(M_f)}{dz} + M_f C_{pf} \frac{d(T_f)}{dz} = h_{fg} \frac{d(M_f)}{dz} \quad (D.18)$$

which, after rearranging, yields

$$\frac{d}{dz}(M_f) = \frac{M_f C_{pf}}{h_{fg} + C_{pf}(T_s - T_f)} \frac{d}{dz}(\bar{T}_f) \quad (D.19)$$

It is assumed that there is no slip between the two phases at the interface, therefore

$$\tau_{gi} = \tau_{fi} = \tau_i \quad (D.20)$$

and since θ is a very small angle, Figure 6.4, then

$$\tau_{giz} = \tau_{fiz} = \tau_i \quad (D.21)$$

Substituting equation (D.2) into equations (D.7) and (D.12), and eliminating the pressure gradient, gives

$$\begin{aligned} & -\frac{(D-2\delta)}{\delta(D-\delta)} \tau_i - \frac{D\tau_w}{\delta(D-\delta)} + \rho_f g - \frac{1}{\pi\delta(D-\delta)} (2U_f - U_g) \frac{dM_f}{dz} + \frac{(D-2\delta)\rho_f U_f^2}{\delta(D-\delta)} \frac{d\delta}{dz} = \\ & \frac{4}{(D-2\delta)} \tau_i + \rho_g g + \frac{4\rho_g U_g^2}{(D-2\delta)} \frac{d\delta}{dz} + \frac{4U_g}{\pi(D-2\delta)^2} \frac{d}{dz} (M_f) \quad (D.22) \end{aligned}$$

or

$$\begin{aligned} & \frac{(D-2\delta)\rho_f U_f^2}{\delta(D-\delta)} \frac{d\delta}{dz} - \frac{4\rho_g U_g^2}{(D-2\delta)} \frac{d\delta}{dz} = \left(\frac{D-2\delta}{\delta(D-\delta)} + \frac{4}{(D-2\delta)^2} \right) \tau_i + \frac{D\tau_w}{\delta(D-\delta)} - \rho_f g \\ & + \rho_g g + \frac{1}{\pi\delta(D-\delta)} (2U_f - U_g) \frac{dM_f}{dz} + \frac{4U_g}{\pi(D-2\delta)^2} \frac{d}{dz} (M_f) \quad (D.23) \end{aligned}$$

$$\left(\frac{(D-2\delta)\rho_f U_f^2}{\delta(D-\delta)} - \frac{4\rho_g U_g^2}{(D-2\delta)} \right) \frac{d\delta}{dz} = \frac{(D-2\delta)^2 + 4\delta(D-\delta)}{\delta(D-\delta)(D-2\delta)} \tau_i + \frac{D\tau_w}{\delta(D-\delta)} - (\rho_f - \rho_g)g + \left(\frac{2U_f - U_g}{\pi\delta(D-\delta)} + \frac{4U_g}{\pi(D-2\delta)^2} \right) \frac{dM_f}{dz} \quad (D.24)$$

and hence

$$\frac{d\delta}{dz} = \left\{ \frac{(D-2\delta)^2 + 4\delta(D-\delta)}{\delta(D-\delta)(D-2\delta)} \tau_i + \frac{D\tau_w}{\delta(D-\delta)} - (\rho_f - \rho_g)g + \left(\frac{2U_f - U_g}{\pi\delta(D-\delta)} + \frac{4U_g}{\pi(D-2\delta)^2} \right) \frac{dM_f}{dz} \right\} / \left\{ \frac{(D-2\delta)\rho_f U_f^2}{\delta(D-\delta)} - \frac{4\rho_g U_g^2}{(D-2\delta)} \right\} \quad (D.25)$$

Substituting the values of τ_i and τ_w (See Chapter 6) into equation (D.25), gives

$$\frac{d\delta}{dz} = \left\{ \frac{D^2}{D^2\delta - 3\delta^2 D + 2\delta^3} \frac{1}{2} \rho_g f_i (U_g - U_f)^2 + \frac{DC\rho_f U_f^2}{2\delta(D-\delta)(Re_f)^n} - (\rho_f - \rho_g)g + \left(\frac{2U_f - U_g}{\pi\delta(D-\delta)} + \frac{4U_g}{\pi(D-2\delta)^2} \right) \frac{dM_f}{dz} \right\} / \left\{ \frac{(D-2\delta)\rho_f U_f^2}{\delta(D-\delta)} - \frac{4\rho_g U_g^2}{(D-2\delta)} \right\} \quad (D.26)$$

re-arranging, gives

$$\frac{d\delta}{dz} = \left\{ \frac{D^2}{2(D^2\delta - 3\delta^2 D + 2\delta^3)} \rho_g f_i (U_g - U_f)^2 + \frac{DC\rho_f U_g^2}{(Re_f)^n} - (\rho_g - \rho_g)g + \left[\frac{2U_f - U_g}{\pi\delta(D-\delta)} + \frac{4U_g}{\pi(D-2\delta)^2} \right] \frac{dM_f}{dz} \right\} / \left\{ \frac{(D-2\delta)\rho_f U_f^2}{\delta(D-\delta)} - \frac{4\rho_g U_g^2}{(D-2\delta)} \right\} \quad (D.27)$$

Consider the non-dimensional terms

$$z^+ = z/L \quad Fr_f = \frac{u_f}{(gL)^{1/2}} = \frac{Q_f}{\pi\delta(D-\delta)(gL)^{1/2}}$$

$$\delta^+ = \delta/L \quad Fr_g = \frac{u_g}{(gL)^{1/2}} = \frac{4Q_g}{\pi(D-2\delta)^2(gL)^{1/2}} \quad (D.28)$$

$$D^+ = D/L$$

$$\rho^+ = \rho_g/\rho_f \quad Re_f = \frac{\rho_f Q_f}{\pi(D-\delta)\mu_f}$$

then equation (D.27) can be made dimensionless by using (D.28), to give

$$\frac{d\delta^+}{dz^+} = \left\{ \frac{D^{+2}}{2(D^{+2}\delta^+ - 3\delta^{+2}D^+ + 2\delta^+3)} \rho_g f_i g Fr_g - Fr_f^2 + \frac{D^+ C \rho_f g Fr_f^2}{2\delta^+(D^+ - \delta^+)(Re_f)^n} \right. \\ \left. - (\rho_f - \rho_g)g \left[\frac{2Fr_f - Fr_g}{\pi\delta^+(D^+ - \delta^+)} \frac{1}{L} \frac{g}{L}^{1/2} + \frac{4Fr_g}{\pi(D^+ - 2\delta^+)^2} \frac{1}{L} \frac{g}{L}^{1/2} \right] \frac{dM_f}{dz} \right\} / \\ \left\{ \frac{(D^+ - 2\delta^+)\rho_f g}{\delta^+(D^+ - \delta^+)} Fr_f^2 - \frac{4\rho_g g}{(D^+ - 2\delta^+)} Fr_g^2 \right\} \quad (D.29)$$

Dividing by $(\rho_f g)$, and re-arranging, yields:

$$\frac{d\delta^+}{dz^+} = \left\{ \frac{D^{+2}}{2D^{+2}\delta^+ - 6\delta^+2D^+ + 4\delta^+3} f_i \rho^+ (Fr_g - Fr_f)^2 + \frac{D^+ C Fr_f^2}{2\delta^+(D^+ - \delta^+)(Re_f)^n} \right. \\ \left. - (1 - \rho^+) \left[\frac{2Fr_f - Fr_g}{\pi\delta^+(D^+ - \delta^+)} + \frac{4Fr_g}{\pi(D^+ - 2\delta^+)^2} \right] \frac{1}{\rho_f (gL)^{1/2}} \frac{dM_f}{dz} \right\} / \\ \left\{ \frac{(D^+ - 2\delta^+) Fr_f^2}{\delta^+(D^+ - \delta^+)} - \frac{4\rho^+ Fr_g^2}{(D^+ - 2\delta^+)} \right\} \quad (D.30)$$

Substituting equation (D.19) into equation (D.30) gives

$$\begin{aligned} \frac{d\delta^+}{dz^+} = & \left\{ \frac{D^{+2}}{2D^{+2}\delta^+ - 6\delta^{+2}D^+ + 4\delta^{+3}} f_i \rho^+ (Fr_g - Fr_f)^2 + \frac{D^+ C Fr_f^2}{2\delta^+ (D^+ - \delta^+) (Re_f)^n} \right. \\ & \left. - (1 - \rho^+) + \left[\frac{2Fr_g - Fr_g}{\pi\delta^+ (D^+ - \delta^+)} + \frac{4Fr_g}{\pi(D^+ - 2\delta^+)^2} \right] \frac{\pi\delta(D - \delta)U_f}{L(gL)^{1/2}} \right. \\ & \left. \frac{Cp_f}{h_{fg} + Cp_f(T_s - T_f)} \frac{dT_f^-}{dz} \right\} / \left\{ \frac{(D^+ - 2\delta^+) Fr_f^2}{\delta^+ (D^+ - \delta^+)} - \frac{4\rho^+ Fr_g^2}{(D^+ - 2\delta^+)} \right\} \end{aligned} \quad (D.31)$$

Consider the non-dimensional terms of

$$\begin{aligned} T^+ &= \bar{T}_f / T_{in} \\ T_s^+ &= T_s / T_{in} \\ HCP^+ &= h_{fg} / Cp_f T_{in} \end{aligned} \quad (D.32)$$

Substituting (D.32) into equation (D.31), gives

$$\begin{aligned} \frac{d\delta^+}{dz^+} = & \left\{ \frac{D^{+2}}{(2D^{+2}\delta - 6\delta^2D^+ + 4\delta^2)} f_i \rho^+ (Fr_g - Fr_f)^2 + \frac{D^+ C Fr_f^2}{2(\delta^+ D^+ - \delta^{+2}) (Re_f)^n} \right. \\ & \left. - (1 - \rho^+) + \left[\frac{2Fr_f - Fr_g}{(\delta^+ D^+ - \delta^{+2})} + \frac{4Fr_g}{(D^+ - 2\delta^+)^2} \right] \right. \\ & \left. \frac{Fr_f \delta^+ (D^+ - \delta^+)}{HCP^+ + (T_s^+ - T^+)} \frac{dT^+}{dz^+} \right\} / \left\{ \frac{(D^+ - 2\delta^+) Fr_f^2}{(\delta^+ D^+ - \delta^{+2})} - \frac{4\rho^+ Fr_g^2}{(D^+ - 2\delta^+)} \right\} \end{aligned} \quad (D.33)$$

As $\delta \ll D$, then equation (D.33) can be written as

$$\frac{d\delta^+}{dz^+} = \left\{ \frac{1}{2\delta^+} f_i \rho^+ (Fr_g - Fr_f)^2 + \frac{C Fr_f^2}{2\delta^+ (Re_f)^n} - (1 - \rho^+) + \left[\frac{Fr_f - Fr_g}{\delta^+ D^+} + \frac{4Fr_g}{(D^+ - 2\delta^+)^2} \right] \frac{\delta^+ D^+ Fr_f}{HCP^+ + (T_s^+ - T^+)} \frac{dT^+}{dz^+} \right\} / \left\{ \frac{Fr_f^2}{\delta^+} - \frac{4\rho^+ Fr_g^2}{(D^+ - 2\delta^+)^2} \right\} \quad (D.34)$$

This is equation 6.27 in Chapter 6 which represents the variation in the film thickness along the test tube.

D.2 Flooding with Uniform Film Including Condensation:

The velocity potential in a stream of gas (vapour) flow with flat interface, Figure 6.6, can be defined as

$$\phi = U_f z + V_f y \quad (D.35)$$

Then

$$u = \frac{\partial \phi}{\partial z} = U_f \quad (D.36)$$

and

$$v = \frac{\partial \phi}{\partial y} = V_f \quad (D.37)$$

The velocity potential can be represented by

$$\phi = U_f z + V_f y + \phi' \quad (D.38)$$

where ϕ' is the velocity potential variation due to the perturbation, then

$$\frac{\partial^2 \phi'}{\partial z^2} + \frac{\partial^2 \phi'}{\partial y^2} = 0 \quad (\text{D.39})$$

seeking a solution of equation (D.39) of the form

$$\phi' = G(t) H(z) I(y) \quad (\text{D.40})$$

gives, from equation (D.39)

$$\frac{1}{H} \frac{\partial^2 H}{\partial z^2} = \frac{1}{I} \frac{\partial^2 I}{\partial y^2} = -\beta^2 \quad (\text{D.41})$$

The constant of separation is assumed negative since a solution sinusoidal in z and exponential in y is required, thus

$$H = A \cos \beta z + B \sin \beta z \quad (\text{D.42})$$

and

$$I = E \cosh \beta y + F \sinh \beta y \quad (\text{D.43})$$

which gives from equation (D.40) (D.44)

$$\phi' = G(t) (A \cos \beta z + B \sin \beta z) (E \cosh \beta y + F \sinh \beta y) \quad (\text{D.45})$$

and consequently

$$\frac{\partial \phi'}{\partial y} = G(t) \beta (A \cos \beta z + B \sin \beta z) (E \sinh \beta y + F \cosh \beta y) \quad (\text{D.46})$$

The boundary conditions are:

- (i) no velocity normal to the wall at some distance h from the wall where $h = 0$ for the liquid phase and ∞ for the gas phase, i.e.

$$\text{or } \left. \begin{array}{l} y = h \\ \\ y = \infty \end{array} \right\} \frac{d\phi'}{dy} = 0 \quad (\text{D.47})$$

(ii) the kinematic condition at the gas (vapour)-liquid interface, i.e.

$$y = \delta, \quad v_g + \frac{\partial \phi'}{\partial y} = \frac{\partial \eta}{\partial t} + u \frac{\partial \eta}{\partial z} + v(\delta, \eta) \quad (\text{D.48})$$

where

$$\eta = \eta_0 \exp(ik(z-ct)) \quad (\text{D.49})$$

Then

$$v_g + \frac{\partial \phi'}{\partial y} = -ik\eta_0 \exp[ik(z-ct)] + uik\eta_0 \exp[ik(z-ct)] + v(\delta, z) \quad (\text{D.50})$$

$$= ik\eta_0(u-c) \exp[ik(z-ct)] + v(\delta, z) \quad (\text{D.51})$$

For flat surface the gas (vapour) velocity normal to the interface can be represented by

$$v_g = - \frac{k_f(T_s - T_f)}{\delta} \frac{1}{\rho_g h_{fg}} \quad (\text{D.52})$$

or

$$v(\delta, z) = - \frac{k_f(T_s - T_f)}{\delta + \eta} \frac{1}{\rho_g h_{fg}} = - \frac{k_f(T_s - T_f)}{\delta \rho_g h_{fg}} \left(1 - \frac{\eta}{\delta}\right) \quad (\text{D.53})$$

$$\therefore v(\delta, z) = V_g \left(1 - \frac{\eta}{\delta}\right) \quad (\text{D.54})$$

$$\therefore v_g + \frac{\partial \phi'}{\partial y} = ik\eta_0 (u-c) \exp[ik(z-ct)] + v_g \left(1 - \frac{\eta}{\delta}\right) \quad (D.55)$$

$$\therefore \frac{\partial \phi'}{\partial y} = \exp[ik(z-ct)] \left[ik\eta_0 (u-c) - \frac{v_g \eta_0}{\delta} \right] \quad (D.56)$$

Now, boundary conditions (D.47), gives from equation (D.46)

$$0 = \beta(E \sin \beta h + F \cosh \beta h) \quad (D.57)$$

$$\text{or } F = -E \tanh \beta h \quad (D.58)$$

when $h \rightarrow \infty$, then

$$F = -E \quad (D.59)$$

Then equation (D.45), becomes

$$\phi' = G(t) (A \cos \beta z + B \sin \beta z) E (\cosh \beta y - \sinh \beta y) \quad (D.60)$$

or

$$\phi' = G(t) (A \cos \beta z + B \sin \beta z) E \exp(-\beta y) \quad (D.61)$$

Applying boundary condition (D.49) to equation (D.61), gives

$$\frac{\partial \phi'}{\partial y} = -E\beta \exp(-\beta \delta) G(t) (A \cos \beta z + B \sin \beta z) \quad (D.62)$$

but from equation (D.56)

$$\frac{\partial \phi'}{\partial y} = \exp[ik(z-ct)] \left[ik\eta_0 (u-c) - \frac{v_g \eta_0}{\delta} \right]$$

hence

$$\beta = k, \quad \frac{B}{A} = i$$

and then equation (D.61) becomes

$$\phi' = G(t)(AE) \exp[k(iz-y)] = G(t)(AE) \exp[ik(z+iy)] \quad (D.63)$$

and

$$\frac{\partial \phi'}{\partial y} = Ek \exp(-k\delta) G(t) A \exp(ikz) = \exp[ik(z-ct)] \left[ik\eta_0(u-c) - \frac{v_g \eta_0}{\delta} \right] \quad (D.64)$$

then

$$G(t) = \left[ik\eta_0(u-c) - \frac{v_g \eta_0}{\delta} \right] \exp(ikct) / (AD)k \exp(-k\delta) \quad (D.65)$$

substituting equation (D.65) into equation (D.63) gives

$$\phi' = \left[i(u-c)\eta_0 - \frac{v_g \eta_0}{k\delta} \right] \exp[-k(y-\delta)] \exp[ik(z-ct)] \quad (D.66)$$

Applying equation (D.66) for the liquid phase when $u = U'_f$,

then

$$\phi'_f = [i(U_f - c)] \eta_0 \exp[ik(y-\delta)] \exp[ik(z-ct)] \quad (D.67)$$

and for the gas(vapour) phase where $u = -U_g$ to give

$$\phi'_g = -\left[i(U_g - c) + \frac{v_g}{k\delta} \right] \eta_0 \exp[-k(y-\delta)] \exp[ik(z-ct)] \quad (D.68)$$

Bernoullis equation can be written as

$$\frac{p}{\rho} + \frac{\partial \phi}{\partial t} + \frac{1}{2} \left(\frac{\partial \phi}{\partial z} \right)^2 + \frac{1}{2} \left(\frac{\partial \phi}{\partial y} \right)^2 = C_1 \quad (D.69)$$

where C_1 is a constant or time dependent function.

Since $\phi = u_f z + v_g y + \phi'$, then equation (D.69) can be written as

$$\frac{p}{\rho} + \frac{\partial \phi'}{\partial t} + \frac{1}{2} \left(U + \frac{\partial \phi'}{\partial z} \right)^2 + \frac{1}{2} \left(v_g + \frac{\partial \phi'}{\partial y} \right)^2 = C_1 \quad (D.70)$$

Note that all perturbed quantities (denoted by (')) are all proportional to perturbation η .

Neglecting terms of order η^2 or above, equation (D.70)

becomes, for the liquid phase, as

$$\frac{p}{\rho_f} + \frac{\partial \phi'_f}{\partial t} + \frac{U_f^2}{2} + U_f \frac{\partial \phi'_f}{\partial z} = C_2 \quad (\text{D.71})$$

and for the gas (vapour) phase as

$$\frac{p}{\rho_g} + \frac{\partial \phi'_g}{\partial t} + \frac{U_g^2}{2} = U_g \frac{\partial \phi'_g}{\partial z} + \frac{V_g^2}{2} + V_g \frac{\partial \phi'_g}{\partial y} = C_3 \quad (\text{D.72})$$

The boundary condition is that at $z = 0$ all perturbed quantities are negligible, thus

$$C_2 = \frac{p_0}{\rho_f} + \frac{U_f^2}{2} \quad (\text{D.73})$$

and

$$C_3 = \frac{p_0}{\rho_g} + \frac{U_g^2 + V_g^2}{2} \quad (\text{D.74})$$

where p_0 is the static pressure at $z = 0$.

Defining a perturbed pressure difference by

$$p' = p - p_0 \quad (\text{D.75})$$

allows equation (D.71) to be rewritten as

$$\frac{p'_f}{\rho_f} + \frac{\partial \phi'_f}{\partial t} + U_f \frac{\partial \phi'_f}{\partial z} = 0 \quad (\text{D.76})$$

and equation (D.72) becomes

$$\frac{p'_g}{\rho_g} + \frac{\partial \phi'_g}{\partial t} - U_g \frac{\partial \phi'_g}{\partial z} + V_g \frac{\partial \phi'_g}{\partial y} = 0 \quad (\text{D.77})$$

Using equation (D.67) gives for the liquid phase

$$\frac{\partial \phi_f'}{\partial z} = -k(U_f - c)\eta_0 \exp[-k(y - \delta)] \exp[ik(z - ct)] \quad (D.78)$$

and

$$\frac{\partial \phi_f'}{\partial t} = kc (U_f - c)\eta_0 \exp[-k(y - \delta)] \exp[ik(z - ct)] \quad (D.79)$$

and hence from equation (D.77)

$$p_f' = \rho_f k (U_f - c)^2 \eta_0 \exp[-k(y - \delta)] \exp[ik(z - ct)] \quad (D.80)$$

For the gas phase, from equation (D.69)

$$\frac{\partial \phi_g'}{\partial z} = -ik \left[i(U_g + c) + \frac{v_g}{k\delta} \right] \eta_0 \exp[-k(y - \delta)] \exp[ik(z - ct)] \quad (D.81)$$

$$\frac{\partial \phi_g'}{\partial t} = ikc \left[i(U_g + c) + \frac{v_g}{k\delta} \right] \eta_0 \exp[-k(y - \delta)] \exp[ik(z - ct)] \quad (D.82)$$

and

$$\frac{\partial \phi_g'}{\partial y} = k \left[i(U_g + c) + \frac{v_g}{k\delta} \right] \eta_0 \exp[-k(y - \delta)] \exp[ik(z - ct)] \quad (D.83)$$

and hence from equations (D.78)

$$p_g' = -\rho_g k \left[i(U_g + c) + \frac{v_g}{k\delta} \right] \left[i(U_g + c) + v_g \right] \eta_0 \exp[-k(y - \delta)] \exp[ik(z - ct)] \quad (D.84)$$

which is equation (6.67) in Chapter 6.